ONE- AND TWO-DIMENSIONAL MASS SPECTROMETRY IN A LINEAR QUADRUPOLE ION TRAP

by

Dalton Thomas Snyder

A Dissertation

Submitted to the Faculty of Purdue University

In Partial Fulfillment of the Requirements for the degree of

Doctor of Philosophy

Department of Chemistry

West Lafayette, Indiana

December 2018

THE PURDUE UNIVERSITY GRADUATE SCHOOL
STATEMENT OF COMMITTEE APPROVAL

Dr. Graham Cooks, Chair
> Department of Chemistry

Dr. Scott McLuckey
> Department of Chemistry

Dr. Dor Ben-Amotz
> Department of Chemistry

Dr. Garth Simpson
> Department of Chemistry

Approved by:
> Dr. Christine Hrycyna
>> Head of the Graduate Program

For Mom, Dad, Nick, Dylan, and Ryan

ACKNOWLEDGMENTS

A PhD is a collaborative achievement, and I have many individuals to thank for their help during my time at Purdue. First and foremost, I must thank my PhD adviser Prof. Graham Cooks for his exceptional guidance and neverending support. I am especially grateful for his suggestions and kind letters of recommendation which led to many opportunities to which I would have otherwise not had access. Brandy McMasters was the other critical piece of the puzzle; our lab would not function properly without her! I also appreciate the support and recommendations from my committee members, namely Prof. Mahdi Abu-Omar (formerly on my committee), Prof. Scott McLuckey, Prof. Dor Ben-Amotz, and Prof. Garth Simpson. Other faculty and staff at Purdue that played significant roles in my graduate career include Ned Gangwer, Betty Dexter, Aaron Harkleroad, Steven Barker, and various members of the Jonathan Amy Facility for Chemical Instrumentation. Dr. Ryan Hilger, Mark Carlsen, and Greg Eakins made particularly notable contributions in terms of electronics design and installation, Dr. Hartmut Hedderich performed gold deposition experiments on various electrodes for surface-induced dissociation experiments, and Randy Repogle fabricated several components that I used.

My labmates, both in and out of Aston Labs, were critical to my development as a person and as a scientist. I thank Dr. Zane Baird, Dr. Adam Hollerbach, and Dr. Wen-Ping Peng for their help with electronics (since usually I had no idea what I was doing). Thanks to Dr. Steve Ayrton for his outstanding figures and his always-enlightening discussions with me regarding ion traps and other scientific things. Dr. Ryan Bain and Dr. Chris Pulliam worked with me and guided me through my first 2-3 years, and I am thankful for the opportunity to work with and befriend both of them. Dr. Alan Jarmusch and Dr. Anyin Li were the scientists I looked up to the most, and as such I almost always trusted their judgement on various matters. Clint Alfaro and Dr. Valentina Pirro were a pleasure to work with on DESI-related projects and were also exceptionally interesting people. Dr. Karen Yanell was always the go-to person for biological studies, quantitation, and reproducibility, and I appreciated her input when provided. Rob Schrader, Lucas Szalwinski, and Kiran Iyer were excellent office-mates through-and-through and cheered me up many times when I was not feeling well. In addition, Rob provided several remarkable figures, Lucas was a pleasure to mentor (and has a bright future), and Kiran and I always appreciated our fair share of beverages and old people jokes. Thanks to all my other labmates for their support as

well, and special thanks to Dr. Joann Max and Casey Smith for collaborating with me on projects (and for fun Wine Wednesdays in the case of Joann).

I was fortunate enough to have several non-Purdue collaborators who helped me and guided me through my graduate studies. Notable individuals from NASA Goddard Space Flight Center include the always inseparable Dr. Desmond Kaplan and Dr. Ryan Danell as well as Dr. Veronica Pinnick, Dr. Friso van Amerom, Dr. Andrej Grubisic, Dr. Will Brinckerhoff, Dr. Marco Castillo, and Dr. Paul Mahaffy. I especially owe Desmond for helping me network at ASMS and for our high-level conversations about ion traps, and Ryan for allowing us to use his RITS ion trap software and for DAQ guidance. I thank my Merck collaborators – Dr. Alice Newman (formerly Pilo) and Dr. Nina Jarrah – for believing in an ion trap scan mode project despite having many detractors. I also thank Dr. Mitch Wells, Dr. Leonard Rorrer, and Dr. Dennis Barket at FLIR Systems, Inc. for the outstanding instrumentation collaboration in which I was happy to be involved. Dr. Jae Schwartz (Thermo Fisher Scientific) also provided guidance on several issues and even pre-reviewed an invited review article, which was greatly appreciated.

I need to thank my non-Purdue friends and family who kept me sane during my time at Purdue and with whom I have had a great four years of fun. Life would not have been nearly as bearable without weekends with 'the neighbors', i.e. Adrian Bohanan and Dr. Allison Heaslip, and many others including Doug and Dan Peo, Corey Denton, Wes and Lindsay Bird, Ben and Matt, Brittany Herriott, Jake and Alyssa Rowe, and (my other neighbors) Brad and Amy. Lastly, I thank my family – mom, dad, Nick, Dylan, and Ryan – for their unending support and kindness for which I am eternally grateful.

TABLE OF CONTENTS

LIST OF TABLES

LIST OF FIGURES

LIST OF SCHEMES

LIST OF SUPPLEMENTARY TABLES

LIST OF SUPPLEMENTARY FIGURES

ABSTRACT

Author: Snyder, Dalton, T. PhD
Institution: Purdue University
Degree Received: December 2018
Title: One- and Two-dimensional Mass Spectrometry in a Linear Quadrupole Ion Trap
Committee Chair: Graham Cooks

Amongst the various classes of mass analyzers, the quadrupole ion trap (QIT) is by far the most versatile. Although it can achieve only modest resolution (unit) and mass accuracy (10^1-10^2 ppm), it has high sensitivity and selectivity, can operate at pressures exceeding 10^{-3} torr, is tolerant to various electrode imperfections, and has single analyzer tandem mass spectrometry (MS/MS) capabilities in the form of product ion scans. These characteristics make the QIT ideal for mass spectrometer miniaturization, as most of the fundamental performance metrics of the QIT do not depend on device size. As such, the current drive in miniature systems is to adopt miniature ion traps in various forms – 3D, linear, toroidal, rectilinear, cylindrical, arrays, etc.

Despite being one of the two common mass analyzers with inherent MS/MS capabilities (the other being the Fourier transform ion cyclotron resonance mass spectrometer), it is commonly accepted that the QIT cannot perform one-dimensional precursor ion scans and neutral loss scans - the other two main MS/MS scan modes - or two-dimensional MS/MS scans. The former two are usually conducted in triple quadrupole instruments in which a first and third quadrupole are used to mass select precursor and product ions while fragmentation occurs in an intermediate collision cell. The third scan can be accomplished by acquiring a product ion scan of every precursor ion, thus revealing the entire 2D MS/MS data domain (precursor ion m/z vs. product ion m/z). This, however, is not one scan but a set of scans. Because the ion trap is a tandem-in-time instrument rather than a tandem-in-space analyzer, precursor ion scans, neutral loss scans, and 2D MS/MS are, at best, difficult.

Yet miniature mass spectrometers utilizing quadrupole ion traps for mass analysis would perhaps benefit the most from precursor scans, neutral loss scans, and 2D MS/MS because they generally have acquisition rates (# scans/s) an order of magnitude lower than their benchtop counterparts. This is because they usually use a discontinuous atmospheric pressure interface (DAPI) to reduce the gas load on the backing pumps, resulting in a ~1 scan/s acquisition rate and

making the commonly-used data-dependent acquisition method (i.e. obtaining a product ion scan for every abundant precursor ion) inefficient in terms of sample consumption, time, and instrument power. Precursor and neutral loss scans targeting specific molecular functionality of interest - as well as 2D MS/MS – are more efficient ways of moving through the MS/MS data domain and thus pair quite readily with miniature ion traps.

Herein we demonstrate that precursor ion scans, neutral loss scans, and 2D MS/MS are all possible in a linear quadrupole ion trap operated in the orthogonal double resonance mode on both benchtop and portable mass spectrometers. Through application of multiple resonance frequencies matching the secular frequencies of precursor and/or product ions of interest, we show that precursor ions can be fragmented mass-selectively and product ions ejected simultaneously, preserving their relationship, precursor ion -> product ion + neutral, in the time domain and hence allowing the correlation between precursor and product ions without prior isolation. By fixing or scanning the resonance frequencies corresponding to the targeted precursor and product ions, a precursor ion scan or neutral loss scan can be conducted in a single mass analyzer. We further show that 2D MS/MS - acquisition of all precursor ion *m/z* values and a product ion mass spectrum for every precursor ion, all in a single scan - is possible using similar methodology. These scan modes are particularly valuable for origin-of-life and forensic applications for which the value of miniature mass spectrometers is readily evident.

CHAPTER 1.   INTRODUCTION

1.1   The Structure of the Quadrupole Ion Trap

Wolfgang Paul in the early 1950s filed a patent for the 3D quadrupole ion trap (QIT) and 2D quadrupole mass filter,[1-3] for which he later shared one-half of the Nobel Prize in Physics in 1989 with Hans Dehmelt.[4] Structurally, the QIT consists of a ring electrode and two endcap electrodes, all with hyperbolic cross sections, and the quadrupole is constructed from a set of four parallel rods arranged in a square array. Through application of a sinusoidal radiofrequency potential (the 'rf') to the ring electrode (QIT), a quadrupole potential is produced.[5-9] For the mass filter, one phase of rf is applied to rods opposite each other – which are electrically connected – while an rf180° out-of-phase is applied to the other pair of rods. The quadrupolar 'field' (a misnomer but nonetheless common) allows trapping of kinetically cooled ions and has become the basis of much of mass spectrometry today.

The quadrupole ion trap can adopt dozens of different structures (**Figure 1.1**) which all produce approximately quadrupolar fields. If endcap lenses are added to a mass filter to trap ions axially along the length of the device, then a 2D linear quadrupole ion trap is obtained.[10,11] The linear ion trap operates similarly to the 3D QIT but offers improved trapping efficiency upon ion injection as well as increased ion storage capacity (dynamic range).[12] The quadrupole electrodes can be made flat instead of curved to ease machining costs and simplify fabrication, resulting in cylindrical[13-15] and rectilinear[16] ion trap geometries but also sacrificing electric field fidelity. The 3D QIT can be wrapped around an axis perpendicular to its endcaps but offset from the center of the device to produce a donut-shaped toroidal ion trap,[17] whose electrodes can once again be simplified to produce flat surfaces.[18,19]
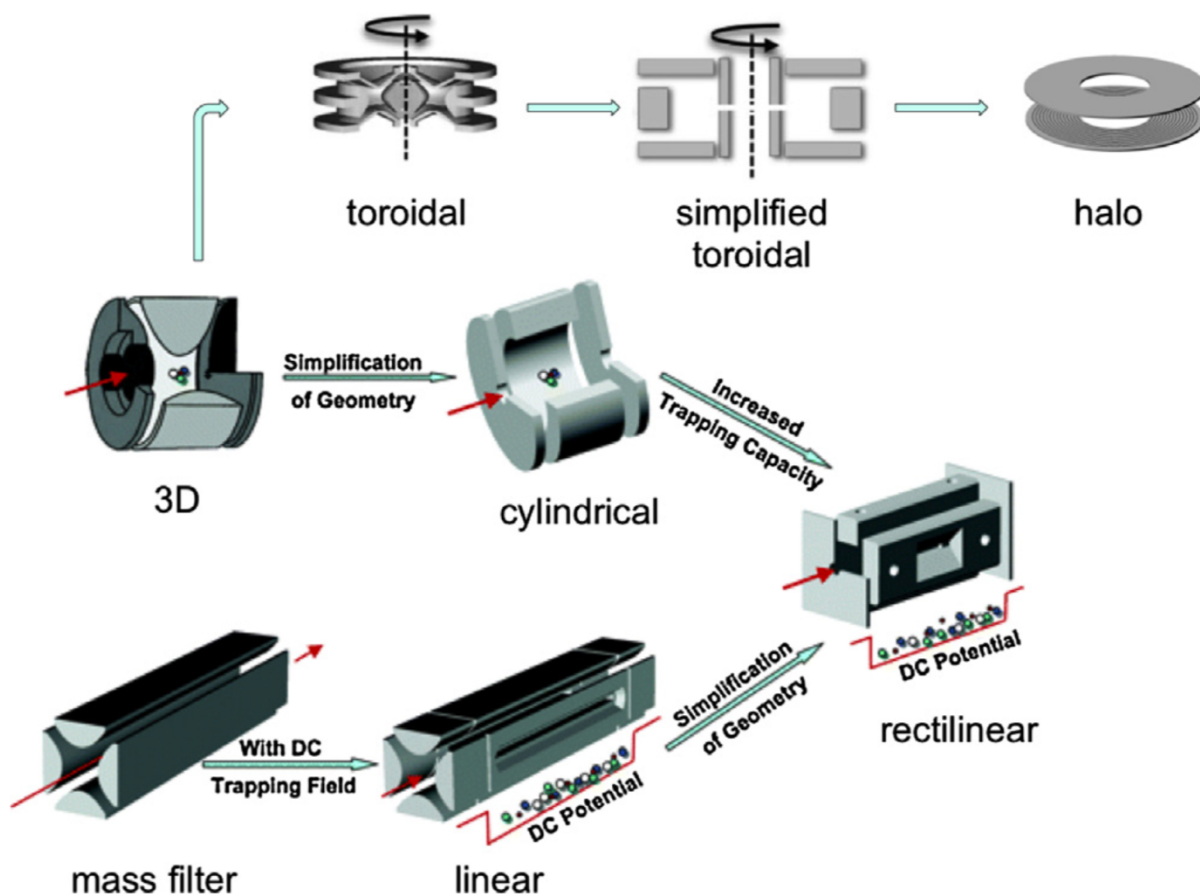
Figure 1.1. Several different electrode geometries which produce approximate quadrupolar potentials. Reproduced from *Chem. Phys. Lett.* **2017***, 668*, 69-89.

1.2 Electric Potential, Equations of Motion, and the Mathieu Parameters

A general characteristic of a quadrupole field is that the electric field strength varies linearly with distance in the quadrupole dimensions (x and y for a device with quadrupole field in two dimensions and r and z for a device with quadrupole field in three dimensions, e.g. a QIT),[9] i.e.

$$\boldsymbol{E} = E_0(\lambda x + \sigma y + \gamma z)$$

Eq. 1.1

Because this equation must satisfy Laplace's equation, we have

$$\lambda + \sigma + \gamma = 0$$

Eq. 1.2

and if we simply assume that

$$\lambda = -\sigma \qquad \text{Eq. 1.3}$$

and

$$\gamma = 0 \qquad \text{Eq. 1.4}$$

(that is, there is only a quadrupole potential in x and y but not z) then eq. 1.1 becomes

$$\mathbf{E} = \lambda E_0 (x - y) \qquad \text{Eq. 1.6}$$

Because the electric field strength is the negative of the derivative of the potential with respect to the coordinates, we have

$$\mathbf{\Phi} = -\frac{1}{2} \lambda E_0 (x^2 - y^2) \qquad \text{Eq. 1.7}$$

If the half-distance between opposing electrodes is r_0 and opposite phases of rf are applied to the two sets of rods (for the quadrupole mass filter or linear ion trap in this case), then this equation becomes

$$\mathbf{\Phi} = \frac{\Phi_0 (x^2 - y^2)}{2r_0^2} \qquad \text{Eq. 1.8}$$

because we have

$$\lambda = -\frac{1}{r_0^2} \qquad \text{Eq. 1.9}$$

For the 3D QIT, eq. 1.8 is

$$\Phi = \frac{\Phi_0(r^2 - 2z^2)}{r_0^2 + 2z_0^2}$$ Eq. 1.10

We can deduce the equations of motion from Newton's second law ($F = ma$, where m is the mass of the ion, F is the electric force on the ion, and a is the acceleration of the ion) and the relation $E = F/qe$ (where E is the electric field strength, q is the integer number of charges on the ion, and e is the elementary charge) so that

$$qeE_u = ma_u$$ Eq. 1.11

where u is x, y, r, or z. Rearranging we obtain

$$a_u - \frac{qeE_u}{m} = 0$$ Eq. 1.12

which, through substitution of the partial derivatives of eq. 1.8, becomes

$$a_x + \frac{qe}{mr_0^2}\Phi_0 x = 0$$ Eq. 1.13

$$a_y - \frac{qe}{mr_0^2}\Phi_0 y = 0$$ Eq. 1.14

Generally, sinusoidal rf potentials (V_{rf}, zero-to-peak) are applied to QITs as well as quadrupole DC potentials (U_{dc}, i.e. the pairs of rods are held at a constant potential offset each other) so that

$$\Phi_0 = U_{dc} - V_{rf}\cos\Omega t$$ Eq. 1.15

where Ω is the angular rf frequency ($\Omega = 2\pi f$, where Ω is the frequency in Hz, usually ~1 MHz) and t is time. With substitution into eqs. 1.13 and 1.14 we obtain

$$a_x + \frac{qe}{mr_0^2}(U_{dc} - V_{rf}\cos\Omega t)x = 0$$ Eq. 1.16

$$a_y - \frac{qe}{mr_0^2}(U_{dc} - V_{rf}\cos\Omega t)y = 0 \qquad\qquad \text{Eq. 1.17}$$

With the following conventional substitutions,

$$a_u = a_x = -a_y = \frac{8qeU_{dc}}{m\Omega^2 r_0^2} \qquad\qquad \text{Eq. 1.18}$$

$$q_u = q_x = -q_y = \frac{4qeV_{rf}}{m\Omega^2 r_0^2} \qquad\qquad \text{Eq. 1.19}$$

$$\xi = \frac{\Omega t}{2} \qquad\qquad \text{Eq. 1.20}$$

the equations of ion motion become

$$\frac{d^2 u}{d\xi^2} + (a_u - 2q_u \cos 2\xi)u = 0 \qquad\qquad \text{Eq. 1.21}$$

Eq. 1.21 is commonly called the 'Mathieu equation' and eqs. 1.18 and 1.19 are the 'Mathieu parameters' that are used to predict ion trajectory stability within quadrupole devices. Note that the factor of '8' and '4' in eqs. 1.17 and 1.18 become '16' and '8' for 3D traps.

We can express solutions to eq. 1.21 as

$$u = \alpha' e^{\mu\xi} \sum_{n=-\infty}^{\infty} C_{2n} e^{2in\xi} + \alpha'' e^{-\mu\xi} \sum_{n=-\infty}^{\infty} C_{2n} e^{-2in\xi} \qquad\qquad \text{Eq. 1.22}$$

where α' and α'' are constants which describe the ions' initial conditions. According to Dawson, C_{2n} and μ are also constants but they do not depend on the initial conditions. This remarkable property differentiates quadrupolar fields from hexapolar, octupolar, and other higher-order fields because *the ion motion (i.e. the ion's secular frequency) does not fundamentally depend on the ion's initial conditions*. The solutions in eqs. 1.22 are such that either i) μ approaches infinity and hence the ion has an unstable trajectory within the mass analyzer or ii) μ remains finite as $t\text{->}\infty$ and hence the ion *may* have a stable trajectory. The specific cases of μ that give rise to stable ion trajectories can be found in Dawson's seminal work but are not discussed further.[9]

For an ion to be successfully trapped in a QIT (or transmitted through a mass filter), it must have stable trajectories in all quadrupole dimensions (x and y for a 2D device or r and z for a 3D device). Ion stability is commonly illustrated by a Mathieu stability diagram, as shown in **Figure 1.2**.[6] Regions of x and y stability are noted; regions of x stability point upward and regions of y stability point downward (or vice-versa). Only ions whose Mathieu a and q parameters fall within the overlapping regions – usually the first stability region, i.e. region A – can have stable trajectories in a quadrupole device and hence can be trapped or transmitted. A close-up of the first region of stability is shown in **Figure 1.3**.
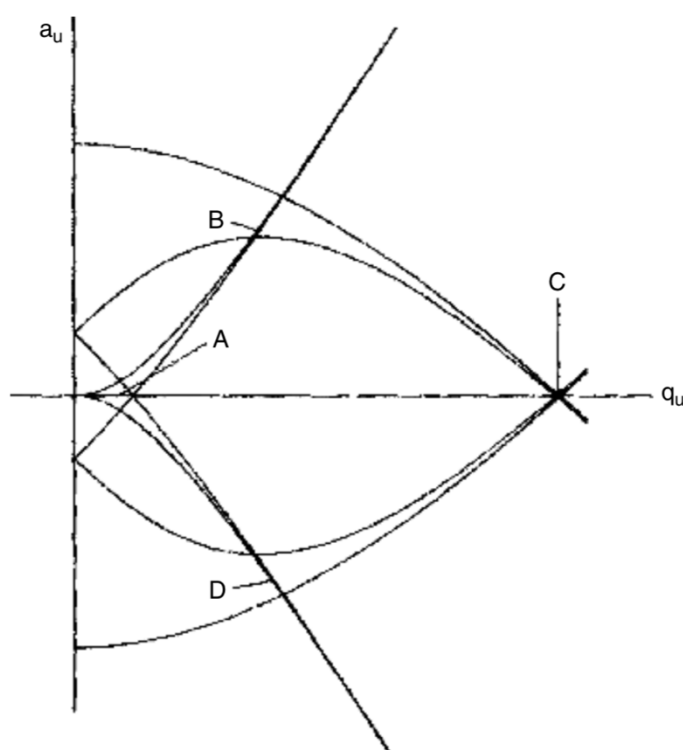
Figure 1.2. Regions of x (pointing downward) and y (pointing upward) stability as predicted by the Mathieu parameters. Regions of overlap (marked A-D) indicate values for which ion motion is stable in both x and y. Reproduced from March, R. E.; Todd, J. F. J. *Quadrupole Ion Trap Mass Spectrometry*; John Wiley & Sons: Hoboken, NJ, 2005.
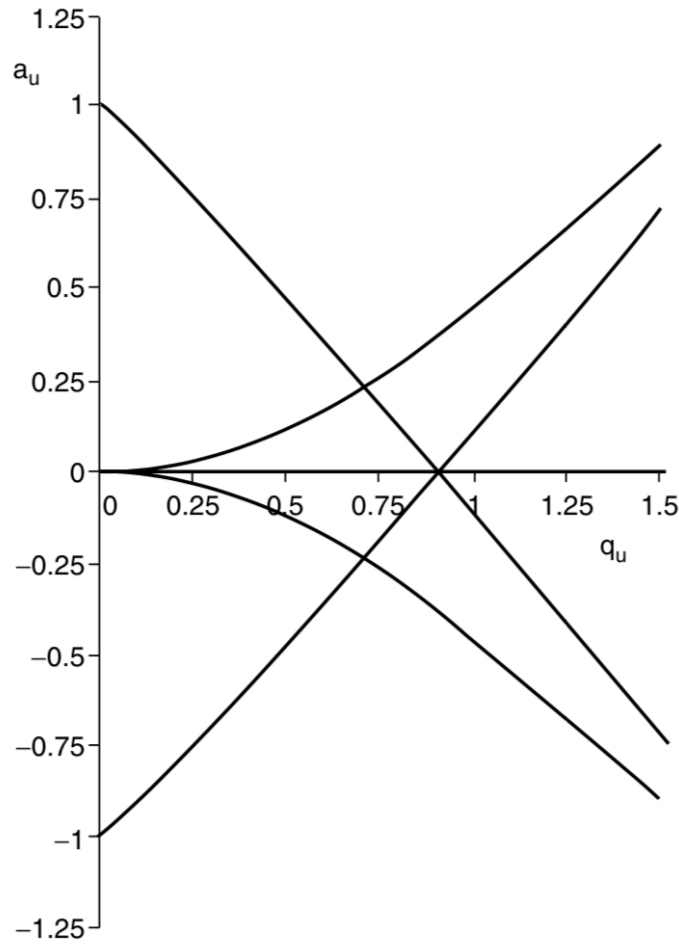
Figure 1.3. Canonical Mathieu stability diagram indicating the first region where ions have stable trajectories in both *x* and *y*. Reproduced from March, R. E.; Todd, J. F. J. *Quadrupole Ion Trap Mass Spectrometry*; John Wiley & Sons: Hoboken, NJ, 2005.

1.3 Secular and Related Frequencies

An ion's Mathieu parameters *a* and *q* can be used to predict not only the ion's stability within a quadrupole field, but also the periodicity of its movement. Each ion in a quadrupole device oscillates at an *m/z*-dependent *fundamental secular frequency* given by

$$\omega_u = \beta_u \Omega / 2$$

Eq. 1.23

and other related frequencies

$$\omega_{u,n} = (n + \tfrac{1}{2}\beta_u)\Omega \quad 0 < n < \infty \tag{Eq. 1.24}$$

and

$$\omega_{u,n} = -(n + \tfrac{1}{2}\beta_u)\Omega \qquad -\infty < n < 0 \tag{Eq. 1.25}$$

where n is is an integer. In other words, the ion's motion comprises contributions from linear combinations of the ion's secular frequency and the main driving rf frequency. Although the main sideband frequencies ($\Omega \pm \omega$) are quite prominent, they are not commonly used in ion trap mass spectrometry. The parameter β_u can be approximated (for $q_u < 0.4$) by

$$\beta_u \approx \sqrt{a_u + \tfrac{1}{2}q_u^2} \tag{Eq. 1.26}$$

but can be calculated through iterative solutions to the following equation

$$\beta_u^2 = a_u + \cfrac{q_u^2}{(\beta_u + 2)^2 - a_u - \cfrac{q_u^2}{(\beta_u + 4)^2 - a_u - \cfrac{q_u^2}{(\beta_u + 6)^2 - a_u - \cdots}}}$$

$$+ \cfrac{q_u^2}{(\beta_u - 2)^2 - a_u - \cfrac{q_u^2}{(\beta_u - 4)^2 - a_u - \cfrac{q_u^2}{(\beta_u - 6)^2 - a_u - \cdots}}}$$

$$\tag{Eq. 1.27}$$

Ions can also be interrogated through quadrupolar excitation at their parametric frequencies[20,21]

$$\omega_{u,n} = |n + \beta_u|\Omega / K \quad -\infty < n < \infty; \; K = 1, 2, \ldots \tag{Eq. 1.28}$$

which requires application of one phase of ac to the *y* rods and the opposite phase to the *x* rods. The main parametric excitation frequency is half of the ion's secular frequency.

1.4   Higher-order Fields and Nonlinear Resonances

Although the Mathieu theory discussed so far is an accurate description of ion motion in a quadrupole potential, it is important to realize that an ideal potential cannot be created. The electric field inside the ion trap will always have contributions from higher-order fields (e.g. hexapole, octupole, decapole, and dodecapole being the prominent members) for several reasons. First, the ion trap cannot have infinitely long or wide rods; the rods must be truncated both radially and axially.[22] There may also be physical imperfections on the rods themselves which cause field nonideality. A quadrupole potential demands electrodes with hyperbolic cross sections, but these can often be difficult to machine and instead circular[23] or rectangular[16] rods are fabricated instead, again introducing higher-order fields.

Mathematically, higher-order fields can be described using the spherical distribution of the potential in a 3D ion trap

$$\Phi(\rho, \theta, 0) = \Phi_0 \sum_{n=0}^{\infty} A_n \frac{\rho^n}{r_0^n} (\cos \theta) \qquad\qquad \text{Eq. 1.29}$$

where ρ and θ are spherical coordinates, A_n is the multipole coefficient of order n, and $P_n cos(\theta)$ is a Legendre polynomial.[24] For a pure quadrupole potential $A_n = 0$ for all n except n = 2, i.e. there are no higher-order fields and the potential varies quadratically from the center of the quadrupole (hence, the electric field strength varies *linearly* with coordinate). In contrast, for higher-order fields (n > 2) the electric field strength increases quadratically for hexapole, cubically for octupoles, and so on. The basic effect of the superposition of these higher-order terms on the quadrupole is to either increase or decrease (depending on the polarity of the higher-order terms) the electric potential *compared to a purely quadrupolar potential*, which has considerable consequences for ion motion and manipulation in an ion trap. The two most prominent repurcussions are the introduction of *nonlinear resonance lines* and a *dependence of ion secular frequency on the ion's position in the trap*.[25]

The addition of higher-order fields to the quadrupole field causes the ions to have small oscillations at overtones (e.g. 2ω, 3ω, 4ω) as well as linear combinations of the rf frequency and those overtones (e.g. Ω - 2ω). A general resonance condition for the ions in the first stability region (**Figure 1.3**) of a 3D trap is

$$n_r \beta_r + n_z \beta_z = 2\nu \qquad \qquad \text{Eq. 1.30}$$

where n_r, n_z, and ν are integers with the constraints that n_r is even for all multipoles, n_z is even for even multipoles, and n_z can be any integer for odd multipoles. Eq. 1.30 can be rewritten in terms of the secular frequencies of the ions and the trapping rf frequency to obtain

$$n_r \omega_r + n_z \omega_z = \nu \Omega \qquad \qquad \text{Eq. 1.31}$$

That is, resonances occur when the ion's secular frequency matches a sideband frequency. Correspondingly, nonlinear resonances occur when the ion's overtone frequency matches a sideband frequency. The most commonly observed higher-order resonances in quadrupole ion traps are the octupole ($\beta_u = 1/2$) and the hexapole ($\beta_u = 2/3$), but another resonance is often observed at the dodecapole line ($\beta_u = 1/3$).[26-28]

A key difference between the secular resonances and higher-order resonances is the amplitude growth of an ion excited at one of its characteristic frequencies ('resonance excitation', see section 1.5) which is given by

$$\frac{dz}{dt} = C_{n-1} z^{n-1} \qquad \qquad \text{Eq. 1.32}$$

For ions excited at their secular frequencies using a supplementary dipole field ($n = 1$), the radial (2D trap) or axial (3D trap) amplitude increases linearly with time. However, for higher-order resonances, the amplitude growth is much faster, resulting in a swift increase in ion kinetic energy and fast ejection from the ion trap. Odd-order multipoles show hyperbolically increasing amplitudes whereas even-order multipoles suppress the nonlinear resonances because the ions experience frequency shifts and fall out of resonance with the nonlinear resonance line.

Non-linear resonance lines have been shown to be both useful and detrimental. For example, if, during ion injection, an ion is placed on a nonlinear resonance line, it may pick up energy from the rf field and quickly be ejected from the ion trap before being detected by the mass scan. This observation has led to the term 'black hole' being used to describe these resonances.[29-31] It has also been reported that long storage times and trap overloading (i.e. space charge effects) exacerbate these problems, likely because under these conditions the ions are more likely to occupy regions closer to the electrodes where high-order fields are more prominent.

Even so, nonlinear resonances can also be useful. Recall that ions ejected at nonlinear resonance lines experience a hyperbolic increase in amplitude growth with respect to time, resulting in fast ion ejection. This effect can be utilized to increase resolution during a resonance ejection mass scan (see section 1.5) if the frequency of the supplementary dipolar ac voltage is chosen to coincide with a nonlinear resonance line (for example, $\beta = 2/3$, or one-third of the rf frequency). Such a method has been termed a 'double resonance ejection' mass scan (or nonlinear resonance ejection).[32,33] A similar scan mode has been applied to traps with asymmetric symmetry (and thus strong hexapole $\beta = 2/3$ lines) to effect a 'triple resonance ejection' scan,[34] wherein a dipolar ac field is applied at the ion's secular frequency and a quadrupolar (parametric) ac is applied at twice the ion's secular frequency. Note that these terms were erroneously used to describe these ejection methods when, in fact, 'double resonance' had already been used to refer to simultaneous resonance excitation of precursor and product ions.[35] Their use should thus be discouraged.

Higher-order fields additionally cause ion secular frequencies to deviate from ideality, particularly close to the trap electrodes where the higher-order multipoles make up a greater proportion of the electric potential than near the center of the trap. For odd-order fields, the potential near one electrode decreases from its ideal (quadrupolar) value; the opposite occurs near the opposite electrode. For even-order fields, the potential near opposite electrodes both decreases or increases for negative and positive higher-order terms, respectively. Because the force on the ion dictates the ion's frequency, if the electric field near an electrode increases from its quadrupolar value, then an ion's secular frequency will correspondingly increase as the ion approaches the electrode. For negative higher-order contributions, an ion's secular frequency decreases as it approaches an electrode. Frequency shifts are prominent if the primary higher-order fields are even but are much less pronounced for odd-order fields.[36] Nonetheless, these frequency shifts affect the

performance metrics of both collision-induced dissociation and resonance ejection, which are discussed in the next section.

1.5   MS and MS/MS in QITs

Even though the QIT was invented in the early 1950s, it was not until the early 1970s that it was successfully used for mass analysis. Fulford and March demonstrated that the ion trap could operate in a mass-selective stability mode using a combination of rf and dc potentials such that the ions with m/z values of interest was brought to the tip of the stability diagram (a = .237, q = .706)[37], ejecting all other ions from the trap. These ions could then be selectively detected using a charged particle detector (e.g. electron multiplier). By injecting new ions and isolating a different m/z bin each time, a mass spectrum could theoretically be obtained, although the method is very inefficient.

It was not until the 1973 disovery of the mass-selective instability scan by Stafford *et al.* that the ion trap became reasonably capable of mass analysis.[38] In mass-selective instability, the rf voltage is ramped linearly so as to bring ions of successively higher m/z to the right-hand side of the stability diagram ($q = 0.908$), at which point the ions are ejected from the trap into an electron multiplier. Because m/z and rf voltage are directly proportional for ejection at a fixed q value (eq. 1.19), ion m/z and time are also linearly related so that a linear fit of the two variables gives the correct mass calibration. Introduction of a small amount of a light buffer gas (helium at ~10^{-5}-10^{-3} torr) improves the performance of the ion trap – particularly resolution – because the ions are collisionally cooled to the center of the trap, reducing their excursions into higher-order fields and narrowing the distribution of positions and kinetic energies that can lead to loss of resolution.

Subsequently, Thermo Finnigan[10] and Sciex[11] produced the first commercial linear ion traps which both used resonance ejection[39-41] as the primary mass scanning methodology. The former linear ion trap ('linear' in **Figure 1.1**) has slits in the x rods and uses resonance ejection at high Mathieu q (usually close to 1/2 the rf frequency, or at a nonlinear resonance line) to radially eject ions into two symmetrically placed detectors. As the rf voltage is ramped linearly, the ions' secular frequencies increase until they come into resonance with the resonance excitation ac waveform, at which point the ions are ejected. If the voltage of the supplementary ac is ramped linearly with the rf voltage, then a linear mass spectrum is obtained.[42] In contrast, the Sciex linear ion trap utilizes the 'cone of reflection' near the fringing fields of the trap (the axial edges) so that when ions are radially excited to higher amplitudes, they experience a significant axial force which

ejects them from the trap in a mass-selective manner.[43] Again, the rf and ac voltages are ramped linearly to obtain a linear mass spectrum.

Other modes of obtaining mass spectra from QITs exist but are not commonly used. From the Mathieu a and q parameters (eqs. 1.18 and 1.19), the parameters that can be altered to make ions successively unstable are the quadrupolar DC[44,45] and the rf frequency[46,47] – both particularly useful for analysis of high m/z ions – as well as the size of the trap[48] and the supplementry ac frequency (i.e. varying the q value of the ac frequency).[49,50]

Auxiliary ac signals can also be utilized to conduct tandem mass spectrometry (MS/MS) experiments via collision-induced dissociation wherein a precursor ion is isolated using either rf/dc mode or using a multi-frequency waveform to eject unwanted ions[51]. The ion to be fragmented is then kinetically excited, collides many times with a neutral background gas, and fragments to form a product ion and a neutral molecule. A low voltage auxiliary ac signal matching the ion's secular frequency is applied to the trap in a dipolar manner to effect kinetic excitation in an ion trap.[52,53] After the product ions are generated, they are collisionally cooled and scanned out via mass-selective instability with resonance ejection. Compared to other methods of dissociation (e.g. photodissociation, triple quadrupole MS/MS, surface-induced dissociation), MS/MS in an ion trap is a slow heating process,[54] requiring hundreds, if not thousands, of collisions in a 10^1 ms period to build up enough internal energy for fragmentation. Higher buffer gas pressures and heavier collision gases can be used, but they increase fragmentation efficiency at the cost of increased scattering and decreased mass spectral resolution.[55] Off-resonance signals can also be used to increase fragmentation efficiency without neutralizing the ions on the electrodes because the ions experience beat patterns, thereby allowing the use of higher collision energies.[56]

Other MS/MS scan modes do exist but are generally only performed on multi-analyzer instruments, most notably the triple quadrupole.[57,58] Consider the dissociation reaction *precursor ion -> product ion + neutral*, or, equivalently, $m_1^+ \rightarrow m_2^+ + m_3$, where m_1, m_2, and m_3 are the masses of the precursor ion, product ion, and neutral, respectively. As described in the prior paragraph, a *product ion scan* selects a precursor ion for fragmentation and determines the product ion m/z values, which are indicative of the molecular structure of the precursor. A *precursor ion scan* fixes the m/z of the observed product ion and scans through precursor m/z values, thereby returning all precursor ion m/z values that fragment to a certain product ion m/z. Similarly, a neutral loss scan detects all precursor ions which have a shared neutral fragment (in this case the precursor

and product ions are detected – not the neutral – only when they share a fixed mass offset).[59] The precursor ion scan and neutral loss scan thus both detect ions which share particular functional groups. Conventionally, ion traps only have access to full scans and product ion scans because it is difficult, with a single mass analyzer, to select a precursor ion, fragment it, and mass select a particular product ion simultaneously.

Because ion traps can only perform product ion scans, when paired with chromatographic techniques, data-dependent MS/MS has become popular for obtaining MS/MS data.[60] Throughout a chromatographic peak the mass spectrometer will collect alternating full scans and MS/MS scans, with the instrument usually choosing the most intense peaks in the full scan for fragmentation. These methods have become particular popular with more recent dual-pressure linear ion traps[61,62] and ion trap-Orbitrap hybrids[63,64] which are capable of nearly 10 Hz MS/MS acquisition rates combined with high resolution full scan capabilities using the Orbitrap.

As mentioned in the previous section, in QITs higher-order fields cause ion frequency shifts which alter the performance of resonance ejection and resonance excitation in various ways. For example, if a positive higher-order (even) field exists within the trap, then the ions' frequencies will increase as the ions are excited because they occupy regions near the electrodes where the higher-order fields are prominent. If a standard mass-selective instability scan with resonance ejection is conducted, then as the ion approaches the point of resonance, its frequency will shift upward *toward* the resonance point, thereby increasing its rate of ejection and improving resolution.[65,66] On the other hand, if the rf voltage is decreased during the mass scan (i.e. if the trap scans from high to low *m/z*), then as the ion approaches the point of resonance and is excited, its secular frequency will increase *away from the resonance point* (because its secular frequency decreases during the scan but then increases when the ion approaches the electrodes), and so ejection will be delayed and resolution will be diminished. Odd-order fields do not cause significant frequency shifts; however, they do create strong higher-order resonances as discussed previously.

MS/MS is also affected by even-order multipoles. As an ion is resonantly excited to generate product ions, its frequency shifts away from the on-resonance ac frequency. The result is that the ion falls out of resonance with the supplementary dipolar ac field. However, the ion will then collisionally cool to the center of the trap and so its frequency will return to an on-resonance condition. Therefore, the ion's motion follows a beat pattern which has been shown to increase

MS/MS efficiency.[23,67,68] Frequency shifts are especially troublesome for small, simplified, and miniaturized ion traps which tend to have significant higher-order multipole contributions.[69]

1.6   Miniature Mass Spectrometers

Traditionally, mass spectrometers are benchtop instruments that are not used outside of the conventional analytical laboratory. The last two decades, however, have seen a noticeable growth in interest and research into miniature and portable mass spectrometers.[70,71] Portable systems have largely been driven by a small set of applications – origin-of-life (i.e. planetary missions), forensics, defense (chemical warfare agent and explosive detection), food authenticity, and agrochemicals.[72] In these particular applications it is important to be able to perform chemical analysis in the field due to time, weight, volume, power, and sample constraints.

Mass spectrometers are one of the most difficult analytical instruments to miniaturize successfully. Although the mass analyzer can be simplified (flat electrodes in **Figure 1.1**) and made suitably small (< 1 μm r_0 is possible[73,74]), the electronics can be miniaturized, and most ion optical elements can be removed while maintaining ~0.2% ion transfer into the trap,[75] the vacuum system is especially troublesome. In particular, smaller, low-power pumps usually do not have the capacity to pump against atmospheric pressure, even if the mass spectrometer inlet orifice is small. Moreover, the pumps and rf system require dozens of watts of power (compared to hundreds of watts for a benchtop system) in order to function properly.

One solution is to use a *discontinuous atmospheric pressure interface (DAPI)*, which is simply a soft silicone tube constricted by a pinch valve that is placed between the inlet capillary and the vacuum chamber.[75] During ion injection, the pinch valve is opened for a period of ~10 ms and ions (from the source) and neutrals (air) are introduced into the ion trap. The valve is then closed, and the instrument is pumped down from ~1 torr to ~10^{-5} torr in a period of ~500 ms so that mass-selective operations can take place. Ion isolation and collision-induced dissociation can also take place (if desired), and finally a mass spectrum is obtained via mass-selective instability with resonance ejection. A second solution is to use a more classical approach with a continuous atmospheric pressure interface and differential pumping, but these solutions usually sacrific either instrument portability or sensitivity.[76-78]

A consequence of utilizing a DAPI system is that, because of the long pump-down time that must precede the mass scan, the acquisition rate decreases from 5-10 Hz – characteristic of

most commercial ion traps – to < 1 Hz.[75,79] A primary question thus addressed in this work is the following: is data-dependent MS/MS feasible on a portable ion trap mass spectrometer, and, if not, what data-independent alternatives exist for these devices?

1.7   Introduction to This Work

This work argues that, because of the low acquisition rates of portable ion traps (~1 scan per second), data-dependent MS/MS is not appropriate, and instead alternative scan modes should be developed. These scan modes should be 1) low-power, 2) simple, and, most importantly, 3) because the ion trap is slow, these scan modes should be *efficient*. That is, the scans should obtain the most MS and MS/MS information possible using the fewest number of scans in the least amount of time, and sample consumption should be minimized.

In this dissertation we develop novel mass scanning methods that satisfy these characteristics and argue their utility and robustness for portable ion trap systems. We begin by developing ac frequency scanning ('secular frequency scanning') at constant rf voltage as a simple, low-power method of mass scanning. We then show that by combining this frequency scanning technique with double resonance methods, precursor and neutral loss scans - largely thought problematic on any single mass analyzer – become possible on a linear quadrupole ion trap. These methods are highly efficient means of moving through the MS/MS data domain to classify compounds in complex mixtures according to their shared molecular functionality. Next, we show that multiplexed versions of precursor, neutral loss, and product scans are possible, giving rise to a new set of scan modes we term 'logical MS/MS'. Lastly, we show that the entire 2D MS/MS data domain can be captured using a single scan and argue that it is a powerful new capability for analysis of complex mixtures using a small, simple ion trap mass analyzer.

PART I. SECULAR FREQUENCY SCANNING IN A LINEAR QUADRUPOLE ION TRAP

CHAPTER 2.   EXPERIMENTAL CHARACTERIZATION OF SECULAR FREQUENCY SCANNING IN ION TRAP MASS SPECTROMETERS

2.1   Abstract

Secular frequency scanning is implemented and characterized using both a benchtop linear ion trap and a miniature rectilinear ion trap mass spectrometer. Separation of tetraalkylammonium ions and those from a mass calibration mixture and from a pesticide mixture is demonstrated with peak widths approaching unit resolution for optimized conditions using the benchtop ion trap. The effects on the spectra of ion trap operating parameters including waveform amplitude, scan direction, scan rate, and pressure are explored, and peaks at black holes corresponding to non-linear (higher-order field) resonance points are investigated. Reverse frequency sweeps (increasing mass) on the Mini 12 are shown to result in significantly higher ion ejection efficiency and superior resolution than forward frequency sweeps that decrement mass. This result is accounted for by the asymmetry in ion energy absorption profiles as a function of ac frequency and the shift in ion secular frequency at higher amplitudes in the trap due to higher order fields. We also found that use of higher ac amplitudes in forward frequency sweeps biases ions toward ejection at points of higher order parametric resonance, despite using only dipolar excitation. Higher ac amplitudes also increase peak width and decrease sensitivity in both forward and reverse frequency sweeps. Higher sensitivity and resolution were obtained at higher trap pressures in the secular frequency scan, in contrast to conventional resonance ejection scans, which showed the opposite trend in resolution on the Mini 12. Mass range is shown to be naturally extended in secular frequency scanning when ejecting ions by sweeping the ac waveform through low frequencies, a method which is similar, but arguably superior, to the more usual method of mass range extension using low q resonance ejection.

2.2 Introduction

Quadrupole and linear ion traps are common mass analyzers due to their excellent sensitivity, relatively high operating pressures (mTorr) compared to other analyzers, tolerance for imperfect electric fields, and capabilities for single analyzer collision-induced dissociation (CID).[69,80] Methods of scanning quadrupole-based analyzers can be deduced from the Mathieu parameters a_u and q_u, which describe the stability of ions in a quadrupolar field[6,7]:

$$a_u = 8zeU / \Omega^2 r_0^2 m \qquad \text{Eq 2.1}$$

$$q_u = 4zeV / \Omega^2 r_0^2 m \qquad \text{Eq 2.2}$$

where z is the integral charge on the ion, u is the respective dimension (x, y, r, or z), e is the unit elementary charge, U is the amplitude of the dc potential applied between the rods, V is the amplitude of the radio frequency (rf) potential applied to the rods, $\Omega = 2\pi f$ is the angular frequency of the rf potential (f = frequency of the rf), r_0 is the characteristic size of the quadrupole or trap (typically the half distance between the rods), and m is the mass of the ion. Assuming the field is purely quadrupolar and solving these parameters for *m/z* with the understanding that z is now the charge of the ion in coulombs, we obtain

$$m/z = 8U / a\Omega^2 r_0^2 \qquad \text{Eq 2.3}$$

$$m/z = 4V / q\Omega^2 r_0^2 \qquad \text{Eq 2.4}$$

The four experimental parameters that determine the stability of an ion in a quadrupolar field are thus i) the amplitude of the dc potential, ii) the frequency of the applied fundamental rf waveform, iii) the radius of the device, and (iv) the rf amplitude.

In a quadrupole mass filter,[1] ions are selected for detection by mass selective stability,[81] wherein the amplitudes of the rf and dc are increased while either keeping their ratio constant (constant resolution) or changing their ratio slightly to increase resolving power with mass and maintain unit resolution. With this method, ions of consecutive masses are successively brought to the apex of the Mathieu stability diagram, causing all other ions to become unstable. If the ramp

of the rf and dc components is linear, then time domain current or voltage data is linearly related to m/z. That is, m/z is directly proportional to the rf/dc amplitude.

By contrast, quadrupole ion traps operate on the basis of mass selective instability.[82] In this technique, typically no dc component is used (U = a_u = 0), placing all ions on the q axis of the Mathieu stability diagram. The rf amplitude is ramped linearly as a function of time, causing ejection of ions of increasing m/z as they are brought successively to the ejection point (q = 0.908). The ions detected are thus those that are *unstable*, whereas only *stable* ions are detected in a conventional quadrupole mass filter. Since m/z is directly proportional to the rf amplitude, the time domain data correspond directly to the mass spectrum. Resonance ejection is a similar scan mode in which a "hole" is created on the q axis of the stability diagram by also applying a small supplementary dipolar ac voltage to eject ions whose secular frequencies match the frequency of the applied ac signal.[83] As before, the rf is ramped, causing ions' secular frequencies to change; when ions of particular m/z come into resonance with the frequency of the applied ac, these ions are mass selectively ejected.

Alternative methods of scanning quadrupoles and ion traps exist but are uncommon. Scanning the frequency of the fundamental rf is a variant on the mass-selective instability scan that has been performed by only a few groups. The first report of rf frequency scanning demonstrated advantages for analysis of high mass ions[84] and subsequent reports demonstrated frequency scanning in a quadrupole mass filter with ions ranging in size from mass 176 Da[46] to microparticles.[85] Frequency scanning has also been reported in specially designed digital ion traps, which do not have rf amplitude scan capabilities but which have demonstrated exceptionally fast scan rates while maintaining reasonable resolution (unit resolution for a 100 Hz scan rate, peak widths FWHM ~2.0 Th for a 1,000 Hz scan rate).[86-88] These scan methods simplify the electronics, but there remain problems of nonlinearity in mass calibration, unexpected peaks, and poor mass resolution.[18] As a result, traditional rf amplitude sweeps have remained the favored method of ion trap operation. It is also theoretically possible to sweep the size of the device (r_0), but this is impossible in practice.[89]

An interesting alternative to sweeping either the rf amplitude or frequency is to instead sweep the frequency of a supplementary ac waveform (**Figure S2.1**), that is, to perform secular frequency scanning using an applied dipolar signal. Each ion then has a set of induced frequencies, $\omega_{u,n}$, dependent upon trap parameters and m/z,[5,12,32,39,90] which can described by

$$\omega_{u,n} = (2n+\beta_u)\Omega/2 \qquad -\infty < n < \infty \qquad\qquad\qquad\qquad \text{Eq 2.5}$$

where n is an integer, u is the axis of interest (x, y, or z) and a new parameter β_u ($0 \le \beta_u \le 1$) which is *m/z* dependent under fixed operating conditions has been introduced. Parametric (quadrupolar) resonances can also be excited in certain circumstances, with the main resonance (n = 0, K=1) occurring at twice the secular frequency. Higher order *quadrupolar* resonances are predicted to occur when

$$\omega_{u,n} = |n+\beta_u|\Omega / K \quad -\infty < n < \infty; K = 1, 2, \qquad\qquad\qquad \text{Eq 2.6}$$

where K is the order of the resonance.[20,21] They have been described by Collings et al. who used parametric (quadrupolar) excitation to observe these signals. These resonances would appear to require parametric excitation although we show below that they can be accessed using dipolar excitation. The parametric excitation experiment is performed by applying ac signals to the ring and endcap electrodes (in a 3D ion trap), with the ring and endcap excitation signals 180 degrees out of phase. Importantly, in order to eject ions using quadrupolar excitation, the excitation force threshold, f_{ex}, must be exceeded.[12] This threshold is given by

$$f_{ex} = \alpha\lambda^{1/K} \qquad\qquad\qquad\qquad\qquad\qquad\qquad\qquad\qquad \text{Eq 2.7}$$

where alpha is a constant and lambda is a damping constant. That is, in order to excite/eject ions at higher order quadrupolar resonances, a higher waveform amplitude is required. Equivalent higher order *dipolar* resonances have not been reported, but we will show that – remarkably - dipolar excitation can eject ions at the higher order quadrupolar resonances due to the coupling of motion in r and z (or x and y) in imperfect ion traps with large higher order field contributions. When n = 0 in Eq 2.5, we have the ion's *fundamental secular frequency*:

$$\omega_{u,0} = \beta_u\Omega/2 \qquad\qquad\qquad\qquad\qquad\qquad\qquad\qquad\qquad \text{Eq 2.8}$$

This is the frequency that is interrogated by resonance excitation/ejection in ion trap instruments operated under dipolar resonance conditions, where, in a 3D ion trap, ac waveforms 180 degrees

out of phase with respect to each other are applied to the endcap electrodes. For small a_u ($a_u < 0.2$) and q_u ($q_u < 0.4$),

$$\beta_u = (a_u + q_u^2 / 2)^{1/2} \hspace{4cm} \text{Eq 2.9}$$

Note that the full definition of β_u can be found in ref. [5]. If no dc potential is applied, as is typical of ion trap operation, then $a_u = U = 0$ and we have

$$\beta_u = (2^{1/2}q_u / 2) = 2^{3/2}zV / \Omega^2 r_0^2 m \hspace{3cm} \text{Eq 2.10}$$

so that

$$\omega_{u,0} = 2^{1/2}zV / \Omega r_0^2 m \hspace{4cm} \text{Eq 2.11}$$

Thus we see that an ion's secular frequency, for low a_u and q_u, is inversely proportional to m/z. This is not a strictly accurate relationship throughout a,q-space, but it is a reasonable approximation in the range of values for which Eq 2.9 applies. This is important because it complicates mass calibration. In order to convert from the time domain to the mass domain, each time point must be converted to an excitation frequency dependent upon the scan parameters and electronic triggers. Each frequency is then converted to a value of beta and subsequently to a q_u value using an iterative algorithm because beta is a continuing fraction in terms of q_u. The q_u value is then used to convert to mass, giving the ejected ion mass as a function of time. Thus, in contrast to the simple linear calibration in rf amplitude scanning, there is no analytical equation available to calibrate mass in secular frequency scanning. Nonetheless, a calibration procedure is demonstrated in ref. [91].

To date, secular frequency scanning has been mentioned in patents[92,93] and review papers[12] but has only been performed sparingly. Welling and co-workers used this method, which they termed "secular scanning", to obtain higher resolution mass spectra when compared to q scanning in a linear ion trap (the resonance was quadrupolar over a limited mass range and with slow frequency scanning),[94] Roth and coworkers used secular frequency scanning in a linear trap for mass selective excitation,[95] and the Austin group at Brigham Young University used it to scan ions

out of the halo ion trap.[19,96,97] Note that in the case of the halo trap, the geometry of the device necessitated the use of ac frequency scanning because simulations indicated that a conventional rf amplitude ramp would cause ions to collide with the electrodes and ceramic holders instead of being ejected out the apertures in the electrodes. However, ac scanning has yet to be systematically characterized despite some clear advantages, particularly the fact that the high amplitude, high frequency rf signal is kept constant which greatly simplifies the electronics since strictly linear rf ramps, which are difficult to generate, are no longer needed. This feature is particularly appealing for miniature instruments.[70,71] More importantly, precursor ion scans using a single ion trap[98,99] can be performed by exciting ions of successive masses as a function of time using a low amplitude dipolar signal while a chosen product ion is ejected by applying a second high amplitude constant frequency ac signal at the product ion's secular frequency. This capability would appear to mark a significant step forward in ion trap mass spectrometry, bringing single ion trap capabilities closer to those of the widely used triple quadrupole. The performance of a triple quadrupole is much superior, but in some applications the small size and simplicity may favor use of an ion trap. These extended ion trap capabilities demand an understanding of the underlying principles, particularly those of secular frequency scanning, in order to improve the performance of precursor scans in single ion traps.

In this paper we show that secular frequency scans can be carried out using either a miniature rectilinear ion trap mass spectrometer or a commercial linear ion trap. We also characterize the effect of scan direction, scan rate, rf amplitude, rf frequency, ac amplitude, and pressure on the spectra and demonstrate facile mass range extension compared to conventional rf amplitude sweeps at low q. "Black holes" occurring at nonlinear resonance points are also investigated.

2.3 Experimental

2.3.1 Instrumentation

Frequency scanning experiments were performed using the Mini 12[100] miniature rectilinear ion trap (RIT)[16] mass spectrometer and a benchtop Thermo LTQ XL linear ion trap (Thermo Scientific, San Jose, California, USA) in the positive ion mode. The former was chosen to assess the effect of higher order fields and higher pressures, whereas the LTQ exhibits higher

performance. The rectilinear ion trap uses electrodes with rectangular cross sections, in contrast to the hyperbolic cross sections of the commercial LTQ. The rf is applied to the y electrodes, while the ac and other waveforms are applied in a dipolar fashion to the x electrodes, which have slits for ion ejection.

Secular frequency scans were performed by outputting a swept frequency sinusoidal waveform of 0.5 - 10 V_{pp} (peak to peak) over a range of 10 - 500 kHz in a scan lasting 300 - 800 ms, unless otherwise specified, from a Sony Tektronix AFG320 arbitrary function generator (Beaverton, Ohio, USA). In the case of the Mini 12, two channels were used to produce a dipolar (180 degrees out of phase) waveform that was applied to the x electrodes after passage through a low pass frequency filter with a cutoff frequency of 500 kHz. Data were recorded using the data system of the Mini 12.[100] The function generator was triggered on a high frequency kilohertz ac waveform of ~7 V_{pp} output from the Mini ac waveform board in a 1 ms segment just prior to the mass scan. The oscilloscope was set to wait for 1 s, the approximate duty cycle of the Mini 12, before accepting further triggers in order to prevent the ac waveform from triggering data acquisition multiple times during a mass scan. See **Figure S2.2**. Unless otherwise specified, all scans were performed using a constant rf amplitude of 6,000 digital-to-analog converter (DAC) units (~195 V_{0-p}) and 0.999 MHz frequency, corresponding to a lower mass/charge cutoff of ~98 Thomson (Th). Note that DAC units and rf and ac amplitudes are directly proportional.

Using the LTQ, secular frequency scans were performed by replacing the resonance ejection waveform generated from the analog board with the same swept frequency waveform as just described. The function generator was triggered at the start of the mass scan using the triggers included in the LTQ Tune diagnostics menu. The rf frequency was tuned to 1.1995 MHz, and the change in rf amplitude built into the Thermo system was minimized by performing "Ultrazoom" scans over the period of the ac frequency scan. Ultrazoom scans occur at a rate of 27 Da/s. This small change in rf amplitude slightly changes resolution, depending on scan direction, but otherwise has a minimal effect on the spectra. The lower mass cutoff (lmco or LMCO) was typically set at 100-200 Th at the beginning of the scan. The LTQ's data system was used to collect data (~2,700 points per second). Unless otherwise specified, all ac scans were linear forward frequency sweeps from low to high frequency (high mass to low mass).

2.3.2   Ionization

Ions studied in both traps were generated by nanoelectrospray ionization (nESI) at ~2,000 V. In the case of the Mini 12 ions were gated into the mass analyzer for ~12 ms, followed by a ~500 ms ion cooling period. The standard Ultrazoom scan function was used in the LTQ.

2.3.3   Simulations

Simulations were performed in ITSIM 6.0[101] using a 2010 MacBook Pro (2.4 GHz Core i5, 3 GB usable RAM, 32-bit Windows 10). One hundred ions of each *m/z* were generated at the start of the simulations with a Gaussian distribution of positions about the center of the trap but zero velocity in x, y, and z. The frequency, but not amplitude, of the supplementary ac waveform applied to the simulated rectilinear trap was ramped linearly (in a forward or reverse direction) versus time while the main trapping rf amplitude and frequency were kept constant. Simulated scan times were shortened to ~3 ms in order to decrease computational time. In order to compensate for the shorter scan time, higher ac amplitudes were used. Collisions were simulated using a hard-sphere collision model at 4 mTorr helium.

2.3.4   Chemicals

Didodecyldimethylammonium bromide and EPA 508.1 herbicide mix (a mixture of alachlor, butachlor, simazine, atrazine, metolachlor, and hexachlorocyclopentadiene) were purchased from Sigma Aldrich (St. Louis, Missouri, USA, and Bellefonte, Pennsylvania, USA, respectively). Hexadecyltrimethylammonium bromide was purchased from Tokyo Chemical Industry Co. (Tokyo, Japan). Benzylhexadecyldimethylammonium chloride was purchased from JT Baker Chemical Co (Phillipsburg, New Jersey, USA). Ultramark calibration solution (4.5 ppm caffeine, 2 ppm MRFA, and 0.0005% Ultramark 1621 in ACN:MeOH:H2O 2:1:1 with 0.5% acetic acid) was purchased from Thermo Fisher (Rockford, Illinois, USA). All reagents were initially dissolved in either HPLC grade methanol (MeOH) or deionized water and then diluted in 50:50 MeOH:H_2O with 0.1% formic acid to obtain their final concentrations, which were generally 1-10 ppm.

2.4   Results & Discussion

The secular frequency scans over a frequency range of 10 - 500 kHz, swept from low to high frequency with an amplitude of 3 V_{pp} (Mini 12) and 1 V_{pp} (LTQ), are shown in **Figure S2.3** for a sample of three tetraalkylammonium ions (2 - 6 ppm) along with the equivalent resonant ejection spectra using the Mini 12 (simulated results shown in b) and the LTQ (d-f). Peak widths are quite broad (~2 ms FWHM) in the RIT, likely due to the low pressure in the trap and the presence of higher order fields, whereas the LTQ shows much sharper peaks (~1 ms FWHM). The spectrum obtained from the LTQ when converted to the mass domain (**Figure S2.3e**), indicated peak widths of ~2-3 Da. Preliminary experiments using an approximately linear mass scan on a cylindrical ion trap showed the ability to resolve bromine isotopic peaks, despite the imperfect geometry (**Figure S2.4**). Under more optimal conditions where the rf amplitude is increased (LMCO = 200 Th), peak widths approaching unit width can be obtained using the LTQ, as discussed later. Resolution decreases with increasing mass due to the nonlinear spacing of ion secular frequencies in terms of mass.

Experimental results illustrating the effect of scan direction on the spectra are shown in **Figure 2.1**. The effect on peak height and width is very pronounced on the Mini 12, where higher order fields are present in large proportions since the fields are only 65% quadrupolar.[16] In this experiment, it was critical to alter the rf amplitude on the Mini 12 so that the ions of interest were ejected at approximately the same time because, as we will show later, secular frequency scans are highly sensitive to pressure. Since the Mini 12 uses a discontinuous atmospheric pressure interface, the pressure in the trap is variable as a function of time, which will affect resolution and sensitivity (see **Figure S2.5** for forward vs. reverse sweeps with ion ejection at different pressures).
In general, reverse frequency sweeps (forward mass scans) result in up to 50% higher signal compared to forward frequency sweeps on the Mini 12, and resolution in the reverse sweep is also significantly better.

The same effect of scan direction on mass spectra is observed in conventional rf scans with resonance ejection.[102] Due to nonlinear fields, ion frequencies shift upward toward the ejection point in a forward resonance ejection spectrum (low mass to high mass), resulting in an increase in sensitivity and resolution; the opposite effect is observed for the reverse rf amplitude sweep since the secular frequency shifts away from the working point.[65] See **Figure S2.6** for reproduced resonance absorption curves of n-butylbenzene, which show the increase of ion secular frequency

at higher ac amplitudes (i.e. in regions with more prominent higher order fields). The effect is much less pronounced on the LTQ since its rods are hyperbolic rather than rectangular.[103]

Note that nonlinear fields cause absorption spectra to shift to higher frequencies only for a positive octopole or other even higher order contribution, as is present in the Mini 12.[16] A positive octopole increases field strength, particularly near the electrodes, which causes ion frequencies of motion to increase correspondingly. The opposite occurs for a negative octopole component. For traps with a negative octopole component, higher resolution and sensitivity would be obtained in the forward frequency sweep.

A rather minor but interesting and unexpected effect of scan direction is illustrated by the red boxes in **Figure 2.1**. The relative spacing between the indicated peaks is identical to the spacing between the main peaks in the spectrum, which indicates that the same ions are being ejected at different frequencies. As we will show later, these frequencies correspond to higher order parametric resonances, which are observed despite using dipolar excitation. In the forward sweep, these resonances, of which there are many as given by eq. 2.6, are encountered before the secular frequency. This could have both a detrimental and favorable effect on resolution and sensitivity. In the forward sweep, the ions would increase their amplitude as they encounter these higher order resonances, which may increase the rate of ejection when their secular frequencies match the ac frequency at a later point in time. However, this effect appears to be very small, likely due to collisional cooling during the long mass scan, so that resolution and sensitivity in forward frequency sweeps is always worse than in reverse sweeps. The parametric resonances are significantly weaker on the LTQ than on the Mini, which indicates that higher order fields play a role. Curiously, the parametric resonances also appear in reverse frequency sweeps, even though they are encountered after the secular frequency. However, secular frequency scanning, particularly with low ac amplitudes, is a relatively weak method of ejection, so a small population of ions is left over after their secular frequencies have already been matched. Thus, these ions are ejected at their parametric resonance frequencies instead.

The effect of scan rate on the spectra is shown in **Figure S2.7.** The scan rate was changed by altering the scan time on the function generator while keeping the scan range constant. The scan rate here is nonlinear since the ac frequency is swept linearly while ion secular frequencies follow an approximately inverse relationship (eq. 2.11). Nonetheless, decreasing the scan rate increases peak separation in time, which is an expected result since ions experience more rf cycles at or near

resonance and since their resonance conditions are further separated in time, but it decreases signal intensity. A similar result is obtained in conventional rf amplitude scans; decreasing the scan rate increases resolution but also decreases S/N, the latter partly due to charge transfer to neutral gas molecules.[102]

The amplitude of the supplementary signal has a significant effect on the appearance of the spectrum, as shown in **Figure 2.2**. Ion intensity decreases, peak width increases, and ion ejection time decreases with increasing ac amplitude for both forward and reverse frequency scans, in agreement with theory.[104] Generally, signals of ~1 V_{pp} or less are enough to generate spectra with high sensitivity and good resolution on the LTQ. If the ac amplitude is too low, however, ions do not gain enough energy to escape the trap, especially in the Mini 12, and at high ac amplitudes some ions are ejected prematurely or even at higher order resonances, particularly when the rf amplitude is also high as discussed later. Sensitivity for ions of different masses is dissimilar due to differences in pseudo-potential well depth, which increases with V and q, and scan rate, which increases with m/z. More rapid ejection at higher ac amplitudes implies that mass calibrations are valid only for one ac amplitude, but fortunately this relationship is approximately linear. While forward and reverse sweeps both show increasing peak width with increasing ac amplitude, they have different optimal ac amplitudes. The forward sweep on the LTQ exhibits the best sensitivity at ~1 V_{pp}, whereas the reverse sweep shows the highest ion intensity at ~4 V_{pp}. This is likely caused by ion frequency shifts at higher ac amplitudes, which will tend to degrade performance in forward sweeps.

The amplitude of the rf waveform has perhaps the most noticeable effect on spectral resolution, as shown in **Figure 2.3** where carbon isotope peaks are resolved with an Ultrazoom scan starting at 200 Th on the LTQ (**Figure 2.3b**, inset). Since each ion's secular frequency is directly proportional to the applied rf voltage (for q < 0.4), increasing the rf amplitude causes ions to be ejected later in the scan. This results in increased resolution because their secular frequencies are further apart. Since secular frequency and mass-to-charge are inversely proportional, high mass ions have secular frequencies that are close to each other, whereas the secular frequencies of low mass ions are better separated in time, which causes resolution to decrease with mass in a linear frequency sweep. However, increasing the rf amplitude also increases each ion's potential well depth ($D_{x,y} = qV_{rf}/4$),[5,12] resulting in less efficient ejection and a loss in sensitivity. **Figure S2.7**

shows a similar effect of rf frequency on the spectra; however, in this case the expected inverse relationship between secular frequency and rf frequency is observed.

Pressure variations are well known to cause substantial changes in mass resolution.[82] Approximately 1 mTorr of a light bath gas such as helium greatly increases resolution and sensitivity in quadrupole ion traps due to collisional cooling, which causes the ion cloud to collapse to the center of the trap where higher order fields are less prominent. However, if the pressure is too high, collisions during the mass scan can cause ions to be ejected at the wrong time, degrading mass resolution. Secular frequency scanning appears to be more tolerant of higher-pressure operation than resonance ejection scans but significantly more affected by low pressure operation (**Figure 2.4**). The pressure in the rectilinear ion trap was altered by varying the amount of time between the opening of the discontinuous atmospheric pressure interface (DAPI) valve[75] and the beginning of the mass scan. In resonance ejection scans, resolution on the Mini 12 is optimum at the lowest pressures achieved, that is, for the scans with collisional cooling times longer than ~600 ms. Sensitivity is largely the same for every resonance ejection scan beyond ~300 ms of cooling. The initial drop in peak intensity can be attributed to collisional ion losses at higher pressure and charge transfer to the background gas,[102] but beyond this no significant difference in ion intensity is observed. This is not the case for secular frequency scans, which appear to be highly pressure sensitive as illustrated in the forward frequency scans in (c) and (d) and reverse scans in (e) and (f). Parts (c) and (e) indicate that the highest resolution is obtained at the higher pressures, particularly for the reverse frequency scan, which shows superior performance in peak width and ion intensities. As the collisional cooling time is increased beyond ~500 ms, the peak width increases dramatically. Sensitivity correspondingly decreases to the point where little to no ion intensity is observed beyond ~500 ms of collisional cooling in (d) and (f).

As mentioned previously, higher order parametric resonances are particularly evident in forward frequency scans since low frequencies, and thus many higher order resonances, are scanned through before the secular frequency. Peaks corresponding to these higher order resonances were observed in several experiments (see **Figure 2.1**), despite the fact that only dipolar excitation was applied. This is further demonstrated and quantified using the Mini 12 with a mixture of five pesticides analyzed by resonance ejection and secular frequency scanning (**Figure 2.5**). The main peaks in the spectrum are protonated herbicides simazine (m/z 203), atrazine (m/z 217), metolachlor (m/z 285), and derivatives of atrazine (m/z 174 and 250, confirmed as derivatives

or metabolites by MS/MS). In the secular frequency scan experiment, both the amplitude of the ac and the rf signals were varied (rf = 6,000 corresponds to ~195 V_{0-p} and rf = 12,000 corresponds to ~386 V_{0-p}). The rf amplitude was increased only *during* the mass scan and not *before* ion injection. At the lower rf amplitude higher order parametric resonances were not observed (**Figure 2.5b**). However, when the rf and ac amplitudes were increased, parametric resonances corresponding to K = 4 were observed. Further increase of the ac amplitude to ~3 V_{pp} resulted in appearance of K = 6 and 8 resonances, and K = 10 resonances were subsequently observed when the ac amplitude was >7 V_{pp}. Note that there is some overlap in the K = 6 and 8 resonances, as shown in **Table 2.1**. Although higher order dipolar resonances have not previously been reported, it is feasible that higher order parametric resonances are being excited due to the coupling of motion in the x and y dimensions, which is a direct result of higher order field components (e.g. hexapole and octapole) introduced by electrode imperfections, electrode truncation, non-ideal geometries, and misalignment. The calculated frequencies of ejection at the higher ac amplitudes corresponded to approximately one-half, one-third, one-fourth, and one-fifth of the secular frequency (**Table 2.1**), or equivalently one-fourth, one-sixth, one-eighth, and one-tenth of the parametric resonance frequency, which is indicative of higher order quadrupolar resonances (K > 1 in eq. 6). These resonances were not limited to the Mini 12; spectra on the LTQ also suffered from these added peaks if the amplitudes of the ac and rf were high enough (see **Figure S2.9** and **Table S2.1**). Since the LTQ has hyperbolic rods compared to the rectangular cross sections in the RIT, the resonances were more difficult to observe, presumably due to weaker coupling of ion motion in x and y. For example, only with a very high LMCO of ~1,000 Da were the parametric resonances observed on the benchtop instrument. Furthermore, the K = 4 resonances were the only ones observed in this case, which is further evidence for x,y-coupled motion as the cause.

In general, higher resonances can only be accessed with higher excitation amplitudes as illustrated in **Figure S2.10**, which is reproduced from Collings *et al.* This shows regions of the Mathieu stability diagram in which the higher order parametric resonances may be accessed. Since the parameter Q is directly proportional to the excitation amplitude and because K increases with Q, higher amplitudes are required for excitation at K > 1 resonances.

An alternative explanation for these findings is possible: electronic coupling between the ac and rf waveforms could accidentally introduce a small supplementary quadrupole field. The need for higher ac and rf amplitudes corroborates this explanation as well. However, though the rf

and ac are coupled together electronically on the LTQ (i.e. the rf is applied to all four rods and the ac is applied only to one pair), this is not the case on the Mini 12. In the latter case, the rf is applied to one rod pair and the ac is applied to the other pair, so there ought to be no coupling between the two. Small perturbations in the sinusoidal excitation could also promote excitation at parametric resonances due to the introduction of higher harmonics. Nonetheless, the more likely cause is the higher order field components because of i) the difference in the accessibility of these resonances on the two different instruments, ii) the observation of parametric resonances on both instruments with two different sets of electronics, and iii) the ac amplitude dependence observed on the Mini 12, which agrees with previous reports (**Figure S2.10**).

In any case, sensitivity and peak width appeared to be improved over that of the fundamental resonance, which has been reported previously.[20,21] Higher resolution at higher order resonances may present an interesting alternative to mass spectral acquisition compared to the fundamental resonances. Furthermore, if the secular frequency scan were used for fragmentation, it may benefit from the higher order fields since ions will gain kinetic energy at several points during the mass scan (the secular frequency and the higher order parametric resonances), promoting more efficient collision-induced dissociation. The fragmentation would be fairly mass selective in time, but different ions of the same mass would presumably fragment at several different times, leading to some overlap in the spectral intensities.

An advantage of secular frequency scanning over conventional rf scanning is mass range extension at low rf amplitudes. Mass range extension can also be accomplished in an ion trap by resonance ejection at a low q value, that is, at a low ac frequency, or by lowering the rf frequency.[84] **Figure S2.11** shows the secular frequency scan mass spectrum of a calibration solution of caffeine (*m/z* 195), the peptide MRFA (*m/z* 525), and Ultramark 1621 (*m/z* 1022-1922, every 100 Th). For reference, resonance ejection at an optimal q value was performed as well (**Figure S2.12**). As shown, the high mass Ultramark calibration ions can be detected at low rf amplitudes by using a relatively low amplitude ac waveform scanned through low frequencies using an appropriate scan time. Despite the closeness of their secular frequencies, the fast frequency scanning, and the large mass range, the Ultramark peaks are resolved in a linear frequency sweep, and their higher order resonances can even be observed using the Mini 12 with a 4 V_{pp} ac amplitude (not shown). The same experiment on the LTQ is shown in **Figure S2.11c** and **S2.11d**. Ion intensity in the secular frequency scan with a LMCO of 1000 Th is double that in the resonance ejection scan with a

LMCO of 50, though the latter is a shorter scan in terms of time and the scan rate is uniform, which contrasts with the secular frequency scan in which the scan rate increases with mass. When converted to the mass domain (not shown), the approximate resolution is ~2 Da FWHM (*m/z* 1422) for the secular frequency scan, but again resolution degrades with increasing mass. Mass range extension in this method is arguably superior to resonance ejection at low q for several reasons: in the latter case (i) ions are also ejected at q=0.908, convoluting the mass spectrum, (ii) higher rf amplitudes are required, (iii) a linear rf amplitude ramp is needed, and (iv) the entire mass spectrum is difficult to obtain due to the low mass cutoff imposed by the supplementary ac (this assumes ions below that cutoff are ejected from the trap prior to the mass scan, due to reason (i)).

One of the main concerns about secular frequency scanning is the presence of "black holes" in the Mathieu stability diagram.[8,105] These occur on iso-β lines where nonlinear higher order resonances corresponding to, for example, hexapole resonances or octopole resonances occur. The RIT is not expected to have hexapole multipole coefficients due to symmetry in the electrodes and electric field.[16] However, the octopolar coefficient in the RIT is ~7.9% of the quadrupolar coefficient and thus contributes substantially to the electric field. Thus, we chose to investigate the nonlinear octopolar resonance at β = ½.[25] **Figure 2.6** shows forward and reverse frequency sweeps when *m/z* 284 is placed just below (i.e. β < 1/2), on (β = 1/2), or just above (β > 1/2) the nonlinear resonance point. In the forward frequency sweep, no signal is observed for peaks at the black hole, regardless of ac amplitude and other relevant parameters. In the reverse frequency sweep, peak splitting is observed at lower ac amplitudes, but use of higher amplitudes (inset in **Figure 2.6b**) diminishes the splitting. Peak splitting has been reported previously in double resonance ejection experiments[32] (i.e. applying a resonance waveform with frequency corresponding to a higher order hexapole or octopole resonance), but the complete lack of peak intensity in the forward frequency sweep is striking. The difference here is that when the resonance point is scanned from low to high frequency, multiple resonances for each ion are encountered before the secular frequency, as shown in **Figure 2.5**. These preliminary excitations cause ions to become translationally excited and to occupy regions closer to the electrodes. Such ions are more susceptible to the higher order resonance points, resulting in a flat intensity profile at the nonlinear resonance point.

2.5   Conclusion

Secular frequency scanning is an electronically simple alternative to conventional rf amplitude or frequency ramping which has advantages in terms of access to ions of high mass. Initial results show poorer resolution, but this can be optimized by tuning the ac amplitude, rf amplitude (or rf frequency), and pressure, or by scanning at a constant rate. Higher order fields and non-optimal pressure also appear to contribute to peak broadening. Imperfect ion traps with large higher order field contributions, such as the Mini 12, through coupling of x- and y-motion of ions excited by a dipolar signal allow parametric excitation with observation of signals at a set of higher order parametric resonances. In normal dipolar secular frequency scan conditions these processes do not make a large contribution to the mass spectra but it is important to recognize their origin.

2.6   Acknowledgements

Figures and Tables
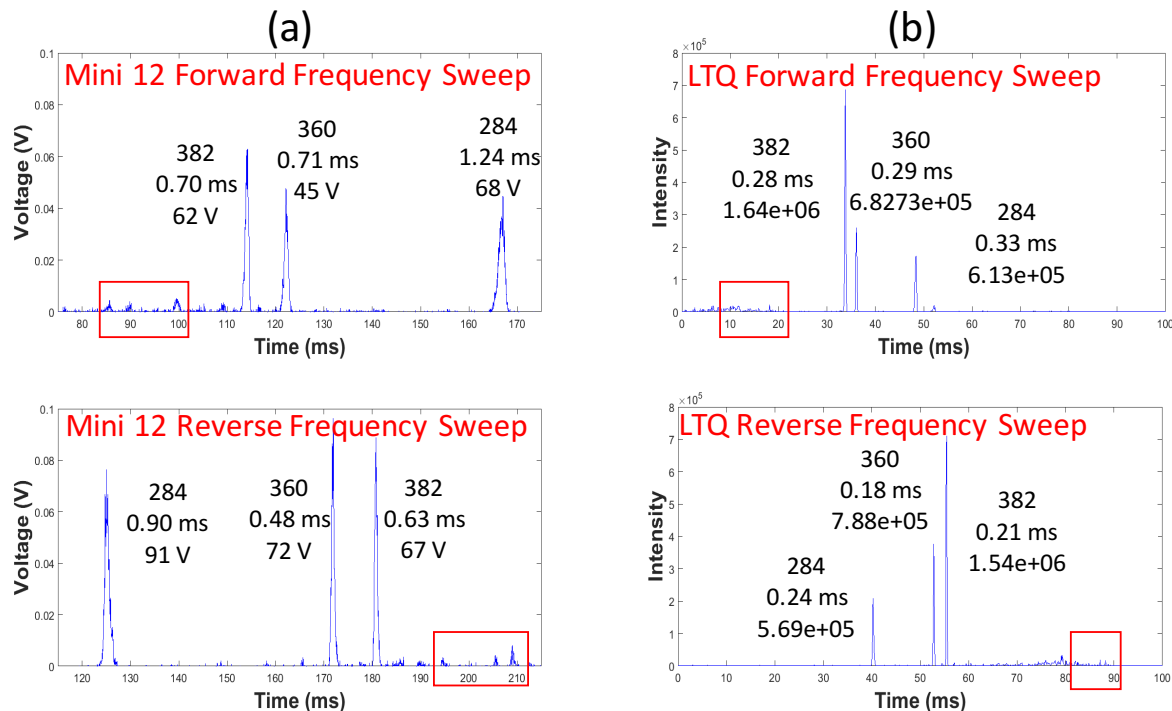
Figure 2.1. Effect of scan direction on the secular frequency scan mass spectra of tetraalkylammonium salts: (a) Mini 12 and (b) LTQ. Scan time was 300 ms from 10 to 500 kHz (or vice versa) with an ac amplitude of 1 V_{pp}. The rf amplitude was 14,000 DAC units (low mass cutoff of ~200 Th) for scans (a). Cooling time on the Mini 12 was 210 ms. Scans (b) performed during an Ultrazoom scan from 200 to 227 Th. Labels show *m/z*, FWHM peak temporal width, and area under the curve. Red boxes indicate peaks showing ejection at higher order parametric resonances.
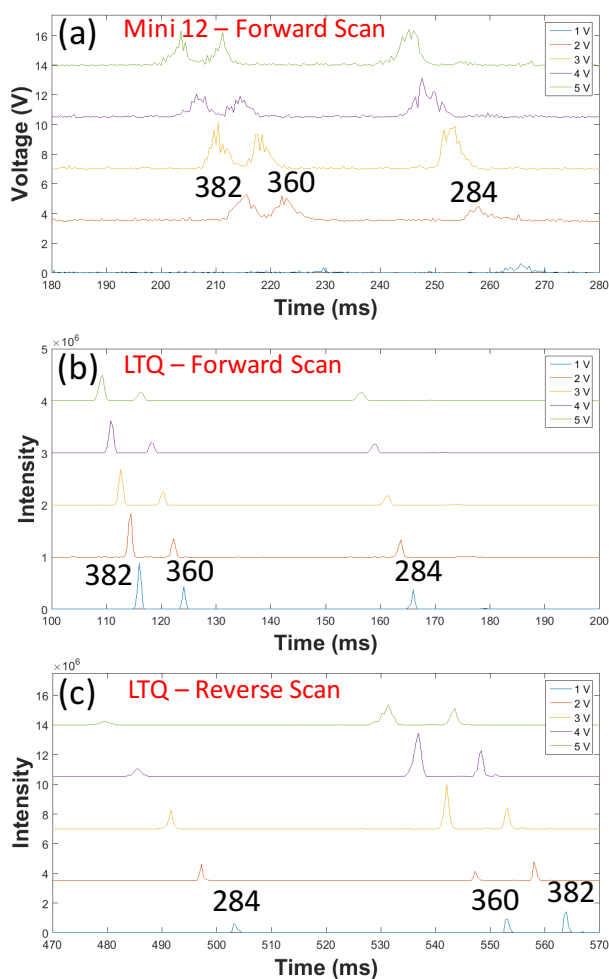
Figure 2.2. Effect of ac amplitude on the secular frequency scan of three quaternary ammonium ions, *m/z* values labeled. Inset voltages are peak-to-peak voltages of the supplementary ac frequency ramp. The rf amplitude was kept at 6,000 DAC units (LMCO = 100 Th on the LTQ) and the frequency of the supplementary ac was swept from 10 to 500 kHz over 800 ms. Shown are (a) a forward frequency scan on the Mini 12 and (b) forward and (c) reverse frequency scans on the LTQ.
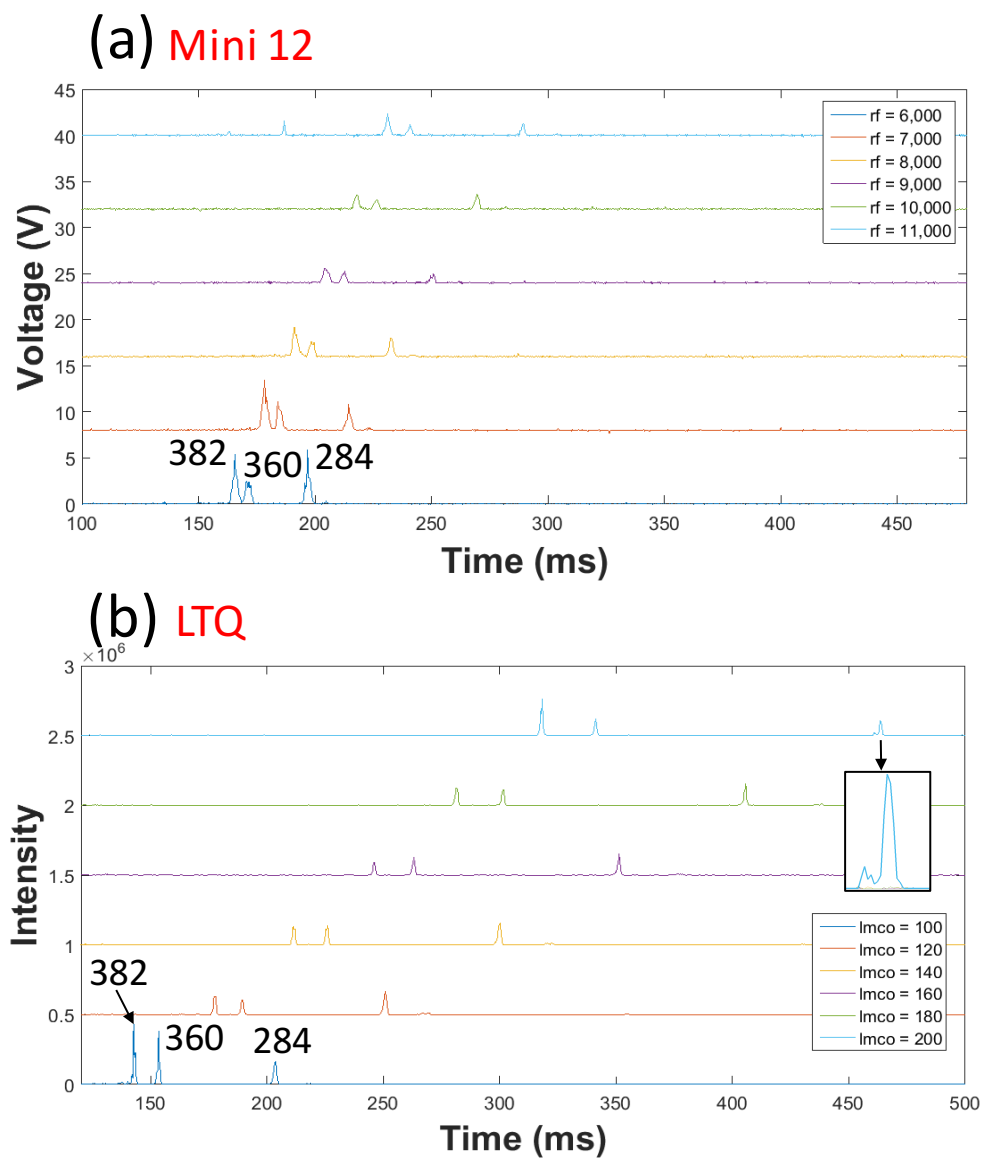
Figure 2.3. Effect of rf amplitude on the secular frequency scan of three quaternary ammonium ions, *m/z* values labeled: (a) Mini 12 and (b) LTQ. Scan parameters were ac amplitude 2 V_{pp}, 10 to 500 kHz, over 800 ms. Inset in (b) shows resolved carbon isotope peaks. Inset legends indicate the rf amplitude either in DAC units or LMCO. Rf = 6,000 DAC units = 195 V_{0-p}. Rf = 12,000 DAC units = 386 V_{0-p}.
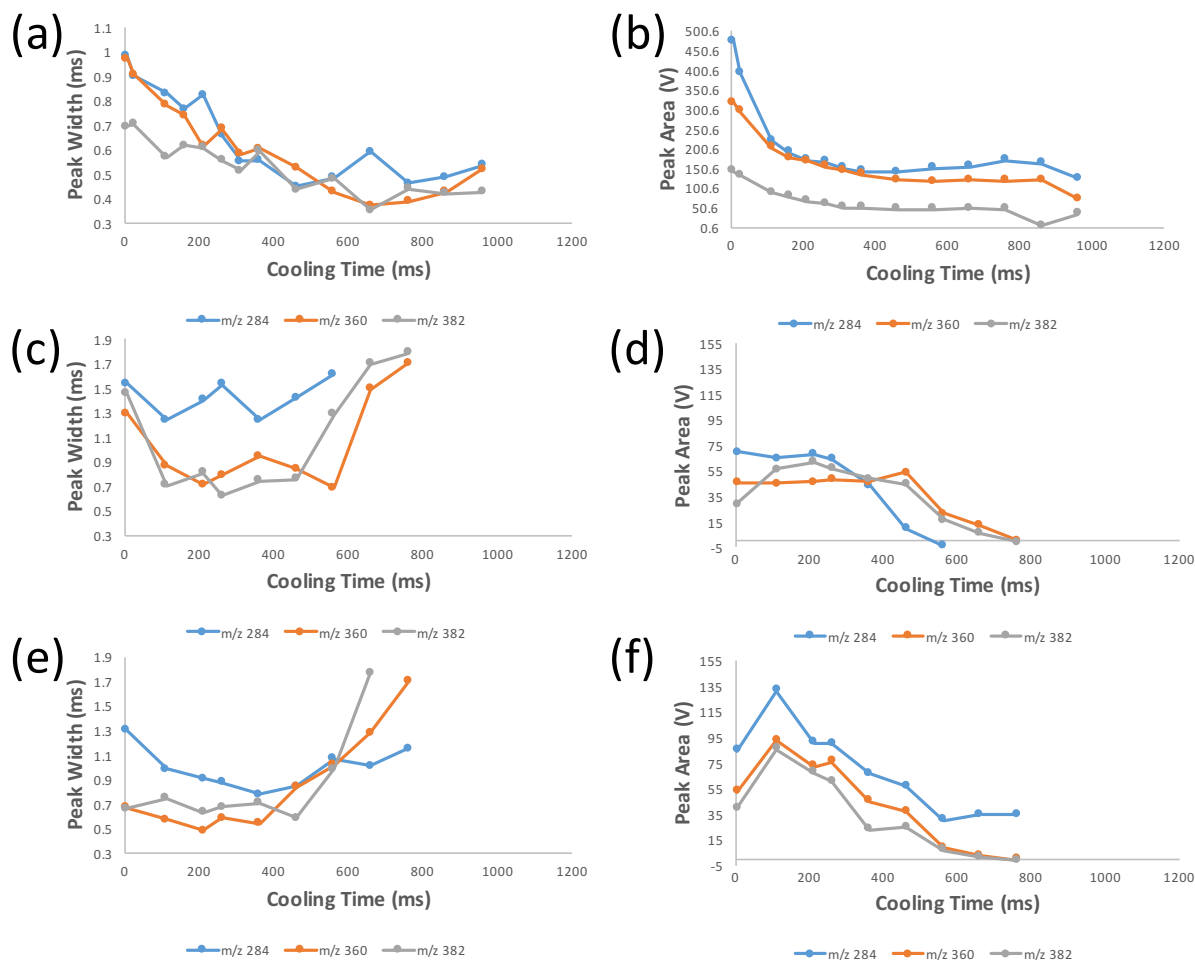
Figure 2.4. Effect of pressure on signal intensity of *m/z* 284, 360, and 382: (a) and (b) resonance ejection, (c) and (d) experimental forward frequency scan, (e) and (f) experimental reverse frequency scan. All experiments were performed on the Mini 12. The resonance ejection scan was 300 ms with a resonance waveform of 345 kHz, 35,000 DAC units. Secular frequency scans were 300 ms, 1 V$_{pp}$, 10-500 kHz or vice versa, with a lower mass cutoff of ~200 Th. Peak area was calculated by summing the intensities across the peak, which could result in a negative value.
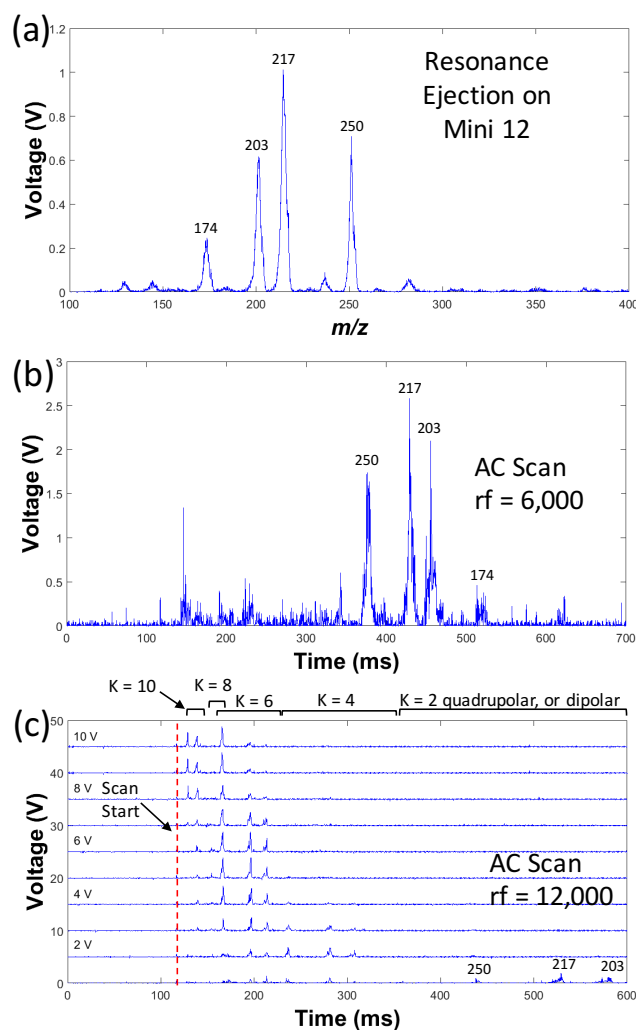
Figure 2.5. Higher order parametric resonances in forward frequency scans. Mass spectra of a mixture of five protonated pesticides, *m/z* values labeled, recorded by (a) resonance ejection using the Mini 12, and (b, c) secular frequency sweeps for different combinations of rf amplitudes (arb. units) and ac amplitudes. Resonance ejection was performed over 300 ms at 345 kHz. The secular frequency sweep was performed over 800 ms from 50 to 500 kHz. The values of K in (c) indicate ejection frequencies that correspond to higher order parametric resonances of K = 2, 4, 6, 8 and 10. See **Table 2.1** for calculations. Note that rf = 6,000 corresponds to ~195 V_{0-p} and rf = 12,000 corresponds to ~386 V_{0-p}.
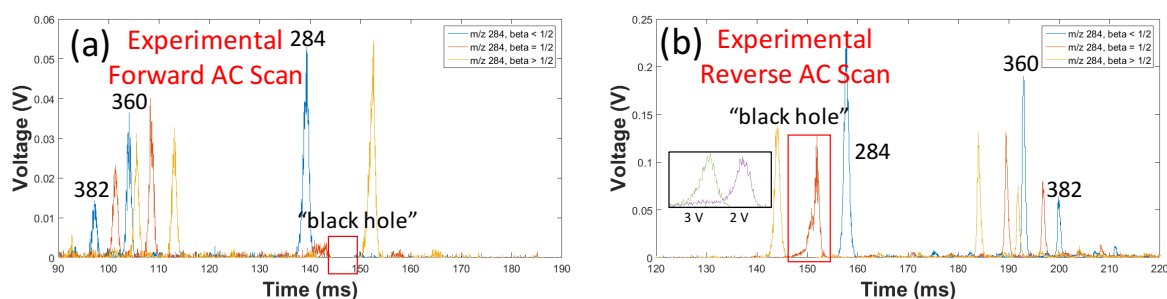
Figure 2.6. Black holes in secular frequency scanning. Shown are secular frequency scan mass spectra of three quaternary ammonium ions *m/z* 284, 360, and 382, where *m/z* 284 was placed below, on, or above the nonlinear octopolar resonance at $\beta = 1/2$. (a) Forward frequency sweep and (b) reverse frequency sweep. Red boxes indicate the peak at the nonlinear resonance point. Scans were performed on the Mini 12 with parameters 10-500 kHz (or vice-versa), 1 V_{pp} ac amplitude, 300 ms in duration, and an rf amplitude such that *m/z* 284 was just below, on, or above the nonlinear resonance point at $\beta = 1/2$. Inset in (b) shows disappearance of peak splitting at higher ac amplitudes.

Table 2.1. Experimental ejection frequencies for ions in **Figure 2.5**, indicating ejection of ions at higher order parametric resonances despite application of only dipolar excitation.[++]

Calibration Parameters		m/z	Experimental Ejection Time (ms)	Experimental Ejection Frequency (kHz)	Calculated β_x	Calculated q_x	Parametric Frequency / Experimental Frequency	Parametric Order
Time (ms)	AC Frequency (kHz)	203	579.6	311.39	0.623	.751	2.00	K = 2 or dipolar
115	50	217	529.2	283.04	0.567	.704	2.00	K = 2 or dipolar
915	500	250	438.4	231.96	0.464	.602	2.00	K = 2 or dipolar
		203	307.6	158.37	0.317		3.93	K = 4
		217	282	143.97	0.288		3.93	K = 4
		250	236.4	118.31	0.237		3.92	K = 4
		203	214	105.71	0.212		5.89	K = 6
		217	197.2	96.26	0.193		5.88	K = 6
		250, 203	166.8	79.15	0.158		5.86, 7.86	K = 6, 8
		217	154.4	72.16	0.144		7.85	K = 8
		203	139.6	63.85	0.128		9.75	K = 10
		217	129.2	58.00	0.116		9.76	K = 10

[++] The two columns on the left were used for calculating the fourth column from the third column. The seventh column is the quotient of the parametric resonance frequency (twice the secular frequency) and the experimental frequency in the fourth column. The parametric order is the K value of the resonance which corresponds to eq. 6. Note that β_x values are calculated from the experimental ejection frequencies. This is not meant to indicate the β_x that the ions reside at (except for the K = 2 case), but rather the β_x values to which the frequencies correspond. q_x values are calculated from β_x only for the K = 2 case since this is where the ions reside on the q axis of the Mathieu stability diagram.

Supplementary Figures
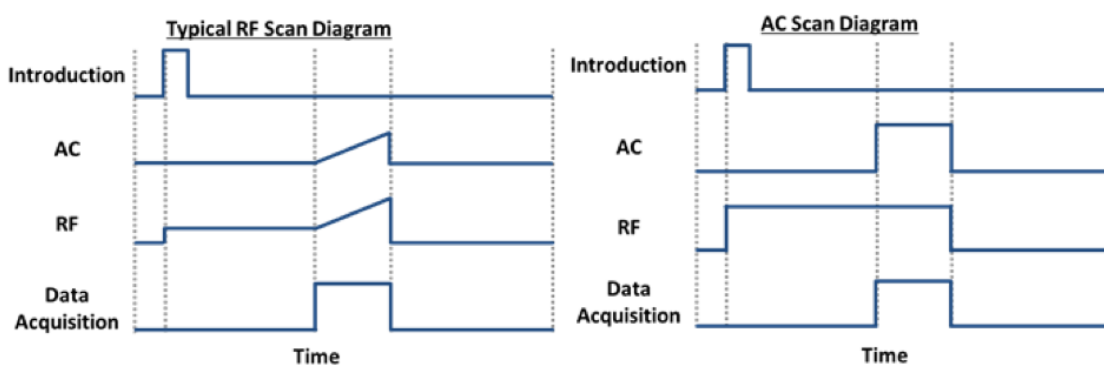
Figure S2.1. Typical scan diagrams (voltage amplitudes) for obtaining a mass spectrum by resonance ejection with an rf amplitude scan and proposed ac frequency sweep ("AC scan" or "secular frequency scan"), enabling acquisition of a mass spectrum with a constant rf amplitude and frequency. During the mass scan, *the frequency of the supplementary ac waveform is swept*, ejecting ions in a mass selective manner.
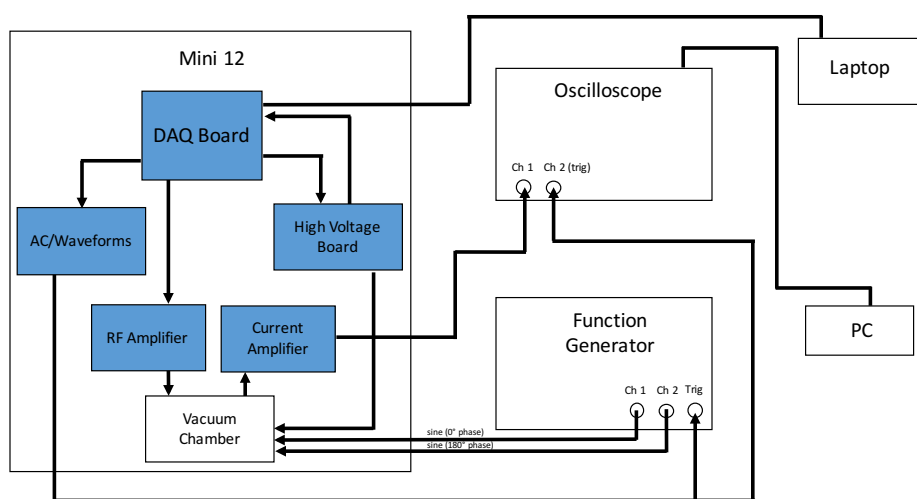
Figure S2.2. Instrumental setup for secular frequency scans on a miniature mass spectrometer.
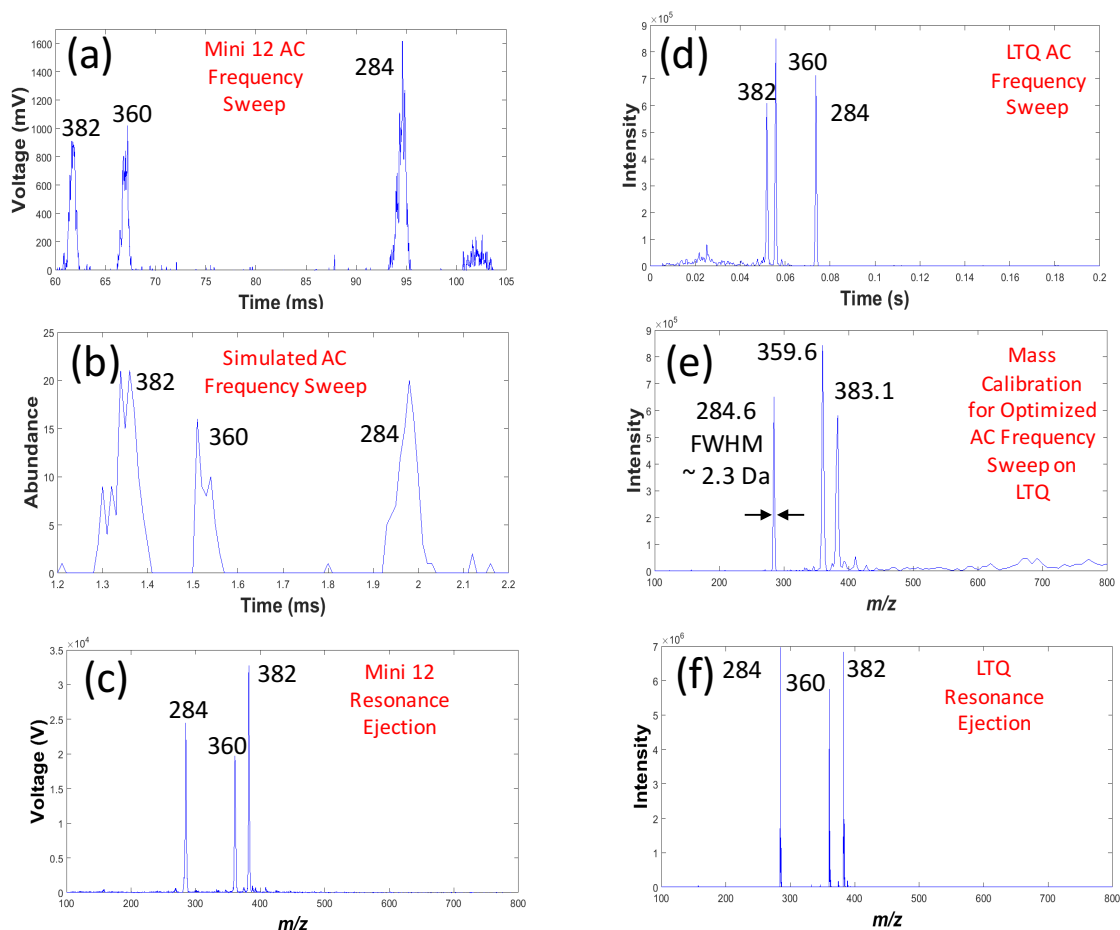
Figure S2.3. Secular (AC) frequency scanning in an ion trap: (a) forward secular frequency scan (reverse mass sweep) of tetraalkylammonium salts (*m/z* 284, 360, and 382) recorded using the Mini 12 (300 ms, 10-500 kHz, 1.5 V_{pp}, LMCO = 100 Th), (b) simulated secular frequency scan (4 mTorr He, 3 ms scan from 10 to 300 kHz, 10 V_{0-p}), (c) resonance ejection using the Mini 12, (d) equivalent secular frequency scan performed using a benchtop LTQ (same conditions as (a), but 1 V_{pp}), (e) scan in (d) converted to the mass domain and (f) comparison to resonance ejection using the LTQ.
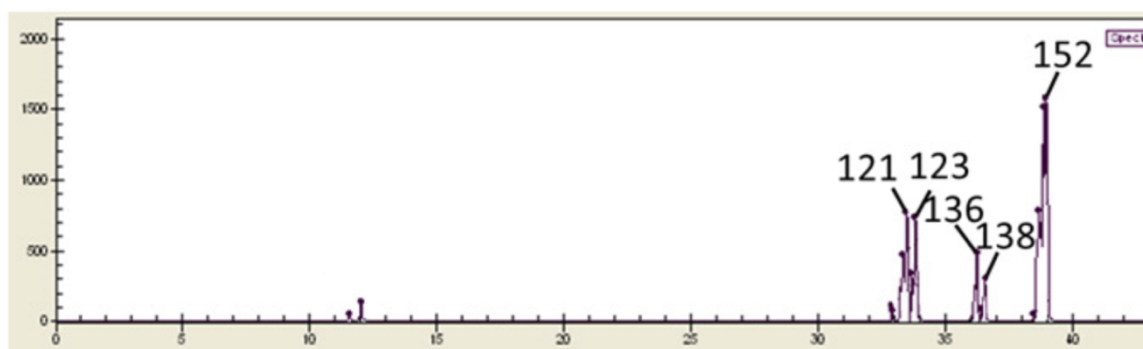
Figure S2.4. Secular frequency scan mass spectrum of 1,3-dibromopropane on a cylindrical ion trap with an internal electron ionization source showing resolved bromine isotope peaks. The lower mass cutoff was ~70 Da, and the ac amplitude was ~0.7 V_{0-p}. The peak at *m/z* 152 is methyl salicylate background from a previous experiment.
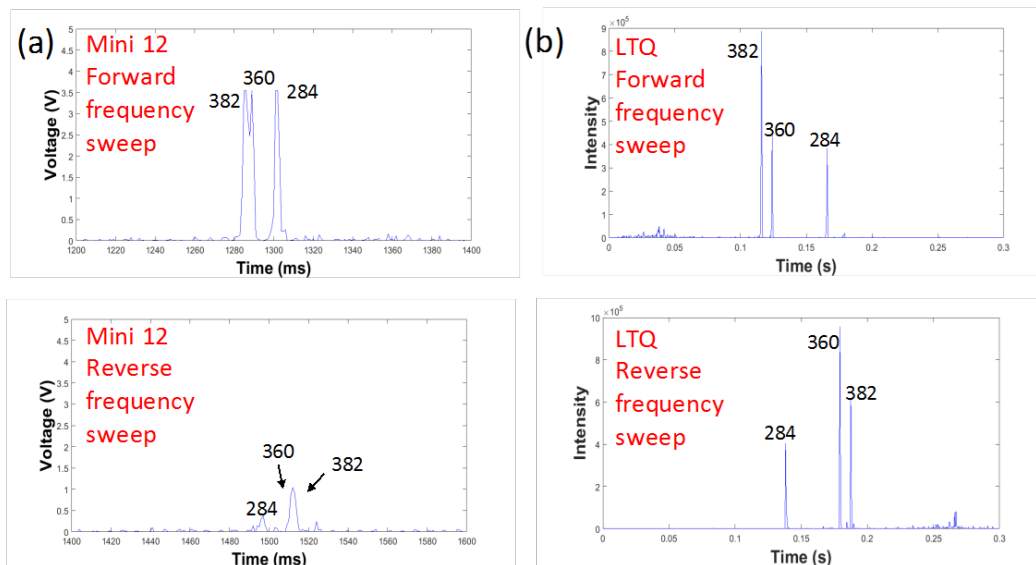
Figure S2.5. Effect of scan direction on the secular frequency scan mass spectra of tetraalkylammonium salts where ions are ejected at different pressures in each scan: (a) Mini 12 and (b) LTQ. Scan time was 300 ms from 10 to 500 kHz (or vice versa) with an ac amplitude of 4 V_{pp} for (a) and 1 V_{pp} for (b). Here resolution and sensitivity *appear* to be superior in the forward sweep, but as we show later in the paper, this is caused by ion ejection later in the scan in the reverse frequency sweep, which drastically reduces resolution and signal intensity, whereas in the forward frequency sweep the ions are ejected at higher pressure near the beginning of the mass scan.
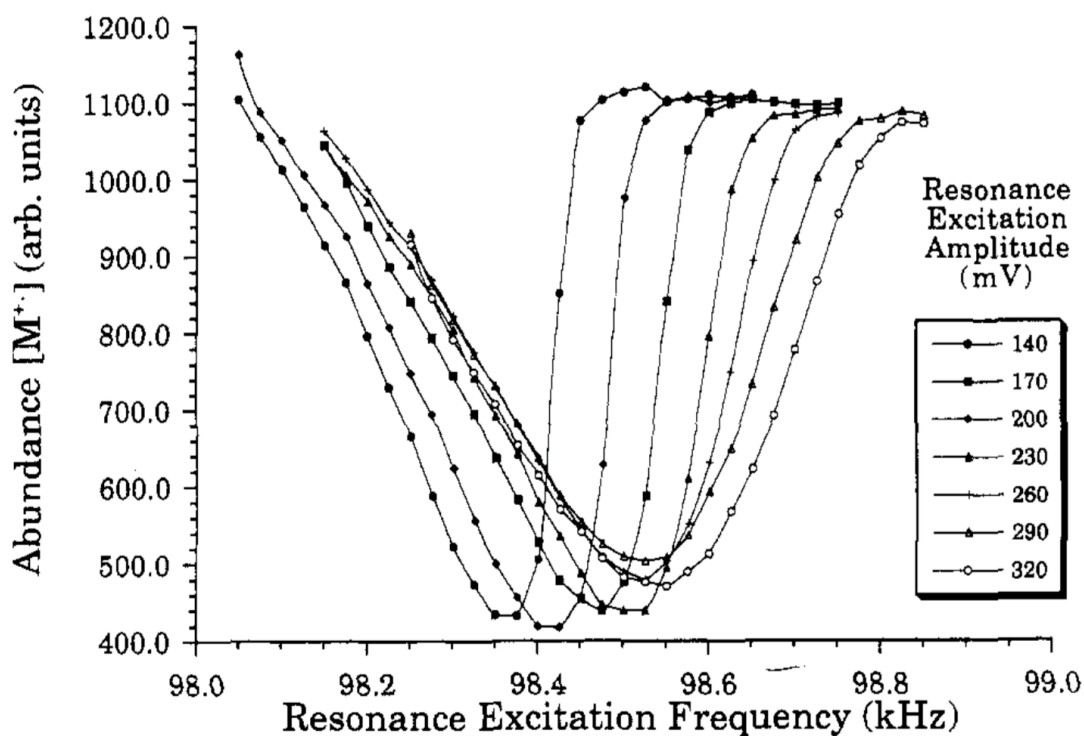
Figure S2.6. Resonance absorption curves for excitation of n-butylbenzene (*m/z* 134). Of considerable interest is (i) the shift of the resonance condition to higher frequencies at higher amplitudes (when ions are far from the center of the trap), and (ii) the asymmetry in the curves, broader at low frequency and sharper at high frequency, particularly for low excitation amplitudes. Reprinted with permission from Williams, J. D.; Cox, K. A.; Cooks, R. G.; Mcluckey, S. A.; Hart, K. J.; Goeringer, D. E. *Anal. Chem.* **1994**, *66*, 725. Copyright 1994 American Chemical Society.
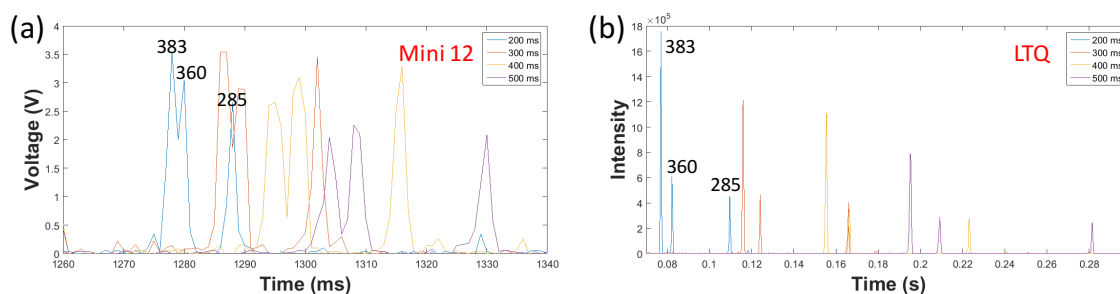
Figure S2.7. Effect of scan rate on the secular frequency scan of tetraalkylammonium salts (*m/z* 285, 360, and 383) demonstrated using (a) Mini 12 and (b) LTQ. Scan rate was altered by changing the scan time (inset) on the function generator while keeping the frequency range the same. Scan range was 10-500 kHz and amplitude was (a) 3 V_{pp} and (b) 1 V_{pp}. The LMCO was set at 100 Th.
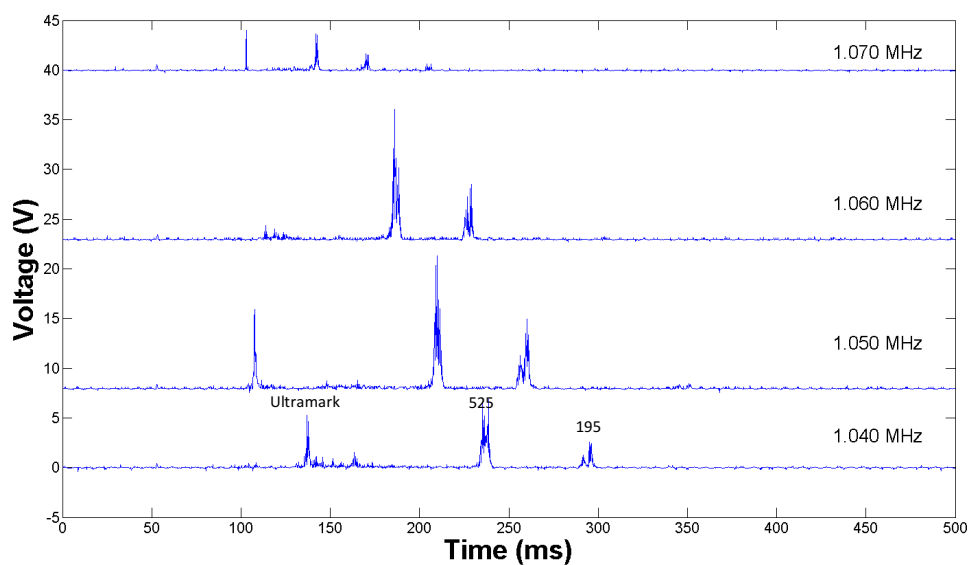
Figure S2.8. Forward frequency scan of a calibration solution of Ultramark (m/z 1022-1922, every 100 m/z), MRFA (m/z 525), and caffeine (m/z 195) showing effect of rf frequency on the spectra. Rf amplitude was held constant at 6,000 DAC steps, ac amplitude was 7 V_{pp}, and scan time was 800 ms.
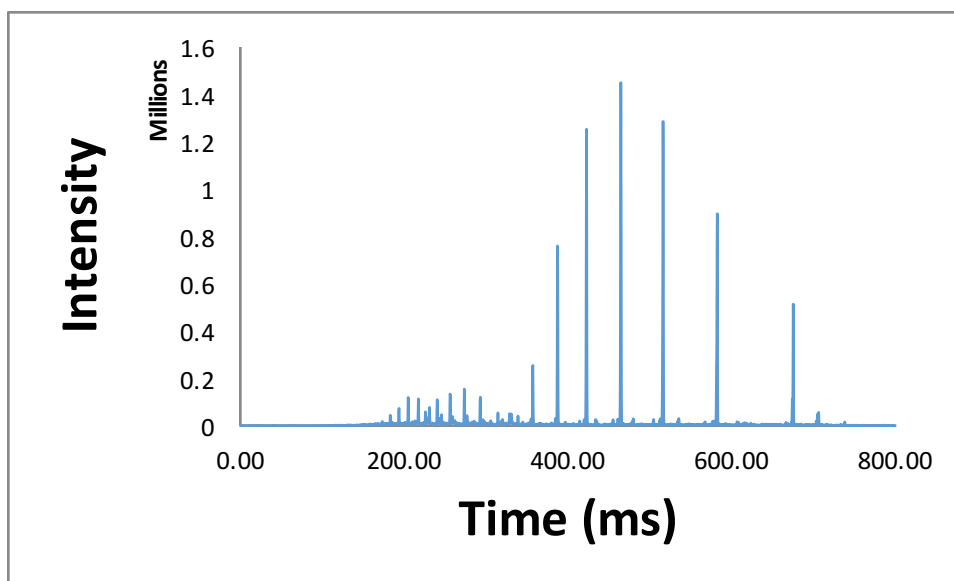
Figure S2.9. Secular frequency scan mass spectrum showing higher order parametric resonances on a benchtop LTQ XL. Ions from an Ultramark 1621 calibration solution were analyzed with a secular frequency scan 10-580 kHz with a 1 V$_{pp}$ amplitude over 800 ms during an Ultrazoom scan starting at 1300 Th. The intense peaks on the right side of the spectrum (>350 ms) are ions ejected at their secular frequency, whereas the same distribution is observed in the 150-350 ms range, indicative of ejection at the K = 4 parametric resonance. See **Table S2.1** for calculations.

Ejection Time (ms)	Ejection Frequency (kHz)	Parametric Frequency / Ejection Frequency	K
0	10	*calibration parameters	
800	580	*calibration parameters	
675.19	491.07	2	2 or dipolar
582.59	425.10	2	2 or dipolar
516.30	377.86	2	2 or dipolar
464.81	341.18	2	2 or dipolar
422.96	311.36	2	2 or dipolar
387.41	286.03	2	2 or dipolar
357.41	264.65	2	2 or dipolar
339.26	251.72	3.90	4
293.33	219.00	3.88	4
256.30	192.61	3.92	4
231.11	174.67	3.91	4
205.19	156.19	3.99	4
183.33	140.62	4.07	4
173.70	133.76	3.96	4

Table S2.1. Calculated times and frequencies of ejection for the scan in **Figure S2.9**. The top two rows of data show the parameters for calculating ejection frequency from ejection time. The data in blue show ion ejection times and frequencies corresponding to those times. These are their experimental secular frequencies. The ions in purple correspond to the ions in blue (first blue ion = first purple ion and so on), but were ejected at a higher order parametric resonance corresponding to K = 4, as calculated in column 3. For the calculation in column 3, it was assumed that the parametric resonance frequency was twice the frequency in blue for each respective ion. Hence, the ratio of the parametric frequency to each blue frequency is exactly 2. The K value corresponds to the order of the parametric resonance.
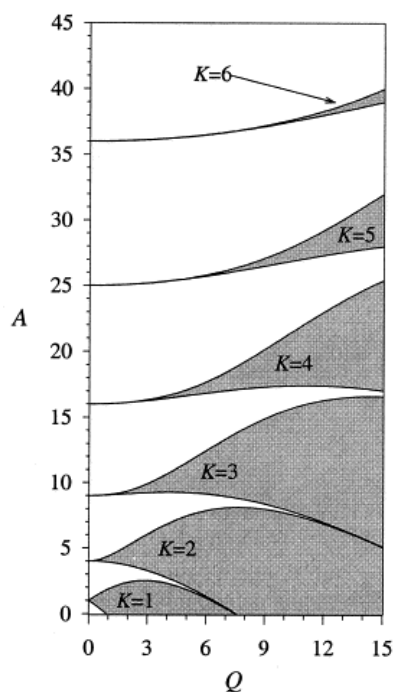
Figure S2.10. Mathieu stability diagram illustrating parametric K = 1 to K = 6 resonances. Shaded areas represent regions of instability. Here Q is directly proportional to the excitation voltage, indicating that the higher order resonances require higher excitation amplitudes. Reprinted from Collings, B.A., Sudakov, M., Londry, F.A.: Resonance shifts in the excitation of the n = 0, K = 1 to 6 quadrupolar resonances for ions confined in a linear ion trap. *J. Am. Soc. Mass Spectrom.* **13**, 577-586 (2002).
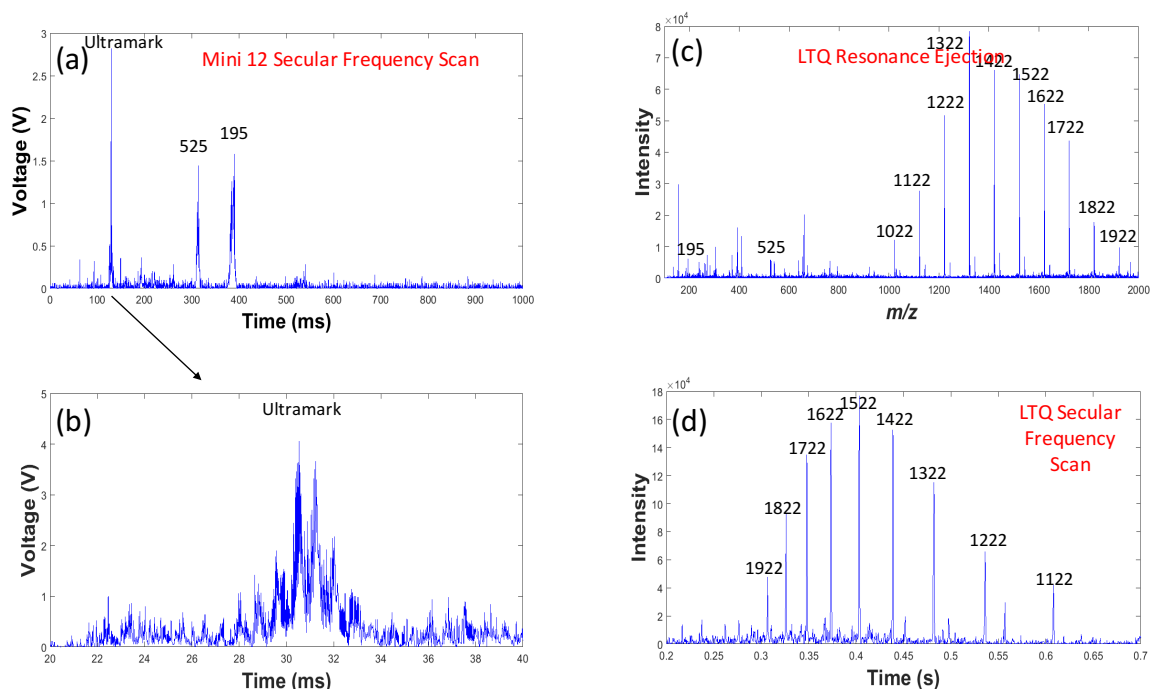
Figure S2.11. Mass range extension on the Mini 12. Secular frequency scans of a solution of caffeine, MRFA, and Ultramark 1621 showing mass range extension at low rf amplitudes: (a) full scan on Mini 12 showing caffeine, MRFA, and Ultramark peaks (3.3 V_{pp}, 10-500 kHz, LMCO = 98 Th, 800 ms scan), (b) zoomed in image showing resolved Ultramark peaks, (c) resonance ejection performed on an LTQ, and (d) secular frequency scan of the Ultramark solution on an LTQ performed over 800 ms, 10-500 kHz, with a 1 V_{pp} amplitude and a lower mass cutoff of 1,000 Th.
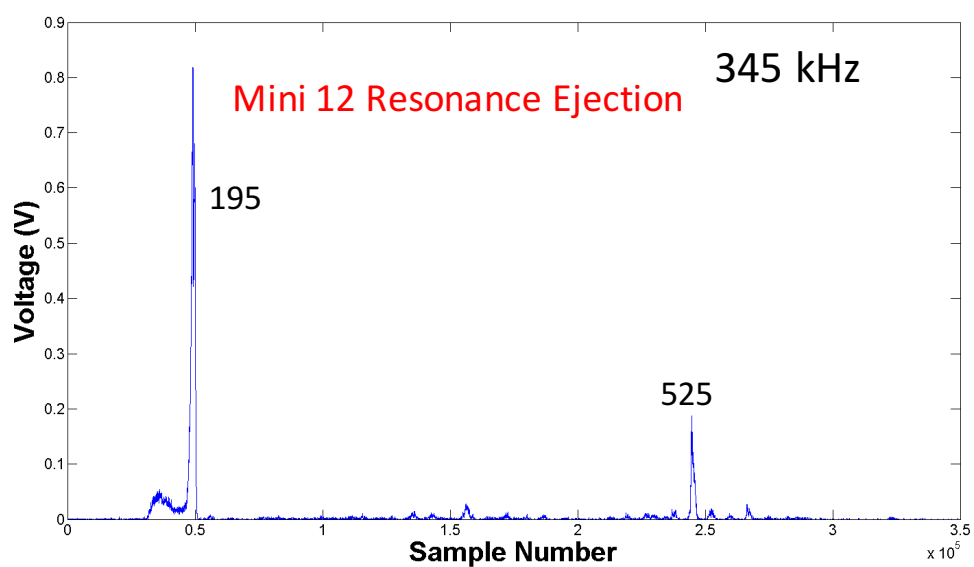
Figure S2.12. Resonance ejection mass spectrum at 345 kHz of a calibration solution of caffeine (*m/z* 195), MRFA (*m/z* 525), and Ultramark 1621 at 345 kHz (not within mass range). Spectrum was acquired on the Mini 12. Sample number is linearly correlated with *m/z*.

CHAPTER 3.   CALIBRATION PROCEDURE FOR SECULAR FREQUENCY SCANNING IN ION TRAP MASS SPECTROMETERS

3.1   Abstract

Rationale: Mass spectra can be recorded using ion traps by scanning the frequency of an ac signal that corresponds to the secular frequency of a trapped ion. There is a considerable simplification in the instrumentation needed to perform such a scan compared to conventional scans of the rf amplitude. However, mass calibration is difficult. An algorithm that can be used to achieve mass calibration is investigated and the factors that affect ion mass assignments are discussed.

Methods: Time domain data, recorded using a commercial benchtop linear ion trap mass spectrometer, are converted to the *m/z* domain using ion Mathieu parameter q_u values which are derived from the dimensionless frequency parameter β_u expressed as a continuing fraction in terms of q_u. The relationship between the operating parameters of an ideal ion trap and ion *m/z* ratio is derived from the Mathieu equations and expressed as an algorithm which through successive approximations yields the Mathieu q_u value and hence *m/z* values and peak widths. The predictions of the algorithm are tested against experiment by sweeping the frequency of a small supplementary ac signal so as to cause mass-selective ejection of trapped ions.

Results: Calibration accuracy is always better than 0.1%, often much better. Peak widths correspond to a mass resolution of 250 to 500 in the *m/z* 100 – 1800 range in secular frequency scans.

Conclusions: A simple, effective method of calibration of mass spectra recorded using secular frequency scans is achieved. The effect of rf amplitude, scan rate, and ac amplitude on calibration parameters are shown using LTQ linear ion trap data. Corrections for differences in ion mass must be made for accurate calibration, and this is easily incorporated into the calibration procedure.

3.2 Introduction

Recently a method has been described for acquiring mass spectra using ion traps in which the frequency of a small supplementary ac signal is ramped through ion secular frequencies over time, a process which we term "secular frequency scanning".[106] It has also been shown that secular frequency scanning can be used as a time-based method of mass selective fragmentation. As a consequence, the combination of a low amplitude secular frequency scan and a high amplitude, constant frequency ejection waveform set at the secular frequency of a particular product ion can be used to record precursor ion spectra in a single ion trap.[99,107]

The attractiveness of recording mass spectra using the secular frequency scan compared to traditional sweeps of the radiofrequency (rf) amplitude is its simplicity since a linear ramp of the rf amplitude is not required. However, as in the rf frequency sweep method,[46] calibration remains difficult due to nonlinearity between the varied parameter (rf frequency or ac frequency) and m/z.[46]

Here, we introduce a simple algorithmic approach for mass calibration of secular frequency scan mass spectra. The algorithm assumes a linear sweep of the ac frequency and a 2D quadrupole trapping field, but nonlinear sweeps and other ion trap geometries can easily be accommodated by modifying the code. The objective is to calibrate for accurate unit mass resolution; exact mass measurements are not possible.

3.3 Theory

Mass calibration in quadrupole ion traps operated in the mass selective instability mode, first described by Stafford *et al.*,[82] is based on the linear relationship between m/z and the rf amplitude, as described by the Mathieu parameters a_u and q_u for a linear ion trap with a 2D trapping field:[5-8,12]

$$a_x = -a_y = 8zeU / \Omega^2 r_0^2 m \qquad \text{Eq 3.1}$$

$$q_x = -q_y = 4zeV_{0-p} / \Omega^2 r_0^2 m \qquad \text{Eq 3.2}$$

where z is the integer charge on the ion, *e* is the unit charge, U is the dc potential on the rods, V_{0-p} is the zero-to-peak (0-p) amplitude of the driving rf potential, Ω is the angular rf frequency ($2\pi f$, where f is the rf frequency), r_0 is the characteristic dimension of the trap (half the distance between

the rods), m is the mass of the ion in kilograms, and x and y are the characteristic dimensions of the 2D quadrupole trapping field. Note that the dimensions in x and y are often different such that r_0 may be replaced by either x_0 or y_0. Similarly, for a 3D quadrupole ion trap we have

$$a_z = -2a_r = -16zeU / \Omega^2(r_0^2 + 2z_0^2)m \qquad\qquad \text{Eq 3.3}$$

$$q_z = -2q_r = 8zeV_{0\text{-p}} / \Omega^2(r_0^2 + 2z_0^2)m \qquad\qquad \text{Eq 3.4}$$

where r and z are the radial and axial dimensions, respectively, and r_0 and z_0 are the half distances between the electrodes in their respective dimensions. More generally, we will refer to any arbitrary characteristic dimension as u. Typically $a_u = U = 0$, so the a_u may be ignored. In terms of *m/z*, we have

$$m/z = 4V_{0\text{-p}} / q_x \Omega^2 r_0^2 \qquad\qquad \text{Eq 3.5}$$

for the linear ion trap and

$$m/z = 8V_{0\text{-p}} / q_z\Omega^2(r_0^2 + 2z_0^2) \qquad\qquad \text{Eq 3.6}$$

for the 3D ion trap. In eqs 3.5 and 3.6 we have combined *e* and z and have limited our discussion to the x and z dimensions since they are typically the direction of ion ejection.

Thus we see that *m/z* and $V_{0\text{-p}}$ are directly proportional. In order to calibrate a quadrupole ion trap, mass standards are analyzed by either resonance ejection or boundary ejection, resulting in an intensity vs. time dataset.[6,8] The time axis is then linearly correlated to *m/z* based on the known monoisotopic mass and charge of each ion, giving a slope and an intercept which are used to convert from the time domain to the *m/z* domain, hence correlating *m/z* and intensity.

Calibration of rf frequency sweeps is inherently more difficult. As given by eqns 3.5 and 3.6, *m/z* is inversely proportional to the *square* of the rf frequency. Nonetheless, frequency sweeps of this kind have been reported in a quadrupole mass filter,[46] quadrupole ion traps,[85,108] and a digital ion trap.[87,88,109] The digital trap is particularly well-suited to these scans because a linear sweep through ion mass can be achieved by changing the period of the digital rf waveform using a square root dependence with respect to time.

A third method of obtaining a mass spectrum with an ion trap is to scan the internal radius (r_0 in eq 3.5 or z_0 in eq 3.6) of the analyzer, but this is mechanically difficult and impractical in that it would require many precise steps to achieve performance similar to standard methods, and the electric field components would change with the varied parameter.[110] Thus, in practice such a scan is impossible.

A secular frequency scan, first reported by Welling *et al.*,[111] has had few adopters in practice,[95] but has most notably been applied in the halo ion trap[19] and its variants.[96,97] In contrast to scans which require a linear rf amplitude ramp, secular frequency scanning is a simpler alternative. This method is based on excitation and/or ejection of ions with a dipolar ac field with frequency corresponding to characteristic frequencies of the motion of ions of particular *m/z* values. The angular frequency components ($\omega_{u,n}$) of ion motion[12] in a pure quadrupole field are given by

$$\omega_{u,n} = (2n+\beta_u)\Omega/2 \qquad -\infty < n < \infty \qquad\qquad\qquad \text{Eq 3.7}$$

where u is the characteristic dimension (x and y for a linear ion trap and r and z for the 3D ion trap), n is an integer, and $\beta_u{}^5$ is a parameter between 0 and 1. Setting n = 0 in eq 3.7, we obtain

$$\omega_{u,0} = \beta_u\Omega/2 \qquad\qquad\qquad\qquad\qquad\qquad\qquad \text{Eq 3.8}$$

which is an ion's *fundamental secular frequency*.

Values of the Mathieu parameter q for an ion can then be derived (or vice-versa) from a continuing fraction expression for β_u in terms of the q_u value, where

$$\beta_u^2 = a_u + \cfrac{q_u^2}{(\beta_u+2)^2 - a_u - \cfrac{q_u^2}{(\beta_u+4)^2 - a_u - \cfrac{q_u^2}{(\beta_u+6)^2 - a_u - \cdots}}}$$

$$+ \cfrac{q_u^2}{(\beta_u-2)^2 - a_u - \cfrac{q_u^2}{(\beta_u-4)^2 - a_u - \cfrac{q_u^2}{(\beta_u-6)^2 - a_u - \cdots}}}$$

$$\text{Eq 3.9}$$

which simplifies in the ion trap since generally $a_u = 0$.[6] A ramp of the ac frequency thus excites ions as a function of time, and if the application time and amplitude of the waveform are sufficient, ions will be ejected from the trap in a non-linear mass-selective manner.

3.4   Algorithm

An overview of the method for mass calibration of secular frequency scan mass spectra is shown in **Figure 3.1**. The first step is to correlate applied ac frequency with each data point in time, which can be determined from the sampling rate of the data system and the scan range and scan time of the waveform generator. These frequencies are then converted to β_u using eq. 3.8. This step assumes that the fundamental secular frequency (eq. 3.8) is being interrogated.

Once β_u values are obtained, they must be converted to Mathieu q_u parameters by solving a truncated version of eq. 3.9. This can be done by using an iterative algorithm, *beta_to_q*, which guesses an initial value of 0.5 for q_u. The value of β_u is bound between 0 and 1 based on the possible values of q_u (typically between 0 and 0.908). Both the left hand side and right hand side of eq. 3.9 are calculated and the difference is obtained. Based on this result, either the left or right bound is changed to coincide with the guessed value of q_u. A new value of q_u is then calculated as the average of the other bound and the current guessed q value. This process repeats until the difference between successive guesses of q_u is less than any arbitrarily specified tolerance. While there are algorithms that converge more quickly (i.e. Newton's algorithm), they generally require taking a derivative, complicating the calculations.

The calculated values of q_u are converted to uncorrected *m/z* ($m_{uncorrected}$) via eq. 3.5 and the known values of V_{0-p}, Ω and r_0, though these values need not be known since they are constant throughout the scan so that any error in the "guessed" values for the parameters is thus incorporated into the slope and intercept calculated in the final step. Note that eq. 3.5 is relevant only for linear ion traps in which a 2D quadrupole trapping field is established. Eq. 3.6 should be used for the 3D ion trap (Paul trap). It should also be emphasized that the characteristic dimensions of a trap, and thus q_u values in different dimensions, may be different. The q_u values used here should be those which correspond to the direction of ion ejection, which is the x direction in the LTQ linear ion trap. For the 3D ion trap, the z direction is typically used for ejection.

Arbitrary sweeps of V_{0-p}, as in the "Ultrazoom" scans[102] that we employed[106] to minimize changes in rf amplitude using a conventional LTQ linear ion trap, can be accommodated by

incrementing V appropriately before each mass is calculated, but this is only necessary in systems like the LTQ where data can only be recorded when $V_{0\text{-}p}$ is being scanned. The standard "Ultrazoom" scan (scan rate of 27 Da/s, ejection at q = 0.88, see **Figure 3.1**) on the LTQ allowed the acquisition of secular frequency scan mass spectra with near-constant rf amplitude without other instrumental or data system modifications. There are no built-in scan functions on this instrument in which the rf amplitude is constant. While the slow rf sweep changes the resolution obtained, this effect is very small.

The last step in the calibration procedure is to take different ion masses into account and to correct for errors in $V_{0\text{-}p}$ and Ω. Ions of greater *m/z* will be ejected more slowly than ions of lower *m/z* due to differences in inertia and differences in ejection frequency. This contrasts with mass shifts in resonance ejection, where ejection delays are principally due to field imperfections and collisions with the surrounding bath gas. [42,84,85,89] The key distinction here is that in resonance ejection all ions are ejected at the *same* frequency; in secular frequency scanning, ions are ejected at *different* frequencies. In addition, the "guessed" values of $V_{0\text{-}p}$, Ω, and the internal radius of the trap (e.g. r_0) may be incorrect, but since they are constant during the scan, they are incorporated into the slope obtained as follows. To take these considerations into account in secular frequency scanning, the true monoisotopic masses of the mass standards are plotted against uncorrected mass data, $m_{uncorrected}$, which generates a linear relationship. A dimensionless slope, s, and an intercept, b (in Th), are then used to convert from $m_{uncorrected}$ to $m_{corrected}$, giving the correct calibration. This procedure is illustrated in **Figure 3.2**, where $m_{uncorrected}$ data from analysis of an Ultramark 1621 calibration solution (details in figure caption) is plotted against the calculated monoisotopic masses of the calibration ions. The result is a linear relationship, the slope and intercept being subsequently incorporated into the final step of the algorithm.

3.5   Results & discussion

Austin and coworkers have shown mass calibrated data for their secular frequency scan experiments in the halo trap,[19,96,97] but quantitative values for calibration accuracy and the effect of scanning parameters on the calibration procedure have not been reported. Using the algorithm in **Figure 3.1** and the slope and intercept from **Figure 3.2**, we were able to obtain quantitative results for both, as shown in **Table 3.1**. For details of the experiments, see ref. 1. In brief, a Thermo LTQ linear ion trap mass spectrometer was used with the resonance ejection waveform replaced

by a swept frequency sinusoidal waveform from an external function generator (Sony Tektronix AFG320) while the standard Ultrazoom scan function was used for rf amplitude control. Thus, system modifications for keeping the rf amplitude constant were not necessary. While the Ultrazoom scan does change the rf amplitude, the effect is very small (scan rate of 27 Da/s, resonance ejection at $q_x = 0.88$) and can largely be ignored. The standard LTQ bath gas pressure of ~1.0 x 10^{-5} Torr was used for collisional cooling. All q values reported from this point on are q_x values since ions are resonantly ejected from the linear ion trap in this dimension (i.e. the resonance ejection waveform is applied in a dipolar fashion between the x rods).

If the last step in the procedure is ignored (i.e. if uncorrected mass values are used for calibration), then the calibrated masses are too high. This is understandable since ions will generally be ejected slightly after their resonance conditions have been met. However, when these values are corrected for the mass-dependent ejection delay and incorrect inputs for trap parameters (e.g. V_{0-p}), calibration error decreases to ~10-600 ppm, which is in reasonable agreement with the typical mass accuracy of a linear ion trap, ~50-100 ppm. Some of the calibration error is due to the mismatch between the LTQ's data system, which records a constant 100 points per integer mass, and the variable scan rate of the secular frequency scan. This results in one data point being acquired every ~0.37 ms. More error can be attributed to the necessity of choosing a built-in scan function, in this case the Ultrazoom scan, to minimize the change in the rf voltage. However, our calculations took this into account by incrementing V at every time step. Even with these difficulties, calibration accuracy was always less than 0.1%, which is sufficient for determining the integer masses of the analytes.

Peak width, calculated as full width at half maximum (FWHM), increases approximately linearly with mass, as shown in the last column of **Table 3.1**. This is the result of scanning the frequency of the ac linearly with time, meaning the scan rate increases with mass. The increase in scan rate is approximately linear for q < 0.4 (the approximation loses significance at q = 0.7).[5]

A second example of mass calibration is shown in **Table 3.2**. The analytes were didodecyldimethylammonium (M^+, m/z 384), hexadecyltrimethylammonium (M^+, m/z 284), and benzylhexadecyldimethylammonium (M^+, m/z 360), as described in a previous experiment.[106] Calibration error is 10-100 ppm, in agreement with **Table 3.1**, and peak widths increase approximately linearly with mass.

The algorithm can further be used to perform secular frequency scans that are linear in mass. This can be accomplished by varying the frequency of the supplemental ac waveform according to eq. 3.5 (or 3.6), 3.8, and 3.9, where an array of m/z values corresponding linearly to time domain points is converted to an array of ac frequencies versus time. The result of applying such a waveform with an arbitrary waveform generator (Keysight 33612A, Newark, SC, USA) to the same linear ion trap is shown in **Figure 3.3a** with linear fit of m/z vs. time in **Figure 3.3b**, which indicates that calibration is linear if this type of scan is performed. Resolution is 0.35 Th FWHM and approximately constant throughout since the scan rate does not change with mass.

We have previously shown that increasing the rf amplitude increases resolution when the ac frequency is swept, that increasing the ac amplitude decreases resolution and sensitivity and ejects ions earlier in the scan, and that increasing scan rate increases resolution.[106] The peak position in time of each ion thus shifts when any of these parameters is altered. Here we explored the effect on the calibration procedure, namely with regard to the slope and intercept incorporated in the final step.

Increasing the rf amplitude increases resolution in secular frequency scanning because ions' secular frequencies are further apart at higher rf amplitudes (eq 3.8), but the rf amplitude is also expected to affect the calibration procedure. This is illustrated in **Figure 3.4**, where the slope and intercept parameters are plotted against the lower mass cutoff (LMCO) of the Ultrazoom scan (corresponding to $q_x = 0.88$). An increase in rf amplitude tends to increase both the slope and intercept. A higher slope indicates a greater delay in ion ejection, whereas a lower slope indicates that ions are ejected more rapidly, that is, closer to their true resonance point. Ions would be expected to be ejected more slowly at higher q values due to greater pseudo-potential well depths, which increase with q and $V_{0\text{-}p}$.[12] Thus, the calculated slope increases with LMCO (rf amplitude). The sharp change in the intercept at LMCO = 800 Th is due to the coupling of the slope and intercept. The slope curve appears to change concavity at LMCO = 800 Th, which results in a sudden increase in the intercept. The intercept is less meaningful than the slope; the slope indicates the rate of ion ejection. A higher slope indicates slower ejection, whereas a lower slope indicates faster ejection.

Changing the scan rate or ac amplitude has a large effect on calibration, as shown in **Figure 3.5**. Note that the scan rate was altered by changing the scan time while keeping the start and end frequencies constant. Thus, a longer scan time will correspond to a lower scan rate. The slope

obtained in the final correction step decreases nonlinearly with increasing scan time, and the intercept correspondingly increases. This can be accounted for by considering the amount of time each ion is at resonance during the scan, which increases with scan time for a constant start and end frequency, resulting in more rapid ejection *relative to the length of the scan.* Both curves level out because further increasing the amount of time each ion is at resonance does not change their ejection time relative to the scan time (i.e. the optimum resonance time has already been attained). The slope and intercept decrease and increase, respectively, in an approximately linear fashion (**Figure 3.5b**) when the ac amplitude increases. This result is the direct consequence of ions being ejected more swiftly when the ac amplitude is high. Fortunately, this can be automatically accounted for in the mass calibration algorithm by inputting the ac amplitude as a variable. Since the relationship between slope/intercept and ac amplitude is linear, a second correction slope and intercept may be incorporated.

As a final note, higher-order fields are known to cause mass shifts in ion traps,[25,33,89,112-115] which thus requires alteration in the calibration procedure or alterations to the ac amplitude to correct for these shifts. These fields are introduced in varying magnitudes due to apertures in the electrodes, electrode truncation and imperfections, and asymmetry in the electrode structure. The octopole and dodecapole terms (A_4 and A_6) are generally the only significant components; odd-order components are usually zero due to trap and electric field symmetry. The mass shifts that such fields cause are due to differences in electric field strength, particularly near the electrodes. A positive contribution from a higher-order term indicates that the field is stronger than a pure quadrupole field; the opposite is true for a negative higher order term. Stronger fields will cause ion oscillatory frequencies to increase (à la eq. 3.5, 3.6, 3.8, and 3.9), whereas weaker fields will have the opposite effect. A further distinction is made between even and odd order terms. Even order fields will either increase or decrease the electric field intensity symmetrically, whereas odd order fields will increase the field intensity near one electrode and decrease it near the opposite electrode. The effect of the odd order field is thus to displace the ion cloud from the center of the trap and decrease the electric field strength acting on the ion cloud because the ions will tend to reside in the region with the lowest field strength, resulting in a downward frequency shift for both positive and negative odd order terms. These are important considerations to take into account when calibrating secular frequency scan mass spectra.

3.6 Conclusion

We have introduced a simple method for mass calibration of secular frequency scan data. Calibration errors less than 0.1% were typical but can be improved by keeping the rf amplitude constant and increasing the data collection rate. The method can be generalized to account for any arbitrary sweep of the ac frequency and rf amplitude and frequency. Secular frequency scans linear in *m/z* can also be performed using this algorithm.

3.7 Acknowledgements

Figures and Tables

$\omega_{u,0}$ vs. Time	

$\beta_u = 2\omega_{u,0} / \Omega$

β_u vs. Time

beta_to_q

q_u vs. Time

q_to_mass

$m_{uncorrected}$ vs. Time

Correct for ejection delay and errors in V_{0-p} and Ω

$m_{corrected}$ vs. Time

Function: *beta_to_q*

Guess q = 0.5; (prev_q is arbitrarily set to 0)
Set left_bound = 0;
Set right_bound = 1;
Set tolerance = 0.000001; % tolerance is arbitrarily set
Set LHS_minus_RHS = 1;   % refers to eq. 9
while (abs(q − prev_q) > tolerance)
        Evaluate LHS of eq. 9;
        Evaluate RHS of eq. 9;
        Calculate LHS_minus_RHS;
        if LHS_minus_RHS > 0
                Set prev_q = q;
                Set q = (q + right_bound) / 2;
                Set left_bound = prev_q;
        elseif LHS_minus_RHS < 0
                Set prev_q = q;
                Set q = (q + left_bound) / 2;
                Set right_bound = prev_q;
        else
                % guess is correct

Function: *q_to_mass**

$m_{uncorrected} = 4eV_{0-p} / (\Omega^2 r_0^2 q m_u)$

Steps for mass correction:
1. Obtain ac scan mass spectrum of mass standards
2. Plot true mass vs. $m_{uncorrected}$
3. Perform linear fit of (2) to obtain slope (s) and intercept (b)
4. $m_{corrected} = s{*}m_{uncorrected} + b$
5. If necessary, correct for AC amplitude

Figure 3.1. Procedure for mass calibration for secular frequency scanning in an ion trap. The applied ac frequency ($\omega_{u,0}$) is linearly correlated with time based on the parameters from the data system and waveform generator (e.g. scan rate, scan frequency range, data collection rate, etc.). These frequencies are then converted to β_u and subsequently to q_u using an iterative algorithm, *beta_to_q*. These q values are then converted to uncorrected masses. The delay in ion ejection, which is mass dependent, is taken into account by linearly correlating true mass and uncorrected mass to obtain a slope (s) and intercept (b). Finally, the corrected mass is obtained by multiplying $m_{uncorrected}$ by s and adding b. Note that m_u is the atomic mass constant.

*Note that changes in V_{0-p} can be taken into account in this step. For example, in the "Ultrazoom" scans on the LTQ, the rf amplitude is incremented such that the scan rate is 27 Da/s at a q_x of 0.88. Thus, V_{0-p} is incremented linearly at each time point, the increment being calculated from the scan rate.
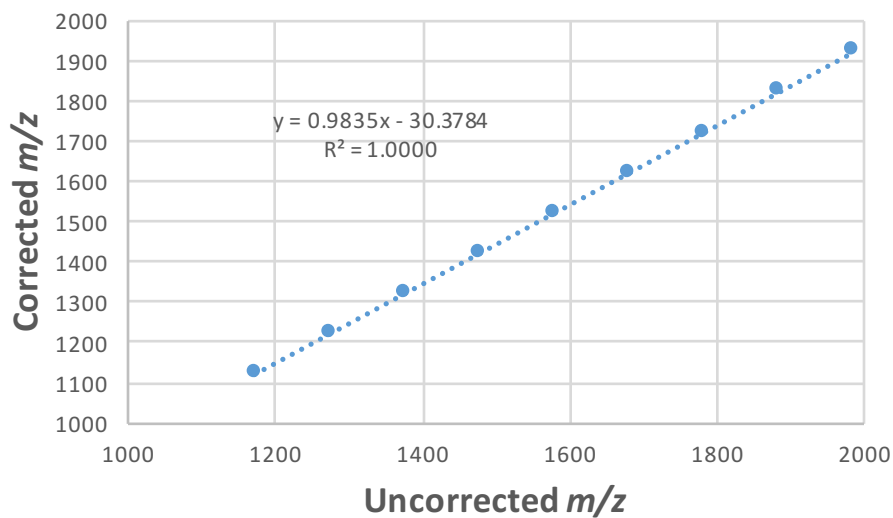
Figure 3.2. Accounting for the mass-dependent delay of ion ejection and incorrect inputs for trap parameters. In the calibration procedure for a linear ac frequency sweep, plotting true mass vs. uncorrected mass gives a linear fit. The slope and intercept are then used to correct for this delay. Data shown are for an LTQ linear ion trap, ac scan of Ultramark 1621 calibration solution, 10-500 kHz, 1.5 V_{pp}, over 800 ms during an Ultrazoom scan beginning at a lower mass cutoff of 1000 Th.
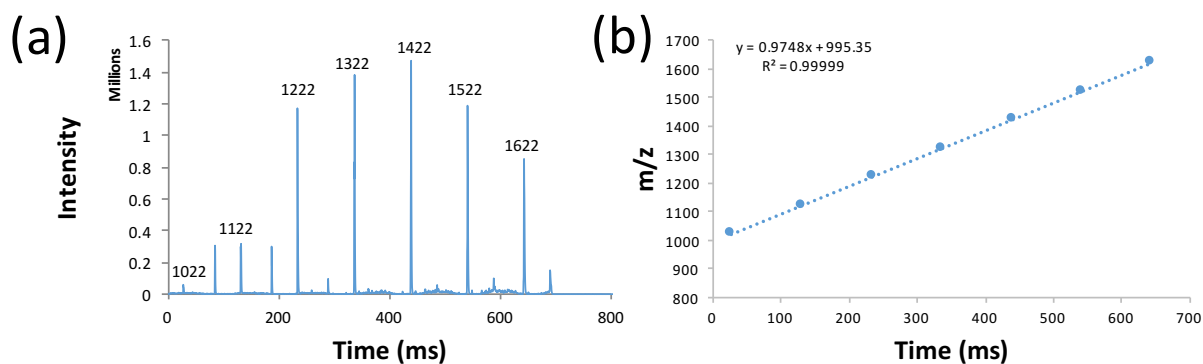
Figure 3.3. Secular frequency scan linear in m/z. Spectrum (a) shows intensity vs. time for an Ultramark 1621 calibration solution analyzed on an LTQ XL with a secular frequency sweep corresponding to a linear *m/z* vs. time relationship. Peak width is constant at 0.35 Th FWHM throughout the scan. Plot in (b) shows linear relationship between m/z and time. Frequency components were calculated from a modified version of the algorithm in Figure 3.1. The scan performed on an LTQ was Ultrazoom from a lower mass cutoff of 1000 to 1027 Da. The secular frequency scan had an amplitude of 1.1 V_{pp} and a length of 800 ms. Nominal masses are labeled.
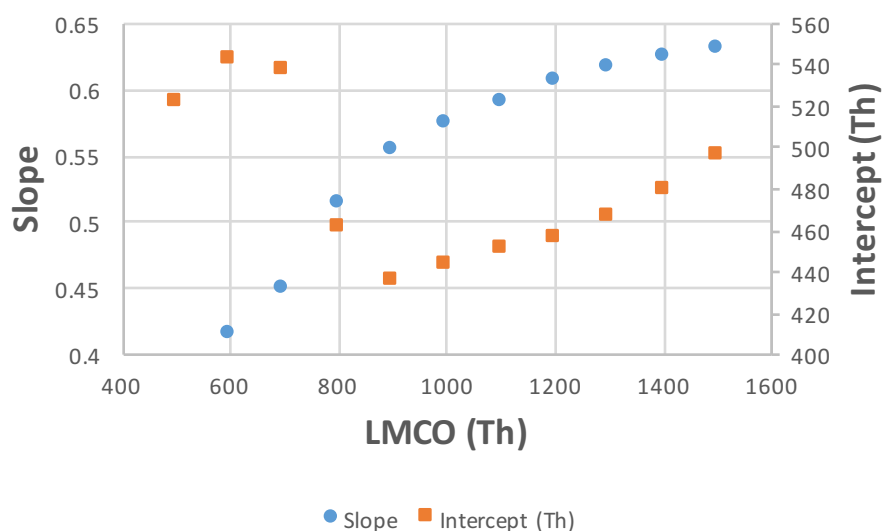
Figure 3.4. Effect of rf amplitude on calibration parameters using an LTQ linear ion trap. As the rf amplitude (LMCO corresponding to $q_x = 0.88$) increases, the slope and intercept in the linear fit generally increase. Scan time was 800 ms with a 1 V_{pp} supplementary ac waveform swept from 10 to 500 kHz. The analytes were Ultramark 1621 calibration solution ions. Slope and intercept refer to the parameters obtained from fitting true mass vs. uncorrected mass, as in **Figure 3.2.**
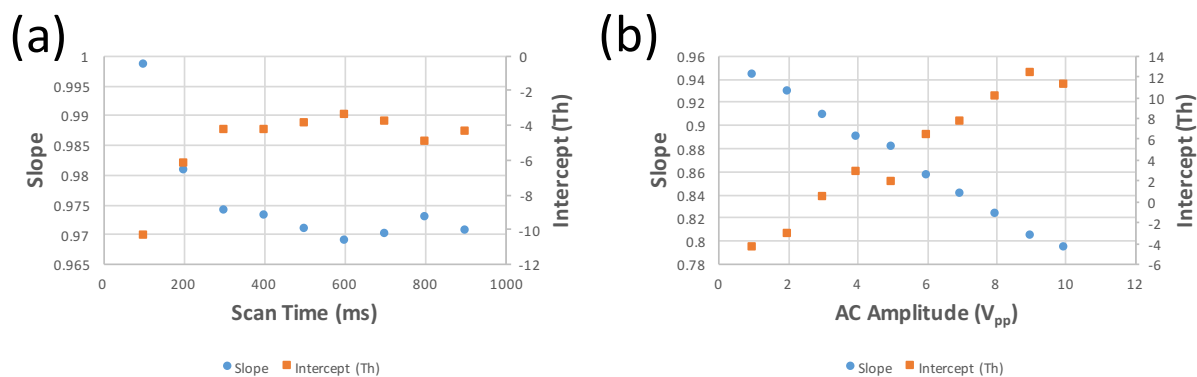
Figure 3.5. Effect of (a) scan rate and (b) ac amplitude on calibration parameters using an LTQ linear ion trap. Slope and intercept refer to the parameters obtained from fitting true mass vs. uncorrected mass, as in **Figure 3.2.** Scans in (a) were 1 V_{pp}, 10-500 kHz over the given scan time, during an Ultrazoom scan beginning at a lower mass cutoff of 100 Th. Scans in (b) were over 800 ms, 10-500 kHz, with the given ac amplitudes, during an Ultrazoom scan beginning at 100 Th. Note that the plot in (a) shows effect of scan *rate* since the scan start and end frequencies were constant but scan time was variable.

Table 3.1. Mass calibration for the scan in **Figure 3.2**. Peak width increases approximately linearly with mass due to the linear sweep of the ac frequency.

Calculated m/z (Th)	Corrected m/z (Th)	Calibration Error (ppm)	FWHM Peak Width (Th)
1121.998	1122.208	188.410	0.86
1221.991	1222.040	39.583	1.81
1321.985	1321.130	646.580	2.32
1421.978	1421.867	78.325	2.39
1521.972	1522.565	389.864	2.87
1621.966	1622.256	178.909	3.38
1721.959	1722.562	350.170	3.13
1821.953	1821.181	423.908	3.57
1921.946	1921.939	4.060	4.04

Table 3.2. Mass calibration for a set of three quaternary ammonium ions. Scan parameters were ac frequency 10-500 kHz, scan time 800 ms, amplitude 1 V_{pp}, LTQ Ultrazoom scan beginning at a lower mass cutoff of 260 Th.

Calculated m/z (Th)	Corrected m/z (Th)	Calibration Error (ppm)	FWHM Peak Width (Th)
284.33	284.35	81.36	0.29
360.36	360.31	130.20	0.63
382.44	382.45	16.54	0.75

CHAPTER 4.   LINEAR MASS SCANS IN QUADRUPOLE ION TRAPS USING THE INVERSE MATHIEU Q SCAN

4.1   Abstract

Rationale: Secular frequency scanning is a method of mass selectively scanning ions out of a quadrupole ion trap by linearly ramping the frequency of the resonance ejection signal *through* ion secular frequencies at constant rf amplitude and frequency. The method is electronically much simpler than resonance ejection, but it requires a complex nonlinear calibration procedure to correlate mass-to-charge with time. The resulting linear relationship between mass-to-charge and time, however, is much preferred.

Methods: A method of secular frequency scanning in quadrupole ion traps is described in which mass-to-charge is linear with time. This method, termed an "inverse Mathieu q scan", contrasts with linear frequency sweeping which requires a complex nonlinear mass calibration procedure, as described previously. In the current method, mass scans are forced to be linear with time by scanning the frequency of the supplementary ac so that there is an inverse relationship between the ejected ion's Mathieu q parameter and time.

Results: In all cases, excellent mass spectral linearity is observed. The rf amplitude is shown to control both the scan range and scan rate, whereas the ac amplitude and scan rate influence the mass resolution. The scan rate depends linearly on the rf amplitude, a unique feature of this scan. Although changes in either rf or ac amplitude affect the positions of peaks in time, they do not change the mass calibration procedure since this only requires a simple linear fit of *m/z* vs. time. Space charge effects are shown to give rise to significant changes in resolution as well as to mass shifts.

Conclusions: A method of secular frequency scanning which provides a linear mass scale has been demonstrated. The inverse Mathieu q scan offers a significant increase in mass range and power savings while maintaining access to linearity, paving the way for a mass spectrometer based completely on ac waveforms for ion isolation, ion activation, and ion ejection.

4.2   Introduction

Methods of scanning ions out of quadrupole ion traps for external detection[7,8,116,117] are generally derived from the Mathieu parameters a_u and q_u, which describe the stability of ions in quadrupolar fields with dimensions u. For the linear ion trap with quadrupole potentials in x and y,[5-8,12,116]

$$q_x = -q_y = 8zeV_{0\text{-}p} / \Omega^2(x_0^2 + y_0^2)m \qquad\qquad \text{Eq 4.1}$$

$$a_x = -a_y = 16zeU / \Omega^2(x_0^2 + y_0^2)m \qquad\qquad \text{Eq 4.2}$$

where z is the integer charge of the ion, e is the elementary charge, U is the dc potential between the rods, $V_{0\text{-}p}$ is the zero-to-peak amplitude of the quadrupolar radiofrequency (rf) trapping potential, Ω is the angular rf frequency, x_0 and y_0 are the half distances between the rods in those respective dimensions, and m is the mass of the ion. When the dimensions in x and y are identical $(x_0 = y_0)$, $2r_0^2$ can be substituted for $(x_0^2 + y_0^2)$. Solving for m/z, we obtain

$$m/z = 4V_{0\text{-}p} / q_x \Omega^2 r_0^2 \qquad\qquad \text{Eq 4.3}$$

$$m/z = 8U / a_x \Omega^2 r_0^2 \qquad\qquad \text{Eq 4.4}$$

Ion traps are generally operated without DC potentials $(a_u = U = 0)$ so that all ions occupy the q axis of the Mathieu stability diagram. In the boundary ejection method, first demonstrated by Stafford and coworkers in the 3D trap[82] and Schwartz et al. in the linear ion trap,[10,93] the rf amplitude is increased so that ions are ejected when their trajectories become unstable at $q = 0.908$, giving a mass spectrum, i.e. a plot of intensity vs. m/z since m/z and rf amplitude (i.e. time) are linearly related.[42]

Resonance ejection is a similar method that improves both resolution and sensitivity.[52,118] A small supplementary ac signal is applied in a dipolar manner across trapping electrodes in order to generate a small dipolar field that oscillates at the applied frequency. When this frequency, generally set near $q_u = 0.88$, matches the secular frequency of an ion in the trap, the ion will be excited or ejected from the trap depending on waveform amplitude and time of application. When the trapping rf amplitude is ramped, all ions' secular frequencies increase, eventually coming into resonance with the weak dipolar field and causing their ejection in order of increasing m/z.

Although a reverse scan can also be performed, resolution and sensitivity generally suffer because of position-dependent ion frequency shifts which are observed with non-zero even higher-order field contributions (e. g. octopole).[36,65,119]

Other variants of resonance ejection are double and triple resonance ejection, in which one or two ac frequencies are applied at nonlinear (hexapole or octopole) resonance points. These scans have been shown to greatly increase resolution and sensitivity in both conventional and miniature instruments.[32,34,74,105] Rhombic ion ejection makes use of multiple frequencies in different directions for reduced space charge effects since ions being ejected will oscillate around the main ion cloud rather than pass through it.[120] Multiple frequencies can also correspond to different ejection points, as in a compressive mass spectrometry scan, which requires acquisition of multiple scans and an algorithm to reconstruct the mass spectrum.[121]

The radius of the trap can theoretically be scanned, but this has not been demonstrated. Instead, a more useful application is an array of traps of different radii for mass selective trapping.[48]

An uncommon method of scanning an ion trap is to scan the main trapping rf frequency.[46] Although useful for analysis of microparticles and other high mass ions since lowering the rf frequency increases the mass range obtainable with a given rf amplitude maximum,[46,47,85,122] calibration is difficult due to the nonlinear relationship between m/z and rf frequency. In addition, many systems which use LC tank circuits are unable to scan the rf frequency while maintaining the resonance of the circuit. Nonetheless, digital ion traps are better suited to frequency scans since they can easily modulate the period of the driving rf while providing linear calibration with an appropriate nonlinear frequency sweep.[86,88,109]

A simple alternative to sweeping the rf parameters in quadrupole ion traps is to instead scan the frequency of the resonance ejection waveform, a method termed "ac scanning," "secular scanning," or "secular frequency scanning," first demonstrated by Welling et al.[111] We should note here that what is scanned is a signal that is in resonance with the secular frequency of ions of different m/z ratios. The ion secular frequency of any particular ion is not scanned. The method is of particular interest for low-power operation of a quadrupole ion trap, for example on a space-based instrument.[50] We also recently experimentally characterized the scan on miniature and benchtop instruments,[106] demonstrated application to single analyzer precursor scans[123] on a miniature mass spectrometer,[99] and implemented a calibration procedure for an ac scan linear in frequency.[91] We also, in that work, briefly discussed an ac scan linear in m/z, which is a highly

attractive variant since mass calibration is simplified. Here, we demonstrate a new mode of secular frequency scanning in which the frequency of the supplementary ac waveform is scanned nonlinearly such that the ejected ion's Mathieu q parameter and time are inversely related, thereby giving a linear *m/z* vs. time calibration. This mode, which we term the "inverse Mathieu q scan", may be particularly well-suited for miniature and portable instruments since a linear rf ramp is not required.[71] Rather, a stable rf signal suffices.

4.3   Theory

The basis for an inverse Mathieu q scan is derived from the nature of the Mathieu parameter q_u (eq. 4.3). In order to scan linearly with *m/z* at constant rf frequency and amplitude, the q_u value of the *m/z* value being excited must be scanned inversely with time t (**Figure 4.1a**) so that

$$q_u = k / (t - j)$$ Eq. 4.5

where k and j are constants determined from the scan parameters. In the mode of operation demonstrated here, the maximum and minimum q_u values (q_{max} and q_{min}), which determine the *m/z* range in the scan, are specified by the user. Because the inverse function does not intersect the q axis (e.g. $q_u = 1/t$), the parameter j is needed for translation so that the first q value is q_{max}. This, of course, assumes a scan from high q to low q, which will tend to give better resolution and sensitivity due to ion frequency shifts mentioned above.

The parameters j and k are calculated from the scan parameters,

$$j = q_{min} \Delta t / (q_{min} - q_{max})$$ Eq. 4.6

$$k = -q_{max} j$$ Eq. 4.7

where Δt is the scan time. Operation in Mathieu q space gives advantages: 1) the waveform frequencies depend only on the rf frequency, not on rf amplitude or the size or geometry of the device, which implies that the waveform only has to be recalculated if the rf frequency changes (alternatively, the rf amplitude can compensate for any drift in rf frequency), and 2) the mass range and scan rate are controlled by the rf amplitude, mitigating the need for recalculating the waveform in order to change either parameter. It is important to note that we purposely begin with an array of q_u values instead of *m/z* values for these very reasons.

Once an array of Mathieu q_u values is chosen, they must be converted to secular frequencies (**Figure 4.1b**), which proceeds first through the calculation of the Mathieu β_u parameter,[8]

$$\beta_u^2 = a_u + \cfrac{q_u^2}{(\beta_u + 2)^2 - a_u - \cfrac{q_u^2}{(\beta_u + 4)^2 - a_u - \cfrac{q_u^2}{(\beta_u + 6)^2 - a_u - \cdots}}} + \cfrac{q_u^2}{(\beta_u - 2)^2 - a_u - \cfrac{q_u^2}{(\beta_u - 4)^2 - a_u - \cfrac{q_u^2}{(\beta_u - 6)^2 - a_u - \cdots}}}$$

Eq. 4.8

a conversion that can be done by using the algorithm described in our prior work on secular frequency scanning.[91] The final step is to convert Mathieu β_u values to secular frequencies (eq. 4.9, 4.10) to give applied ac frequency vs. time (**Figure 4.1c**). Each ion has a set of secular frequencies,

$$\omega_{u,n} = |2n + \beta_u|\Omega/2 \qquad -\infty < n < \infty$$

Eq. 4.9

where n is an integer, amongst which is the primary resonance frequency, the *fundamental secular frequency*,

$$\omega_{u,0} = \beta_u\Omega/2$$

Eq. 4.10

This conversion gives an array of frequencies for implementation into a custom waveform calculated in a mathematics suite (e.g. Matlab).

Evans-Nguyen et al.[50] used a logarithmic sweep of the ac frequency for secular frequency scanning, but, as described here, the relationship between secular frequency and *m/z* is not logarithmic, resulting in very high mass errors during mass calibration. This can be clearly observed in **Figure 4.1** plots **a** and **c**, which show an inverse relationship for the excited ion's Mathieu q_u parameter and time and the more complex relationship between time and applied frequency in an inverse Mathieu q scan, respectively. The curvature clearly differs between the two plots.

In theory, once the Mathieu q_u parameters are converted to secular frequencies, a waveform is obtained. However, this waveform *should not* be used for secular frequency scanning due to jagged edges observed throughout the waveform (i.e. phase discontinuities). In the mass spectra,

this is observed as periodic spikes in the baseline intensities (see Snyder, et al., Figure 3a[91]). Instead, in order to perform a *smooth* frequency scan, a new parameter ϕ is introduced. This corresponds to the phase of the sinusoid at every time step (e.g. the ith phase in the waveform array, where i is an integer from 0 to $v*\Delta t-1$). Instead of scanning the frequency of the waveform, we will instead scan the phase of the sinusoid in order to maintain a continuous phase relationship. The relationship between ordinary (i.e. not angular) frequency f and phase ϕ is

$$f(t) = (1/2\pi)(d\phi/dt)(t) \qquad\qquad \text{Eq. 4.11}$$

so that

$$\phi(t) = \phi(0) + 2\pi\int_0^t f(\tau)d\tau \qquad\qquad \text{Eq. 4.12}$$

where variable τ has been substituted for time t in order to prevent confusion between integration limit t and the time variable in the integrand. Thus, the phase of the sine wave at a given time t can be obtained by integrating the function that describes the frequency of the waveform as a function of time, which was previously calculated.

We begin with the phase of the waveform set equal to zero:

$$\phi(0) = 0 \; (t = 0) \qquad\qquad \text{Eq. 4.13}$$

The phase is then incremented according to eq. 4.14 and 4.15, which accumulates (integrates) the frequency of the sinusoid, so that

$$\Delta = \omega_{u,0} \, / \, v \qquad\qquad \text{Eq. 4.14}$$

$$\phi(i+1) = \phi(i) + \Delta \qquad\qquad \text{Eq. 4.15}$$

where v is the sampling rate of the waveform generator. Note that $\omega_{u,0}$ is the *angular secular frequency* ($2*\pi*f_{u,0}$, where $f_{u,0}$ is the ordinary secular frequency in Hz) in units of radians/sec. Thus, sweeping through phase ϕ (**Figure 4.1d**) instead of frequency gives a smooth frequency sweep.

Because the relationship between secular frequency and time is approximately an inverse function, the phase will be swept according to the integral of an inverse function, which is a logarithmic function (**Figure 4.1d** is approximately logarithmic with time). However, because the relationship between secular frequency and *m/z* is *only approximately an inverse relationship*, the

phase ϕ will deviate from the log function and thus cannot be described analytically (due to eq. 4.8).

4.4 Experimental

4.4.1 Chemicals

Didodecyldimethylammonium bromide was purchased from Sigma Aldrich (St. Louis, Missouri, USA), hexadecyltrimethylammonium bromide was purchased from Tokyo Chemical Industry Co. (Tokyo, Japan), and benzylhexadecyldimethylammonium chloride was purchased from JT Baker Chemical Co (Phillipsburg, New Jersey, USA). In general, concentrations were 5-10 µg/ml. Pierce ESI LTQ calibration solution (containing Ultramark 1621[124]) was obtained from Thermo Fisher (Rockford, IL, USA). A reference spectrum for this calibration solution can be found on the manufacturer's website (currently, https://www.thermofisher.com/order/catalog/product/88322).

4.4.2 Ionization

Ions were generated by nanoelectrospray ionization (nESI) at ~1500 V using 5 µm nanospray tips pulled from borosilicate glass capillaries (1.5 mm O.D., 0.86 I.D., Sutter Instrument Co.) by a Flaming/Brown micropipette puller (Sutter Instrument Co. model P-97, Novato, CA, USA).

4.4.3 Instrumentation

All experiments were performed using a Thermo LTQ linear ion trap[10] (San Jose, CA, USA) with the rf frequency tuned to 1.175 MHz. The rf amplitude of the instrument was kept *approximately constant* by using the "Ultrazoom" feature (rf scan rate of 27 Da/s) set at an appropriate lower mass cutoff (LMCO). All LMCO values reported herein describe the *m/z* value at q = 0.908. Rf voltages are also reported, in units of V_{0-p} (rod to ground). Helium at a pressure of 1 mtorr was used for collisional cooling.

The resonance ejection waveform was replaced by a custom waveform generated in Matlab using the method described above. The waveform was generally 0.3 s in length with the waveform generator (Keysight 33612A, Newark, SC, USA) sampling rate set to 10 MSa/s. Note that it is

important to oversample the waveform to maintain the fidelity of the frequency scan. Here we sample at ~16 times the highest frequency (~600 kHz) in the frequency sweep.

The ac waveform was triggered at the beginning of the mass scan using the triggers in the LTQ Tune diagnostics menu and was swept from high frequency to low frequency so that an inverse relationship between the excited ion's Mathieu q parameter and time was obtained, thereby giving a linear *m/z* calibration (see **Figure 4.1**). Generally, q_{max} was set to 0.908 and q_{min} was 0.05. In most scans, the rf amplitude was set at 1290 V_{0-p} so that the LMCO was *m/z* 460, which resulted in a scan rate of ~30,000 Da/s.

Data were obtained from either the single-ended or differential output(s) on the LTQ electrometer board and recorded using an oscilloscope (Tektronix TDS 2024C, Beaverton, OR, USA, or Agilent Technologies InfiniiVision MSO-X 4154A, Santa Clara, CA, USA) which was triggered using the "Sync" output on the waveform generator. This increased the density of data points in time compared to the LTQ data collection rate of 1 point every 0.37 ms. All spectra and data points are based on the average of 16 scans.

4.5   Results & Discussion

4.5.1   Secular frequency scanning linear in m/z

Figure 4.2 shows the mass spectra obtained from analyzing an Ultramark 1621 calibration solution with an inverse Mathieu q scan (scan rate here was 30,000 Da/s). These scans are indicative of several effects: 1) the linearity of the scan, 2) the effect of ac amplitude on resolution, and 3) the effect of space charge on resolution with respect to *m/z*. As shown in the insets, linearity is excellent in both the high and low ac amplitude cases. Ultramark 1621 peaks are expected from *m/z* 922 to *m/z* 2022, with equal spacings of 100 *m/z*. The most noticeable features of the spectra are the significant differences in resolution with respect to both *m/z* and ac amplitude. Since the ac frequency sweeps from high Mathieu q to low q, low mass ions are ejected first. They therefore experience a greater space charge effect than the high mass ions that are scanned out later. This gives rise to differences in resolution with mass, quantified later. Increasing the ac amplitude greatly increases the resolution in the scan, evident in **Fig. 4.2b**, in part due to a reduction in space charge broadening at higher ac amplitudes.[125] Peak width is approximately constant in this scan. Overall, resolution in panel **a** was quite low, ranging from ~20 to ~200, whereas resolution in panel

b ranged from ~120 to ~850. In the absence of space charge, resolution is expected to improve (see below).

The calibration plots in (c) and (d) show *m/z* vs. ejection time; both show excellent linearity. The slope of the curve is the experimental scan rate and the *m/z* intercept is the *apparent* LMCO, both of which are discussed later.

4.5.2   Wide mass range with linear calibration

Although mass range extension has been demonstrated with low q resonance ejection,[126] secular frequency scanning linear in frequency,[106] secular frequency scanning with a logarithmic frequency sweep,[50] and rf frequency sweeping,[85,122] there has usually been an inevitable tradeoff with either resolution or mass calibration. With an inverse Mathieu q scan there is no such tradeoff. Although the initial waveform calculation is not intuitive or analytical and can take a significant amount of time, it need only be performed once for a given rf frequency and device.

Unlike resonance ejection, the mass range is no longer limited by the maximum value of the trapping rf amplitude. Instead, the highest mass obtainable ought to correspond to the highest mass ion trapped; this in turn is determined by the pseudo-potential well depth (when this limits ion trapping, or otherwise it is generally pressure-limited)[12] or by the lowest q value the waveform scans through:

$$m/z_{max} = 4V_{0\text{-p}} / q_{min} \, \Omega^2(r_0^2) \hspace{4cm} \text{Eq. 4.16}$$

Figure 4.3 illustrates the wide mass range (*m/z* 500 to *m/z* 3,500) over which this scan allows data to be collected with excellent resolution, even with fast scanning (26,000 Da/s). For comparison, the LTQ resonance ejection mode yields unit resolution up to *m/z* 2,000 while scanning at ~16,666 Da/s, although a "high mass" low q resonance ejection mode also exists, which extends the mass range to *m/z* 4,000 but scans are then significantly slower and resolution and sensitivity suffer.

With an inverse Mathieu q scan, resolution, sensitivity, and ease of calibration are all maintained. **Figure 4.3a,b**, shows scans in the absence of significant space charge effects using an injection time of 5 ms. Panel **a** shows a scan linear in *m/z*, whereas panel **b** shows a scan linear in frequency. As expected from the approximately inverse relationship between *m/z* and secular

frequency, a high degree of nonlinearity between *m/z* and time is observed at low mass (**Figure 4.1b**). For a truly linear mass scale, the low mass ions would have ejection times closer together than they are with a linear frequency sweep. In other words, low mass ions have secular frequencies that are farther apart compared to high mass ions.

4.5.3   Resolution

Theoretically, the resolution in resonance ejection with either an rf amplitude ramp or ac frequency sweep should be numerically equivalent to the frequency resolution, as described by Goeringer et al[127] as well as Makarov.[66] In particular, in the absence of higher order fields and space charge effects, the mass resolution should vary inversely with the scan rate in terms of frequency units per unit time. However, the scan rate only changes significantly at high Mathieu q, so this cannot account for the observed differences in resolution, seen clearly in **Figure 4.1c**. The slope of the curve (i.e. the scan rate) changes dramatically below a Mathieu q of ~0.3, but most ions will have low Mathieu q parameters, so the scan rate for most ions is approximately the same.

As shown in **Figure 4.3c**, the resolution ranged from ~400 to ~1500 (FWHM) and generally increased with mass since peak width was constant. When the frequency was scanned linearly, resolution again generally decreased with Mathieu q. Since the scan rate in radians/sec^2 is constant for this kind of scan, the difference in scan rate cannot account for the difference in resolution in this scan either Differences in ejection q values and potential well depths also contribute to differences in resolution, which is well known from the theory of resonance ejection.[125,127,128] Usually resolution in resonance ejection decreases at low Mathieu q; however, the opposite effect is observed here. It may be the case that space charge decreases the resolution of low mass ions relative to high mass ions as would be expected, even in the case where space charge is controlled. Because low mass ions occupy the center of the ion cloud, a resonance ejection scan is analogous to peeling an onion from the inside out, thereby resulting in an increase in resolution with *m/z*. For now, the exact mechanism of resolution increase at low q is unknown.

Resolution also depends on ac amplitude and scan rate. Surprisingly, resolution for all ions increased up to the maximum amplitude of the generator (**Figure 4.4a**), which contrasts with our previous results using linear frequency sweeping which showed significant peak broadening at ac amplitudes higher than ~1 V$_{pp}$.[106] This could be due to the faster scan rate in these experiments

relative to the scans applied previously.[10,66,125] Surprisingly, for *m/z* 1422, the resolution *increased* with scan rate (**Figure 4.4b**), which should not be the case. The scan rate is calculated as the slope of the calibration equation (*m/z* versus time), peak width was determined as full width at half maximum (FWHM), and resolution was calculated as m/Δm (Δm = FWHM peak width). For this experiment, the scan rate was changed not by altering the rf amplitude, but rather by varying the mass scan time Δt while keeping the scan range the same.

In order to quantify the effects of space charge, we used a simple mixture consisting of three precharged ions (quaternary amines, *m/z* 284, 360, and 382). The resolution of each ion as a function of scan rate is given in **Figure 4.4c**. For the ion ejected first in the scan (*m/z* 284), which experiences the most space charge effects while being ejected, resolution increased with scan rate. However, for the other two ions, resolution decreased with scan rate, which is the expected result. This implies that increasing the scan rate can somewhat compensate for space charge effects, which has also been observed in resonance ejection.[125] Presumably the ejected ions have fewer cycles through the rest of the ion cloud at high scan rates, reducing the interaction time and thereby resulting in less of a decrease in resolution.

Although unit resolution is not demonstrated here, the scan rate can be decreased and ac amplitude can be increased further in order to increase the resolution. The pressure can also be optimized for this scan. In addition, the time required to calculate the waveform and import it to a function generator increases with the length of the waveform, which is determined by the sampling rate and scan time. This paper, however, is concerned primarily with empirical observations rather than resolution optimization.

4.5.4   Space charge effects

As shown in **Figure 4.2a**, which was the result of a mass scan for a relatively long 50 ms injection time, space charge effects appear to play a significant role in determining both resolution and peak position. The resolution as a function of Mathieu q parameter for an inverse Mathieu q scan with a long 50 ms injection time is shown in **Figure 4.5a** for ions with different *m/z* and therefore different Mathieu q parameters. Absolute resolution is significantly decreased from the scan in **Figure 4.3a** since the injection time is 40 ms longer. The profile of resolution as a function of q is also significantly different. Most notable is that low mass ions (high q) suffer significantly from space charge effects, resulting in quite low resolution (R~20). As discussed previously, this

is because these ions are ejected first, when the ion cloud is relatively dense.[84,112,120] Additionally, a deep potential well causes a physically tight ion packet and increases space charge effects, an effect made worse by the distribution of ions of different *m/z*, with low mass ions at the center of the cloud and high mass ions near the periphery.[129] Curiously, high mass ions also appear to suffer from resolution degradation. We speculatively attribute this to non-optimal ac amplitudes for the high mass ions. In general the optimal resolution in resonance ejection will be obtained by ramping the ac amplitude linearly with *m/z* (i.e. time).[42] Here the ac amplitude was kept constant, which may contribute to loss of resolution at high mass.

The resolution as a function of injection time for a single peak (*m/z* 1422) in the mass spectrum is shown in **Figure 4.5b**. As expected, resolution decreases with injection time due to greater space charge effects.[118] However, more notable is the large mass shift observed at high injection times. These high values are likely due to the fast mass scanning performed here (scan rate ~30,000 Da/s).

4.5.5   Scan rate and low mass cut off

The scan rate in an inverse q scan can be derived from the Mathieu q parameter. Differentiating eq. 4.3 with respect to t, and assuming the trap parameters are kept constant, we obtain

$$d(m/z)/dt = -4V_{0\text{-}p} \, / \, q^2 \, \Omega^2(r_0^2) * (dq/dt) \qquad \text{Eq. 4.17}$$

From eq. 4.5 we obtain

$$dq/dt = -k \, / \, (t\text{-}j)^2 \qquad \text{Eq. 4.18}$$

Substituting this into eq. 4.17, we have

$$d(m/z)/dt = [-4V_{0\text{-}p} \, / \, [k \, / \, (t-j)]^2 \, \Omega^2(r_0^2)] * [-k \, / \, (t - j)^2] \qquad \text{Eq. 4.19}$$

so that

$$d(m/z)/dt = 4V_{0\text{-}p} \, / \, k \, \Omega^2(r_0^2) \qquad \text{Eq. 4.20}$$

Thus, one expects the scan rate to depend linearly on the rf amplitude, a unique feature of this scan. As we showed in **Figure 4.4**, the scan rate can also be altered by keeping the mass scan range (begin and end q values) the same but altering the mass scan time Δt.

These results are verified in **Figure 4.6**. To generate panel **a**, the Ultramark 1621 calibration solution was examined with a 0.3 s inverse Mathieu q scan from a q of 0.908 to 0.05 while varying the rf amplitude from scan to scan. Mass-to-charge was fit linearly with time in order to generate a calibration curve, the slope of which was determined to be the scan rate. As shown in panel **a**, the experimental and theoretical scan rates are linearly determined by the rf amplitude for a fixed waveform and agree quite closely. The small differences observed between the theoretical and experimental values can be explained by any nonlinear contribution to the electric field (e.g. hexapole and octopole fields), which will change the field strength in the trap and thereby change each ion's Mathieu q parameter. The scan rate will also vary with ac amplitude, which contributes to this error.

The mass range should also depend linearly on the rf amplitude, with the first and last masses, m/z_{min} and m/z_{max}, respectively, calculated from

$$m/z_{min} = 4V_{0-p} / q_{max} \Omega^2(r_0^2) \hspace{3cm} \text{Eq. 4.21}$$

and eq. 4.16. The calculated and experimental LMCO in these experiments also agreed quite closely. Experimentally, the LMCO is the m/z value that calibrates to time t = 0, which is not necessarily the lowest m/z ion in the trap. In general, higher ac amplitudes led to a higher *apparent* LMCO, which approached the theoretical value as the ac amplitude was increased. This is because when the ac amplitude is increased all ions are ejected at earlier points in the scan, which causes the calibration line (m/z vs. ejection time) to shift leftward toward t = 0, thereby increasing the apparent LMCO. As noted above, any nonlinear contribution to the electric field will also tend to change the LMCO, and thus experimental LMCO may deviate from the theoretical value (which assumes a pure quadrupole field).

Panel **b** in **Figure 4.6** shows the effect of ac amplitude on ion ejection time, which is a nearly linear relationship. Because the slope of ejection time vs. ac amplitude may be different for ions of different masses,[84,112] this leads to varying *apparent* scan rates, which are experimentally calculated in panel **c**. These were determined from the slope of the best fit line of m/z versus experimental ejection time (i.e. the calibration equation). This is a similar result to the change in

slope when calibrating a secular frequency scan linear in frequency, as described previously.[91] That is, a higher ac amplitude will tend to increase the rate of ion ejection, but this increase will not necessarily be uniform across Mathieu q space. Since the apparent scan rate increases when the ac amplitude increases, we can deduce that higher mass ions experience a greater shift in ejection time (toward earlier times) than low mass ions, which we observed when plotting the calibration equations at different ac amplitudes on the same plot (compare **Figure 4.2c,d**).

4.6   Conclusion

We have demonstrated a method of secular frequency scanning (scanning through ions of different secular frequency and hence mass/charge) which is linear with mass. The method is unique in that the only instrumental parameter that affects the required frequencies is the rf frequency. The waveform need not be recalculated since scan rate (and LMCO) are determined by the rf amplitude. Space charge appears to play a significant role in peak broadening in these scans, and high masses were shown to be easily accessible while maintaining resolution, sensitivity, and ease of calibration.

Unit resolution may be possible using these experiments, although there are tradeoffs with scan time. The scan time here was set at 0.3 s, which is short considering we are working out to high mass (over 8,000 Th, not explicitly shown). To increase resolution one would need to increase the scan time; the waveform would therefore contain more points. This means it would take longer to calculate the waveform and load it into memory, although a better approach would be to calculate a battery of scan functions ahead of time rather than calculating them in real time. Control of space charge would also improve resolution, but we were not able to utilize automatic gain control in these experiments.

While this method requires complex waveform calculation, it may be particularly well-suited for miniature mass spectrometers. We imagine a miniature system based solely on ac waveforms for ion isolation, ion activation, and ion ejection. Ion isolation may be performed by stored waveform inverse Fourier transform or by a similar frequency-based method, ion activation could proceed via resonance excitation, and the method demonstrated here could form the basis for the mass scan. Such a system would have low power consumption and simplify the electronics of the mass spectrometer since the feedback required for the linear rf amplitude ramp would no longer be required. Instead, only a stable rf at constant amplitude and frequency would be needed.

4.7 Acknowledgements
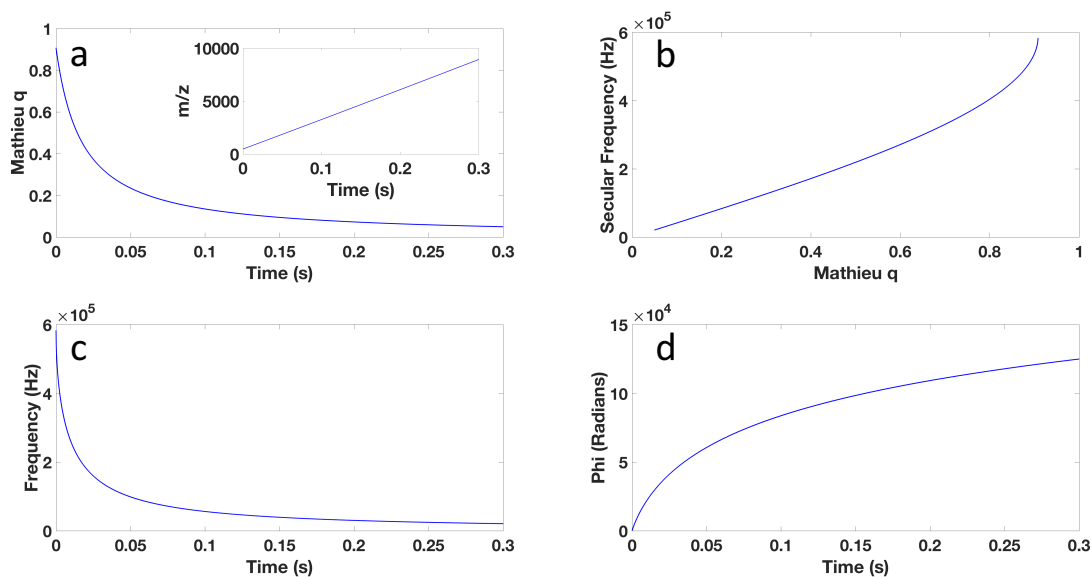
Figures

Figure 4.1. Calculating the custom waveform for the inverse Mathieu q scan: (a) plot of excited ion's Mathieu q parameter vs. time, showing an inverse relationship which gives a linear *m/z* vs. time relationship, (b) plot of secular frequency vs. Mathieu q parameter, (c) applied ac frequency vs. time for an inverse Mathieu q scan, and (d) the scan of sinusoidal phase ϕ (for smooth frequency scanning) as a function of time. Note that (d) is obtained by integrating (c).
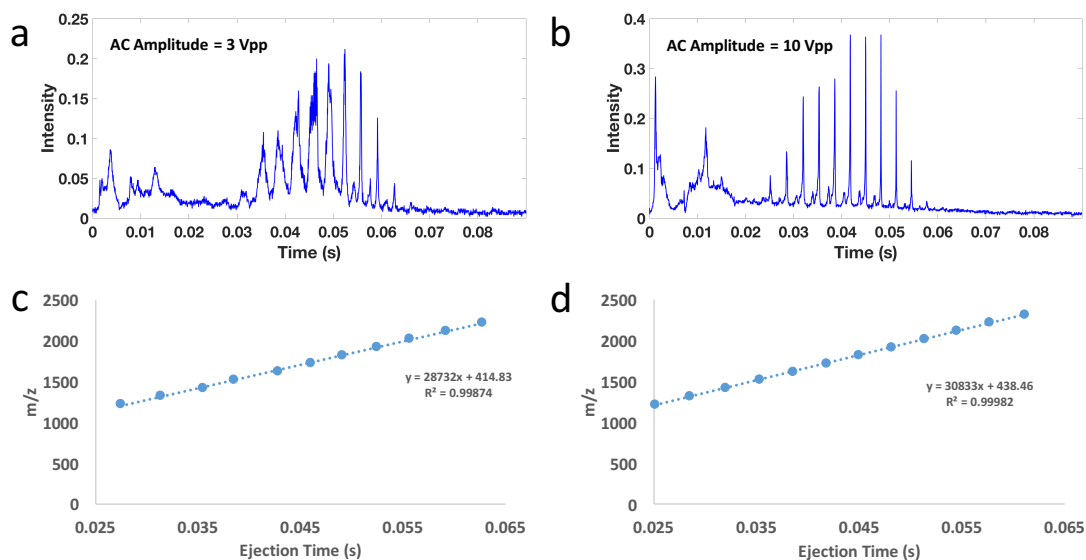
Figure 4.2. Secular frequency scanning linear in *m/z* (inverse Mathieu q scan): (a) plot of intensity vs. time for an Ultramark 1621 calibration solution obtained with an rf amplitude of ~1290 V$_{0-p}$ (LMCO of ~460 Da) and ac amplitude of 3 V$_{pp}$ where the ac frequency was scanned inversely with the excited ion's Mathieu q$_u$ parameter from 0.908 to 0.05, and (b) the same spectrum with a higher ac amplitude. Panels (c) and (d) show best fit lines for *m/z* versus time (i.e. mass calibration) for panels (a) and (b), respectively. The scan speed was approximately 30,000 Da/s.
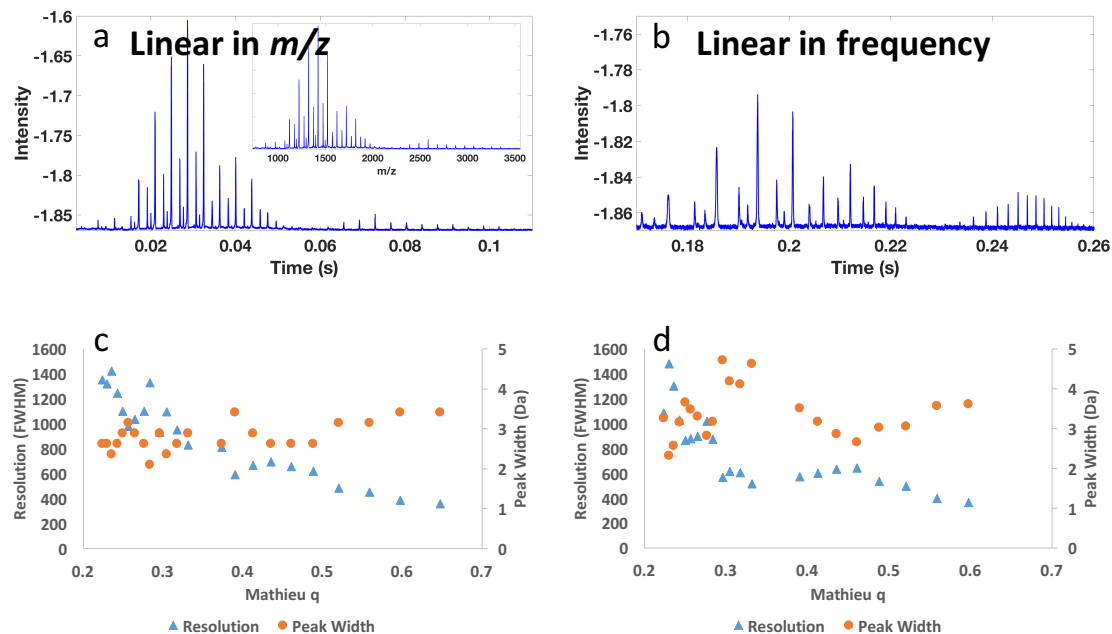
Figure 4.3. Resolution in inverse Mathieu q scans: plot of intensity vs. time for Ultramark 1621 calibration solution obtained with a secular frequency scan (a) linear in *m/z* (inset shows mass calibrated spectrum) and (b) linear in frequency, both of which show a wide mass range (*m/z* 500 to *m/z* 4,000) at low rf amplitudes. (c) and (d) show resolution and peak width vs. time for scans (a) and (b), respectively. Intensities are negative because a differential signal was obtained from the LTQ electrometer board. The scan rate in (a) was approximately 26,000 Da/s. The rf amplitude was ~1290 V$_{0\text{-p}}$. Injection time was 5 ms.
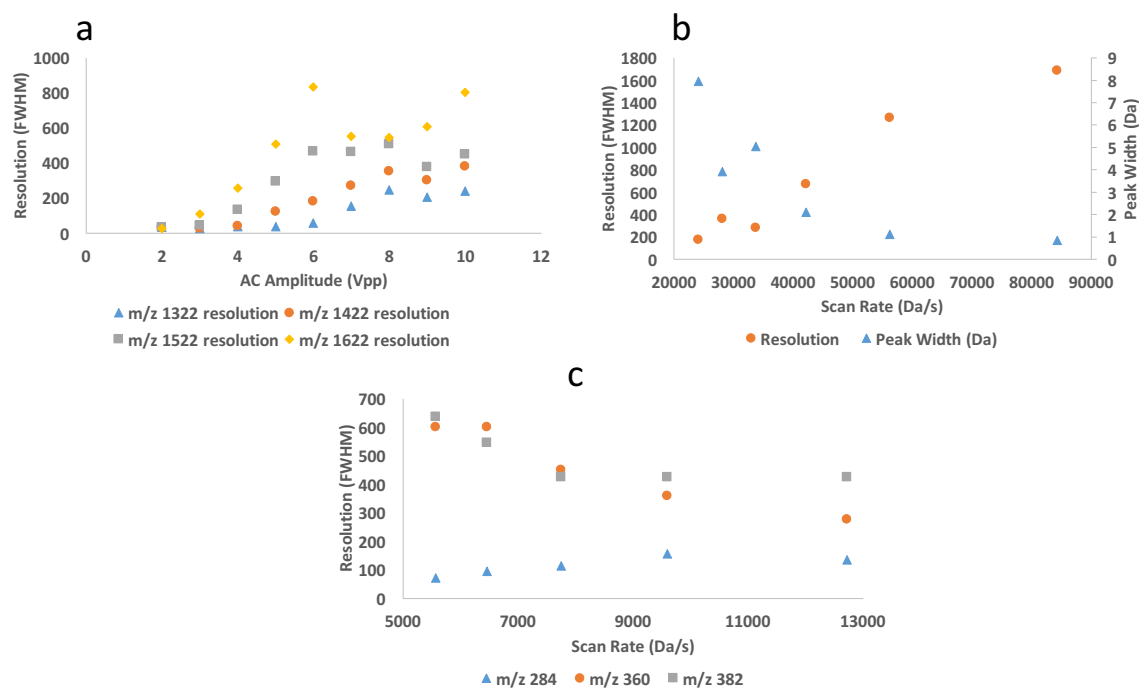
Figure 4.4. Resolution in inverse Mathieu q scans: (a) shows resolution for selected Ultramark 1621 calibrant ions as a function of ac amplitude, (b) is resolution as a function of scan rate for *m/z* 1422 (scan rate was varied by keeping rf amplitude constant and changing the mass scan time but keeping the scan range the same), and (c) shows resolution vs. scan rate for a mixture of 3 quaternary ammonium ions, indicating that resolution decreases with scan rate for ions that experience less space charge, whereas the opposite is true for ions that experience more space charge effects (those ejected earlier in the scan).
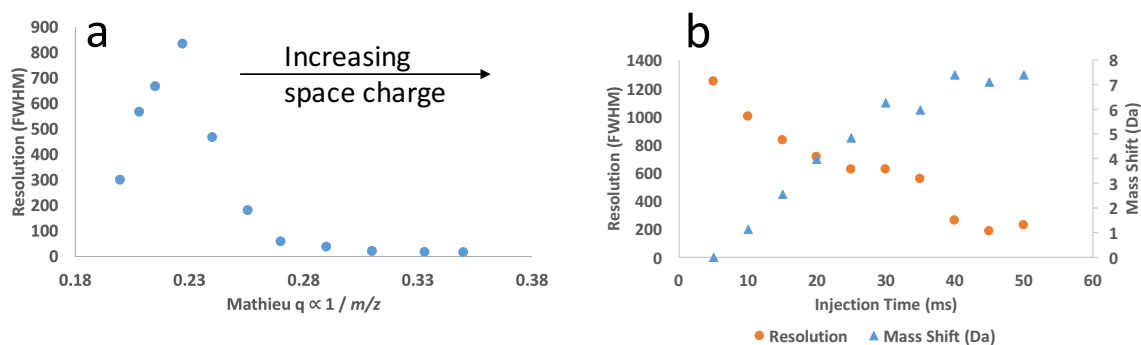
Figure 4.5. Space charge effects in secular frequency scanning: (a) shows decreasing resolution with Mathieu q parameter due to increasing space charge effects (50 ms injection time), and (b) shows resolution and mass shifts for *m/z* 1422 as a function of injection time. The rf amplitude and frequency were held constant and an inverse Mathieu q scan was performed on Ultramark 1621 calibrant ions (*m/z* 1022-2022, every 100 Th). Each point in (a) represents an ion of a different *m/z*. The scan rate was approximately 30,000 Da/s (rf amplitude of ~1290 V_{0-p}).
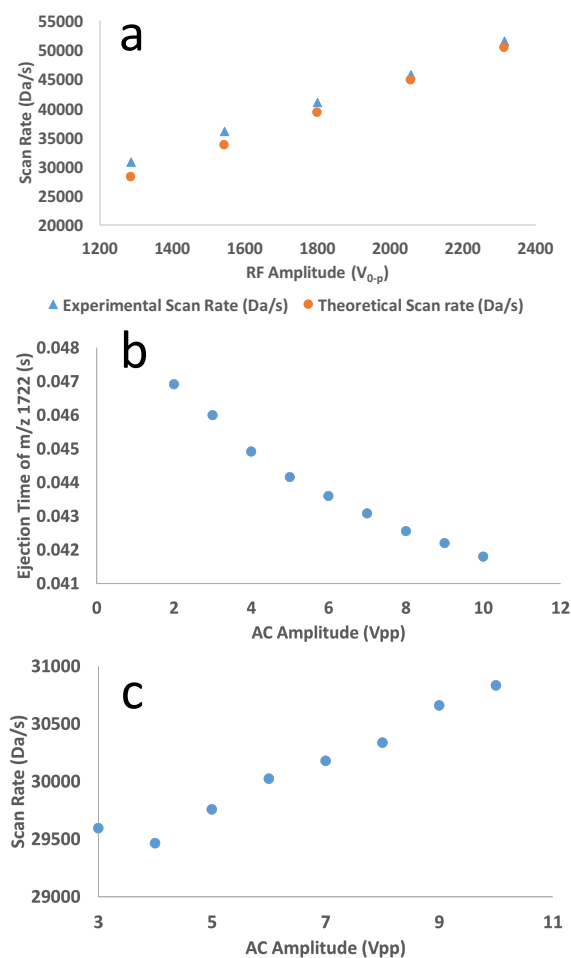
Figure 4.6. Effect of ac amplitude and rf amplitude on scan rate. For a constant ac waveform, the rf amplitude (directly proportional to the LMCO) linearly determines the scan rate (a). (b) higher ac amplitudes result in faster ion ejection, though high mass ions will experience a greater shift in ejection time, which results in an increase in apparent scan rate (c).

CHAPTER 5.   IMPROVING MASS ASSIGNMENTS IN QUADRUPOLE ION TRAPS OPERATED USING AC SCANS: THEORY AND EXPERIMENTAL VALIDATION

5.1   Abstract

Two theoretically equivalent methods of improving mass assignments in quadrupole ion traps operated using ac frequency scans are described side-by-side. Both use the inverse Mathieu q scan under constant rf conditions. In a first method, the ac amplitude is varied quadratically as a function of the Mathieu q parameter so as to force mass shifts to be constant with respect to ion *m/z*, thereby giving a precisely linear relationship between *m/z* and time. The average mass error improves by a factor of four when using the quadratic regression of ac amplitude vs. Mathieu q compared to constant ac amplitude conditions, assuming a linear mass calibration procedure. The quadratic relationship is also predicted by theory. In a second, simpler method, the ac signal amplitude is kept constant during the inverse Mathieu q scan and a quadratic relationship between *m/z* and time is used for mass calibration. Although the mass calibration is not linear in this case, the complicated amplitude optimization process is bypassed while retaining the same degree of mass accuracy. Importantly, in this case no parameter aside from the overall ac amplitude needs to be optimized, which is an advantage over the standard resonance ejection method in which the ac amplitude must be optimized for a given rf amplitude scan. Average mass error as low as 0.1 Da is shown to be possible in the two ac scan methods, which compares reasonably well with commercial resonance ejection data. This performance is adequate for ion traps used on planetary exploration missions and other in situ measurements, for which the ac frequency scanning method is particularly applicable.

5.2 Introduction

The Mathieu parameters for the linear quadrupole ion trap are defined as[7-9,12,130]

$$a_x = -a_y = \frac{8zU}{mr_0^2\Omega^2}$$

<div align="right">Eq. 5.1</div>

$$q_x = -q_y = \frac{4zV}{mr_0^2\Omega^2}$$

<div align="right">Eq. 5.2</div>

where z is the elementary charge, U is the DC potential applied to the rods in a quadrupolar manner, V is the zero-to-peak amplitude of the trapping radiofrequency (rf) potential, m is the mass of the ion, r_0 is the half distance between opposite electrodes, and Ω is the rf frequency in angular units (rad/s).

Based on the Mathieu parameters, the variables that can be utilized to give a mass spectrum are well known to be the rf amplitude (i.e. boundary[82] and resonance ejection[131]), the rf frequency[46,47], the dc amplitude[45,132], and the radius of the trap (though this has not been demonstrated directly). However, a fifth option also exists, an alternative which requires the trapping rf conditions to be kept constant and the frequency of a supplemental ac (resonance ejection) voltage to be scanned through ion fundamental secular frequencies,

$$\omega_{u,0} = \frac{\beta_u\Omega}{2}$$

<div align="right">Eq. 5.3</div>

so that an ion is ejected when the frequency of the supplemental voltage matches the ion's induced frequency of motion.[49,50] Such a scan has been termed a 'secular frequency scan'.[106] A useful variant of the secular frequency scan is the 'inverse Mathieu q scan',[133] in which the ac frequency is scanned nonlinearly under constant rf trapping conditions to give an inverse relationship between the ejected ion's q parameter and the ion's ejection time. All of these mass scanning methods (aside from ac frequency scanning) are described in gold standard references,[7-9] and the ac frequency scan methods are described in a more recent review.[134]

The ac frequency scanning method under constant rf conditions is the topic of interest in the current paper because it may be particularly advantageous for miniature low-power ion traps used in planetary exploration. Even though all commercial benchtop ion trap mass spectrometers use resonance ejection (rf and ac amplitude ramping) for the mass scan, for miniature mass spectrometers the ac frequency scan under constant rf conditions is more appropriate.[71,106,135] The ac frequency scan is electronically simpler because precision is needed in the kHz frequency

domain rather than the kV voltage domain. Mass range is also superior in the ac frequency scan mode (for a given maximum rf voltage) because ions at low q values can be ejected using a relatively low rf voltage. Moreover, power savings and simpler trap electronics are expected for the ac frequency scan mode compared to resonance ejection because the trap can be operated under lower rf amplitude conditions and hence with a smaller rf coil and without the feedback electronics needed for the precisely linear rf amplitude ramp. These characteristics are particularly important for flight or rover instruments planned for planetary, comet, or atmospheric exploration, for example the quadrupole mass spectrometer aboard Curiosity's[136-138] Surface Analysis at Mars suite of instruments and the planned linear ion trap mass spectrometer (LITMS) on the Mars Organic Molecule Analyzer (MOMA) (ExoMars, planned 2020 launch).[139] Despite the advantages of the ac frequency scan for these particular applications, there are some disadvantages, including the nonlinear mass scale [91] and lower resolution at low Mathieu q values. The former problem can be solved by implementing nonlinear ac frequency scanning in the form of the inverse Mathieu q scan. Solutions to the latter problem are currently being investigated. Furthermore, we have observed poor mass accuracy (1-2 Da mass errors) in inverse Mathieu q scan mass spectra when using a linear mass calibration procedure.

The questions addressed here are thus: 1) how must the ac amplitude of the custom inverse Mathieu q scan vary with *m/z* in order to obtain an exactly linear mass scale?, and 2) can the ac amplitude be held constant during the frequency sweep and instead can a different, but still simple, mass calibration procedure be adopted so that no scan parameter need be optimized?

To answer these questions, we must first consider previously-developed theory and methods for calibration of the gold standard rf mass scanning method: the rf amplitude ramp method (resonance ejection), which has been commercialized for many years on both benchtop and small ion trap systems. Theory predicts that the relationship between rf amplitude and *m/z* ought to be linear (eq. 5.2); however, several experimental variables prevent this relationship from holding across a wide mass range. Mass shifts are caused by space charge effects, the presence of higher-order fields, collisions with bath gas molecules, ion fragmentation, the variation in amplitude of the supplemental ac voltage, the change in rf amplitude as an ion is being ejected, and the rate of the rf amplitude scan.[84,89,112,140,141] Interestingly, mass shifts can also be compound-dependent and thus can be used, under certain limited circumstances, to differentiate between isobars.[89,142,143] All of these effects would be expected to also contribute to mass shifts in the ac

frequency scan mode of operation, and hence a theoretical understanding of the factors controlling mass shifts, particularly for mass calibration, must be achieved.

There have been at least two methods of compensating for mass shifts as a function of m/z when scanning the trapping rf voltage in the resonance or boundary ejection mode. In one study, CsI clusters were used for mass calibration, and apparent mass shifts were calculated as a function of m/z.[84] The relationship between mass shift and m/z was shown to be linear so that spectra could be corrected based on the calibration spectrum. This procedure required no instrumental modifications to the then-standard Thermo Finnigan ion trap electronics, and thus the supplemental ac amplitude was kept constant during the mass scan. An internal calibration procedure has also been described.[112] Because analytes and calibrant ions were subjected to the same injection and trapping conditions, mass errors were shown to be minimized. However, a peak-matching procedure was required at low scan rates due to the large difference in mass between the nearest calibrant ion and the analyte of interest.

Modern commercial benchtop mass spectrometers must scan the supplemental ac voltage linearly with time along with the rf voltage so that apparent mass shifts are proportional to ejected ion m/z.[10,42] For example, the Thermo Fisher LTQ linear ion trap system linearly scans the ac voltage applied to the x electrodes. This process requires automated optimization of both the rf voltage scan and the ac voltage scan to achieve a linear calibration and optimum resolution across the instrument's mass range, a process which takes several minutes to complete. Similarly, the commercial MDS Sciex linear ion trap ramps the ac and rf voltages as well.[11]

Following the past three decades of resonance ejection development, in this paper we describe, both experimentally and theoretically, two equivalent solutions for improving mass assignments in the inverse Mathieu q scan mode: a first solution in which the ac amplitude is varied as a function of the Mathieu q parameter and a linear mass calibration procedure is used, and a second solution in which the ac amplitude is constant during the mass scan and instead a quadratic fit of m/z vs. time is used. Experimentally, both methods are found to be adequate in terms of mass accuracy, but the latter method is much easier to implement and it further simplifies the ac frequency scan mode compared to the resonance ejection mode.

5.3 Theory

We begin with the theory developed by Doroshenko and Cotter.[42] The equation relating the shift in ejection time (Δt) from the ideal ejection time (t_e) of an ion of mass m that is resonantly ejected from a quadrupole ion trap using an excitation ac frequency w_{ac} with force F_{ac} (proportional to the ac amplitude) is

$$r_0 = \frac{F_{ac}}{2mw_{ac}\sqrt{\frac{1}{\tau^2}+a^2\Delta t^2}} \qquad\qquad \text{Eq. 5.4}$$

where τ is the collisional relaxation rate, Δt is a small apparent time shift relative to the ideal (theoretical) ejection time t_e due to the ejection of the ion at the wing of the absorption line (instead of the line center), r_0 is the previously-defined half-distance between opposite rods, and a is the frequency scan rate. In other words, t_e is reached when the ion's secular frequency matches the excitation ac frequency and is thus the theoretical ejection time, whereas Δt is the difference between this value and an ion's actual ejection time. The absorption line (i.e. amplitude of oscillation vs. excitation frequency), characteristic of a damped harmonic oscillator with constant oscillation frequency, is described by a Lorentzian function.

The inverse Mathieu q scan uses a nonlinear sweep of the ac frequency such that

$$q = \frac{k}{t_e - j} \qquad\qquad \text{Eq. 5.5}$$

where k and j are constants which depend on the start and end Mathieu q values of the frequency scan as well as the mass scan time (see ref. [133]), giving

$$t_e = \frac{k}{q} + j \qquad\qquad \text{Eq. 5.6}$$

Eq. 5.6 assumes that ions are ejected exactly at the center of the absorption line when the secular frequency exactly matches the excitation ac frequency; however, in reality they are ejected earlier at their *apparent* ejection time

$$t_a = t_e - \Delta t \qquad\qquad \text{Eq. 5.7}$$

for positive Δt (which we assume is the centroid of the mass peak over which the ions are ejected), implying that eq. 5.6 becomes

$$t_a = \frac{k}{q} + j - \Delta t \qquad\qquad \text{Eq. 5.8}$$

so that

$$\Delta t = \frac{k}{q} + j - t_a \qquad\qquad \text{Eq. 5.9}$$

The frequency scan rate, a, can be found by calculating the rate of change of the excitation frequency with respect to time, which we assume is proportional to the rate of change of the ejected ion's Mathieu q parameter with respect to time

$$a = \frac{dw_{ac}}{dt} = \frac{d\gamma q}{dt} = \frac{d}{dt}\left(\frac{\gamma k}{t_e - j}\right) = \frac{-\gamma k}{(t_e - j)^2} = \frac{-\gamma k}{(\frac{k}{q} + j - j)^2} = \frac{-\gamma q^2}{k} \qquad\qquad \text{Eq. 5.10}$$

where we have used the Dehmelt approximation to assume that the secular frequency is proportional to the Mathieu q parameter ($w_{ac} = \gamma q$).[144] We should note here that the Dehmelt approximation is only valid for low Mathieu q values ($q < 0.4$), but it remains a reasonable approximation up to $q = 0.7$. As we will see later, use of this approximation did not create noticeable disagreements between theory and experiment, even at high Mathieu q parameters.

Assuming the force on the ion is proportional to the ac voltage ($F_{ac} = zCV_{ac}$, where C is a coefficient of proportionality and V_{ac} is the ac voltage) yields

$$r_0 = \frac{F_{ac}}{2mw_{ac}\sqrt{\frac{1}{\tau^2} + a^2\Delta t^2}} \approx \frac{-zCV_{ac}}{2mw_{ac}a\Delta t} = \frac{-qCV_{ac}}{2\alpha w_{ac}a\Delta t} = \frac{-qCV_{ac}}{2\alpha\gamma qa\Delta t} = \frac{-CV_{ac}}{2\alpha\gamma a\Delta t} \qquad \text{Eq. 5.11}$$

where $m/z = \alpha/q$. Solving for the ac amplitude, we have

$$V_{ac} = \frac{-2\alpha\gamma r_0}{C}\Delta t a = \frac{-2\alpha\gamma r_0}{C}\Delta t\left(\frac{-\gamma q^2}{k}\right) = \frac{2\alpha\gamma^2 r_0}{kC}\Delta t q^2 \qquad\qquad \text{Eq. 5.12}$$

Thus we see that to have Δt = constant during the frequency scan (so the major dependence of t_a upon q in eq. 5.8 is preserved) the ac voltage should be proportional to q^2. That is, the ac amplitude ought to be closely approximated by a quadratic function of the Mathieu q parameter, assuming a perfectly linear mass scale is desired.

If the linearity of the mass scale is not important, but rather only a simple relationship between *m/z* and time is desired, then the preceding derivation can be used further to deduce the true relationship between *m/z* and time for the inverse Mathieu q scan. Suppose we keep the ac amplitude in Eq. 5.12 constant throughout the mass scan and replace Mathieu q with α(*z/m*), giving us

$$\left(\frac{m}{z}\right)^2 = \frac{2\alpha^3\gamma^2 r_0}{kCV_{ac}}\Delta t \qquad\qquad \text{Eq. 5.13}$$

Eq. 5.13 implies that if the ac amplitude is kept constant during an inverse Mathieu q scan, then the deviation between an ion's actual and theoretical ejection time depends quadratically on the m/z of the ion. For the inverse Mathieu q scan $t \propto m/z$ (to a close approximation) so that we should have $\Delta(m/z) \propto (m/z)2$. That is, the mass error from the linear fit of m/z vs. time should vary quadratically with the m/z of the ion. As shown in **Figure 5.1**, it is experimentally confirmed that there is an apparent quadratic relationship between mass error and m/z when using a linear fit for mass calibration of the inverse Mathieu q scan data for a selected Ultramark mixture analyzed at a scan rate of 16,000 Da/sec. An equivalent plot of ejection delay vs. m/z (i.e. eq. 5.13) indeed also indicates that the former varies as the latter squared (not shown). Hence, one ought to be able to use a quadratic mass calibration procedure instead of a linear one and thereby improve mass assignments without ac amplitude modulation.

Presented here are comparative results between these two methods of improving mass assignments in quadrupole ion traps using the inverse Mathieu q scan: 1) a method in which a linear mass scale is realized by modulating the ac amplitude according to Eq. 5.12, and 2) a simpler method in which the ac amplitude is kept constant and instead a quadratic mass calibration procedure is adopted instead of a linear procedure.

5.4   Experimental

5.4.1   Ionization

Nanoelectrospray ionization (nESI) with a 1500 V potential was used to generate ions for all experiments. Nanospray tips of 5 μm internal diameter were pulled from borosilicate glass capillaries (1.5 mm O.D., 0.86 I.D., Sutter Instrument Co.) by a Flaming/Brown micropipette puller (Sutter Instrument Co. model P-97, Novato, CA, USA).

5.4.2   Chemicals

Cesium hydrogencarbonate and tridecafluoroheptanoic acid (TFHA) were purchased from Sigma-Aldrich Co. (St. Louis, MO, USA) and were both dissolved in the same methanol/water solution so that the final concentration of cesium and TFHA was 2 mM. When electrosprayed, this solution generates CsTFHA clusters that are useful for mass calibration.[145] Pierce ESI LTQ

calibration solution (containing Ultramark 1621 calibrant) was purchased from Thermo Fisher (Rockford, IL, USA).

5.4.3   Instrumentation

All scans were performed using a benchtop Thermo LTQ linear ion trap mass spectrometer (San Jose, CA, USA) with rf frequency tuned to 1.185 MHz.

Inverse Mathieu q scan mass spectra were obtained during 'Ultrazoom' scans (during which the rf amplitude was slowly scanned, 27 Da/s, closely approximating constant rf conditions). The rf amplitude ramp is undesirable for ac frequency scanning, but it was the closest available approximation to a fixed rf when using this commercial instrument. Even so, the slow rf ramp does not fundamentally change the mass calibration or ac amplitude optimization procedures.

The inverse Mathieu q scan waveform was calculated according to our prior work,[133] imported to an arbitrary waveform generator (Keysight 33612A, Newark, SC, USA) set to a sampling rate at 10 MSa/sec and triggered at the beginning of the mass scan using the triggers in the 'Diagnostics' menu in the LTQ Tune software. Typical parameters for the frequency sweep were 300 ms length, $q_{start} = 0.908$, $q_{end} = 0.15$, and constant ac amplitude. In the cases where the ac amplitude was varied as a function of Mathieu q ($\propto 1/t$), additional lines of code were added to the Matlab program used for calculating the frequency sweep in order to generate a varied-amplitude waveform.

The differential output from the LTQ electrometer board was monitored on an external oscilloscope (Keysight InfiniiVision MSOX3024T, Newark, SC, USA). All spectra and data points are based on an average of 16 single mass scans.

5.5   Results & Discussion

5.5.1   Improving mass assignments for the inverse Mathieu q scan

The original goal of the inverse Mathieu q scan was to create a linear relationship between m/z and time,[133] or, in a broader sense, to simplify the relationship between m/z and time when operating an ion trap in the ac frequency scan mode for mass analysis. However, as shown in **Figure 5.1** and Eq. 5.13, the true relationship between m/z and time is not linear because of the non-constant frequency scan rate. As described in Eq. 5.12 and 5.13, there are two theoretically

equivalent methods of improving mass assignments compared to this simple case in which the ac amplitude was kept constant while a linear regression was used for mass calibration.

If a precisely linear mass scale is desired for an ion trap operating in the inverse Mathieu q scan mode, then the ac amplitude *must* be varied during the mass scan because the natural relationship between *m/z* and time in this mode is slightly quadratic, as indicated in Eq. 5.13. A general method for optimizing the ac amplitude for the inverse Mathieu q scan, can be described as follows:

1. Using calibration standards that produce ions that fall over the appropriate range of Mathieu q values (at a particular fixed rf amplitude), record time domain mass spectra by varying the ac amplitude *between* scans but keeping the ac amplitude constant *during* each scan.
2. Plot ejection time (s) vs. ac amplitude (V) for each calibrant ion and perform a linear regression on each plot, obtaining a slope and and intercept for each *m/z* (i.e. Mathieu q value).
3. Using the same scan rate and rf amplitude as in (1), calculate ideal ejection times (s) for each calibrant ion, assuming a perfect linear relationship between *m/z* and time.
4. Using the slope ($\Delta s/\Delta V$) and intercept (s at V=0) obtained in (2), calculate the ac amplitude needed for each *m/z* value to be ejected at the time determined in (3).
5. Convert *m/z* to Mathieu q and plot the optimized ac amplitude vs. Mathieu q parameter for each calibrant ion.
6. Perform a polynomial regression of order n (n > 1, where n is an integer, normally 2), relating ac amplitude (V) to Mathieu q parameter.
7. Vary the ac amplitude according to the regression in (6).

For the experiments performed here, we chose a Pierce ESI LTQ tune solution containing caffeine, the peptide MRFA, and phosphazine Ultramark 1621 ions (m/z 922-2022, spaced every 100 Da)[124] as well as a separate solution containing cesium hydrogencarbonate and tridecafluoroheptanoic acid (TFHA) salts that form CsTFHA clusters up to *m/z* 10,000 in electrospray ionization.[145]

The Ultramark 1621 calibration solution was analyzed using the inverse Mathieu q scan with scan time 300 ms from Mathieu q = 0.908 to 0.15 at an rf amplitude of 2620 V_{0-p} (mass scan rate 16,000 Da/s). The ac amplitude, constant *during* each scan, was varied *between* scans from 2.5 V_{p-p} to 5.0 V_{p-p} in 0.5 V_{p-p} increments and the ejection times of each of the calibrant ions were plotted against the ac amplitude. The relationship between ejection time and ac amplitude was approximately linear, which has been shown previously,[84] so a least squares linear regression was

performed for each calibrant ion. The slope and intercept, with units (s/V_{p-p}) and (s), respectively, were then plotted against the Mathieu q parameters of the calibrant ions, as shown in **Figure 5.2a**. In all cases, an increase in ac amplitude causes the ions to be ejected sooner. Moreover, as the Mathieu q parameter increases, the slope apparently increases in magnitude. This relationship indicates that ions with lower *m/z* values respond to changes in excitation amplitude to a greater degree than ions with higher *m/z* values, which we have also observed when sweeping the ac frequency linearly.[91] On the other hand, the intercept tends to increase with the Mathieu q parameter, although this is not physically meaningful because ions cannot be ejected if the ac amplitude is 0 V_{pp}.

Once the slope and intercept are determined, the ideal ac amplitude for each Mathieu q parameter must be calculated from ideal ejection times. The ideal ejection times can be determined, for example, by plotting *m/z* vs. time for one of the scans in step (1) and using the linear regression (*not* the data points themselves) as the ideal relationship. For all data shown here, ideal ejection times were calculated from the best fit linear regression of *m/z* vs. time for a 5 V_{p-p} ac amplitude. Once this linear regression is performed, the *m/z* values of the calibrant ions are plugged back into the regression to determine the ideal ejection times.

The next step is to determine the relationship between the Mathieu q parameter and the ideal ac amplitude. The ideal ejection times are converted to optimized ac amplitudes by subtracting the intercept in step (2) (**Figure 5.2a**, blue circles) and dividing by the slope, also from step (2) (**Figure 5.2a**, orange squares). The optimized ac amplitudes are then plotted against the Mathieu q parameters of the calibrant ions. Finally, the data is fit to a quadratic function. The resulting optimization of ac amplitude as a function of Mathieu q is shown in **Figure 5.2b**. The frequency swept waveform itself is also shown in **Figure 5.2**. As with typical mass calibrations, the optimization *is only valid for the chosen mass range and scan rate*. The scan rate for these first experiments was 16,000 Da/s which matches the commercial LTQ resonance ejection scan rate so that fair comparisons could be made between the two methods.

We also note that the very slow rf amplitude (V_{rf}) ramp that we necessarily used to approximate constant rf amplitude conditions contributes to the first order term in the quadratic fit because, according to ref. [42], for our particular experimental system the scan rate is

$$a = \frac{dw_{ac}}{dt} = \frac{-\gamma q^2}{k} - f \frac{dV_{rf}}{dt} q \qquad \text{Eq. 5.14}$$

where f is some coefficient and the latter term is caused by the slow rf ramp so that eq. 5.12 becomes

$$V = \frac{2\alpha\gamma r_0}{c} a\Delta t = \frac{2\alpha\gamma r_0}{c}\left(\frac{-\gamma}{k}q^2 - f\frac{dV_{rf}}{dt}q\right)\Delta t \qquad\qquad \text{Eq. 5.15}$$

In fact, the slow rf ramp does not even change the ac amplitude optimization or the mass calibration procedure; rather, it only contributes to the first order term in the quadratic fit. Preliminary experiments performed on a breadboard linear ion trap mass spectrometer at NASA Goddard Space Flight Center confirmed the quadratic nature of the AC amplitude vs. Mathieu q curve which provided strict linearity in *m/z* vs. time. Curiously, the first order coefficient remained, despite the unchanging rf amplitude. Thus, there must be other factors, not just the unwanted rf ramp, that contribute to the first order term. These factors are not discussed further because they do not fundamentally alter the optimization procedure.

In order to validate the optimization procedure and the quadratic nature of *m/z* vs. time for the constant ac amplitude case, we compared mass errors obtained from two inverse Mathieu q scans, one in which the ac amplitude was constant and one in which the ac amplitude was varied according to the quadratic regression in **Figure 5.2b**. In the case of the constant ac amplitude scan both linear and quadratic fits of *m/z* vs. were performed and compared to the ac amplitude modulation case with linear fit of *m/z* vs. time. **Table 5.1** shows experimental ejection times, monoisotopic *m/z* values, and calibrated *m/z* values for each of the Ultramark 1621 in the constant ac amplitude case with linear mass calibration, and the absolute values of the experimentally determined mass errors. The average mass error in this case was 0.66 Da because the mass scale is not precisely linear if the ac amplitude is not modulated during the mass scan. This average error is approximately an order of magnitude higher than the average mass error from the commercial internally-optimized resonance ejection method, which had an average error of 0.07 Da just after optimization.

Table 5.2 shows individual mass errors for each peak in the Ultramark mass spectrum as well as the average mass error for the case where the ac amplitude was modulated according to **Figure 5.2b** and a linear mass calibration was performed. By varying the ac amplitude, the average mass error is decreased by a factor of 4.7 to 0.14 Da because the mass scale is forced into linearity by the changing ac amplitude as a function of *m/z*. As described in Eq. 5.13, the same results can be obtained by calibrating the data in **Table 5.1** according to a quadratic function of *m/z* vs. time,

which gives an average mass error of 0.11 Da (**Table 5.1**, last two columns), slightly better than the ac amplitude modulation case.

We do note additionally that it appears that the ion *m/z* 1322 falls on the hexapole nonlinear resonance line at $\beta = 2/3$, resulting in an abnormally high mass error for this particular point. If the calibrant ion on the nonlinear resonance line is ignored, then the average mass error drops dramatically to 0.097 Da (65 ppm average mass error, assuming *m/z* 1500) for the amplitude modulation case, and 0.09 Da for the quadratic mass calibration case. Although this average error does not quite match the commercial instrument's average error in the typical resonance ejection mode, varying the ac amplitude linearly is much easier than varying it nonlinearly with respect to time. Furthermore, the LTQ's ac amplitude optimization procedure is completely automated using the integrated electronics. Most importantly, ions are ejected at different Mathieu q values in the ac frequency scan case, whereas all ions are ejected at the same q value in resonance ejection. We particularly noticed degradation of both mass accuracy and resolution when calibrant ions were placed at lower Mathieu q parameters.

Although resolution is not the topic of this paper, unit resolution was observed over a broad mass range at a scan rate of 16,000 Da/s (**Figure 5.3**), which is the commercial resonance ejection scan rate. Resolution tended to degrade at lower Mathieu q values, which is expected.[127] Unit resolution was observed from the lower-mass cutoff to between 2 and 2.5x the lower-mass cutoff using a scan rate of 16,000 Da/s. Peaks at nonlinear resonance lines appeared broader than expected and also exhibited peak splitting (*m/z* 1321 in **Figure 5.3**).[106] Calibrant ion data that coincided with these nonlinear resonance lines were ignored when optimizing the ac amplitude, so they did not alter the results in any way, aside from biasing the average mass error in the final average error calculations.

In order to further validate both the ac amplitude optimization procedure as well as the quadratic nature of *m/z* vs. time for a constant ac amplitude inverse Mathieu q scan, we repeated the previously-described experiments using a different set of ions, CsTFHA clusters produced from electrospray ionization of a solution of cesium hydrogen carbonate and tridecafluoroheptanoic acid.[145] The ions produced from this solution fall over a broader range of q parameters, thereby giving a larger mass range for optimization and calibration. Both the Ultramark 1621 mixture and the CsTFHA mixture were used to optimize the ac amplitude at an rf amplitude of 1308 V_{0-p} (mass scan rate 8,000 Da/s). The results are shown in **Figure 5.4**.

Although it is somewhat alarming that the quadratic fits deviate quite a lot from each other, especially at high q, experimentally both returned better average mass errors than their constant ac amplitude counterparts (**Table 5.3**). The constant ac amplitude scan with linear mass calibration gave quite high average mass errors of 2.17 Da and 2.84 Da for the Ultramark 1621 and CsTFHA solutions, respectively. The 'Ultramark' ac amplitude modulation in **Figure 5.4** gave much better mass accuracy, averaging 0.49 Da error when a linear mass scale was assumed. The quadratic ac amplitude modulation for the CsTFHA clusters (blue circles in **Figure 5.4**) improved mass errors to 0.35 Da, on average, again with a linear mass calibration method. The mass error for the Ultramark solution under these conditions (LMCO ~500 Da) would be expected to be higher because the calibrant ions are at lower Mathieu q values than the cluster ions. Note that only the relative ejection times of the ions – not the absolute times – determine the calibration linearity. Hence, two different ac amplitude optimizations (as in **Figure 5.4**) can both be 'correct' in the sense that they both increase mass accuracy relative to the constant amplitude, linear calibration case.

In principle, higher order polynomials can also be fit to the ac amplitude vs. Mathieu q data points, and the fit would be expected to improve with the order of the polynomial since the curvature of the amplitude vs. q plot could be better approximated. Using a fifth order polynomial fit of $V_{ac} = -152.26q^5 + 311.78q^4 - 220.1q^3 + 28.384q^2 + 25.341q - 1.4061$, we obtained average mass errors of 0.15 Da and 0.22 Da for the Ultramark ions and CsTFHA clusters (**Table 5.3**), respectively, an order of magnitude decrease in error from the constant amplitude case, and a 30-75% reduction in average mass error compared to the quadratic amplitude approximation. Higher order polynomials could similarly be applied to mass calibration, although they are not justified by theory.

In applying a quadratic fit of *m/z* vs. time instead of a linear fit to the constant ac amplitude data used to create **Table 5.3**, we obtained results (**Table 5.3**, sixth row) that mirror the mass accuracy obtained by optimizing the ac amplitude quadratically with respect to Mathieu q. The average mass errors were 0.48 and 0.22 Da for the Ultramark and CsTFHA mixtures, respectively. This result should not be surprising because we have solved the same problem in two different ways: in one approach the ac amplitude is modulated to eject ions such that the ejection delay does not vary with *m/z*, and in the second the mass calibration itself takes the varying ejection delays into account.

We now take a moment to comment on the Dehmelt approximation that we used to assume the secular frequency is proportional to the ion's Mathieu q value, an approximation only valid for q < 0.4. Even though the validity of the approximation is questionable over a large range of high Mathieu q values, the data in **Figures 5.2** and 5.**4** and **Tables 5.1** and **5.2** do not show a clear degradation of mass assignments at high q. It is thus clear that neither the ac amplitude optimization procedure nor the quadratic mass calibration is complicated by the invalidity of the Dehmelt approximation at high Mathieu q. In fact, it is the low q calibrant ions that suffered from higher mass errors, principally because their frequency dispersions as a function of *m/z* are smaller.

5.5.2   The case of the secular frequency scan

Finally, we briefly comment on the more general case of the secular frequency scan in which the ac frequency is ramped linearly with respect to time ($w_{ac} = lt + w_0$).[50,91,106] The scan rate in this case is

$$a = \frac{dw_{ac}}{dt} = l$$

<div align="right">Eq. 5.16</div>

so that

$$V_{ac} = \frac{2\alpha\gamma r_0}{c}l\Delta t$$

<div align="right">Eq. 5.17</div>

That is, in the case of the linear secular frequency scan, the ac amplitude should theoretically have no dependence on ion *m/z*. This is a remarkable feature of the secular frequency scan, which is clearly the simplest of the ion trap mass scan techniques, but unfortunately the one for which mass calibration is comparatively complicated.

5.6   Conclusion

We have demonstrated two methods for improving mass assignments in quadrupole ion traps using the inverse Mathieu q scan. Compared to the constant ac amplitude case, the varied ac amplitude waveforms decrease average mass errors, on average, by a factor of four, but with higher-order polynomial fits they can decrease mass errors by an order of magnitude. A simple quadratic fit of *m/z* vs. time of data acquired using a constant ac amplitude waveform returns similar results in terms of mass accuracy but is much easier to implement. The results compare

well with the automated optimization method of a commercial instrument which gives approximately half the average mass error as the calibrated ac amplitude case. However, further improvements to the calibration procedure, and perhaps even procedural automation, may partially bridge this gap.

5.7   Acknowledgements

Figures and Tables
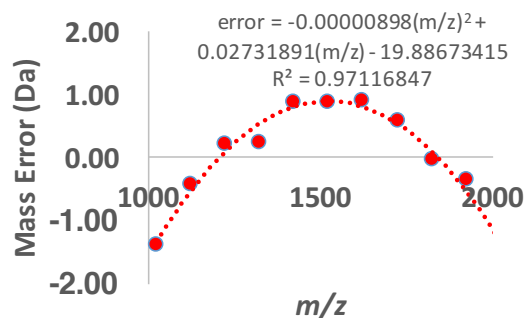
Figure 5.1. Mass error as a function of *m/z* for an inverse Mathieu q scan from q = 0.908 to q = 0.15 over 300 ms with a fixed rf amplitude of 2620 V$_{0-p}$ (mass scan rate 16,000 Da/s) and a fixed ac amplitude. A linear fit of *m/z* was performed, and mass errors were calculated. Note the systematic mass errors aside from *m/z* 1322, which falls on a hexapole nonlinear resonance line and hence does not fall on the quadratic fit.
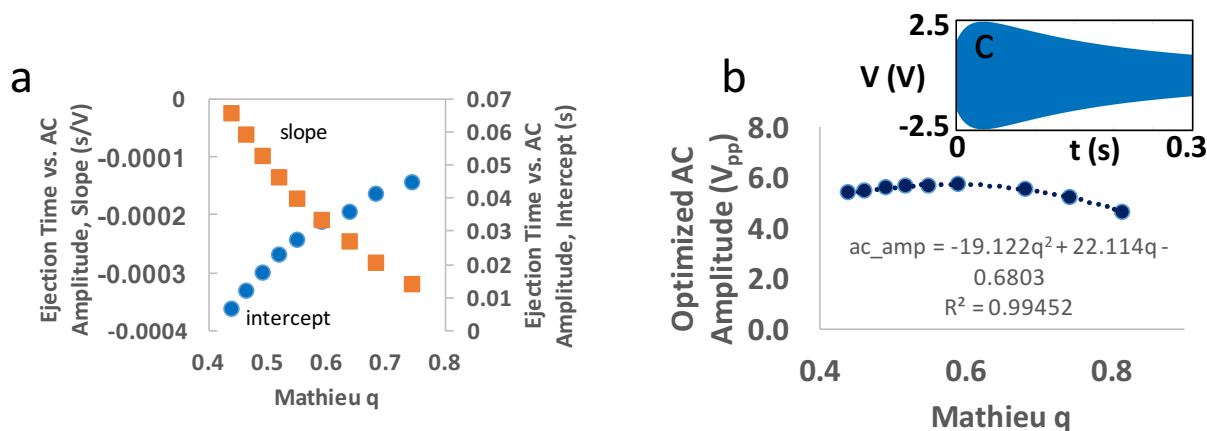
Figure 5.2. Procedure for optimizing the ac amplitude in inverse Mathieu q scans for exactly linear mass calibration: ion ejection time vs. ac amplitude is plotted for each calibrant *m/z* and a linear regression is performed, giving (a) slopes and intercepts. The desired ejection time for a perfectly linear *m/z* vs. time relationship is then fabricated and the required ac amplitude for each of those calibrant ions is calculated from coefficients in (a). A quadratic regression (b) then gives the calibrated ac amplitude as a function of Mathieu q, hence as a function of time. The inset (c) shows waveform voltage as a function of time. To acquire this data an Ultramark 1621 calibration solution was analyzed with a 300 ms inverse Mathieu q scan of the given ac amplitude from Mathieu q = 0.908 to q = 0.15. The rf amplitude was 2620 V$_{0\text{-}p}$, resulting in a mass scan rate of 16,000 Da/s.
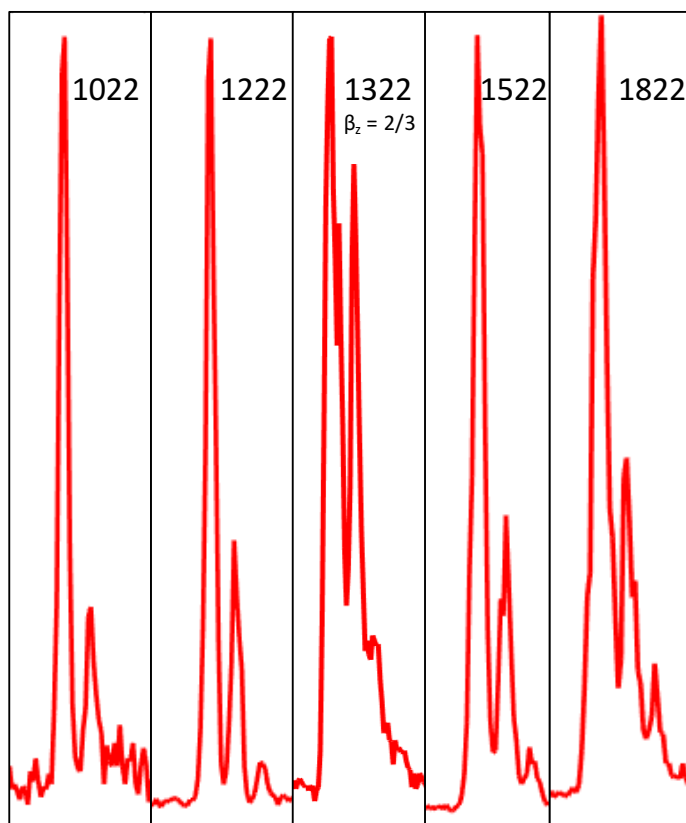
Figure 5.3. Peaks for selected masses from the Ultramark 1621 calibration solution analyzed with an inverse Mathieu q scan at a scan rate of 16,000 Da/s. Note that *m/z* 1322 lies on the hexapole nonlinear resonance line $\beta = 0.66$.
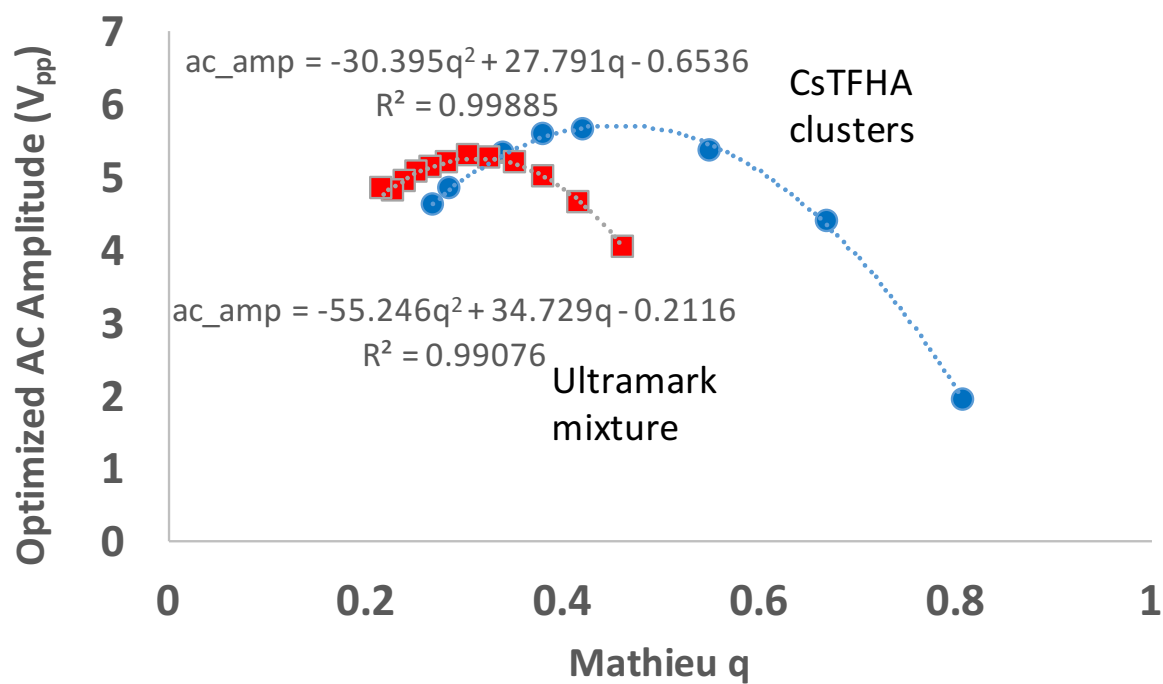
Figure 5.4. AC amplitude optimization equations for (red squares) the Ultramark 1621 mixture and (blue circles) CsTFHA clusters. The rf amplitude was 1300 $V_{0\text{-}p}$ (scan rate 8,000 Da/s) but the inverse Mathieu q scan parameters, aside from ac amplitude, were the same as **Figure 5.1**.

Table 5.1. Experimental mass errors for the Ultramark 1621 calibrant ions using an inverse Mathieu q scan with constant ac amplitude. Linear mass calibration was used to generate columns 3 and 4 and quadratic mass calibration was used to generate columns 5 and 6.

Ejection Time (s)	Calculated *m/z*	Calibrated *m/z* Linear Mass Calibration	|Mass Error| (Da) Linear Mass Calibration	Calibrated *m/z* Quadratic Mass Calibration	|Mass Error| (Da) Quadratic Mass Calibration
0.006619	1021.99	1020.60	1.39	1021.95	0.04
0.01298	1121.99	1121.57	0.43	1122.10	0.11
0.01932	1221.99	1222.21	0.22	1222.11	0.12
0.02562	1321.98	1322.21	0.23*	1321.67	0.32*
0.03196	1421.97	1422.85	0.87	1422.04	0.06
0.03826	1521.97	1522.85	0.88	1521.95	0.02
0.04456	1621.96	1622.86	0.89	1622.05	0.09
0.05084	1721.95	1722.54	0.58	1722.01	0.05
0.0571	1821.95	1821.91	0.04	1821.82	0.13
0.06338	1921.94	1921.59	0.35	1922.14	0.19
0.06961	2021.94	2020.49	1.45	2021.83	0.11
		Average:	0.66		0.11

The experimental conditions are the same as **Figure 5.1**. The mass calibration equation was $m/z = 15{,}873.5t + 915.5$ for linear mass calibration and $m/z = 2{,}261.9t^2 + 15{,}700.9t + 917.9$ for quadratic mass calibration.
*lies on nonlinear resonance line $\beta = 0.66$ (hexapole).

Table 5.2. Experimental mass errors for the Ultramark 1621 calibrant ions using an inverse Mathieu q scan with ac amplitude optimized according to a quadratic function of Mathieu q.

Ejection Time (s)	Calculated *m/z*	Calibrated *m/z* Quadratic Amplitude vs. q, Linear Mass Calibration	|Mass Error| (Da) Quadratic Amplitude vs. q, Linear Mass Calibration
0.006712	1021.99	1021.94	0.041
0.01303	1121.998	1122.10	0.11
0.01934	1221.991	1222.14	0.15
0.0256	1321.985	1321.38	0.60*
0.03196	1421.978	1422.20	0.23
0.03826	1521.972	1522.08	0.11
0.04457	1621.966	1622.11	0.15
0.05087	1721.959	1721.99	0.032
0.05717	1821.953	1821.86	0.088
0.06348	1921.946	1921.89	0.048
0.06979	2021.94	2021.932	0.008
		Average:	**0.14**

The experimental conditions were the same as **Figure 5.1**, except the ac amplitude was optimized according to: $V_{ac} = -19.122q^2 + 22.114q - 0.6803$ (Figure 2b). The mass calibration equation was as follows: $m/z = 15,853.1t + 915.5$. *lies on nonlinear resonance line $\beta = 0.66$ (hexapole).

Table 5.3. Average mass errors for each ac amplitude optimization and mass calibration combination.

AC Amplitude Optimization Procedure, Mass Calibration	Average Mass Error (Da)	
	Ultramark 1621	CsTFHA Clusters
Constant ac amplitude, linear mass calibration	2.17	2.84
Quadratic regression, linear mass calibration	0.49	0.35
Quintic regression, linear mass calibration	0.15	0.22
Constant ac amplitude, quadratic mass calibration	0.48	0.22

The rf amplitude was 1300 V_{0-p}. The inverse Mathieu q scan parameters were the same as Figure 5.4, except the ac amplitude was calibrated according to either (quadratic) $V_{ac} = -30.395q^2 + 27.791q - 0.6536$ or (quintic) $V_{ac} = -152.26q^5 + 311.78q^4 - 220.1q^3 + 28.384q^2 + 25.341q - 1.4061$. Scan rate was 8,000 Da/s.

CHAPTER 6. ION ISOLATION AND MULTIGENERATIONAL COLLISION-INDUCED DISSOCIATION USING THE INVERSE MATHIEU Q SCAN

6.1 Abstract

Rationale: In a bid to develop a mass spectrometer using ac frequency scanning for ion isolation, ion activation, and ion ejection, we have developed scan functions for each process using the inverse Mathieu q scan.

Methods: Ion isolation is accomplished by frequency hopping, that is, by skipping past the ranges of frequencies corresponding to the ions to be isolated during the frequency sweep. Multigenerational collision-induced dissociation is demonstrated by scanning the frequency of excitation from low to high so that multiple generations of fragment ions can be observed in the product ion mass spectra. Because the excitation frequency is scanned quickly across a large range, fragmentation of some precursor ions can be too limited. However, by first fixing the excitation frequency on the precursor ion and then scanning the frequency using the inverse Mathieu q scan, a higher abundance of product ions can be obtained.

Results: Isolation of a single mass-to-charge (m/z) as well as nonadjacent m/z ions is demonstrated with isolation efficiency greater than 70%. Fragmentation of caffeine and noroxycodone is demonstrated, the latter of which shows multiple generations of product ions.

Conclusion: The results demonstrated here provide strong evidence that an ion trap mass spectrometer can be operated without using an rf amplitude ramp for any operation, and instead ac frequency scanning can be used for all mass selective operations.

6.2 Introduction

Mass-selective operations in quadrupole ion traps encompass ion injection, ion isolation, ion excitation, and ion ejection.[5-8] Here, the isolation and excitation steps are emphasized.

Typically isolation and excitation take advantage of each ion's secular frequency, that is, the mass-to-charge (m/z) dependent oscillation frequency that is characteristic of each ion. In ion traps, ions of particular m/z values can be isolated by ejecting unwanted species from the trap while retaining the ion(s) to be isolated. Isolation can be performed by setting the rf and dc potentials on the quadrupole rods such that the ion of interest is placed at the apex of the Mathieu stability diagram, thereby removing other ions from the trap since their trajectories will be unstable.[146] Some alternative methods use a radiofrequency (rf) amplitude sweep, often with a resonance ejection signal at a Mathieu q value just below the q value of the ion to be isolated, to remove unwanted ions from the trap.[147] Sweeping the frequency of the resonance ejection (ac) signal at constant rf amplitude can also be used,[147] but the most common method is based on applying a sum of sine waves of different frequencies or equivalently a set of ac signals created using the stored waveform inverse Fourier transform technique or filtered noise field.[51,148-150] These ac resonance methods cause ions over a broad m/z range except those of chosen m/z values to be ejected. For digital ion traps, which are of increasing interest because of their electronic simplicity and potential power savings,[151] isolation can be accomplished by modulating the duty cycle of the trapping rectangular waveform.[152]

Ion activation in quadrupole ion traps usually takes the form of resonance excitation,[52,131] wherein a single-frequency signal corresponding to the ion's secular frequency is applied in a dipolar manner, causing the ion to gain kinetic energy and collide with bath gas molecules, inducing fragmentation. Many variants of resonance ejection exist, which either give higher-energy fragmentation, extend the mass range of collected product ions, simplify the isolation waveform, or shorten the period of activation.[153-161] Ions can be excited by moving them close to the boundary of the stability diagram as well in boundary-activated dissociation.[162] Other methods such as infrared multiphoton dissociation,[163] UV photodissociation,[164,165] and surface-induced dissociation (SID)[166] also can be used, but radiation methods are generally not mass-selective and collection of product ions after surface-induced dissociation is inefficient in quadrupole ion traps.[167]

Our goal is to develop an ion trap mass spectrometer based completely on ac waveforms for ion isolation, ion excitation, and ion ejection. In particular, the precise linear rf voltage ramp that is required for the mass scan and some isolation methods is undesirable because of the higher power consumption and the additional electronics needed to ensure rf ramp linearity in the mass

scan. To be clear, we are interested in a mass spectrometer with rf amplitude that can be tuned between operations and scans but which is not desired to ramp linearly with high precision, as is needed in the mass scan and some isolation and fragmentation methods. Tunability of the rf amplitude is still needed, however, in order to manipulate ions' q values for ion isolation, fragmentation, and mass scanning because the rf amplitude will determine isolation performance, energy deposition into precursor ions and fractional product ion mass range during CID, and mass range and mass scan rate during the mass scan.

Similarly, scans of the rf frequency, which is typically near 1,000 kHz, are more difficult to implement than ac frequency scans and are inherently nonlinear with *m/z*, complicating mass calibration. Low amplitude ac signals are much more readily implemented and controlled (particularly the ac frequency) and hence are particularly advantageous for space-based and other portable and miniature instruments.[50,70,71,168] This consideration has led us, in the last two years, to develop methods of secular frequency scanning for ion trap mass spectrometers.[106] In the secular frequency scan, the rf amplitude and frequency are held constant while the frequency of a small amplitude supplementary resonance ejection signal is ramped through ion secular frequencies. If the frequency scan is linear with time, then a nonlinear mass spectrum is obtained, which must be calibrated to obtain the linear mass spectrum.[91] A further important advantage of the secular frequency scan is that it allows for single analyzer precursor scans to be performed in ion traps,[99,123] furthering the capabilities of these already advantageous devices.

Further work on the frequency scan has resulted in a nonlinear ac frequency sweep called the "inverse Mathieu q scan".[133,135] With this method, the ac frequency is swept nonlinearly such that the Mathieu q parameter of the ion being ejected varies inversely with time. Because mass-to-charge and Mathieu q are inversely related

$$m/z = 4V_{0\text{-}p} \,/\, q\Omega^2 r_0^2 \qquad\qquad\qquad \text{Eq. 6.1}$$

where $V_{0\text{-}p}$ is the zero-to-peak rf amplitude (volts), Ω is the angular rf frequency (radians/second), and r_0 is the half distance between the quadrupole rods (meters), the relationship between *m/z* and time is linear. As a result, the calibration procedure for the inverse Mathieu q scan is the same as boundary and resonance ejection; a linear fit between *m/z* and time is all that is required.

The ability to obtain linear mass spectra using an ac frequency sweep has overcome the biggest hurdle to developing an ac-based mass spectrometer. However, it additionally may be

desirable to be able to use an ac frequency sweep method for both ion isolation and ion activation in order to keep the instrument as operationally simple as possible. In this paper, we add to the demonstrated use of ac scans for ion ejection the demonstration that ion isolation and multigenerational collision-induced dissociation in an ion trap can be performed using ac scans in the inverse Mathieu q scan mode.

6.3   Experimental

6.3.1   Ionization

Nanoelectrospray ionization using a 1.5 kV potential was used to generate ions from a borosilicate glass capillary with a ~5 um tip diameter (1.5 mm O.D., 0.86 mm I.D., Sutter Instrument Co.). The capillaries were pulled to a point using a Flaming/Brown micropipette puller from Sutter Instrument Co. (model P-97, Novato, California, USA).

6.3.2   Chemicals

Pierce ESI LTQ calibration solution containing caffeine (*m/z* 195), the peptide MRFA (*m/z* 524), and Ultramark 1621[124] was purchased from Thermo Fisher Scientific (Rockford, IL, USA). A typical mass spectrum of this solution can be found on the manufacturer's website (currently, https://www.thermofisher.com/order/catalog/product/88322). Noroxycodone was purchased from Cerilliant (Round Rock, TX, USA) and was dissolved in methanol at a concentration of 10 μg/mL.

6.3.3   Instrumentation

Experiments were performed using a Thermo LTQ Orbitrap XL mass spectrometer (San Jose, CA, USA). The "normal" scan rate of 16,666 Da/s was used for boundary ejection with the rf frequency tuned to 1,175 kHz. The isolation and activation waveforms were replaced with waveforms generated by a Keysight 33612A arbitrary waveform generator (Newark, SC, USA). The waveforms were triggered at the beginning of the isolation period (~13 ms in length followed by a ~30 ms activation period) using the triggers in the "Diagnostics" menu in the LTQ Tune software.

Isolation and activation waveforms were calculated in Matlab using a custom program similar to the one previously described.[133] The isolation waveform (**Figure 6.1**) was an inverse Mathieu q scan with a user-defined isolation q value (q_{iso}) and isolation width (Δq), both defined

in terms of Mathieu q space (these values are easily converted to the frequency domain). The program begins with an array of Mathieu q values (**Figure 6.1a**), with a user-defined start and end q value (typically 0.908 and 0.05, respectively, for isolation). The program then removes q values that satisfy the relationship $q_{iso} - \Delta q/2 < q < q_{iso} + \Delta q/2$ to give a smaller array of q values, which are then converted to β parameters using a function *beta_calculator*.[91] The β values are then converted to frequencies and subsequently given phases, as described previously.[91] The resulting waveform was exported from Matlab as a .csv file (column vector) and imported to the arbitrary waveform generator, set on channel 1 to a sampling rate of 10 MSa/sec. The frequency sweep excites ions over a broad range of *m/z* values, and if the amplitude and time of application are sufficient, the ions will be ejected from the trap. Because some q values are taken out of the frequency scan, a "notch" or frequency hop is created in a similar manner to stored waveform inverse Fourier transform notches.[51,148,169,170] In the case of the frequency scan, a "jump" is observed in the waveform (**Figure 6.1b**, inset), and the width of the jump (in frequency units or Mathieu q units) is determined by Δq. Because the waveform sweeps through the phase of the sinusoid instead of frequency, phase continuity is maintained regardless of any frequency jumps and thus no discontinuities are observed in the waveform. Multiple frequency hops may be incorporated by specifying additional q_{iso} and Δq values.

Ion activation was performed after ion isolation, again using the inverse Mathieu q scan. The activation waveform was set on channel 2 of the function generator and was also triggered on the isolation event but was set to delay the activation signal for ~13 ms, the duration of isolation. The ion to be isolated was set at a Mathieu q_x value of 0.83, after which point it was placed at q_x = 0.3 for activation. For activation, the frequency of the ac waveform was swept so that the first q_x value interrogated was 0.15 and the last value was 0.908. That is, the frequency was swept nonlinearly from low to high frequency (high to low *m/z*), the opposite direction of the isolation scan. Unlike isolation, the activation waveform did not skip q values. The amplitude of the excitation was typically a constant 200 mV$_{pp}$, whereas the amplitude of the isolation waveform was constant in the range ~2 - 6 V$_{pp}$, depending on the *m/z* of the ion to be isolated.

After ion isolation and/or excitation, ions were detected by boundary ejection using an analytical rf amplitude ramp. For isolation efficiency calculations, the peak area of the isolated ion before and after isolation was compared. It is a future goal to incorporate the inverse Mathieu q

scan for all isolation, activation, and ejection methods in a single ion trap, but this was not possible on the commercial instrument used for this work.

6.4   Results & Discussion

The development of a miniature mass spectrometer using ac frequency sweeps for all mass-selective operations necessitates the investigation of a set of simple, effective, and efficient isolation, activation, and mass scan techniques. The mass scan has recently been explored in the form of the inverse Mathieu q scan,[133] in which the frequency of the ac is swept nonlinearly so that a linear relationship between the *m/z* of the ion to be ejected and time is obtained. The inverse Mathieu q scan can further be used for both isolation and ion activation, and the same program can be used to generate all frequency swept waveforms, as described in this paper. Implementing ac frequency sweeps for all mass-selective operations is expected to extend mass range, decrease power consumption, and minimize the need for rf correction electronics needed for the precise analytical rf ramp.

Using the procedure in **Figure 6.1a** and the frequency sweep in **Figure 6.1b**, we were able to isolate caffeine from an LTQ calibration mixture (caffeine, MRFA, and Ultramark 1621) with high efficiency (~100%) and an apparent isolation width of ~2 - 3 Da (**Figure 6.2b**). The full scan is shown in **Figure 6.2a** for comparison. The peptide MRFA (*m/z* 524) could also be isolated with ~62% efficiency (**Figure 6.2c**), despite its low intensity relative to other peaks in the spectrum. Note that the scale in panel c has been magnified by a factor of 10.

In these experiments, several variables were altered, including the q_{iso} value at which the ion was isolated, the ac amplitude, the total time of the frequency sweep, the frequency sweep range, the number of bursts of the frequency sweep (that is, the number of consecutive applications of the isolation waveform), and the isolation window Δq. We found that optimal values were 4 ms sweep time from q = 0.908 to 0.05, q_{iso} = 0.83, three bursts, and Δq = 0.02. The reasoning for each of these choices is given below.

The isolation q value was varied (0.2, 0.5, and 0.83 were tested) and it was determined that a q_{iso} of 0.83 was optimal. Isolation using a sum of sines in the LTQ linear ion trap is also performed by placing the ion of interest at a q of 0.83 and applying the isolation waveform for ~13 ms,[103] so it is perhaps not surprising that the we obtained the best results at this value as well. Presumably, the pseudo-potential well depth is near a maximum value at 0.83, which makes

isolation easier since other ions will be more easily ejected. Ion secular frequencies are also quite far apart near the stability boundary, making the isolation of adjacent *m/z* species easier. In principle, however, isolation can be performed at other q values, but the isolation width and isolation efficiency will vary.

The ac amplitude is a key factor in an isolation experiment. The amplitude should be high enough to eject ions over a wide *m/z* range but not so high that the ion to be isolated is also ejected. **Figure 6.3a** shows the effect of varying the ac amplitude, which in our experiments was kept constant throughout each scan. Isolation widths of 2 - 3 Da could routinely be obtained with >90% isolation efficiency for any *m/z* value placed at q = 0.83, although higher ac amplitudes are needed for higher *m/z* ions because potential well depth increases approximately linearly with the rf amplitude according to the Dehmelt approximation.[144] For isolation of caffeine, increasing the ac amplitude beyond ~1.5 V_{pp} results in an improved isolation width at the cost of at least 50% of the analyte ions. Greater than an order of magnitude signal loss is observed when decreasing the isolation width (via ac amplitude increase) to < 1 Da. We should note that the effects of signal loss are amplified when the waveform isolation width Δq, specified in terms of Mathieu q units, is decreased, as shown in **Figure 6.3b**. In particular, only small decreases in isolation width are observed for large differences in Δq, but the corresponding loss of ion intensity is unacceptably high. We tried many variants of inverse Mathieu q scanning in order to obtain unit isolation width with near 100% efficiency, including varying the ac amplitude, varying the number of frequency sweeps and frequency sweep range, and implementing a coarse and then fine isolation window, but no combination resulted in unit isolation width without a considerable loss in signal intensity.

Figure 6.4 compares the variation in the user-defined isolation window Δq as well as the number of successively applied frequency sweeps. Each 'burst' is a single frequency sweep, and 'multiple bursts' implies consecutive application of the sweep. Panels (a) and (b) share the same number of frequency bursts but vary the isolation window width. Despite the narrower window, panel (b) still shows chemical noise that is also present in panel (a), which has a much wider window (0.02 vs .0002, in frequency units a window of 20 kHz vs. 0.4 kHz). Increasing the number of bursts, as in (c) and (d) gets rid of this chemical noise, but in the case of the narrower isolation width (d) also attenuates the ion signal by an unacceptable amount. Only 7.5% of the original signal remains. In contrast, for the wider isolation width, 92% of the original signal remains.

Because the number of bursts appears to be more important than a narrow isolation window and a high ac amplitude, we shortened the duration of the isolation sweep to 4 ms and applied 3 bursts, which made the total isolation time for this technique 12 ms, comparable to the 13 ms needed for isolation on the commercial LTQ. Fortunately, nearly 70% of the original ion intensity remains after isolation (**Figure 6.5a**), and an isolation width of ~3 Da is obtained. Because the waveform sweeps through phase space rather than frequency space, phase continuity is maintained and any arbitrary number of frequency hops (equivalent to 'notches' in SWIFT) can be incorporated, as in **Figure 6.5b** which shows the simultaneous isolation of both caffeine and MRFA (intensities should not be compared with panel a, separate full scans for each are not shown). Note that the isolation window in terms of Mathieu q units was not the same for the two ions. Presumably this is because 1) the ions are at different q values and thus have different potential well depths, 2) the higher *m/z* ions have secular frequencies that are much closer together than the low *m/z* ions, and 3) the amplitude of the ac waveform is kept constant (but can in principle be altered to any desired level at any time).

Collision-induced dissociation can also be accomplished using the inverse Mathieu q scan. For example, **Figure 6.6a** is a product ion mass spectrum from collision-induced dissociation of caffeine (and its carbon-13 isotope peak) at q = 0.3 using three bursts of an inverse Mathieu q scan from 0.15 to 0.908. Note that the direction of the frequency sweep is from low to high such that high *m/z* ions are first to fragment during the CID step, followed by low *m/z* ions later in the CID step. Because the precursor ion (*m/z* 195) is only on resonance for a very short period of time during the frequency sweep, very limited fragmentation is observed, even at higher ac amplitudes. To address this, we created a waveform which has a constant frequency set at the q value of the ion to be fragmented (q = 0.3 in this case) for 4 ms followed by an inverse Mathieu q scan from q = 0.3 to q = 0.908. Because the precursor ion is initially given more time at resonance, a higher intensity of fragment ions *m/z* 138, 110, etc. is observed (**Figure 6.6b**). However, the additional resonance time was not needed for noroxycodone (**Figure 6.6c**), which produced abundant fragment ions with three bursts of a 4 ms frequency sweep. Because the frequency sweep is such that ions are fragmented from high to low *m/z*, the inverse Mathieu q scan produces several generations of product ions and is hence a multigenerational CID technique.[171,172] This characteristic is clear in the product ion spectrum of noroxycodone, which in a typical MS^2 experiment loses only water to produce a highly abundant ion at *m/z* 284. Due to the

multigenerational capabilities of the inverse Mathieu q scan, the water loss product also fragments during the CID step, generating, for example, the MS[3]-like product ions at *m/z* 229 and *m/z* 187.

We should not assume the inverse Mathieu q scan, alone, is a generalizable method for CID because many unreactive ions simply will not fragment readily enough. Instead, the more generalizable method is that of **Figure 6.6b**. The ac frequency should first be fixed on the precursor ion of interest for a tunable period of time, during which the precursor ion fragments. Then, if multigenerational spectra are desired, the fixed ac frequency should be immediately followed by an inverse Mathieu q scan from low to high q. For the frequency sweep, the frequency range, amplitude, and sweep time should also all be tunable.

6.5   Conclusion

We have demonstrated efficient ion isolation using the inverse Mathieu q scan, with efficiencies approaching 100% for isolation widths of 2 - 3 Da, as well as multigenerational collision-induced dissociation using a reverse inverse Mathieu q scan, which scans from low to high frequency. The next step in this ongoing line of work is to fully implement the inverse Mathieu q scan for isolation, activation, and ejection on a miniature mass spectrometer.

For comparison, in conventional instruments, various ac waveforms (e.g. SWIFT, single frequency resonance excitation, resonance excitation with an analytical rf amplitude ramp, etc.) are used for isolation and activation and an analytical rf amplitude ramp effects the mass scan. The set of inverse Mathieu q scan techniques may be advantageous because, unlike most mass spectrometers, the same scan can accomplish all three steps of CID: isolation, activation, and ejection.

6.6   Acknowledgements
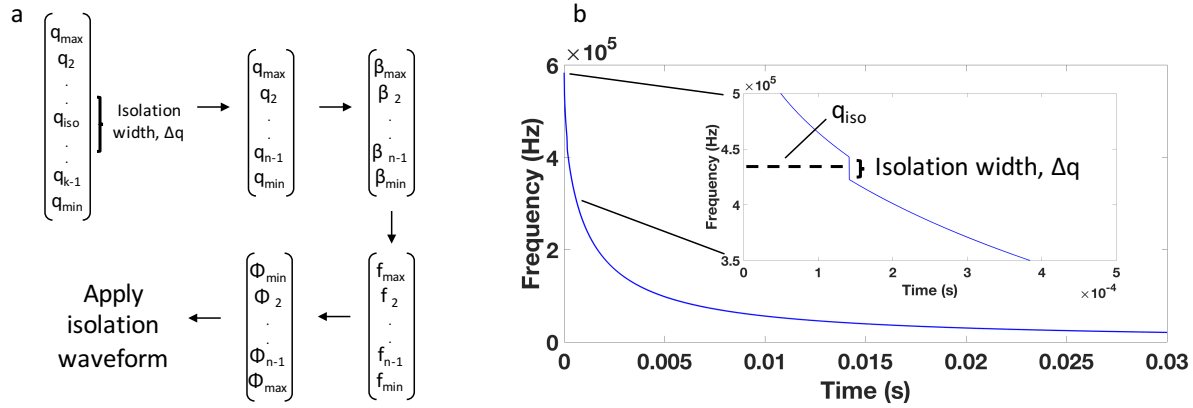
Figures

Figure 6.1. Waveform calculation for ion isolation in a quadrupole ion trap using the inverse Mathieu q scan: (a) an array of Mathieu q values is created and those values within the isolation range ($q_{iso} - \Delta q/2 < q < q_{iso} + \Delta q/2$) are removed from the array. The remaining q values are converted to β values and then to frequencies and finally phases. Panel (b) shows applied frequency as a function of time for an inverse Mathieu q isolation scan from q = 0.908 to q = 0.05 over 30 ms with an isolation notch at q = 0.83 and a width Δq of 0.02 (in Mathieu q units, equivalent to 20 kHz in frequency units). Inset emphasizes the frequency hop in the isolation waveform.
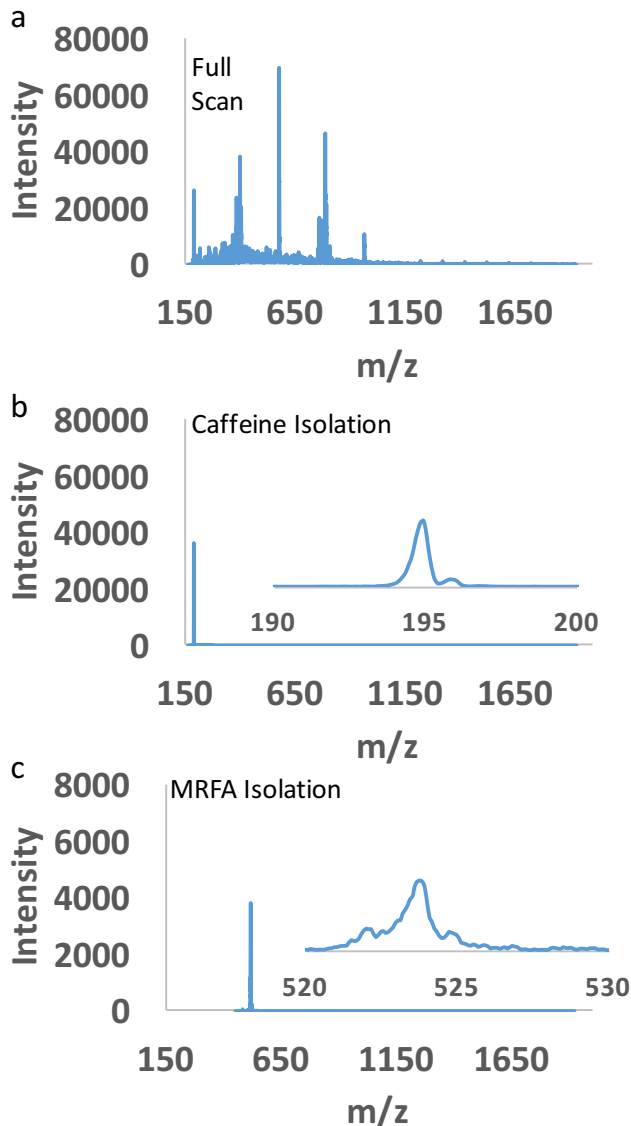
Figure 6.2. Ion isolation in a linear ion trap using the inverse Mathieu q scan. Panel (a) shows the full scan boundary ejection mass spectrum of a mixture of caffeine (*m/z* 195), MRFA (*m/z* 524), and Ultramark 1621 ions. In (b) caffeine is isolated with ~100% efficiency using four consecutive bursts of an inverse Mathieu q scan from 0.908 to 0.05, where each burst was 30 ms in length and 1.3 V_{pp}. In (c) the peptide MRFA is isolated with 62% efficiency using the same method with a 3.6 V_{pp} isolation waveform.
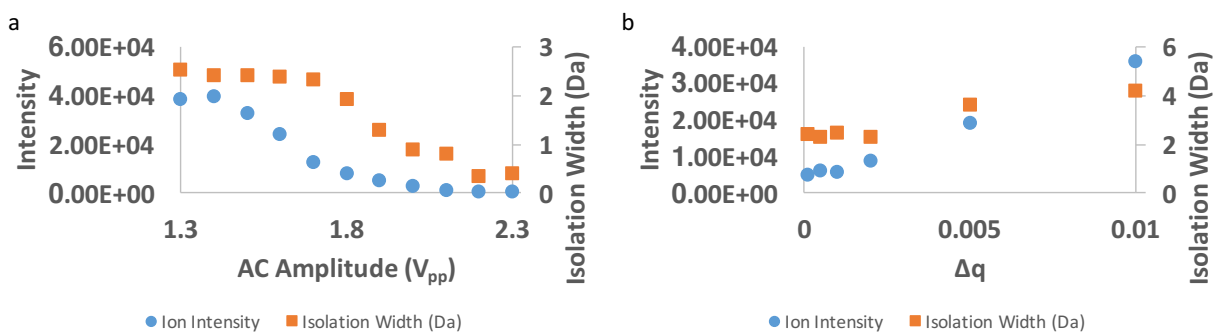
Figure 6.3. Effect of the (a) ac amplitude and (b) Δq of the inverse Mathieu q scan on isolation efficiency and isolation width. In this experiment, caffeine was isolated at a q of 0.83 while 4 bursts of a 30 ms inverse Mathieu q scan with a frequency hop ('notch') at q = 0.83 ($\Delta q = 0.02$ for panel a) was applied. For (b) the ac amplitude was constant at 1.3 V_{pp}.
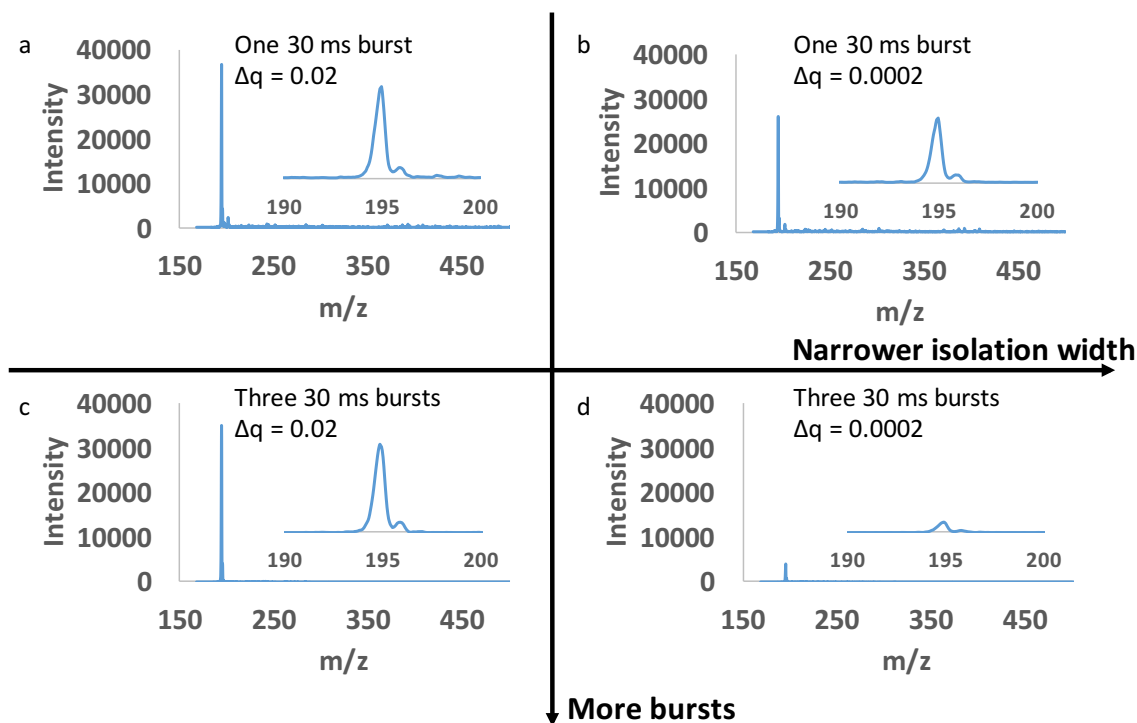
Figure 6.4. Effect of waveform isolation width Δq (in Mathieu q units) and number of bursts on isolation using the inverse Mathieu q scan. Isolation efficiency decreases drastically when the isolation width is decreased (b and d). However, increasing the number of bursts while using a relatively wide isolation width (c) retains the analyte ions while improving the isolation. In all cases, caffeine was isolated at a q_{iso} of 0.83 and the given number of bursts of a 1.3 V_{pp} isolation waveform was applied during isolation.
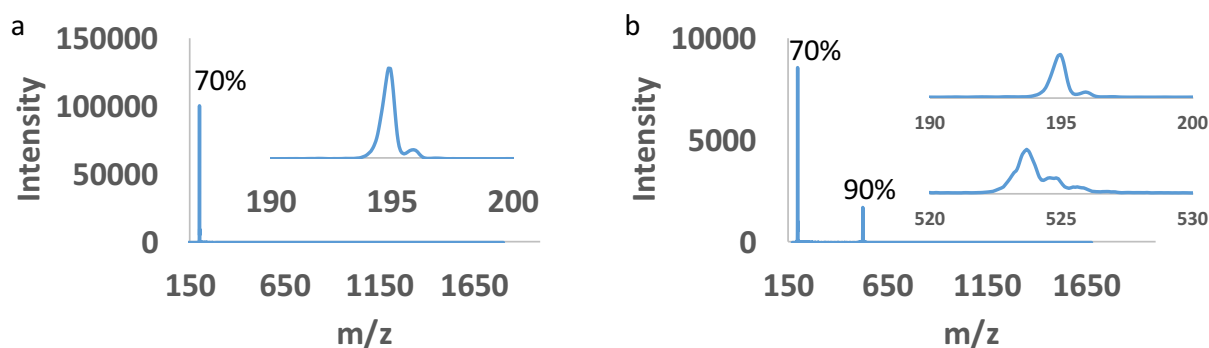
Figure 6.5. (a) Isolation of caffeine using a 1.3 V_{pp} inverse Mathieu q scan over 12 ms (three 4 ms bursts), showing retention of 70% of the analyte ions. (b) Dual notch isolation waveform of amplitude 3.2 V_{pp} using notches at q = 0.83 and 0.305 was used to isolate caffeine and MRFA simultaneously. The width of isolation for caffeine was 0.02 and was 0.04 (in Mathieu q units) for MRFA. Note that isolation efficiencies are calculated with respect to the full scan taken just before each respective experiment. The intensities in the two panels should not be compared.
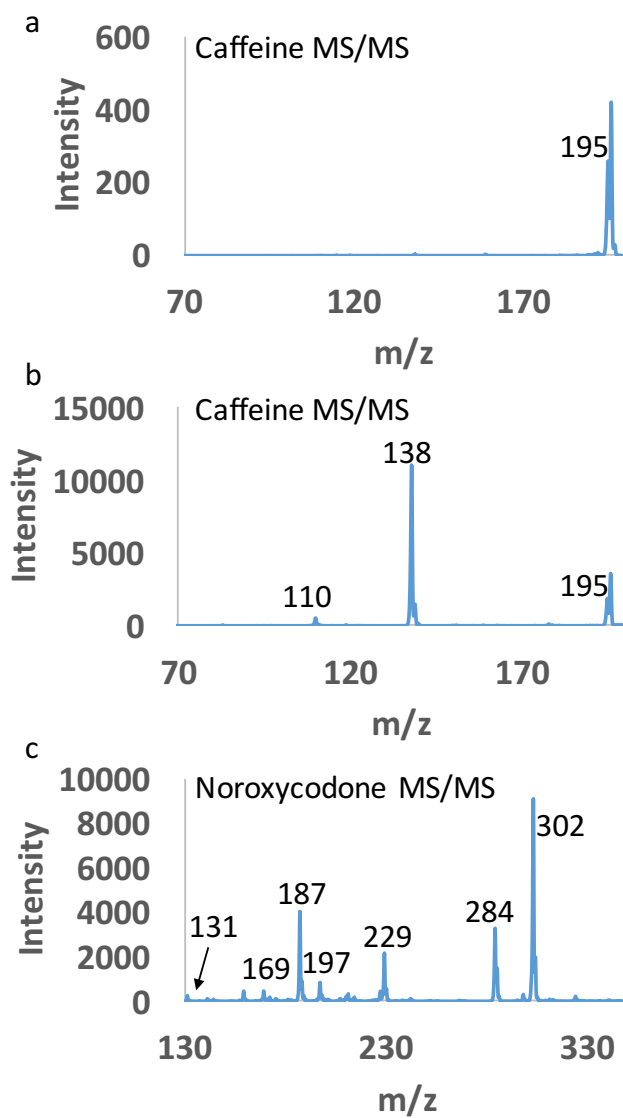
Figure 6.6. Multigenerational collision-induced dissociation using the inverse Mathieu q scan, following ion isolation using the technique in **Figure 6.1**: (a) inverse Mathieu q scan CID of caffeine using 3 bursts of a 4 ms scan with amplitude ~250 mV$_{pp}$, where caffeine was placed at q = 0.3. Very little fragmentation is observed because the precursor ion is not given much time at resonance. However, if the resonance waveform is altered so that the ac frequency stays on the resonance frequency of caffeine for 4 ms followed by a frequency ramp (b), then more efficient fragmentation is observed. In (c), the multigenerational capabilities of the inverse Mathieu q scan for CID are observed with noroxycodone. The precursor ion (*m/z* 302) first fragments at q = 0.3 by losing water (to *m/z* 284) (the lone product ion in MS^2), but the frequency scan also causes fragmentation of the water loss product, yielding MS^3-like ions as well.

CHAPTER 7.   EXTENDING THE MASS RANGE OF A MINIATURE ION TRAP MASS SPECTROMETER USING THE INVERSE MATHIEU Q SCAN

7.1   Abstract

The mass/charge range of a mass spectrometer operated in either the boundary or resonance ejection mode is usually limited by the highest radiofrequency (rf) voltage that can be attained, although lowering the resonance ejection Mathieu q value (q_{eject}) can increase this range at the expense of resolution and unintended boundary ejection can result in spectral complexity. High voltage requirements are particularly troublesome for miniature instruments, which have tight electronic constraints and closely-spaced electrodes prone to discharging. Here we demonstrate an alternative approach to mass range extension based on a method scanning the resonance ejection frequency nonlinearly in the form of an inverse Mathieu q scan. The results show an increase in mass range of up to 3.5 times on both a benchtop LTQ linear ion trap and the Mini 12 miniature linear ion trap mass spectrometer without instrumental modifications, and unit resolution is observed on the benchtop instrument by controlling the scan rate and minimizing space charge effects.

7.2   Introduction

Miniaturization of mass spectrometers has been the subject of extensive investigation over the past two decades, resulting in the development of more than thirty complete systems from both academic and commercial laboratories.[70,71,168] These devices can be designed for targeted or general applications ranging from environmental[72,173] and drug[174,175] screening to bacterial discrimination[176] and hazardous[177] or explosive[178] compound detection. For such applications, usually only modest performance is required – unit resolution over a mass range from 50 Da to < 1,000 Da and detection limits in the ppm range.

Ionization of complex samples for miniature mass spectrometers commonly is performed using either a spray- or plasma-based ambient ionization method due to the experimental simplicity; moreover, little to no sample workup is required. Common ambient spray sources are desorption electrospray ionization,[179,180] paper spray ionization,[100,181-183] leaf spray ionization,[72,184,185] and relay electrospray,[186] along with their closely related variants.[187,188] Plasma sources, though generally limited to volatile analytes,[189,190] include low-temperature plasma,[191-193] dielectric barrier discharge ionization,[194] and desorption atmospheric pressure chemical ionization.[195] In the experiments using pure samples or simple mixtures described here, nanoelectrospray ionization (nESI) sufficed.

The vacuum system is perhaps the most troublesome component for miniaturization because i) it is the most power-hungry subsystem and ii) small pumps inherently have small pumping capacities. Point (ii) is particularly cumbersome because mass analyzers require good vacuum in order to obtain high sensitivity and resolution. The standard configuration for miniature mass spectrometers is to use either a continuous membrane introduction interface,[196,197] an analytically limited option, or to use a discontinuous interface (i.e. DAPI or PP-API)[75,198] with a 5 L/min diaphragm pump and a 10 L/s turbo pump.[199] This latter choice provides analytical versatility and good performance at some cost in terms of analysis time. Continuous atmospheric pressure interfaces enabled by differential pumping do exist,[76,190] but they trade performance for continuity. Demonstrations of ion trap mass analysis at relatively high pressures, from 15 mtorr[200] up to ~1 torr,[74] signal possible reduction in the need for high performance pumps.

Ion traps are preferable to other mass analyzers in miniature instruments because they operate at higher pressure, their resolution does not *inherently* depend on device size, and they have capabilities for single analyzer tandem mass spectrometry.[71] Geometry is usually simplified in smaller traps for ease of fabrication,[69,201] as in cylindrical (simplified from 3D quadrupole ion trap [1]),[13,15,32,202,203] rectilinear[100,193,204] (linear 2D[10,11]), and halo[19,96,97] (toroidal[17,18,205,206]) ion traps.

The performance requirements of ion traps in miniature mass spectrometers usually include unit mass resolution with ppm or lower detection limits and a mass/charge range approaching *m/z* 1,000. Higher performance may be achieved without sacrificing simplicity and ease of operation. Resolution scales inversely with operating pressure and directly with rf frequency.[74,104,207,208] In addition, space charge effects will tend to increase with smaller traps,[209] and sensitivity also tends to degrade with pressure.

The subject of this paper is mass range, which in miniature ion traps is primarily determined by the maximum rf voltage ($V_{0-p,max}$) obtainable during the resonance ejection scan. The highest mass-to-charge value accessible for a linear ion trap is

$$m/z_{max} = 8V_{0-p,max} / q_x \Omega^2(x_0{}^2 + y_0{}^2) \qquad \text{Eq. 7.1}$$

where q_x is the Mathieu parameter at which the resonance ejection signal is set, Ω is the angular rf frequency, and x_0 and y_0 are the internal radii of the quadrupole field. Mass range in a quadrupole ion trap is additionally dependent upon i) the pressure in the device and in the ion optics and ii) the Dehmelt pseudo-potential well depth ($D_{x,y} = qV_{RF} / 4$) of analyte ions.[144] In general, in order to trap high m/z ions, a higher pressure must be used in order to collisionally cool the ions, which will tend to have high kinetic energies and low pseudo-potential well depths.

Experimentally, mass range can be extended by i) decreasing or scanning the main rf drive frequency,[46,47] ii) decreasing the size of the trap, or iii) decreasing the Mathieu resonance q_{eject} value (i.e. using a lower resonance frequency).[84,126] Both (i) and (ii) require instrumental modification, whereas (iii), resonance ejection, is the more common method due to its simplicity. However, resolution inevitably suffers at lower resonance q_{eject} values and spectral complexity from associated boundary ejection can be problematic. A fourth alternative, which is adopted in this study, is to scan the resonance ejection frequency at constant rf amplitude, viz. to perform a secular frequency scan.

In secular frequency scanning a linear ramp of the resonance ejection frequency is applied at constant rf amplitude and frequency.[106] Our original aim in exploring this scan was motivated by the possibility of performing very simple single analyzer precursor scans in a miniature mass spectrometer.[99] Although this type of precursor scan can be done, its performance is limited by the range of q values over which ions are fragmented. Nonetheless, we investigated the secular frequency scan (or ac scan) further as a simple alternative to resonance or boundary ejection. Even though resolution was shown to be inferior in these frequency scans, we will show here that it can be improved and unit resolution can be achieved on a benchtop instrument in instances where space charge effects are controlled and scan rate is lowered.

Two of the principal concerns with ac scanning are i) the effects of nonlinear resonance points and ii) the nonlinear relationship between m/z and secular frequency (and hence time). We showed that nonlinear resonance points resulted in either blank intensity profiles or broadened mass peaks, depending on scan direction.[106] However, in hyperbolic traps, these effects will tend

to be minimal. We also demonstrated the complex nonlinear calibration procedure needed for secular frequency scanning.[91] In this method, applied resonance frequencies are correlated to *m/z* through the Mathieu parameters q and β, and a final linear fit using calibration standards gives the correct calibration. Because calibration will change with rf amplitude, rf frequency, ac amplitude, and start and end ac frequencies, it is preferable to have a linear calibration procedure, which we have recently demonstrated.[133] In that work we showed that by scanning the frequency of the resonance ejection signal so that an inverse relationship between the Mathieu q parameter of the ejected ion and time is obtained, a linear relationship then exists between *m/z* and time, a feature which has been sought for years.

7.3   Experimental

7.3.1   Chemicals

Renin substrate tetradecapeptide (angiotensinogen 1-14), neurotensin, insulin-like growth factor fragment 3-40, bovine serum albumin, cesium hydrogencarbonate, and perfluoroheptanoic acid were purchased from Sigma-Aldrich Co. (St. Louis, MO, USA). Human Ghrelin was purchased from Phoenix Pharmaceuticals, Inc. (Belmont, CA, USA). Trimethylamine hydrochloride and polyethylene glycol (PEG) 4,400 and 14,000 were purchased from Aldrich Chemical Company, Inc. (Milwaukee, WI, USA). Concentrations for salts were ~2 mM in methanol/water. Bovine serum albumin was dissolved in water at 20 μg/mL. Polymers were dissolved in methanol/water at ~1 mM with 5,000 ppm triethylamine added as charge reducing agent. Peptides were dissolved in water to concentrations of ~200 μM.

7.3.2   Ionization

In all experiments ions were produced by nESI at ~1500 V using 5 μm nanospray tips pulled from borosilicate glass capillaries (1.5 mm O.D., 0.86 I.D., Sutter Instrument Co.) by a Flaming/Brown micropipette puller (Sutter Instrument Co. model P-97, Novato, CA, USA).

7.3.3   Instrumentation

Experiments were performed using both a benchtop Thermo LTQ[10] linear ion trap mass spectrometer (San Jose, CA, USA) as well as the Mini 12[100] miniature mass spectrometer developed in-house at Purdue University.

For conventional resonance ejection scans on the LTQ, the rf frequency was tuned to 1.175 MHz and built-in scan functions were used with automatic gain control (AGC) turned on. The "normal" scan rate is 16,666 Da/s at an ejection frequency of 490 kHz, whereas the "high mass" (i.e. low q resonance ejection) scan uses a lower scan rate of 2,500 Da/s at 200 kHz (q = 0.46) which increases the upper mass/charge limit from 2,000 Th to 4,000 Th (Th = Thomson = mass-to-charge).

The inverse Mathieu q scan was performed using the LTQ by substituting a swept frequency resonance ejection signal for the LTQ's built-in fixed resonance signal during an Ultrazoom scan with a given lower mass cutoff (LMCO) (proportional to the rf amplitude). As we have described previously, the Ultrazoom scan is a very slow scanning method that allows the rf amplitude to remain nearly constant. We chose this scan method because, of all the built-in scans on the LTQ, the Ultrazoom scan most closely approximates constant rf amplitude conditions.

The resonance ejection signal was constructed in Matlab using the algorithm previously described.[133] Briefly, the resonance frequency is scanned to maintain an inverse relationship between Mathieu q and time, thereby giving a linear mass scan. The waveform was imported to an arbitrary waveform generator (Keysight 36612A, Newark, SC, USA) with sampling rate set to 10 MSa/s. The ac waveform was triggered at the beginning of the mass scan using the triggers in the LTQ Tune diagnostics menu. In general, the scan time was 0.3 s and the highest and lowest Mathieu q values interrogated were 0.908 and 0.05. The amplitude of this resonance signal was generally 2-10 V_{pp}. Automatic gain control (AGC) was turned off during the inverse Mathieu q scan to prevent triggering the ac waveform on the AGC scan. Data were collected using either the built-in hardware and software of the LTQ or, in cases where resolution was of interest or where a higher density of data points was desired, as a differential signal from the LTQ electrometer board (collected with an oscilloscope, Tektronix TDS 2024C, Beaverton, OR, USA).

For scans using the Mini 12 mass spectrometer (rf frequency = 0.999 MHz), the waveform generator was triggered using a high frequency ac waveform output from the ac/waveform board. The discontinuous atmospheric pressure interface was held open for 12 ms and the collisional cooling time was set to 300 ms. The Mini 12 data collection system was sufficient for the inverse Mathieu q scan.

All spectra were calibrated by comparing mass spectral peak locations in cesium tridecafluoroheptanoic acid clusters[145] to standard spectra obtained using the LTQ's "high mass" scan (low q resonance ejection).

7.4   Results & Discussion

7.4.1   Mass range extension using a benchtop mass spectrometer

In this study we are concerned with extending the mass range of a mass spectrometer *without instrumental modifications*. That is, the goal is to increase mass range while keeping rf amplitude within readily achievable ranges and maintaining the rf frequency and trap size at constant and typical values.

Figure 7.1 compares several spectra obtained by low q resonance ejection (left column) with data acquired using the inverse Mathieu q scan (right) on a commercial LTQ linear ion trap. Panels (a) and (b) compare typical spectra obtained for bovine serum albumin (66 kDa). The two spectra are nearly identical in terms of the charge state profile and resolution. Because the scan rate in the inverse Mathieu q scan is much higher (82,000 Da/s compared to 2,500 Da/s), fewer ions are lost (e. g. to charge transfer to the background gas) before they are ejected, therefore resulting in higher sensitivity and observation of more charge states. The inverse Mathieu q scan requires a fairly high LMCO in order to observe these ions. The higher LMCO will increase these ions' Mathieu q values, which i) increases their potential well depth so they are not removed from the trap prematurely by the constant amplitude frequency sweep, and ii) puts them within the Mathieu q range of the scan, which here was set from 0.05 to 0.908. That is, ions with q values below 0.05 will not be detected, though in practice the q range can be extended even further.

It is also important to note that for a given frequency sweep the scan rate, scan range, and resolution will depend on the rf amplitude, the rf frequency, and the trap size. Since the rf amplitude is the only adjustable parameter, it will determine the scan rate and scan range. A higher LMCO (i.e. rf amplitude) will increase the mass range but it will also increase the scan rate. In contrast, in the resonance ejection experiment, the scan rate is constant; it is set by the rate of change of the rf amplitude with respect to time as well as the resonance q parameter, trap size, and rf frequency. The total scan time for a resonance ejection scan will thus increase with the mass range.

The uppermost m/z value will additionally be limited by the ac amplitude, which here is kept constant. Higher ac amplitudes are typically needed to eject ions of higher mass, despite their lower pseudo-potential well depth, but ac amplitudes that are too high will tend to eject these ions before their resonance conditions are met, decreasing the *apparent* mass range.

Figure 7.1 panels (c) and (d) compare spectra of cesium tridecafluoroheptanoic acid (CsTFHA) clusters. While the mass range of the low q resonance ejection scan has a maximum of ~m/z 4,000, which is determined by the maximum rf amplitude, the inverse Mathieu q scan has a (theoretically) limitless range. In fact, mass range will be limited by other factors, particularly pressure and pseudopotential well depth. Clusters beyond m/z 7,000 were detected using the ac frequency scan. Despite the higher scan rate of 52,300 Da/s, the frequency scan results in nearly identical resolution to resonance ejection, which had the much more favorable slow scan rate of 2,500 Da/s. Note that the inset of panel (d) was observed using an oscilloscope. The apparent resolution of the full mass scan is much lower because the built-in data system of the LTQ significantly undersamples the data.

Panels (e) through (h) show mass range extension applied to polymer analysis. Polyethylene glycol 4400 (PEG4400, MW = 4,400 Da) and PEG14000 (MW = 14,000 Da) were charged reduced using trimethylamine and subsequently analyzed by low q resonance ejection and the inverse Mathieu q scan. As above, the commercial low q resonance ejection mass scan has a maximum m/z of 4,000 Th and thus fails to detect the +1 charge state of PEG4400 and the +1/+2 charge states of PEG14000. However, we were able to detect these ions using the inverse Mathieu q scan *without changing the rf frequency, ion optics, trap size, or pressure*. In panel (f) the +1 charge state of PEG4400 is detected, though a relatively high LMCO (rf amplitude) is again required. The +2 charge state of PEG14000 is shown in panel (h). These data were observed using an external oscilloscope with memory limited to 2,500 points (but variable sampling rate), so only a small mass range is observable per scan.

While the mass range of a resonance ejection frequency sweep (i.e. inverse Mathieu q scan) is limitless theoretically, there are practical limitations. We were able to observe ions with $m/z >$ 10,000 on the benchtop instrument, which is shown in **Figure 7.2**. The +1 charge state of PEG14000 was observed, though the signal-to-noise is relatively low. This is a 5x improvement over conventional resonance ejection and a 2.5x improvement over the commercial low q

resonance ejection scan. While the *m/z* values appear too low, the difference in *m/z* between the peaks is 44 Th, which does indicate the presence of the +1 charge state.

7.4.2 Summary of comparison of inverse Mathieu q scans to low q resonance ejection

Given that low q resonance ejection is perhaps the most comparable method to the inverse Mathieu q scan, comparisons should be made. These are summarized in **Table 7.1**, which shows calculated scan rates, low and high mass limits obtained from the experimental calibration of CsTFHA clusters, and resolution achieved for selected peaks using either resonance ejection at the given frequency or the inverse Mathieu q scan. This analysis was performed for data acquired using the commercial benchtop LTQ.

For the same rf voltage ramp, scan rate will increase when the resonance ejection q value (frequency) is lowered, which is in agreement with the Mathieu equations. Loss of low mass ions is modest because there is only a small fraction of the ion population with high q values. The increase in scan rate and selection of non-optimal values for ejection q results in resolution degradation, as one would expect. However, although the inverse Mathieu q scan loses ions at the low mass end of the spectrum (in order to bring high *m/z* ions within the scan range set from Mathieu q of 0.908 to 0.05), the mass range is extended without loss of resolution if the scan rate and space charge are controlled. Nearly unit resolution is obtained (**Figure 7.1b**, inset) despite the high scan rate and large mass range. Given that the peak width in inverse Mathieu q scans has been shown to be nearly constant as a function of *m/z*,[133] we believe that unit resolution is achieved throughout the mass spectrum. The mechanism of resolution improvement using the inverse Mathieu q scan is not currently known.

Note that in **Figure 7.1b** space charge was carefully controlled, whereas it was not controlled in many of the other frequency scan spectra because automatic gain control was not available in the frequency scan mode. In addition, the scan rate varies a great deal as a function of rf amplitude, so the resolution between scans will vary due to the difference in scan rate. For example, peak width in **Figure 7.1f** was approximately 6 Da, which was 6 times higher than **Figure 7.1e**. However, the scan rate in the former was ~40 times higher, so the comparison between these two spectra is not fair.

The case for the inverse Mathieu q scan is made even clearer by considering other factors. No linear rf ramp is needed in this scan, which is particularly appealing for miniature instruments

since rf correction is often troublesome and requires specialized circuitry. In addition, the potential for discharges is mitigated, and, unlike resonance ejection at low q, there are no interferences from boundary ejection. Also, unlike other frequency scan methods (specifically rf frequency scanning), resolution is maintained at high mass since the rf frequency is constant, and, furthermore, mass calibration is linear when using the inverse Mathieu q scan. In contrast, when scanning the rf frequency, the resolution will degrade at lower rf frequencies (high *m/z*) because ions have fewer cycles through the rf field[210,211] and the mass calibration will inherently be nonlinear unless the drive frequency is scanned nonlinearly. Since many instruments already have software and electronics for complex waveform calculation and synthesis (e.g. the stored waveform inverse Fourier transform, which is implemented on the Mini 12), the inverse Mathieu q scan merely requires software implementation rather than hardware changes (aside from waveform memory expansion, perhaps).

The inverse Mathieu q scan, may, however, complicate the instrument electronics if the impedance or frequency response of the electronics and electrodes is variable as a function of frequency. This would result in a variable ac amplitude as a function of time, which would affect mass accuracy, mass resolution, and sensitivity. The frequency sweep on an LTQ linear ion trap was measured from both the x and y electrodes (note that in these experiments only the x electrodes were used for ejection). **Figure 7.3** shows the measured oscilloscope traces in green and yellow. In both cases, the amplitude of the ac waveform is constant throughout the scan except for a very small portion at the highest frequencies where the amplitude decreases slightly. Given that very few ions reside at these highest frequencies, we expect that the change in impedance as a function of frequency has a minimal effect on the spectra presented here.

7.4.3   Mass range extension using a miniature mass spectrometer

In the conventional resonance ejection mode at a Mathieu q value of ~0.81, the mass range of the Mini 12 mass spectrometer is limited to < *m/z* 1,000.[176] Gao *et al.* showed extension of this range to *m/z* 1,300 by lowering the rf frequency on the Mini 11,[212] which uses similar electronics.

The inverse Mathieu q scan was easy to translate to the Mini 12. The rf frequency on the Mini 12 is 999 kHz, which is lower than the LTQ's 1.175 MHz, and the pressure in the trap is substantially higher during ion injection, so high mass ions ought to be easier to trap. The only instrumental parameter that was altered was the rf amplitude during ion injection, which was

increased by ~30% from normal scans on the Mini 12 in order to successfully trap ions of high *m/z*. The custom inverse Mathieu q frequency sweep was triggered on the Mini 12 by outputting a high frequency (kHz) ac signal from the Mini 12 ac/waveform board to an external function generator, and a scan time of 0.3 s was used, the same as that applied to the LTQ (although the duty cycle on the Mini 12 was much reduced because of the need to close the DAPI value to achieve requisite vacuum for mass analysis).

Figure 7.4 shows the results of the inverse Mathieu q scan on the Mini 12 for the same analytes as shown in **Figure 7.1**. Panel (a) is the mass spectrum of bovine serum albumin. Resolution is degraded by the higher order fields, lower rf frequency, increased space charge effects, and the pressure in the trap, but charge states are resolved. Mass range extension up to > *m/z* 2,000 was observed. Note that the ions around *m/z* 600 were also observed on the LTQ, but were not shown in the corresponding figure. The charge states appear to be substantially lower on the Mini 12, a feature which will be discussed later.

Panel (b) is the mass spectrum of CsTFHA clusters. For this experiment, the ion transfer capillary (at atmospheric pressure) was heated by wrapping it with heating tape in order to increase the desolvation of these clusters. However, the highest *m/z* observed was *m/z* 1,100, which represents only a modest increase in mass range. This is likely due to the ion source conditions in the Mini 12, not the mass scan.

The analysis of polymers PEG4400 and PEG14000 in panels (c) and (d), respectively, was more successful. Scan rates were 21,600 Da/s and 24,500 Da/s, respectively (compared to the conventional resonance ejection scan rate of 3,000 Da/s). In the case of PEG4400, charge states +2 through +5 were detected, although peaks were not necessarily resolved. The highest observed *m/z* was approximately ~2,500 Th in this scan. For PEG14000, both the +11 and +4 charge states were detected for a maximum detected *m/z* of 3,500 Th, an extension of 3.5x over conventional resonance ejection.

7.4.4 Comparison between LTQ and Mini 12

There are several differences observed in the spectra when comparing LTQ data (**Figure 7.1**) to Mini 12 data (**Figure 7.4**). For one, unit resolution is not obtained from the Mini 12, which is expected due to the imperfections in trap geometry, pressure, lower rf frequency, high scan rate, and increased space charge effects in a miniature trap. The LMCO (rf amplitude) on the Mini 12

was, in general, lower because of its lower rf frequency (0.999 MHz compared to the LTQ's 1.175 MHz). The same mass range could be achieved with a lower rf amplitude because of this. However, other differences, namely in vacuum and source conditions, result in more nuanced differences in performance.

Regarding differences in vacuum conditions, the LTQ uses differential pumping to transfer ions from atmospheric pressure (760 torr) to ~1 torr in the transfer optics just beyond the source and finally to ~mtorr or less in the ion trap itself. This process would be expected to be much gentler than the corresponding journey on the Mini 12, where ions go from 760 torr to ~mtorr or lower pressures over a very short distance, the length of the inlet capillaries. This harsher transfer will tend to cause fragmentation (as is well known) and to unfold proteins and polymers, resulting in higher charge states, which is evident when comparing **Figure 7.4a** to **Figure 7.1a**. We also analyzed the peptides renin substrate tetradecapeptide (angiotensinogen 1-14), neurotensin, insulin-like growth factor fragment 3-40, and human ghrelin and observed higher charge states (not shown).

The second major difference between the benchtop and miniature instrument is found in the ion source. Nanoelectrospray ionization was used in both cases, but the ion transfer capillary on the LTQ is heated, whereas it is not on the Mini 12. There is also no curtain gas, sheath gas, or skimmer/tube lens system on the Mini 12, so desolvation will be inherently less efficient than on the LTQ, resulting in lower sensitivity and more difficulty in generating dry clusters (**Figure 7.4b**). Regardless, the improvement in mass range here was approximately 3.5x when compared to conventional resonance ejection at high q.

7.5 Conclusion

We have demonstrated mass range extension using the inverse Mathieu q scan on both a benchtop and a miniature mass spectrometer. This required no instrumental modifications – only implementation in software for systems that already synthesize complex injection/isolation/activation waveforms – and it maintained linear mass calibration. The ease of implementation on a miniature mass spectrometer will be determined by the frequency response of the electronics and trap electrodes, but in the case of the LTQ studied here near-flat frequency response was observed.

The inverse Mathieu q scan was shown to increase the mass range of a benchtop mass spectrometer by almost 2.5x and increase the mass range of a miniature instrument by 3.5x over conventional and low q resonance ejection without altering the rf frequency or trap size. Despite the high scan rate and unconventional method, unit resolution was achieved on the LTQ under conditions in which the scan rate and space charge were controlled, matching the resolution obtained by resonance ejection using a lower scan rate.

7.6 Acknowledgements
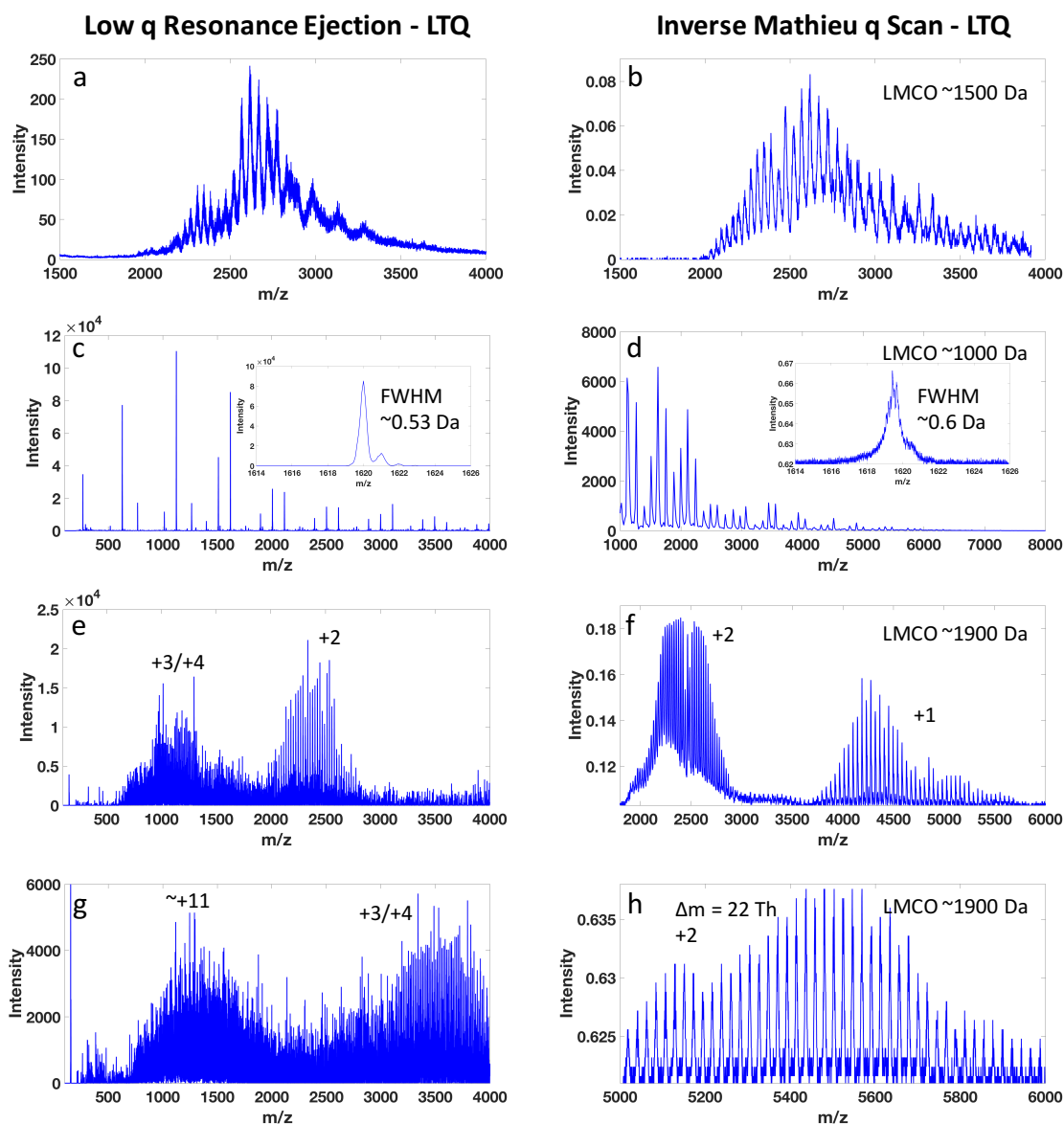
Figures

Figure 7.1. Mass range extension using a benchtop LTQ linear ion trap mass spectrometer by (a), (c), (e), (g) low q resonance ejection at q = 0.46 and (b), (d), (f), (h) the inverse Mathieu q scan with the given LMCO. Analytes were (a), (b) bovine serum albumin (66 kDa), (c), (d) cesium tridecafluoroheptanoic acid clusters with inset resolution, (e), (f) polyethylene glycol 4,400 (MW = 4,400 Da), and (g), (h) polyethylene glycol 14,000 (MW = 14,000 Da). Note the apparent resolution in the full MS in (d) is lower than the actual resolution because the data system undersamples the spectrum.
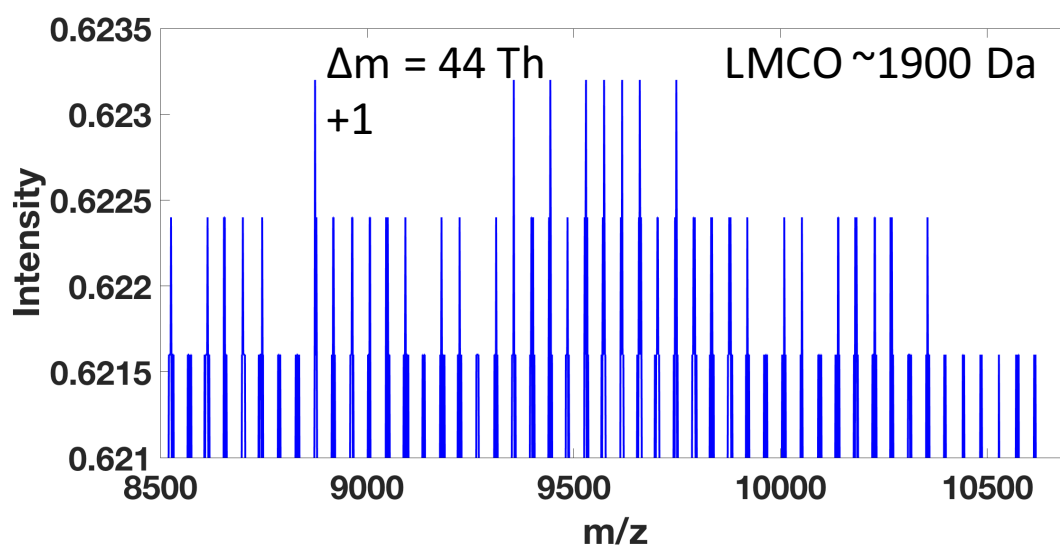
Figure 7.2. LTQ mass spectrum of the +1 charge state of polyethylene glycol 14,000 (MW = 14,000 Da) using the inverse Mathieu q scan, showing peak separations by 44 mass units and mass range extension to > *m/z* 10,500.
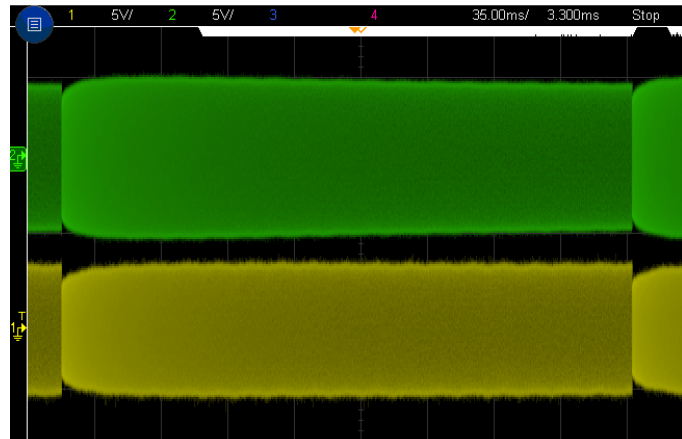
Figure 7.3. Oscilloscope trace of inverse Mathieu q scan measured on the x (green) and y (yellow) electrodes showing change in amplitude as a result of the frequency response of the electronics. Horizontal axis is time (300 ms frequency sweep) and vertical axis shows ac voltage. Rf voltage was off during the measurement.
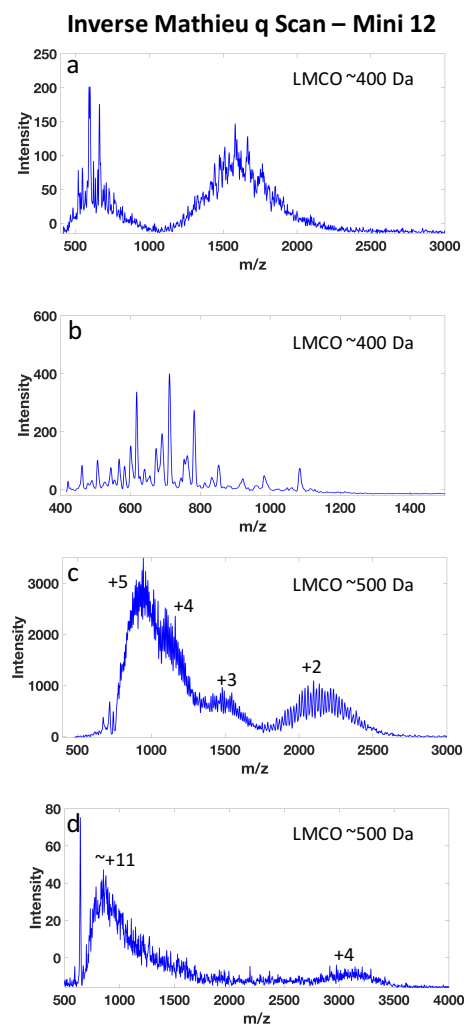
Figure 7.4. Mass range extension on the Mini 12 miniature mass spectrometer using the inverse Mathieu q scan. Mass spectra of (a) bovine serum albumin, (b) cesium tridecafluoroheptanoic acid clusters, (c) polyethylene glycol 4400, and (d) polyethylene glycol 14000. The scan rate in (a)/(b) and (c)/(d) was 21,600 Da/s and 24,500 Da/s, respectively.

Table 7.1. Comparison of scan parameters and results for mass range extension by low q resonance ejection and inverse Mathieu q scan*

Resonance Frequency (kHz)	q_{eject}	Scan Rate (Th/s)	Low Mass (Th)	High Mass (Th)	Peak Width at m/z 1620 (FWHM)	Resolution at m/z 1620 (FWHM)
490	0.88	16,700	**50**	2,000	0.7501	2159.712038
390	0.78	18,600	57	2,240	1.12	1446.428571
290	0.63	23,100	72	2,775	1.55	1045.16129
190	0.44	33,290	110	4,000	1.34	1208.955224
90	0.21	112,000	254	13,000	3.5	462.8571429
Inverse Mathieu q Scan†	Variable (0.50)	52,300	900	**16,600**	**0.63**	**2571.428571**

*The analysis was performed on a benchtop LTQ linear ion trap and the analytes were CsTFHA clusters.

† See inset in Figure 7.1. q_{eject} is variable as a function of *m/z*, and *m/z* 1620 was ejected at q_{eject} = 0.50

CHAPTER 8.   UNIQUE CAPABILITIES OF AC FREQUENCY SCANNING AND ITS IMPLEMENTATION ON A MARS ORGANIC MOLECULE ANALYZER ION TRAP

8.1   Abstract

A limitation of conventional quadrupole ion trap scan modes which use rf amplitude control for mass scanning is that, in order to detect a subset of an ion population, the rest of the ion population must also be interrogated. That is, ions cannot be detected out of order; they must be detected in order of either increasing or decreasing mass-to-charge (*m/z*). However, an ion trap operated in the ac frequency scan mode, where the rf amplitude is kept constant and instead the ac frequency is used for mass-selective operations, has no such limitation because any variation in the ac frequency affects only the subset of ions whose secular frequencies match the perturbation frequency. Hence, an ion trap operated in the ac frequency scan mode can perform any arbitrary mass scan, as well as a sequence of scans, using a single ion injection; we demonstrate both capabilities here. Combining these two capabilities, we demonstrate the acquisition of a full mass spectrum, a product ion spectrum, and a second-generation product ion spectrum using a single ion injection event. We further demonstrate a "segmented scan" in which different mass ranges are interrogated at different rf amplitudes in order to improve resolution over a portion of the mass range, and a "periodic scan" in which ions are continuously introduced into the ion trap to achieve a nearly 100% duty cycle. These unique scan modes, along with other characteristics of ac frequency scanning, are particularly appropriate for miniature ion trap mass spectrometers. Hence, implementation of ac frequency scanning on a prototype of the Mars Organic Molecule Analyzer mass spectrometer is also described.

8.2   Introduction

The development of miniature mass spectrometers has spanned several decades, from the fabrication of the first miniature ion trap mass analyzers[15,69,209,213] to the commercial release of

small vacuum pumps.[199] These two advances bookmark a series of developments that led to the decrease in size of the entire mass spectrometer from hundreds of pounds, still typical of most benchtop systems, to miniature systems weighing 4 – 25 kg.[70,71,214] Despite the years of development and hundreds of papers on the topic,[71] miniature mass spectrometers are just now beginning to join the mainstream market with applications ranging from pharmaceuticals,[7] to forensics[215,216] to planetary exploration.[50,138,139,217]

The quadrupole ion trap (QIT) is the most popular mass analyzer for miniature systems because of its tolerance for poor vacuum and electrode imperfections, while still exhibiting high sensitivity and providing tandem mass spectrometry (MS/MS) capabilities. Many variants of the device have been fabricated, such as 2D and 3D traps,[1,2,11,218] cylindrical structures,[13,15,219,220] the rectilinear ion trap,[204] and toroidal and halo traps[17-19,97,205,206,221,222]. Even so, the method of operating individual traps has changed surprisingly little in the past 30 years. Conventionally, the trapping radiofrequency (rf) amplitude is ramped (increased) linearly over the time of the mass scan, thereby ejecting ions when their trajectories become unstable, either at the Mathieu stability boundary or at the frequency corresponding to a supplementary resonance ejection (ac) signal.

Frequency scanning technologies also exist, most notably in the digital ion trap (DIT).[86-88,151,223-229] These mass analyzers use high-frequency switching technology to alternate between HIGH and LOW voltage states. Because the duty cycle and the period of the main trapping waveform can easily be manipulated with high precision, ion isolation, collision-induced dissociation, and mass scanning can all be performed with relatively simple electronics. These versatile technologies are certainly promising, but they have yet to see commercialization.

A second frequency scanning technology that has recently emerged is the "secular frequency scan",[19,49,106] in which the trapping parameters are kept constant and instead the supplementary ac frequency is ramped through the ion secular frequencies. This mode of operation is particularly amenable to miniaturization because the electronics are simplified compared to the rf amplitude ramp case: the rf does not need to be varied during the mass scan, and lower rf amplitudes can be used to access higher mass-to-charge (*m/z*) values.[50] Unfortunately, there is a nonlinear relationship between *m/z* and the ac frequency, thus degrading resolution at low Mathieu q and requiring complicated calibration procedures.[91] Alternatively, the ac frequency can be scanned nonlinearly using the "inverse Mathieu q scan" to give an approximately linear

relationship between *m/z* and time,[133] though small frequency-dependent mass shifts preclude an ideally linear relationship.[230]

Certainly, the ability to obtain nearly linear mass spectra using a ramp of the low voltage supplementary frequency is an important step in the development of miniature instruments. The electronics needed do not require a complete overhaul of already-existing systems, as adoption of digital technology would, and, more importantly, the trapping conditions are constant during the mass scan. As we will show here, this unique characteristic of ac frequency scanning allows quadrupole ion traps to be operated in modes either unavailable to or analytically challenging for devices where the trapping conditions vary (that is, when the range of stable masses varies with the scanning parameter, whether trapping voltage or frequency). These new scan modes include the previously-described periodic (continuous) frequency scan[231] as well as three new modes described here: the *arbitrary mass scan*, the *multiscan* and the *segmented scan*. We further describe the first implementation of ac frequency scanning using a Mars Organic Molecule Analyzer prototype mass analyzer, for which the ac frequency scan is a particularly appropriate choice.

8.3   Experimental

8.3.1   Chemicals

Cesium hydrogencarbonate, tridecafluoroheptanoic acid, monobutyl phthalate, and perfluorotributylamine were purchased from Sigma-Aldrich Co. (St. Louis, MO, USA). Cesium hydrogencarbonate and either tridecafluoroheptanoic acid or monobutyl phthalate were dissolved in methanol/water at 2 mM and used to produce cluster ions from electrospray ionization.[145] Pierce ESI LTQ calibration solution containing caffeine, the peptide MRFA, and Ultramark 1621 was purchased from Thermo Fisher (Rockford, IL, USA).

8.3.2   Instrumentation

Scans were developed using a Thermo LTQ linear ion trap mass spectrometer (San Jose, CA, USA) at Purdue University. Ions were produced by nanoelectrospray ionization (nESI) using a voltage of 2 kV. Nanospray tips (5 μm diameter) were pulled from borosilicate glass capillaries (1.5 mm O.D., 0.86 I.D.) using a Flaming/Brown micropipette puller (Sutter Instrument Co., model P-97, Novato, CA, USA). Constant rf amplitude conditions were closely approximated using "Ultrazoom" scans wherein the rf amplitude is slowly ramped at the minimum allowed rate of 27

Da/s. Without access to the proprietary Ion Trap Control Language (ITCL) the rf amplitude cannot be held precisely constant during the mass scan segment.

AC frequency scanning waveforms were constructed in Matlab[133] and imported to a Keysight 33612A arbitrary waveform generator (Newark, SC, USA). The sampling rate was set to 10 MSamples/s. AC waveforms were triggered at the beginning of the mass scan using the triggers in the LTQ Tune diagnostics menu. An oscilloscope (Keysight InfiniiVision MSOX3024T) was used to collect the differential output signal from the electrometer board using test points 'TP7' and 'TP8'. Note that because a *differential* signal was obtained from the LTQ, reported signal intensities can be negative, but the sign of the signal has no physical meaning with respect to the measured mass spectra. All spectra are the average of at least 10 scans.

A Mars Organic Molecule Analyzer (MOMA) prototype instrument, developed at NASA Goddard Space Flight Center (GSFC), was used for later portions of this work. The mass analyzer internal to this instrument is identical to the design of the final MOMA instrument being built for operation on Mars.[139] MOMA is a key organic detection instrument on the ExoMars rover which is based around a linear ion trap (LIT) mass spectrometer. MOMA will analyze samples using two independent ionization sources, an electron ionization (EI) source coupled to a pyrolysis oven and gas chromatograph (pyr/GC) and a laser desorption ionization (LDI) source for direct analysis of crushed rock samples. All of the MOMA data presented here were collected in the EI mode, although the described techniques are equally applicable to the LDI mode of operation. The MOMA LIT design and geometry is derived from the Thermo LXQ instrument,[232] a discontinued model of the popular LTQ instrument. The primary difference is that the LXQ (and by extension MOMA) is the use of a single set of hyperbolic rod segments to define the ion trapping region rather than the three segments as used in the LTQ configuration. The MOMA LIT is further differentiated from the LXQ as the primary radial trapping dimension (r_0) for the MOMA LIT was chosen to be 3 mm versus 4 mm for the later Thermo design and the rod length is 27.75 mm instead of the later 37 mm. This choice serves to decrease the analyzer mass and volume (a 25% reduction for all dimensions compared to the LXQ), which is desirable for a space-based mission, but more importantly, it reduces the RF power requirements necessary for achieving a given mass range. The MOMA prototype instrument is controlled by custom software (RITS, Danell Consulting) written in National Instruments LabVIEW (Austin, TX) and driven by a combination of custom and commercial RF and DC voltage supplies.[233]

8.4   Results & Discussion

There are five general methods for obtaining a mass spectrum using a quadrupole ion trap: 1) scanning the rf voltage, 2) scanning the rf frequency, 3) varying the trap radius, 4) scanning the quadrupolar dc voltage, and 5) scanning a resonance excitation (ac) frequency. The common feature of methods 1) – 4) is that the variation in scanning parameter changes the stable mass range in the ion trap. It is thus impossible, using one of these four techniques, to interrogate a subset of the ion population in the trap without also interrogating (i.e. changing the Mathieu parameters of) the rest of the ion population. For example, to scan an ion out using an analytical rf voltage ramp, not only does the ion of interest get ejected, but other ions on the scan line are also ejected as they approach the stability boundary. Moreover, the secular frequencies of all the ions in the trap vary as a function of the scanning parameter.

By contrast, scan method 5 is unique because the trapping conditions do not change as a function of the varied ac frequency. Only the subset of ions whose secular frequencies match the perturbation frequency are affected. No other ions are excited, and their secular frequencies (defined by their Mathieu a and q values) are static. This characteristic – constant trapping conditions – makes possible new quadrupole ion trap scan modes which are not accessible, or at best are analytically complex, using any of the other scan methods.

8.4.1   The arbitrary mass scan

We begin with the "arbitrary mass scan" in which the ac frequency is scanned such that ions are detected out of order (i.e. not strictly from low to high mass-to-charge). **Figure 8.1a** shows an example of a typical full ac scan mass spectrum of cesium tridecafluoroheptanoic acid (CsTFHA) clusters recorded using nanoESI on the LTQ at Purdue. Because the ac frequency is scanned (via an inverse Mathieu q scan) from high frequency to low frequency, the mass spectrum is recorded from low m/z to high m/z, with an approximately linear relationship between m/z and time.

A limitation of scans based on changing boundary conditions (e.g. rf amplitude ramp) is that the mass spectrum *must* be obtained from low to high m/z (or vice-versa, in rare cases). Ions of intermediate m/z cannot be detected without first ejecting ions of higher or lower m/z. An exception is if a resonance excitation signal of constant frequency is placed to coincide with ions of intermediate m/z. However, this experiment will either suffer from 1) coincidence of resonance

and boundary ejection peaks,[234] or 2) require prior clearing of the low or high m/z ions, thus resulting in a loss of mass information.

However, as demonstrated in **Figure 8.1b**, the ac frequency can be scanned so that intermediate m/z ions are detected first, followed by low m/z and finally high m/z ions. A plot of the relationship between frequency, m/z, and time for the arbitrary mass scan is shown in **Figure 8.1d**. This scan is performed 1) without loss of any mass information, and 2) without interferences from boundary ejection. Of course, the mass spectrum must be reconstructed as shown in **Figure 8.1c**. Ions of the same m/z are detected in both the single ac scan and arbitrary mass scan cases, though a single ghost peak is observed at t = 0 in **Figure 8.1b** and m/z ~1300 in **Figure 8.1c**. Furthermore, the relative intensities are different between the two scans. However, differences in space charge effects can account for this variation. Specifically, in a conventional mass scan, the low m/z ions suffer from the most space charge during ion ejection. However, in the arbitrary mass scan performed here, ions of intermediate m/z were scanned out first. Hence, space charge effects were increased for these ions but decreased for the low m/z analytes.

Note that the ghost peak is quite often observed when the ac frequency scan is initialized, even though the frequency sweep begins at zero phase and hence zero voltage. The cause of this signal spike is currently unknown; however, it is possible that the initial burst of voltage from the application of the ac waveform ejects ions of certain m/z values, hence giving a ghost peak.

8.4.2   The multiscan

A second unique scan mode available to the ac frequency scan ion trap is the "multiscan". This mode takes advantage of the tunability of the ion ejection efficiency when using ac frequency scans. Specifically, ions may be left in the trap even after a mass scan, particularly if the scan speed is high or the ac amplitude is low. By contrast, for methods like boundary or resonance ejection, even if ions are not ejected by the (fixed) resonance ejection signal, they will certainly be ejected at the boundary. Hence, no ions in the scan range can reside in the trap after an analytical rf amplitude ramp, preventing further mass measurements from being made without replenishment of the ions. Although ion replenishment is easily achieved in the laboratory, for space science applications – which have significant resource constraints - any reduction in sample consumption, scan time, number of ion injections, or power reduction is beneficial.

Figure 8.2a shows a single ac scan mass spectrum from the LTQ of cesium monobutyl phthalate clusters using 5 V_{pp} ac amplitude. Although some ions are left over in the trap after this scan (not shown), the number of ions left can be increased simply by decreasing the ac amplitude. As shown in **Figure 8.2b**, if the ac amplitude is decreased to 1.1 V_{pp} then a "double scan" can be performed in which sequential mass scans give two full scan mass spectra. Similarly, if the ac amplitude is lowered even more, a "triple scan" can yield three consecutive full scan mass spectra (**Figure 8.2c**). Thus, even if a mass scan leaves ions in the trap, which would decrease the instrument's overall sensitivity, the leftover ions can subsequently be scanned out by using another frequency scan.

The ability to obtain a full scan mass spectrum while leaving a substantial population of ions in the trap presents a unique opportunity to perform experiments unavailable to ion traps operated in the conventional manner. For example, one can obtain a full scan mass spectrum, select one of the ions observed in the mass scan, isolate that ion, fragment it, and scan out the product ions to produce an MS^2 product ion spectrum. All of these steps can be performed with a single ion injection without prior knowledge of the mass contents. **Figure 8.3** illustrates this concept with the cesium monobutyl phthalate clusters. In this case, after ion injection, a low amplitude (0.8 V_{pp}) inverse Mathieu q scan was used to obtain a full mass scan. Subsequently, without injection of another ion packet, *m/z* 841, a prominent ion in the full scan, was isolated at q = 0.245 (inset) using three bursts of a notched inverse Mathieu q scan [235] and it was then fragmented using a low voltage resonance excitation signal at its secular frequency. Finally, a full scan of the product ions was obtained, revealing *m/z* 487 as the sole product ion. Although a conventionally-operated quadrupole ion trap can easily perform MS^2 scans using a single ion packet, it cannot be used to obtain *both full scan and product ion scan* data using a single ion injection without loss of information. If a full scan is obtained using the rf to eject ions, then a product ion scan cannot be obtained using the same ion packet. If a product ion scan is obtained, then a full scan of the precursor ions cannot be obtained. The ac frequency scan ion trap has no such limitation.

Multiscan capabilities can also be used to obtain further product ion data. **Figure 8.4** shows the application of the multiscan as far as MS^3, wherein the following steps were performed on a single ion packet (in order): i) full mass scan, ii) isolation of precursor ion *m/z* 841, iii) CID of *m/z* 841, iv) full mass scan, v) isolation of MS^2 ion *m/z* 487, vi) CID of *m/z* 487, and finally vii) a full

mass scan, revealing MS^3 ion *m/z* 339. Again, this seven-stage experiment was performed with only a single ion injection event.

In these experiments, due to instrument control limitations, we were required to know the *m/z* information of the precursor ions *prior to ion injection* in order to successfully isolate and fragment them. However, in practice, one need not know anything about the ions prior to injection in order to perform multiscan experiments because the first full mass scan provides this information. The computer that runs the instrument could then process this data while keeping the leftover ions in the trap, and it could subsequently isolate and fragment one of those precursor ions from the same ion packet in a data dependent operation. This selection could be based on any number of metrics: ion intensity, *m/z*, isotope ratios, etc.

8.4.3   Implementation of ac frequency scanning at NASA Goddard Space Flight Center

The capabilities of these ac frequency scan modes are uniquely applicable and useful for any resource-constrained ion trap instrument, such as the MOMA instrument currently under development at the Goddard Space Flight Center. The rf supply in a small ion trap-based instrument makes up a significant portion of the power requirements of the overall system. Specifically, the ability to achieve higher performance (particularly in terms of mass range) without the increased power draw typical of trapping voltage scans, is a very attractive proposition. Additionally, the samples that are analyzed in such a mission can be quite limited in amount and can sometimes only be captured at discrete time points. Trace molecules may only exist in particular locations and also within particular layers of rock while automated selection of source parameters (e.g. laser energy) can result in accelerated sample consumption. More efficient use of the ions that are generated can result in direct improvement in the ultimate information yield from a mission.

In order to evaluate the real-world capabilities of these scan modes when implemented on a miniaturized instrument (such as MOMA), tests were conducted using MOMA breadboard instrumentation. This breadboard system has the same central ion trap design as the flight instrumentation that will travel to Mars on the ExoMars rover, and therefore the performance obtained from these tests is representative of what could be achieved with a space-based device. The ac frequency scan experiments on the MOMA breadboard instrument were performed using

perfluorotributylamine (PFTBA), the standard calibrant species for EI operations on the MOMA instrument which provides ion mass peaks over the entire EI mode mass range from *m/z* 69 to 502.

Initial experiments included exploration of mass range, sensitivity, resolution, mass accuracy, and mass calibration. In general, the full mass range of PFTBA could be acquired using an inverse Mathieu q scan (15 kDa/sec) at an rf amplitude of 140 V_{pp}, and unit (or nearly unit) resolution was achieved over a mass range from the lower mass cutoff (LMCO) to approximately 2 to 2.5 times the LMCO. Similar sensitivities were achieved in resonance ejection and ac scanning at high Mathieu q, but at low q the sensitivity of resonance ejection was several times higher. It was further confirmed that a quadratic fit of *m/z* vs. time gave mass accuracies rivaling those obtained via resonance ejection.[230] Nonetheless, of particular interest here are the new scans modes demonstrated at Goddard.

8.4.4   The segmented scan

Additional unique scan modes were accessible at Goddard due to the flexibility of the system control software and hardware, particularly the ability to control the rf amplitude during each segment of the overall scan (not just during the mass scan) as well as the ability to record data during several adjacent or nonadjacent mass scan segments. These abilities allowed the implementation of a third scan mode, the "segmented scan", which was compared to the already-implemented resonance ejection scan method.

One of the main concerns with ac frequency scanning is that because ions are ejected at variable Mathieu q_{eject}, the resolution will depend on the difference between an ion's secular frequency and the secular frequencies of ions of similar *m/z* values. For ions at low q, the frequency dispersion is very small so that resolution suffers immensely. In contrast, at high q, ion secular frequencies are further apart, allowing higher resolution scans to be performed. Hence, in standard resonance ejection experiments the supplemental ac frequency is typically set very close to the stability boundary where the frequency dispersion is at a maximum. For the ac frequency scan, the resolution at low q is quite low, and hence one method of increasing resolution for these higher *m/z* ions is to bring them to higher q values during the mass scan. That is, one solution is to *segment* the mass scan into sections with differing rf amplitudes. In each segment the ac frequency sweep is repeated to obtain a separate mass spectrum at each rf amplitude (and hence each at a different

mass range). Note that only a single ion injection is needed to acquire all of the segments. No ion replenishment between segments is necessary.

For example, a single inverse Mathieu q scan of PFTBA calibrant ions on the Goddard breadboard linear ion trap at a mass scan rate of 15 kDa/s gave unit resolution up to *m/z* 131 when the rf amplitude was 140 V_{pp}, approximately corresponding to a lower mass cutoff of ~50 Da (green triangles in **Figure 8.5**). However, resolution degraded severely for higher *m/z* ions, to a peak width of 5.8 Da for *m/z* 502 due to the lower frequency dispersion at low q. These results are significantly worse than the resolution obtained for a normal resonance ejection scan at the hexapole line $\beta = 2/3$ (orange squares).

If the mass spectrum is instead segmented into two sections, the first covering the lower mass range *m/z* 69 to *m/z* 131 (approximatley twice the LMCO) and the second covering *m/z* 264 to *m/z* 502, then a considerable increase in resolution is observed. Peak widths decreased from 2.0 Da, 3.1 Da, 4.4 Da, and 5.8 Da to 0.65 Da, 0.81 Da, 1.3 Da, and 2.8 Da, respectively, for *m/z* 264, 300, 414, and 502. A further increase in resolution would be observed by decreasing the scan rate and by further segmenting the scan. For the segmented scan, power consumption could be lower than in resonance ejection (depending on the specifics of the implementation) and a precise linear rf ramp would not be needed. Instead, a "switching" mode of operation could be employed wherein a set of 3-4 rf amplitudes would be available during the mass scan, each of which would require separate mass calibration. In any case, the rf amplitude ramp mode of operation will have higher resolution and sensitivity, though it also requires more complicated and higher power electronics.

8.4.5   The periodic scan

The fourth and final scan mode demonstrated in this work is a "periodic scan" wherein the ion trap is operated with a 100% duty cycle by continuously injecting ions and periodically scanning them out of the trap for detection. Here we define the duty cycle as the ratio of time that the trap accepts ions from an external source to the total time of operation for one scan. Because ion traps are pulsed mass analyzers that require both ion injection and collisional cooling, the typical duty cycle is relatively low (~4%). However, if no discrete injection and cooling steps are implemented, then the trap can be operated at nearly 100% duty cycle. This experiment is similar to the high speed digital frequency scanning previously implemented on a 3D ion trap,[87] although

we, in contrast, employ no discrete cooling time, as described in patent US20150034820 (which also describes the digital frequency scanning methodology).[236]

While the periodic scan is not *unique* to the ac frequency scan mode of operation, we believe that it is *more appropriate* for this mode than for any mode in which the trapping conditions change. The detector is not pulsed but is instead operated in a continuous fashion. Hence, any ions outside the stability boundary will be immediately ejected and detected as chemical noise. For scan modes in which the boundary *m/z* value changes as a function of time, the noise on the detector should also vary because different ions will be unstable at different times. In contrast, for the ac frequency scan the stability boundary *m/z* does not change so the noise on the detector should only vary with the variations in the source, not the trap itself. Moreover, ions of different *m/z* will have the same average collisional cooling times (which are determined by the mass scan rate) and the same duty cycles in the ac frequency scan mode. For other modes, a preference for high mass ions ought to be observed because their duty cycles are higher. The higher mass ions are stable and are allowed to cool for a longer period of time than low mass ions because the LMCO will be less than the higher mass ion's *m/z* for a proportionally longer total time. The ac scan should have no such bias except as determined by space charge conditions.

Table 8.1 compares the resolution obtained from an inverse Mathieu q scan in the normal pulsed mode (4% duty cycle) and the periodic mode (100% duty cycle). Resolution is degraded somewhat due to space charge effects, particularly for higher *m/z* ions that naturally have lower frequency dispersions, but remains acceptable for the lower mass range. Note that although the ions are continuously being injected, no clear increase in signal intensity was observed on either the Goddard ion trap or at Purdue. Even so, it is the increased number of scans per unit time that is perhaps more important for space science purposes. Because there are no cooling or injection steps in the experiment, the periodic scan may be particularly useful for chromatographic applications. Gas chromatography has been particularly popular on planetary missions. For example, both the Viking lander and the Surface Analysis at Mars suite coupled a gas chromatograph with either a magnetic sector or a quadrupole mass filter.[138,237] An increase of an ion trap duty cycle may therefore provide a means to better monitor dynamically-evolving populations from a chromatograph.

8.4.6 Unifying principles of ac frequency scanning and applicability to planetary exploration

Finally, we comment on the utility of the scan modes demonstrated here. The unifying principles in this paper are 1) constant trapping parameters, and 2) more efficient ion usage. The second characteristic simply means that ions are not lost to boundary conditions so long as their initial conditions are favorable to trapping. We do not mean to imply that the ac frequency scan ejects ions more efficiently than resonance or boundary ejection, but rather that multiple operations can be performed with a single ion packet. More efficient ion usage and the ability to perform multiple operations or monitor dynamic ion populations as a function of time could be a highly advantageous capability for miniature instruments. Space science ion trap instruments (for example, the mass spectrometer aboard the ExoMars rover[139]) are a natural fit for the scans demonstrated here since they have limited mass, power and volume, as well as the number of ion injection events.

8.5 Conclusion

We have demonstrated four modes of operation for the ac frequency scan ion trap: the "arbitrary mass scan", the "multiscan", the "segmented scan", and the "periodic scan". These modes are all enabled via ac frequency scanning and are performed under constant trapping conditions. As such, ions are not forced out of the trap at the stability boundary when the scanning parameter is varied, but instead are selectively ejected at chosen (static) Mathieu q values. These scan modes allow new experiments to be performed with widely-used electronic systems, and hence they extend the capabilities of existing instruments without requiring physical modifications.

8.6 Acknowledgements

Figures and Tables

a. Single AC Scan

b. Arbitrary Mass Scan

c. Arbitrary Mass Scan Reconstructed Mass Spectrum

d. *m/z* and Frequency Domain
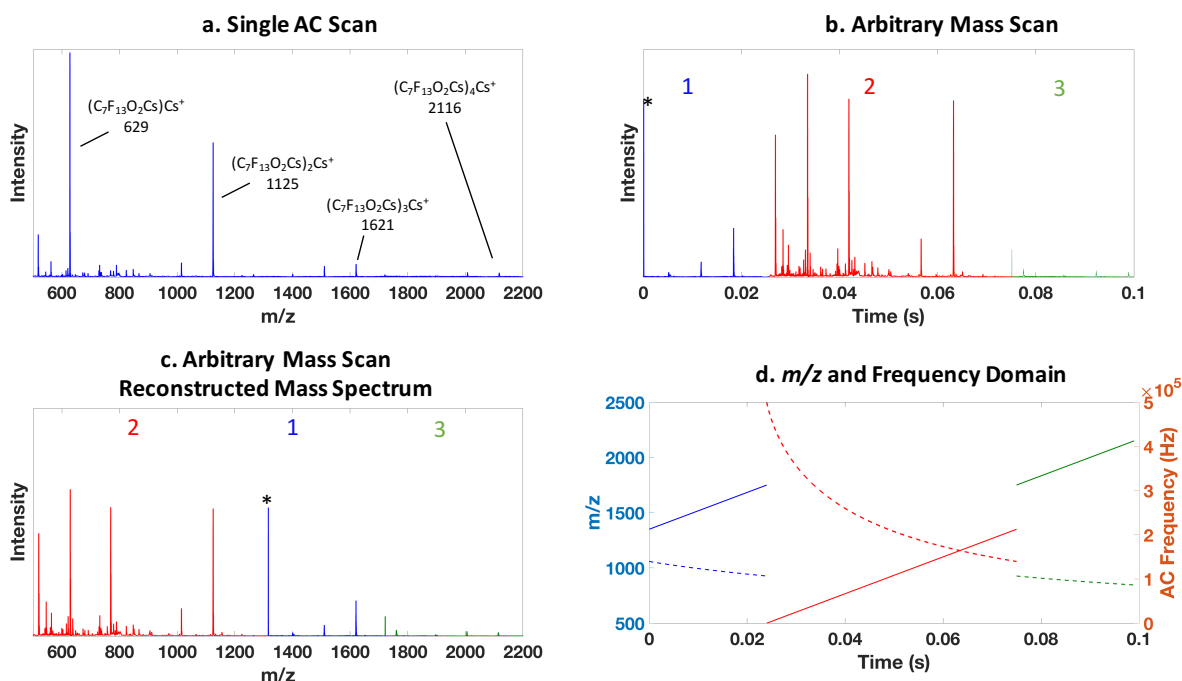
Figure 8.1. The arbitrary mass scan. Spectrum (a) shows full inverse Mathieu q scan mass spectrum of CsTFHA cluster ions, whereas (b) shows an arbitrary mass scan wherein intermediate *m/z* ions were ejected first, followed by lower *m/z* ions and finally higher *m/z* ions, color coded to show the time intervals. Spectrum (c) shows the reconstructed mass spectrum (*indicates ghost peak) and (d) indicates the *m/z* (solid lines) and AC frequency (dashed lines) vs. time relationships in the three segments that comprise (b). The rf amplitude was 1300 V_{0-p}, scan rate was 16,600 Da/s, the relationship between Mathieu q and ac amplitude was calibrated using a quadratic function, and the inverse Mathieu q scan spanned q = 0.908 to 0.15.
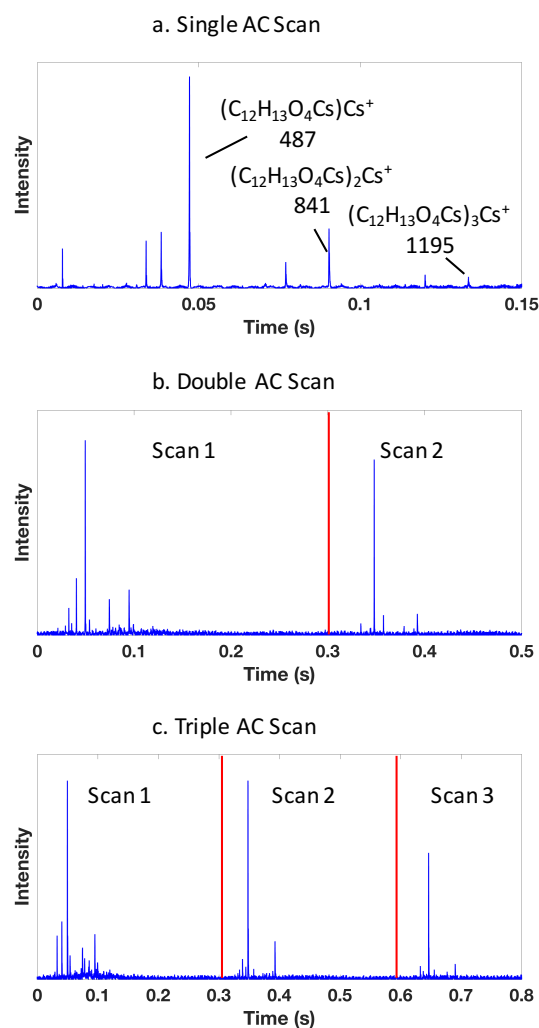
Figure 8.2. The multiscan. Spectrum (a) shows a single inverse Mathieu q scan of cesium monobutyl phthalate clusters with rf amplitude fixed at 1300 $V_{0\text{-}p}$, scan rate 16,600 Da/s, 5 V_{pp} fixed ac amplitude. Spectrum (b) shows a double ac frequency scan using an amplitude of 1.1 V_{pp}, and (c) shows a triple ac scan using an amplitude of 0.8 V_{pp}. In all cases, only one ion packet was injected into the trap at t < 0 and the full vertical lines indicate the beginning of a subsequent scan.
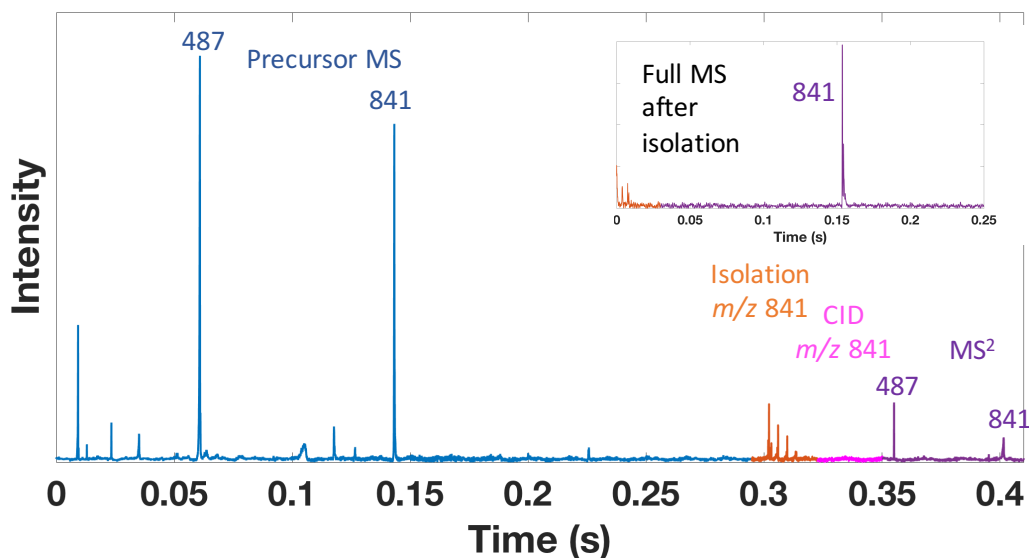
Figure 8.3. Application of multiscan to MS^2. After ion injection, a low voltage inverse Mathieu q scan (0.8 V$_{pp}$) is used to obtain a full scan mass spectrum of cesium monobutyl phthalate clusters; then *m/z* 841 is isolated using 3 bursts of a 1.2 V$_{pp}$, 15 ms inverse Mathieu q scan with notch at q = 0.245. Subsequently the isolated ion (inset) is subjected to a 0.2 V$_{pp}$ resonance excitation signal at its secular frequency (104 kHz), and finally the product ions of *m/z* 841 are scanned out with a 2 V$_{pp}$ frequency scan to reveal *m/z* 487 as a fragment. The entire experiment was performed using a single ion packet injected at t < 0.
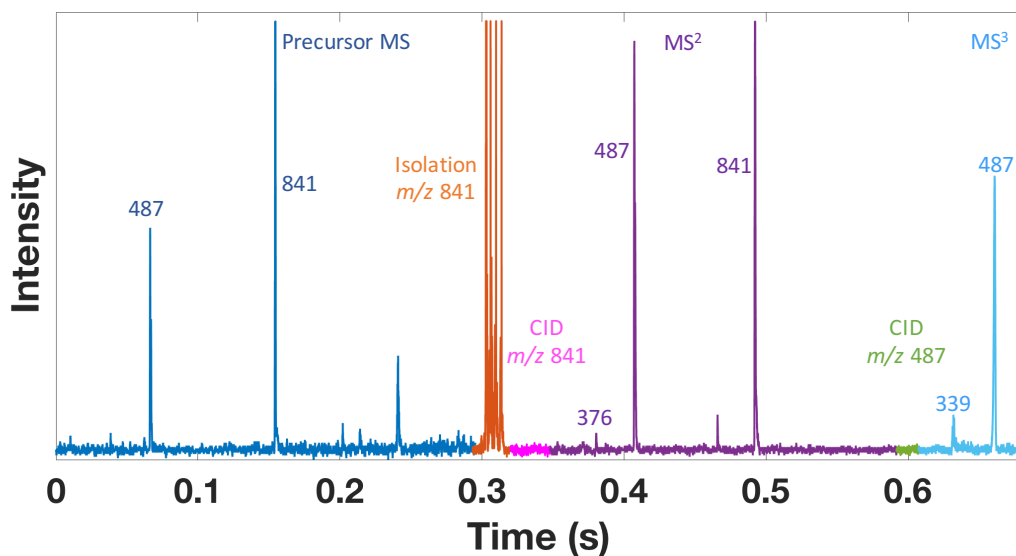
Figure 8.4. Application of multiscan to a single ion population subjected to five successive operations to MS^3. After ion injection, cesium monobutyl phthalate clusters are scanned out of the ion trap using a low voltage (0.8 V$_{pp}$) inverse Mathieu q scan, after which *m/z* 841 is isolated and fragmented, followed by a full mass scan, fragmentation of product ion *m/z* 487 (16 ms, 197 kHz, 160 V$_{pp}$), and finally a full scan (0.5 V$_{pp}$), revealing MS^3 ion *m/z* 339. The entire seven stage experiment was performed using a single ion packet injected at t < 0.
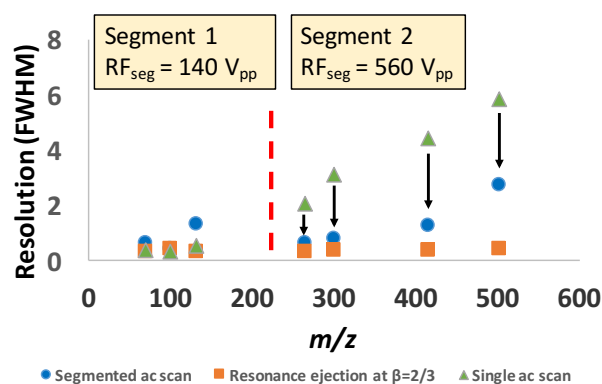
Figure 8.5. Comparison of resolution (expressed simply as full width at half maximum, FWHM) obtained from a singly-segmented inverse Mathieu q scan, resonance ejection at β = 2/3 (hexapole), and a double-segment inverse Mathieu q scan at an rf amplitude of 140 V_{pp} followed by 560 V_{pp}. Experiment was performed with PFTBA on a MOMA prototype at a scan rate of 15 kDa/sec.

Table 8.1. Peak Width (Da) in periodic frequency scanning

m/z	100% Duty Cycle	4% Duty Cycle
69	0.72	0.72
100	1.20	0.75
131	1.49	0.98
264	5.00	2.07

Resolution (FWHM) vs. *m/z* for PFTBA test ions analyzed with either 100% duty cycle (periodic scan) or 4% duty cycle (normal mode of operation). Scan rate was 15 kDa/s. Data acquired using the MOMA prototype. Sample was PFTBA. RF amplitude was 140 V_{pp}.

PART II. PRECURSOR AND NEUTRAL LOSS SCANS IN A LINEAR QUADRUPOLE ION TRAP

CHAPTER 9.   SINGLE ANALYZER PRECURSOR SCANS USING AN ION TRAP

9.1   Abstract

Rationale: Precursor ion and neutral loss scans are general survey methods of tandem mass spectrometry (MS/MS) used for detecting structurally related compounds. Until now they have only been performed in multiple analyzer instruments, e.g. triple quadrupoles and hybrid MS/MS instruments. Implementation of precursor ion scans in single mass analyzers would be advantageous in reducing instrument complexity.

Methods: Adoption of secular frequency scanning as a method of mass selective excitation is shown to enable precursor scans in a single ion trap. A small supplementary ac signal is swept in frequency so as to cause mass-selective excitation of trapped ions. Simultaneously, a higher fixed amplitude ac signal is applied at the fixed secular frequency of a product ion, ejecting the mass-selected product ion and providing temporal data corresponding to a precursor ion spectrum.

Results: Precursor scanning in a single ion trap is demonstrated using a mixture of three illicit drugs: cocaine, 3,4-methylenedioxyamphetamine (MDA), and 3,4-methylenedioxymethamphetamine (MDMA). Acquisition of the spectra as a function of the frequency of the product ejection waveform demonstrates that the signals acquired represent precursor ion scans.

Conclusions: Secular frequency scanning is a nonconventional method of mass scanning that in combination with product ion ejection enables precursor scans in single ion traps. This phenomenon is demonstrated here for a miniature linear ion trap, but the concepts described also apply to quadrupole mass filters.

9.2   Introduction

Precursor and neutral loss scans are notably absent from a single ion trap's repertoire, despite the ion trap's attractiveness as a mass analyzer. Serial arrays of two or more traps and/or

beam-type analyzers in various configurations are used to perform precursor scans,[238-246] but this comes at the cost of instrument complexity, increased size and cost, and, in many cases, a required third stage (*e.g.* an rf-only quadrupole for collision-induced dissociation, CID).[247-249]

The triple quadrupole mass spectrometer is the premier instrument for carrying out survey scans (precursor and neutral loss scans).[249] In order to perform a precursor scan, the first quadrupole is scanned so that the rf-only collision cell generates fragments in a mass selective manner in the order of the mass scan. The third quadrupole is set on a particular product ion so that signal is detected only when a precursor of that product ion is fragmented. Other combinations of mass analyzers that can be used to perform precursor scans are the quadrupole time-of-flight mass spectrometer,[250] quadrupole mass filters in tandem with ion traps (Qq-traps and QqQ-traps)[244,245] or sectors (BEQQ),[251] and multiple sector instruments (e.g. BEBE),[242] but again these come at the cost of greater power consumption and instrumental complexity.

The usefulness of single mass analyzers in complex mixture analysis would be considerably increased were they capable of precursor ion scans which allow recognition of classes of compounds and molecules with particular functional groups. Examples of precursor scan applications are particularly widespread in proteomics and phytochemical studies, but they are useful for many other complex matrices as well. Examples include determination of protein/peptide modification sites (*e.g.* phosphorylation, methylation, and glycosylation),[239,252-259] as well as detection of phosphopeptides,[248,252] identification of cross-linked peptides,[260] determination of glycosylated compounds,[257,261,262] characterization of alkaloids,[263] phospholipids,[264-266] and other phytochemicals in plants,[267] analysis of physiological metabolic products,[265,268] and determination of pharmaceutical residues in water.[269,270]

Single ion traps have not been shown previously to provide precursor ion spectra. Conventional methods of mass selective ion detection preclude such scans. In particular, in order to perform precursor scans in a single ion trap, the conventional mass selective instability scan,[271] in which the amplitude of the rf is ramped linearly with time to eject ions in order of increasing *m/z*, must be abandoned in favor of a more flexible and versatile scan method.

We recently extended[106] the use of secular frequency scanning from the halotrap [19] to other types of ion traps as an instrumentally simplified alternative to ramping the amplitude of the radio-frequency (rf) waveform. In this method, the frequency of a small supplementary ac waveform is scanned through the secular frequencies of the trapped ions. When the frequency of this waveform

matches the resonance frequency of an ion, the ion's amplitude increases, effecting either CID (low amplitude waveform) or ion ejection (high amplitude waveform). This scanning technique has not been widely adopted, but its simplicity has led to a few interesting applications,[272-274] most notably in the halo ion trap.[19] Since a linear ramp of the rf amplitude is not needed, the technique may be most suitable for miniature instruments, which benefit from low-power operation and simple electronics.[275,276]

While resolution is noticeably worse in secular frequency scans, there are further advantages beyond its elegance and simplicity. As we will show in this paper, application of secular frequency scanning enables additional functionality, namely precursor scans, in single ion traps.

9.3   Experimental

9.3.1   Instrumentation

All frequency scanning experiments were performed using the Mini 12[277] miniature rectilinear ion trap (RIT)[16] mass spectrometer operating in the positive ion mode. Product scans were performed by synthesizing two dipolar waveforms composed of a high amplitude, fixed frequency component and a low amplitude, swept frequency component. The former was generated by the Mini 12 ac/waveforms board, whereas the latter was obtained from a Sony Tektronix AFG320 arbitrary function generator (Japan). The two were combined using two summing operational amplifiers (LM318H, National Semiconductor, Coppell, Texas, USA), one for each polarity, and high-frequency ambient noise was filtered out using low-pass frequency filters with a cutoff frequency of 500 kHz. Unless otherwise specified, scans were forward frequency scans (high to low mass) 300 ms in length with a scan range of 50-250 kHz and a constant rf amplitude and constant frequency of 0.999 MHz, corresponding to a lower-mass cutoff of 98 Thomson (Th). The swept frequency waveform had an amplitude of ~0.15-0.3 V_{pp} (peak-to-peak), whereas the constant frequency ejection waveform had a ~3 V_{pp} amplitude. Data were acquired using a Tektronix TDS 2024C four-channel digital storage oscilloscope (Beaverton, Oregon, USA). Both the function generator and oscilloscope were triggered by a high frequency kilohertz ac waveform of ~2 V output (0 to peak) from the Mini ac/waveform board in a 1 ms segment just prior to the mass scan. The oscilloscope was set to wait for ~1 s to acquire further spectra in order to prevent multiple acquisitions due to the oscillating trigger waveform.

9.3.2   Ionization and Ion Introduction

Ions were generated by nanoelectrospray ionization at ~2,000 V. The discontinuous atmospheric pressure introduction (DAPI) valve on the Mini 12 was opened for 12 ms to allow for ion introduction. The ions were then allowed to cool for 500 ms, which was then followed by the mass scan.

9.3.3   Chemicals

Cocaine, 3,4-methylenedioxyamphetamine (MDA), and 3,4-methylenedioxymethamphetamine (MDMA) were purchased from Cerilliant (Round Rock, Texas, USA). HPLC grade methanol was purchased from Fisher Scientific (Fair Lawn, New Jersey, United States). Deionized water was obtained from a Thermo Fisher Scientific EasyPure II system (Marietta, Ohio, USA). 88% formic acid was obtained from Mallinckrodt Chemicals (Phillipsburg, New Jersey, USA). Reagents were initially dissolved in either HPLC grade methanol (MeOH) or deionized water and then diluted in 50:50 MeOH:H_2O with 0.1% formic acid to obtain their final concentrations (~1 ppm).

9.4   Results & Discussion

The ability to perform precursor scans in a single ion trap is a direct consequence of the adoption of secular frequency scanning as the primary method of mass selective ion interrogation. In secular frequency scanning, a small supplementary ac signal is varied in frequency so that ions are excited in a mass-selective manner. If the amplitude of the waveform is high, ions are ejected from the trap as the ac comes into resonance with each ion's secular frequency or related characteristic frequency, and the full mass spectrum is obtained. However, if the amplitude of this signal is low and if the time of application is appropriate, ions of different m/z values will be fragmented at different times, with efficiencies which depend on the ion structure and q value.

Mass selective fragmentation in time further allows a single trap to be used to carry out tandem mass spectrometry (MS/MS) operations that are otherwise unavailable to tandem-in-time instruments, but possible in tandem-in-space instruments. All that is needed is the ability to selectively interrogate product ions. This can be accomplished by applying a *second* dipolar ac waveform at the product ion's secular frequency. The amplitude of this signal should be high enough that the product ions of interest are immediately ejected as they are formed during the

excitation scan, but not so high that enough energy is provided to adjacent ions to escape the trap and be detected, thereby resulting in a loss of mass information.

The process is illustrated in **Figure 9.1**. On the Mathieu stability diagram, the secular frequency scan ("scanned excitation") fragments ions of successive *m/z* values, the order depending on scan direction. Forward frequency (and thus reverse mass) scans show much higher efficiency in traps with higher order field components, as we have shown.[106] A second higher amplitude AC signal is then fixed on a product ion ("fixed hole") so that ejection is rapid, preserving the mass selective nature of the experiment. **Figure 9.1b** shows the frequencies, in time, that are required to perform the scan. We chose to ramp the low amplitude waveform linearly from low to high frequency due to electronic simplicity, resulting in an approximately inverse relationship between *m/z* and time.

Figure 9.2 shows the secular frequency scan for a mixture of three illicit drugs, cocaine ([M+H]$^+$, *m/z* 304), 3,4-methylenedioxymethamphetamine (MDMA, [M+H]$^+$, *m/z* 194), and 3,4-methylenedioxyamphetamine (MDA, [M+H]$^+$, *m/z* 180) along with precursor scans recorded with the higher amplitude, constant frequency ejection waveform set (a) off resonance (210 kHz) and (b) on the resonance frequency of *m/z* 182, which is the sole product ion of cocaine (whereas both MDA and MDMA fragment to *m/z* 163). No signal is observed in the off resonance case because there are no ions corresponding to the applied ejection frequency and the amplitude of the swept waveform is deliberately set too low for ion ejection. However, when the ejection signal is set on 153 kHz, the resonance frequency of ion *m/z* 182, only a single peak due to the cocaine transition (*m/z* 304 -> *m/z* 182) is detected. The corresponding full mass scan via a secular frequency sweep is shown in (c) for reference. Note that a blank experiment in which no ejection frequency was applied resulted in a blank spectrum (not shown).

Unambiguous confirmation of this experiment as a precursor scan is shown in **Figure 9.3**, where the frequency of the ejection waveform was changed. Only when the frequency of this waveform matched the fundamental resonance of *m/z* 182 (153 kHz) or a higher order resonance (153 kHz / 2 = 76 kHz) is the cocaine signal observed. Small signals are also detected slightly below the resonance frequency (e.g. 70 kHz and 145 kHz) due to broad resonance absorption, which is well characterized experimentally in the classic paper by Williams and coworkers[65] and theoretically by Makarov,[278] which we have discussed elsewhere.[106] In brief, due to fields beyond the quadrupole field, namely the octapolar and dodecapolar fields, ions absorb resonance energy

farther below their resonance frequency than above. In other words, their resonant absorption spectra are asymmetric. Due to the high slope just above resonance, a sharp drop-off of signal is observed (which Makarov termed "quenching") in the 155 kHz and 80 kHz spectra in **Figure 9.3**. Due to the small slope below resonance, the product ion *m/z* 182 is able to gain enough kinetic energy to escape the trap, even if the ejection waveform is set slightly below resonance. Optimization of the field is likely to improve this aspect, as the rectilinear trap is only ~65% quadrupolar.

9.5   Conclusion

Secular frequency scanning is an unconventional method of mass scanning that enables further MS/MS scans, specifically precursor scans, to be performed in single ion traps, expanding the range of applications for such devices. While broad resonance absorption curves may limit the resolution of precursor scans, the ability to perform precursor survey scans in single mass analyzers is likely to have favorable consequences in areas where small light instruments are needed to examine complex samples, as in planetary exploration, environmental monitoring, and some commercial applications.

9.6   Acknowledgements
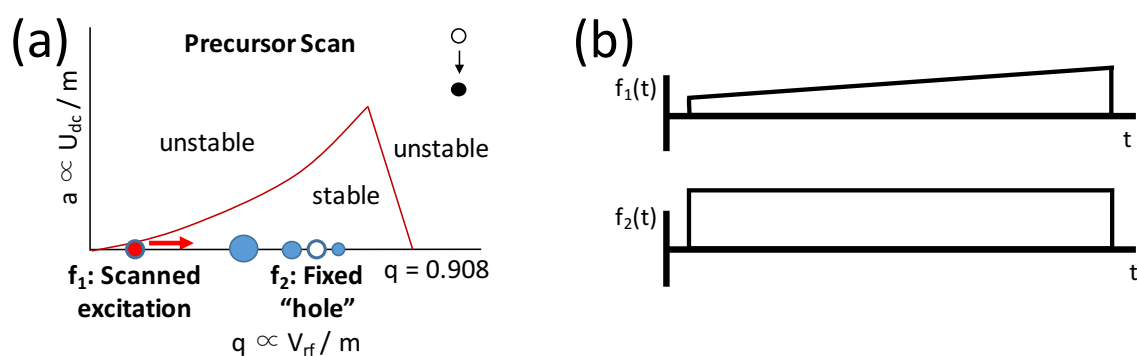
Figures

Figure 9.1. Precursor ion scan in a single ion trap: (a) illustration of single analyzer precursor scans in context of the Mathieu stability diagram, and (b) required frequencies of ac waveforms as a function of time. The swept frequency ac waveform, which has frequency f_1, has a low amplitude so as to mass selectively fragment precursor ions, whereas the second waveform with constant frequency f_2 has a high amplitude to eject particular product ions immediately upon formation.
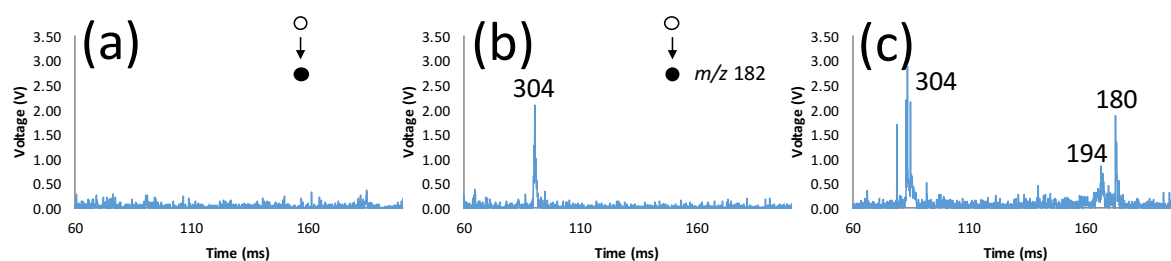
Figure 9.2. Ion trap precursor ion scan performed on a mixture of three illicit drugs, cocaine ([M+H]$^+$, *m/z* 304), MDMA ([M+H]$^+$, *m/z* 194), and MDA ([M+H]$^+$, *m/z* 180). In (a), the constant frequency waveform is set off resonance (210 kHz), resulting in a blank spectrum. In (b), the ejection waveform is set on 153 kHz, the resonance frequency of *m/z* 182, a product of cocaine, resulting in a detectable cocaine signal. Finally, (c) shows the secular frequency scan mass spectrum for reference, obtained using a higher amplitude ac frequency sweep.
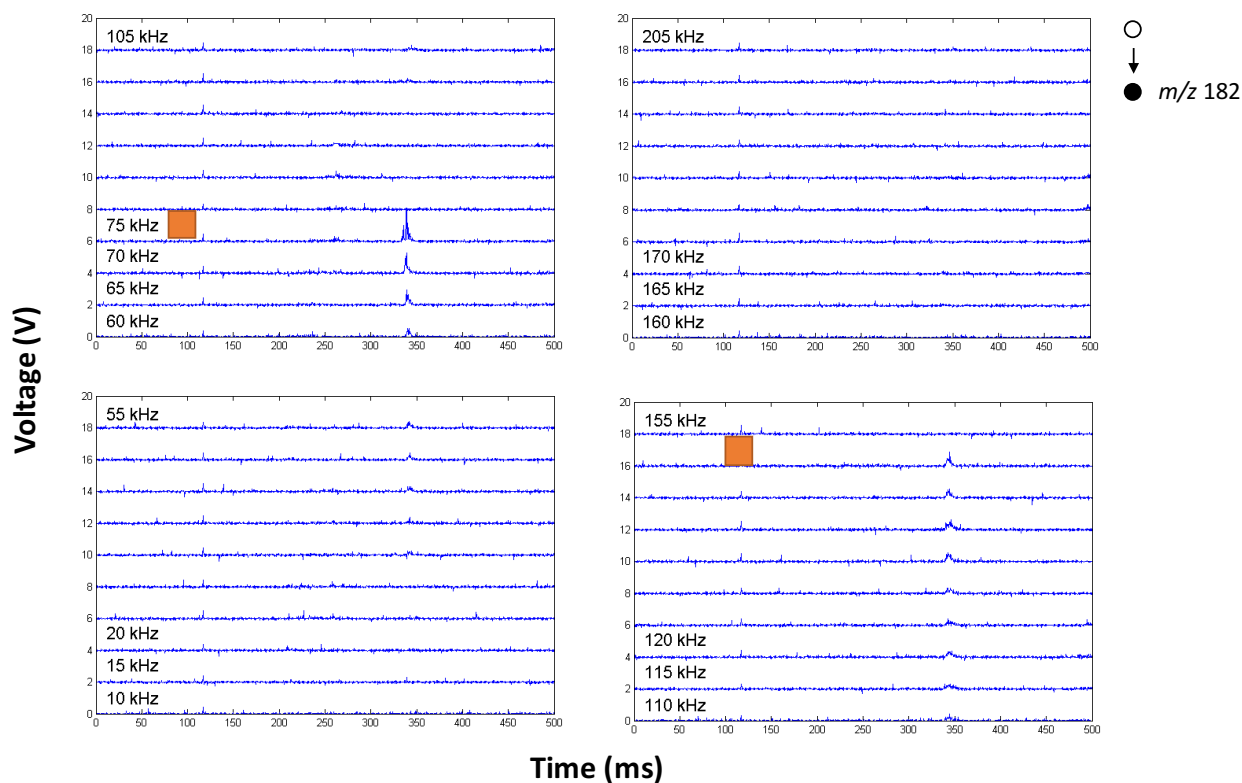
Figure 9.3. Temporal appearance of the precursor ion scan of cocaine ([M+H]$^+$, m/z 304) when the ejection waveform (frequency specified in each spectrum) is set on the product ion of cocaine, m/z 182 ([M+H]$^+$), while a second ac waveform of lower amplitude is swept linearly in frequency as a function of time. Figure is read in order of increasing ejection frequency from bottom left to top left and then bottom right to top right. Only when the ejection frequency is set on the fundamental or a higher order resonance (indicated by orange squares, the fundamental being ~150 kHz) of the product ion is the cocaine signal detected. Ejection of cocaine slightly off resonance indicates that resonant absorption spectra in the rectilinear trap are quite broad. The mass excitation scan took place over 800 ms from 10 to 300 kHz with a 0.3 V$_{pp}$ ac waveform.

CHAPTER 10.   SINGLE ANALYZER PRECURSOR ION SCANS IN A LINEAR QUADRUPOLE ION TRAP USING ORTHOGONAL DOUBLE RESONANCE EXCITATION

10.1 Abstract

Reported herein is a simple method of performing single analyzer precursor ion scans in a linear quadrupole ion trap using orthogonal double resonance excitation. A first supplementary ac signal applied to the y electrodes is scanned through ion secular frequencies in order to mass-selectively excite precursor ions while, simultaneously, a second fixed-frequency ac signal is applied orthogonally on the x electrodes in order to eject product ions of selected mass-to-charge ratios towards the detector. The two ac signals are applied *orthogonally* so as to preclude the possibility of i) inadvertently ejecting precursor ions into the detector, which results in artifact peaks, and ii) prevent beat frequencies on the x electrodes from ejecting ions off-resonance. Precursor ion scans are further implemented while using the inverse Mathieu q scan for easier mass calibration. The orthogonal double resonance experiment results in single ion trap precursor scans with far less intense artifact peaks than when both ac signals are applied to the same electrodes, paving the way for implementation of neutral loss scanning in single ion trap mass spectrometers.

10.2 Introduction

Miniature mass spectrometers[70,71] are desirable analytical tools for many specialized applications ranging from pharmaceutical reaction monitoring[279] to forensics,[215,216,280] chemical agent analysis,[193,281-284] and planetary exploration.[139,285] Because the quadrupole ion trap is tolerant of mtorr pressures and electric field imperfections and also has single analyzer product ion MS/MS capabilities,[201,286] it is the ideal mass analyzer for miniaturization. Hence, miniature instruments have increasingly been trending toward quadrupole ion traps over higher-resolution but more complex alternatives.[13,15,17-19,71,97,202,204,205,219,287-292]

Even so, quadrupole ion traps by themselves do not currently perform precursor ion or neutral loss scanning, two of the four main types of MS/MS experiments.[293] This is an unfortunate omission since both types of scans are particularly useful for analyzing complex mixtures for ions with similar functional groups.[239,240,243,248,252,255,257,258,260,265,294,295] Planetary exploration and forensics, in particular, may benefit from single analyzer precursor ion scanning capabilities since small organic molecules such as aryls with common substituents and various classes of drugs often have similar fragmentation patterns. For planetary exploration, a data-independent precursor ion scan would help increase the efficiency of ion utilization and decrease power and sample consumption compared to obtaining product ion spectra of several precursor ions (and thereby reconstructing the precursor ion spectrum). This data-dependent precursor ion scan would require multiple ion injections from the same source material.

The difficulty in performing a precursor scan in a single analyzer stems from its three requirements: i) mass selection of precursor ions, ii) fragmentation of the mass-selected precursors, and iii) mass analysis of the resulting product ions. Conventionally the simultaneous mass selection of precursor and product ions has required multi-analyzer instruments such as the triple quadrupole (or pentaquadrupole).[58,296] Other instruments that can perform precursor ion scans are multisector mass spectrometers,[294] quadrupole time-of-flight instruments,[248,257,295] and triple quadrupoles used in tandem with ion traps (e.g. Q-traps).[240] As mentioned previously, none of these configurations is ideal for miniaturization due to the sheer size, power consumption, and complexity of multi-analyzer mass spectrometers.

It is commonly thought that single quadrupole ion traps can perform product ion scans but that they do not have data-independent precursor or neutral loss scanning capabilities. However, some two and a half decades ago Yost *et al.* demonstrated, in principle, precursor ion scanning in a 3D quadrupole ion trap using a double resonance technique.[123] A first scanned ac frequency was applied to the endcaps in order to mass selectively excite precursor ions, thereby providing the functionality of the first and second quadrupole in a triple quadrupole system. The function of the third quadrupole, detection of a particular product ion *m/z*, was implemented in the ion trap with a *second* ac frequency fixed on the product ion of interest. Ideally, a signal would only occur at the detector when a product ion with *m/z* value corresponding to this second frequency was produced by fragmentation of a precursor ion. Because the precursor ions are fragmented mass selectively in time with a swept frequency sinusoid, the correlation between precursor and product ion – as

well as mass information – is preserved in the ejection time of the product ion (in principle, a neutral loss scan can similarly be performed by scanning both ac frequencies at a constant mass offset, but this has not been demonstrated).

Since this initial development, precursor and neutral loss spectra in single ion traps have almost always been recorded either using data-dependent acquisition,[297,298] requiring multiple ion injections and thus multiple mass scans, or using data-independent activation methods that also require multiple ion injections[299] or by methods which rely on data deconvolution.[300] Furthermore, none of these methods are single scans; rather, they all require *multiple scans*. For miniature and portable instruments – especially for planetary exploration and other situations where power and sample mass are limited - these methods are unsuitable.

We have previously implemented a double resonance precursor ion scan using the Mini 12[100] miniature linear ion trap mass spectrometer developed at Purdue University.[99] In the process of optimizing this scan mode, many artifact peaks were observed, and furthermore mass calibration was difficult because the ac frequency was scanned linearly, giving a nonlinear relationship between *m/z* and time.[91] We postulated that artifact peaks were caused by i) beat frequencies resulting from the application of multiple ac frequencies on the same pair of rods, and ii) accidental ejection of precursor ions as the first ac frequency was scanned. In this follow-up publication, we demonstrate single analyzer precursor scans in a linear quadrupole ion trap using *orthogonal* double resonance excitation. In comparison to the previously-demonstrated *parallel* excitation experiment, orthogonal excitation largely removes artifact peaks. Precursor ion scanning is also demonstrated in conjunction with the inverse Mathieu q scan, which forces an approximately linear relationship between *m/z* and time, thereby simplifying mass calibration compared to the linear frequency sweep case.

10.3 Experimental

10.3.1 Chemicals

Amphetamine, methamphetamine, 3,4-methylenedioxyamphetamine, 3,4-methylenedioxymethamphetamine, oxycodone, noroxycodone, and ketamine were purchased from Cerilliant (Round Rock, TX, USA) and dissolved in methanol. Final drug concentrations of 1 - 5 ppm were used for all experiments. Pierce ESI calibration mixture containing caffeine, the peptide MRFA, and the phosphazine Ultramark 1621 was purchased from Thermo Fisher

(Rockford, IL, USA). Cesium hydrogencarbonate, tridecafluoroheptanoic acid (TFHA), monobutyl phthalate (MBP), and sodium sulfate were purchased from Sigma-Aldrich Co. (St. Louis, MO, USA) and were dissolved in 50:50 methanol:water at a concentration of 3 mM. For generating CsTFHA or CsMBP cluster ions, the cesium hydrogencarbonate and either TFHA or MBP were dissolved in the same solution and electrosprayed as is.

10.3.2 Ionization

Ions were generated by nanoelectrospray ionization (nESI) at 1500 V using 5 μm nanospray tips pulled from borosilicate glass capillaries (1.5 mm O.D., 0.86 I.D.; Sutter Instrument Co., Novato, CA, USA) by a Flaming/Brown micropipette puller (model P-97; Sutter Instrument Co.). The flow rate in the nanoelectrospray performed here is on the order of 10 nL/min [301]. The positive ion mode was used for all experiments. Ion injection time was generally set at 50 ms but was manually optimized to prevent trap overloading. Automatic gain control was not used in this study.

10.3.3 Instrumentation

A Thermo Instruments (San Jose, CA, USA) LTQ linear ion trap mass spectrometer running LTQ XL 2.7 software was used for all experiments. The commercial rf coil was modified so that dipolar ac signals could be applied simultaneously to both the x and y rods while also applying the high voltage trapping rf signal in a quadrupolar manner. Otherwise the instrument was used as supplied commercially.

Generally, ac frequency scanning is performed at constant trapping (rf frequency and amplitude) conditions. However, ion trap control language (ITCL) code was not available, so instead ac frequency scanning was performed during an Ultrazoom scan. The Ultrazoom scan is the closest available approximation to constant rf conditions, as the rf amplitude is swept slowly at a rate corresponding to 27 Da/s. For experiments performed here, the starting Ultrazoom mass is reported because rf voltage readbacks are not provided by the manufacturer.

Orthogonal precursor ion scans were accomplished by applying on the y electrodes a swept frequency sinusoid for mass-selective precursor ion excitation while simultaneously applying to the x electrodes a second fixed-frequency signal corresponding to the secular frequency and hence *m/z* of a particular product ion.[99,123] The result of this orthogonal double resonance[35,131] experiment is a single analyzer precursor scan. All supplemental ac waveforms were supplied by a Keysight

33612A arbitrary waveform generator (Newark, SC, USA). Channel 1 supplied the ejection signal to the x electrodes and channel 2 supplied the swept frequency resonance excitation signal to the y electrodes. The generator was triggered at the start of the mass scan using the triggers built in to the LTQ Tune "Diagnostics" menu.

10.4 Results & Discussion

10.4.1 Single analyzer precursor ion scans

In order to perform a single analyzer precursor scan, the functions of the three quadrupoles in a triple quadrupole mass spectrometer must be condensed onto a single analyzer. For the quadrupole ion trap, this conundrum translates into the use of multiple supplemental ac frequencies for ion excitation and ejection. A first frequency ("scanned excitation frequency" in **Figure 10.1a**) is scanned through a range of ion secular frequencies in order to excite the precursor ions in the trap mass selectively as a function of time. A second frequency ("fixed ejection frequency" in **Figure 10.1a**), set on the frequency corresponding to the product ion of interest, is used to eject product ions of a particular *m/z*. The resulting scan table is shown in **Figure 10.1b**. Because ion secular frequencies depend on the trapping rf voltage and frequency, both must be kept constant during the precursor scan. Instead of using an rf ramp for mass scanning, the first ac frequency is swept either linearly or nonlinearly, and the selection affects mass calibration. The second frequency, the product ion ejection frequency, is fixed. In this study, the amplitudes of both precursor excitation and product ejection waveforms were kept constant, although they could have been varied in order to alter the normalized collision energy that each precursor ion experiences or to vary with precursor ion potential well depth. However, the ac amplitude will also affect mass calibration, so they were not varied in this work.

10.4.2 Orthogonal vs. parallel precursor ion scans

The key aspect of the current precursor scan experiment that differentiates it from previous implementations is the use of the orthogonal dimension for ion excitation. Few studies have used the y dimension in linear ion traps for mass selective operations because the detector lies in the orthogonal x direction. Rhombic ion excitation is one such case where orthogonal excitation signals are used to resonantly eject ions.[120] The resulting rhombic ion motion was shown to

decrease space charge effects compared to typical single-direction resonance ejection. Here we use orthogonality for double resonance excitation.

The orthogonality in the precursor scan is critical to removing artifact peaks, which can result from beat frequencies as well as unintended precursor ion ejection caused by the excitation ac frequency sweep. For example, **Figure 10.2a** shows a full scan mass spectrum from 200 to 140 kHz of the peptide MRFA from the Pierce ESI LTQ calibration mixture, which also contains caffeine and Ultramark 1621. The orthogonal precursor scan of *m/z* 288 (shown in **Figure 10.2b**), the most abundant fragment of MRFA in LTQ CID (see **Table 10.1** for precursor and product ion relationships), returns a single peak (m/z 524) corresponding to the time at which the precursor ion forming the m/z 288 product ion fragments. Using the ejection time of MRFA (ejection time 0.169 s in the precursor scan compared to 0.17 s in the full mass scan) as a reference for its secular frequency, 166 kHz, we calculate the secular frequency of *m/z* 288 as 335 kHz, in close agreement with the experimental value of 331 kHz.

Note that because the product ions are generated far from the center of the trap, they may experience substantial secular frequency shifts compared to their precursor ions, which can contribute to differences between calculated and experimentally observed secular frequencies. Also, ions are not ejected on resonance; rather, they are ejected slightly beforehand, which can further increase the error in secular frequency calculations based on ejection time. Furthermore, because the rf amplitude is being ramped, ion secular frequencies will shift slightly during the scan, increasing the error in calculated secular frequencies. This effect, in particular, likely has the greatest affect on the results presented here. Nonetheless, errors within perhaps 10 kHz were chosen to be acceptable in these calculations.

The parallel variant of the precursor ion scan, in which both supplemental ac waveforms are applied to the x electrodes, returns the result in **Figure 10.2c**. Essentially the parallel experiment records a full scan mass spectrum because the excitation ac waveform ejects the precursor ions into the detector. If the excitation amplitude is decreased from 1.1 V_{pp} to 300 mV_{pp}, then only the MRFA peak is left. However, the high signal intensity (10^2 counts) indicates that the precursor ion is still being ejected, and there is no way to unambiguously determine the relative contributions of the full scan and the precursor ion scan. Hence, although the orthogonal variant appears to lose sensitivity (a factor of 100 in this case), it returns less ambiguous results than the parallel variant. Moreover, the 100x drop in sensitivity should be interpreted as a 'worst case

scenario' because we are unfortunately forced to ramp the rf very slowly on our commercial instrument, and as the rf amplitude increases the ions' secular frequencies increase. The ac frequency is scanning from high to low (in the *opposite* direction of the shift in ion frequencies via the rf ramp) and hence the time each ion has on resonance is quite short. By keeping the rf constant and by scanning more slowly, we expect that much higher sensitivity will be observed.

10.4.3 Application to amphetamines

Many amphetamines as well as designer drugs[302-304] give similar fragments in their product ion scans[305] and the protonated molecules also fragment quite readily in ion traps. The latter characteristic is particularly important for precursor ion scans in ion traps because of the slow heating CID process[54] and also because the precursor ions are on resonance for a very short period of time, which can lead to limited (if any) fragmentation. The short on-resonance time is further exacerbated by the slow rf ramp necessarily applied using the LTQ, which causes ion secular frequencies to drift. On a more customized instrument, the rf ramp would not be an obstacle.

A full ac scan mass spectrum of a mixture of amphetamine (amp), methamphetamine (map), 3,4-methylenedioxyamphetamine (mda), and 3,4-methylenedioxymethamphetamine (mdma) is shown in **Figure 10.3a**. Because amphetamine and methamphetamine both fragment readily to *m/z* 119, the precursor ion scan shows both peaks. The calculated secular frequency of *m/z* 119 under these conditions is 200 kHz, in agreement with the experimental value of 206 kHz. Under these conditions the product ion's secular frequency is calculated to shift by 7 kHz (from ~202.5 kHz to ~209.1 kHz) during the rf scan period between ejection of amp and mdma, which can contribute to both loss of signal intensity and error in secular frequency calculations. A similar precursor ion scan of *m/z* 163, the primary fragment of both mda and mdma, again yields both corresponding peaks. Once again, the calculated and experimental secular frequency of the product ion agreed within 10 kHz.

10.4.4 Multigenerational precursor ion scans

One of the unique features of quadrupole ion trap precursor ion scanning is direct access to multigenerational scans without need for another analyzer. We and others have previously documented multigenerational collision-induced dissociation scans wherein multiple generations of fragment ions can be produced by sweeping the rf amplitude from high to low while a fixed excitation frequency is applied for CID[153,172,305,306] or by applying multiple resonance frequencies

corresponding to, for example, fixed neutral loss fragments.[299] A similar experiment can be performed in ion traps by sweeping the ac frequency in the unconventional direction (low to high) so that high mass ions are first to fragment, followed by their product ions.[306] For example, **Figure 10.4a** shows a full ac scan mass spectrum from 100 to 360 kHz (the opposite direction to that used in **Figure 10.3**). Resolution and sensitivity are much worse in this mode due to ion frequency shifts, as has been documented previously,[24,36,50,119,307,308] which is further compounded by the rf ramp.

A precursor ion scan of *m/z* 119 gives only protonated amphetamine (m/z 136) (and a broad peak due to its unwanted rf ramp resonance ejection). Nonetheless, using the relationship *m/z* 136->119->91, we can perform a *multigenerational precursor ion scan* by setting the product ion ejection frequency on *m/z* 91 (experimentally 261 kHz, calculated 253 kHz) and observing the transition *m/z* 119->91 at t = 0.135 s, which corresponds to a secular frequency of 187 kHz for the *m/z* 119 ion, in agreement with the calculated value. This peak is *not* observed in the full mass scan because it can only be produced by first fragmenting *m/z* 136 (at t = 0.095 s) and subsequently fragmenting its product ion *m/z* 119 (at t = 0.135 s) and finally ejecting the second generation product ion *m/z* 91. This experiment is akin to setting the third and fifth analyzers in a pentaquadrupole mass spectrometer[296,309-311] on *m/z* 119 and *m/z* 91, respectively, and scanning the first quadrupole through a range of precursor ion *m/z* values. However, the pentaquadrupole is considerably more complex and is not amenable to portable and miniature instruments, particularly those for planetary exploration. Of course, the relationship between *m/z* 136 and *m/z* 91 is only clear in the ion trap data when both the single and multigenerational precursor scans are compared (or if the forward and reverse precursor scans are compared). Otherwise, the relationship would be ambiguous.

10.4.5 Precursor ion scanning of cluster ions

The tightly controlled nature of the commercial LTQ – that is, the forced use of the Ultrazoom scan to approximate a fixed rf amplitude – restricted our experiments to ions that fragment quite readily. Furthermore, there was a lower limit to the ac frequency scan rate, again forced by the use of an rf ramp. With more customized instrumentation, however, the excitation scan could be slowed to give each ion more time on resonance, thereby increasing the quantity of product ions formed. As a result of these restrictions, cluster ions were ideal for precursor ion scanning because i) they fragment readily with very little resonance time, ii) they form similar

product ions, and iii) the precursor ions fall over a wide mass range. This last characteristic made simple mass calibration possible, as discussed later.

Precursor ion scans were performed in the positive ion mode on cesium tridecafluoroheptanoic acid clusters (**Figure 10.5a-d**), cesium monobutyl phthalate clusters (**Figure 10.5e-f**), and on sodium sulfate clusters (**Figure 10.6**). In the case of the cesium-containing clusters, at both high and low *m/z* clean precursor ion spectra were obtained (**b**, **d**, and **f**). These spectra mimicked the full scan mass spectra (**a**, **c**, and **e**) because the clusters in the full scan fragment easily to similar product ions. For example, for higher mass CsTFHA clusters, *m/z* 629 was a common fragment, and for lower mass CsTFHA clusters, *m/z* 133 was a common fragment. The CsMBP clusters shared *m/z* 841 as the common product ion; hence, a precursor ion scan of this product ion (**Figure 10.5e**) mirrored the full scan data (**Figure 10.5f**).

10.4.6 Linear mass calibration

All of the data shown up to this point was obtained using linear frequency sweeping. Linear frequency sweeping gives each ion the same amount of time on resonance because the scan rate in frequency units per unit time is constant. However, the mass spectral data then must be calibrated using the nonlinear Mathieu parameters, which is not ideal.[91] For another example, a full scan of sodium sulfate cluster ions is shown in **Figure 10.6a**. The precursor ion scan of *m/z* 660 (**Figure 10.6b**), a common product ion, gives a single stage MS-like spectrum. However, the nonlinear nature of the relationship between ion secular frequency and time makes calibration unintuitive. Instead, the excitation waveform can be replaced by a nonlinear frequency sweep in the form of an inverse Mathieu q scan (as shown in **Figure 10.6b**), which excites the precursor ions such that there is an approximately linear relationship between the excited ion's *m/z* and time.[133] **Figure 10.6c** shows the same precursor ion spectrum wherein the excitation scan was an inverse Mathieu q scan from q = 0.908 to q = 0.15 taken over 300 ms. As shown in panel **d**, there is an approximately linear relationship between *m/z* and time, making calibration simple. Note, however, that because the excitation frequency is scanned nonlinearly, the precursor ions will have the about the same number of secular oscillations but different amounts of time on resonance, which can affect the relative intensities of the peaks observed.

10.5 Conclusion

We have demonstrated precursor ion scanning in single quadrupole ion trap mass analyzers using an orthogonal double resonance technique. In combination with nanoelectrospray, the data-independent precursor ion scan uses minimal sample yet maintains reasonable sensitivity, characteristics ideal for resource-limited situations (e.g. a miniature ion trap mass spectrometer on Mars).

Orthogonal activation suffers from fewer artifact peaks than parallel activation and therefore allows for higher energy deposition into the precursor ions without fear of precursor ion detection. Unlike triple quadrupole and other double analyzer instruments, the choice of scan direction in the ion trap can be used to access higher order precursor scanning experiments by successively fragmenting precursor and product ions in the same excitation sweep. Furthermore, a linear relationship between *m/z* and time can be observed if the precursor ion excitation scan is an inverse Mathieu q scan. Cluster ions are ideal calibrants for these scans because they share product ions, fragment quite readily, and fall over a wide mass range.

Further work is needed in order to characterize resolution and sensitivity in order to understand the performance of single analyzer precursor scans compared to multi-analyzer scans.

The results demonstrated here pave the way for further utilization of precursor ion scanning as well as implementation of neutral loss scanning and double resonance multiple reaction monitoring scans in single ion trap mass analyzers using orthogonal excitation. These scans will further solidify the quadrupole ion trap's emerging standing as the most versatile of mass analyzers as well as the one most amenable to miniaturization.

10.6 Acknowledgements
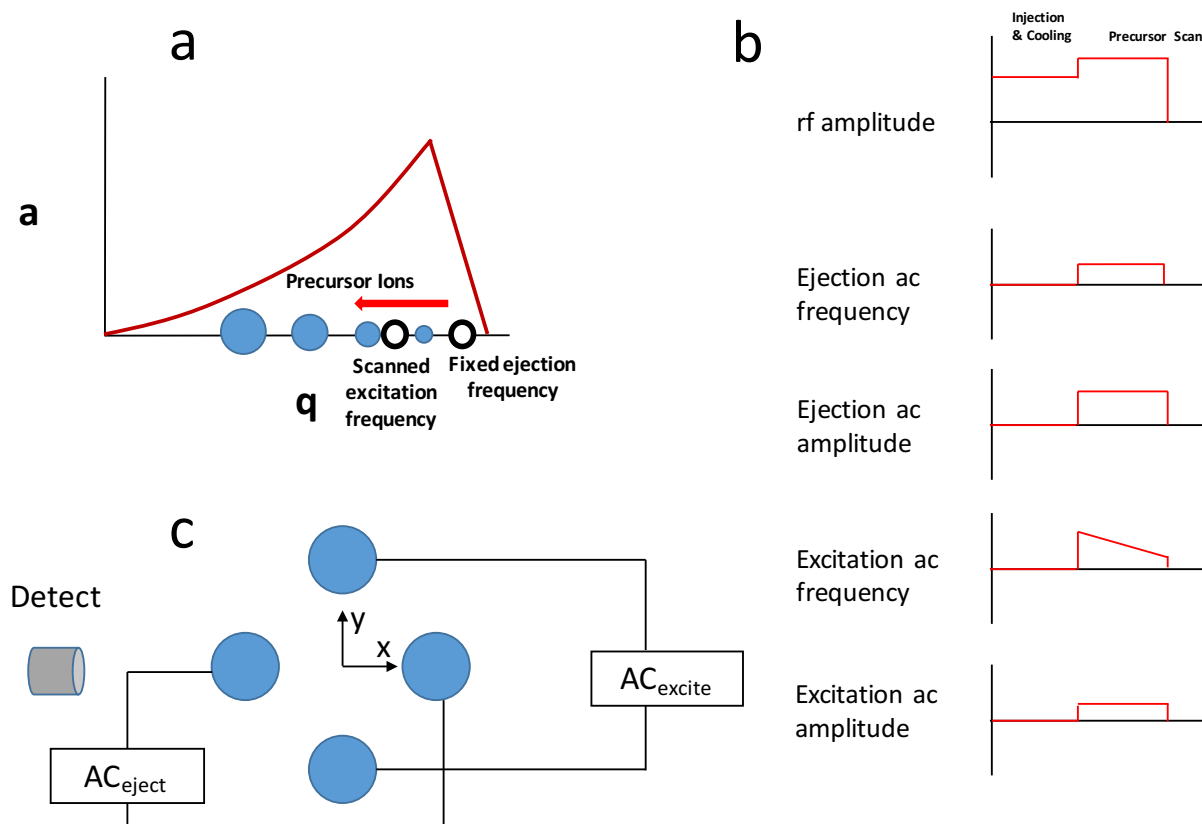
Figures

Figure 10.1. Single analyzer precursor ion scans in a quadrupole ion trap using orthogonal double resonance excitation: (a) illustration of precursor ion scanning on the Mathieu stability diagram, where a first ac frequency is scanned through ion secular frequencies to excite precursors while simultaneously a second ac signal is fixed on a particular product ion, (b) scan table for the precursor scan, and (c) schematic of orthogonal ac signals applied to the rods of an LTQ linear ion trap.
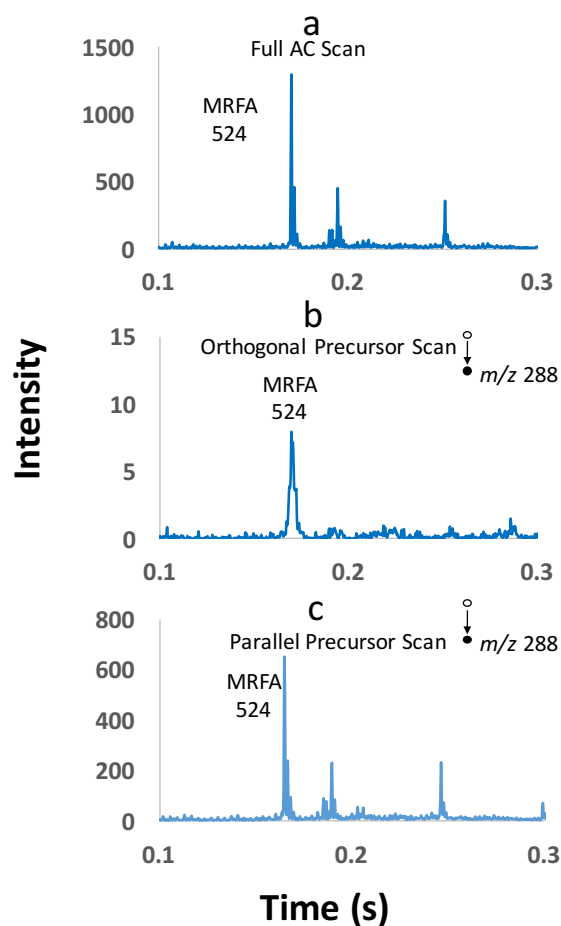
Figure 10.2. Comparison of parallel and orthogonal precursor ion scans. (a) Shows full ac scan mass spectrum of MRFA, (b) shows orthogonal precursor scan of *m/z* 288, and (c) shows parallel precursor scan of *m/z* 288 wherein both excitation and ejection signals were applied to the x electrodes. The excitation signal was scanned from 200 to 140 kHz over 0.3 s with an amplitude of 1.1 V_{pp}. The ejection signal was set at a frequency of 331 kHz, 1 V_{pp}. The Ultrazoom scan started at *m/z* 240.
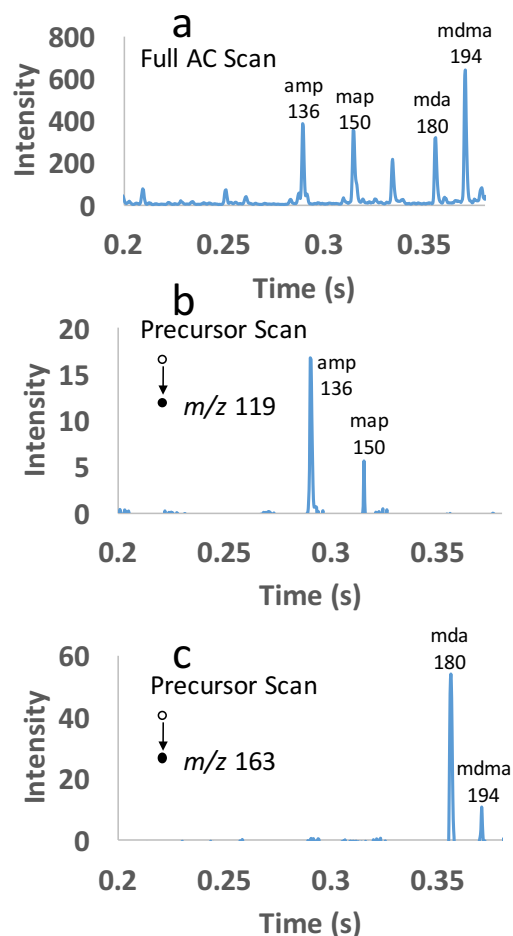
Figure 10.3. Orthogonal double resonance precursor ion scanning of amphetamines. (a) full ac frequency scan mass spectrum of amphetamine (amp), methamphetamine (map), 3,4-methylenedioxyamphetamine (mda), and 3,4-methylenedioxymethamphetamine (mdma), (b) orthogonal precursor ion scan of m/z 119, and (c) orthogonal precursor ion scan of m/z 163. The excitation signal on the y electrodes was scanned from 360 to 100 kHz over 400ms with an amplitude of 260 mV$_{pp}$. The ejection signal on the x electrodes was set at (b) 206 kHz, 260 mV$_{pp}$, or (c) 151.6 kHz, 240 mV$_{pp}$. The Ultrazoom scan started at m/z 60. For (b) and (c), resonance ejection background signal was subtracted from the raw signal.
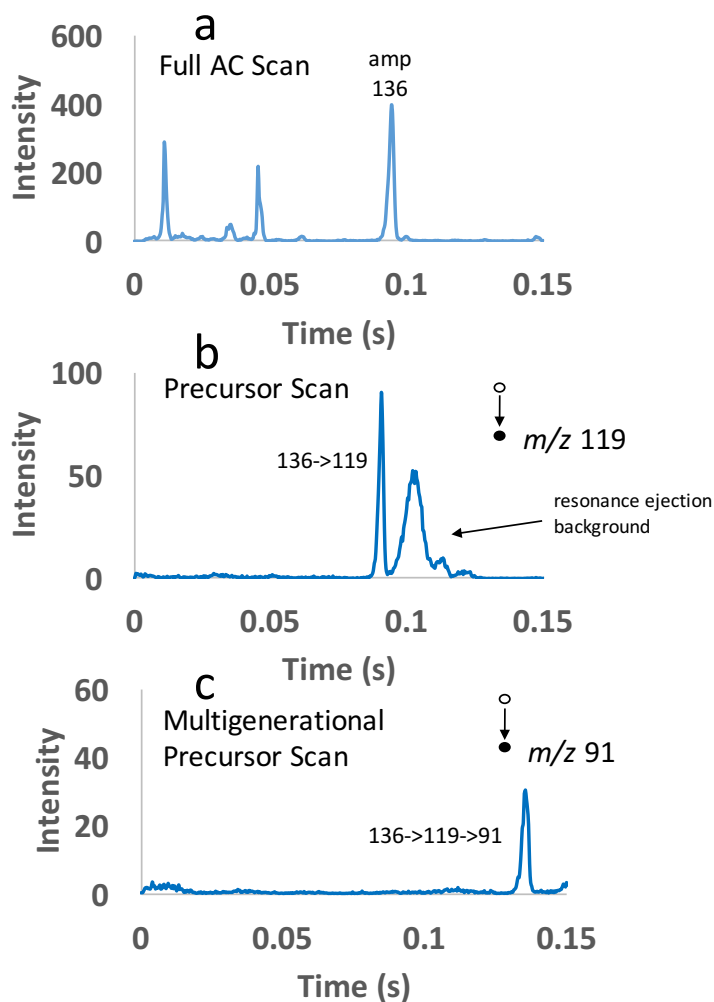
Figure 10.4. Multigenerational precursor ion scanning in a single linear ion trap. (a) shows full scan mass spectrum from high to low mass (low to high frequency), (b) shows single generation precursor ion scan of *m/z* 119, and (c) shows multigenerational precursor ion scan of *m/z* 91 (a product ion of *m/z* 119 and second generation product ion of *m/z* 136). The excitation signal on the y electrodes was scanned from 100 to 360 kHz with an amplitude of 240 mV$_{pp}$ over 0.4 s. The ejection signal on the x electrodes was set at (b) 188 kHz (240 mV$_{pp}$) or (c) 261 kHz (240 mV$_{pp}$). The Ultrazoom scan started at *m/z* 90.
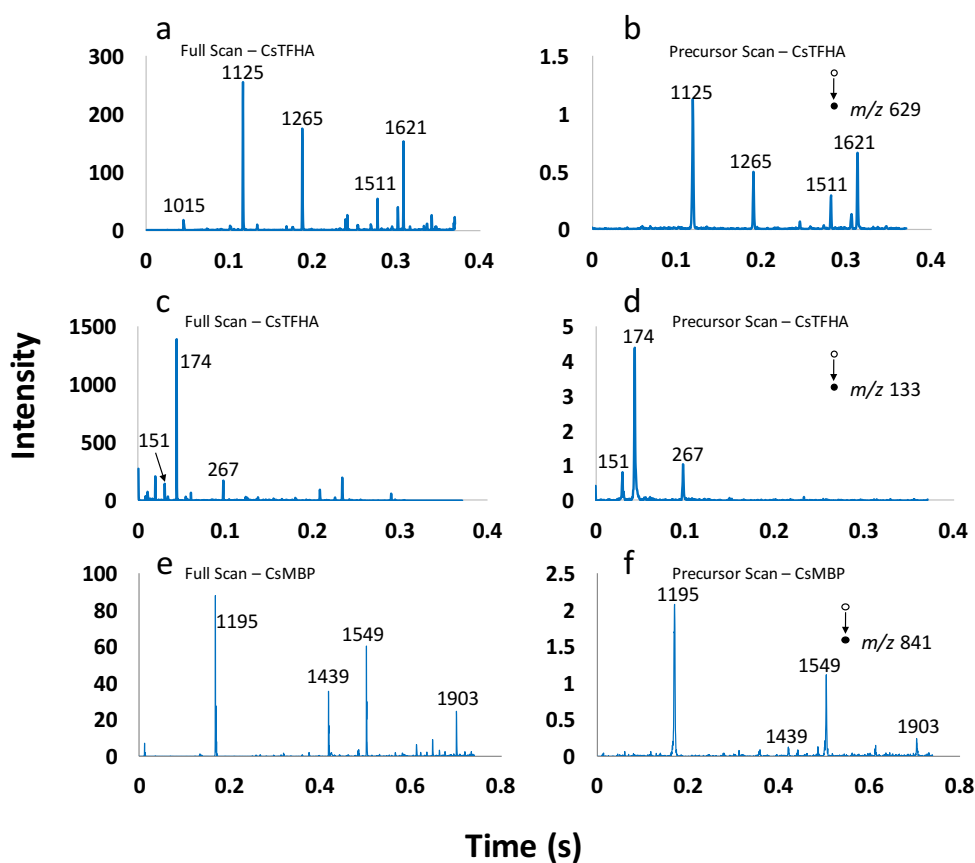
Figure 10.5. Single analyzer precursor ion scans of cesium salt clusters: (a) full ac frequency scan of CsTFHA clusters from *m/z* 1000 to 2000, (b) precursor ion scan of *m/z* 629, (c) full ac scan of CsTFHA clusters from *m/z* 100 to 500, (d) precursor ion scan of *m/z* 133, (e) full ac scan of CsMBP clusters from *m/z* 1000 to 2000, and (f) precursor ion scan of *m/z* 841.
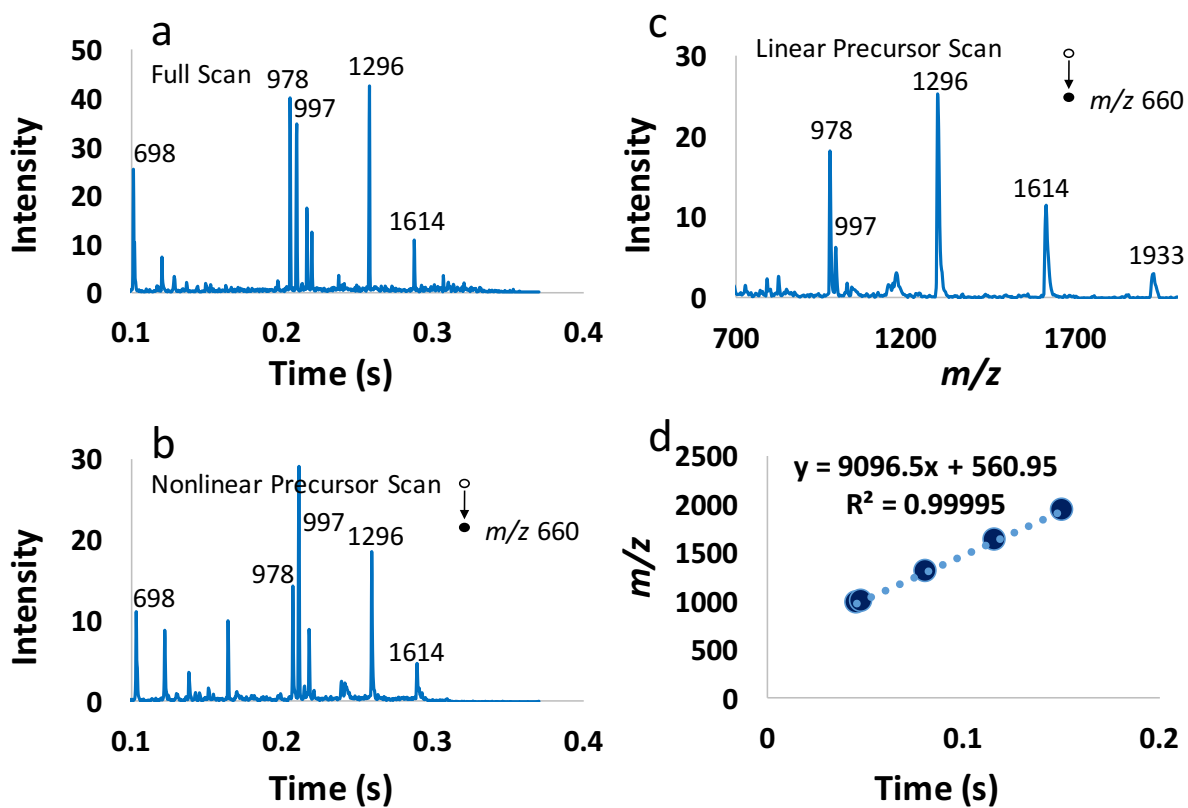
Figure 10.6. Linear mass calibration in single analyzer precursor ion scans: (a) full ac scan of NaSO$_4$ clusters, (b) nonlinear precursor ion scan of *m/z* 660 (linear frequency sweep), (c) precursor ion scan of *m/z* 660 using the inverse Mathieu q scan for excitation, and (d) linear mass calibration for the scan in (c).

Table 10.1. Precursor and product ion nominal *m/z* values for compounds in this study. Data acquired on an LTQ linear ion trap at q = 0.25. Normalized collision energy was generally 25 (arb. units) but was increased in some cases (e.g. MRFA). Bold values indicate the most abundant product ions, which were the ones used for precursor ion scanning.

Analyte	Precursor *m/z*	MS/MS *m/z*
Caffeine	195	**138** 110
MRFA	524	507, 489, 454, 435, 418, 407, 376, **288**, 271, 229
Amphetamine (amp)	136	**119** (->91 in MS^3), 91
Methamphetamine (map)	150	**119** (->91 in MS^3), 91
3,4-Methylenedioxyamphetamine (mda)	180	**163**
3,4-Methylenedioxymethamphetamine (mdma)	194	**163**
Oxycodone (oxy)	316	**298**
Noroxycodone (noxy)	302	**284**
Ketamine (ket)	238	**220**
Cesium tridecafluoroheptanoic acid clusters (CsTFHA)	151	**133**
	174	**133**
	267	**133**
	1125	356, **629**, 996
	1265	**629**, 769
	1511	**629**, 1015
	1621	**629**, 1125
Cesium monobutyl phthalate clusters (CsMBP)	1195	487, **841**
	1439	487, 731, **841**, 1085
	1549	487, **841**, 1195

Table 10.1 continued

	1903	**841**, 1195, 1549
Sodium sulfate clusters	698	**660**
	828	**660**
	978	**660**
	997	360, **660**
	1030	394, 550, **660**
	1046	409, **660**, 858, 994
	1296	**660**, 978
	1614	**660**, 978, 1297, 1551, 1588

CHAPTER 11.   SINGLE ANALYZER NEUTRAL LOSS SCANS IN A LINEAR QUADRUPOLE ION TRAP USING ORTHOGONAL DOUBLE RESONANCE EXCITATION

11.1 Abstract

In this follow-up paper to our previous work on single analyzer precursor ion scans in a linear quadrupole ion trap (Snyder, D. T.; Cooks, R. G.; "Single analyzer precursor ion scans in a linear quadrupole ion trap using orthogonal double resonance excitation", *J. Am. Soc. Mass Spectrom.* **2017**, *28*, 1929-1938.), we now report the development of single analyzer neutral loss scans in a linear quadrupole ion trap using orthogonal double resonance excitation. Methodologically, there are three key differences between single analyzer precursor ion scans and neutral loss scans under constant radiofrequency (rf) conditions: 1) in the latter experiment both excitation and ejection frequencies must be scanned, whereas in the former the ejection frequency is fixed, 2) the need to maintain a constant neutral loss while incrementing both precursor and product ion masses - complicated by the complex relationship between secular frequency and mass - requires use of two simultaneous frequency scans, both linear in mass, and 3) because the ejection frequency is scanned, a third ac signal occurring between the ac excitation and ac ejection frequency scans must also be applied and scanned in order to reject artifact peaks caused by ejection of unfragmented precursor ions. Using this methodology, we demonstrate neutral loss scans on a commercial linear ion trap using mixtures of illicit drugs and acylcarnitines. We also demonstrate neutral loss scanning on a *Populus deltoides* leaf and on a lignin sample, both significantly more complex mixtures.

11.2 Introduction

The beginnings of tandem mass spectrometry (MS/MS or MS^n) date back to the first mass-analyzed ion kinetic energy spectrometer (MIKES) developed at Purdue University.[312-316] Tandem MS, the production and mass analysis of fragment ions from mass-selected precursor ions, is

particularly useful for complex mixture analysis and has served as the backbone of fields as diverse as proteomics,[298,299,317] forensics,[318,319] environmental monitoring,[205,320] and biomarker discovery.[321,322]

Amongst the activation methods for MS/MS are collision-induced dissociation (CID),[323] ultraviolet photodissociation,[164,324,325] infrared multiphoton dissociation,[326] electron transfer dissociation,[327] surface-induced dissociation,[166,328,329] and others. Collision-induced dissociation has been especially notable in the development of the suite of MS/MS scan modes which includes three prominent members - product ion scans, precursor ion scans, and neutral loss scans[58,293] – as well as other notable modes - doubly charged ion scans,[330] reaction intermediate scans,[331] multiple reaction monitoring,[332] and functional relationship scans.[333] Of interest in this work is the neutral loss scan, which is readily implemented in multi-analyzer instruments such as the triple quadrupole[58] but not previously accessible with any single mass analyzer operated in a data-independent mode.

Although neutrals are not directly measurable by mass spectrometers, they are indirectly accessible by a variety of methods and they carry important analytical information. The two most prominent techniques for probing neutral species are neutralization-reionization mass spectrometry (NRMS)[334-336] and the neutral loss scan.[337] The NRMS experiment neutralizes a mass-selected ion, usually by charge exchange or CID, and the resulting neutral undergoes energetic collisions which produce neutral fragments that are re-ionized and mass analyzed. Hypervalent and other unusual species can be produced and characterized,[338-340] a unique capability.

By contrast, in a neutral loss MS/MS experiment a precursor ion is mass-selected by a first mass analyzer and undergoes activation to produce a product ion and a neutral. The product ion is mass selected for detection by a second analyzer. For the neutral loss scan, the relationship between the precursor ion mass-to-charge ratio (m/z) and the product ion m/z is fixed – that is, the neutral mass is constant - and as such it describes a shared molecular functionality of a group of precursor ions. In comparison, the precursor ion scan selects a fixed product ion m/z which might also correspond to a common functionality in all precursor ions which yield this fragment.

Because mass selection of both precursor and product ion is necessitated in precursor ion and neutral loss scans, the prevailing wisdom in mass spectrometry has been that multiple mass analyzers are required. However, Yost et al. demonstrated in principle that a single 3D ion trap

could perform a single analyzer precursor ion scan by using multiple simultaneous resonance frequencies corresponding to precursor and product ion.[123] In other words, the precursor ion is mass-selectively activated via CID by a first scanned resonance frequency, and product ions of a selected *m/z* (determined by the resonance frequency) are then simultaneously ejected upon their formation by a second fixed resonance frequency. The correlation between *m/z* and time is thus preserved in the ejection time of the product ion.

The first published implementation of the single analyzer precursor ion scan in a linear ion trap[99] used the Mini 12[100] miniature rectilinear ion trap mass spectrometer developed at Purdue University. In that experiment, the two resonance frequencies were applied in a *parallel* fashion on the same pair of electrodes; however, beat frequencies and unintentional ejection of precursor ions during excitation caused artifact peaks, which significantly hampered the utility of this scan mode. Subsequently, we developed an *orthogonal* version of the precursor scan experiment in which precursor ion excitation and product ion ejection frequencies were applied to orthogonal electrode pairs, thereby mitigating both problems simultaneously.[341]

Here we demonstrate the corresponding neutral loss scan mode in a single linear ion trap, also using orthogonal double resonance excitation. The implementation of neutral loss scans, as well as precursor ion scans, in a single mass analyzer is motivated by the constraints placed upon miniature and portable mass spectrometers,[70,71] for which simple, power-efficient electronics, lenient vacuum conditions, and small footprints are imperative. These considerations eliminate multiple-analyzer mass spectrometers as candidate analyzers in a portable system. The constraints are further exacerbated in space science, where power consumption and instrument volume are of the utmost concern.[139] The ultimate goal in this work is the eventual implementation of both precursor ion and neutral loss scans on the next-generation linear ion traps developed at NASA Goddard Space Flight Center for detection of organic compounds on Mars.

11.3 Experimental

11.3.1 Chemicals

Acetyl-L-carnitine (C_2 side chain) hydrochloride, propionyl-L-carnitine (C_3), isobutyryl-L-carnitine (C_4), isovaleryl-L-carnitine (C_5), and hexanoyl-L-carnitine (C_6) were purchased from Sigma Aldrich (St. Louis, MO, USA). These compounds were dissolved and diluted in 50:50 methanol/water. Amphetamine, methamphetamine, 3,4-methylenedioxyamphetamine, and 3,4-

methylenedioxymethamphetamine were purchased from Cerilliant (Round Rock, TX, USA) and were diluted in methanol to concentrations between 0.25 and 1 ppm. Pierce ESI LTQ calibration mixture containing caffeine, the peptide MRFA, and Ultramark 1621[124] was obtained from Thermo Fisher (Rockford, IL, USA). Organosolv switchgrass lignin was prepared as previously described[342] and dissolved initially in 50:50 water:tetrahydrofuran but then diluted further in 50:50 methanol:water.

11.3.2 Ionization

Nanoelectrospray ionization (nESI) was used for production of analyte ions in the majority of this study. Typical operating parameters were 1,500 V spray voltage using 5 μm nanospray tips pulled from borosilicate glass capillaries (1.5 mm O.D., 0.86 I.D.; Sutter Instrument Co., Novato, CA, USA) by a Flaming/Brown micropipette puller (model P-97; Sutter Instrument Co.).

A leaf from a *Populus deltoides* tree (latitude 40.464, longitude -86.968) was analyzed by leaf spray ionization tandem mass spectrometry.[184,261] For this experiment, a triangle (~8 mm height, 5 mm width) was cut from the leaf, held in a copper clip, and 5 kV was applied to the leaf after addition of 20 μL of methanol/water in order to generate ions for analysis.

The positive ion mode was used for all experiments. Ion injection time was generally set at 5 ms but was manually optimized to prevent trap overloading. Automatic gain control was not used in this study.

11.3.3 Instrumentation

A Thermo Scientific LTQ linear ion trap mass spectrometer (San Jose, CA, USA) with rf frequency tuned to 1.164 MHz was used for all experiments. The dimensions of the trap are $x_0 =$ 4.75 mm, $y_0 = 4$ mm, and 3 axial sections of 12, 37, and 12 mm.[10] As described previously,[341] the commercial rf coil was modified with an extra Thermo LTQ low pass filter board (part 97055-91120) and Thermo LTQ balun board (part 97055-91130) in order for low voltage ac signals to be applied to both x and y electrodes of the linear ion trap.[10] As supplied commercially, the LTQ can only apply supplementary ac voltages to the x electrodes, the direction in which the detector lies, but in this study orthogonality of excitation and ejection signals is crucial to obtaining unambiguous results.

In contrast to our previous study on single analyzer precursor ion scans, the rf voltage in this study was fixed by substituting the rf modulation signal between the main rf amplifier board

and the rf detector board with a DC signal from an external function generator. The DC signal was directly proportional to the output voltage from the coil, as indicated by the calibrated lower-mass cutoff (LMCO) and mass scan rate values (**Table 11.1**). For example, a modulation signal of 210 mV$_{pp}$ provided a LMCO of ~100 Th. Due to electronic constraints, the amplitude of the modulation signal did not vary through the scan period and was constant through the ionization, ion cooling, and mass scan time segments. The duty cycle of the modulation signal was ~90%, the remaining time being used to pulse the analyzer to zero voltage and thus clear the trap of ions after every scan.

Neutral loss scans were performed by simultaneously applying three swept-frequency sinusoidal inverse Mathieu q scans to the x and y electrodes of the linear ion trap, as shown in the Mathieu stability diagram in **Figure 11.1a** and the scan table in **Figure 11.1b**. In general, all the inverse Mathieu q scans started at Mathieu q = 0.908 (start frequency of 580 kHz) and ended at q = 0.15 (end frequency of 62 kHz) 300 ms later. These scans give an approximately linear relationship between excited/ejected ion *m/z* and time.[133,230] Note that because the same frequency sweeps were used throughout this study, a higher rf voltage (and hence LMCO) will result in lower activation time for each precursor ion since the scan rate is proportional to the rf voltage.

A first frequency sweep was used for ion excitation, a second frequency sweep was used for precursor ion rejection after its excitation (artifact rejection), and a third frequency sweep was used for product ion ejection. The former two ac signals were summed and applied to the y electrodes and the third signal was applied to the x electrodes (**Figure 11.1c**), viz. in the dimension in which ions are detected. The frequency sweeps were all calculated in Matlab and applied by two synced Keysight 33612A 2-channel waveform generators (Newark, SC, USA). For application of two simultaneous frequency sweeps to the y electrodes, the two channels of one of the generators were summed into a single channel, a built-in feature of these Keysight units. The second Keysight generator supplied the product ion ejection frequency sweep and the dc signal for rf modulation.

In order to maintain a constant mass offset between the excitation frequency sweep and the ejection frequency sweep - a requirement for a neutral loss scan - the delay time between application of the excitation sweep and ejection sweep had to be varied. Because t $\propto$ *m/z*, to a close approximation, for the inverse Mathieu q scan, a time offset between two identical frequency sweeps corresponds to a constant mass offset throughout the mass scan. The time offset could be

approximated from the calibrated mass scan rate. Once the time offset was selected and verified experimentally, the time offset between the excitation frequency sweep and the artifact reject sweep was made approximately half the offset between the excitation and ejection sweeps. The artifact rejection sweep ejects into the y electrodes precursor ions that survive the excitation sweep, as we will discuss later, and is an important difference between single analyzer precursor ion scans and neutral loss scans.

The function generators were triggered just before the ionization period using the triggers built into the LTQ 'Diagnostics' menu, and the trigger delays were then adjusted so that the neutral loss scan started at the beginning of the LTQ's data acquisition period (i.e. mass scan). For a built-in scan function, the commercial 'Ultrazoom' scan was chosen. However, the 'Ultrazoom' selection as used here did not control the scan rate or rf amplitude; it only controlled the length of data acquisition and digitization rate of the detection electronics. Each spectrum displayed here is an average of 20 scans.

11.4 Results & Discussion

11.4.1 Comparison between single analyzer precursor ion scans and neutral loss scans

In previous work we demonstrated single analyzer precursor ion scans in a linear ion trap using orthogonal double resonance excitation at constant rf amplitude, that is, using sweeps of the low voltage ac frequency.[341] In order to mass-selectively fragment precursor ions as a function of time, a first swept-frequency sinusoidal ac signal is applied to the y electrodes. To eject a particular product ion, a second ac signal with fixed frequency corresponding to that of the product ion is applied simultaneously to the x electrodes (direction in which ions are detected). The orthogonality of the excitation and ejection ac signals is key to preventing artifacts from being observed in the mass spectrum since precursor ions can be unintentionally ejected during the excitation frequency sweep. Thus, a signal is observed at the detector only when a precursor ion fragments to the product ion whose secular frequency is selected for ejection. Mass information is preserved in the ejection time of the product ion, which correlates to the fragmentation time of the precursor ion.

Neutral loss scans in a single linear ion trap have similarities to precursor ion scans but are significantly more complex. The difficulty stems from the following differences: 1) the ejection frequency must be scanned and hence it will eject both undesired precursor ions that survive fragmentation as well as the desired product ions formed during fragmentation, and 2) the

excitation and ejection frequency sweeps must have a constant mass offset through the entire mass scan (a difficult task due to the complex relationship between secular frequency and ion m/z).

The first problem can be mitigated by scanning a third frequency for 'artifact rejection' (**Figure 11.1a** and **11.1b**). The artifact rejection frequency sweep must occur between the excitation and ejection frequency sweeps. Hence, during the simultaneous sweep of all three frequencies, precursor ions will first fragment because of the y-dimension excitation, neutral loss products will simultaneously be ejected into the detector by the dipolar x-direction ejection sweep, and leftover precursor ions will be ejected into the y electrodes by the artifact rejection sweep.

The second problem is maintenance of a constant mass offset between the excitation and ejection frequencies. The fact that the relationship between ion secular frequency and m/z cannot be described analytically but instead requires a numerical or analytical (i.e. a finite equation) approximation[8,91,343] makes calculation of the frequency sweeps difficult unless the relationship between m/z and time is linear, as is the case for the inverse Mathieu q scan.[133,135,230] By using this nonlinear frequency sweep for excitation, ejection, and artifact rejection, a simple experimental parameter, the delay time between the frequency sweeps, then determines the mass of the neutral loss (**Figure 11.1b**). This fortunate relationship is only applicable to the inverse Mathieu q scan because $t \propto m/z$ and therefore $\Delta t \propto \Delta m/z$.

Of course, the amplitude of each of the three frequency sweeps needs to be adjusted according to the intended function. The excitation sweep should have the lowest amplitude so that it activates, not ejects, precursor ions. The artifact rejection and product ion ejection sweeps should both have higher amplitudes in order to eject precursor and product ions, respectively. The former should be adjusted to 1) prevent premature ejection of precursors but also 2) to efficiently eject precursors after activation. Importantly, the smaller the neutral loss mass, the closer each frequency sweep will be and hence the lower the amplitude that will be used for artifact rejection. The product ion ejection amplitude should be adjusted for sensitivity and resolution. In this work, the excitation signal was a few hundred millivolts, whereas the rejection and ejection sweeps were generally 3-6 times higher in amplitude. See **Table 11.1** for all experimental parameters.

To sum up the neutral loss scan experiment, a first inverse Mathieu q scan activates precursor ions, and simultaneous sweeps of two additional inverse Mathieu q scans with appropriate time delays reject leftover precursor ions and eject product ions of a constant mass offset. The three ac waveforms are identical inverse Mathieu q scans which allows one to easily

maintain a constant mass offset. The excitation and artifact reject sweeps are applied in the y dimension to reduce artifacts from ejection of precursor ions, and the ejection sweep is applied in the x direction, where the detector is placed (**Figure 11.1c**). The amplitude of each signal is adjusted for its intended function.

11.4.2 Validation of neutral loss scanning by double resonance excitation

In order to experimentally validate whether neutral loss scans are viable using a single linear ion trap, particularly with respect to artifact rejection, we began experiments with a very simple LTQ calibration mixture containing caffeine, the peptide MRFA, and Ultramark 1621 phosphazine molecules. To validate artifact rejection, only the low mass range (i.e. region surrounding the m/z of protonated caffeine) was considered. **Figure 11.2a** shows a full mass scan in this mass range (LMCO = 100 Th) using a 300 ms inverse Mathieu q scan from Mathieu q = 0.908 to q = 0.15. Only caffeine, m/z 195, is present in high abundance and hence it should also be the only ion detected in a neutral loss scan of 57 Da (m/z 195->138). As shown in **Figure 11.2b-e**, only the neutral loss scan with all three ac frequency sweeps applied simultaneously gives an unambiguous mass spectrum (panel **b**). With the artifact rejection frequency off (**Figure 11.2c**), several peaks are observed to confound the data, and with either the excitation (**Figure 11.2d**) or ejection (**Figure 11.2e**) frequencies off, virtually no ions are detected. Note the different intensity scales for each plot. For the neutral loss scan, the full width at half maximum (FWHM) for caffeine is 0.6 Da.

11.4.3 Screening of illicit drugs

Previously we demonstrated the application of precursor ion scans to amphetamine analysis and showed that amphetamine (amp) and methamphetamine (map) can be detected via a precursor ion scan of m/z 119, and 3,4-methylenedioxyamphetamine (mda) and 3,4-methylenedioxymethamphetamine (mdma) can be detected using a precursor ion scan of m/z 163.[341] Analogously, a neutral loss scan of 31 Da returns map and mdma (**Figure 11.3b**, compare to full scan in panel **a**) whereas a neutral loss scan of 17 Da (NH_3) reveals amp and mda, despite their low intensity (<25 counts) in the full mass scan. For the latter scan, differences in fragmentation efficiency or differences in precursor ion Mathieu q parameter can account for the relative intensity shifts from the full scan to the neutral loss scan. Remarkably, neither neutral loss scan shows beat frequency effects or other artifacts which may be caused by simultaneous

excitation of multiple ions. Also note how cleanly the neutral loss scans of 31 Da and 17 Da distinguish the four amphetamines. The FWHM peak width in these spectra was ~0.9 Da.

11.4.4 Screening of acylcarnitines

In the premier demonstration of data-dependent ion trap precursor ion and neutral loss scanning, Yost *et al.* analyzed acylcarnitines, which offer similar product ions as well as similar neutral losses.[344] The Yost method required a complex sequence of scan segments and algorithms in order to select precursor ions for activation as well as to resonantly eject product ions without also ejecting other precursor ions. Although that method would be expected to yield higher sensitivity and resolution than the method proposed here (because each precursor ion is given more time on resonance and more time for product ion collisional cooling), the complexity and inefficiency of the scan with respect to electronics, data system, time, and hence power consumption makes it unsuitable for resource-constrained ion traps. Using the reported common neutral loss of 59 Da, we were able to perform a similar but data-independent neutral loss experiment with acetyl-, propionyl-, isobutyryl-, isovaleryl-, and hexanoyl-L-carnitine using a single ion injection (5 ms injection time) and a single 300 ms mass scan period. As shown in **Figure 11.4b** (compare to full scan in panel **a**), all of the acylcarnitines are detected, although only ~4% of the precursor ion intensity is observed due to the short activation time. The intensity in the neutral loss scan can be increased by decreasing the scan rate, giving precursor ions longer resonance times and thus increasing the conversion of precursor ions to product ions. For example, if the scan rate is decreased by a factor of three, then the efficiency of conversion of precursor ions to detected product ions becomes ~10%. Other peaks were observed between the main analyte peaks. These correspond to the sodiated analytes, which clearly exhibit higher conversion of precursor ions to product ions, likely due to the stabilization of the molecules via a salt bridge interaction.

11.4.5 Screening of phenolic glycosides in a Populus deltoides leaf

Moving to a complex mixture is a significant step for any scan mode, as additional complexity can easily result in addition of artifact peaks as well as suppression of analyte signal. As an initial demonstration of analysis of complex mixtures using a data-independent single analyzer neutral loss scan, we chose an individual leaf of a *Populus deltoides* tree.[261] The *Populus* genus is well-known to contain phenolic glycosides, which are defense chemicals that deter

herbivores and decrease their fitness.[345,346] Previously they have been analyzed by leaf spray ionization tandem mass spectrometry using a triple quadrupole mass spectrometer.[261] Potassiated salicortin and HCH salicortin (structures in ref. [261]) were previously observed as the dominant ions in the full scan, as they were in this study (**Figure 11.5a**). It was also noted previously that neutral losses of 44 Da in the positive ion mode (CO_2, as confirmed by exact mass measurement on an LTQ Orbitrap XL with < 1.0 ppm error) are common amongst the phenolic glycosides due to their unique (and shared) side chains, and hence a neutral loss scan ought to filter out most other chemicals.

A neutral loss scan of 44 Da (**Figure 11.5b**) revealed both potassiated salicortin as well as the potassium adduct of HCH salicortin. About 3% of the precursor ions were converted to detected product ions, in line with the data in the previous case. Despite the chemical complexity of the leaf, virtually no other peaks were observed in the neutral loss spectrum, perhaps because losses of CO_2 are not common in the positive ion mode. The peak width in this case was ~1 Da FWHM.

11.4.6 Screening of components in switchgrass lignin

The previous experiment provides evidence that a complex mixture can be vastly simplified using a single data-independent neutral loss scan in a single quadrupole ion trap. One might think, however, that ions of lower abundance than salicortin were not detected in the neutral loss scan because they were present at low concentrations. We therefore examined a mixture with a large set of ions of varying abundances that could be detected using a single neutral loss scan.

Organosolv switchgrass lignin is a complex mixture of phenolic compounds and carbohydrates – as well as other molecules with similar functionality – that has previously been characterized by HPLC-MS/MS in a linear quadrupole ion trap coupled to a Fourier transform ion cyclotron resonance mass spectrometer.[342] The study was performed primarily in negative ion mode because most of the ions produced in the positive ion mode lose 18 Da (water) in MS/MS, and hence MS/MS spectra in positive mode do not distinguish the various classes of molecules. However, for the purposes of determining the dynamic range of the neutral loss scan, the positive ion mode provides a reasonable set of analytes for examination.

As previously described and as shown in **Figure 11.6a**, the full scan mass spectrum of organosolv lignin is complex, but most of the molecules present in the full scan lose 18 Da in MS/MS. As shown in **Figure 11.6b**, a neutral loss scan of 18 Da returns not just the ions of high abundance, but also those of low abundance. Of course, the ions of interest must be labile enough

to fragment in a relatively short period of time (~1 ms), and so the neutral loss scan will inherently be biased against molecules that do not fragment readily. Another limitation of the ion trap neutral loss scan is that the selectivity is limited by secular frequency spacing and bandwidth. It is hence difficult to distinguish neutral losses of similar mass. As shown in **Figure 11.6b**, not only were water loss products detected, but also the loss of 17 Da (152->135). Exciting and ejection ions at varying Mathieu q exacerbates this problem. The sensitivity is limited by the limited activation time that each ion experiences, which in these experiments varied from ~350 μs to 1 ms. As noted previously, however, the conversion efficiency of precursors to products can be increased by slowing the scan rate.

11.5 Conclusion

Since the initial development of linear quadrupole ion traps approximately a decade and a half ago,[10,11] it has been the prevailing wisdom that single ion traps cannot perform data-independent precursor and neutral loss scans, two of the three main types of MS/MS experiments. As we have shown in this and the related paper on precursor ion scans, quadrupole ion traps are extraordinarily versatile devices with access to all three major MS/MS scan types.

Compared to previous variants of data-dependent neutral loss scanning, this double resonance neutral loss scan offers high efficiency in terms of time, rf power, and sample consumption. The demonstrated method is completely data-independent and only requires a single mass scan segment and a single ion injection, making it particularly suitable for planetary exploration and other applications where significant constraints are imposed upon the instrument.

11.6 Acknowledgements

Figures and Tables

Figure 11.1. Methodology for single analyzer neutral loss scans in a linear quadrupole ion trap. (a) As shown on the Mathieu stability diagram, three supplementary ac frequencies are scanned simultaneously at the same mass scan rate in order to excite precursor ions and simultaneously eject product ions of a constant mass offset from the precursors, while a third intermediate frequency is scanned to reject artifactual unfragmented precursor ions. A scan table of the experiment is shown in (b), and (c) shows the directionality of the low voltage frequency sweeps (trapping rf not shown). Adapted with permission, from *J. Am. Soc. Mass Spectrom.* **2017**, *28*, 1929-1938., Springer, 2017.
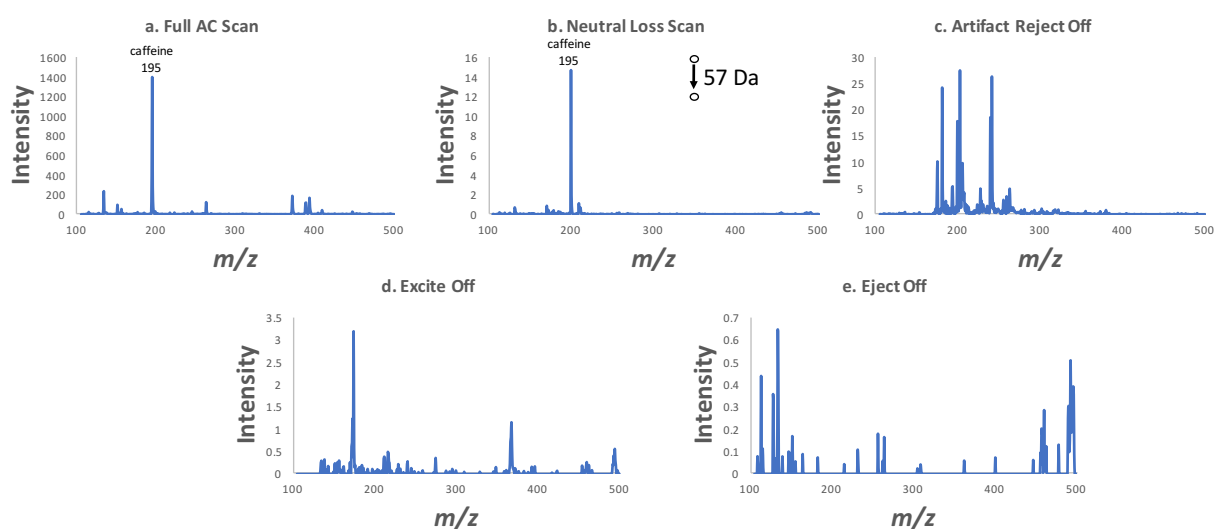
Figure 11.2. Only the combination of three ac frequency sweeps performed at the same mass scan rate gives an unambiguous neutral loss scan. (a) Full ac scan using LTQ ESI of caffeine in Pierce calibration mixture, (b) neutral loss scan of 57 Da, and neutral loss scans with (c) artifact reject frequency off, (d) precursor ion excitation frequency off, (e) product ion ejection frequency off. Note the different intensity scales.
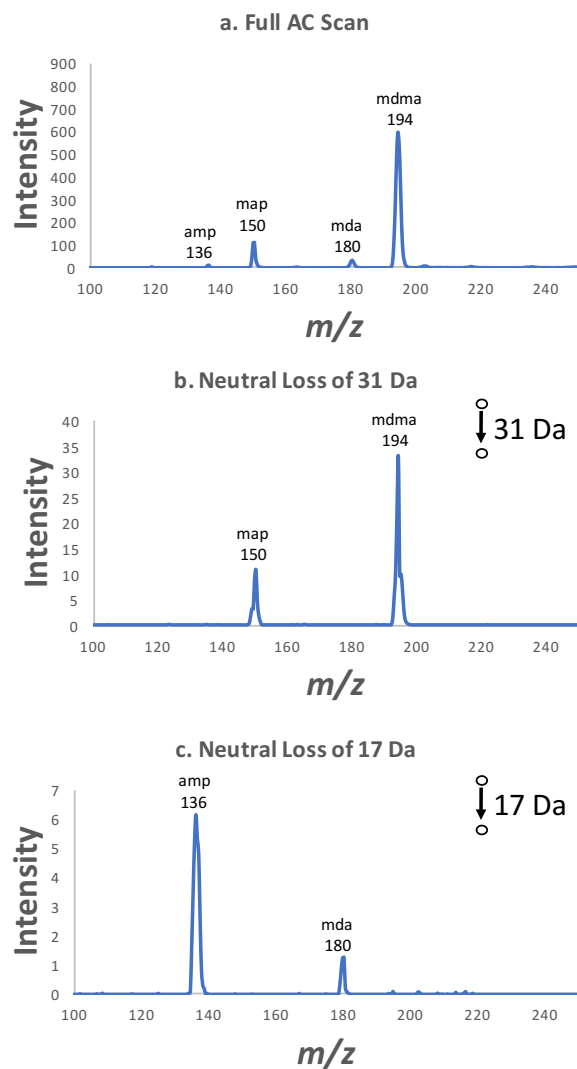
Figure 11.3. Single analyzer neutral loss scans of amphetamines:
(a) full scan mass spectrum of amphetamine (amp),
methamphetamine (map), 3,4-methylenedioxyamphetamine (mda),
and 3,4-methylenedioxymethamphetamine (mdma), (b) neutral
loss scan of 31 Da, and (c) neutral loss scan of 17 Da.
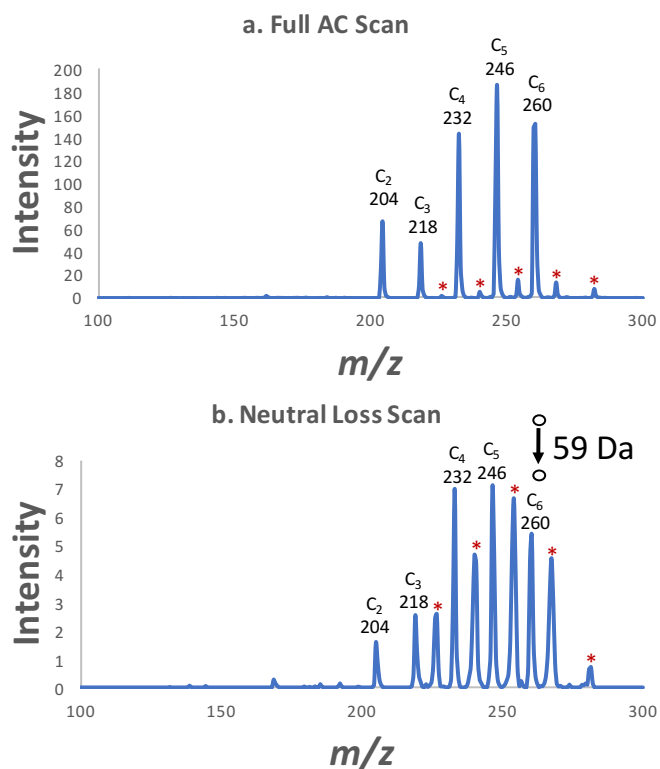
Figure 11.4. Single analyzer neutral loss scanning of acylcarnitines: (a) full ac scan of acetylcarnitine (*m/z* 204), propionylcarnitine (*m/z* 218), isobutyrylcarnitine (*m/z* 232), isovalerylcarnitine (*m/z* 246), and hexanoylcarnitine (*m/z* 260), and (b) neutral loss scan of 59 Da. Peaks marked with * are sodium adducts.
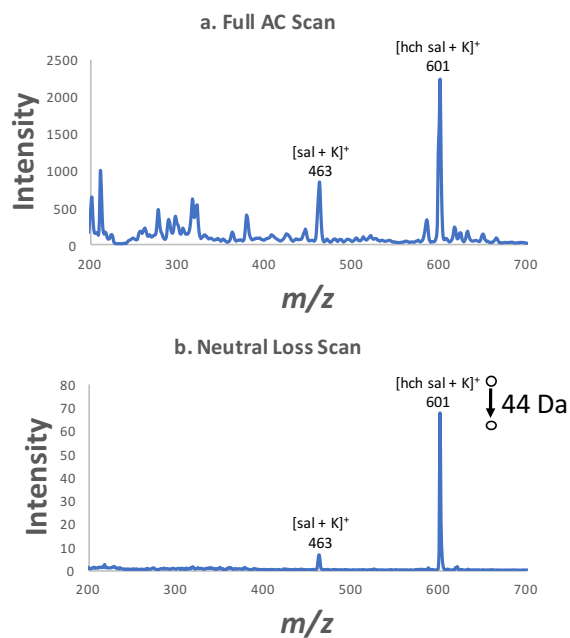
Figure 11.5. Single analyzer neutral loss scanning of a *Populus deltoides* leaf: (a) full scan mass spectrum and (b) neutal loss scan of 44 Da, targeting phenolic glycosides salicortin (sal) and HCH salicortin (hch sal).
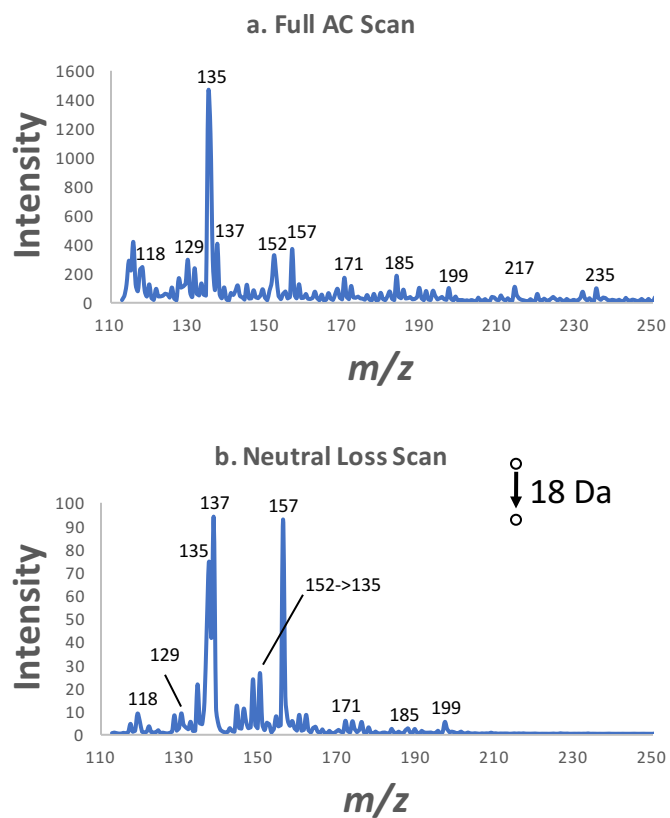
Figure 11.6. Single analyzer neutral loss scan of organosolv switchgrass lignin: (a) full scan mass spectrum and (b) neutral loss scan of 18 Da.

.

Table 11.1. Experimental parameters for all neutral loss scans performed in this work.

Figure	RF Modulation[1] (mV$_{pp}$)	LMCO (Th)	Scan Rate (Th/s)	Excitation Amplitude (mV$_{pp}$)	Artifact Reject Amplitude (mV$_{pp}$)	Eject Amplitude (mV$_{pp}$)	Excite Delay[2] (ms)	Artifact Reject Delay (ms)	Eject Delay (ms)	NL[3] (Da)
2b	210	100	1,740	400	2,700	1,200	75	91.35	112.6	57
3b	150	70	1,140	150	440	400	75	85.35	99.6	31
3c	150	70	1,140	140	190	400	75	80.35	94.5	19
4b	210	100	1,740	600	3,400	1,200	75	91.35	107.6	59
5b	300	200	2,900	400	2,000	1,600	75	79.35	87	44
6b	200	110	1,580	500	700	700	135	140	147	18

[1]RF Modulation is the dc voltage substituted between the rf detector board and rf amplifier and is proportional to the rf amplitude (i.e. determines the LMCO).
[2]Delay time indicates trigger delay between the beginning of the ionization phase to the application of the waveform. The difference between the excite delay and eject delay is directly proportional to the neutral loss mass.
[3]NL = neutral loss

CHAPTER 12.   PRECURSOR AND NEUTRAL LOSS SCANS IN AN RF SCANNING LINEAR QUADRUPOLE ION TRAP

12.1 Abstract

Methodology for performing precursor and neutral loss scans in an rf scanning linear quadrupole ion trap is described and compared to the unconventional ac frequency scan technique. In the rf scanning variant, precursor ions are mass selectively excited by a fixed frequency resonance excitation signal at low Mathieu q while the rf amplitude is ramped linearly to pass ions through the point of excitation such that *m/z* varies linearly with time. Ironically, a nonlinear ac frequency scan is still required for ejection of the product ions since their frequencies vary nonlinearly with the linearly-varying rf amplitude. In the case of the precursor scan, the ejection frequency must be scanned so that it is fixed on a product ion *m/z* throughout the rf scan, whereas in the neutral loss scan it must be scanned to maintain a constant mass offset from the excited precursor ions. Both simultaneous and sequential permutation scans are possible; only the former are demonstrated here. The scans described are performed on a variety of samples using different ionization sources: protonated amphetamine ions generated by nanoelectrospray ionization (nESI), explosives ionized by low-temperature plasma (LTP), and chemical warfare agent simulants sampled from a surface and analyzed with swab touch spray (TS). We lastly conclude that the ac frequency scan variant of these MS/MS scans is preferred due to electronic simplicity. In an accompanying manuscript, we thus describe the implementation of orthogonal double resonance precursor and neutral loss scans on the Mini 12 using constant rf voltage.

12.2 Introduction

Invented by Wolfgang Paul in the mid-twentieth century (though not used for mass analysis until much later),[1,4,347] the quadrupole ion trap (QIT) has become one of the most important tools

for chemical analysis, largely due to high sensitivity but also because of selectivity and ease of applicability. Other key developments in the history of the QIT are the development of mass-selective instability,[38] the first demonstration of collision-induced dissociation,[52] the invention of linear ion traps with quadrupolar potentials in two dimensions instead of the QIT's three,[10,11,43] and the implementation of resonance ejection (both radial[348] and axial[43]) on linear ion traps. Dual linear ion traps (LITs) (e.g. Thermo Velos),[61] triple quadrupole linear ion traps (e.g. SCIEX QTRAP)[244,245] and LIT-Orbitrap[349,350] or LIT-TOF[351] have recently become commonplace in modern instrument suites. Another important development, though less recognized, was the first demonstration of the precursor ion scan in the QIT.[352] This method used simultaneously two resonance (low voltage ac) frequencies to activate precursor ions mass selectively as a function of time while also targeting a fixed product ion for ejection from the ion trap, all while keeping the main trapping rf voltage constant during the mass scan. Subsequently, data-dependent scans became the predominant method for precursor and neutral loss 'scanning' in single 2D and 3D ion traps.[298,299,344,353] These are not single scans but are instead sets of scans from which precursor and neutral loss spectra are reconstructed.

Recent work has shown that data-independent precursor and neutral loss scans, usually accomplished with large, high-power, multi-analyzer instruments, are possible in single *linear* quadrupole ion traps as well by using orthogonal double resonance excitation.[135,230,341] These scans are methodologically similar to the 3D trap precursor scan implemented years ago, but precursor ions are excited and product ions are ejected orthogonally so as to prevent cross-talk between the two processes. The scans have further been developed into simultaneous and sequential MS/MS combinations and permutations in which multiple precursor scans are combined with neutral loss and product scans to maximize information gain from a single ion injection event.[230] To date, however, all data-independent precursor and neutral loss scans in a single QIT/LIT have involved scans of the low voltage ac frequency at constant rf voltage.[50,91,205,306,307,354] Under these conditions, the ions' secular frequencies do not vary during the scan,[12] making MS/MS scans easy to implement. Conventional ion traps, on the other hand, do not typically use ac frequency scanning for mass selective operations but instead use highly precise linear ramps of the rf voltage (e.g. in mass selective instability with resonance ejection) or multi-frequency waveforms[51,148,355] for ion manipulation.

Here we demonstrate the corresponding precursor and neutral loss scans as well as some simultaneous combinations of precursor and neutral loss scans using an rf scanning linear quadrupole ion trap. We also compare this method with the ac frequency scan method developed previously. As we will see in the next section, the rf scan requires high precision not only in the rf voltage scan but also in the nonlinear ac frequency scan that targets product ions for ejection from the trap as the precursor ions fragment. We demonstrate these scans on a variety of samples using several different ambient ionization sources. The ambient ion sources combined with fully fleshed-out single analyzer MS/MS capabilities strengthen the capabilities of miniature mass spectrometers, for which these scans are particularly appropriate.[70,71]

12.3 Theory

We begin with the standard Mathieu q parameter for the linear ion trap while assuming conditions in which Mathieu a = 0 (i.e. no quadrupolar DC potential on the trap rods)[7,9,356]

$$q = \frac{4zeV_{rf}}{r_0^2\Omega^2 m}$$
Eq. 12.1

where V_{rf} is the zero-to-peak amplitude of the main trapping sine wave (rf), m is the mass of the ion, r_0 is the half distance between the rods, Ω is the angular rf frequency, and z is the integer charge of the ion, and e is the elementary charge. We assume from this point on that the term 'ze' collapses so that z is assumed to be the charge of the ion in coulombs. In the experiments demonstrated here, the rf amplitude is ramped linearly so that

$$V_{rf} = \frac{dV_{rf}}{dt}t + V_0$$
Eq. 12.2

where dV_{rf}/dt = constant and V_0 is the rf voltage at the start of the mass scan. In the precursor ion scan, there are two waveforms (**Figure 12.1**). First, a constant frequency sine wave at low Mathieu q is used for excitation of precursors ions where m/z is linearly related to time (because the rf voltage is scanned linearly). The product ion ejection frequency must be scanned so that it always ejects the selected product ion m/z. The product ion m/z is fixed and corresponds to a Mathieu parameter q_{pro}, but because the rf voltage is scanned, the product ion's Mathieu q parameter during the scan varies according to

$$q_{pro} = \frac{4z\left(\frac{dV_{rf}}{dt}t + V_0\right)}{r_0^2\Omega^2 m}$$
Eq. 12.3

meaning that the product ion ejection frequency for the precursor ion scan is simply varied so that a linear relationship between Mathieu q and time is maintained. The frequency scan rate depends on the rf voltage scan rate. We can then convert from Mathieu q to parameter β (see ref. [91]) and subsequently to ion secular frequency ω using the relationship $\beta = 2\omega/\Omega$, thereby giving the appropriate frequency sweep (**Figure 12.1**, precursor ion scan, AC$_{eject}$). This frequency scan must occur exactly in tandem with the rf scan so that resonance ejection of ions of similar m/z to the target ion does not occur. Therefore, high precision in both the rf voltage scan and ac frequency scan is required.

For the neutral loss scan, the product ion's mass-to-charge ratio $(m/z)_{pro}$ changes as a function of time so as to maintain a constant mass offset, N, from the excited precursor ion m/z $(m/z)_{pre}$, which is excited at a frequency corresponding to Mathieu parameter q_{exc} = constant)

$$\left(\frac{m}{z}\right)_{pre} - \left(\frac{m}{z}\right)_{pro} = N \qquad \text{Eq. 12.4}$$

so that

$$q_{pro} = \frac{4V_{rf}}{r_0^2\Omega^2[(m/z)_{pre}-N]} = \frac{4(\frac{dV_{rf}}{dt}t+V_0)}{r_0^2\Omega^2(\frac{4\frac{dV_{rf}}{dt}t}{q_{exc}r_0^2\Omega^2}+(\frac{m}{z})_0-N)} \qquad \text{Eq. 12.5}$$

where $(m/z)_0$ is the first precursor ion excited during the scan. Eq. 12.5 then simplifies to

$$q_{pro} = \frac{(\frac{dV_{rf}}{dt}t+V_0)q_{exc}}{\frac{dV_{rf}}{dt}t+(m/z_0-N)(\frac{1}{4}q_{exc}r_0^2\Omega^2)} \qquad \text{Eq. 12.6}$$

which is a nonlinear frequency sweep (**Figure 12.1**, neutral loss scan AC$_{eject}$) that also must be calculated and loaded into an arbitrary waveform generator.

We note here that these equations were not used to calculate waveforms; they merely provide the theoretical foundation for the frequency scans. The method used in this work for calculating the frequency sweeps is described in the next section.

It is also worth briefly discussing the differences in implementation between the current work and previous work.[135,230,341] The former we refer to as the 'RF Scan' variant and the latter as the 'AC Scan' (or 'Constant RF') variant. In both cases, precursor ions are fragmented in the y

dimension in the linear ion trap so that there is a linear relationship between fragmentation time and m/z. In the 'RF Scan' this is accomplished by linearly ramping the rf voltage while simultaneously applying a constant frequency auxiliary waveform in the y dimension. In the 'AC Scan' case fragmentation is accomplished by using an inverse Mathieu q scan[354] (a nonlinear frequency sweep with linear relationship between m/z and time) while the rf voltage is held constant. In the precursor scan the product ions are then ejected with application in the x dimension (simultaneous with the excitation in y) of either 1. ('RF Scan') the nonlinear frequency sweep described in Eq. 12.3, where Mathieu q is directly related to frequency, or 2. ('AC Scan') a fixed frequency sine wave. For the neutral loss scan, the x dimension waveform is either 1. ('RF Scan') the nonlinear frequency sweep described in Eq. 12.6, or 2. ('AC Scan') a second inverse Mathieu q scan at constant mass offset from the excitation frequency sweep. In the case of the neutral loss scan, an 'Artifact Reject' frequency sweep must also be included to reject, into the y rods, precursor ions that do not fragment when they are excited. The 'Artifact Reject' is generally identical to the product ion ejection frequency in terms of the curvature of frequency vs. time but is offset in frequency so as to be between the excitation and ejection frequencies.

12.4 Experimental

12.4.1 Chemicals

Amphetamine (m/z 136), methamphetamine (m/z 150), 3,4-methylenedioxyamphetamine (m/z 180), and 3,4-methylenedioxymethamphetamine (m/z 194), were purchased from Cerilliant (Round Rock, TX, USA) and dissolved in methanol. These analytes were detected in the protonated form in the positive ion mode. HPLC grade methanol was purchased from Fisher Scientific (Hampton, NH, USA).

Explosives including 1,3,5-trinitrobenzene (m/z 213, M$^-$), 2,6-dinitrotoluene (m/z 183, [M+H]$^-$), 4-amino-2,6-dinitrotoluene (m/z 197, M$^-$), and 2,4,6-trinitrotoluene (m/z 227, M$^-$) were purchased from Sigma-Aldrich (St. Louis, MO, USA) and dissolved in methanol. These compounds were detected in the negative ion mode using low-temperature plasma ionization. Chemical warfare agent (CWA) hydrolysis products (i.e. simulants) ethyl methylphosphonate (m/z 123), isopropyl methylphosphonate-D$_7$ (m/z 144), cyclohexyl methylphosphonate (m/z 177), and pinacolyl methylphosphonate (m/z 179), all m/z values for [M-H]$^-$, were also purchased from Sigma and dissolved in methanol. CWAs were detected in the negative ion mode.

12.4.2 Nanoelectrospray ionization

Nanoelectrospray ionization[301] using a 1.5 kV potential was utilized for analysis of amphetamines. Borosilicate glass capillaries (1.5 mm O.D., 0.86 mm I.D.) from Sutter Instrument Co. (Novato, CA, USA) were pulled to 2 μm tip diameters using a Flaming/Brown micropipette puller (model P-97, Sutter Instrument Co.). The nanospray electrode holder (glass size 1.5 mm) was purchased from Warner Instruments (Hamden, CT, USA) and was fitted with 0.127 mm diameter silver wire, part number 00303 (Alfa Aesar, Ward Hill, MA), as the electrode.

12.4.3 Low-temperature plasma ionization

The low-temperature plasma (LTP) probe and its use for the detection of explosives have been described elsewhere in detail.[191,357] The probe consists of a glass tube (o.d. 5.95 mm, i.d. 3.88 mm) with an internal, stainless steel, grounded electrode of diameter 1.57 mm. A copper tape electrode surrounds the outside of the tube, and the glass serves as a dielectric barrier. Alternating high voltage was applied by a PVM500 plasma driver purchased from Information Unlimited (Amherst, NH, USA) with voltage of 0.7-2.5 kV at a frequency of 21 kHz. Helium discharge gas was used at a flow rate of 0.4 L/min. Samples of 2 μL of explosives dissolved in methanol were placed on a glass slide, allowed to dry, and then moved to a custom-built holder mounted on a 3D moving stage. The glass slide was placed directly under the mass spectrometer inlet while the end of the LTP probe was 5 mm from the sample and inclined at an angle of 45°.

12.4.4 Swab touch spray ionization

Swab touch spray experiments were performed using sterile rayon minitip swabs (model 160C) purchased from Copan Diagnostics (Murrieta, CA, USA). The swabs possess an aluminum handle and are mounted in a plastic cap that serves as a convenient holder. The swabs are commercialized for purposes other than ESI probes for MS analysis. However, they have been used without modification from their commercial form.[358,359] Swab touch spray experiments were performed by soaking the rayon tip with methanol (approx. 40-50 μL) and then touching an area of a microscope glass slide that was previously spiked with a methanolic solution (which was let dry) containing ethyl methylphosphonate, isopropyl methylphosphonate-D_7, cyclohexyl methylphosphonate, and pinacolyl methylphosphonate (500 ng of absolute material, each, deposited on the slide).

The swabs were placed vertically in front of the mass spectrometer using a custom ion source system. Electrospray was generated using methanol-ethanol 1:1 v/v as solvent system. Electrospray was initiated after addition of solvent directly on the swab tip via a fused silica capillary and external syringe pump. The syringe pump flow rate was set at 50 µL/min for about 30 s, accounting for dead volume and wetting the swab tip. When the swab tip was visibly wet, high voltage (−6.0 kV) was applied directly to the metallic handle. Solvent flow rate was changed to 20 µL/min. A red laser was used to visualize the spray plume.

12.4.5 Instrumentation

All experiments were performed using a Thermo LTQ linear ion trap (Thermo, San Jose, CA, USA) with rf frequency tuned to 1.1635 MHz. The device has hyperbolic rod cross sections with y_0 of 4.00 mm and x_0 of 4.75 mm. Each rod is cut into three axial sections of 12, 37, and 12 mm length. The middle sections have a 0.25 mm slot cut 30 mm along the rod's total length. The instrument was modified as described previously[135] to enable application of low voltage AC waveforms on both the x and y electrodes of the linear ion trap. All excitation and artifact rejection waveforms were applied to the y rods and all ejection waveforms were applied to the x rods. Helium at a pressure of 1 mTorr was used for collisional cooling and collision-induced dissociation.

For both neutral loss and precursor ion scan modes, a supplementary constant amplitude sine wave of fixed frequency (between 100 and 200 mV_{pp} amplitude, usually between 130 kHz (q = 0.31) and 200 kHz (q = 0.46) was applied to the y-electrodes to provide excitation for dissociation of precursor ions while the 'Ultrazoom' scan function was used to linearly ramp the rf amplitude with high precision, thereby fragmenting precursor ions linearly with respect to time from low to high m/z. The 'Ultrazoom' scan as commercially implemented ejects ions at a Mathieu q parameter of ~0.834 with a scan rate of 27 Da/sec. We, however, replaced the auxiliary ac waveform with a first excitation waveform of constant frequency (usually at a Mathieu q of 0.3) and amplitude and a second waveform of scanned frequency for product ion ejection. The product ion ejection waveform, described mathematically in the previous section, was a nonlinear frequency sweep with amplitude ~600 mV_{pp} applied to the x-electrodes at the same time as the rf ramp and constant frequency excitation signals. For neutral loss scans, a nonlinearly swept sine wave of constant amplitude and of lower frequency than the excitation waveform was used to reject leftover precursor ions to prevent them from being ejected by the product ion ejection frequency sweep. The supplementary waveforms were triggered at the start of the mass scan using

the 'scan out' trigger in the LTQ Tune Diagnostics menu. Automatic gain control was turned off for all experiments so that ion injection time was controlled manually and usually set at 10 ms. For DESI experiments, 600 ms injection times were used.

12.4.6 Waveform calculation

Product ion ejection waveforms were calculated in Matlab (Mathworks, Natick, MA) using an algorithm whose description follows. The commercial LTQ's 'Ultrazoom' scan was used to precisely control the rf amplitude, especially the linearity of the voltage ramp which ultimately determines the feasibility of these scan modes. Since the LTQ does not report the rf voltage to the user, the algorithm for calculating product ion ejection waveforms must be calibrated. It was experimentally determined that the Ultrazoom scan ejects ions at a frequency corresponding to Mathieu q = 0.834, and the scan rate at this q value is 27 Da/sec. The start and end masses entered into the LTQ Tune software thus correspond to the *m/z* value at q = 0.834 at the start and end of the scan, respectively. The varied ejection *m/z*, linearly related to time due to the linearity of the rf ramp, and constant q_{eject} were used to calculate the rf amplitude as a function of time through eq. 1 (assuming a quadrupole coefficient of 1), with the rf frequency set at 1.1635 MHz and radius of $x_0 = 0.00475$ m. This rf amplitude was then used to calculate the q value of the product ion as a function of time, and the q value was then converted to the ion's secular frequency which was incorporated into an ac waveform using a phase accumulator as described previously [354]. The waveform (i.e. voltage vs. time) was exported from Matlab as a column vector (.csv) and imported into one of two Keysight 33612A function generators (Newark element14, SC, USA). The sampling rate for all waveforms was 10 MSa/sec.

An important difference between the precursor ion scan and the neutral loss scan is that in the former the ejection frequency stays on a fixed *m/z*, whereas in the latter the product ion *m/z* is scanned to maintain a constant mass offset from the activated precursor ions. For the precursor ion scan, a constant *m/z* was converted to Mathieu q and then to secular frequency for each time point. For the neutral loss scan, the excited precursor ion *m/z* was calculated through eq. 12.1 and the corresponding product ion *m/z* (m/z_{pre} - *N*) was then converted to Mathieu q and hence secular frequency. For the neutral loss scan it is important to include another frequency sweep on the y electrodes for artifact rejection because precursor ions leftover after the excitation event will otherwise be unintentionally ejected and detected via the product ion ejection frequency sweep.[135] For the rf ramp neutral loss scan, the product ion ejection waveform was also used for artifact

rejection, except the sampling rate of the waveform generator was set lower (e.g. 7 MSa/sec), thereby creating a waveform with similar curvature but lower frequencies than the product ion ejection waveform (green trace in **Figure 12.1**). Thus, precursor ions surviving excitation were then neutralized on the y electrodes and therefore not detected.

12.5 Results & Discussion

12.5.1 Nanoelectrospray Ionization of Amphetamines

We first turn to a familiar system to acquire precursor and neutral loss spectra by scanning the rf voltage in a linear quadrupole ion trap: analysis of amphetamines ionized by nanoelectrospray ionization. Previously we demonstrated precursor[341] and neutral loss[135] scans in an ac frequency scanning ion trap (at constant rf voltage) as well as simultaneous and sequential MS/MS combinations and permutations.[230] All of these scan modes can also be implemented while the rf amplitude is ramping linearly, though the implementation here is much more difficult because the ion secular frequencies vary nonlinearly as a function of the rf amplitude. For example, the four amphetamines shown in the full scan mass spectrum in **Figure 12.2a** (amphetamine, methamphetamine, 3,4-methylenedioxyamphetamine, and 3,4-methylenedioxymethamphetamine) can be subdivided into different subsets based on 1) shared product ions (panels b-d) or 2) shared neutral losses (panels e-f). Amphetamine and methamphetamine are detected with a precursor ion scan of *m/z* 119 and 3,4-methylenedioxyamphetamine and 3,4-methylenedioxymethamphetamine are detected with a precursor ion scan of *m/z* 163. All four compounds can be detected using a simultaneous double precursor ion scan (panel d) wherein the two product ion ejection frequencies used in panels b and c were summed and applied as a dipolar resonance ejection signal on the x electrodes of the linear ion trap while the precursor ions were excited at a single fixed frequency.

Similarly, panel e shows a neutral loss scan of 17 Da to detect amphetamine and 3,4-methylenedioxyamphetamine, and a neutral loss scan of 31 Da detects the other two analytes. A simultaneous double neutral loss scan of 17 Da and 31 Da (panel g) again detects all the analytes in a single scan. In this case the precursor ion excitation frequency and artifact rejection frequency sweep remain the same but the two product ion ejection frequencies (neutral loss of 17 and neutral loss of 31) are summed and applied to the x electrodes simultaneously.

We now show that single ion trap precursor and neutral loss scans are useful for a wide variety of analytes ionized using several different ambient ionization sources. In particular, the

ambient methods pair well with single analyzer MS/MS capabilities for applications in which miniature mass spectrometers are desired. As demonstrated here, these applications include low-temperature plasma ionization for detection of explosives on surfaces and swab touch spray ionization of chemical warfare agent simulants.

12.5.2 Low-temperature Plasma for Detection of Explosives on Surfaces

The target applications for single analyzer MS/MS scans are those which have significant resource constraints in terms of instrument size and power, access to sample, sample amount, and instrument portability. Detection of explosives is one application that can benefit from on-site instrumentation. Ambient plasma ionization methods (e.g. low-temperature plasma[191,192,360]) have been shown to be effective at detecting a wide array of alkyl and aryl nitrates and related compounds directly from surfaces with high sensitivity using both benchtop and portable instrumentation.[357,361] A general survey scan that fits this class of compounds is a neutral loss of 30, the neutral fragment corresponding to NO. Although not all aromatic nitrates fragment in this manner, many do so quite readily (see ref. [357]) and hence they can be simultaneously detected and confirmed by an MS/MS transition in a single mass scan segment. **Figure 12.3a** shows a full scan mass spectrum of four such analytes, namely 2,6-dinitrotoluene (*m/z* 183), 4-amino-2,6-dinitrotoluene (*m/z* 197), 1,3,5-trinitrobenzene (*m/z* 213), and 2,4,6-trinitrotoluene (*m/z* 227), ionized from a room-temperature glass slide using low-temperature plasma ionization. A neutral loss scan of 30 Da is then shown in **Figure 12.3b**. As little as 20 ng of each material was detected directly from the glass surface using the neutral loss scan. 2,6-dinitrotoluene was not detected at 20 ng due to inefficient fragmentation but can be detected at higher concentrations.

12.5.3 Swab Touch Spray Ionization of Chemical Warfare Agent Simulants

Swab touch spray ionization[358,359] is a recently-developed variant of ambient touch spray ionization[362] wherein a rayon swab on an aluminum handle is used to collect material (e.g. oral fluid, solids from a surface,[363] fibers in a forensic analysis) and subsequently solvent and high voltage are applied for ionization. In the experiment performed here, a mixture of chemical warfare agent simulants (500 ng each of ethyl methylphosphonate (*m/z* 123), isopropyl methylphosphonate-D$_7$ (*m/z* 144), cyclohexyl methylphosphonate (*m/z* 177), and pinacolyl methylphosphonate (*m/z* 179), where all *m/z* values refer to [M-H]$^-$) was deposited on a glass slide

which was then allowed to dry, and then the slide was swabbed using a methanol-soaked rayon swab. The swab was then placed in a 3D-printed holder, 9:1 methanol/ethanol was continually supplied to the swab at a rate of ~20 uL/min, and -6 kV was applied to generate ions. **Figure 12.4a** shows the full scan mass spectrum from this experiment; each of the CWA analytes is noted. A scan mode particularly suitable for these analytes is a precursor ion scan of *m/z* 95, which corresponds to the fragment ion $CH_3P=O(OH)O^-$ (i.e. a methylphosphonate ion). The result from a precursor ion scan of *m/z* 95 is shown in **Figure 12.4b**. All four CWAs are detected, though the signal-to-noise ratio is low due to inefficient fragmentation (He is used as collision gas on the LTQ). Note that isopropyl methylphosphonate-D_7 fragments to *m/z* 96 but is also be detected as a low abundance signal using the same precursor scan because of the closeness of the secular frequencies of the product ions. Further information about sensitivity and product ion selectivity can be found in the next chapter.

One of the interesting features of this spectrum is the 'humps' that are observed in the baseline. These may be caused by differences between the product ion's actual secular frequency at a given point during the scan and the applied product ion ejection frequency, which can cause unintended resonance ejection as the applied ac frequency and product ion's secular frequency drift away from each other. This characteristic makes calibration and optimization of the nonlinear frequency sweep quite difficult, especially in comparison to the ac frequency scan variant where the rf amplitude (and ion secular frequency) is constant.[341] When the rf is varied, the nonlinear ac frequency sweep must always line up, to a high degree of accuracy, with the highly precise rf voltage ramp so that the frequency sweep always targets the product ion of interest and not adjacent *m/z* ions. Other unwanted peaks can be observed when a precursor ion or product ion formed from fragmentation during the scan is ejected due to boundary instability (although this was not shown in any spectra here). Sometimes these peaks can be distinguished from the precursor scan peaks by peak width; the former can be wider. In contrast, in the constant rf version of the precursor scan the product ion ejection frequency must merely be tuned to the product ion's fixed secular frequency, which is much easier to tune.

12.5.4 Comparison of AC Frequency Scanning and RF Voltage Scanning for Ion Trap MS/MS

We now compare the two demonstrated variants of precursor and neutral loss scanning, paying particular attention to operational aspects of the scans. In previous experiments[135,230,341] the

rf amplitude was kept constant during the scan and instead the inverse Mathieu q scan (nonlinear ac frequency scan with linear mass scale[354]) was used for mass selective ion fragmentation while either a fixed frequency (precursor scan[341]) or scanned inverse Mathieu q scan (neutral loss[135]) was used to eject a particular product ion while the precursor ions fragmented. In the current experiments, the rf amplitude is used more conventionally in that it is ramped linearly with time while a fixed frequency ac signal is used for precursor ion fragmentation. A nonlinearly scanned frequency is used for product ion ejection (**Table 12.1**). Conveniently, both MS/MS variants return data for which m/z is linearly related to time. In the ac frequency scan (constant rf) case, if the ac frequency is instead scanned linearly, then calibration is considerably more complicated.[91] In both the rf voltage scan case and ac frequency scan case, sequential and simultaneous scans are possible; however, for the rf scan care must be taken not to eject the precursor ions at the Mathieu stability boundary (q = 0.908). In both scans, multigenerational capabilities[172,305] are possible if the precursor ions are fragmented from high to low m/z, the direction opposite to that demonstrated in this paper. Unit resolution is observed in all of these scan modes for scan rates near 10^2 Da/sec (the slowness of which is necessitated to obtain reasonable conversion of precursor ions to product ions). An advantage of the rf scan variant is identical fractional product ion mass range for all precursor ions since fragmentation is performed at constant frequency. Additionally, the collision energy can be ramped linearly with the rf amplitude without significantly altering mass calibration.[42] For the ac frequency scan case the collision energy vs. time relationship would be considerably more complex.

Importantly, the ac frequency scan variant – at constant rf - is significantly simpler. For a precursor ion scan, a simple single frequency need be tuned for ejection of the product ion and a simple time offset between identical frequency scans is required for the neutral loss scan. There are also fewer artifact peaks because 1) the rf is not scanned and hence no ion's secular frequency changes during the scan, and 2) the stable mass range in the ion trap does not vary with the scanning parameter, meaning fewer precursor ions and product ions generated during fragmentation will be ejected due to boundary instability. Hence, the ac frequency scan method ought to be the preferred MS/MS variant due to its simplicity and also because it generates more reliable data with fewer artifacts. A description of this mode of operation implemented on the Mini 12 mass spectrometer is described in the next chapter.

12.6 Conclusion

We have demonstrated an alternate scan mode in which precursor and neutral loss scans are possible in a single linear quadrupole ion trap using rf voltage scans combined with ac frequency scans. The scans are compatible with a wide range of ambient ionization sources and useful for a variety of purposes, including detection of explosives and chemical warfare agent simulants by low-temperature plasma ionization and touch spray ionization, respectively, analysis of amphetamines by nanoelectrospray ionization, detection of active ingredients in pharmaceutical tablets by DESI, and drug analysis by paper spray ionization. These cases and the corresponding ionization methods are merely illustrative, not comprehensive.

Compared with the ac frequency (constant rf) scan variant, the rf voltage scan version offers similar performance in terms of mass spectral resolution and fragmentation efficiency but can suffer from a greater proportion of artifact peaks due to boundary ejection and 'unsyncing' of the rf voltage scan and product ion ejection frequency scan. In addition, the rf scan variant is significantly more complex, requiring simultaneous and highly precise scans of rf voltage and ac frequency. Nonetheless, because commercial mass spectrometers operate in the rf scan mode this method may be more appropriate for applications where only current instrumentation is available.

12.7 Acknowledgements

Figures and Tables
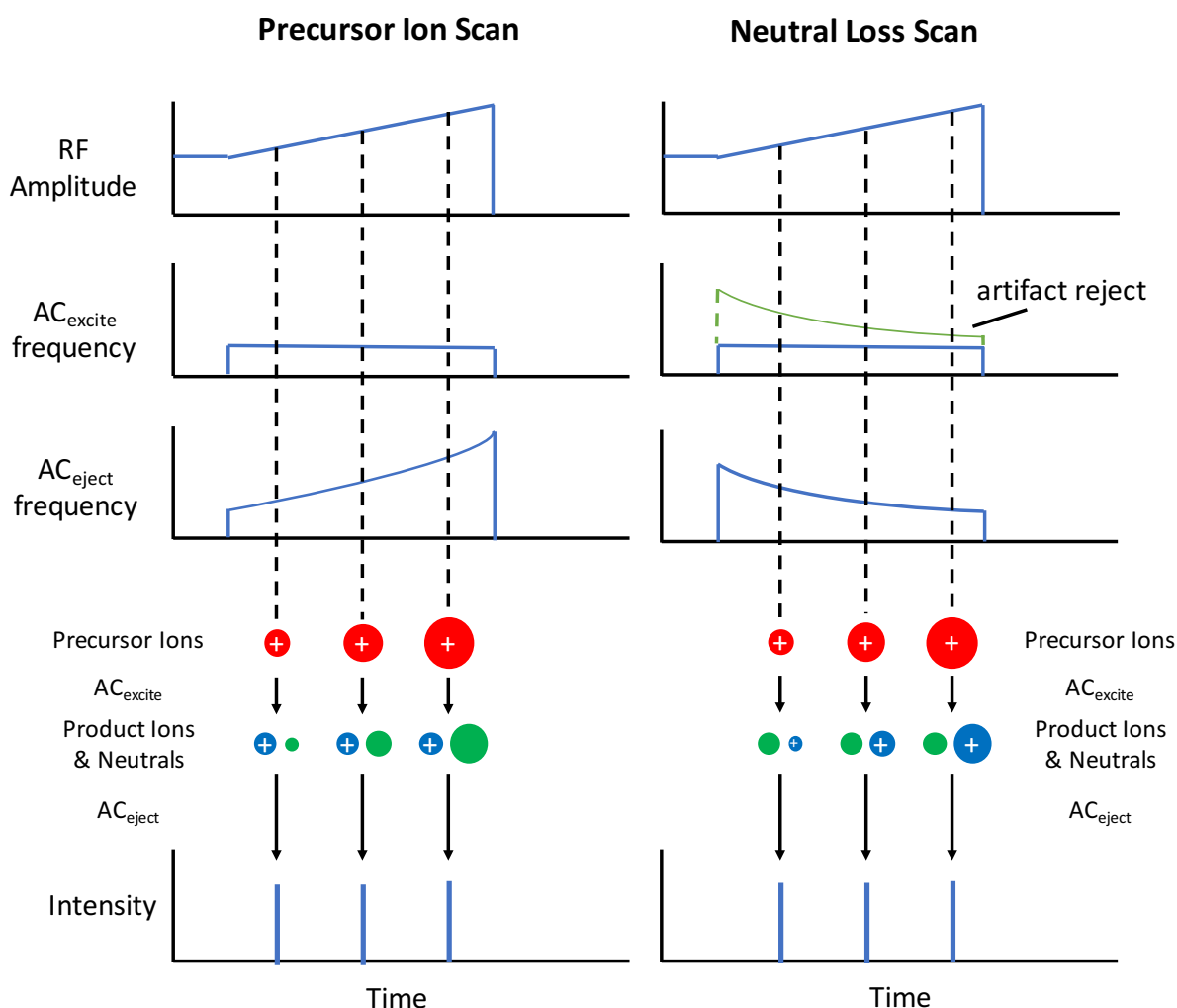
Figure 12.1. Scan table for precursor ion scans and neutral loss scans in an rf scanning linear quadrupole ion trap. The precursor ion excitation frequency is applied in the y dimension (where there is no detector) along with an artifact rejection frequency sweep (in the case of the neutral loss scan), whereas the product ion ejection frequency is placed on the x electrodes. Precursor ions fragment with a linear relationship between *m/z* and time and either a constant product ion *m/z* is ejected and detected or product ions with a shared mass offset from their respective precursor ions.
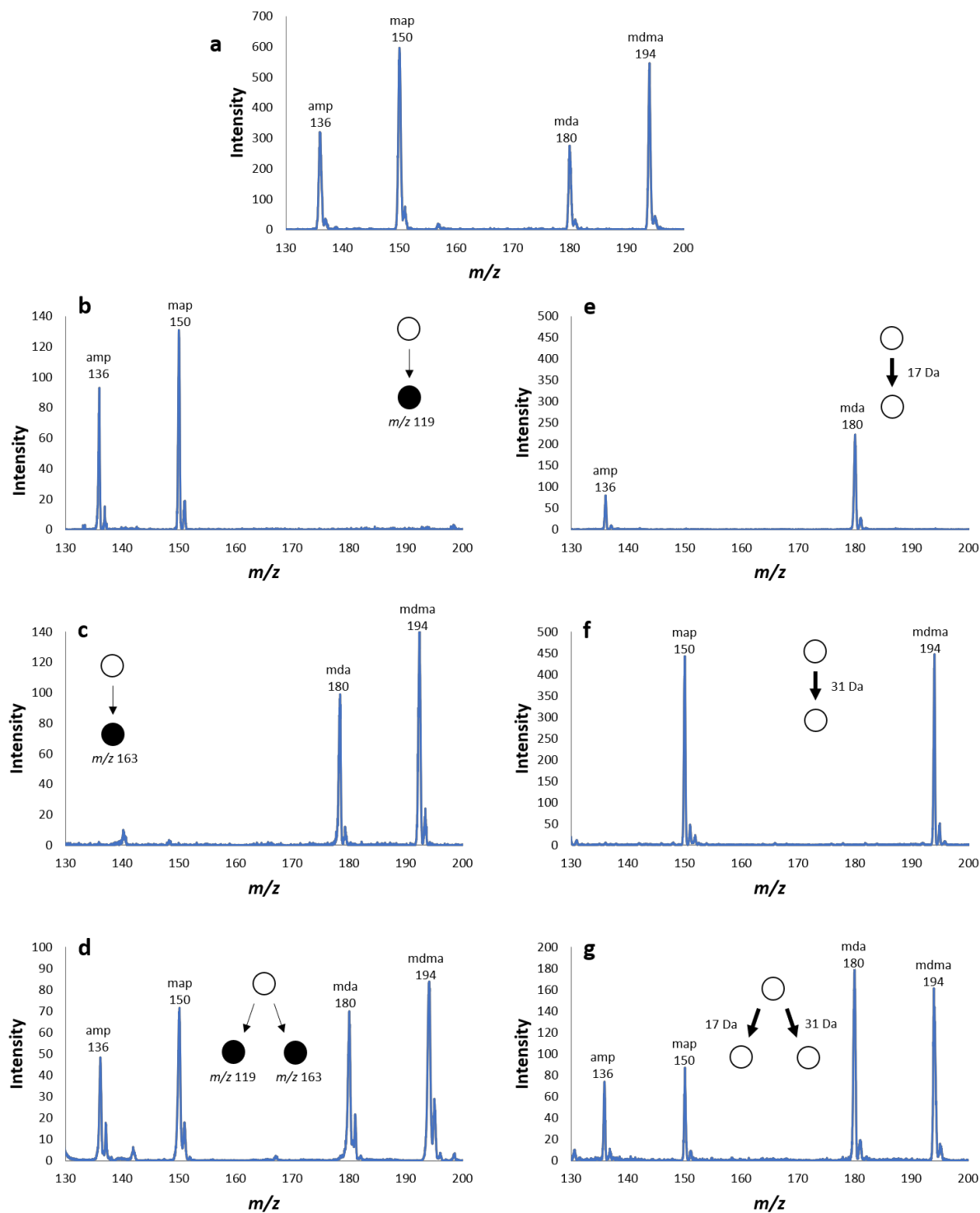
Figure 12.2. Precursor and neutral loss scans using an rf scanning linear ion trap: (a) full scan mass spectrum of amphetamine, methamphetamine, 3,4-methylenedioxyamphetamine, and 3,4-methylenedioxymethamphetamine, (b) precursor ion scan of *m/z* 119, (c) precursor ion scan of *m/z* 163, (d) simultaneous precursor ion scan of *m/z* 119 and 163, (e) neutral loss scan of 17 Da, (f) neutral loss scan of 31 Da, and (g) simultaneous neutral loss scan of 17 Da and 31 Da.
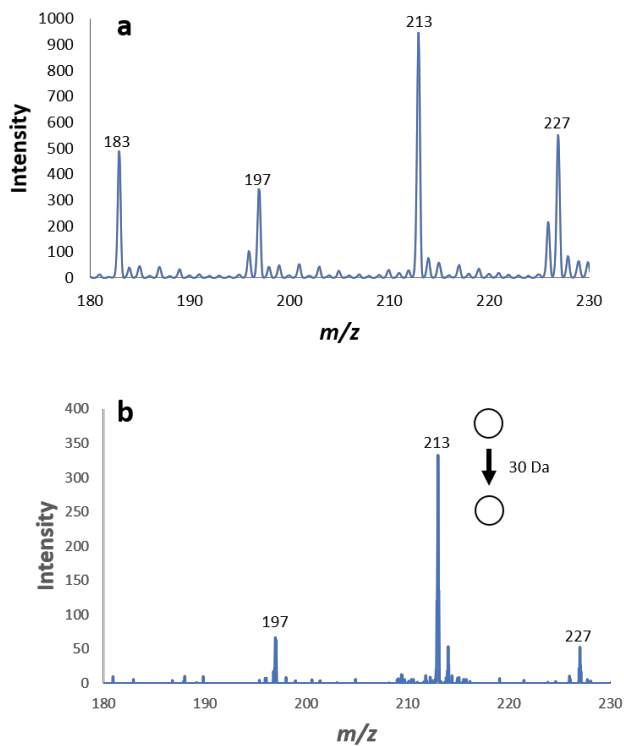
Figure 12.3. Neutral loss scan of explosives ionized by low-temperature plasma: (a) full resonance ejection mass scan of 20 ng each 1,3,5-trinitrobenzene (*m/z* 213), 2,6-dinitrotoluene (*m/z* 183), 4-amino-2,6-dinitrotoluene (*m/z* 197), and 2,4,6-trinitrotoluene (*m/z* 227), and (b) neutral loss scan of 30 Da.
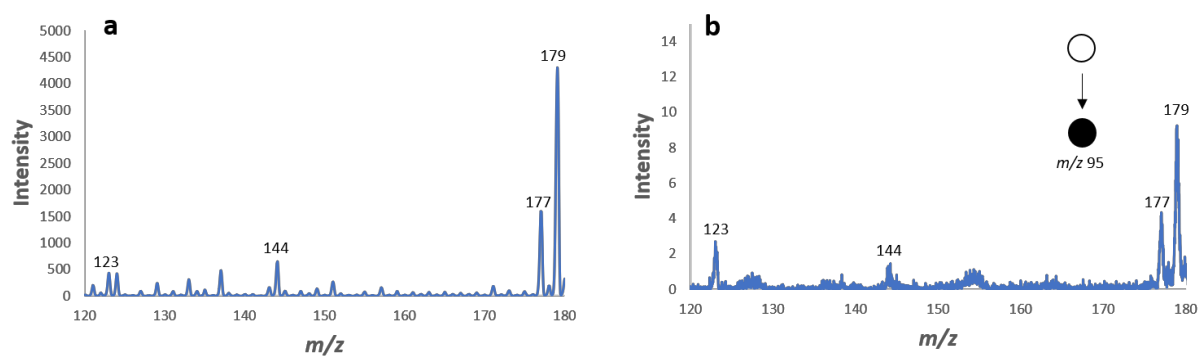
Figure 12.4. Precursor ion scan of chemical warfare agent simulants sampled from a glass substrate and ionized by swab touch spray: (a) full scan mass spectrum of 500 ng each ethyl methylphosphonate (*m/z* 123), isopropyl methylphosphonic acid-D$_7$ (*m/z* 144), cyclohexyl methylphosphonate (*m/z* 177), and pinacolyl methylphosphonate (*m/z* 179), all [M-H]⁻, and (b) precursor ion scan of *m/z* 95.

Table 12.1. Comparison of ac scan and rf scan variants

Parameter / Scan Variant	AC Frequency Scan		RF Amplitude Scan	
	Precursor	**Neutral Loss**	**Precursor**	**Neutral Loss**
RF Amplitude	Fixed		Ramped linearly	
Precursor ion excitation frequency	Scanned linear in frequency or mass	Scanned linear in mass	Fixed	
Artifact rejection frequency	None	Scanned linear in mass	None	Fixed or scanned
Product ion ejection frequency	Scanned	Scanned linear in mass with fixed mass offset from precursor	Scanned nonlinearly to stay on product ion's secular frequency	Scanned nonlinearly with fixed mass offset from precursor
Mass Calibration (m/z vs. time)	~Linear with inverse Mathieu q scan, nonlinear with any other frequency sweep		Linear	
Simultaneous permutations possible?	Yes		Yes	
Sequential permutations possible?	Yes		Yes	
Multigenerational possible?	Yes, scan from high to low mass (low to high frequency)		Yes, scan from high to low mass (high to low rf amplitude)	
Advantages	Simpler to implement; fewer interferences from boundary ejection		linear mass scale with linear rf ramp; ions fragmented at same q parameter	
Disadvantages	Mass scale nonlinear for linear frequency scan; precursors fragmented at variable q parameter		Interferences from boundary ejection; difficult to align rf voltage scan with ac frequency scan simultaneously	
Reference	135,230,341		This paper	

CHAPTER 13.   IMPLEMENTATION OF PRECURSOR AND NEUTRAL LOSS SCANS ON A MINIATURE ION TRAP MASS SPECTROMETER AND PERFORMANCE COMPARISON TO A BENCHTOP LINEAR ION TRAP

13.1 Abstract

Implementation of orthogonal double resonance precursor and neutral loss scans on the Mini 12 miniature rectilinear ion trap mass spectrometer is described and performance is compared to a commercial Thermo LTQ linear ion trap. The ac frequency scan version of the technique at constant rf voltage is used here because it is operationally much simpler to implement. Remarkably, the Mini 12 shows up to 2 orders of magnitude higher sensitivity compared to the LTQ. Resolution on the LTQ is better than unit at scan speeds of ~400 Th/s, whereas peak widths on the Mini 12, on average, range from 0.5 Th to 2.0 Th full width at half maximum and depend heavily on the precursor ion Mathieu q parameter as well as the pump-down time that precedes the mass scan. Both sensitivity and resolution are maximized under higher pressure conditions (low pump down time) on the Mini 12. The effective mass range of the product ion ejection waveform was found to be 5.8 Th on the Mini 12 in the precursor ion scan mode vs. 3.9 Th on the LTQ. In the neutral loss scan mode, the product ion selectivity was between 8 and 11 Th on the Mini 12 and between 7 and 8 Th on the LTQ. The effects of nonlinear resonance lines on the Mini 12 were also explored.

13.2 Introduction

Although product ion scans are common on single quadrupole ion traps, the two other main MS/MS scans (precursor scan and neutral loss scan)[293] are generally thought problematic on a single analyzer. Conventionally these two survey scans are implemented on triple quadrupole mass spectrometers[58] wherein the first and third quadrupoles mass select particular precursor and product ions while an intermediate rf-only quadrupole serves as a collision cell. Such a scan is complicated on most single mass analyzers due to the difficulty in not only mass selecting multiple

ions simultaneously, but also activating the precursor ion via collision-induced dissociation. A single quadrupole ion trap, however, can do both and hence can perform precursor and neutral loss scans via double resonance, that is, by simultaneously activating precursor ions and ejecting mass-selected product ions by applying multiple resonance (i.e. low voltage auxiliary) frequencies[135,230,341,352].

Although single analyzer precursor and neutral loss scans do not compare favorably with data-dependent methods[344] on commercial mass spectrometer systems in terms of mass spectral resolution, sensitivity, and speed, they are more attractive on some miniature systems (see **Introduction S13.1** in SI). Not only does the mass analyzer need to decrease in size on these smaller spectrometers[201,364-367], but so do the electronics and data acquisition systems, the ion optics (if there are any), and most importantly the vacuum system. Because small vacuum pumps, usually a 10 L/s turbo pump backed by a 5 L/min diaphragm pump,[199] struggle to pump a single chamber to <1 torr with a continuous atmospheric pressure interface, the discontinuous atmospheric pressure interface (DAPI) has become an attractive alternative.[75,198] Continuous interfaces do exist on miniature spectrometers, but they are usually 2-3 orders of magnitude less sensitive than their discontinuous counterparts (e.g. Mini 10, 11, 12, S).[100,193,197,212,287] Although efforts have been made to miniaturize ICRs,[368] the Orbitrap,[369] sector instruments,[370,371] and even a triple quadrupole mass spectrometer,[372] for the reasons above – especially vacuum system constraints - the quadrupole ion trap has become the predominent analyzer for miniaturization. Conventionally this would limit miniature mass spectrometers to the full scan mode and the product ion scan mode, and in combination with the long pump down time characteristic of DAPI systems (10^{-1}-10^{0} s), reconstructing precursor and neutral loss spectra from data-dependent sets of product ion scans becomes less feasible. However, if operated unconventionally in the ac frequency scan mode,[49,50,205] precursor and neutral loss scan modes become available, somewhat mitigating the need for another analyzer for higher resolution or improved MS/MS capabilities and providing an attractive alternative over conventional data-dependent modes.

In this study, we implemented capabilities for precursor ion scanning and neutral loss scanning on a Mini 12 miniature rectilinear ion trap mass spectrometer and compared their performance to that obtained on a commercial Thermo LTQ linear ion trap. Both resolution and limit of detection were characterized as well as detection efficiency and mass-to-charge selectivity. Nonlinear resonance lines were also explored.

13.3 Experimental

13.3.1 Chemicals

Amphetamine (m/z 136), methamphetamine (m/z 150), 3,4-methylenedioxyamphetamine (m/z 180), 3,4-methylenedioxymethamphetamine (m/z 194), and 3,4-methylenedioxyethylamphetamine (m/z 208) were purchased from Cerilliant (Round Rock, TX, USA). HPLC grade methanol was purchased from Fisher Scientific (Hampton, NH, USA). Formic acid was purchased from Sigma-Aldrich (St. Louis, MO, USA). All analytes were diluted in methanol with 0.1% formic acid. A concentration of 1 ppm was used for all experiments except when a calibration curve was made.

13.3.2 Ionization

Nanoelectrospray ionization using a 1.5 kV potential was utilized for all experiments. Borosilicate glass capillaries (1.5 mm O.D., 0.86 mm I.D.) from Sutter Instrument Co. (Novato, CA, USA) were pulled to 2 μm tip diameters using a Flaming/Brown micropipette puller (model P-97, Sutter Instrument Co.). The nanospray electrode holder (glass size 1.5 mm) was purchased from Warner Instruments (Hamden, CT, USA) and was fitted with 0.127 mm diameter silver wire, part number 00303 (Alfa Aesar, Ward Hill, MA), as the electrode.

13.3.3 Instrumentation

Experiments were performed on the homebuilt Mini 12 miniature ion trap mass spectrometer. The Mini 12 has a rectilinear ion trap (RIT, x_0 = 5.0 mm, y_0 = 4.0 mm, length 43.2 mm) with slits of length 15.0 mm and width 1.0 mm on the x electrodes.[100,193,204] The main trapping radiofrequency (rf) voltage (~5 kV_{pp} max, 1.017 MHz) is generated by an LC tank circuit (**Figure 13.1**, black) and is normally applied only to the y rods while the x rods are either grounded or used for applying low voltage ac signals. Endcap lenses operated at ~50 V keep ions trapped axially. A single conversion dynode with electron multiplier (model 397, DeTech Detector Technology, Inc., MA) is used for detection. The ion trap typically operates in the resonance ejection mode [10] and has custom-designed electronics for linearly ramping the rf voltage, applying low voltage ac frequencies to the x rods for stored waveform inverse Fourier transform isolation (or activation)[51,148,169] and collision-induced dissociation (MS^n), and low and high voltage DC signals

for the endcap electrodes and conversion dynode/electron multiplier, respectively. High voltage (up to 5 kV) can also be supplied by the Mini 12 for ionization.

The Mini 12 uses a discontinuous atmospheric pressure interface.[75] Ions and neutrals are admitted into the Mini 12 RIT by opening the DAPI valve for ~12 ms, after which the valve is closed and a wait time is used for collisional cooling. During this time, the pressure in the ion trap drops from 10^{-1} torr to between 10^{-3} and 10^{-5} torr, during which mass analysis or collision-induced dissociation takes place.

The performance of the Mini 12 was compared to that of a commercial LTQ linear ion trap mass spectrometer (Thermo Finnigan, San Jose, CA, USA). The LTQ has a three-section linear ion trap with hyperbolic cross sections. The dimensions of the device are $x_0 = 4.75$ mm, $y_0 = 4$ mm, and three axial sections of lengths 12, 37, and 12 mm. The rf frequency was tuned to 1.166 MHz. The LTQ uses helium (ion gauge reading 0.60×10^{-5} torr) as the cooling and collision gas, whereas the Mini 12 uses air with a base pressure of 10^{-5} torr. Importantly, the Mini 12 uses a single electron multiplier with conversion dynode as the detector, whereas the LTQ uses two, one on either side of the linear ion trap.

The Mini 12 rf circuit was modified as shown in **Figure 13.1**, in red. A center-tapped iron core toroidal transformer (Laird Technologies LFB090050-000, Earth City, MO, USA) enabled coupling of low voltage ac signals on the y electrodes. The coils on the toroid do not overlap in order to improve isolation between the rf and ac signals. The ac signal is applied to the primary winding, and the two outputs of the secondary winding are applied to the two y rods, giving a dipolar ac signal between the rods. The rf signal is a single phase on the y rods, and low voltage ac signals are applied directly to the x rods. The LTQ rf coil was modified as described previously[135,341] with an extra Thermo LTQ low pass filter board (part 97055−91120) and Thermo LTQ balun board (part 97055−91130) in order for low voltage ac signals to be applied to both x and y electrodes of the linear ion trap.

Two Keysight 33612A arbitrary waveform generators (Chicago, IL, USA) were used to apply low voltage ac waveforms to the x and y electrodes of each linear ion trap. One generator supplied the waveform for the x electrodes and one supplied the waveform for the y electrodes. The sampling rate of arbitrary waveforms was set at 10 megasamples per second.

13.3.4 Waveforms

Precursor ion scans require application of 1) an ac frequency sweep (at constant rf voltage) for mass-selective precursor ion excitation and 2) a fixed frequency of higher amplitude for ejection of a particular product ion.[99,341,352] Neutral loss scans require three simultaneous and identical frequency sweeps with appropriate trigger delays: a first sweep for precursor ion excitation, a second sweep for ejection of leftover precursor ions into the y electrodes, and a third frequency sweep for ejection of the neutral loss product ions. The trigger delay between precursor excitation and product ion ejection is directly proportional to the neutral loss. Generally, excitation amplitude was 200-300 mV_{pp} and ejection amplitude was 600-800 mV_{pp}. Excitation and artifact rejection signals were applied to the y rods and ejection signals were applied to the x rods, usually each in a dipolar fashion. All frequency sweeps in this work are inverse Mathieu q scans[354] that linearize the mass scale with respect to time by sweeping the ac frequency nonlinearly. These waveforms generally started at Mathieu q = 0.908 and ended at q = 0.3 with a sweep time of 600 ms. They were calculated in Matlab according to previously-described methods [354] and imported to the Keysight waveform generators.

13.3.5 Scan functions

The Mini 12 scan function is as follows: ion injection (DAPI open), 12 ms; cooling (DAPI closed, instrument pump down), 700 ms; ramp rf voltage up to operating point, 100 ms; mass scan, 600 ms; reset for next scan, 1 ms. The function generators were triggered by a 5 V pulse that normally operates the 'Sample Pump' as a 24 V pulse. A voltage divider was used to obtain the former from the latter. Data were acquired at 312,500 samples per second and were digitally smoothed using a 30-point triangle filter.

The LTQ was operated in the 'Ultrazoom' mode with an ion injection time of 10 ms. The rf voltage was constant throughout ion injection, cooling, and the mass scan and was controlled externally by substituting the coil modulation signal (proportional to the rf amplitude) on the rf detector board with a dc signal from an external function generator. Automatic gain control was turned off throughout this study, but space charge was not observed at 1 ppm concentration as demonstrated in SI **Figure S13.1**. The three function generators were triggered by the 'Injection' trigger in the LTQ Tune 'Diagnostics' menu. The data collection rate on the LTQ was approximately 2,700 samples per second.

In all experiments, *m/z* 119 had its working point at a Mathieu q value of 0.57 on LTQ vs. 0.53 on the Mini 12.

13.3.6 Data interpretation

Data were analyzed in either Matlab (Mathworks, Natick, MA, USA) or Excel (Microsoft, Redmond, WA, USA). Spectra were mass calibrated separately using a linear fit of *m/z* vs. time. In most cases, Mini 12 spectra are the average of 3 separate scans, whereas the LTQ data is the average of 10 scans. In the case of the LTQ, the only scan saved was the average spectrum and hence error bars will not be shown for LTQ data. All ion intensities are baseline-subtracted integrated intensities. Resolution is dimensionless and is reported as m/Δm, where m is the *m/z* value of the precursor ion (Th) and Δm is the measured full (peak) width at half maximum intensity (FWHM), also in Th.

13.4 Results & Discussion

Five amphetamine standards were chosen for this study: amphetamine (*m/z* 136->*m/z* 119), methamphetamine (*m/z* 150->*m/z* 119), 3,4-methylenedioxyamphetamine (*m/z* 180->*m/z* 163), 3,4-methylenedioxymethamphetamine (*m/z* 194->*m/z* 163), and 3,4-methylenedioxyethylamphetamine (*m/z* 208->*m/z* 163). Of interest here is not any particular class of compounds or implementation with a particular ion source, but rather performance metrics. Characterized here are mass spectral resolution, sensitivity, detection efficiency, product ion selectivity, pressure effects, and nonlinear resonance lines. We further compare the performance of the Mini 12 to a benchtop LTQ linear ion trap in both the precursor ion and neutral loss scan mode, an overview of which is shown in **Table 13.1**.

13.4.1 Performance of Precursor and Neutral Loss Scans

A full scan mass spectrum of the 5-component amphetamine mixture obtained on the Mini 12 is shown in **Figure 13.2a**. Fragmentation is observed even in the full scan, with *m/z* 163, *m/z* 119, and *m/z* 91 all present. This fragmentation can be attributed to the large pressure change during ion injection, during which the precursor ions will tend to fragment. The lower limit of the mass spectra here is set at *m/z* 120 since the lowest *m/z* fragment interrogated is *m/z* 119, and hence any precursor or neutral loss scan peaks below this are artefactual for singly charged ions.

Both a precursor ion scan of *m/z* 119 (for amphetamine and methamphetamine) and *m/z* 163 (for the other three) are shown in **Figure 13.2b, c**. A double simultaneous precursor ion scan is then shown in **Figure 13.2d**. This spectrum was obtained by applying the resonance frequency of *m/z* 119 on one of the x rods and simultaneously applying the resonance frequency of *m/z* 163 on the other x rod while sweeping the excitation frequency on the y rods. The corresponding neutral loss scans of 17 Da and 31 Da are shown in panels e and f. Note that *m/z* 163 (a fragment of *m/z* 180, 194, and 208) is detected because it fragments to *m/z* 133 and 135 and the neutral loss scan does not have unit selectivity. Corresponding precursor and neutral loss scans on the LTQ are shown in **Figure S13.2** (helium bath gas) and **Figure S13.3** (nitrogen bath gas). The use of nitrogen as bath gas increases the integrated signal intensity but also compromises resolution.

13.4.2 Sensitivity and Limit of Detection

Sensitivity and limit of detection are two performance metrics that were characterized on both the Mini 12 and LTQ. The precursor ion scan of *m/z* 119 was used for this experiment. The concentrations of amphetamine and methamphetamine were varied over 4 orders of magnitude from 10 ppb (viz. ng/mL) to 100 ppm (viz. µg/mL). The integrated signal intensity was plotted against concentration to obtain a semi-quantitative calibration curve. Because internal standards were not used, the linearity of the plots is less than ideal. Therefore, we defined the limit of detection as the mass spectrum with signal-to-noise ratio of 3. On the Mini 12 (**Figure 13.3a**), the limit of detection for the precursor ion scan was 10 ppb, whereas the detection limit using the same frequency scan rate for excitation on the LTQ was 1 ppm (**Figure 13.3c**). Note that the LTQ uses two detectors whereas the Mini 12 uses one. For comparison, the LTQ's product ion scan mode (q_{exc} = 0.25, 30 ms excitation time, normalized collision energy of 25) yielded a limit of detection of 1 ppb for both *m/z* 136 and *m/z* 150 (**Figure S13.4**).

The remarkable difference between limits of detection on the Mini 12 and LTQ in the precursor ion scan mode can likely be explained by several factors. First, the Mini 12 uses air as collision gas whereas the LTQ uses helium, which affects fragmentation efficiency and collisional damping (the latter being important to cool the product ions to the center of the trap before they are ejected in the x dimension). The higher operating pressure on the Mini 12 helps with these processes. Substituting nitrogen for helium in the LTQ gave a limit of detection of 250 ppb on the LTQ in the precursor ion scan mode (**Figure S13.5a**), and the sensitivity (slope of the calibration curve) increased by a factor of 2.6 for *m/z* 136 and 5.8 for *m/z* 150.

A calibration curve was also constructed for the neutral loss scan of 31 Da. Solutions used for this experiment consisted solely of methamphetamine and 3,4-methylenedioxymethamphetamine at various concentrations. The calibration curve on the Mini 12 for both *m/z* 150 and 194 is shown in **Figure 13.3b**. Surprisingly, even at 1 ppm concentration there is loss of calibration linearity. The limit of detection (S/N = 3) was found to be 250 ppb, much higher than the precursor ion scan and reasonably comparable to the LTQ's 500 ppb detection limit in the neutral loss scan mode using helium as bath gas (**Figure 13.3d**). Using nitrogen as bath gas on the LTQ resulted in a limit of detection of 250 ppb (**Figure S13.5b**) due to a doubling in sensitivity.

Both the severe increase in limit of detection and loss of calibration curve linearity on the Mini 12, even at high concentrations (1 ppm), are somewhat puzzling. Space charge may play a role here but is unlikely to be the only factor since it was not observed at 1 ppm in the full scan mode or in the other MS/MS scan modes on the Mini 12 and LTQ. However, there are key differences between the precursor scan and neutral loss scan that are worth considering. We postulate that the loss in calibration linearity is due to frequency shifts in the Mini 12 ion trap.[33,119] As the precursor ions are excited, they approach the y electrodes where their secular frequencies shift. Because the product ions are then generated close to the y electrodes, their secular frequencies are shifted relative to their 'true' or predicted secular frequencies. Their y oscillations then dampen rapidly in the ion trap due to collisions with air molecules, returning their secular frequencies to the 'normal' predicted values. At the same time, their x amplitudes increase via the ejection frequency sweep, again shifting their frequencies. It is this combination of frequency shifts, excacerbated by the fact that the precursor and product ion ejection waveforms must be swept at a *constant mass offset* that may cause loss of calibration linearity and also an increase in limit of detection.

13.4.3 Detection Efficiency

We next measured the percentage of precursor ions that were converted to product ions that were detected, which we define as the 'detection efficiency'. The detection efficiency is thus affected by fragmentation efficiency of the precursor ions, product ion collisional cooling, and product ion ejection efficiency. Detection efficiency was calculated as the ratio, expressed as a percent, of integrated peak intensity for ions of a selected *m/z* in the precursor or neutral loss scan to the integrated peak intensity measured using mass-selective instability with resonance ejection

(see **Discussion S13.1** in SI). As shown in **Figure 13.4a**, the detection efficiency on the Mini 12 was two orders of magnitude higher, 44% for amphetamine and 70% for methamphetamine vs. 0.4% and 0.3%, respectively, than that for the LTQ (helium bath gas) in the precursor scan of *m/z* 119. If we consider, though, that the LTQ has two detectors to the Mini 12's one, then the corresponding detection efficiencies on the LTQ were 0.2% and 0.15%, respectively. Substituting nitrogen for helium in the LTQ resulted in 2.6% and 4.8% efficiencies. For the neutral loss scan of 31 Da, the Mini 12 yielded 38% and 67% efficiencies for *m/z* 150 and 194, respectively, to the LTQ's 1.1% and 2.6% using helium gas (**Figure 13.4b**). Nitrogen improved LTQ efficiencies to 10.4% and 8.0%.

13.4.4 Resolution and Product Ion Selectivity

Resolution in ac frequency scanning depends heavily upon the frequency dispersion of the trapped ions as well as their secular frequency bandwidths.[106] It is thus important to characterize both *mass spectral resolution* as well as the *product ion selection window*.

At an rf amplitude of 7000 DAC units (LMCO ~70 Th), peak widths were 1.48 and 1.86 Th for *m/z* 136 and 150, respectively, whereas for an rf amplitude of 9,500 DAC units (LMCO ~92 Th), peak widths decreased to 0.93 and 0.87 Th. Unfortunately, at higher rf amplitudes artifact peaks were observed because the amphetamine precursor ions fragment to *m/z* 91 as well, and so if the precursors fragment while the LMCO > 91 Th, the product ion *m/z* 91 will inadvertently be detected by boundary instability. In the case of the LTQ, unit resolution was observed for a LMCO of 87 Th, with approximate peak widths of 0.5 Th for *m/z* 136 and 150. In nitrogen, the peak width for *m/z* 136 was 1.1 Th and for *m/z* 150 was 0.9 Th. On both the Mini 12 and LTQ resolution degraded at lower Mathieu q values due to decreased secular frequency dispersion.

We define the product ion selection window for the precursor ion scan as *Δ(m/z)*, or the width (in Th) of the intensity vs. product ion ejection frequency curve as measured at half maximum amplitude. In other words, the product ion selection window describes the range of *m/z* values that are targeted by the ejection frequency in the MS/MS scan: *(m/z)_{precursor} -> (m/z)_{product} ± Δ(m/z)/2*. In this experiment, a precursor ion scan of *m/z* 119 was performed on amphetamine and methamphetamine and the ejection frequency was altered from its ideal value of 201 kHz (Mini 12, q = 0.53) and 253 kHz (LTQ, q = 0.57). The integrated intensities of *m/z* 136 and 150 were recorded. On the Mini 12 the FWHM of the curve was 5.6 Th (**Figure 13.5a**), compared to approximately 3.9 Th (*m/z* 136) and 4.3 Th (*m/z* 150) on the LTQ using helium (**Figure 13.5b**).

In other words, on the Mini 12 ions between m/z 121.5 and m/z 115.9 were selected for ejection from the trap by applying an 800 mV$_{pp}$ excitation signal corresponding to the secular frequency of m/z 119.

In order to determine the product ion selection window (in Th) for the neutral loss scan of 31 Da, the trigger delay between the precursor excitation frequency sweep and both the artifact rejection sweep and product ejection sweep was varied while keeping the difference between the artifact rejection trigger delay and product ejection trigger delay constant. The same rf amplitude, frequency scan rate, and ac voltages were used in this experiment as compared to the precursor scan experiment. The integrated intensities of methamphetamine and 3,4-methylenedioxymethamphetamine were plotted with respect to the trigger delays, and the results are shown in **Figure 13.5c** (Mini 12) and **13.5d** (LTQ, helium). For the Mini 12, the approximate product ion selection windows were 8.6 Th and 11 Th for m/z 150 and 194, respectively. For the LTQ, those widths were 7.1 Th and 7.8 Th, respectively. Other factors, such as mass scanning rate, that affect resolution are mentioned in **Discussion S13.2**.

13.4.5 Effect of Cooling Time

Although not a significant concern on a benchtop instrument which operates at constant pressure in the ion trap volume, pump down time on the Mini 12 must be carefully considered. The Mini 12 uses a discontinuous atmospheric pressure interface[75] composed of a silicone tube that is constricted by a pinch valve except for when ions are introduced. During ion introduction, a low voltage pulse opens the valve, thereby letting ions and neutrals into the vacuum chamber. The ions are then trapped and cooled, and the chamber is pumped down to operating pressure. Because the pressure in the Mini 12 varies as a function of time, it is critical to optimize it for the given scan mode.

The effect of cooling time (i.e. instrument pump down) on the sensitivity and resolution of the precursor ion scan of m/z 119 is shown in **Figure 13.6a** and **13.6b**, respectively. At low cooling times (high pressure), the peak width is minimized (panel **b**) at 0.94 and 0.56 Th for m/z 136 and 150, respectively, resulting in the best resolution. At high cooling times, the peak widths increase substantially to 2.5 and 3.3 Th, respectively, and the ion intensity also decreases, likely due to inefficient fragmentation at low pressure. In the middle (~750 ms), however, there is optimal ion intensity and reasonable peak width (1.0 and 1.1 Th peak widths for m/z 136 and 150).

13.4.6 Nonlinear Resonance Lines

Nonlinear resonance lines cause the rapid uptake of energy from the rf field so that any ion whose working point lies on the resonance line can be rapidly ejected even before a mass scan takes place.[7,29-31,34,373] Their effects on the spectra described here are thus important to consider, especially since the Mini 12 uses a single-section rectilinear ion trap which is only 65% quadrupolar with $A_4/A_2 = 7.9\%$ and $A_6/A_2 = -17.2\%$.[204] In contrast, the LTQ houses a 3-section trap (to minimize ion excursion into fringe fields near the endcaps) with hyperbolic cross sections.[10] Using the precursor ion scan of m/z 119 on the Mini 12 (while varying the rf voltage to change the ion's working point), we found that when m/z 136 had its working point placed at a black hole octupole line at $\beta = 1/2$ during the scan, the peak disappeared (**Figure 13.7**, left). Moving the precursor ion working point away from the 'black hole' increased the intensity of m/z 136 until it was far enough away that the nonlinear resonance appeared to have no effect (**Figure 13.7**, right). These are identical results to our prior secular frequency scanning study.[106] When the *product ion* (m/z 119) was placed on or near the octupole nonlinear resonance line, no effect was observed. This is perhaps because the product ion is intended to be immediately ejected by the product ion ejection frequency so that any additional energy uptake due to the nonlinear resonance only helps in this process. However, the resolution did not increase compared to when the product ion was placed away from the nonlinear resonance line (experiment described in **Discussion S13.3**). We believe this is because the resolution is largely determined by the slow fragmentation of the precursor ions rather than the comparatively fast ejection of the product ions.

13.5 Conclusion

Precursor and neutral loss scans using orthogonal double resonance excitation have been successfully implemented on a miniature rectilinear ion trap. Compared to a selected benchtop instrument, the Mini 12 offers up to 2 orders of magnitude higher sensitivity in the precursor scan mode and 2x better sensitivity in the neutral loss scan mode. Future work should focus on improving the product ion selection window, which limits the selectivity of both types of MS/MS scans, as well as reducing the contribution of artifact peaks (from boundary instability).

The scans demonstrated here are particularly valuable for miniature instruments that use discontinuous interfaces, as they have very low duty cycles and will also be expected to have higher sensitivity by using a heavier collision gas. A goal of this work is to implement these scan

modes at NASA Goddard Space Flight Center for possible use in future planetary missions.[79,374] This would build on the importance of mass spectrometry in many NASA and European Space Agency missions including the Rosetta project[375,376] and the more recent development of the Sample Analysis at Mars suite and Mars Organic Molecule Analyzer.[139,217]

13.6 Acknowledgements
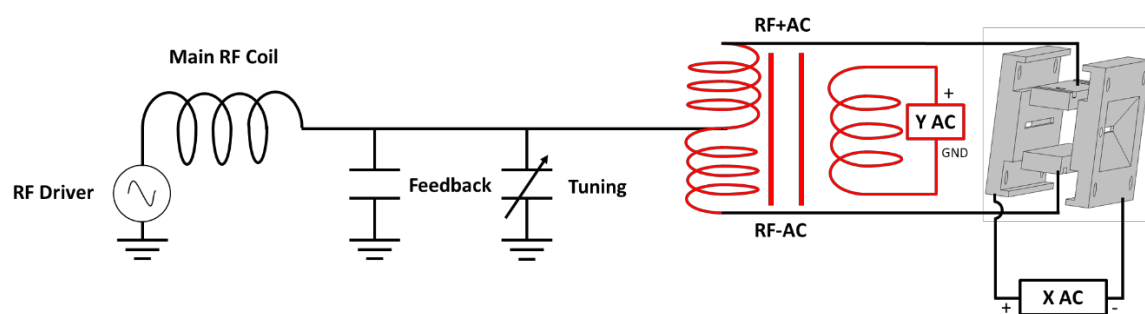
Figures

Figure 13.1. Schematic of existing Mini 12 rf coil coupled to the rectilinear ion trap (black) and center-tapped toroidal transformer (red) used to couple low voltage ac signals onto the y rods.
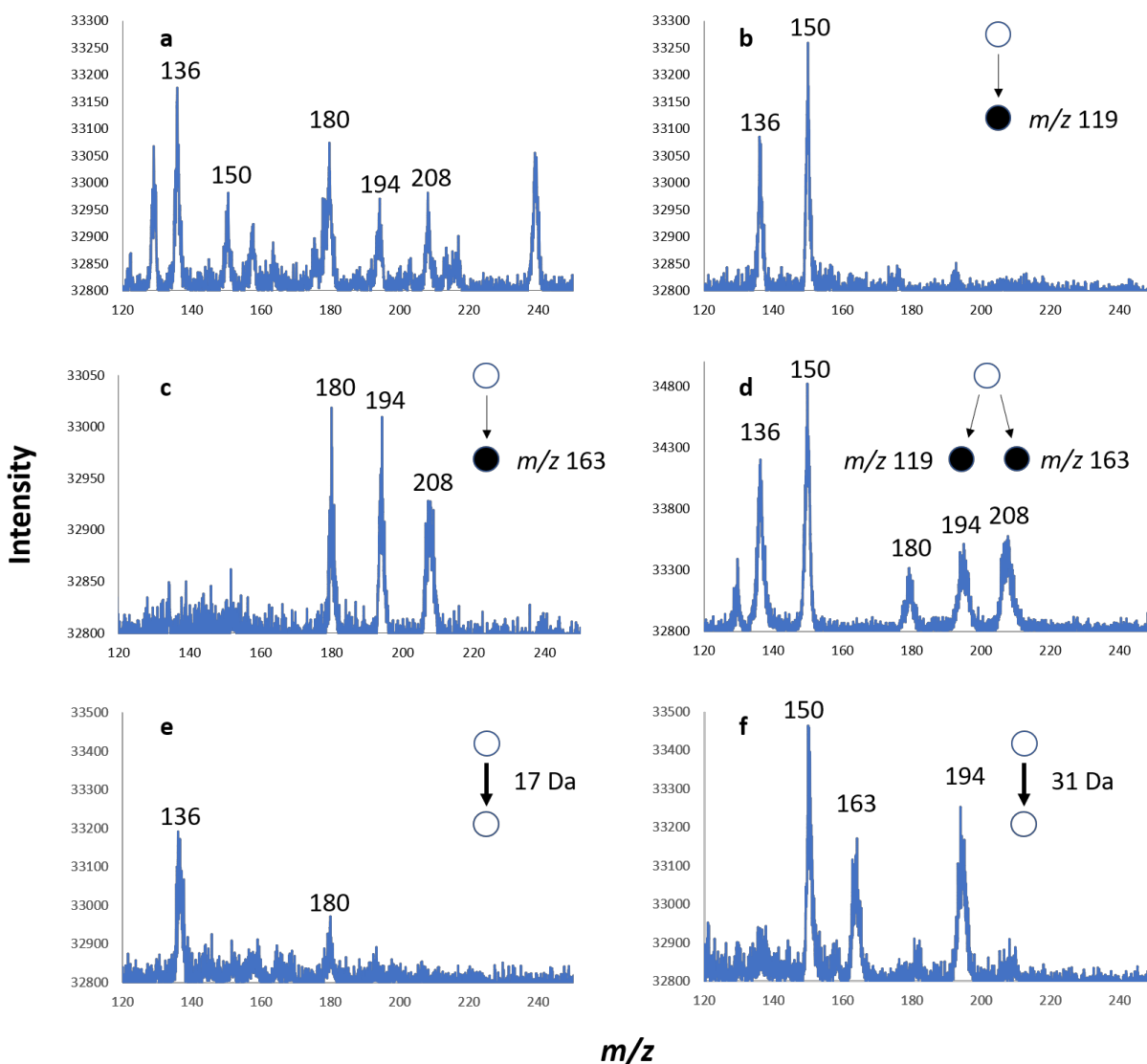
Figure 13.2. Precursor and neutral loss scans on the Mini 12 mass spectrometer: (a) full ac frequency scan mass spectrum of five amphetamines (*m/z* 136, 150, 180, 194, and 208), (b) precursor ion scan of *m/z* 119, (c) precursor ion scan of *m/z* 163, (d) double simultaneous precursor scan of *m/z* 119 and *m/z* 163, (d) neutral loss scan of 17 Da, and (f) neutral loss scan of 31 Da. These data can be compared to corresponding LTQ spectra in the Supplemental Information (**Figures S13.1**, **S13.2**, **S13.3**).
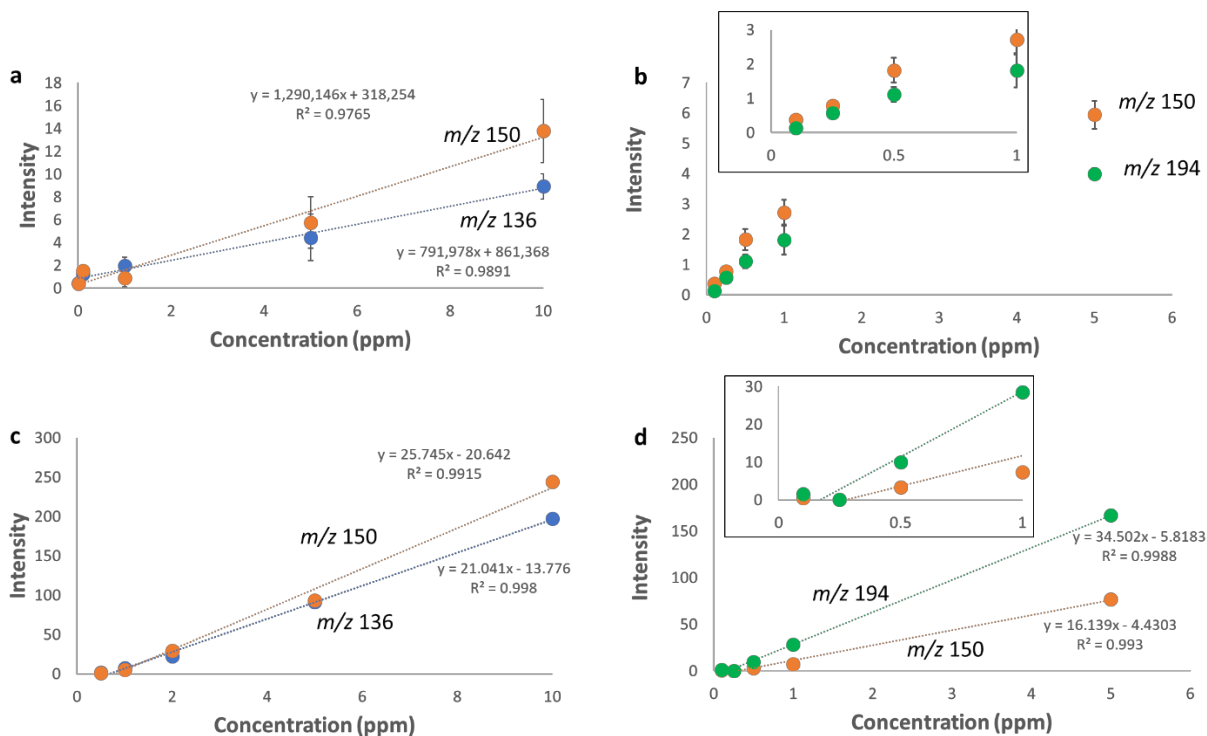
Figure 13.3. Calibration curves for the precursor ion scan of *m/z* 119 on (a) Mini 12 and (b) LTQ (helium bath gas) as well as the neutral loss scan of 31 Da on (c) Mini 12 and (d) LTQ (helium bath gas). LTQ calibration curves using nitrogen are shown in **Figure S13.5**.
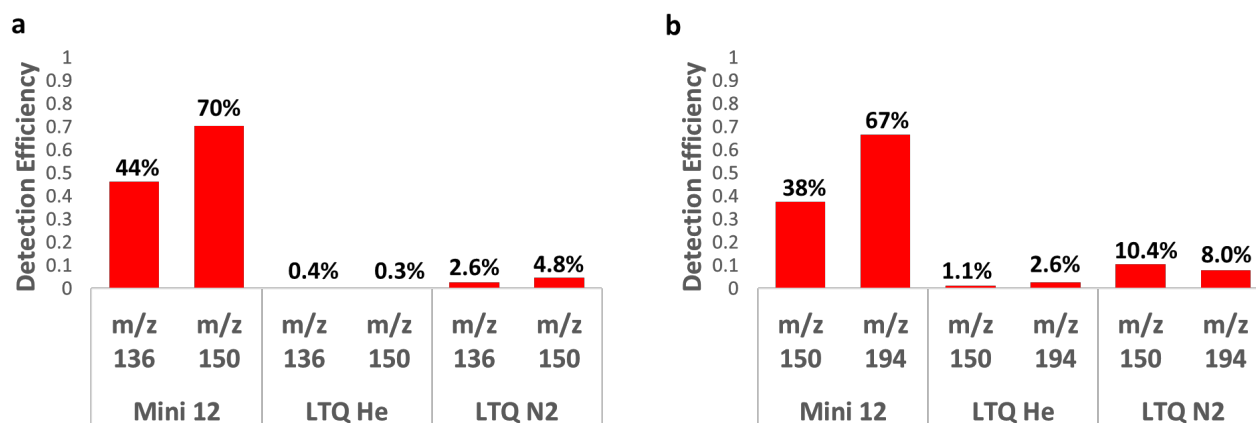
Figure 13.4. Detection efficiencies for (a) precursor ion scan of *m/z* 119 and (b) neutral loss scan of 31 Da on the Mini 12 and LTQ (helium or nitrogen bath gas). The detection efficiency was calculated as the ratio of MS/MS scan intensity to full MS scan intensity (and expressed as a percent) for the selected ion.
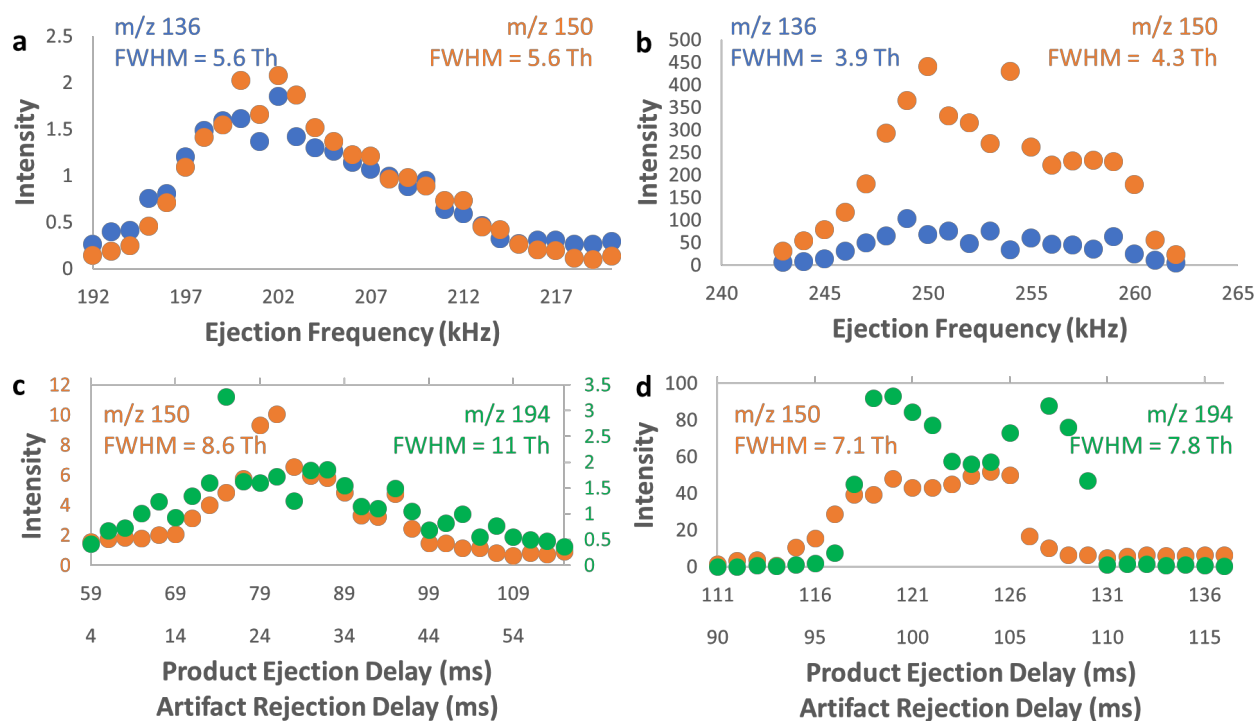
Figure 13.5. Product ion selection selection window in the precursor ion scan of *m/z* 119 on (a) Mini 12 and (b) LTQ; and product ion selection window for the neutral loss scan of 31 Da on (c) Mini 12 and (d) LTQ. FWHM = full width at half maximum of the ion intensity vs. ejection frequency (for the precursor scan) or trigger delay (for the neutral loss scan), which describes the range of product ion *m/z* values that are targeted by the given scan.
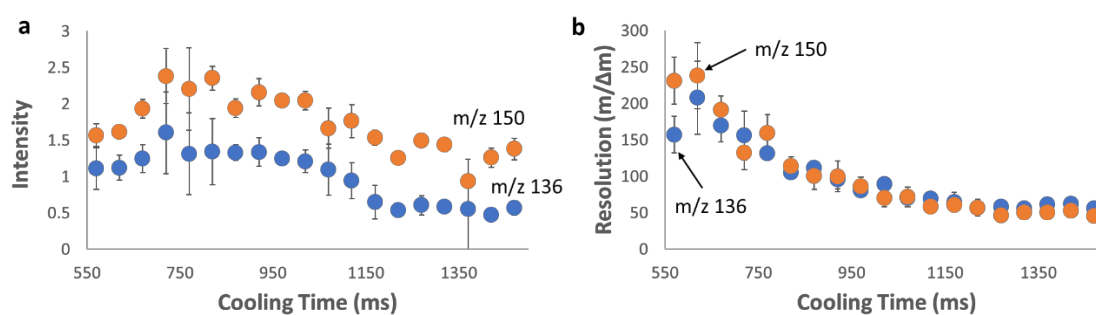
Figure 13.6. Effect of cooling time on precursor ion scan of *m/z* 119: (a) ion intensity vs. cooling time and (b) mass spectral resolution vs. cooling time. Data acquired on the Mini 12.
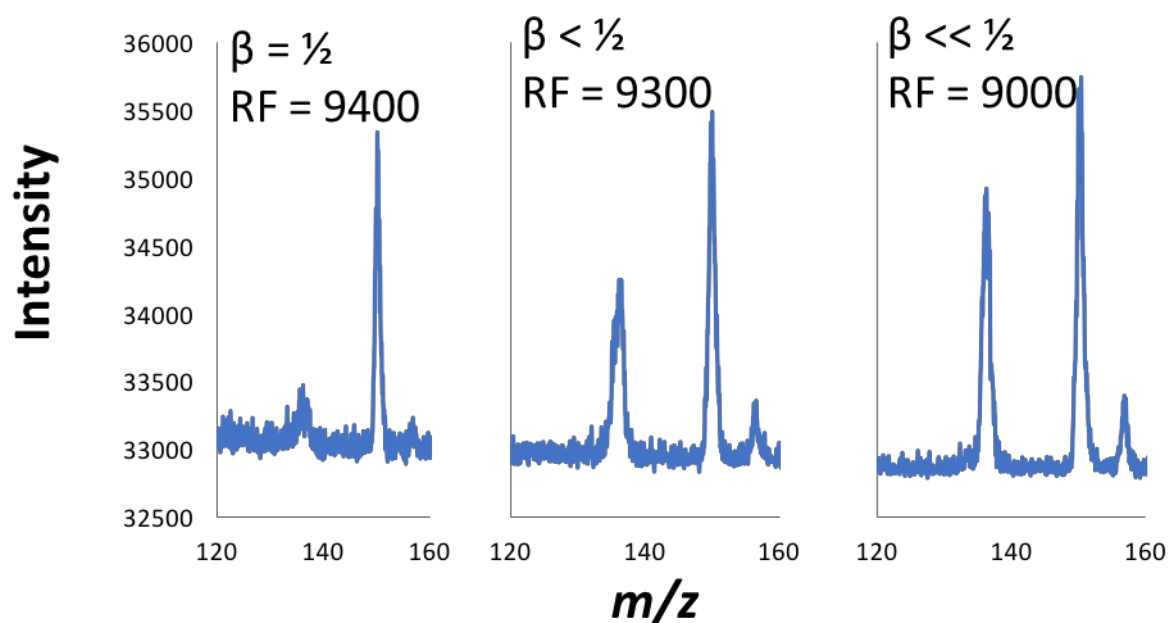
Figure 13.7. Effect of the octupole ($\beta = 1/2$) nonlinear resonance line on precursor ion scan of *m/z* 119. Precursor ion *m/z* 136 had working point either (left) on the nonlinear resonance line, (middle) slightly below the nonlinear resonance line, and (right) far away from the nonlinear resonance line. The working point of the ions was altered by changing the rf voltage (reported in DAC units) during the precursor ion scan.

Table 13.1. Performance of precursor and neutral loss scans on LTQ (helium bath gas) and Mini 12 (air)

Performance Metric	LTQ Pre	Mini 12 Pre	LTQ NL	Mini 12 NL
Resolution (m/Δm) at *m/z* 150	300	150	300	150
Product Ion Selection Window	3.9 Th , 4.3 Th	5.6 Th, 5.6 Th	7.1 Th, 7.8 Th	8.6 Th, 11 Th
Limit of Detection (ppb)*	1,000	10	500	250
Detection Efficiency*	0.3 - 0.4%	40 - 80%	1 - 3%	40 - 70%

. Pre = precursor ion scan of *m/z* 119. NL = neutral loss scan of 31 Da.

*LTQ has two detectors and Mini 12 has a single detector.

In these experiments, the rf voltage was set such that *m/z* 119 was placed at q = 0.53 (Mini 12) or q = 0.57 (LTQ)

SUPPLEMENTARY INFORMATION

Introduction S13.1: Value of Precursor and Neutral Loss Scans for Miniature Ion Traps

Precursor and neutral loss scans on single ion traps can be accomplished in one of two ways. First, a series of data-dependent product ion scans can be used to reconstruct precursor and neutral loss spectra. Usually this method requires an ion injection, fragmentation, and mass scan event for each precursor ion of interest. On benchtop ion trap instruments, which have mass scan rates on the order of 10^4 Th/s[10,11,43,61,244] and overall acquisition rates (number of scans per second) on the order of 10^1 Hz, data-dependent operations are feasible, useful, and high-performance.

However, the pumping limitations[199] of most miniature ion trap systems require use of a discontinuous atmospheric pressure interface,[75] i.e. a pinch valve within the inlet system that is closed except during ion introduction. Mass scan rates for these instruments are on the order of 10^3 Th/s and acquisition rates are on the order of 10^{-1} - 10^0 Hz. The primary reason for reduction in the repetition rate is the need to pump out the neutrals that are introduced with analyte ions when the DAPI valve is opened. For example, the Mini 12[100] and the Mars Organic Molecule Analyzer linear ion trap[79] both acquire one spectrum every 1-3 s. In such an instrument, data-dependent operations are less feasible because of the lower acquisition rate. If, instead, data-independent precursor and neutral loss scans – which, using a single scan, search over a large mass range for selected product ions or neutral losses - could be implemented, this would be a useful feature for interrogating complex mixtures. They could be used to search for functionally similar molecules, and subsequent to these scans one could use product ions scans on the 'candidates' observed in the precursor or neutral loss scan. We believe such a mode would be more time- and sample-efficient than relying solely on product ion scans.
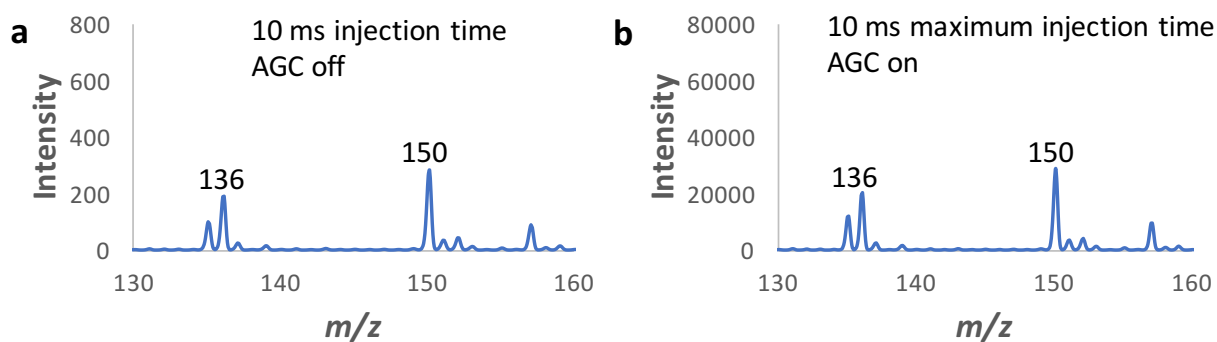
Figure S13.1. Comparison of AGC On vs. Off Full resonance ejection mass spectrum of amphetamine (*m/z* 136) and methamphetamine (*m/z* 150) with (a) manual 10 ms injection time and automatic gain control (AGC) off and (b) 10 ms maximum injection time and AGC on. Note the minimal space charge observed in panel a. Data acquired on LTQ.
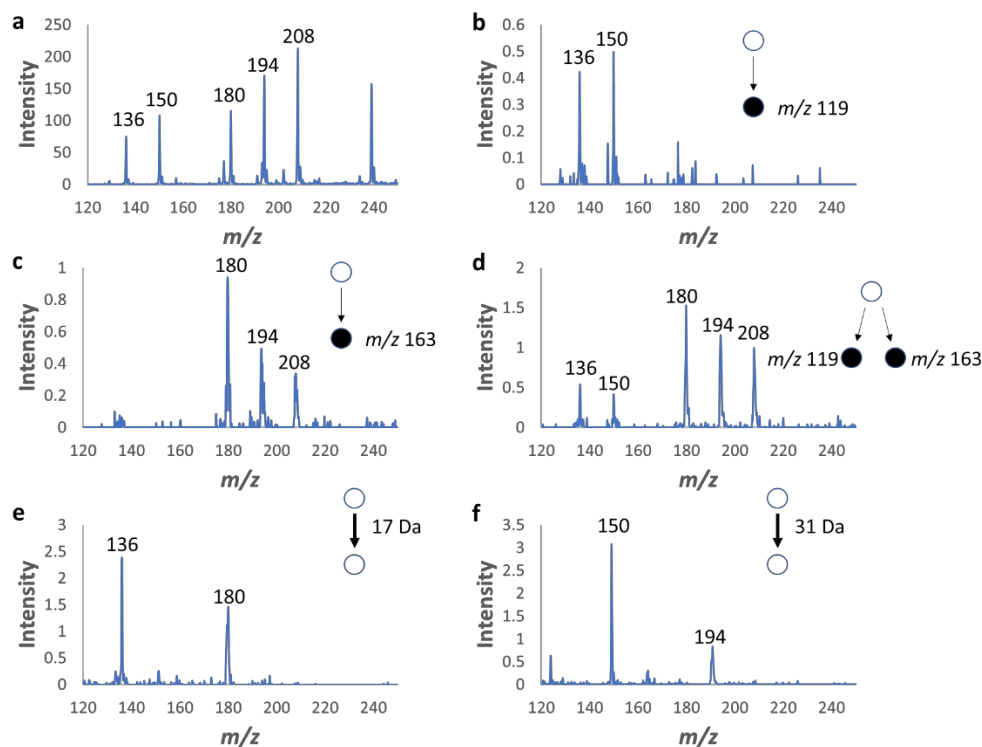
Figure S13.2. LTQ Mass Spectra Using Helium Precursor and neutral loss scans on a benchtop LTQ using helium as bath gas (ion gauge reading 0.6E-5 torr): (a) full resonance ejection mass spectrum of 1 ppm each of five amphetamines (*m/z* 136, 150, 180, 194, and 208), (b) precursor ion scan of *m/z* 119, (c) precursor ion scan of *m/z* 163, (d) double simultaneous precursor scan of *m/z* 119 or 163, (e) neutral loss scan of 17 Da, and (f) neutral loss scan of 31 Da. The scan rate in panel (a) was 16,000 Th/s and the scan rate in the other panels was 470 Th/s.
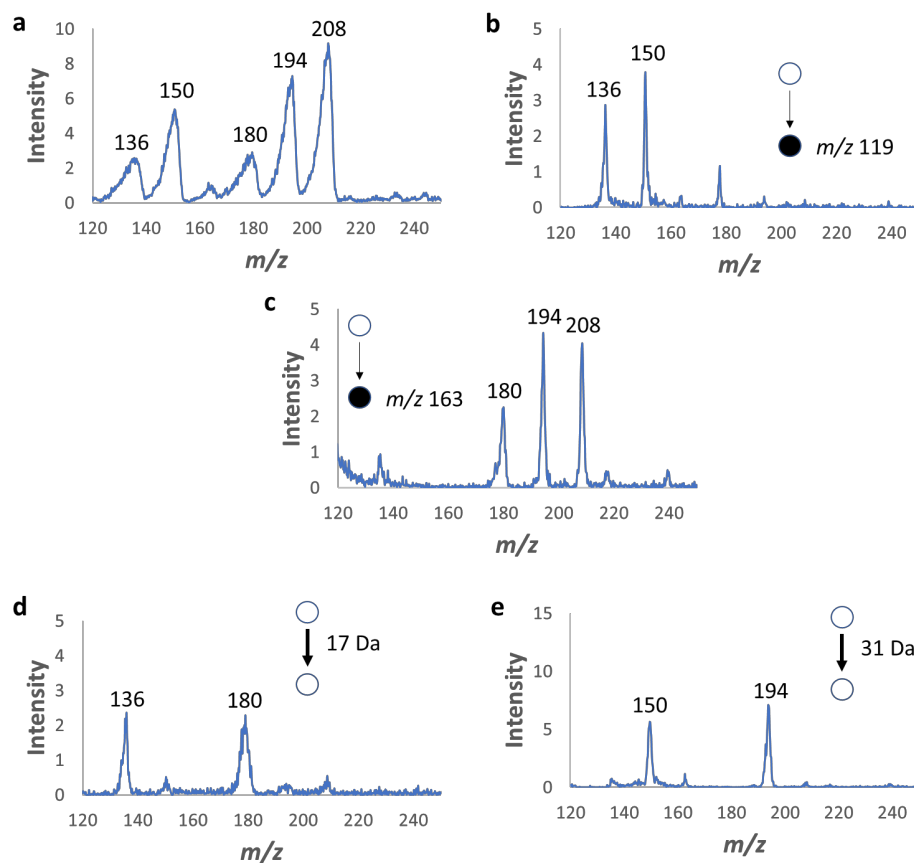
Figure S13.3. LTQ Mass Spectra Using Nitrogen Precursor and neutral loss scans on a benchtop LTQ using nitrogen as bath gas (ion gauge reading 2.6E-5 torr): (a) full resonance ejection mass spectrum of 1 ppm each of five amphetamines (*m/z* 136, 150, 180, 194, and 208), (b) precursor ion scan of *m/z* 119, (c) precursor ion scan of *m/z* 163, (d) neutral loss scan of 17 Da, and (f) neutral loss scan of 31 Da. Note that the low resolution in panel (a) is the result of the combination of nitrogen as bath gas and fast scan rate (16,000 Th/s), not space charge. The scan rate in panels (b) – (e) was 470 Th/s. In panel (b), a contamination peak (*m/z* 177) which
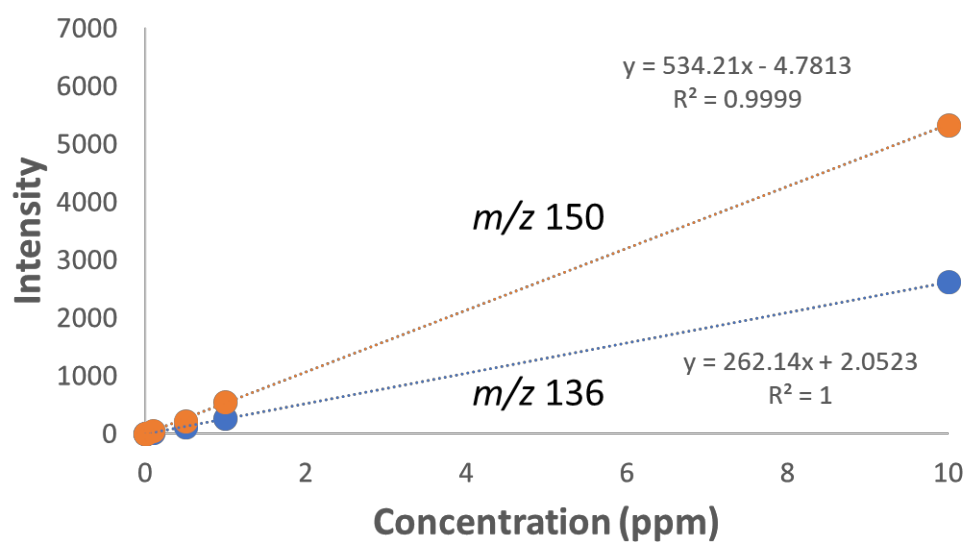
Figure S13.4. LTQ Calibration Curve Using Product Ion Scanning LTQ calibration curve for amphetamine (*m/z* 136) and methamphetamine (*m/z* 150) using product ion scanning with helium as bath gas (q_{excite} = 0.25, activation time = 30 ms, normalized collision energy = 25, injection time = 10 ms). The intensity plotted is that of the most abundant product ion, *m/z* 119. The limit of detection for both precursors was 1 ppb.

285
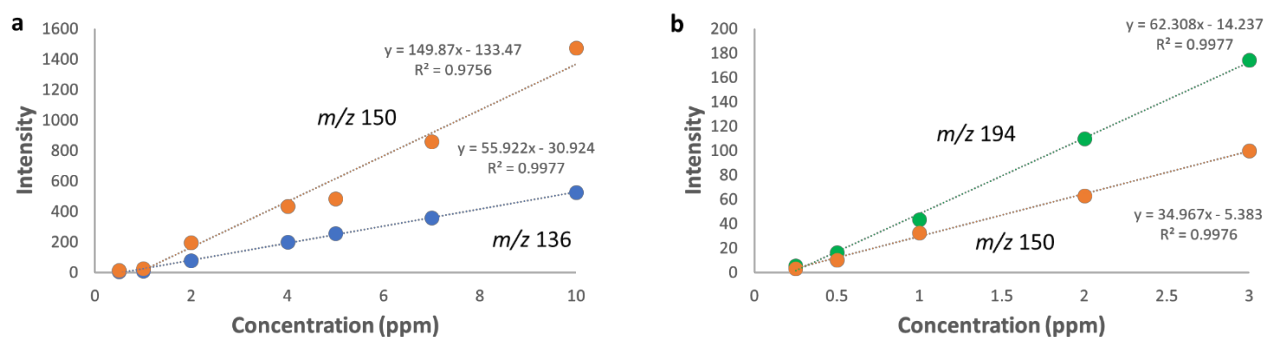
Figure S13.5. LTQ Calibration Curves Using Nitrogen LTQ calibration curves (using nitrogen as bath gas) for (a) precursor ion scan of *m/z* 119 and (b) neutral loss scan of 31 Da. The solution in panel a contained amphetamine and methamphetamine, and the solution in b contained methamphetamine and 3,4-methylenedioxymethamphetamine. The limits of detection were (a) 500 ppb and (b) 250 ppb.

Discussion S13.1: Calculation of 'Detection Efficiency'

The sensitivity of the precursor and neutral loss scans is affected by several factors. First, a precursor ion must be successfully converted to a product ion when it is excited in the y dimension. Next, the product ion must also be ejected from the trap in the orthogonal dimension. Importantly the product ion's kinetic energy needs to dampen in y so it is ejected through the x electrode slits instead of hitting the electrode and being lost. In other words, the fragmentation efficiency of the precursor ion, the ejection efficiency of the product ion, collisional damping of the product ion, ion-neutral scattering, and ion neutralization all affect the 'detection efficiency', which we define as the number of precursor ions of a given *m/z* that are successfully trapped and converted to product ions of a selected *m/z* which are then detected.

To measure the total number of precursor ions of a given *m/z* we used the LTQ's normal resonance ejection scan function with a 10 ms injection time (AGC off) and integrated the peak intensity. To measure the number of product ions detected, we used either a precursor ion scan of *m/z* 119 or a neutral loss scan of 31 Da, again with a manual 10 ms injection time, and integrated each peak. The detection efficiency of, say, *m/z* 136->119 was the intensity of *m/z* 119 from the precursor ion scan divided by the intensity of *m/z* 136 from the full scan.

Discussion S13.2: Factors Affecting Resolution

There are many factors that affect the resolution for a linear quadrupole ion trap. These include mass scanning rate, space charge effects, nonlinear resonance lines, working point (i.e. the ion's Mathieu q parameter), the closeness of the electric potential to an ideal quadrupole potential, the bath gas pressure and composition, fringe field effects (near the endcaps), and the rf frequency. Given that many of these factors were already unequal between the Mini 12 and LTQ because of the differing rf frequencies, vacuum systems (continuous vs. discontinuous interface), and mass analyzer geometries, we decided not to attempt to 'level the playing field' but instead to 1) use the same frequency scan rate (but not *mass scan* rate) for excitation on both instruments, and 2) use similar Mathieu q values for the product ion. Other factors, including bath gas composition and pressure, rf frequency, and mass analyzer geometry were left as is, i.e. at optimized or standard values.

Discussion S13.3: Nonlinear Resonance Line Experiments

In these experiments, a solution of amphetamine and methamphetamine was subjected to a precursor ion scan of *m/z* 119. The frequency scan rate of the excitation waveform was kept constant, as was the rf frequency, but the product ion ejection frequency had to be varied to always coincide with *m/z* 119. In a first experiment, the rf amplitude (which on the Mini 12 is specified in DAC units directly proportional to voltage) was varied until precursor ion *m/z* 136's working point was placed at the octupole line. It was evident when *m/z* 136 was on or near the line because the peak intensity in both the full scan and precursor scan (Figure 13.7) was decreased dramatically. In addition, we know the relationship between excitation frequency and time, and if *m/z* 136 is excited/detected at (or near) the time at which the excitation frequency sweep passes through the octupole nonlinear resonance frequency (a quarter of the rf frequency), then we know that *m/z* 136 has working point at (or near) the octupole nonlinear resonance frequency.

The same logic applies for placing the product ion *m/z* 119's working point at the octupole line. In addition, we can set the product ion ejection frequency at the octupole line frequency and vary the rf amplitude over a small range of values and see what effect the nonlinear resonance line has on the mass spectra when the product ion's working point is at or near that line.

CHAPTER 14.   SIMULTANEOUS AND SEQUENTIAL MS/MS SCAN COMBINATIONS AND PERMUTATIONS IN A LINEAR QUADRUPOLE ION TRAP

A version of this chapter has been published in a peer-reviewed journal as:
Snyder, D. T.; Szalwinski, L. J.; Cooks, R. G. Sequential and simultaneous MS/MS combinations and permutations in a linear quadrupole ion trap. *Anal. Chem.* **2017**, *89*, 11053-11060.

14.1 Abstract

Methods of performing precursor ion scans as well as neutral loss scans in a single linear quadrupole ion trap have recently been described. In this paper we report methodology for performing *permutations* of MS/MS scan modes, that is, ordered combinations of precursor, product, and neutral loss scans, following a single ion injection event. Only particular permutations are allowed; the sequences demonstrated here are 1) multiple precursor ion scans, 2) precursor ion scans followed by a single neutral loss scan, 3) precursor ion scans followed by product ion scans, and 4) segmented neutral loss scans. 5) The common product ion scan can be performed earlier in these sequences, under certain conditions. Simultaneous scans can also be performed. These include multiple precursor ion scans, precursor ion scans with an accompanying neutral loss scan, and multiple neutral loss scans. We argue that the new capability to perform complex simultaneous and sequential MS^n operations on single ion populations represents a significant step in increasing the selectivity of mass spectrometry.

14.2 Introduction

The drive to miniaturize mass spectrometers has encouraged the development of a wealth of unconventional ionization sources, atmospheric pressure interfaces, vacuum systems, and mass analyzer combinations.[70,71] Both continuous[76,377] and discontinuous[75,198] atmospheric pressure interfaces have been developed, allowing the coupling of ambient spray and plasma ionization methods with portable systems.[191,318,360,378] The standard analyzer geometry has evolved from the 3D quadrupole ion trap (Paul trap)[1] to cylindrical,[13] rectilinear,[204] linear,[10,11] toroidal,[17,18,205] and halo traps,[19,97] as well as ion trap arrays,[209,379-381] two-plate linear ion traps,[382] wire ion traps,[366,383] and other unusual devices.

By contrast, the fundamental way in which mass analysis is performed in quadrupole ion traps has varied very little. Mass-selective instability,[82] usually with resonance ejection[10,131] either radially[10] or axially[11,43] has remained the dominant form of mass analysis in both 2D and 3D ion traps.[7-9] Improvements in resolution, sensitivity, and space-charge tolerance can be made through nonlinear resonance ejection[33,34,119] and orthogonal excitation during the ejection process.[120] Ion ejection can furthermore be made unidirectional through careful selection of multipole components,[34,384] rf/ac phase relationship,[34] and ac signal components.[385]

Despite the minimal variance in ion trap mass analysis over the past three decades, three unconventional mass scanning methodologies have appeared in the ion trap literature: digital ion trap frequency scanning,[86,88,386] sinusoidal rf frequency scanning,[387] and ac frequency scanning.[19,49,50,91,135,205,354] Digital technology is promising, especially with regards to high spectral resolution and scan speed, but it requires a complete overhaul of existing instrumentation and has a higher power consumption than for conventional methods. Rf frequency scanning can similarly improve resolution and mass range. The ac frequency scanning technique, in contrast, is not particularly high performance yet it offers increased instrument versatility while requiring virtually no instrument modifications.[374]

Among the unique capabilities made accessible by ac frequency scanning (also known as secular frequency scanning) are data-independent single analyzer precursor ion scans and neutral loss scans.[99,123,135,341] These simple scans, of which the precursor variant was demonstrated on a 3D ion trap some 25 years ago,[123] require simultaneous orthogonal excitation of precursor and product ions for fragmentation of a particular precursor ion in concert with the ejection and detection of a particular product ion. In the case of the precursor ion scan, the product ion m/z, and hence secular frequency under constant rf conditions, is fixed, whereas in the neutral loss scan the difference between precursor ion and product ion m/z is fixed, and with an added 'artifact rejection' (to neutralize unfragmented precursor ions) scan this requires a triple frequency scan for implementation. In comparison, previous implementations of precursor and neutral loss 'scans' have largely been data-dependent sequences[299,344] of resonance excitation[52] and resonance ejection and hence are not actually 'scans', but rather are sequences of scans from which precursor and neutral loss spectra can be reconstructed.

Both the precursor ion scan and the more difficult neutral loss scan that we ~~have~~ demonstrated [55] show relatively low conversion of precursor ions to detected product ions using

conventional scan rates (thousands of Th per second). For example, in cases where each precursor ion is given ~3 ms to fragment, typical estimated conversions are 5-10%, which implies that perhaps 90% of the precursor ions are left in the ion trap after a precursor ion scan. For the neutral loss scan, this is not the case because the precursor ions must be cleared from the ion trap during the scan to prevent artifact peaks. Nonetheless, the inefficiency in fragmentation in the precursor scan allows certain *MS/MS permutations* to be performed. These are ordered combinations of the three main MS/MS scan types: precursor ion scans, product ion scans, and neutral loss scans. The zero-dimensional multiple reaction monitoring experiment is not a scan and is not considered because if isolation is performed strictly, no ions will remain after this experiment which can only be the endpoint of an experimental sequence. By performing multiple scans on the same ion population, the information obtained from those ions can be maximized, a particularly useful characteristic for resource-constrained ion traps with relatively low duty cycles and when sample size and/or access is highly limited. The allowed combinations of scans are multiple precursor ion scans, precursor ion scans followed by a neutral loss scan, precursor ion scans followed by product ion scans, and segmented neutral loss scans, as well as simultaneous precursor and neutral loss scans, all of which are demonstrated here for simple mixtures of illicit drugs.

14.3 Experimental

14.3.1 Chemicals

Amphetamine (*m/z* 136), methamphetamine (*m/z* 150), 3,4-methylenedioxyamphetamine (*m/z* 180), 3,4-methylenedioxymethamphetamine (*m/z* 194), 3,4-methylenedioxyethylamphetamine (*m/z* 208), cocaine (*m/z* 304), noroxycodone (*m/z* 302), oxycodone (*m/z* 316), buphedrone HCl (*m/z* 178), N-ethylcathinone (*m/z* 178), morphine (*m/z* 286), codeine (*m/z* 300), and 6-monoacetylmorphine (*m/z* 328) were purchased from Cerilliant (Round Rock, TX, USA). HPLC grade methanol was purchased from Fisher Scientific (Hampton, NH, USA). All analytes were detected in the protonated form in the positive ion mode. Oral fluid samples were were spiked with amphetamine standards and subsequently diluted ten-fold in 95:4.9:0.1 acetonitrile:water:formic acid.

14.3.2 Ionization

Nanoelectrospray ionization using a 1.5 kV potential was utilized for all experiments. Borosilicate glass capillaries (1.5 mm O.D., 0.86 mm I.D.) from Sutter Instrument Co. (Novato, CA, USA) were pulled to 2 μm tip diameters using a Flaming/Brown micropipette puller (model P-97, Sutter Instrument Co.). The nanospray electrode holder (glass size 1.5 mm) was purchased from Warner Instruments (Hamden, CT, USA) and was fitted with 0.127 mm diameter silver wire, part number 00303 (Alfa Aesar, Ward Hill, MA), as the electrode.

14.3.3 Instrumentation

All scans were performed using a Finnigan LTQ linear ion trap mass spectrometer (San Jose, CA, USA) modified previously to perform orthogonal excitation.[135,341] The ion trap has dimensions $x_0 = 4.75$ mm, $y_0 = 4$ mm, and three axial sections of lengths 12, 37, and 12 mm. The rf frequency was tuned to 1.166 MHz. The rf amplitude was held constant throughout ionization, ion cooling, and mass scan segments by substituting the rf modulation signal between the rf detector board and rf amplifier with a low voltage DC pulse (~190 mV, ~700 ms period, 90% duty cycle) from an external function generator. All ac waveforms were generated by using two Keysight 33612A (Chicago, IL, USA) arbitrary waveform generators. Inverse Mathieu q scans were calculated in Matlab,[133] exported as .csv files, and imported to the waveform generators. The inverse Mathieu q scan is a nonlinear sweep of the low voltage ac frequency (performed at constant rf voltage) that linearizes the mass scale in contrast to the result of linear frequency sweeping.[388] Scan rates were in the range 200-500 Th/s and the lower-mass cutoff was usually set at 90 Th.

Precursor ion scans were performed by applying to the y electrodes of the linear ion trap a low voltage (~200 mV$_{pp}$) swept frequency (an inverse Mathieu q scan)[133] for precursor ion excitation while simultaneously applying a higher voltage (~600 mV$_{pp}$) fixed frequency to the x electrodes at a particular product ion's secular frequency.[341]

Similarly, neutral loss scans required three identical inverse Mathieu q scans with appropriate trigger delays.[135] A first frequency scan (~200 mV$_{pp}$) was used for precursor ion excitation, a second frequency scan (~600 mV$_{pp}$) with trigger delay was applied to reject into the y electrodes remaining precursor ions subsequent to their excitation, and finally a third frequency sweep (~600 mV$_{pp}$) with a trigger delay larger than the artifact delay was used for product ion ejection. The fixed neutral loss selected was directly proportional to the time delay between the

excitation and ejection sweeps. Each scan was calibrated separately using a linear fit of *m/z* vs. time.

Permutation scans were performed by applying the appropriate waveforms back-to-back or simultaneously. For sequential precursor ion scans, the excitation frequency sweep was applied twice in sequence. During the first sweep a first product ion ejection frequency was applied to target a first product ion, and during the second sweep a different frequency was applied to target a different product ion *m/z*. For the double (simultaneous) precursor ion scan, a single inverse Mathieu q scan was applied to the y electrodes for ion excitation while a dual frequency sine wave was applied to the x electrodes to target two product ions for ejection. To perform a precursor scan and neutral loss scan sequentially, an inverse Mathieu q scan was applied twice in sequence for ion excitation. During the first sweep a single frequency was applied to the x electrodes to target ions of a fixed *m/z* for ejection, and during the second sweep two trigger-delayed frequency sweeps (artifact rejection and product ion ejection) were applied to complete the neutral loss scan. For simultaneous precursor and neutral loss scans the waveforms required for each scan were summed and applied to the appropriate electrodes simultaneously. Hence, an excitation scan and artifact rejection scan were applied to the y electrodes while a fixed frequency and time-delayed frequency scan were summed and applied to the x electrodes. For the precursor ion scan followed by the product ion scan, a precursor ion scan was performed first, after which a selected precursor ion (not isolated) was excited at its secular frequency. A full ac frequency sweep then gave the product ion mass spectrum. Segmented neutral loss scans were simply back-to-back neutral loss scans (targeting different neutral losses) at different rf amplitudes. Simultaneous neutral loss scans were performed by using two single frequency sweeps on the y electrodes for ion excitation and artifact rejection while simultaneously applying two frequency sweeps on the x electrodes, one for each neutral loss. Only one ion injection event was used for each permutation, and automatic gain control was turned off. Injection time was varied from 5 ms to 25 ms, depending on sample concentration (generally 1-10 ppm, viz. g/L). Each mass spectrum shown here is the average of 10 scans.

14.5 Results & Discussion

Precursor ion scans and neutral loss scans are possible in single quadrupole ion traps using double resonance excitation, that is, by simultaneously exciting a precursor ion and ejecting a particular product ion so that the detection of that product ion occurs at the unique time during which its precursor fragments. Unlike CID in beam-type instruments (e.g. sectors and triple quadrupoles), CID in ion traps requires a relatively long time to increase internal energies because 1) helium is used as the collision partner and 2) collision energies are quite small. Hence many collisions – and thus more time – are required for fragmentation in ion traps. For the precursor scans and neutral loss scans, the low fragmentation efficiency translates into relatively low sensitivity for conventional scan rates. However, precursor ion scans – if performed under low ac amplitude conditions – do not clear the ion trap completely and thus if only a small fraction of the precursor ions are converted to product ions, then the rest of the ions are left in the trap for reexamination. This characteristic makes available permutations of MS/MS scan modes.

The full range of allowed MS/MS permutations is shown in **Table 14.1**. Multiple precursor ion scans can be performed on the same ion population so long as the precursor ions are not ejected and fully fragmented. Precursor ion scans can also be followed by a single neutral loss scan. Because the neutral loss scan clears the ion trap with an 'artifact rejection' frequency sweep, no subsequent scans are possible using a single ion injection event. Any number of product ion scans can succeed precursor ion scans as well. Finally, although two neutral loss scans cannot interrogate the same mass range (for a single ion injection event), one ion packet can be used for a segmented neutral loss scan wherein different neutral loss scans are performed over different mass ranges. Simultaneous scans are also allowed. Multiple precursor ion scans may be performed concurrently as well as precursor scans with neutral loss scans and finally multiple simultaneous neutral loss scans. In each of the scans the AC amplitudes are optimized while constant RF amplitude is used.

14.5.1 Multiple Precursor Ion Scans in Sequence

Multiple precursor ion scans are allowed because each precursor ion scan (at scan rates of hundreds of Th per second) converts a small fraction of precursor ions to product ions. Permutations of precursor ion scans could be useful for scanning an analyte population for different molecular functionalities and for monitoring more than one class of molecules. An

example of a double sequential precursor ion scan is shown in **Figure 14.1b** (compare to full scan in panel a). In this example amphetamines are monitored using a precursor ion scan of *m/z* 163 and cocaine is monitored using a precursor ion scan of *m/z* 182. All three amphetamines in this simple mixture could be detected at ~1 ppm with no artifact peaks and about 8% conversion of precursor ions to product ions at a scan rate of ~450 Da/s. Note that mdea was detected with S/N ~ 10, but is hard to see without an expanded intensity axis. The same precursor ion scan could, in principle, be performed multiple times, allowing for signal averaging or signal accumulation, somewhat mitigating the relatively low sensitivity of the method.

14.5.2 Precursor Ion Scans Followed by a Neutral Loss Scan

Precursor ion scans can be followed by a single neutral loss scan. Because the neutral loss scan clears the trap of ions, no other scans are possible subsequently. Nonetheless, like permutations of precursor ion scans, precursor ion scans followed by a neutral loss scan may be useful for examining an ion population for different functional groups. **Figure 14.2b** (full scan in panel a) shows a precursor ion scan of *m/z* 182 (the most abundant product ion of cocaine) followed by a neutral loss scan of 18 Da, which targets opioids oxycodone and noroxycodone. In the case of the neutral loss scan, unit resolution is observed at a scan rate of 470 Da/s and at most 17% of the precursor ions are converted to detected product ions. In principle, multiple precursor ion scans could be followed by a single neutral loss scan; however, the electronic constraints of our system limited the number of sequential scans we could perform.

14.5.3 Precursor Ion Scans Followed by Product Ion Scans

Product ion scans may follow precursor ion scans as well. A useful example of the utility of this scan mode is shown in **Figure 14.3**, where isobaric buphedrone and N-ethylcathinone were detected in the full scan in panel a, from a mixture with methamphetamine, and also in a precursor ion scan of *m/z* 160 (panel b, blue). A product ion scan of *m/z* 178 (panel b, orange) then confirms that both isobars are present since *m/z* 91 and 147 are unique to buphedrone and *m/z* 133 is unique to N-ethylcathinone. Note that no isolation was performed prior to the product ion scan (and hence methamphetamine was also detected in the final mass scan), although in principle it would usually precede the product ion scan.

14.5.4 Segmented Neutral Loss Scans

Because neutral loss scans clear the precursor ions from the ion trap via the 'artifact rejection' frequency sweep, no other scan modes may follow them. Hence, although neutral loss scans may not be repeated in the same mass range, segmented neutral loss scans are still allowed. These are similar to segmented full mass scans documented previously[374] wherein different mass ranges are interrogated at dissimilar rf amplitudes to improve resolution and mass accuracy across a portion of the mass range. Neutral loss scans can also be 'segmented' so that different mass ranges can be analyzed for different neutral losses. Segmenting the neutral loss scan allows better mass spectral resolution to be obtained for higher mass ions, which have lower secular frequency dispersions compared to lower mass ions. Moreover, often different classes of molecules will occupy different mass ranges so that multiple classes of molecules could be monitored with a single ion injection event (e.g. fatty acids and complex phospholipids in tissue). **Figure 14.4b** shows a segmented neutral loss scan of a mixture of methamphetamine, mdma, noroxycodone, and oxycodone (all of which were detected in the full scan in panel a). A first neutral loss scan of 31 Da was initiated at a low mass cutoff of ~91 Th, and a second neutral loss scan of 18 Da was carried out at a low mass cutoff of ~165 Th (i.e. using a higher rf amplitude). Both spectra exhibit unit resolution at a scan rate of 230 Da/s (first scan) and 415 Da/s (second scan) and with approximately 4% conversion of precursor ions to detected product ions.

14.5.5 Simultaneous Scans

One of the disadvantages of performing multiple discrete MS/MS scans in sequence is that an insufficient number of ions may remain after the first scan for several reasons. It is possible that most of the precursor ions are fragmented in the first scan, or if enough collision energy is imparted to the precursors then they may collide with the orthogonal electrodes (y direction, in our case) and hence be lost before any other scans take place. In this case it is possible to perform *simultaneous* MS/MS scans. That is, one may perform multiple simultaneous precursor ion scans, simultaneous precursor and neutral loss scans, and simultaneous neutral loss scans.

Figure 14.5 gives examples of all three cases. In **Figure 14.5a** a full ac frequency scan of methamphetamine, mdma, and mdea is shown. Methamphetamine fragments to *m/z* 119 and the latter two drugs fragment to *m/z* 163. Hence, all three amphetamines can be targeted (**Figure 14.5b**) by doing a simultaneous precursor ion scan of both product ion *m/z* values, which is accomplished

by using a dual frequency waveform (332 kHz and 227 kHz) for product ion ejection. An important characteristic of these spectra is the resolution observed. Although unit resolution was not observed in the full scan due to space charge effects (i.e. the trap was purposely overloaded with ions), unit resolution was observed in the MS/MS scan. The cause of the resolution increase is likely the orthogonal excitation that causes the product ions to circle the bulk of the ion cloud just before ejection, and hence better resolution is observed compared to the full scan mode wherein the precursor ions were only excited in one dimension. This effect has been previously documented in the study of "rhombic" ion excitation.[120]

A simultaneous precursor and neutral loss scan can similarly be performed by applying the following waveforms simultaneously: 1) a frequency scan in y for precursor ion activation, 2) a fixed frequency sine wave in x for product ion ejection (precursor scan), 3) a frequency scan in y for precursor ion rejection (artifact rejection) after activation, and 4) a frequency scan in x, with fixed mass offset from the excitation frequency scan, for neutral loss product ion ejection into the detectors. **Figure 14.5c** shows a single neutral loss scan of 85 Da on a simple solution of morphine, codeine, and 6-monoacetylmorphine, which detects the transitions m/z 286->201 and m/z 300->215. By simultaneously performing a precursor ion scan of m/z 286 (a product ion of 6-mam), 6-mam also appears in the MS/MS spectrum. Of course, whether each ion is ejected by the precursor scan or the neutral loss scan is ambiguous. Nonetheless, a simultaneous scan would still be useful, for example, in providing broad coverage of the amphetamines, which fragment either to m/z 163 or m/z 119. In this case it is not critical to know which fragment is produced by an unknown amphetamine, but a subsequent product ion scan would make the assignment clear.

Finally, an example of a simultaneous neutral loss scan performed on a mixture of amphetamine, methamphetamine, 3,4-methylenedioxyamphetamine, and 3,4-methylenedioxymethamphetamine is shown in **Figure 14.5f**. The individual neutral loss scans (shown in **Figure 14.5e**) are loss of 17 Da and loss of 31 Da (one ion injection each). Because each of these scans detects two of the amphetamines, all four of the amphetamines can be targeted by simultaneous neutral loss scans of 17 Da and 31 Da. This experiment required the following waveforms: 1) precursor ion excitation frequency sweep on the y electrodes, 2) artifact rejection sweep to eject unfragmented precursor ions into the y electrodes, 3) product ion ejection frequency sweep on the x electrodes for the 18 Da loss, and 4) product ion ejection frequency sweep on the x electrodes for the 31 Da loss.

14.5.6 Performance of MS/MS Scans on Oral Fluid

The final experiment performed in this work was utilization of the MS/MS scan modes in the case of a complex mixture. Oral fluid was chosen as an appropriate sample, as it has previously been examined for illicit drugs by swab touch spray tandem mass spectrometry.[359] In this work amphetamine standards were spiked into the oral fluid at concentrations ranging from 1 ppm to 100 ppm and subsequently the sample was diluted ten-fold in 50:4.9:0.1 acetonitrile:water:formic acid to improve nanospray performance. A full scan of the nanosprayed solution containing the drugs at 100 ppb final concentration (each is 1 ppm in oral fluid) is shown in **Figure 14.6a**. The four amphetamine peaks are buried in the mass spectrum. A simultaneous double precursor ion scan, **Figure 14.6b**, of *m/z* 119 and *m/z* 163 reveals all four amphetamines, although clearly the scan was performed near the limit of detection. The same scan with 5x higher concentration of amphetamines is shown in panel c. Both spectra are remarkably clean and free from artifacts.

14.5.7 Duty Cycle and Sensitivity

The scans demonstrated here on a commercial benchtop instrument are quite slow (10^2 Th/s) compared to data-dependent scans (10^4 Th/s for each scan in the sequence). However, when translated to miniature instruments that use discontinuous interfaces,[75] these data-independent scans will be more practical. For example, the Mini 12[100] takes ~700 ms to pump down after ion injection (when the DAPI valve is opened briefly) and uses an approximately 300 ms mass scan in the resonance ejection mode. Operating this system in a data-dependent mode would hence require several ion injection and cooling events, thereby using tens of seconds of instrument runtime, not including signal averaging. In comparison, a sequential or simultaneous MS/MS permutation scan would require ~1 s total and would therefore be faster than the data-dependent mode while still retaining selectivity and increase in signal-to-noise from MS/MS transitions. Lastly, in comparison to the product ion scan mode, precursor and neutral loss scans in ion traps are considerably less sensitive, perhaps 2 orders of magnitude. Some of the loss of sensivity may be compensated for by using air as cooling and collision gas, which is common on miniature instruments. Work is currently underway to implement the full MS/MS suite on a miniature system and will be the subject of a future report.

14.6 Conclusion

Permutations of MS/MS scan modes have been demonstrated on a single linear ion trap. Using one ion injection event, the information obtained from the injected ions can be maximized by performing particular ordered combinations of precursor ion scans, product ion scans, and neutral loss scans. Simultaneous precursor ion scans or precursor and neutral loss scans are also possible, expanding the range of analytes that can be detected with a single MS/MS scan. These scan modes are particularly important for resource-constrained instruments with limited instrument volume, power, or samples such as those examined using an ion trap for Mars origin of life studies or a portable instrument for forensic analyses in the field.

14.7 Acknowledgements
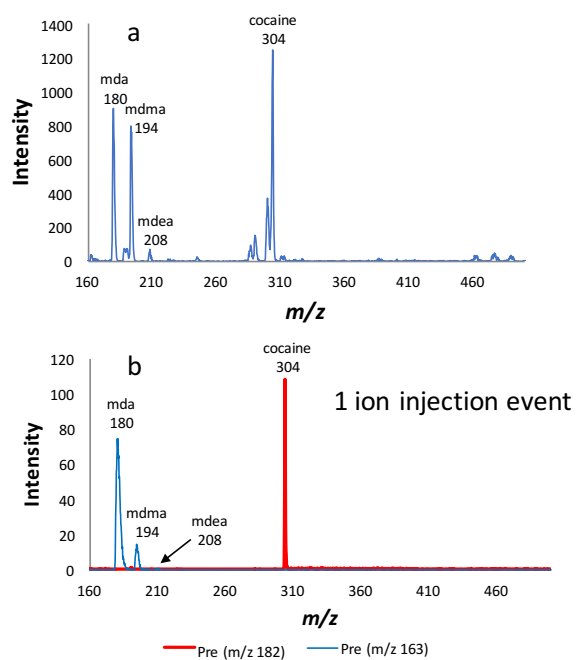
Figures

Figure 14.1. Permutations of precursor ion scans: (a) full ac scan mass spectrum of 3,4-methylenedioxyamphetamine (mda), 3,4-methylenedioxymethamphetamine (mdma), 3,4-methylenedioxyethylamphetamine, and cocaine, and (b) precursor ion scan of m/z 163 followed by precursor ion scan of m/z 182 using the same ion population.
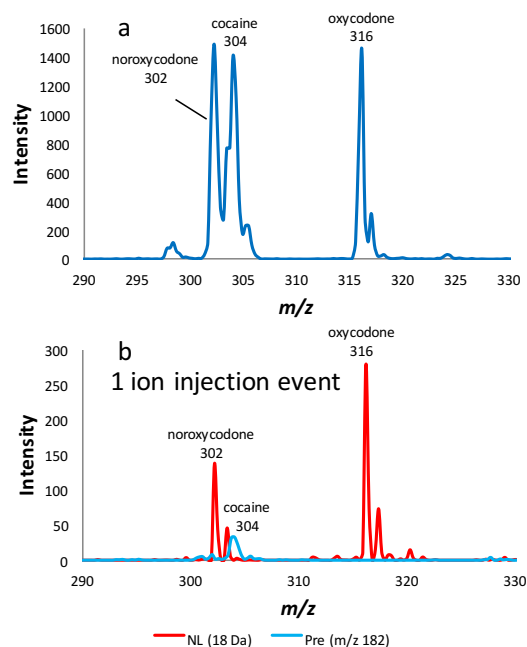
Figure 14.2. Permutation of precursor ion scans and neutral loss scans: (a) full ac scan mass spectrum of cocaine, noroxycodone, and oxycodone, and (b) precursor ion scan of *m/z* 182 followed by neutral loss scan of 18 Da.
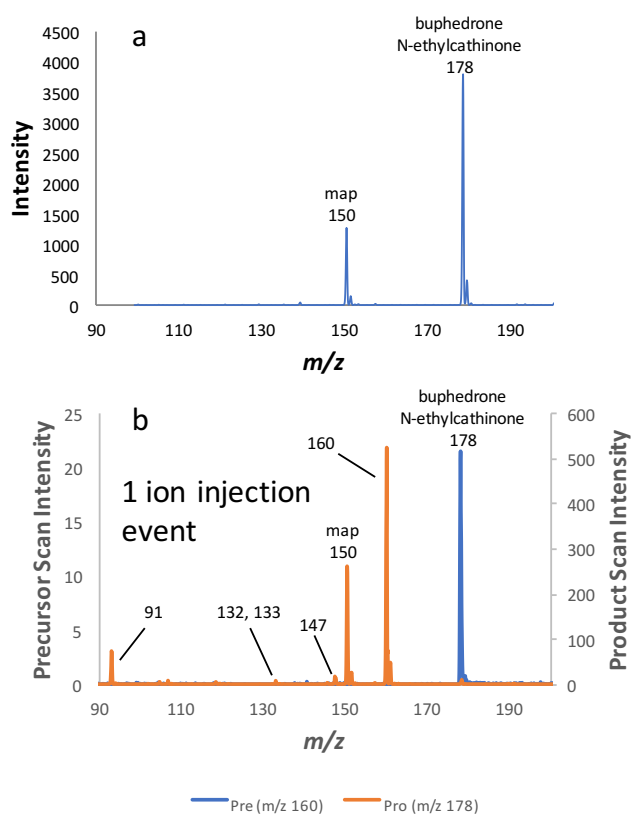
Figure 14.3. Permutation of precursor ion scan and product ion scan: (a) full rf scan mass spectrum of buphedrone, N-ethylcathinone, and methamphetamine, and (b) precursor ion scan of *m/z* 160 followed by product ion scan of isobars at *m/z* 178, confirming that both buphedrone and N-ethylcathinone are present. Note that *m/z* 178 was not isolated before the product ion scan and hence *m/z* 160 is present (though not fragmented) in (b).
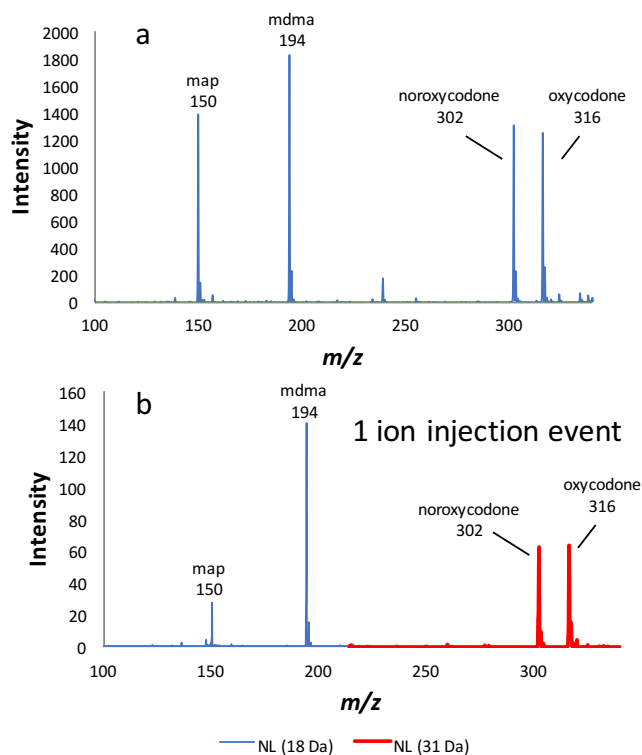
Figure 14.4. Segmented neutral loss scan: (a) full rf ramp resonance ejection mass spectrum of methamphetamine (map), 3,4-methylenedioxymethamphetamine (mdma), noroxycodone, and oxycodone, and (b) segmented neutral loss of 31 Da (at a LMCO of 91 Da) and subsequently 18 Da (at a LMCO of 165 Da) using a single ion injection. No signal was observed with the precursor ion excitation signal off.
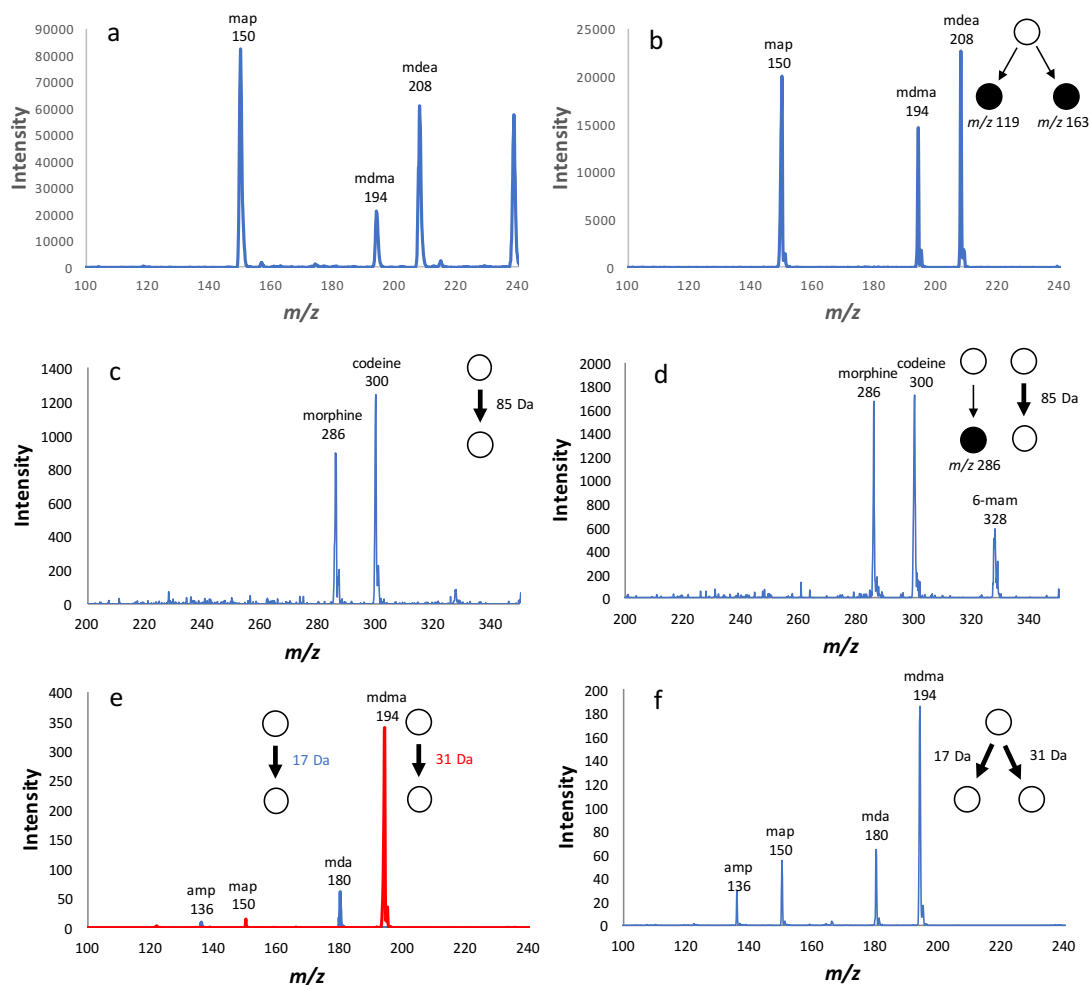
Figure 14.5. Simultaneous MS/MS scans: (a) full ac frequency scan of protonated methamphetamine, 3,4-methylenedioxymethamphetamine, and 3,4-methylenedioxyethylamphetamine, (b) simultaneous double precursor ion scan of *m/z* 119 and *m/z* 163, (c) single neutral loss scan of 85 Da of a mixture of morphine, codeine, and 6-monoacetylmorphine, (d) simultaneous precursor ion scan of *m/z* 286 and neutral loss scan of 85 Da, (e) separate neutral loss scans of 17 Da (blue) and 31 Da (red) performed on amphetamine, methamphetamine, 3,4-methylenedioxyamphetamine, and 3,4-methylenedioxymethamphetamine, and (f) simultaneous neutral loss scan of 17 Da and 31 Da
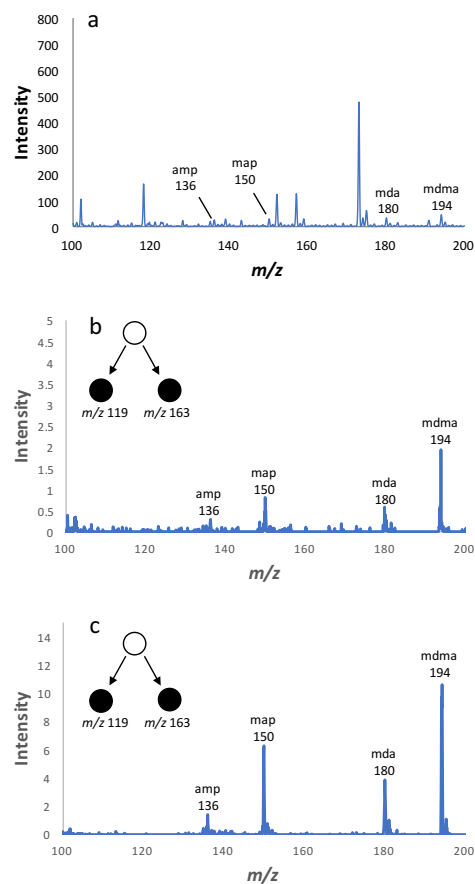
Figure 14.6. Simultaneous double precursor ion scan of
oral fluid spiked with amphetamines: (a) full scan of 10%
oral fluid with final concentration 100 ppb amp, map, mda,
and mdma (1 ppm in oral fluid), (b) simultaneous double
precursor ion scan of *m/z* 119 and 163, and (c) the same

Table 14.1. MS/MS permutations available to the linear ion trap[a,b]

MS/MS Permutation	Advantages over single stage MS/MS	Example	Experimental Scan Rate (Th/s)	Experimental LMCO (Th)
Pre^n	Broad coverage of molecular functionality; increased coverage of a set of related analytes (e.g. amphetamines)	Figure 14.1	469	93
Pre^n-NL	Coverage of several classes of compounds; increasing information yield from particularly uninformative MS/MS experiments (e.g. NL of water)	Figure 14.2	475	99
Pre^n-Pro^n	Extensive MS/MS domain mapping; confirmation of precursor ion identity, esp. isobars	Figure 14.3	226	85
NL^n (segmented)	Ability to work with several classes of compounds that generally lie in different m/z ranges	Figure 14.4	230, 415	91, 165
Simultaneous Pre^n	Broader analyte coverage in a single mass scan, although presentsmore ambiguity than discrete scans	Figure 14.5b	240	93
Simultaneous Pre^n-NL	Broader analyte coverage in a single mass scan, although presents more ambiguity than discrete scans	Figure 14.5d	342	128
Simultaneous NL^n	Monitor multiple classes of compounds in a single scan, though there is ambiguity in precursor->product relationships	Figure 14.5f	214	83

Pre = precursor ion scan; NL = neutral loss scan; Pro = product ion scan

n = a positive integer

[a] Product ion scans can also be performed earlier in the sequence provided the masses of the fragments do not fall into ranges of interest in the other scan types

[b] Multiple reaction monitoring (MRM) experiments can also be done at the end of any permutation but they are not considered further as they are not *scans*.

PART III. LOGICAL MS/MS

CHAPTER 15.   LOGICAL MS/MS SCANS: A NEW SET OF OPERATIONS FOR TANDEM MASS SPECTROMETRY

15.1 Abstract

A new set of operations for tandem mass spectrometry is described. Logical MS/MS operations categorize compounds in mixtures based on characteristic structural features as revealed by MS/MS behavior recorded in multiple fragmentation pathways. This approach is a conceptual extension of tandem mass spectrometry in which interrogation of the full data domain is performed by simultaneous implementation of precursor and neutral loss scans. This process can be thought of as moving through the 2D MS/MS data domain along multiple scan lines simultaneously, which allows experiments that explore the 2D data domain of MS/MS to be couched in terms of logical operations, AND, NAND (not and), OR (inclusive or), XOR (exclusive or), NOT, etc. Examples of particular logical conditions are all precursor ions that fragment to both of two selected product ions (logical AND), or all precursor ions that do not produce a specified fragment ion (logical NOT). These and other operational modes (TRUE/FALSE, XOR, OR, etc.) complement and extend the existing set of conventional MS/MS scans, namely product scans, precursor scans, and neutral loss scans. We describe the implementation of logical MS/MS scans on a commercial linear ion trap mass spectrometer using simple mixtures of amphetamines and fentanyl analogues and argue their utility for complex mixture analysis.

15.2 Introduction

Wolfgang Paul and colleagues obtained a patent for the first quadrupole devices, the mass filter and the 3D ion trap (QIT), in the early 1950s.[1,2,4,6,9] Paul shared the Nobel Prize in Physics in 1989 with Hans Dehmelt, who was the first to trap a subatomic particle (an electron).[144,389] Fulford and March first demonstrated that ions could be mass-selectively stored in what was then called the Quadrupole Ion STORage (QUISTOR) device operated in mass-selective stability (rf/dc) mode,[37] and nearly three decades after the invention of the ion trap, Stafford *et al.* introduced the more convenient mass-selective instability scan, a linear ramp of the trapping radiofrequency (rf) signal which is used to eject ions in order of their mass-to-charge ratio (*m/z*).[38] Resonance ejection was subsequently developed and is now the predominant technique for mass analysis in both 2D

and 3D traps,[10,11,39,43] with the notable advantages of increased resolution,[102,127,390] sensitivity, and mass range.[40,41] Resonance ejection is methodologically similar to mass-selective instability but ejects ions at any specified Mathieu q value by matching the ions' secular frequencies with a supplemental low-voltage ac frequency, usually at high Mathieu q, while ramping the rf voltage. Other less-used, but still notable, modes of mass analysis include rf frequency scanning[46,47] (including in the digital ion trap[86-88,223]), dc voltage scanning,[44] and ac frequency scanning.[49,50,91,106,133,205,391]

A remarkable feature of the quadrupole ion trap is the capacity to perform various tandem mass spectrometry (MS/MS or MS^n) operations in a single device,[392] a capability that usually requires multiple mass analyzers and a separate collision cell (e.g. in hybrid instruments or in a triple quadrupole[58]). In a QIT, an ion can be excited with a low voltage ac waveform with frequency component(s) matching the ion's secular frequency or other related frequency, causing dissociation. A subsequent scanout then yields a product ion mass spectrum.[39,52] Performing multiple fragmentation steps tandem-in-time can yield higher order MS^n spectra as well,[53] increasing analytical selectivity while also improving signal-to-noise.

Although not widely used as such, ion traps can also conduct precursor ion scans[99,123,341] and neutral loss scans,[393,394] modes that usually depend on multiple mass analyzers for simultaneous mass selection of precursor and product ions. To implement these capabilities, multiple simultaneous resonance frequencies are used to mass-select (and fragment) a precursor ion while also ejecting one or more selected product ions with a second ac frequency, which can correspond to a fixed product m/z or a fixed neutral loss. The more common scanning methodology is to acquire sets of data-dependent product ion scans from which precursor or neutral loss spectra can be reconstructed,[60] a method which takes advantage of the increasingly rapid scanning capabilities of modern ion trap systems[63] but also acquires superfluous data.

The beginnings of tandem mass spectrometry as an analytical technique date back to the first mass-analyzed ion kinetic energy spectrometer (MIKES) developed by Beynon and Cooks at Purdue University.[314,395] Since then, MS/MS techniques have been developed for hybrid instruments[244,396-398] and Fourier transform ion cyclotron resonance traps,[399] time-of-flight instruments, and quadrupole ion traps. In almost every MS/MS scan developed to date,[59] either the precursor ion m/z is fixed and the product ion m/z is varied (closed circle with arrow pointing to open circle), the product ion m/z is fixed while the precursor m/z is scanned (open circle with arrow

pointing to closed circle), or a selected neutral loss relationship is fixed (two open circles with a bold arrow between them).[59] The neutral loss scan is a subset of the functional relationship scans, in which there is a specified mathematical relationship between precursor ions and product ions.[400] In a plot of precursor *m/z* vs. product *m/z*, the product ion scan is illustrated by a horizontal line, the precursor ion scan is a vertical line, and the neutral loss scan is a diagonal. Higher order MS^3 scans expand the working space to three dimensions, and so on.

In this work we describe a set of scan modes for tandem mass spectrometry – termed 'logical MS/MS scans' - which are complementary to the existing set of three main MS/MS scan modes (namely product ion scans, precursor ion scans, and neutral loss scans). Logical MS/MS scans use logical operations to categorize compounds in mixtures based on characteristic structural features as revealed by MS/MS behavior along multiple fragmentation pathways. An example is a NOT operation, which detects precursor ions that do not fragment to a selected product *m/z* (or, alternatively, do not undergo a selected neutral loss). The NOT operation is exactly complementary to either a precursor ion scan or neutral loss scan. Here we demonstrate the implementation of logical MS/MS operations on a linear ion trap. The operations explicitly demonstrated here include TRUE/FALSE, OR, XOR, AND, NOT, and NOR.

15.3 Experimental

15.3.1 Chemicals

Amphetamine (MW 135 Da), methamphetamine (MW 149 Da), 3,4-methylenedioxyamphetamine (MW 179 Da), 3,4-methylenedioxymethamphetamine (MW 193 Da), 3,4-methylenedioxyethylamphetamine (MW 207 Da), fentanyl (MW 336 Da), acetyl fentanyl (MW 322 Da), butyryl fentanyl (MW 350 Da), furanyl fentanyl (MW 374 Da), *cis*-3-methylfentanyl (MW 350 Da) hydrochloride, acryl fentanyl (MW 334 Da) hydrochloride, carfentanil oxalate (MW 394 Da), norcarfentanil (MW 290 Da), remifentanil (MW 376 Da) hydrochloride, sufentanil (MW 386 Da) citrate, and alfentanil (MW 416 Da) hydrochloride were purchased from Cerilliant (Round Rock, TX, U.S.A.). Samples were diluted to total concentrations between 1 and 10 µg/mL (mixtures with more components had lower concentrations of individual components) in 50:50 methanol/water with 0.1% formic acid added to improve ionization. All analytes were detected in the protonated form in the positive ion mode. HPLC grade methanol was purchased from Fisher Scientific (Hampton, NH, U.S.A.). Product ion spectra for all compounds

used in this study are shown in **Table S15.1** for reference, and chemical structures with color-coded fragments are given in **Scheme 15.1**.

15.3.2 Ionization

All analytes were ionized in the positive ion mode by nanoelectrospray ionization. Briefly, 1.5 kV was applied to a nanospray electrode emitter (glass size 1.5 mm), which was purchased from Warner Instruments (Hamden, CT, U.S.A.) and fitted with 0.127 mm diameter silver wire, part number 00303 (Alfa Aesar, Ward Hill, MA), as the electrode. Borosilicate glass capillaries (1.5 mm O.D., 0.86 mm I.D.) from Sutter Instrument Co. (Novato, CA, U.S.A.) were pulled to 2 μm tip diameters using a Flaming/Brown micropipette puller (model P-97, Sutter Instrument Co.).

15.3.3 Instrumentation

A Finnigan LTQ linear ion trap (San Jose, CA, USA) was used for all experiments.[10] The internal dimensions of the three-section trap are as follows: $x_0 = 4.75$ mm, $y_0 = 4$ mm, axial sections of length 12, 37, and 12 mm. The rf frequency was tuned to 1.166 MHz and the rf amplitude was held constant throughout the ionization, cooling, and mass scan periods by substituting the rf modulation signal usually supplied by the instrument with a ~600 ms DC pulse (90% duty cycle) of amplitude between 160 mV and 280 mV (corresponding to approximate low-mass cutoffs of 76 Th and 159 Th, respectively, scaling linearly with the DC pulse amplitude) supplied from an external function generator. Nitrogen was used as bath gas at an ion gauge reading of 1.3×10^{-5} torr. Helium was not used because it yielded poor fragmentation efficiency in the LTQ in the scan modes demonstrated here.

The LTQ rf coil was modified as described previously[341,393,394] to allow low voltage ac signals from external function generators to be coupled onto the main rf on the x and y rods. The rf is applied in a quadrupolar fashion while each pair of ac signals is dipolar. Low voltage ac waveforms were applied by two Keysight 33612A (Newark element14, Chicago, IL, U.S.A.) function generators with 64 megasample memory upgrades for each channel. All waveforms (aside from single frequencies) were calculated in Matlab (Mathworks, Natick, MA) and imported to the function generators as .csv column vectors. For ion excitation, the ac amplitude was between 100 mV_{pp} and 200 mV_{pp} for single frequencies and ~2 V_{pp} for broadband (multi-frequency) waveforms. For ion ejection or artifact rejection, the ac amplitude was 500 mV_{pp} for single frequency waveforms and 3.8 V_{pp} for broadband waveforms. Ion excitation waveforms and artifact rejection

waveforms were always applied to the y electrodes, while product ion ejection waveforms were always applied to the x electrodes for ejection of mass-selected ions into the detectors. Function generators were triggered during the ionization step using triggers in the LTQ Tune 'Diagnostics' menu, and their outputs were delayed so they applied waveforms during the mass scan segment, during which the data acquisition rate was approximately 28.7 kHz (the 'normal' scan mode with 'high' mass range chosen in the 'LTQ Tune' software).

15.3.4 Waveform Calculation

Inverse Mathieu q scans were calculated via a program in Matlab as described previously.[133] The inverse Mathieu q scan is a nonlinear ac frequency sweep with approximately linear mass scale.[133,230] The starting frequency always corresponded to Mathieu q = 0.908, the end frequency corresponded to q = 0.15, and the scan time was set at 600 ms (**Figure S15.1a**).

Broadband ac waveforms were also calculated in Matlab and had general characteristics of a 5 MHz sampling rate, 1 kHz frequency spacing, and phases distributed quadratically with frequency in order to obtain a flat amplitude profile with respect to time. Broadband waveforms contained zero, one, or two notches, with each notch being 10 kHz wide. For broadband waveforms whose frequency components did not vary with time (e.g. in TRUE/FALSE scans), the waveform spanned 300 kHz (q = 0.654) to 50 kHz (q = 0.12) (**Figure S15.1b**) to prevent selected product ions from being ejected while precursors were excited. In cases where the inverse Mathieu q scan was used for ion excitation, the frequencies present in the broadband ejection waveform were varied with time so that at any given point in the broadband waveform the lower bound of the frequencies included in the waveform was 10 kHz higher than the corresponding frequency being applied in the inverse Mathieu q scan at the same point in time (see **Figure S15.1c-f**). This ensures that precursor ions are not ejected by the broadband waveform before they are excited by the inverse Mathieu q scan. For example, if the inverse Mathieu q scan was exciting an ion with secular frequency 300 kHz, then at that time point only frequencies above 310 kHz were represented in the sum of sines broadband waveform. All waveform calculation programs are included in the **Supplemental Information** (**Programs S15.1-4**) for reference.

15.4 Results & Discussion

15.4.1 What Is a Logical MS/MS Operation?

Logical MS/MS is an extension of tandem mass spectrometry in which interrogation of the data domain is performed by *simultaneous* implementation of the precursor and neutral loss scans (or complementary NOT/NOR scans), conceptually illustrated as moving through the 2D MS/MS data domain along multiple scan lines simultaneously. This allows experiments which explore the 2D data domain of MS/MS to be couched in terms of logical operations, AND, NAND, OR, XOR, NOT, etc. We emphasize that such logical operations are a means to connect the MS/MS data to the structural properties of the set of constituent molecules. Logical operations are *efficient* ways of connecting the data to particular structural properties of interest, e.g. which of the compounds in the mixture is a fentanyl?

For the case of two selected product ions (or two selected neutral fragments, viz. neutral losses), there are sixteen possible logical operations which include: 1) FALSE, 2) AND, 3) BUT NOT, 4) LEFT PROJECTION, 5) NOT…BUT, 6) RIGHT PROJECTION, 7) XOR (exclusive OR), 8) OR (inclusive), 9) NEITHER…NOR (NOR for short), 10) IFF (if and only if), 11) RIGHT COMPLEMENTATION (which we refer to as NOT), 12) IF, 13) LEFT COMPLEMENTATION (also NOT), 14) IF…THEN, 15) NAND, and 16) TRUE. Precursor ions can be grouped on a Venn diagram (**Figure 15.1a**) according to whether they share one product ion (region 2 or 3), two product ions (region 4), or none (region 1). Precursor ions residing in the same region of the Venn diagram thus also occupy the same scan lines on the 2D MS/MS domain (**Figure 15.2b**). An AND (example shown) scan, for example, would thus traverse two scan lines simultaneously and detect ions residing on both lines.

In each of the following sections we describe the interpretation of each logical operation with respect to precursor and product ion relationships, using the symbolism shown in **Table 15.1**, and we also describe implementation of these scans using a linear quadrupole ion trap (**Table 15.2**). All ion trap implementations assume the rf voltage is constant during the scan events, which simplifies the experiments because the ions' secular frequencies remain constant throughout the scan. It is possible to perform these scans using the more common ion trap operation with varying rf voltage, but this implementation is much more difficult and is not recommended.

15.4.2 TRUE/FALSE Operation

A TRUE/FALSE operation determines whether any precursor ions of unknown mass-to-charge fragment to a selected product ion *m/z*. This scan is not a precursor ion scan or a neutral loss scan because the *m/z values of the precursor ions are not obtained during the scan*. Instead, only a true or false result is obtained. That is, either the sample contains ions of a particular molecular class associated with a product ion *m/z* or neutral mass (TRUE) or it does not (FALSE). The symbol for this scan is similar to the precursor scan symbolism except that the open circle used for the scanned precursor *m/z* is substituted with an open square. It is our interpretation that an open circle corresponds to a varied (but *known*, i.e. scanned) mass-to-charge value[59] whereas the newly proposed open square corresponds to a *range* of mass-to-charge values that is excited *simultaneously*. Because no instrumental parameter is scanned, the *m/z* values of the precursors is not obtained.

Using a linear ion trap system, a TRUE/FALSE scan can be performed by first ejecting precursor ions whose *m/z* values match the selected product ion *m/z*, subsequently exciting a range of precursor ions using a broadband ac waveform, and finally applying a single frequency ac waveform to eject the targeted product ion *m/z*. The broadband waveform used here has frequency representation from q = 0.654 to q = 0.12 (1 kHz frequency spacing) in order to excite precursor ions but not eject the targeted product ions, which are purposely placed at working points above q = 0.654 so they are retained in the trap. Precursor ions with *m/z* matching the product ion were rejected using a single frequency applied for 10 ms, the broadband waveform was applied for 50 ms to fragment the precursor ions simultaneously, and finally the product ion's secular frequency was applied for 10 ms to eject and detect it.

We applied a TRUE/FALSE scan to a set of eight fentanyl analogues: acetyl fentanyl, acryl fentanyl, fentanyl, butyryl fentanyl, *cis*-3-methylfentanyl, furanyl fentanyl, sufentanil, and alfentanil. As shown in **Table S15.1** and **Scheme 15.1**, five of these analogues (the fentanyls) share a product ion at *m/z* 188, the single methylated analogue has a product ion at *m/z* 202, and the two fentanils share a neutral loss of 148/149 Da. A TRUE/FALSE scan of *m/z* 188 (**Figure 15.2a**) gives the expected 'true' as an answer, whereas the corresponding scan for *m/z* 185 gives 'false' (**Figure 15.2b**), showing mass selectivity. A TRUE/FALSE scan of *m/z* 202 (**Figure 15.2c**) also gives 'true' because of *cis*-3-methylfentanyl.

A TRUE/FALSE scan is useful because multiple 'scans' can be performed in rapid succession to target several different product ions. We performed two in succession (for product ions m/z 188 and m/z 202) in ~5 ms (**Figure 15.2d**), which is 240 times faster than the corresponding slow ion trap precursor scan which spans 600 ms for a single scan in our implementation. A TRUE/FALSE scan, in which no precursor m/z information is obtained, hence can be used to improve the efficiency of sample analysis so that a conventional precursor ion scan (which *does* retrieve the precursor ion m/z values) is only run when a value of 'true' is returned from a TRUE/FALSE scan, which should result in fewer wasted MS/MS survey scans.

15.4.3 OR Operation

An inclusive OR operation determines which precursor ions either fragment to one of two selected product ions or fragment via one of two neutral losses without distinguishing the the ions which fall on the particular scan lines. Ions thus can fall into either region 2, 3, or 4 in the Venn diagram. On the 2D MS/MS plot, an OR operation involves traversing two precursor ion (or neutral loss) scan lines *simultaneously*. Symbolically, we propose modifying the symbolism for a double precursor or neutral loss scan previously proposed in ref. [394] to include the downward facing carrot between the two product ion circles to represent logical 'or'.

Performing an inclusive OR operation on a linear ion trap simply requires excitation of precursor ions in one dimension (here the y dimension) via an ac frequency sweep with simultaneous ejection of two selected product ions in the x direction. For the precursor ion scan, two dipolar ac frequencies are used to eject two different product ions,[341,394] whereas for a double neutral loss scan, two swept ac frequencies are used to access the two different neutral losses (see ref. [393]). **Figure 15.3a** shows a double precursor ion scan of m/z 119 and m/z 163 on a set of five amphetamines. The two lower molecular weight amphetamines fragment to m/z 119 and the other three fragment to m/z 163. As shown in the fast Fourier transforms of the peaks at m/z 150 and m/z 180 in **Figure 15.3b**, the two peaks are indistinguishable (despite resulting from resonance ejection of different m/z product ions), and hence it is ambiguous as to whether each peak is due to the ejection of m/z 119, m/z 163, or both. In the case of the inclusive OR operation, it does not matter because they need not be distinguished. For an exclusive or (XOR), described next, methodology is needed to differentiate product ions of different m/z observed at the detector.

15.4.4 XOR Operation

An XOR (exclusive or) operation, symbolically a downward-facing carrot with a bar underneath, determines the precursor ions that fragment exclusively to one of two mass-selected product ions. That is, the ions must fall into region 2 or 3 of the Venn diagram but not into 4. Like the inclusive OR operation, an XOR operation traverses multiple precursor or neutral loss scan lines simultaneously, but in the XOR case we need a method of distinguishing different resonance ejection processes, assuming only a single scan is performed. (Otherwise one could perform two sequential scans targeting the two selected product ions.)

We recently developed *frequency tagging* as a method for distinguishing resonantly ejected product ions from those ejected due to boundary instability ('artifacts') in ion trap precursor and neutral loss scans (Snyder, Szalwinski, Cooks, to be published). In this method, two closely spaced frequencies are used to resonantly eject product ions. The peak shapes of resonantly ejected ions are modulated according to the difference between the two frequencies (the beat frequency). For example, if an ion has a secular frequency at 200 kHz and a dual frequency waveform containing 200 kHz and 201 kHz is applied for resonance ejection, then the peak will have beats (maxima and minima) with frequency of 1 kHz. This method can also be used to distinguish resonantly ejected ions with different *m/z* values if two different beat frequencies are used for two different product ions, thus allowing us to distinguish peaks from regions 2, 3, and 4 of the Venn diagram. A fast Fourier transform of the peak in the mass spectrum can recover the beat frequency and thus determine on which of multiple simultaneously traversed scan lines a precursor/product ion pair resides. Note that ions in region 4 will have contributions from both beat frequencies whereas ions from regions 2 or 3 will have a single beat frequency.

Figure 15.3c shows an XOR precursor ion scan for a mixture of five amphetamines wherein product ions of *m/z* 119 were resonantly ejected with a beat frequency of 1 kHz while product ions of *m/z* 163 were ejected with a beat frequency of 2 kHz, all in a single scan. As shown in the peak FFTs in **Figure 15.3d**, *m/z* 150 (which fragments to *m/z* 119) and *m/z* 180 (which fragments to *m/z* 163) are now clearly distinct, with peak modulation frequencies that correspond to the appropriate beat frequency.

A similar experiment can be performed with neutral losses as shown in **Figure 15.4**. The spectrum in (a) shows a full scan of a mixture of five fentanils whereas (b-d) show the results of single neutral losses of 31/32 Da (indistinguishable because of limited resolution in the ion trap

neutral loss scan), 60 Da, and 148 Da using beat frequencies of 1 kHz, 1.5 kHz, and 1 kHz, respectively. An XOR neutral loss of 148 Da or 60 Da is shown in panel (e), and the peak shapes and FFTs in panel (g) show unambiguously that sufentanil almost exclusively displays a neutral fragment of 148 Da (i.e. its peak has a beat frequency of 1 kHz as shown in panel g) while carfentanil has a neutral fragment of 60 Da (i.e. its peak has a beat frequency of 1.5 kHz in panel g).

In what cases would an XOR operation be useful? The XOR scan allows precursor and neutral loss scans to be *multiplexed* via frequency tagging. Not only can two precursor or two neutral loss scans be performed simultaneously (while also *differentiating* the peaks from each scan line), but precursor and neutral loss scans can be performed together as a 'simultaneous combination'.[394] The capability to multiplex precursor and neutral loss scans therefore improves ion trap scan efficiency in terms of time, sample consumption, and instrument power.

15.4.5 AND Operation

An AND operation detects ions that fragment to both of two selected product ions or to both of two neutral fragments (region 4). The upward carrot is used as a logical 'and' symbol. On the 2D MS/MS diagram, *we must traverse two scan lines simultaneously and be able to determine which precursor ions lie on both lines*. To accomplish the latter, frequency tagging is implemented once again.

Figure 15.3e gives an example of an AND scan using amphetamine ions. In a first experiment, a precursor ion scan of *m/z* 119 using a 1 kHz frequency tag yielded a peak at *m/z* 136 whose FFT yielded the medium blue curve in panel (f). Only a peak at 1 kHz is observed. Next, a precursor scan *of m/z* 91 using a 2.5 kHz frequency tag yielded a peak with FFT given by the light blue curve in panel (f). Again, only a 2.5 kHz frequency is observed. An AND scan combines both frequency tags on the x electrodes of the linear trap while simultaneously exciting the precursors in y using a frequency sweep. Note the presence of only one beat in the individual scans but both beats in the combined AND scan (panel (g), darkest blue), thus making it clear with a single scan that *m/z* 136 fragments to both *m/z* 119 and *m/z* 91. Note that *m/z* 150 also lies on both scan lines (FFT not shown to avoid conjestion) .

Figure 15.4f gives an example of a neutral loss AND operation, again using frequency tagging on the set of five fentanils. The AND scan in panel (f) can detect those ions which lose 31/32 Da and 60 Da. Peaks which lie on both scan lines will have beats corresponding to both 1

kHz and 1.5 kHz. Panel (h) clearly shows that sufentanil only has the neutral loss of 31 Da (1 kHz beat), whereas carfentanil has a neutral loss of both 32 Da (1 kHz) and 60 Da (1.5 kHz).

In what cases could an AND scan be useful? An AND scan clearly *increases the selectivity of precursor and neutral loss scans*. In **Figure 15.4f,h**, while the neutral loss scan of 31/32 Da could not differentiate the neutral fragments of sufentanil and carfentanil despite the neutral loss originating from different molecular functionalities (see **Scheme 15.1**), the AND neutral loss of 31/32 Da and 60 Da does differentiate them because it targets a second neutral loss from the ester side chain of carfentanil. In contrast, sufentanil has a methoxy group that gives the neutral loss of 31 Da but does not yield other notable neutral loss.

15.4.6 NOT Operation

A NOT operation detects precursor ions that do not produce a particular fragment ion or fragment neutral. The NOT operation is therefore the exact complement of the precursor or neutral loss scan. On the 2D MS/MS diagram, instead of traversing a single scan line or two scans lines, we must traverse an infinite number of scan lines but also exclude ions from one selected line. The NOR operation is an extension of this but excludes ions from more than one selected scan line.

NOT operations are denoted by horizontal bars either over the product ion circle (precursor scan) or over the neutral loss mass (neutral loss scan). When considering two circles in a Venn diagram, a NOT operation would detect ions which fall within regions 1 or 2 (NOT 3), or 1 or 3 (NOT 2). A simpler interpretation is a single-circle diagram. In this case a NOT operation would detect ions outside the circle, i.e. precursor ions which do not produce a selected product ion.

In the ion trap, a NOT precursor ion scan can be performed by sweeping an excitation frequency through precursor ion secular frequencies (to fragment the precursors) while simultaneously ejecting all product ions except the selected product *m/z* using a notched broadband waveform. Because we do not want to eject the precursor ions with the broadband waveform and because the product ion mass range varies with the excited precursor *m/z*, we constructed a specialized broadband sum of sines waveform whose frequency components are always higher than the excitation frequency (see **Figure S15.1c,e**). To keep the selected product ion in the trap (the NOT ion), a static notch is also implemented into the waveform (**Figure S15.1d,f**). In our implementation, the notch is 10 kHz wide, and the lowest frequency at any given time in the broadband waveform is 10 kHz higher than the corresponding frequency of the excitation frequency sweep (again, this is to prevent the ejection of precursors before they are fragmented).

Figure 15.5a shows the full scan of the 8-component fentanyl mixture used in **Figure 15.2**. A precursor ion scan of *m/z* 188 (**Figure 15.5b**), the most abundant product ion of most of the fentanyl analogues, detects the fentanyls but not the methylated analogue and not the fentanils. The fentanils have a quaternary carbon which changes the primary route of fragmentation to a neutral loss of either 31, 32, 60, or 148 Da, depending on the substituents. The complementary NOT scan of *m/z* 188, shown in panel (c), detects the remaining three fentanyl analogues. The other five fentanyls are still detected – but with significantly diminished intensity - because they have product ions other than *m/z* 188, although they are almost all < 10% in abundance. Clearly the NOT scan is only useful for molecular classes which have a single high abundance product ion, or it should be used in comparison to a full scan mass spectrum. Without the full scan, it would be unclear which ion intensities were diminished by excluding particular product ions. For cases where molecular classes have two high abundance product ions, then the NOR operation may be useful.

The neutral loss NOT scan is similar but has important procedural differences. It is not feasible to scan the notch in the broadband ejection waveform because as the notch is scanned, so too will all the neutral loss products be scanned out even though they were in the notch at one point during the scan, hence giving an artifact peak. That is, because the neutral loss product *m/z* is varied, it cannot always be in the static notch. A better way to do the experiment is to instead eject the neutral loss product ions into the y electrodes, preventing them from being ejected in x, where the LTQ detectors are. A neutral loss NOT scan thus requires the following waveforms: 1) an inverse Mathieu q scan for precursor ion excitation in the y dimension, 2) a broadband waveform with no notch for product ion ejection in x (**Figure S15.1c,e**), and 3) an inverse Mathieu q scan for rejection of the selected neutral loss product ions into the y electrodes. Anecdotally, this neutralization implementation also works for a NOT precursor scan, though waveform 3 is replaced by a single frequency sine wave.

The spectrum in **Figure 15.6a**, which appears to be a full scan, is a NOT neutral loss scan *without* waveform 3. That is, precursor ions are mass-selectively excited via an inverse Mathieu q scan and all product ions of those precursor ions are ejected toward the detector via a broadband waveform that has no notch. In other words, *the scan detects precursor ions that form any product ion*. Note that a square is once again used for the product ions because the product ion *m/z* is neither fixed nor scanned, i.e. not known. All product ions are ejected simultaneously.

If product ions that satisfy a neutral loss of 148 Da are neutralized on the y rods using a trigger-delayed inverse Mathieu q scan (recall that for the inverse Mathieu q scan, t α *m/z*, so that the trigger delay is proportional to the neutral loss mass), then their detection can be prevented, giving a NOT neutral loss scan as shown in **Figure 15.6b**. Again, it is worth noting that the diminished peaks (acryl fentanyl, fentanyl, *cis*-3-methylfentanyl, sufentanil, and alfentanil) still have some intensity because they have other neutral losses as well, but a neutral loss of 148 Da is by far the most abundant fragmentation pathway for these ions. Similarly, a NOT neutral loss of 177 Da (**Figure 15.6c**) decreases the abundance of furanyl fentanyl since it is the only precursor ion in the mixture that has such a loss. We again note that by themselves these scans are not easy to interpret, but with comparison to a full scan mass spectrum, logical conclusions about the precursor ions' fragmentation pathways can be made.

15.4.7 NOR Operation

The final logical MS/MS operation demonstrated here is the NOR scan. The NOR scan, symbolically an upwards facing carrot with bars over *both* product ions (or neutral loss masses), detects precursor ions that do not produce either of two selected product ions or product neutrals, i.e. only ions in region 1 outside the circles. The NOR scan traverses an infinite number of scan lines, as did the NOT scan, and can be thought of as two (or more) simultaneous NOT scans.

In the ion trap, this can be accomplished by modifying the singly notched broadband waveform used in the NOT precursor scan to have two notches. For the NOR neutral loss scan, yet another trigger-delayed inverse Mathieu q scan must be used to reject product ions that satisfy the second selected neutral loss into the y electrodes, preventing their detection. **Figure 15.5d** shows a NOR precursor ion scan of *m/z* 188 and *m/z* 269. The former rejects acetyl fentanyl, acryl fentanyl, fentanyl, butyryl fentanyl, and furanyl fentanyl, and the latter rejects alfentanil, leaving *cis*-3-methylfentanyl and sufentanil. Similarly, **Figure 15.6d** shows a NOR neutral loss of 148 Da and 177 Da. The former largely rejects acryl fentanyl, fentanyl, sufentanil and alfentanil, and the latter largely rejects furanyl fentanyl. As stated previously, this scan should be particularly useful for classes of compounds which have two dominant product ions or product neutrals.

15.4.8 Other Operations

Other logical MS/MS operations are proposed here but are not implemented. It may be possible to do these operations on other instruments or on the ion trap in the future, but currently

the ion trap implementation is unknown. For example, a NAND scan would detect precursor ions that do not fragment to one selected product ion or do not fragment to a second selected ion. If for a NAND precursor ion scan two notches are implemented in the broadband ejection waveform, then the result will be a NOR scan, not a NAND. It is thus not possible to only reject precursor ions that fragment to both selected product ions without also rejecting those precursors which fragment only to one. That is, ions from regions 2, 3, and 4 cannot be differentiated if they are not detected and frequency tagged. The IFF and IF/IF…THEN operations have similar complications on the ion trap.

15.5 Conclusion

A new set of logical MS/MS operations was described and demonstrated. Logical operations access in a single scan the logical connection between precursor ions and one or more product ions and may be useful for certain applications where precursor ions of a particular class share structural features that are expressed through common product ions or neutral losses, or in cases where dominant ions of similar molecular class are not of interest and can be excluded using a NOT or NOR operation. Additional selectivity and sensitivity as well as multiplexed capabilities can be gained through simultaneous acquisition of multiple fragmentation channels via frequency tagging. Although only the ion trap implementation was shown here, implementations on other mass spectrometer types are readily imagined.

15.6 Acknowledgements

Schemes

Acetyl fentanyl

Acryl fentanyl

Fentanyl

Butyryl fentanyl

cis-3-methylfentanyl

Furanyl fentanyl

Sufentanil

Alfentanil

Norcarfentanil

Remifentanil

Carfentanil

Amphetamine

Methamphetamine

3,4-Methylenedioxy methamphetamine(MDMA)

3,4-Methylenedioxy amphetamine(MDA)

3,4-Methylenedioxy-N-ethylamphetamine(MDEA)

m/z 188   m/z 119

m/z 202   m/z 163

148 Da   32 Da

31 Da   60 Da
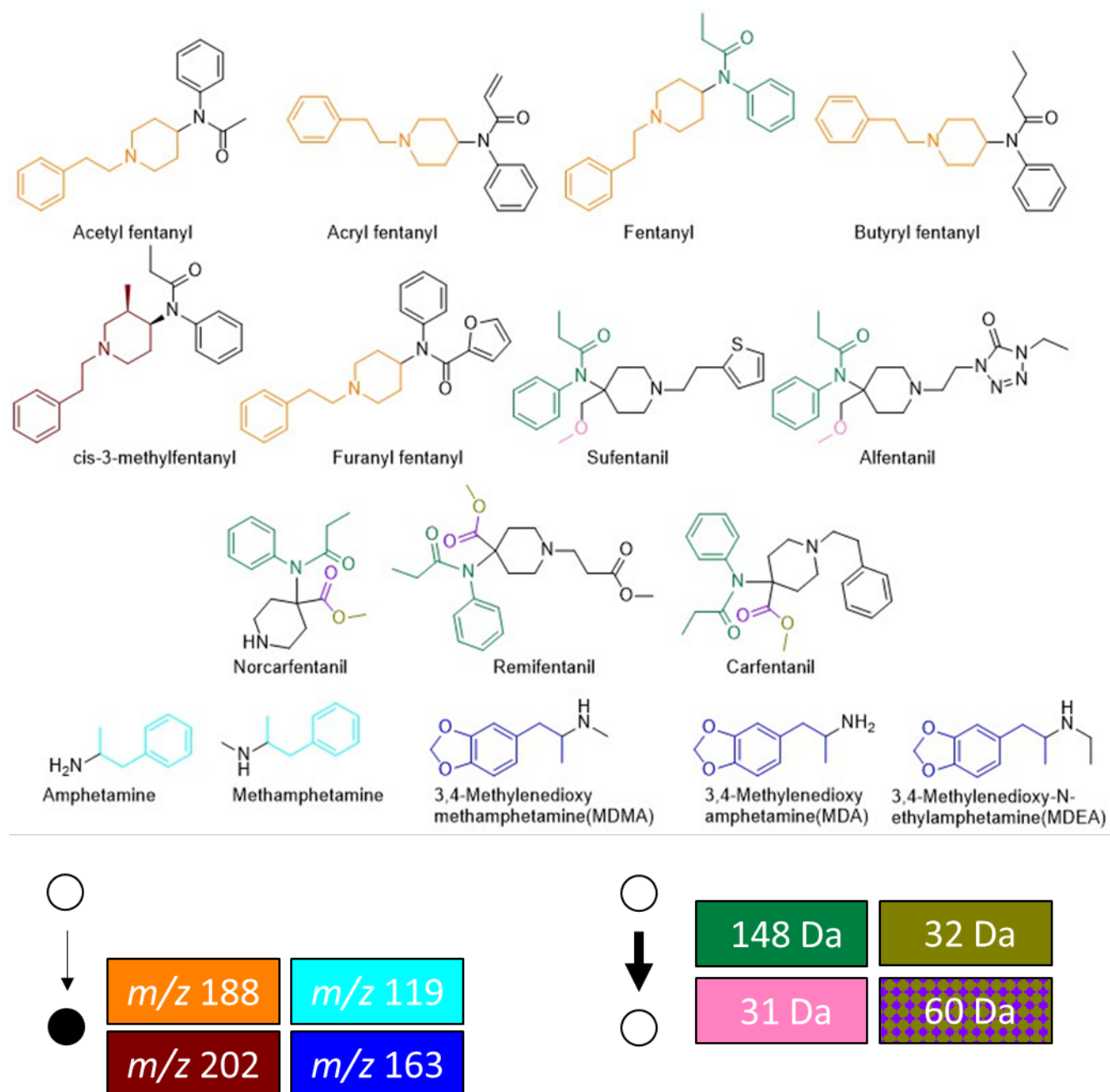
Scheme 15.1. Structures (above) and experimentally observed masses of product ions (below, left) and neutral fragments (below, right) for compounds used in this study.

Figures and Tables
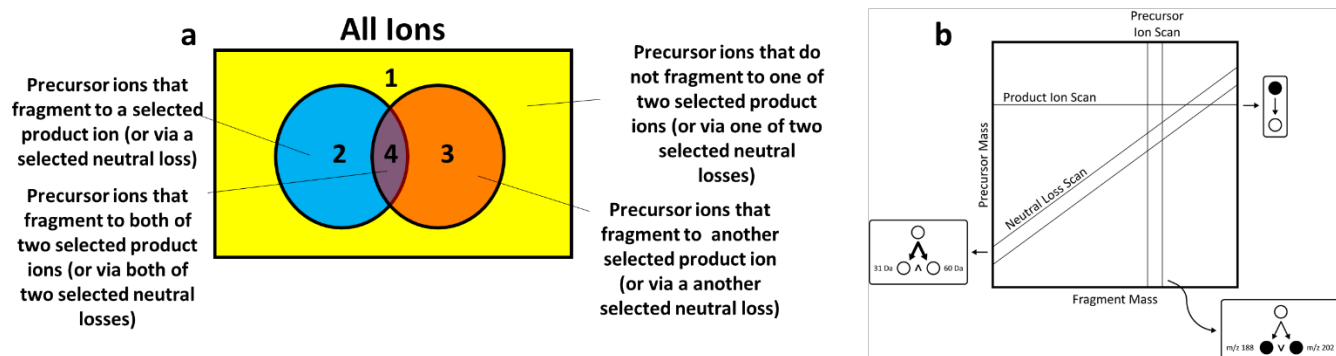
Figure 15.1. (a) Venn diagram representation of ion populations with respect to logical MS/MS experiments. Precursor ions may fragment to just two product ions and corresponding neutrals in the cases considered here. (b) 2D MS/MS domain with (i) single product ion scan, (ii) neutral loss scan of 31 Da AND 60 Da, and (iii) precursor ion scan of *m/z* 188 OR *m/z* 202.
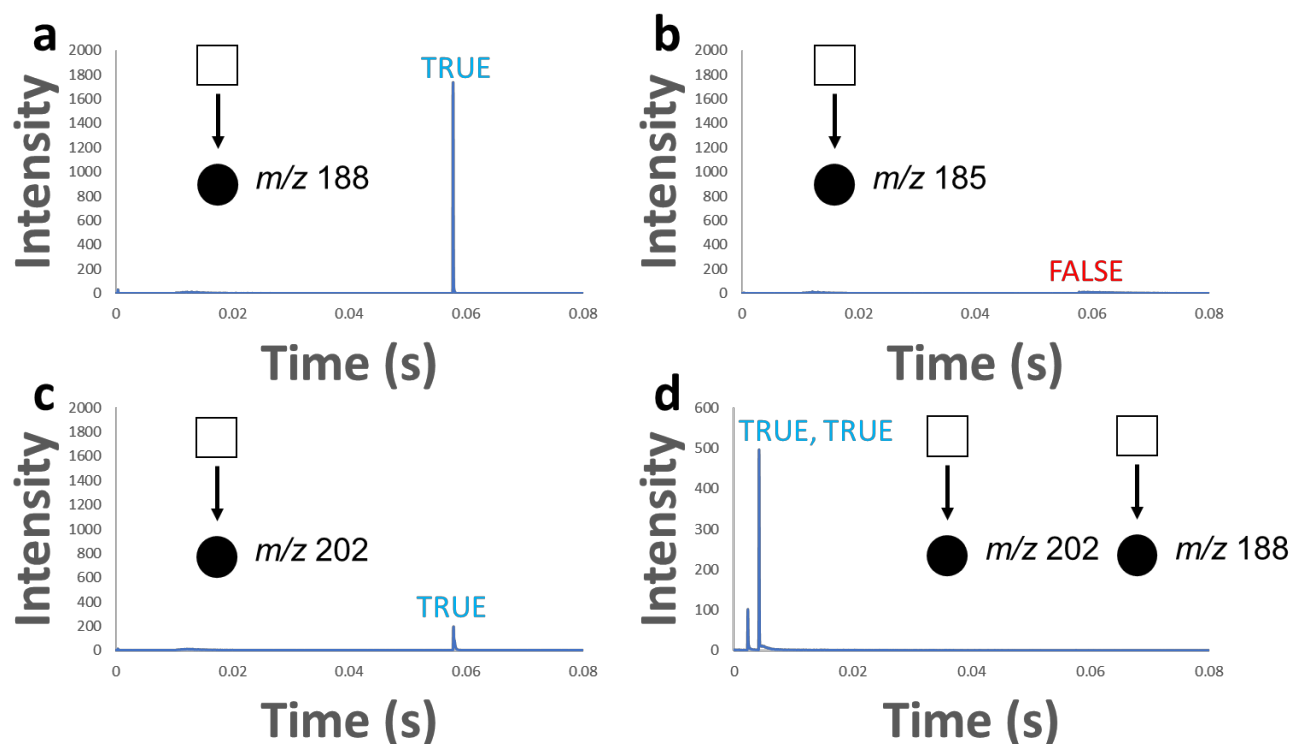
Figure 15.2. Logical TRUE/FALSE scans: (a) TRUE/FALSE scan performed on a set of eight fentanyl analogues (acetyl fentanyl, acryl fentanyl, fentanyl, butyryl fentanyl, *cis*-3-methylfentanyl, furanyl fentanyl, sufentanil, and alfentanil) wherein *m/z* 188 precursors were ejected for 10 ms, precursor ions were then excited with a broadband sum of sines for 50 ms, and finally *m/z* 188 product ions were ejected using a single frequency sine wave, resulting in TRUE, (b) the same set sequence but targeting *m/z* 185, resulting in FALSE, (c) the same sequence targeting *m/z* 202 for a result of TRUE (*cis*-3-methylfentanyl), and (d) optimized sequential TRUE/FALSE scans showing that precursor ions fragmenting to *m/z* 202 and/or *m/z* 188 are present in the sample (though their *m/z* values are not measured in this scan).
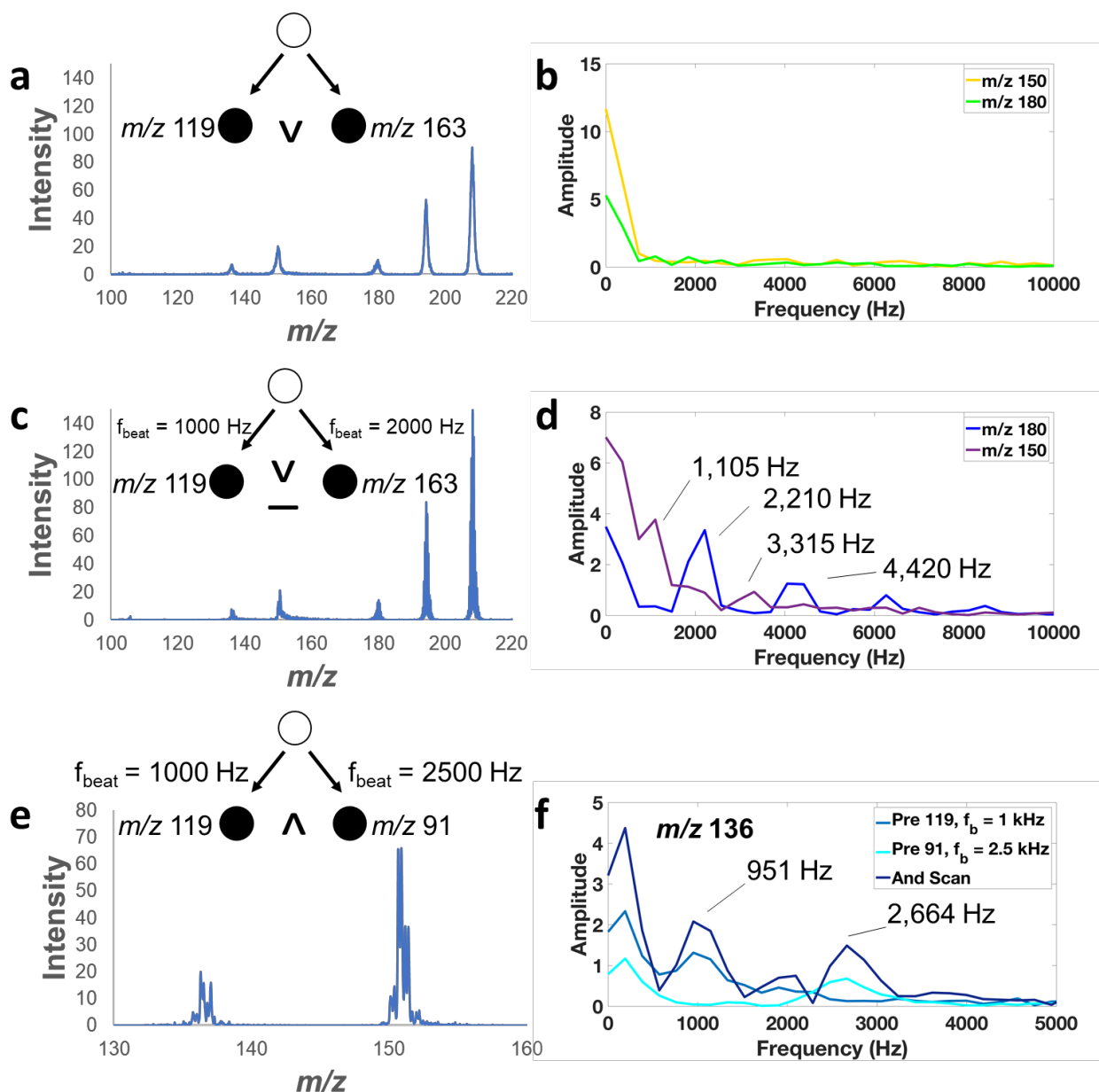
Figure 15.3. Logical OR/AND precursor ion scans: (a) conventional double precursor ion scan of *m/z* 119 and *m/z* 163 applied to a solution of five amphetamines, (c) OR scan using two different beat frequencies for resonance ejection of *m/z* 119 and *m/z* 163, and (e) AND scan using two different beat frequencies for ejection of *m/z* 119 and *m/z* 91. No difference between the two resonance ejection processes is apparent in the fast Fourier transform (FFT) of the peaks in (a) in plot (b), but when using frequency tagging it becomes apparent in (d) that *m/z* 180 fragments to *m/z* 163 and *m/z* 150 fragments to *m/z* 119, and in (f) it is readily observed in the peak FFTs that *m/z* 136 and *m/z* 150 from plot (e) fragment to both targeted product ions and are thus AND peaks.
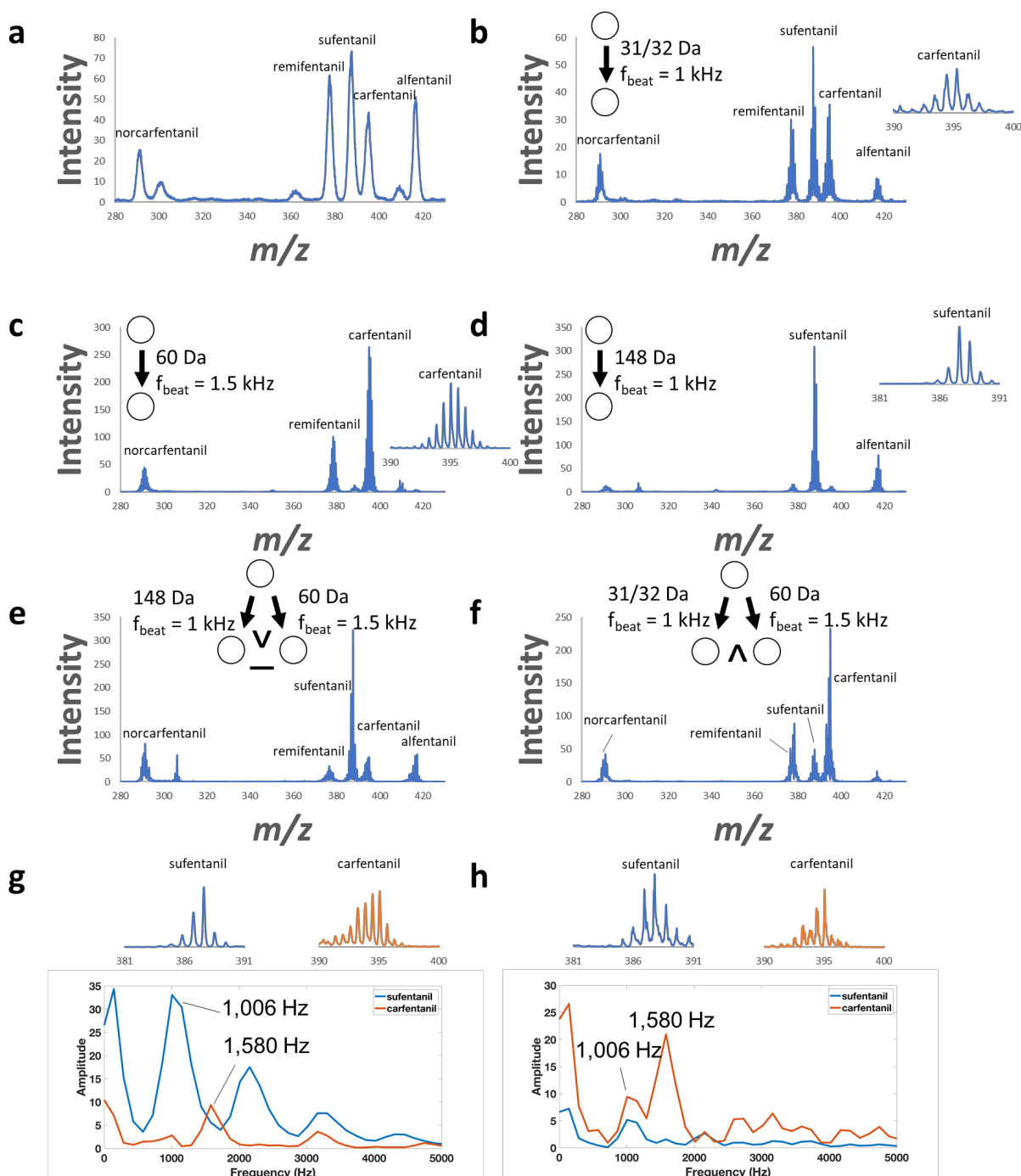
Figure 15.4. Logical XOR/AND neutral loss scans: (a) full scan of five fentanils, (b) neutral loss scan of 31/32 Da using a beat frequency of 1 kHz, (c) neutral loss scan of 60 Da using a beat frequency of 1.5 kHz, (d) neutral loss scan of 148 Da with beat frequency 1 kHz, (e) XOR neutral loss scan of 148 Da (1 kHz beat) or 60 Da (1.5 kHz beat), (f) AND neutral loss scan of 31 Da (1 kHz beat) and 60 Da (1.5 kHz beat), (g) peak shapes and FFTs for two peaks in (e), and (h) peak shapes and FFTs for two peaks in (f).
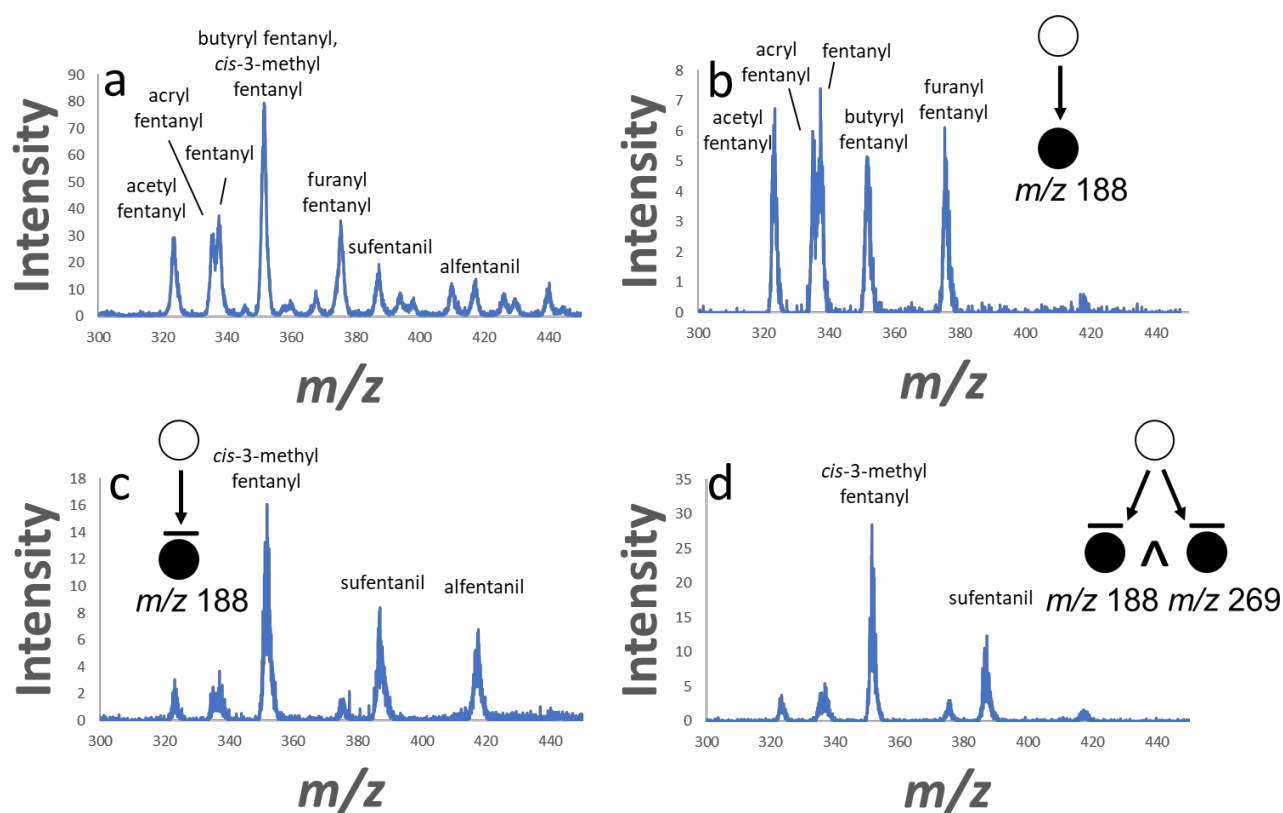
Figure 15.5. Logical NOT/NOR precursor ion scans: (a) full scan mass spectrum of eight fentanyl analogues (acetyl fentanyl, acryl fentanyl, fentanyl, butyryl fentanyl, *cis*-3-methylfentanyl, furanyl fentanyl, sufentanil, and alfentanil), (b) precursor ion scan of *m/z* 188, (c) NOT scan of *m/z* 188, showing ions that do not fragment to *m/z* 188, and (d) NOR scan of *m/z* 188 and *m/z* 269 showing ions that do not fragment to either selected product ion.
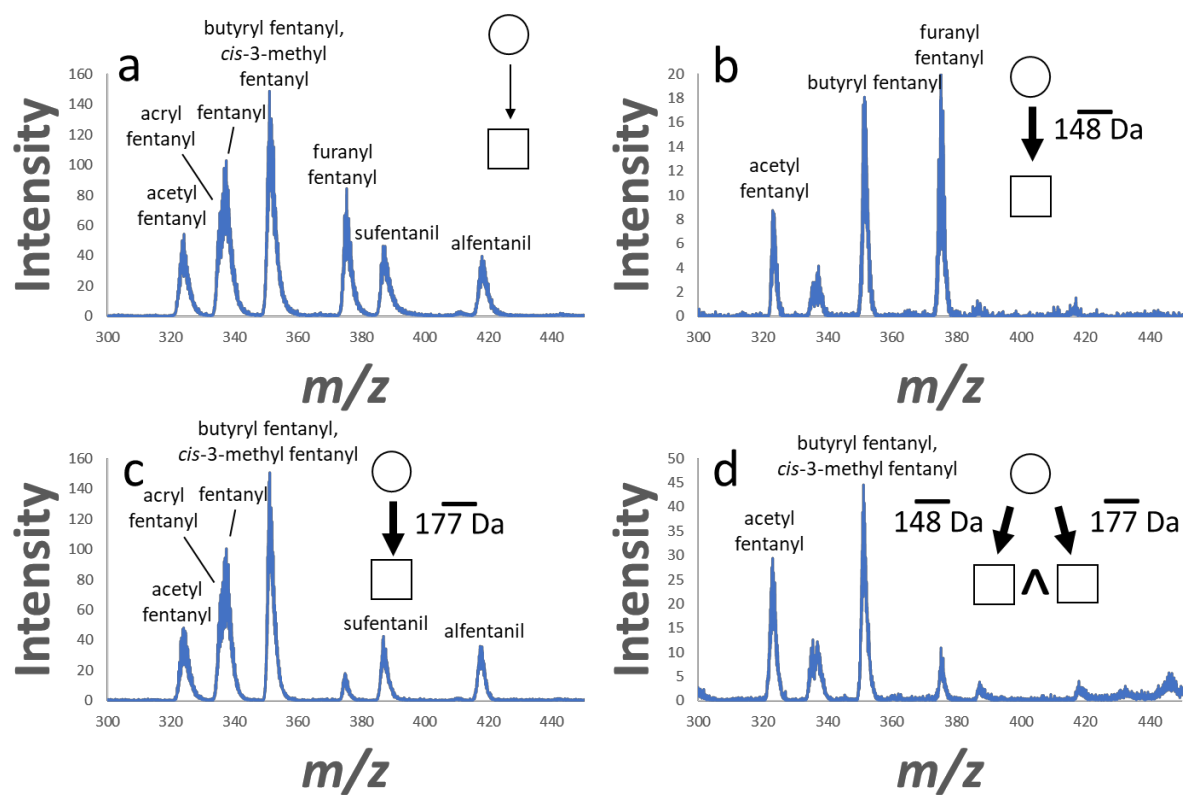
Figure 15.6. Logical NOT/NOR neutral loss scans: (a) arbitrary neutral loss scan detecting all precursor ions which fragment via any arbitrary neutral loss, (b) NOT neutral loss scan of 148 Da, detecting all precursor ions which give any neutral loss that is not 148 Da, (c) NOT neutral loss scan of 177 Da, and (d) NOR neutral loss scan of 148 Da and 177 Da.

Table 15.1. Proposed logical MS/MS operations, terminology, symbolism, and interpretation. For logical operations, generally only the precursor ion symbolism is shown. For the neutral loss variants, closed circle product ions are replaced with open circles, the arrows are bolded, and any 'not' black bars are shown above the fixed neutral loss mass (as shown for NOT) instead of above the product ion circle (for fixed mass charged species).
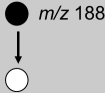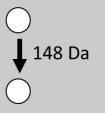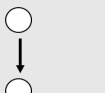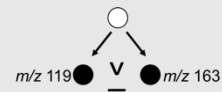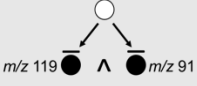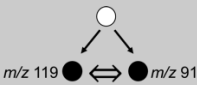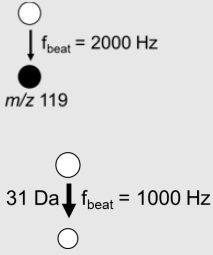
	Operation	Symbol	Region*	Interpretation
Existing Operations	**Product Ion Scan**	● m/z 188 → ○	N/A	Detects product ions of a mass-selected precursor ion
	Precursor Ion Scan	○ → ● m/z 188	2 or 3	Detects precursor ions of a mass-selected product ion
	Neutral Loss Scan	○ ↓ 148 Da ○	2 or 3	Detects precursor ions that fragment to product ions with a selected (fixed) mass offset from the precursor ions; a subset of the functional relationship scans
	Functional Relationship Scan	○ → ○	N/A	Detects precursor ions whose product ions satisfy a given mathematical relationship with respect to the precursors, e.g. product ions whose m/z is half the precursor ion m/z
	Single/Multiple Reaction Monitoring	● m/z 337 → ● m/z 188	N/A	Detects ions that satisfy the specified transition from a fixed precursor m/z to a fixed product m/z
New LOGICAL Operations	**TRUE/FALSE**	□ → ● m/z 188	2,4 or 3,4 (TRUE) None (FALSE)	Detects whether any ion in the mass analyzer fragments to a mass-selected product ion; precursor ion m/z values are not obtained
	AND	m/z 119 ● ∧ ● m/z 91	4	Detects precursor ions that fragment to both of two mass-selected product ions
	BUT NOT NOT…BUT	m/z 119 ● ∧ ● m/z 91	2 (BUT NOT) 3 (NOT…BUT)	Detects precursor ions that fragment exclusively to one of two mass-selected product ions but not the other
	LEFT/RIGHT PROJECTION	See 'Precursor Ion Scan'	2,4 (LEFT) 3,4 (RIGHT)	A precursor ion scan
	XOR (exclusive OR)	m/z 119 ● ∨ ● m/z 163	2,3	Detects precursor ions that fragment to either of two mass-selected product ions but not both

Table 15.1 continued

	OR (inclusive)	m/z 119 ● ∨ ● m/z 163	2,3,4	Detects precursor ions that fragment to either of two mass-selected product ions or both
	NOT (also called LEFT/RIGHT COMPLEMENTATION for binary systems)	↓ ● m/z 188 ↓ 148 Da	1,3 (LEFT) 1,2 (RIGHT)	Detects precursor ions that do not fragment to a particular product ion
	NOR	m/z 119 ● ∧ ● m/z 91	1	Detects precursor ions that do not fragment to either of two selected product ions
	IFF (if and only if)	m/z 119 ● ⟺ ● m/z 91	1,4	Detects precursor ions that fragment to both of two mass-selected products ions or that fragment to neither
	IF **IF…THEN**	m/z 119 ● ∨ ● m/z 91	1,2,4 (IF) 1,3,4 (IF…THEN)	Detects precursor ions that do not fragment to one of two particular product ions or that fragment to one of those ions
	NAND	m/z 119 ● ∨ ● m/z 91	1,2,3	Detects precursor ions that do not fragment to both of two particular product ions
Ion Trap Scans	**Frequency tagging**	↓ f_{beat} = 2000 Hz ● m/z 119 31 Da ↓ f_{beat} = 1000 Hz	N/A	Resonance ejection of ions modulated at a particular beat frequency, f_{beat}; uses two closely spaced frequencies to form the beat frequency; useful for distinguishing resonantly ejected ions from boundary ejected ions and for distinguishing different resonance ejection processes

*Region corresponding to the Venn diagram in **Figure 15.1**

Table 15.2. Proposed implementation of LOGICAL MS/MS on linear quadrupole ion traps

	Operation	Ion Trap Implementation*
Existing Operations	Product Ion Scan	Resonance excitation followed by a full mass scan
	Precursor Ion Scan	Resonance excitation of precursors with simultaneous ejection of a selected product ion with a fixed ac frequency
	Neutral Loss Scan	Three simultaneous frequency sweeps with constant mass (time) offset
	Functional Relationship Scan	Three simultaneous frequency scans with variable mass offset
New Logical Operations	TRUE/FALSE	**(Pre)** Broadband excitation of precursors followed by ejection of fixed *m/z* via single frequency; **(NL)** none, unless precursor ion *m/z* values are known beforehand
	AND	Double precursor ion scan or double neutral loss scan using two different beat frequencies; peaks must correspond to both beats
	NOT…BUT, BUT NOT	Double precursor ion scan or neutral loss scan using two different beat frequencies; peaks must correspond to one beat but not the other
	LEFT/RIGHT PROJECTION	See 'Precursor Ion Scan' above
	XOR (exclusive OR)	Double precursor ion scan or neutral loss scan using two different beat frequencies; peaks must correspond to either beat but not both
	OR (inclusive)	Double precursor ion or neutral loss scan; no beat frequency required although can be used to differentiate regions 2,3,4
	NOT	**(Pre)** Single frequency sweep for precursor ion excitation with singly notched broadband waveform for product ion ejection; **(NL)** no notch in broadband waveform; reject NL products into y electrodes with frequency sweep
	NOR	**(Pre)** Single frequency sweep for precursor ion excitation with doubly notched broadband waveform for product ion ejection **(NL)** Single frequency sweep for precursor ion excitation; broadband waveform for product ion ejection; two additional frequency sweeps for neutralization of neutral loss product ions on y rods
	IFF (if and only if)	Not currently known; cannot differentiate regions 2,3,4
	IF, IF…THEN	Not currently known; cannot differentiate regions 2,3,4
	NAND	Not currently known; cannot differentiate regions 2,3,4

*Assumes rf voltage is constant throughout the scan

SUPPLEMENTAL INFORMATION

Table S15.1. Table of fragmentation data for each compound used in this study. Helium was used as collision gas on a Thermo LTQ linear ion trap. Parameters were q = 0.25, normalized collision energy = 35, 30 ms activation time.

Name	MW (amu)	m/z ([M+H]+)	MS2 m/z (RA)	NL (Da)
amphetamine	135.1	136.17	119.08 (100)	17
			91.08 (1)	45
methamphetamine	149.12	150.17	119.08 (100)	31
			91.08 (9)	59
3,4-methylenedioxyamphetamine	179.09	180.17	163.08 (100)	17
3,4-methylenedioxymethamphetamine	193.11	194.17	163.08 (100)	31
			137.08 (0.3)	57
3,4-methylenedioxyethamphetamine	207.13	208.17	163.08 (100)	45
			135.08 (0.3)	73
			72.08 (3)	136
acetyl norfentanyl	218.3	219.3	202.18 (12)	17
			177.18 (6)	42
			136.09 (8)	83
			84.09 (100)	135
acetyl fentanyl	322.44	323.4	202.18 (4)	121
			188.27 (100)	135
butyryl fentanyl	350.5	351.4	282.36 (11)	69
			231.18 (4)	120
			230.18 (3)	121
			189.18 (100)	162
			188.18 (76)	163
furanyl fentanyl	374.48	375.5	198.18 (100)	177
			188.18 (85)	188
fentanyl	336.47	337.36	281.27 (8)	56
			216.18 (10)	121
			188.18 (100)	149
isobutyryl fentanyl	350.49	351.4	281.27 (5)	70
			230.18 (5)	121
			188.18 (100)	163
valeryl fentanyl	364.25	365.4	281.27 (9)	84
			244.27 (4)	121
			188.18 (100)	177
acryl fentanyl	334.46	335.27	214.18 (10)	121
			188.18 (100)	147
			146.18 (3)	189

Table S15.1 continued

			105.09 (10)	230
p-fluorofentanyl	354.46	355.3	299.27 (5)	56
			234.18 (14)	121
			188.18 (100)	167
			150.18 (4)	205
			146.18 (4)	209
4-fluoroisobutyryl fentanyl	368.5	369.3	299.25 (5)	70
			248.17 (4)	121
			188.17 (100)	181
cis-3-methylfentanyl	350.5	351.4	295.27 (5)	56
			230.27 (11)	121
			202.27 (100)	149
sufentanil	386.55	387.4	356.36 (74)	31
			239.18 (100)	148
			238.18 (68)	149
alfentanil	416.52	417.4	386.45 (95)	31
			269.27 (100)	148
			268.27 (68)	149
			237.27 (1)	180
			236.27 (1)	181
			198.18 (7)	219
			197.18 (8)	220
			171.18 (1)	246
			170.18 (3)	247
remifentanil	376.45	377.36	345.27 (100)	32
			317.27 (26)	60
			285.27 (8)	92
			228.18 (2)	149
carfentanil	394.5	395.36	363.27 (100)	32
			335.36 (40)	60
			246.27 (2)	149
norcarfentanil	290.36	291.3	259.27 (100)	32
			231.27 (4)	60
			186.18 (2)	105
			142.09 (2)	149
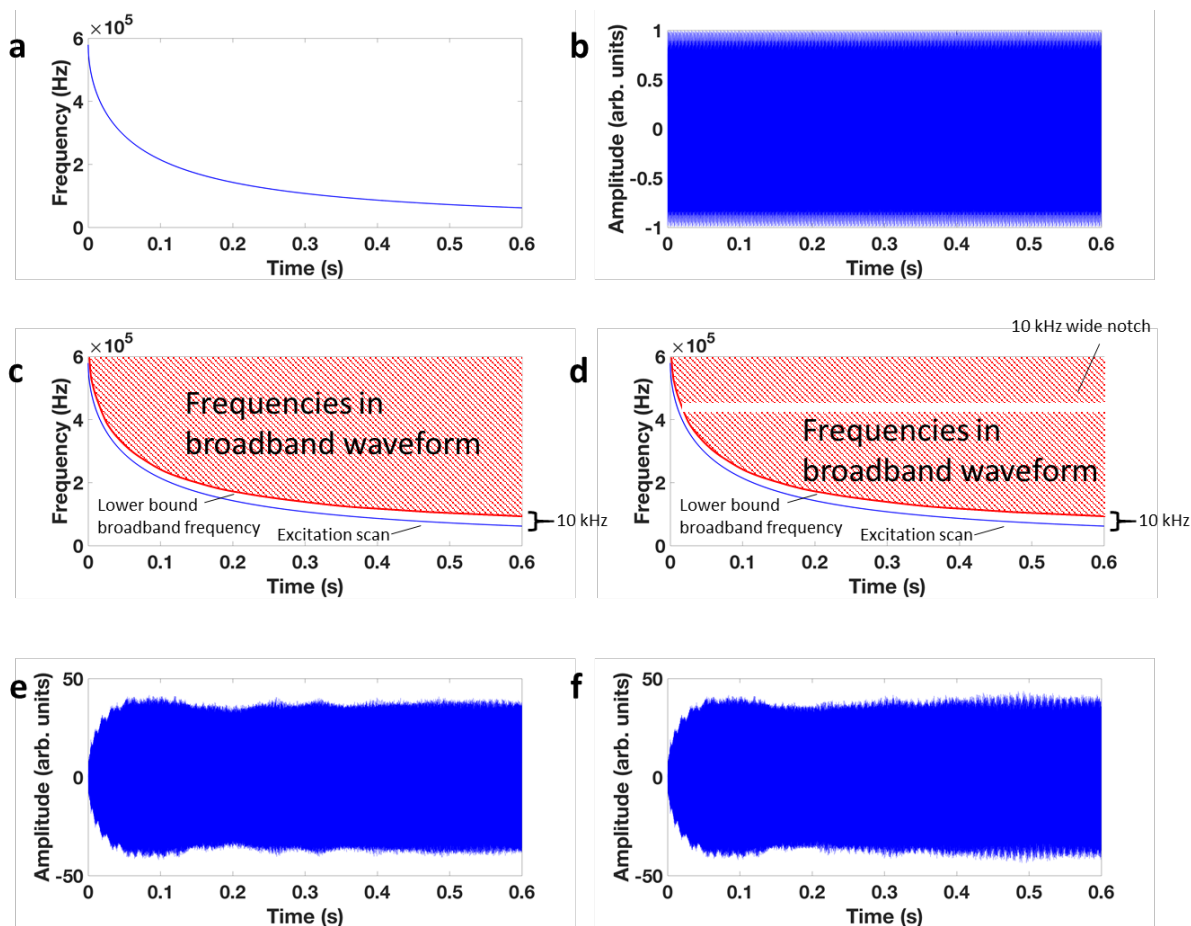
Figure S15.1. Illustrative waveforms used in this study: (a) frequency vs. time profile for an inverse Mathieu q scan over 600 ms from q = 0.908 to q = 0.15, (b) a broadband sum of sines waveform with 1 kHz frequency spacing from 300 kHz (q = 0.654) to 50 kHz (q = 0.12) and a quadratic phase relationship with respect to frequency, (c) frequency vs. time relationship for a broadband waveform with frequency lower bound 10 kHz higher than the inverse Mathieu q scan in (a), (d) the same frequency profile as (c) but with a 10 kHz wide notch, (e) a waveform with the profile in (c), and (f) a waveform with the profile in (d) where the notch at 157 kHz is 10 kHz wide (used for a NOT precursor scan). Voltage is shown in arbitrary units because they end up scaled by the waveform generator.

Program S15.1: Program for calculating an inverse Mathieu q scan with (in this case) 600 ms mass scan time and start and end Mathieu q values of 0.908 and 0.15, respectively.

```
% Program: Inverse_Mathieu_q_Scan.m
% Calculates an Inverse Mathieu q Scan, i.e. an ac frequency sweep with
% approximately linear mass scale


% Define variables
scan_time = 0.6;                % mass scan time in seconds
begin_q = 0.908;                % starting Mathieu q value
end_q = 0.15;                   % ending Mathieu q value
sampling_rate = 5000000;        % sampling rate of waveform - must match
                                % function generator (Sa/s)
rf_frequency = 1166000;         % trap rf frequency in Hz
num_points = ceil(sampling_rate * scan_time);   % number of points in the
                                                % waveform
time = linspace(0, num_points-1, num_points)*scan_time/num_points;
                                % time variable
begin_amplitude = 1;            % p-p voltage to start at if doing an
                                        % amplitude ramp
end_amplitude = 1;              % p-p voltage to end at if doing an amplitude
                                        % ramp
phi(1) = 0;                     % initial phase of waveform, best to set at 0
                                        % so scan starts at 0 voltage


% Calculate Mathieu q values as a function of time
% Assume sweep according to q = k / (t-j)
% where q is Mathieu q value to interrogate,
% t is time, and k and j are constants to be calculated
j = end_q*scan_time / (end_q - begin_q);
k = -begin_q*j;
q_values = k ./ (time - j);


% Assume linear ramp of ac amplitude
% If begin and end amplitude are the same, then amplitude is constant
amplitudes = linspace(begin_amplitude,end_amplitude,num_points);


% Preallocate memory for frequency, beta, and waveform voltage as a function %
of time
```

```matlab
frequencies = zeros(num_points,1);
betas = zeros(num_points,1);
waveform = zeros(num_points,1);


% Use a phase accumulator (phi) to do a nonlinear frequency sweep, convert
% Mathieu q to beta, then to frequency, and finally to phase accumulator
for i = 1:num_points
    betas(i) = beta_calculator(q_values(i));
    frequencies(i) = betas(i)*rf_frequency/2;
    waveform(i) = amplitudes(i)*sin(phi(i));
    delta = 2*pi*frequencies(i)/sampling_rate;
    phi(i+1) = phi(i) + delta;
end
```

Program S15.2: Program for converting from Mathieu q to parameter beta (which is directly proportional to secular frequency).

```matlab
function [beta] = beta_calculator(q)


% Function: beta_calculator
% Accepts an ion's Mathieu q value and calculates the ion's beta value


% Initial guess
beta = 0.5;
prev_beta = 0;


% Bounds
left_bound = 0;
right_bound = 1;


% Tolerance defines accuracy of result
tolerance = 0.00001;
LHS_minus_RHS = 1;       % LHS = left hand side of the equation for calculating
                         % beta; RHS = right hand side


% Iterate the calculation until the difference between the LHS and RHS of the
% equation for calculating beta is below a specified tolerance
while (abs(beta - prev_beta) > tolerance)
    % Left hand side of beta equation
    LHS = beta^2;
    q_sq = q^2;


    % Right hand side of beta equation
    RHS   =    q_sq/((beta+2)^2   -   q_sq/((beta+4)^2   -   q_sq/((beta+6)^2   -
q_sq/((beta+8)^2-q_sq/((beta+10)^2)))) + q_sq/((beta-2)^2 - q_sq/((beta-4)^2 -
q_sq/((beta-6)^2-q_sq/((beta-8)^2-q_sq/((beta-10)^2)))));


    LHS_minus_RHS = LHS - RHS;


    % Guess not close enough
    if LHS_minus_RHS < 0
        prev_beta = beta;
```

```matlab
            beta = (beta + right_bound) / 2;
            left_bound = prev_beta;
        elseif LHS_minus_RHS > 0
            prev_beta = beta;
            beta = (beta + left_bound) / 2;
            right_bound = prev_beta;
        else
        % do nothing, guess was close enough
        end
end
end
```

Program S15.3: Program for creating a broadband sum of sines waveform for ion excitation. Phases are distributed quadratically vs. frequency to ensure a flat amplitude profile.

```matlab
% Program: sum_sine_excitation
% Creates a broadband waveform with no notches for excitation
% or ejection of ions over a wide mass range

sampling_rate = 5000000;                    % waveform generator sampling rate
                                            % (Sa/s)
rf_freq = 1166000;                  % trapping rf frequency in Hz
start_freq = 300000;                        % where the notch starts (Hz)
end_freq = 50000;                   % where the notch ends (Hz)
freq_resolution = 1000;                 % difference between adjacent
                                        % frequencies (Hz)
waveform_length_s = 0.1;                    % length of waveform in s
phase_fudge_factor = 0.001;         % determines how phases are distributed
num_points = round(waveform_length_s*sampling_rate);  % number of points in
                                                    % the waveform


% Initialize arrays for the waveform, frequency vs. time, and phase as a
% function of frequency
master_waveform = zeros(num_points,1);
frequencies = linspace(start_freq,end_freq,num_frequencies);
num_frequencies = length(frequencies);
phases = zeros(num_frequencies,1);


% Distribute phases so that master waveform has flat amplitude profile
% Assumes phases are quadratically related to frequency
for i=1:num_frequencies
    phases(i)                         =                        (frequencies(i)-
frequencies(1))^2*waveform_length_s/(2*(frequencies(num_frequencies)-
frequencies(1))*phase_fudge_factor);
end

% Make time array
time = linspace(0,waveform_length_s,waveform_length_s*sampling_rate).';


% Build master waveform
for i=1:num_frequencies
```

```
    master_waveform                 =                 master_waveform                 +
        sin(2*pi*frequencies(i).*time+phases(i));
end


% normalize amplitude to 1
master_waveform = (1/max(master_waveform))*master_waveform;
```

Program S15.4: Program for calculating a notched broadband waveform for a NOT scan (precursor scan variant). The broadband waveform varies as a function of time so that the included frequencies are always above the corresponding inverse mathieu q scan frequency at each time point. A fixed notch is also implemented so as to prevent the ejection of a selected product ion. Thus, this scan (in conjunction with an inverse Mathieu q scan for precursor ion excitation) detects all precursor ions that do not exclusively produce the selected product ion. To create a NOR scan broadband waveform, two notches are implemented instead of one. For neutral loss variants, no notches are used and instead the neutral loss products are neutralized on the y rods by an inverse Mathieu q scan.

```matlab
% Program: Not_Scan (precursor scan version)
% Calculates a notched broadband waveform that varies with time so that the
% lowest frequency at any given time point is above the corresponding
% frequency for the specified inverse Mathieu q scan. This prevents
% precursor ions from being ejected by the broadband waveform before they are
% fragmented by the inverse Mathieu q scan. The notch is fixed and placed so
% as to prevent the ejection of a selected product ion, thereby ejecting all
% product ions except the selected ion.


% Define variables
scan_time = .6;                             % scan time in seconds
begin_q = 0.908;                     % Mathieu q value to start at
end_q = 0.15;                          % Mathieu q value to end at
sampling_rate = 5000000;             % sampling rate of waveform (Sa/s)
rf_frequency = 1166000;              % trap rf frequency in Hz
num_points = ceil(sampling_rate * scan_time);   % number of points in waveform
time = linspace(0, num_points-1, num_points)*scan_time/num_points;
                              % time variable
frequency_resolution = 1000;         % spacing between adjacent frequencies (Hz)
distance_from_lower_bound = 10000;       %  frequency  distance  between  the
inverse
                              % Mathieu q scan and the lowest frequency
                              % in the broadband waveform
phase_fudge_factor = 0.0001;           % used for phase overmodulation
notch_frequency = 157000;                  % center frequency of notch in Hz
notch_width = 10000;                         % frequency width of notch in
Hz


% Calculate Mathieu q values as a function of time for an inverse Mathieu q
% scan
```

```matlab
% Assume sweep according to q = k / (t-j)
j = end_q*scan_time / (end_q - begin_q);  k = -begin_q*j;
q_values = k ./ (time - j);


% Convert from Mathieu q to frequency; 'lower_bound_frequencies' contains the
% lower bound frequency of the broadband waveform as a function of time, i.e.
% the frequency that the inverse Mathieu q scan is applying as a function of
% time
lower_bound_frequencies = zeros(num_points,1);
betas = zeros(num_points,1);
for i = 1:num_points
    betas(i) = beta_calculator(q_values(i));
    lower_bound_frequencies(i) = betas(i)*rf_frequency/2;
end


% Build frequencies array
num_frequencies                     =                     floor(abs(rf_frequency/2-
lower_bound_frequencies(end))/frequency_resolution); % total number of
                                                     % frequencies in waveform
frequencies                                                               =
linspace(rf_frequency/2,lower_bound_frequencies(end),num_frequencies);
                %


% Distribute phases so that master waveform has flat amplitude profile
phases = zeros(num_frequencies,1);
for i=1:num_frequencies
    phases(i)                       =                       (frequencies(i)-
frequencies(1))^2*scan_time/(2*(frequencies(num_frequencies)-
frequencies(1))*phase_fudge_factor);
end


% Build final waveform point by point
waveform = zeros(num_points,1);
for i=1:num_points
    for n=1:length(frequencies)
        % This frequency is above the lower bound and is not in the notch, so
        % include it!
        if ((frequencies(n) > lower_bound_frequencies(i) +
```

```
        distance_from_lower_bound) && ~((frequencies(n) < notch_frequency
        + notch_width/2) && (frequencies(n) > notch_frequency —
        notch_width/2)))
        waveform(i) =
        waveform(i) + sin(2*pi*frequencies(n)*time(i) + phases(n));
    end
  end
end
```

PART IV. TWO-DIMENSIONAL MASS SPECTROMETRY IN A LINEAR QUADRUPOLE ION TRAP

CHAPTER 16.   TWO-DIMENSIONAL MASS SPECTROMETRY IN LINEAR QUADRUPOLE ION TRAPS VIA FREQUENCY TAGGING

16.1 Abstract

An experimental method for correlating precursor and product ion *m/z* values without prior isolation has been developed for the linear quadrupole ion trap. Precursor ions are mass-selectively excited using a nonlinear ac frequency sweep at constant rf voltage while, simultaneously, all possible product ions of the excited precursor ions are ejected from the ion trap using a time-varying broadband waveform. The fragmentation time of the precursor ions correlates with the ejection time of the product ions, allowing the time axis to be correlated to precursor ion mass-to-charge and also allowing the correlation between precursor and product ions. Additionally, product ions' *m/z* values are encoded by a second frequency - the first being the ion's secular frequency - induced from the nonlinear spacing of the frequency components of the broadband ejection waveform. That is, the product ion *m/z* values are encoded by unique beat frequencies in the broadband waveform and hence they are 'frequency tagged' ions. We demonstrate the utility of this method for analyzing structurally related precursor ions, including chemical warfare agent simulants, fentanyls and other opioids, amphetamines, cathinones, antihistamines, and tetracyclic antidepressants. Remarkably, some isobars with similar fragmentation patterns (e.g. cathinones) are readily discriminated from each other without performing a discrete product ion scan.

16.2 Introduction

Two-dimensional mass spectrometry (2D MS/MS or 2D MS) is a method for correlating precursor ions and product ions without isolation of the former.[401,402] Its origin can be traced to a 1987 paper by Pfändler *et al.* in which it was proposed to be useful for studying ion/molecule collisions via a series of rf pulses and delay/reaction times in a Fourier transform ion cyclotron resonance (FT-ICR) cell.[403] Subsequently, Guan and Jones described the theory of 2D MS in ICRs[404] and Pfändler provided the first experimental evidence for precursor-product ion correlations using ion/molecule reactions.[405] Experimentally, 2D MS in ICRs requires an excitation pulse (a frequency sweep), a varied time delay, and an encoding pulse identical to the excitation pulse, followed by a conventional detection pulse, after which the induction current is

measured and ion *m/z* obtained from the Fourier transform of the detected transient. As the time delay is varied between pulse sequences (each requiring a new ion injection), the abundance of fragment ions varies periodically according to the cyclotron frequency of the precursor ions because the encoding pulse will have a different phase relationship with respect to each precursor ion *m/z* and will thus excite some ions but de-excite others. This causes some precursor ions to fragment more than others if a radius-dependent activation mode is used (IRMPD, for example). Because each precursor ion *m/z* has a different cyclotron frequency, the periodicity of the product ion abundances (with respect to the time delay) generated from different precursor ions will also be unique. The product ion *m/z* values are obtained from FFTs of the detected transients, whereas the precursor ion *m/z* values are determined from FFT of product ion abundance vs. delay time.

Other advances include new pulse sequences using stored waveform inverse Fourier transform (SWIFT)[401,402] for ion radius modulation and denoising algorithms for data analysis.[406,407] More recently van Agthoven and coworkers have proposed an optimized pulse sequence in which two encoding pulses with optimized voltage amplitudes are separated by a delay time, and after the second pulse the ion signal is observed during the detection period.[408] In addition, others have demonstrated increased precursor ion resolution using nonuniform sampling.[409] Usually infrared multiphoton dissociation is used for fragmentation[410] but several implementations have used electron capture dissociation.[411,412] After decades of development, 2D MS in FT-ICRs is finding extensive use in applications for analysis of small molecule biologics (cholesterol),[413] peptides and glycopeptides,[412,414] proteins,[411,415,416] and polymers.[417] Even so, 2D MS in ICRs still faces multiple challenges: limited precursor ion resolution (requiring overnight runs to obtain unit precursor ion mass resolution), high sample consumption (one injection per time delay increment because fragmentation is irreversible), and loss of resolution during collision-induced dissociation (hence, laser-based methods are prominent).[409]

To date, 2D MS has only been experimentally demonstrated on FT-ICR instruments; it has yet to garner theoretical or experimental interest in the arguably similar – and much cheaper, simpler, and feasible for miniaturization - quadrupole ion trap (QIT). This is an odd omission given that many waveform methods (e.g. SWIFT, frequency 'chirps') that originated on ICRs were successfully translated to quadrupole traps.[51,148] After all, both ICRs and QITs are ion frequency analyzers with MS/MS capabilities, although the QIT is indirectly so (the ions' frequencies are indirectly measured via resonance ejection at a fixed frequency, whereas in the ICR the frequencies

are measured directly via ion excitation and charge detection). Simulated evidence that 2D MS is possible in a linear ion trap has been published by O'Connor's group.[418] In these simulations, SWIFT was used to radially excite ions as a laser pulse fragmented ions at the center (the un-modulated ions). According to the work, the intensities of product ions were modulated corresponding to the secular frequency of the excited precursors, as is the case for the similar ICR experiments. Despite this simulated evidence, no experimental data of 2D MS on linear ion traps has emerged. Furthermore, the requirement of a laser for dissociation and a second mass analyzer for determination of product ion *m/z* limits the overall applicability of this method. Moreover, such a method would not be feasible for portable ion traps which are of interest to us and which would benefit most from the efficiency of acquiring the entire 2D MS/MS domain with, say, a single scan.

Herein we propose a 'frequency tagging' method[419,420] for 2D MS on quadrupole ion traps using simple collision-induced dissociation for precursor ion fragmentation and show experimental evidence that *precursor and product ion m/z values can both be obtained and correlated in a single scan*. In this work we use a nonlinear frequency sweep for time-dependent fragmentation of precursor ions from low to high *m/z* in one dimension of the linear trap and eject all product ions of those precursor ions as they are being formed by using a broadband sum of sines waveform applied in the orthogonal dimension. The sum of sines is encoded with beat frequencies proportional to the product ion secular frequencies, thus modulating peak shapes according to those beat frequencies. By taking the fast Fourier transform of each peak, the beat frequencies of the ejected product ions – hence, the product ions' secular frequencies – can be recovered for every precursor ion without isolation. Secular frequency can then be converted to ion *m/z*, and subsequently product ion frequency spectra can be converted to the mass domain, thereby yielding a product ion spectrum for every precursor ion.

This work follows our recent experimental demonstration of precursor and neutral loss scans on a single linear ion trap in which orthogonal double resonance was used for mass analysis.[341,393,421,422] The 2D MS/MS can be thought of as conducting every possible precursor ion scan at once (or, correspondingly, every possible neutral loss or product ion scan). Experimentally, the linear ion trap 2D MS method is most similar to the precursor ion scan, which we have argued will be most useful for miniature or portable instruments[69-71,421,423] with low acquisition rates (e.g. DAPI systems[75]). On such instruments data-dependent product ion scans are less feasible than

data-independent acquisition. It thus may be important to be able to acquire as much data as possible in each scan, i.e. perform 2D MS.

16.3 Experimental

16.3.1 Chemicals

All drug standards were purchased from Cerilliant (Round Rock, TX, USA) and were either used as provided or diluted in 50:50 methanol/water with 0.1% formic acid. All other standards were purchased from Sigma (St. Louis, MO, USA) and prepared similarly.

16.3.2 Ionization

Nanoelectrospray ionization was used for all experiments herein. In order to generate ions, 1.5 kV was applied to a nanospray electrode holder (glass size 1.5 mm), which was purchased from Warner Instruments (Hamden, CT, U.S.A.) and fitted with 0.127 mm diameter silver wire, part number 00303 (Alfa Aesar, Ward Hill, MA). Borosilicate glass capillaries (1.5 mm O.D., 0.86 mm I.D.) from Sutter Instrument Co. (Novato, CA, U.S.A.) were pulled to 2 μm tip diameters using a Flaming/Brown micropipette puller (model P-97, Sutter Instrument Co.).

16.3.3 Instrumentation

All data was generated on a Thermo LTQ linear quadrupole ion trap (San Jose, CA, USA). The LTQ ion trap has an rf frequency of 1.166 MHz and dimensions of $x_0 = 4.75$ mm, $y_0 = 4$ mm, axial sections of length 12, 37, and 12 mm.[10] In these experiments, the rf amplitude was constant throughout injection, cooling, and mass scan stages, as described previously.[393] Because the mass range is limited when the rf amplitude is not varied (ions at low q are not generally useful), the experiments were subdivided into a 'low mass' mode (LMCO = 73 Th) and a 'high mass' mode (LMCO = 105 Th). The LTQ used in this work was previously modified to be able to apply low voltage ac signals to both the x and y rods. The data collection rate in the 'normal' scan rate mode with 'high' selected as the mass range was 28.732 kHz, which is fixed by the LTQ data system and cannot be changed (but does vary between different scan modes). The helium normally used in the LTQ was substituted with nitrogen at an ion gauge reading of 1.4×10^{-5} torr. Nitrogen increases fragmentation efficiency but also decreases resolution.[55]

Waveform Generation: Two waveforms were used in these experiments; both were calculated in Matlab (Mathworks, Natick, MA, USA), exported as .csv files and imported into one of two Keysight 33612A arbitrary waveform generators (purchased from Newark element14, Chicago, IL, USA) with 64 megasample memory upgrades. One generator supplied the waveform for precursor ion excitation in the y dimension while the other supplied a broadband sum of sines for product ion ejection in the x dimension.

A first waveform was a frequency sweep applied in the y dimension of the LTQ ion trap in order to mass-selectively fragment precursor ions as a function of time. The frequency sweep was an inverse Mathieu q scan[133] (nonlinear frequency sweep with linear mass scale vs. time) from Mathieu q = 0.908 to q = 0.15 over 600 ms. This excitation sweep always had a peak-to-peak amplitude of 350 mV$_{pp}$.

The second waveform, applied in the x dimension, was a broadband sum of sines used to eject all product ions of the excited precursor ions; the product ions' *m/z* values were encoded in the beats in the waveform so that beat frequency and product ion secular frequency were directly proportional. A master array contained main frequencies that were spaced every 10 kHz from Mathieu q = 0.908 to q = 0.15, with the lowest frequency being 73 kHz. Beat frequencies were then encoded by adding a second frequency per main frequency, with a starting beat frequency of 500 Hz and subsequent spacings of 600 Hz, 700 Hz, 800 Hz, etc (i.e. the beat increased by 100 Hz per 10 kHz). The lowest main frequencies (corresponding to the highest *m/z* ions) had the smallest beat frequencies, and the highest main frequencies (lowest *m/z* ions) had the highest beat frequencies. The frequencies in the waveform were therefore 73 kHz and 73.5 kHz, 83 kHz and 83.6 kHz, 93 kHz and 93.7 kHz, and so on until half the rf frequency was met. Phase overmodulation using a quadratic function of phase vs. frequency (common with Stored Waveform Inverse Fourier Transform methods)[51,148,169] was used to maintain an approximately constant voltage amplitude (6 V$_{pp}$) as a function of time.

The ejection waveform was built point-by-point, and, critically, only frequencies at least 10 kHz above the precursor ion's frequency were included in each point. That is, the frequency components of the sum of sines waveform varied because the excited precursor ion mass varied and thus the product ion mass range varied as a function of time. The excited precursor ion's frequency is known because it equals the frequency applied by the excitation waveform (the inverse Mathieu q scan). For example, if at time 0.1 s the inverse Mathieu q scan is applying a

frequency of 300 kHz to fragment a precursor ion, then at that time point the sum of sines waveform will only include frequencies above 310 kHz.

This particular waveform was not the only waveform that successfully encoded product ion frequencies. The main frequency spacing can be altered from 10 kHz and the difference between adjacent beat frequencies (100 Hz in this work) can also be altered. Moreover, there need not be 'main frequencies.' For example, one could encode the frequencies as follows: 73 kHz, 73.5 kHz (+0.5 kHz compared to adjacent frequency), 74.1 kHz (+0.6 kHz), 74.8 kHz (+0.7 kHz), 75.6 kHz (+0.8 kHz), and so on. Several different waveforms were successful, but we will only show data for the particular encoding described in the previous paragraphs.

All mass and frequency spectra are the result of an average of 10 scans. Fast Fourier transforms were calculated in Matlab using 301 points per peak and a sampling rate of 28.732 kHz, as described previously. Only frequencies above 300 Hz are shown in the spectra and used for statistical analysis. Peaks below this frequency correspond to the width of each mass peak which is not useful. Software precursor ion scans were also performed in Matlab after the total ion current in the frequency spectra was normalized to 1. Principal component analysis (PCA) was conducted in OriginPro 2018 (OriginLab Corporation, Northampton, MA, USA) using built-in PCA tools

16.4 Results & Discussion

16.4.1 What is frequency tagging?

Frequency tagging[419,420] (**Figure 16.1a**) is a method of tagging ions resonantly ejected from a quadrupole ion trap with a secondary frequency observable at the detector, the primary frequency being the ion's fundamental secular frequency which is usually not observed except when measuring charge induction current in the ion trap.[424] Any ion in the trap can be frequency tagged by applying a dual frequency sine wave that is the sum of the ion's secular frequency and a second frequency very close to the secular frequency. For example, an ion whose secular frequency is 300 kHz can be tagged with a 2 kHz frequency if a dual frequency sine wave containing 300 kHz and 302 kHz is used for resonance ejection (or excitation). The 2 kHz beat is observed in the mass spectral peak at the detector (**Figure 16.1a, peak shape**). The peak can be the result of a precursor ion scan, a neutral loss scan, or a full scan. A fast Fourier transform of the mass spectral peak results in recovery of the beat frequency, and if beat frequency and the secular frequency are

related in some predetermined or pre-programmed (but calibratable) fashion, then this relationship can be used to relate beat frequency to product ion *m/z*.

In this work we used frequency tagging to perform 2D MS/MS in a linear quadrupole ion trap. There are three key pieces of information obtained in a 2D MS/MS experiment: 1) precursor ion *m/z*, 2) product ion *m/z*, and 3) the relationship between the precursor ions and the product ions (i.e. from which precursor ion did each product ion originate?). In our implementation of 2D MS/MS, these three pieces of information are obtained as follows. 1) Precursor ion *m/z* is linearly related to time because the precursor ions are fragmented from low to high *m/z* using an inverse Mathieu q scan ('Excitation Voltage vs. Time' in **Figure 16.1**). 2) Simultaneously, a broadband sum of sines waveform – with encoded beat frequencies – is used to eject the product ions as they are being formed from fragmentation of the precursors. Product ion *m/z* is recovered from fast Fourier transform of each mass spectral peak, where beat frequency is linearly related to secular frequency based on a pre-programmed relationship (which is then directly correlated to product ion *m/z*). **Figure 16.1b** shows the experimentally observed relationship between secular frequency and beat frequency, and converting secular frequency to *m/z* gives the plot in **Figure 16.1c**. The calibration is shown in blue and the experimental values in red. 3) Product ions are ejected from the ion trap at the same time as their respective precursor ions are fragmented and hence their relationship is preserved in time, as was the case in our implementation of precursor and neutral loss scans.[99,341,393,421,422] The application of two waveforms, an inverse Mathieu q scan for precursor ion fragmentation and a broadband beat-encoded sum of sines for product ion ejection, thus allows us to obtain the entire MS/MS domain with one scan.

16.4.2 2D MS/MS using frequency tagging

A simple mixture of 5 amphetamines was analyzed using this 2D MS/MS method. The mass calibrated spectrum in **Figure 16.2a** gives the *m/z* values of the precursor ions as a function of time, thus satisfying requirement #1 of 2D MS/MS. Note the unique beats in each peak which will be used to recover product ion *m/z*. It is also critical to remember that although the precursor ion *m/z* correlates with time, *the precursor ions are never detected*. Only the product ions are observed at the detector.

Requirement #3, association between fragmented precursor ion *m/z* and generated product ion *m/z*, is satisfied by taking the fast Fourier transform of any given peak in the spectrum. Because we know that each peak is due only to one precursor ion, we can be sure that any peaks in the fast

Fourier transform of the mass peak are product ions formed from fragmentation of the selected precursor ion. Of course, this does not hold if there is substantial overlap or if there are isobars (in that case the FFT will give peaks from both precursors, as we will demonstrate later).

In order to obtain the product ion m/z (requirement #2), we must be able to associate the peaks in the beat frequency domain (after FFT) with particular m/z values. Experimentally this can be done by taking FFTs of peaks of known standards and correlating beat frequency with the known product ion m/z. Because in our case beat frequency and secular frequency are directly proportional, we can calculate the calibrated relationship between beat frequency and m/z, as shown in **Figure 16.1c** and compare it to experimental values, shown as red diamonds. These calibrations can now be used to confidently assign m/z values in the frequency spectra. Note that the calibration shown is only applicable to 'high mass' mode. In 'low mass' mode the rf voltage is lower and thus the relationship between m/z and secular frequency (and beat frequency) is different.

Amphetamine and methamphetamine share product ions at m/z 91 and 119, and this is evident in the FFTs (**Figure 16.2b**) of the peaks in the mass spectrum (**Figure 16.2a**). A peak at 3436 Hz corresponds to m/z 91 and 2386 Hz corresponds to m/z 119. Because beat and secular frequency are proportional in our implementation, lower m/z ions will have higher beat frequencies. Similarly, amphetamines mda, mdma, and mdea fragment to m/z 163, m/z 135, and m/z 133 at 1527 Hz and 2005 Hz, respectively. Additional peaks in the frequency spectra correspond to harmonics (i.e. two and three times the beat frequency) as well as other, less predictable beats and combination frequencies. Because of these additional peaks, frequency spectra are not converted into the mass domain. However, these peaks do serve to provide a unique pattern for each precursor ion and may be useful for distinguishing similar spectra.

16.4.3 2D MS/MS for analysis of fentanyls

We next applied 2D MS/MS to analysis of opioids of the fentanyl class, which have become a serious health risk due to their extreme potency and wide range of analogues.[425,426] When subject to CID in the ion trap, many of these compounds fragment almost exclusively to m/z 188[427] and so their frequency spectra should be markedly similar. A full scan of a mixture of 16 fentanyl analogues appears in **Figure 16.3a**. The precursor ion masses are directly proportional to time, allowing for the spectrum to be mass calibrated. The beats in each peak are indicative of the product ion m/z values and be recovered through FFTs. As shown in **Figure 16.3b**, 4-ANPP (a

fentanyl precursor), acetyl fentanyl, 4-fluoroisobutyryl fentanyl, fentanyl, furanyl fentanyl, p-fluorofentanyl, isobutyryl fentanyl, butyryl fentanyl, valeryl fentanyl, and acryl fentanyl all fragment to *m/z* 188 and hence have almost identical frequency spectra. *Cis*-3-methylfentanyl has a prominent product ion at *m/z* 202 which is noticeably frequency shifted (about 240 Hz) from *m/z* 188. Acetyl norfentanyl is a metabolite and hence fragments differently as well.

Notably, butyryl, isobutyryl, and *cis*-3-methylfentanyl are isobaric (*m/z* 351) and so their peaks overlap in the mass spectrum if they are in a mixture together. We tested whether we could observe all three components in a 1:1:1 mixture. The frequency spectrum in **Figure 16.3c** (bottom) indicates a primary product ion at *m/z* 188. Presumably the peak at *m/z* 202 overlaps significantly and is not observed. However, the harmonic (1.86 kHz x 2 = 3.72 kHz) is observed because it is twice as far from the harmonic of *m/z* 188 compared to the fundamental frequencies, and thus it is umambiguous that methylated fentanyl is in the spectrum. Later we will give statistical evidence that all three components are evident in the frequency spectrum. Butyryl and isobutyryl fentanyl are nearly indistinguishable, though.

Quaternary fentanils (emphasis on the 'il') share neutral losses – e.g. 31 Da, 32 Da, 60 Da, 148 Da are examples - instead of product ions. In the frequency domain the similarities are not obvious, which is a weakness of the current method. The frequency domain must be converted to the mass-to-charge domain and then to neutral losses to make any reasonable conclusions about similarities between spectra. **Figure S16.1** shows the frequency spectra of alfentanil and sufentanil (which share neutral losses of 31 Da and 148/149 Da) and norcarfentanil, carfentanil, remifentanil (which share neutral losses of 32 Da, 60 Da, and 149 Da).

16.4.4 2D MS/MS for analysis of other molecular classes

Frequency tagging spectra of other molecular classes – focusing on classes that share product ions rather than neutral losses – are shown in **Figure S16.2/S16.3**. Chemical warfare agent simulants cyclohexyl methylphosphonate, isopropyl methylphosphonate-d7, and pinacolyl methylphosphonate fragment exclusively to *m/z* 95 (*m/z* 96 for the deuterated analytes) in the negative ion mode and thus have very similar frequency spectra, including strong harmonics. Tetracyclic antidepressants amoxapine, loxapine, and clozapine share *m/z* 272 but otherwise have dissimilar spectra in both the mass and frequency domain. Antihistamines pheniramine, chlorpheniramine, brompheniramine, and diphenhydramine share *m/z* 167 (or *m/z* 168), as noted on the spectra, but also have other dissimilar product ions. Other opioids (along with caffeine as a

reference spectrum) were analyzed, with results in **Figure S16.3**. These spectra were more difficult to deconvolute and are not labeled but will be statistically analyzed later.

16.4.5 Analysis of isobaric cathinones

A challenge in mass spectrometry is differentiating isobars, particularly if those isobars fragment similarly. Not only will their product ion spectra appear similar, but so will their 2D MS/MS frequency spectra. As shown in **Figure 16.4**, isobaric cathinones (*m/z* 178) buphedrone and *N*-ethylcathinone share product ions at *m/z* 160 and 132 and are nearly indistinguishable. However, three other cathinone isobars, namely pentedrone, 3,4-dimethylmethcathinone, and 4-methylethcathinone are – remarkably – readily distinguished. Although they share water loss (*m/z* 174), they also have unique MS^2 ions *m/z* 132, *m/z* 161, and *m/z* 147. As we showed previously, mixtures of isobars can also be identified if standard spectra of the individual components are known.

16.4.6 Statistical analysis of beat frequency spectra

After acquiring frequency spectra for 47 compounds of various molecular classes and normalizing the integrated intensity of each spectrum to 1, we performed principal component analysis to statistically distinguish molecular classes. **Figure 16.5a** shows the PCA plot with each molecular class color coded with the same color as their frequency spectra. Clearly the fentanyls group together because of their strong similarities as well as methylphosphonates (chemical warfare agent simulants), and methylenedioxyamphetamines. Tetracyclic antidepressants clozapine, loxapine, and amoxapine also group closely together, and isobars buphedrone and *N*-ethylcathinone are close. Fentanils are scattered because they have neutral losses in common instead of a fixed product ion *m/z* and this particular analysis will group based on shared product ions. Other opioids, cathinones, and antihistamines do not separate well because they have more complex fragmentation patterns and because the frequency resolution – hence mass resolution - of the product ions is quite low. **Figure 16.5b** shows loading plots and the fentanyl frequency spectrum for reference. Clearly, *m/z* 188 is the strongest contributor to principal component 1 and thus gives good separation between fentanyls and other classes. Principal component 2 focuses on higher mass peaks than *m/z* 188 (lower frequencies) and provides better separation amongst some of the other classes.

The three points circled in red are isobaric fentanyls (*m/z* 351). Isobutyryl and butyryl fentanyl have nearly identical product ion spectra (product ion *m/z* 188) which is evident in their frequency spectra and in the PCA plot, and *cis*-3-methylfentanyl fragments instead to *m/z* 202 and thus falls in an entirely different location. An isobaric mixture of 1:1:1 isobutyryl:butyryl:*cis*-3-methyl fentanyl was analyzed by frequency tagging and it appropriately lies between the circled individual components on the PCA plot.

16.4.7 Software ion scan functions of 2D MS/MS data

Principal component analysis is only one way to analyze the frequency tagging data and furthermore is not necessarily the best method of analysis. We can also reconstruct precursor ion 'spectra' from the recorded frequency spectra, i.e. perform 'software ion scans'.[428] For example, a reconstructed precursor scan of *m/z* 188 (**Figure 16.6**, blue) yields the fentanyls as the most abundant analytes. A software precursor scan of *m/z* 132 yields three of the cathinones, a precursor scan of *m/z* 272 yields the tetracyclic antidepressants amoxapine, clozapine, and loxapine (as well as some fentanils which have very broad peaks in their frequency spectra), and a reconstructed precursor scan of *m/z* 167 shows the pheniramines as prominent ions with that functionality. The low frequency and mass resolution of the product ions does mean that there is substantial overlap in the spectra, and improvements to the resolution should be the next major step in this work. Note that the amphetamines and CWAs were analyzed at different rf amplitudes and were not included in these reconstructed 'spectra'.

16.5 Conclusion

We have demonstrated a method of performing two-dimensional mass spectrometry in a single linear quadrupole ion trap using frequency tagging. The method should be especially promising for ion traps with low acquisition rates or for cases where sample or instrument power is precious, as a single scan can be used to obtain a remarkable amount of information.

Of course, improvements to this technology should be sought. These include minimizing the contributions of harmonics (or dealing with them during data analysis), increasing product ion resolution and mass accuracy, and seeking refinements to waveform construction, data acquisition, and analysis. It may also be possible to perform 2D MS/MS in a quadrupole ion trap without using frequency tags (for example, if the product ions' frequencies themselves could be observed at the

electron multiplier), in which case product ion resolution should naturally improve as more cycles are observed in each mass spectral peak.

16.6 Acknowledgements
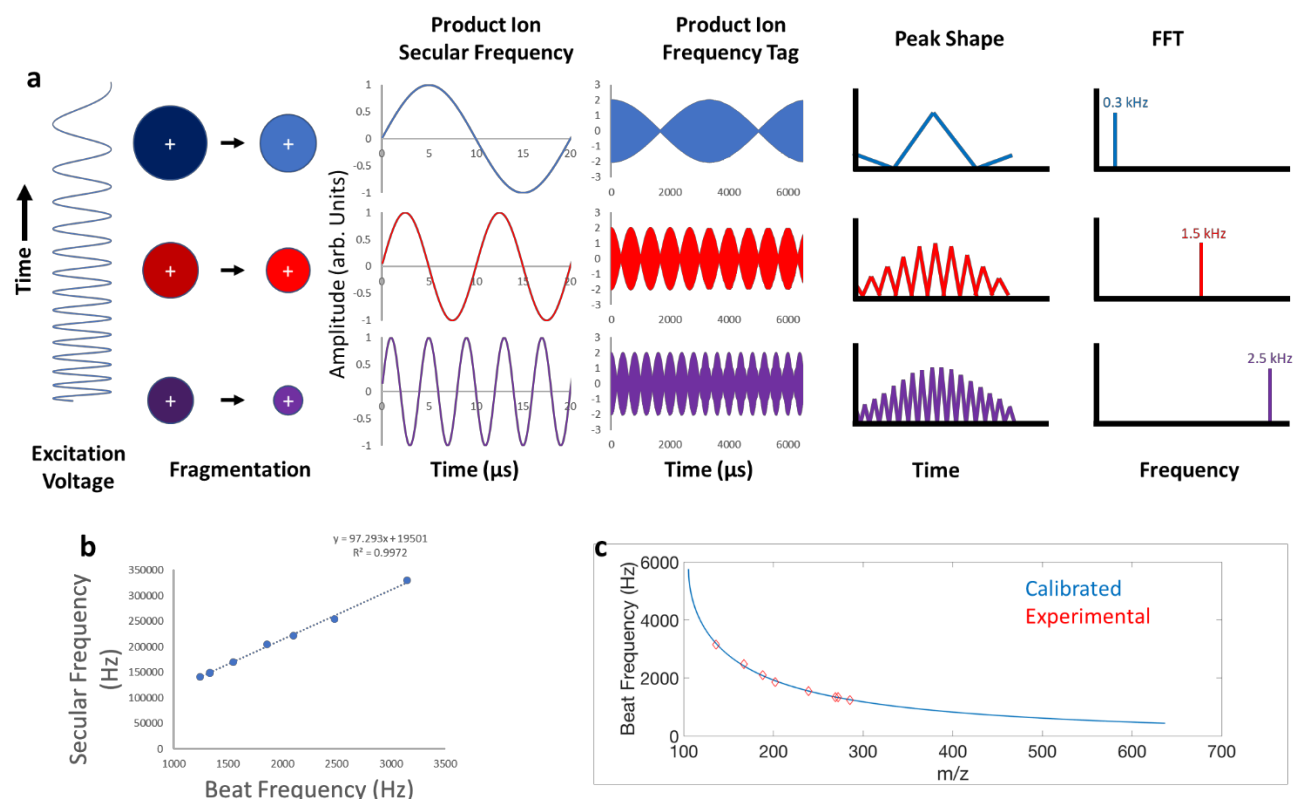
Figures

Figure 16.1. Frequency tagging mass spectrometry for 2D MS/MS. (a) Precursor ions are fragmented from low to high *m/z* via a frequency sweep ('Excitation Voltage'), forming product ions. Each product ion is 'tagged' with a secondary frequency by resonance excitation with two frequencies close to its secular frequency, the difference of which creates a beat frequency that modulates the mass spectral peak shapes. When product ions are generated they are immediately ejected and detected by a broadband sum of sines with encoded beat frequencies, but the ejection process follows the programmed beat pattern and hence the mass spectral peaks also show beats. (b) The beat frequencies, related linearly to product ion secular frequency, can be recovered by taking the fast Fourier transform of each peak. The beats can be plotted against the experimental secular frequencies for calibration. (c) Experimental vs. calibrated relationship between beat frequency and product ion *m/z* in 'high mass' mode (LMCO ~100 Th) on the LTQ.
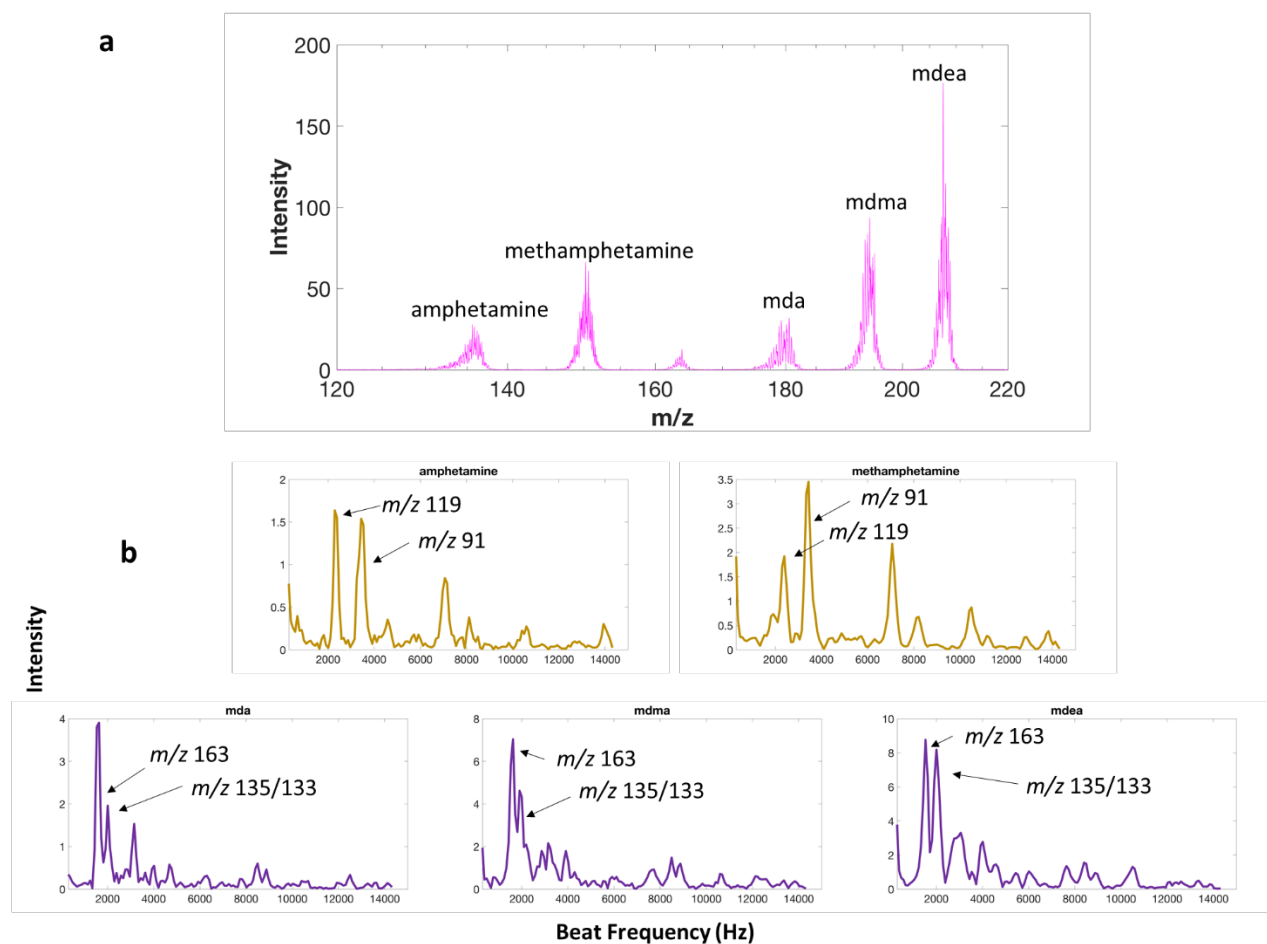
Figure 16.2. (a) Frequency tagging mass spectrum in 'low mass' mode on the LTQ for five amphetamines (note the beats in each peak) and (b) frequency spectrum of each peak. Frequencies that correspond to known product ions are marked.
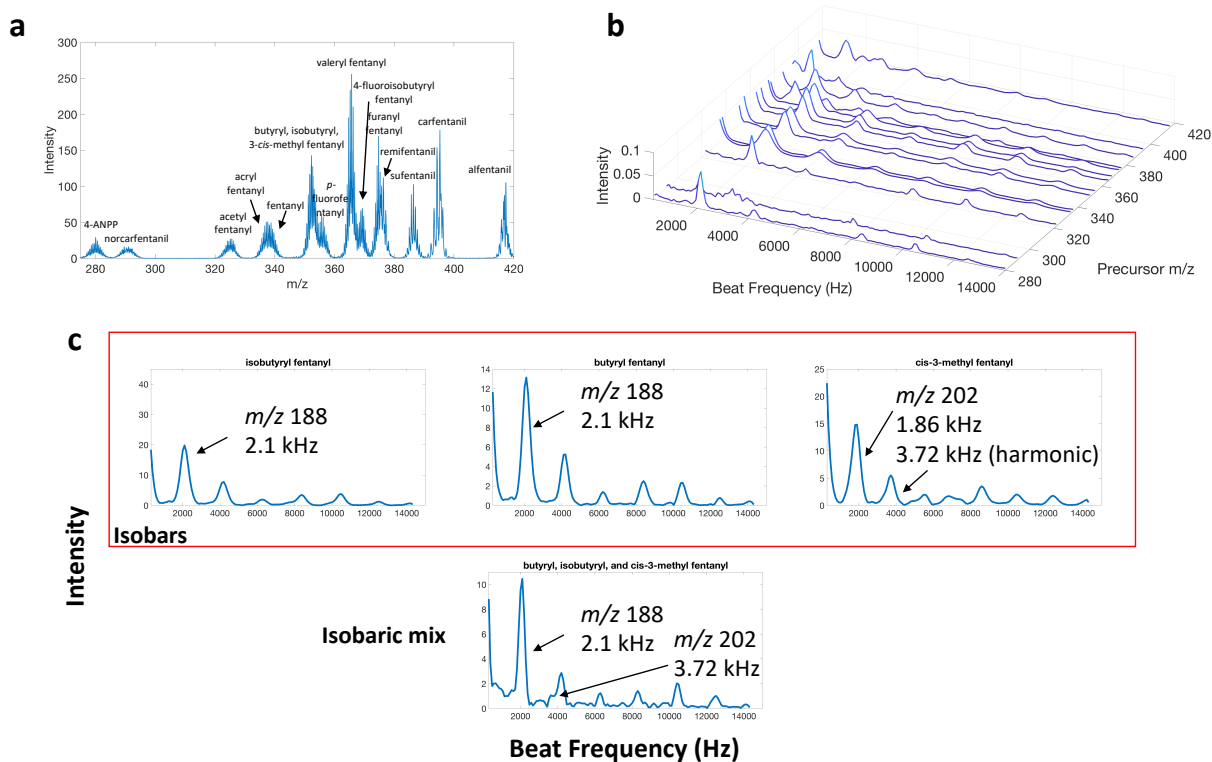
Figure 16.3. 2D MS/MS of a mixture of 16 fentanyl analogues. (a) Full scan mass spectrum of the mixture (note the beats in the spectra), (b) beat frequency spectra for each precursor ion, (c) comparison of frequency spectra of three isobaric fentanyls and three-component mixture. Known product ions are marked. Data was acquired in 'high mass' mode.
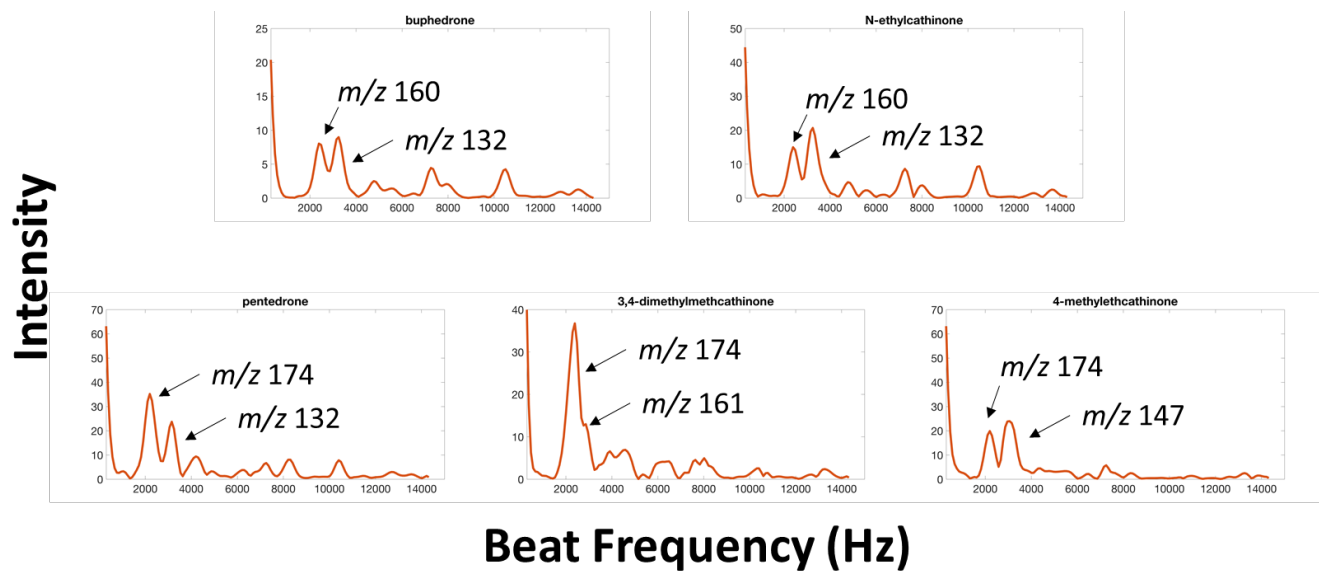
Figure 16.4. Frequency spectra of sets of cathinone isobars: *m/z* 178 isobars (a) buphedrone and (b) *N*-ethylcathinone; *m/z* 192 isobars (c) pentedrone, (d) 3,4-dimethylcathinone, and (e) 4-methylethcathinone. Data was acquired in 'high mass' mode.
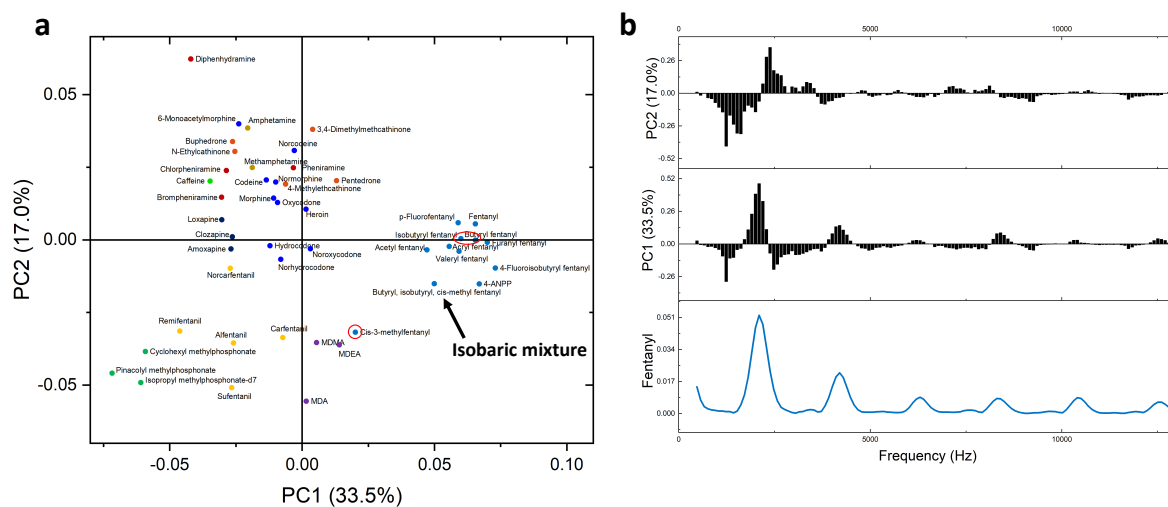
Figure 16.5. (a) Principal component analysis of all frequency spectra acquired on the LTQ (with isobars circled in red and isobaric mixture noted) and (b) loadings for each frequency with fentanyl FFT as the reference.
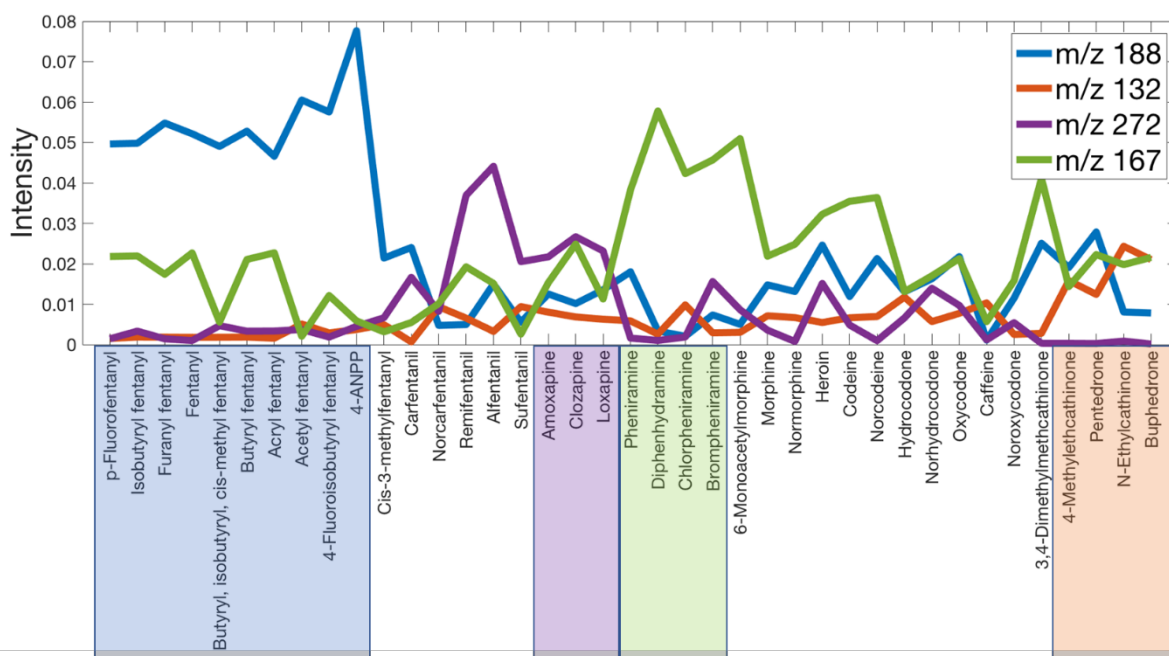
Figure 16.6. Reconstructed software precursor ion scans for selected product ions.

Supplemental Information
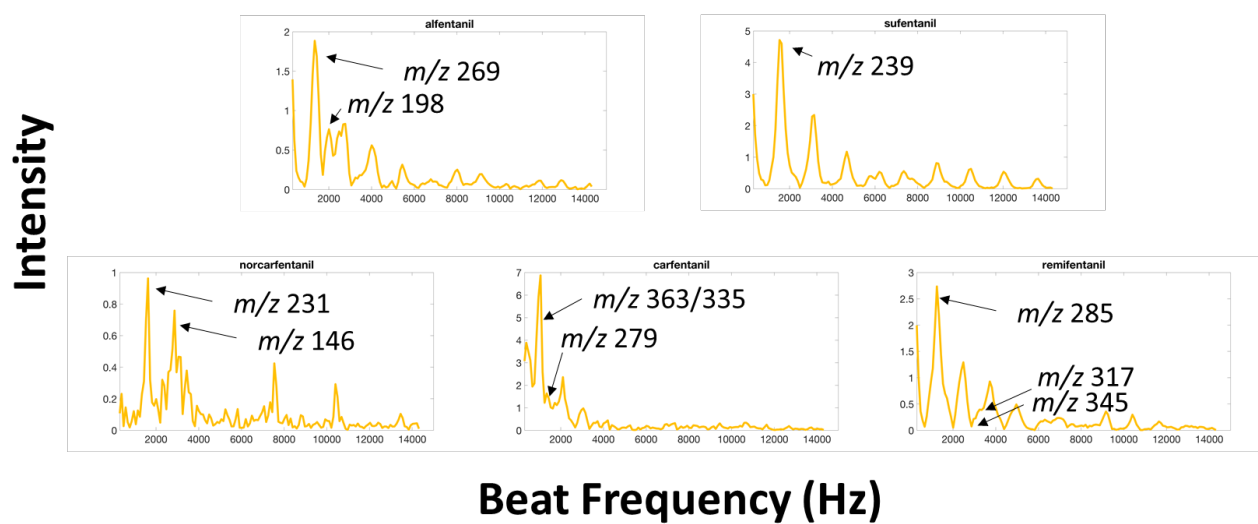
Figure S16.1. Frequency tagging spectra of five fentanils in 'high mass' mode.
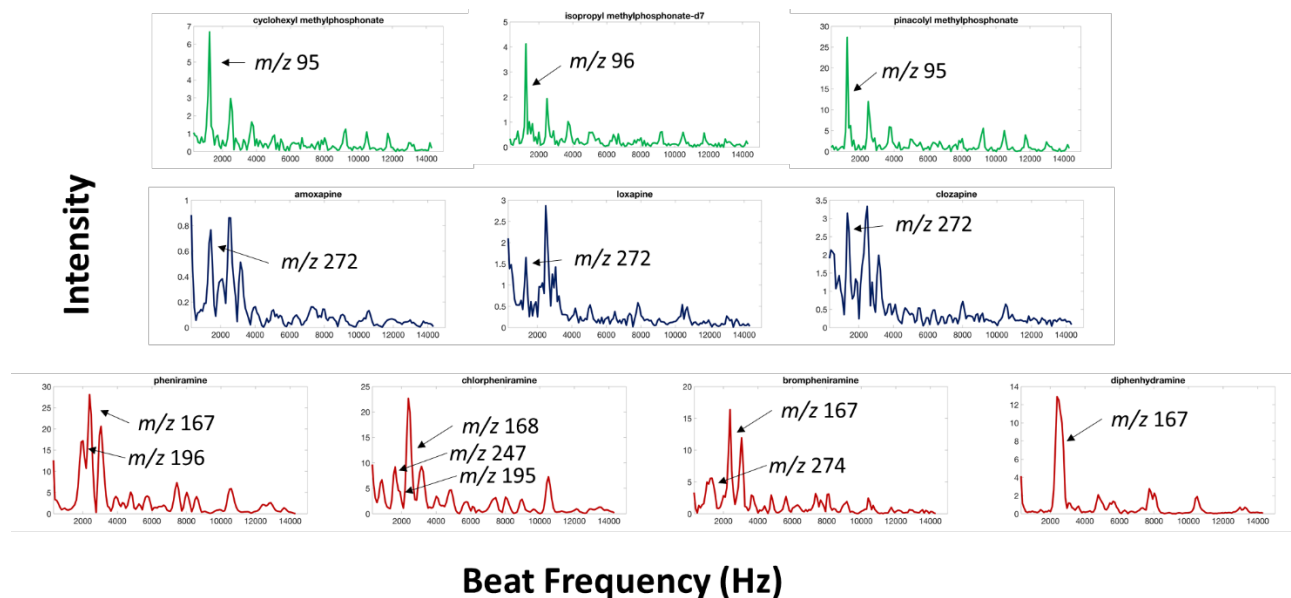
Figure S16.2. Frequency tagging spectra for (top, green) three chemical warfare agent simulants, (middle, dark blue) three tetracyclic antidepressants, and (bottom, red) four antihistamines. The chemical warfare agent spectra were obtained at a LMCO of 65 Th; other data was obtained in 'high mass' mode (LMCO 100 Th).
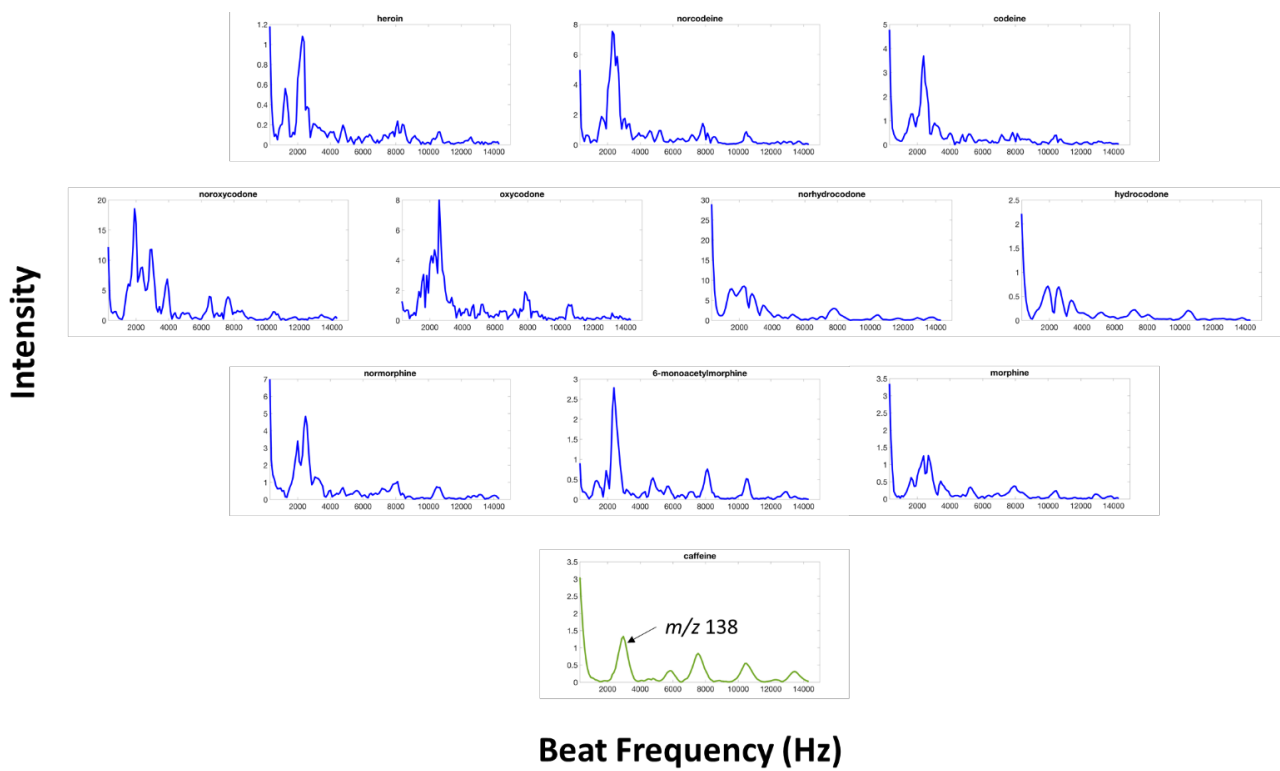
Figure S16.3. Frequency tagging spectra of opioid standards and metabolites as well as caffeine. All data was acquired in 'high mass' mode.

CHAPTER 17. TWO DIMENSIONAL MASS SPECTROMETRY IN A LINEAR QUADRUPOLE ION TRAP USING ION MICROPACKET DETECTION

17.1 Abstract

A method of correlating precursor and product ions in a linear quadrupole ion trap without ion isolation – that is, two-dimensional mass spectrometry – is described herein and compared to a previously described 'frequency tagging' method. Like 'frequency tagging', precursor ions are mass-selectively activated by a nonlinear frequency sweep at constant rf voltage while a broadband waveform is used to eject all possible product ions of each precursor ion. Precursor ion m/z is deduced from fragmentation time, which also correlates in time with the ejection of the product ions. Instead of inducing a low-kHz secondary frequency to differentiate the product ions at the electron multiplier detector, the ions' secular frequencies themselves are determined by detecting the product ion micropackets as they are ejected using a fast current amplifier and MHz data acquisition system. A fast Fourier transform of each mass spectral peak recovers the secular frequency of each product ion (or twice the secular frequency if two detectors are used) which can then be related to product ion m/z through the Mathieu parameters. We show here that the ion micropacket method has several notable advantages over frequency tagging, specifically that product ion resolution is improved by at least a factor of 4 and that harmonic overlap is reduced. Moreover, the resolution of the precursor ions is improved by using helium instead of nitrogen without significantly compromising the resolution of the product ions.

17.2 Experimental

17.2.1 Chemicals

Standards were purchased from Cerilliant (Round Rock, TX, USA) and were diluted in 50:50 methanol/water with 0.1% formic acid to ~5 ppm (µg/mL) concentration.

17.2.2 Instrumentation

All ions were generated using nanoelectrospray ionization with a 1.5 kV potential. Data was acquired on a Thermo LTQ linear quadrupole ion trap (San Jose, CA, USA). The LTQ ion trap has rf frequency 1.163 MHz, radial dimensions of $x_0 = 4.75$ mm and $y_0 = 4$ mm, and three

axial rod sections of length 12, 37, and 12 mm.[10] The rf voltage was held constant throughout the mass scan period to prevent the ions' secular frequencies from changing during the scan. Helium was used as bath gas at an ion gauge reading of 1.3×10^{-5} torr.

Low voltage ac waveforms supplied by two Keysight 33612A function generators (Chicago, IL, USA) were coupled onto the x and y rods of the linear ion trap as described previously.[341,393] A first waveform was an inverse Mathieu q scan from q = 0.908 to q = 0.15 over 600 ms applied on the y rods to excite and fragment precursor ions. A second waveform was a broadband sum of sines constructed in Matlab and applied to the x electrodes (the detection dimension). This waveform is used to simultaneously eject all product ions of the excited precursor ions. Frequencies were equally spaced (1 kH spacing) from 583 kHz to 62 kHz and their phases were distributed quadratically with frequency.[169] The broadband waveform was built point-by-point so that the frequency components included in each point were always at least 10 kHz above the corresponding frequency in the accompanying inverse Mathieu q scan since each precursor ion has a different product ion mass range (and thus will have a different product ion frequency range). In other words, each time point in the broadband waveform consisted of a different set of frequencies to coincide with different product ion mass ranges.

17.2.3 Data acquisition and analysis

Data were obtained directly from the electron multipliers of the LTQ using a combination of a fast transimpedance (current) amplifier and either a Keysight MSOX3024T oscilloscope (Chicago, IL, USA) or a National Instruments USB-6343 DAQ device with BNC termination (Austin, TX, USA). The amplifier consists of a current to voltage conversion followed by a two-stage current feedback operational amplifier (CFA) circuit. The CFAs allow the circuit to achieve a very high gain without the linear tradeoff in bandwidth, as with traditional voltage feedback operational amplifiers. The total gain of the circuit is around 3,000,000 V/A with a bandwidth of 225MHz. The oscilloscope was generally operated with a sampling rate between 50 and 100 MHz and acquired ~1.9 ms of data (but could only save 16,000 points of data), whereas the the DAQ device had a fixed sampling rate of 2 MHz and could acquire and save data over 600 ms (1.2 million points). Fast Fourier transforms (FFTs) of the oscilloscope data (16,000 points over 1.9 ms) were conducted in Matlab, whereas Labview was used to obtain FFTs of DAQ data (using 10 ms windows containing 20,000 points each). All spectra are the average of 20 scans.

17.3 Results & Discussion

17.3.1 What is an Ion Micropacket?

Ions can only be ejected during certain 'allowed' periods in a quadrupole ion trap operated in the resonance ejection mode.[429] This has been observed through both simulation[429,430] and experiment[56] by several groups using a variety of ion trap configurations. As ions are resonantly excited for ejection through application of an auxiliary frequency, they oscillate coherently and are ejected such that the rate of appearance of the micropackets at the detector corresponds to the excitation frequency (*not* the ion secular frequency). If a detector is placed on either side of the ion trap, then the micropackets are observed at a frequency corresponding to *twice* the auxiliary frequency since the ions are equally likely to be ejected through either x electrode slit.[429,431] The frequency of ejection can be determined through Fourier transform of each mass spectral peak, assuming the detection electronics are fast and sensitive enough to observe the micropackets.

For example, **Figure 17.1a** shows oscilloscope traces of five peaks from an ac frequency scan mass spectrum of a set of amphetamines. Because the electrometer board on the LTQ filters the signal from the electron multipliers, we chose to bypass it and use an external transimpedance amplifier instead. As shown in **Figure 17.1b**, the ion micropackets of *m/z* 208 are clearly observed at regularly spaced intervals, the frequency of which can be obtained by calculating the fast Fourier transform of the peak (**Figure 17.1c**). The auxiliary frequency at the time of ion ejection as well as the second and third harmonics are observed. For *m/z* 208, the primary peak (second harmonic) is 339.6 kHz, implying that the precursor ions were ejected at 339.6/2 = 169.8 kHz. A third harmonic of the secular frequency is observed at 508.4 kHz, and a second harmonic of 339.6 kHz is observed at 677.1 kHz. In this last case 677.1 kHz is not a harmonic of the ion's ejection frequency but rather a harmonic of *twice* the ion's ejection frequency. Notably, the second harmonic (the frequency of ejection doubled) is the dominant peak, again because ions can be detected in the positive and negative x directions. When only a single detector is used, then the ejection frequency itself is the dominant peak (not shown).

Although this manuscript primarily demonstrates the use of ion micropackets for two-dimensional mass spectrometry, they are also useful for determining which peaks in ion trap precursor and neutral loss spectra are artefactual.[431] For example, **Figure 17.1d** displays four oscilloscope traces from a precursor ion scan of *m/z* 163, which ideally should only detect *m/z* 180, 194, and 208. However, *m/z* 150 produces fragments that are unstable during the scan and are

hence immediately ejected and detected alongside the resonantly ejected *m/z* 163 ions. Panel (e) is the trace of the peak at *m/z* 208. Although it is less evident than panel (b), there is regularity in the appearance of the product ion micropackets which is evidenced by the Fourier transforms in panel (f). In this case it is the *product ion micropackets* that are observed instead of the precursor ion micropackets. The experimental frequency of ejection was 217 kHz and thus the ion micropackets are observed at 434 kHz. For the artifact (*m/z* 150), no frequency information is evident in the Fourier transform (orange trace) because boundary ejection is chaotic, whereas resonance ejection is orderly.

17.3.2 2D MS/MS Using Ion Micropackets

Ion micropackets can also be used for two-dimensional mass spectrometry scans in a quadrupole ion trap. Experimentally, the 2D MS/MS scan is identical to the precursor ion scan in that precursor ions are excited in the y dimension using an ac frequency sweep (with constant rf voltage) while the product ions are ejected toward the detectors in the x dimension through application of another auxiliary waveform. In the case of the precursor scan, only a single *m/z* need be targeted, requiring a single frequency. For a 2D MS/MS scan, all possible product ions of the excited precursors must be ejected using a broadband waveform. As described in the experimental section, because the possible range of product ion *m/z* values changes with the excited precursor ion *m/z*, the frequency coverage of the broadband sum of sines also varies with time. In the experiments herein, the frequency spacing of the waveform was 1 kHz from start frequency 62 kHz to end frequency 583 kHz, but only frequencies at least 10 kHz above the y dimension excitation frequency were included in the corresponding broadband waveform at each time point.

Figure 17.2a shows the two-dimensional mass spectrum of the same set of five amphetamines. Note the beats in the peaks which are caused by the broadband waveform frequency spacing and distribution of phases. The ion micropackets are also present within these beat patterns and can be determined via Fourier transform of the individual peaks (**Figure 17.2b**). Peaks widths of 10 ms containing 20,000 points were used for the FFTs. Amphetamine and methamphetamine fragment to *m/z* 91 and *m/z* 119, and these peaks are noted. The shared product ions of 3,4-methylenedioxyamphetamine, 3,4-methylenedioxymethamphetamine, and 3,4-methylenedioxyethylamphetamine are also labeled. All labeled peaks are frequency doubled (second harmonic of the secular frequency) since these have higher intensity than the primary frequency and also give better resolution, which is unsurprising. We can calibrate the secular

frequency to *m/z* conversion through Mathieu parameters using the known product ion *m/z* values and the center of the product ion frequency profiles in panel (b). Based on these data, mass calibrated product ion spectra in **Figure 17.2c** were generated. Clearly the resolution at low *m/z* (high Mathieu q) is best (approaching unit for *m/z* 91), which is expected and discussed later.

Figure 17.3a is a 2D MS spectrum of a set of 16 fentanyl analogues and metabolites with product ion frequency spectra given in panel (b). The similarities between many of the analytes is notable, with *m/z* 188 being the primary fragment. For the isobaric mixture of butyryl, isobutyryl, and *cis*-3-methyl fentanyl, both *m/z* 188 (butyryl, isobutyryl) and *m/z* 202 (*cis*-3-methyl) are observed at the second harmonic. Norcarfentanil, carfentanil, and remifentanil share a neutral loss of 32 Da and 60 Da, which is noted, whereas sufentanil and alfentanil give neutral losses of 31 Da and 148 Da. In the case of alfentanil the neutral loss of 31 Da is not observed because that particular product ion's secular frequency (114 kHz) is within 10 kHz of the precursor ion's frequency (105 kHz) and so is not ejected when it is formed. The broadband waveform could, in principle, be altered to eject ions closer in frequency to the precursor ion, but this risks premature excitation and ejection of the precursor ions.

17.3.3 Improved Product Ion Resolution

One of the primary motivations for measuring the ejection frequency of the product ions at the detector is to improve the resolution of our previous 'frequency tagging' 2D MS method. In 'frequency tagging' low kHz beat frequencies were observed in the mass spectral peaks at the detector, with mass resolutions (m/Δm) of 15 and 13 for *m/z* 91 and *m/z* 119 of amphetamine and 10 for *m/z* 163 of MDMA (**Figure 17.4**). In order to improve the resolution, either the beats must be measured for a longer period of time (i.e. the mass spectral resolution must worsen), or a higher frequency must be measured. Conveniently, the ion micropacket method measures frequencies that are hundreds of kHz and thus should return higher resolution than the frequency tagging method. For *m/z* 91 and *m/z* 119 of amphetamine, much improved mass resolutions of 120 and 48 were obtained, and for MDMA the resolution of *m/z* 163 was increased to 20.6. We do note that these resolution values are likely fundamentally limited by ion secular frequency bandwidths and off-resonance excitation effects. Moreover, the product ions are distributed over Mathieu q space when they are formed and ejected so that higher mass resolution will almost always be obtained for the lower *m/z* product ions which have greater frequency dispersions in the ion trap than higher

m/z ions. Even so, it may be possible to improve the frequency resolution further by improving the phasing of the broadband ejection waveform or by optimizing the amplitude of the waveform.

A second advantage of the micropacket method over the frequency tagging method is that less overlap is observed in the frequency spectra. This is especially notable for the fentanyls which showed 6 peaks over a 10 kHz frequency range using frequency tagging but only two peaks (the secular frequency and second harmonic) over a 1 MHz range in the micropacket method. The third harmonic was not observed because it would not satisfy the Nyquist criterion.

17.3.4 Pressure Effects and Ion Dephasing

Even though the micropacket method shows clear advantages in terms of frequency resolution and reduction of harmonic overlap, there are additional challenges over the frequency tagging method. First, detection of the micropackets requires faster and more sensitive detection electronics, particularly the current amplifier, in order to measure signals that are hundreds of kHz instead of tens of kHz or less.

A second challenge is that the ion phase with respect to the ac waveform must be carefully controlled. The ion micropacket technique only works properly if the ion micropackets are ejected at regularly spaced intervals, that is, if the ions do not get dephased through irregularities in the waveforms or through collisions with the background gas. **Figure 17.5a** is a plot of the peak at ~315 kHz in **Figure 17.2b** (precursor ion *m/z* 136, product ion *m/z* 119) at various helium pressures. These spectra were digitally filtered using a 50-point moving average; the beats in the smoothed peaks are observed because there is a peak in the FFT every 1 kHz (due to the 1 kHz spacing in the broadband waveform). At low helium pressure (e.g. 0.52×10^{-5} torr), very little fragmentation is observed so that the frequency spectrum is blank because very few micropackets are measured. As the pressure increases, several effects are evident. First, the observed frequency shifts up, which has been attributed by Whitten *et al.*[207] to the addition of a drag term to the equations of motion, shifting the ions' Mathieu a and q parameters and thus their secular frequencies. Strangely, in nitrogen (**Figure 17.5b**), the apparent frequency shifted higher as the pressure decreased, which implies that factors other than drag are responsible for the shift. Also notable is that at higher pressures in helium, the product ion intensities increased, presumably due to greater fragmentation efficiency. In nitrogen, on the other hand, higher pressures led to decreased intensity in the FFT due to ion dephasing.[89,114,408] Although the overall ion current decreased ~25% from the lowest pressure to the highest-pressure spectrum, this cannot account for the entire loss of frequency

information. Instead, the more scattering collisions with nitrogen must knock the ions out of phase with the frequencies in the broadband waveform, causing a loss of frequency information. Helium is light enough that, even at the higher-pressure settings, frequency information was not lost. FT-ICRs experience more pronounced phase shift problems and instead use other dissociation methods such as IRMPD and ECD to keep the background pressure low.[401,408,414,416] Similar techniques could similarly benefit 2D MS in quadrupole ion traps.

17.4 Conclusion

A method of conducting two-dimensional mass spectrometry scans in a linear quadrupole ion trap by simultaneously fragmenting precursor ions and ejecting product ions while detecting the product ion micropackets at the detector has been demonstrated. The micropacket technique offers better resolution and reduced harmonic overlap than frequency tagging but also requires faster detection electronics. Due to ion dephasing effects, it may be desirable to implement an alternative method of dissociation instead of CID. For example, infrared multiphoton dissociation is used in ICR 2D MS for this very reason and may also be suitable for the quadrupole ion trap.

17.5 Acknowledgements
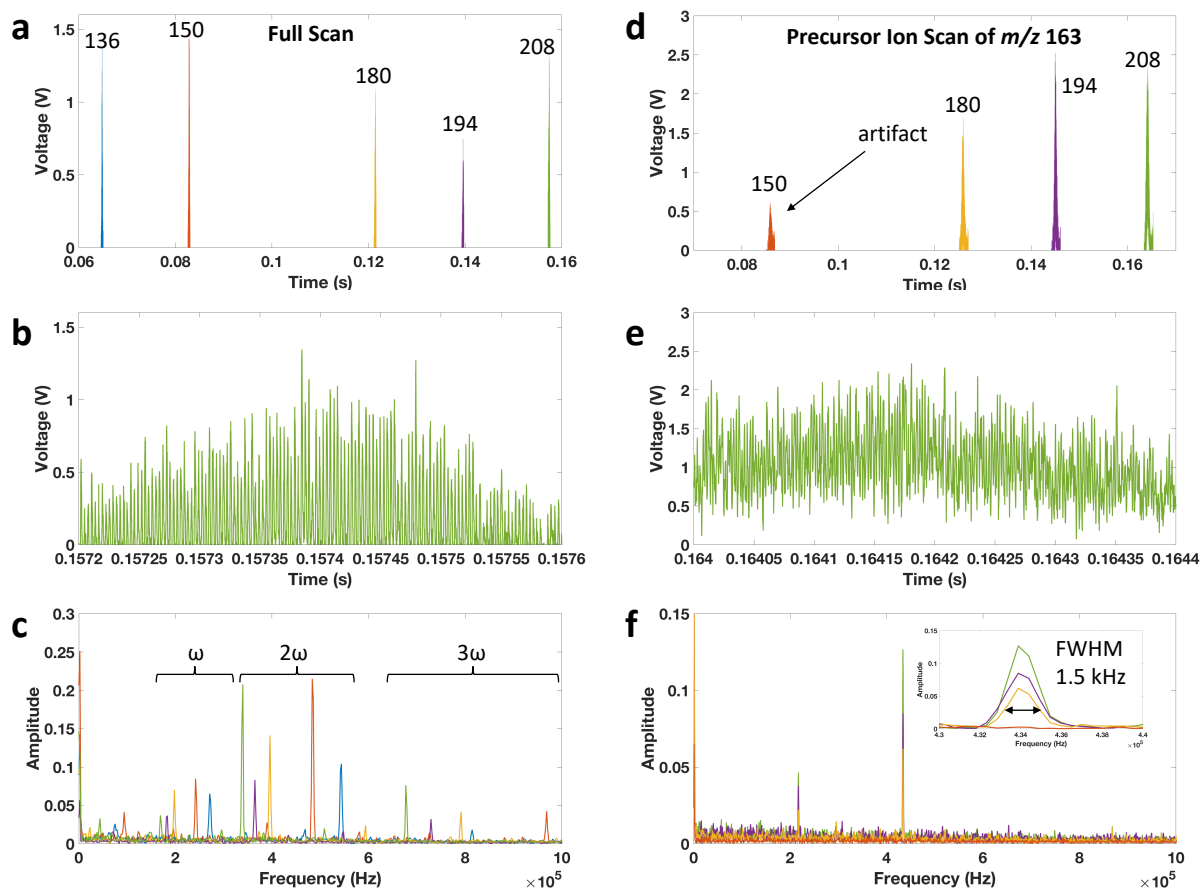
Figures

Figure 17.1. Ion micropacket detection in various modes of operation: (a) oscilloscope traces of each peak from a full scan of a set of five amphetamines and (d) a precursor ion scan of *m/z* 163, showing one artifact at *m/z* 150, (b),(e) zoomed in traces of *m/z* 208 showing the ion micropackets, and (c),(f) fast fourier transforms of each peak from (a) and (d), respectively.
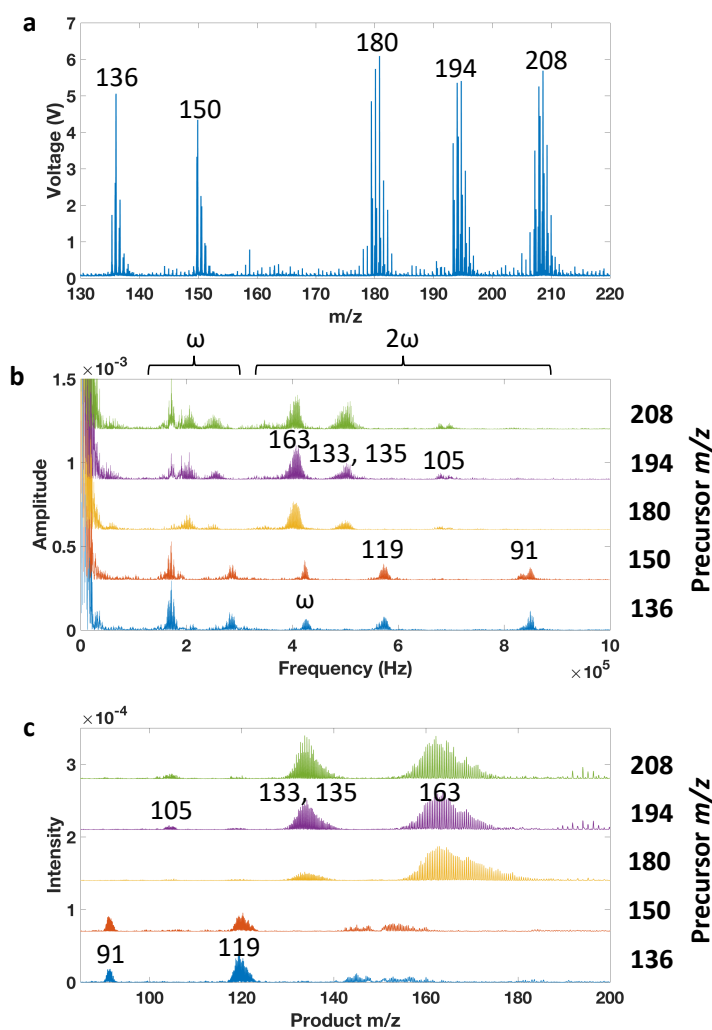
Figure 17.2. 2D MS using ion micropacket detection. (a) mass calibrated spectrum of five amphetamines and (b) frequency spectra (i.e. product ion spectra) of each peak. Known product ion *m/z* values are marked.
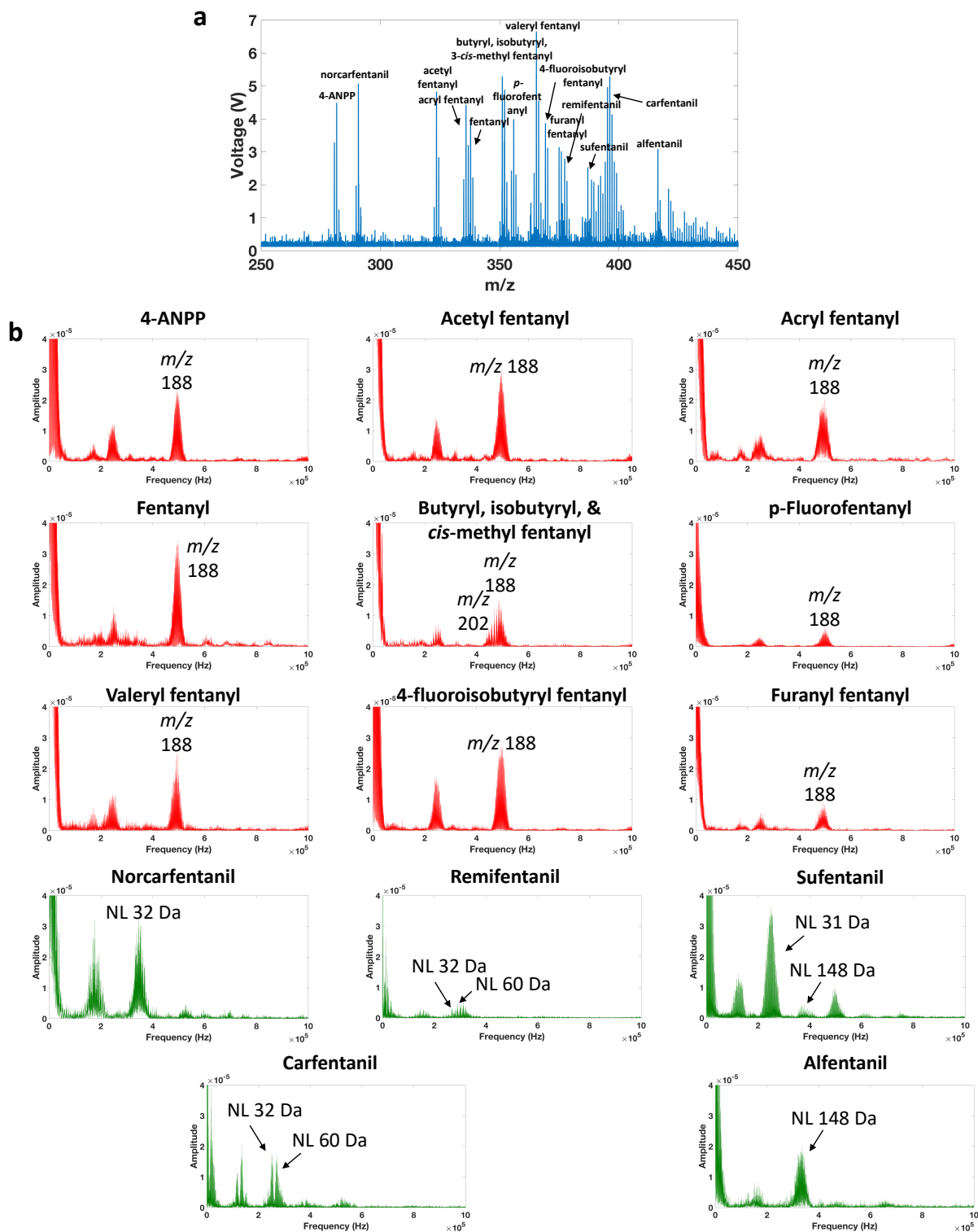
Figure 17.3. 2D MS of fentanyl analogues. (a) mass calibrated spectrum of sixteen fentanyl analogues and (b) frequency spectra (i.e. product ion spectra) of each peak. Known product ion *m/z* values are marked.
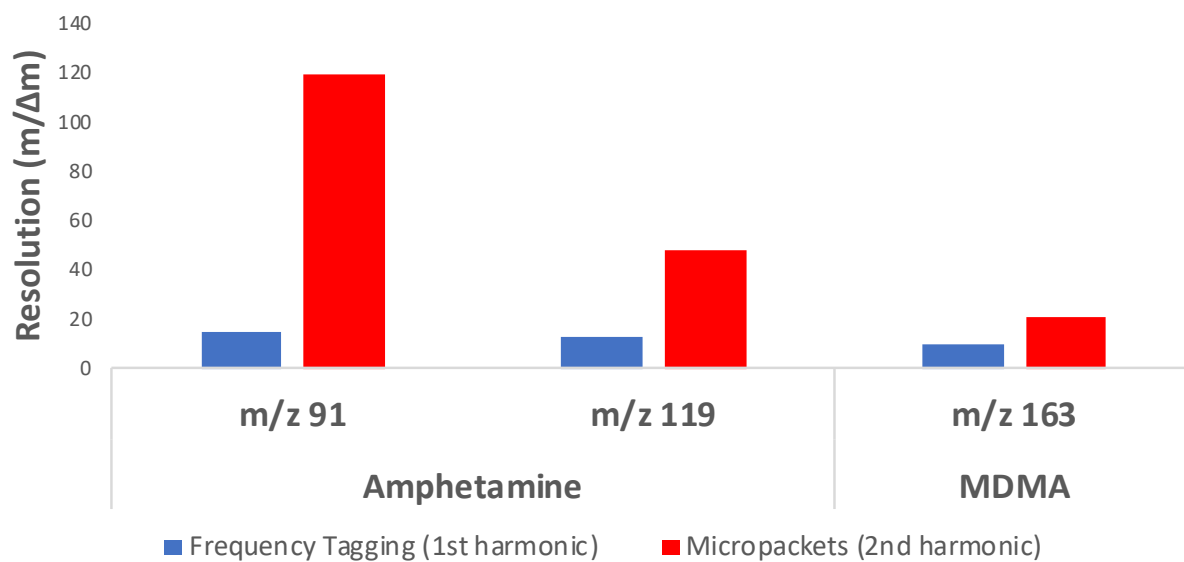
Figure 17.4. Product ion resolution comparison between 2D MS using frequency tagging (blue, 1st harmonic) and the ion micropacket method (red, 2nd harmonic).
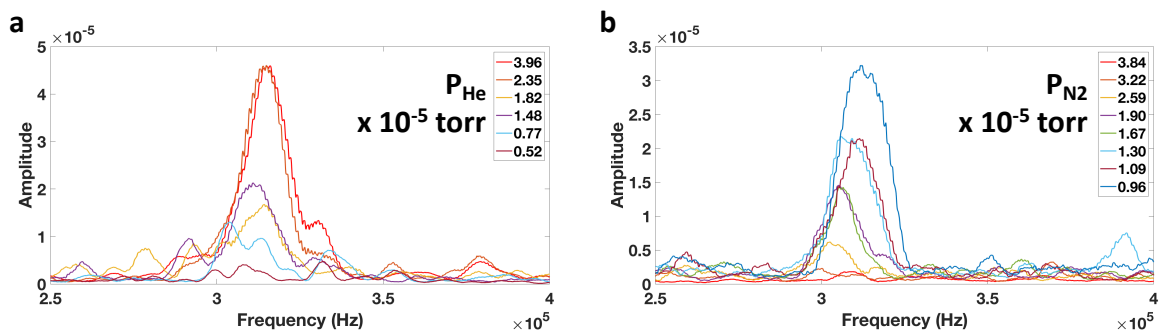
Figure 17.5. Effect of (a) helium and (b) nitrogen pressure on the FFT of *m/z* 136 in Figure 3b. The frequency spectra were smoothed using a 50-point moving average.

REFERENCES

(1) Paul, W.; Steinwedel, H. *Z. Naturforsch. Sect. A* **1953**, *8*, 448-450.

(2) Paul, W.; Reinhard, H. P.; Vonzahn, U. *Zeitschrift Fur Physik* **1958**, *152*, 143-182.

(3) Wolfgang, P.; Helmut, S., Apparatus for separating charged particles of different specific charges, U.S. Patent US2939952A, 1960.

(4) Paul, W. *Rev. Mod. Phys.* **1990**, *62*, 531.

(5) March, R. E. *J. Mass Spectrom.* **1997**, *32*, 351-369.

(6) March, R. E.; Todd, J. F. J. *Quadrupole Ion Trap Mass Spectrometry*; John Wiley & Sons: Hoboken, NJ, 2005 Quadrupole Ion Trap Mass Spectrometry.

(7) March, R. E. *Mass Spectrom. Rev.* **2009**, *28*, 961-989.

(8) March, R. E.; Todd, J. F. J. *Practical Aspects of Trapped Ion Mass Spectrometry*; CRC Press Taylor & Francis Group: Boca Raton, FL, 2010; Vol. IV.

(9) Dawson, P. H. *Quadrupole mass spectrometry and its applications*; Elsevier, 2013 Quadrupole mass spectrometry and its applications.

(10) Schwartz, J. C.; Senko, M. W.; Syka, J. E. *J. Am. Soc. Mass Spectrom.* **2002**, *13*, 659-669.

(11) Hager, J. W. *Rapid Commun. Mass Spectrom.* **2002**, *16*, 512-526.

(12) Douglas, D. J.; Frank, A. J.; Mao, D. *Mass Spectrom. Rev.* **2005**, *24*, 1-29.

(13) Fulford, J. E.; March, R. E.; Mather, R. E.; Todd, J. F. J.; Waldren, R. M. *Can. J. Spectrosc.* **1980**, *25*, 85-97.

(14) Wells, J. M.; Badman, E. R.; Cooks, R. G. *Anal Chem* **1998**, *70*, 438-444.

(15) Badman, E. R.; Johnson, R. C.; Plass, W. R.; Cooks, R. G. *Anal. Chem.* **1998**, *70*, 4896-4901.

(16) Ouyang, Z.; Wu, G.; Song, Y.; Li, H.; Plass, W. R.; Cooks, R. G. *Anal Chem* **2004**, *76*, 4595-4605.

(17) Lammert, S. A.; Plass, W. R.; Thompson, C. V.; Wise, M. B. *Int. J. Mass Spectrom.* **2001**, *212*, 25-40.

(18) Lammert, S. A.; Rockwood, A. A.; Wang, M.; Lee, M. L.; Lee, E. D.; Tolley, S. E.; Oliphant, J. R.; Jones, J. L.; Waite, R. W. *J. Am. Soc. Mass Spectrom.* **2006**, *17*, 916-922.

(19) Austin, D. E.; Wang, M.; Tolley, S. E.; Maas, J. D.; Hawkins, A. R.; Rockwood, A. L.; Tolley, H. D.; Lee, E. D.; Lee, M. L. *Anal. Chem.* **2007**, *79*, 2927-2932.

(20) Collings, B. A.; Douglas, D. J. *J. Am. Soc. Mass Spectrom.* **2000**, *11*, 1016-1022.

(21) Collings, B. A.; Sudakov, M.; Londry, F. A. *J. Am. Soc. Mass Spectrom.* **2002**, *13*, 577-586.

(22) Tian, Y.; Higgs, J.; Li, A.; Barney, B.; Austin, D. E. *J Mass Spectrom* **2014**, *49*, 233-240.

(23) Michaud, A. L.; Frank, A. J.; Ding, C.; Zhao, X.; Douglas, D. J. *J Am Soc Mass Spectrom* **2005**, *16*, 835-849.

(24) Wang, Y.; Franzen, J. *Int. J. Mass Spectrom. Ion Processes* **1994**, *132*, 155-172.

(25) Franzen, J. *Int. J. Mass Spectrom. Ion Proc.* **1994**, *130*, 15-40.

(26) Dawson, P. H.; Whetten, N. R. *Int. J. Mass Spectrom. Ion Phys.* **1969**, *2*, 45-59.

(27) Alheit, R.; Kleineidam, S.; Vedel, F.; Vedel, M.; Werth, G. *Int. J. Mass Spectrom. Ion Processes* **1996**, *154*, 155-169.

(28) Chu, X. Z.; Holzki, M.; Alheit, R.; Werth, G. *Int. J. Mass Spectrom. Ion Processes* **1998**, *173*, 107-112.

(29) Guidugli, F.; Traldi, P. *Rapid Commun. Mass Spectrom.* **1991**, *5*, 343-348.

(30) Morand, K. L.; Lammert, S. A.; Cooks, R. G. *Rapid Commun. Mass Spectrom.* **2005**, *5*, 491.

(31) Eades, D. M.; Johnson, J. V.; Yost, R. A. *J. Am. Soc. Mass Spectrom.* **1993**, *4*, 917-929.

(32) Moxom, J.; Reilly, P. T.; Whitten, W. B.; Ramsey, J. M. *Rapid Commun. Mass Spectrom.* **2002**, *16*, 755-760.

(33) Franzen, J. *Int. J. Mass Spectrom. Ion Processes* **1993**, *125*, 165-170.

(34) Splendore, M.; Marquette, E.; Oppenheimer, J.; Huston, C.; Wells, G. *Int. J. Mass Spectrom.* **1999**, *191*, 129-143.

(35) Asam, M. R.; Glish, G. L. *J. Am. Soc. Mass Spectrom.* **1997**, *8*, 987-995.

(36) Wang, Y.; Huang, Z.; Jiang, Y.; Xiong, X.; Deng, Y.; Fang, X.; Xu, W. *J. Mass Spectrom.* **2013**, *48*, 937-944.

(37) Fulford, J. E.; March, R. E. *Int. J. Mass Spectrom. Ion Phys.* **1978**, *26*, 155-162.

(38) Stafford, G. C.; Kelley, P. E.; Syka, J. E. P.; Reynolds, W. E.; Todd, J. F. J. *Int. J. Mass Spectrom. Ion Processes* **1984**, *60*, 85-98.

(39) Fulford, J. E. *J. Vac. Sci. Technol.* **1980**, *17*, 829.

(40) Kaiser, R. E.; Louris, J. N.; Amy, J. W.; Cooks, R. G. *Rapid Commun. Mass Spectrom.* **1989**, *7*, 225-229.

(41) Kaiser, R. E.; Cooks, R. G.; Stafford, G. C.; Syka, J. E. P.; Hemberger, P. H. *Int. J. Mass Spectrom. Ion Processes* **1991**, *106*, 79-115.

(42) Doroshenko, V. M.; Cotter, R. J. *Rapid Commun. Mass Spectrom.* **1994**, *8*, 766-776.

(43) Londry, F. A.; Hager, J. W. *J. Am. Soc. Mass Spectrom.* **2003**, *14*, 1130-1147.

(44) Todd, J.; Penman, A.; Smith, R. *Int. J. Mass Spectrom. Ion Processes* **1991**, *106*, 117-135.

(45) Prentice, B. M.; McLuckey, S. A. *Anal. Chem.* **2012**, *84*, 7562-7569.

(46) Landais, B.; Beaugrand, C.; Capron-Dukan, L.; Sablier, M.; Simonneau, G.; Rolando, C. *Rapid Commun. Mass Spectrom.* **1998**, *12*, 302-306.

(47) Schlunegger, U. P.; Stoeckli, M.; Caprioli, R. M. *Rapid Commun. Mass Spectrom.* **1999**, *13*, 1792-1796.

(48) Badman, E. R.; Cooks, R. G. *Anal. Chem.* **2000**, *72*, 5079-5086.

(49) Welling, M.; Schuessler, H. A.; Thompson, R. I.; Walther, H. *Int. J. Mass Spectrom. Ion Processes* **1998**, *172*, 95-114.

(50) Evans-Nguyen, T.; Becker, L.; Doroshenko, V.; Cotter, R. J. *Int. J. Mass Spectrom.* **2008**, *278*, 170-177.

(51) Guan, S.; Marshall, A. G. *Anal. Chem.* **1993**, *65*, 1288-1294.

(52) Louris, J. N.; Cooks, R. G.; Syka, J. E. P.; Kelley, P. E.; Stafford, G. C.; Todd, J. F. J. *Anal. Chem.* **1987**, *59*, 1677-1685.

(53) Louris, J. N.; Brodbeltlustig, J. S.; Cooks, R. G.; Glish, G. L.; Vanberkel, G. J.; Mcluckey, S. A. *Int. J. Mass Spectrom. Ion Processes* **1990**, *96*, 117-137.

(54) McLuckey, S. A.; Goeringer, D. E. *J. Mass Spectrom.* **1997**, *32*, 461-474.

(55) Danell, R. M.; Danell, A. S.; Glish, G. L.; Vachet, R. W. *J. Am. Soc. Mass Spectrom.* **2003**, *14*, 1099-1109.

(56) Hager, J. W. *J. Am. Soc. Mass Spectrom.* **2009**, *20*, 443-450.

(57) Yost, R. A.; Enke, C. G. *J. Am. Chem. Soc.* **1978**, *100*, 2274-2275.

(58) Yost, R. A.; Enke, C. G. *Anal. Chem.* **1979**, *51*, 1251-1264.

(59) Schwartz, J. C.; Wade, A. P.; Enke, C. G.; Cooks, R. G. *Anal. Chem.* **1990**, *62*, 1809-1818.

(60) McClellan, J. E.; Quarmby, S. T.; Yost, R. A. *Anal. Chem.* **2002**, *74*, 5799-5806.

(61) Second, T. P.; Blethrow, J. D.; Schwartz, J. C.; Merrihew, G. E.; MacCoss, M. J.; Swaney, D. L.; Russell, J. D.; Coon, J. J.; Zabrouskov, V. *Anal. Chem.* **2009**, *81*, 7757-7765.

(62) Li, L.; Zhou, X.; Hager, J. W.; Ouyang, Z. *Analyst* **2014**, *139*, 4779-4784.

(63) Olsen, J. V.; Schwartz, J. C.; Griep-Raming, J.; Nielsen, M. L.; Damoc, E.; Denisov, E.; Lange, O.; Remes, P.; Taylor, D.; Splendore, M.; Wouters, E. R.; Senko, M.; Makarov, A.; Mann, M.; Horning, S. *Mol. Cell. Proteomics* **2009**, *8*, 2759-2769.

(64) Senko, M. W.; Remes, P. M.; Canterbury, J. D.; Mathur, R.; Song, Q.; Eliuk, S. M.; Mullen, C.; Earley, L.; Hardman, M.; Blethrow, J. D. *Anal. Chem.* **2013**, *85*, 11710-11714.

(65) Williams, J. D.; Cox, K. A.; Cooks, R. G.; Mcluckey, S. A.; Hart, K. J.; Goeringer, D. E. *Anal. Chem.* **1994**, *66*, 725-729.

(66) Makarov, A. A. *Anal. Chem.* **1996**, *68*, 4257-4263.

(67) Zhao, X.; Granot, O.; Douglas, D. J. *J Am Soc Mass Spectrom* **2008**, *19*, 510-519.

(68) Xiong, C.; Zhou, X.; Zhang, N.; Zhan, L.; Chen, Y.; Chen, S.; Nie, Z. *J Am Soc Mass Spectrom* **2015**, *26*, 1338-1348.

(69) Badman, E. R.; Graham Cooks, R. *J. Mass Spectrom.* **2000**, *35*, 659-671.

(70) Ouyang, Z.; Cooks, R. G. *Annu. Rev. Anal. Chem.* **2009**, *2*, 187-214.

(71) Snyder, D. T.; Pulliam, C. J.; Ouyang, Z.; Cooks, R. G. *Anal. Chem.* **2016**, *88*, 2-29.

(72) Pulliam, C. J.; Bain, R. M.; Wiley, J. S.; Ouyang, Z.; Cooks, R. G. *J. Am. Soc. Mass Spectrom.* **2015**, *26*, 224-230.

(73) Kornienko, O.; Reilly, P. T. A.; Whitten, W. B.; Ramsey, J. M. *Rapid Communications in Mass Spectrometry* **1999**, *13*, 50-53.

(74) Blakeman, K. H.; Wolfe, D.; Cavanaugh, C.; Ramsey, J. M. *Anal. Chem.* **2016**, *88*, 5378-5384.

(75) Gao, L.; Cooks, R. G.; Ouyang, Z. *Anal. Chem.* **2008**, *80*, 4026-4032.

(76) Zhai, Y.; Feng, Y.; Wei, Y.; Wang, Y.; Xu, W. *Analyst* **2015**, *140*, 3406-3414.

(77) Zhai, Y.; Jiang, T.; Huang, G.; Wei, Y.; Xu, W. *Analyst* **2016**, *141*, 5404-5411.

(78) Si, X.; Hu, L.; Xu, W.; Li, H.; Li, C. *International Journal of Mass Spectrometry* **2017**, *423*, 15-19.

(79) Li, X.; Danell, R. M.; Pinnick, V. T.; Grubisic, A.; van Amerom, F.; Arevalo, R. D.; Getty, S. A.; Brinckerhoff, W. B.; Southard, A. E.; Gonnsen, Z. D.; Adachi, T. *Int. J. Mass Spectrom.* **2017**, *422*, 177-187.

(80) Peng, Y.; Austin, D. E. *TrAC* **2011**, *30*, 1560-1567.

(81) Miller, P. E.; Denton, M. B. *J. Chem. Educ.* **1986**, *63*, 617-622.

(82) Stafford, G. C.; Kelley, P. E.; Syka, J. E. P.; Reynolds, W. E.; Todd, J. F. J. *Int. J. Mass Spectrom. Ion Proc.* **1984**, *60*, 85-98.

(83) Goeringer, D. E.; Whitten, W. B.; Ramsey, J. M.; Mcluckey, S. A.; Glish, G. L. *Analytical Chemistry* **1992**, *64*, 1434-1439.

(84) Kaiser, R. E.; Cooks, R. G.; Stafford, G. C.; Syka, J. E. P.; Hemberger, P. H. *Int. J. Mass Spectrom. Ion Proc.* **1991**, *106*, 79-115.

(85) Nie, Z.; Cui, F.; Chu, M.; Chen, C.-H.; Chang, H.-C.; Cai, Y. *Int. J. Mass Spectrom.* **2008**, *270*, 8-15.

(86) Ding, L.; Sudakov, M.; Kumashiro, S. *Int. J. Mass Spectrom.* **2002**, *221*, 117-138.

(87) Wang, D.; van Amerom, F. H.; Evans-Nguyen, T. *Anal. Chem.* **2013**, *85*, 10935-10940.

(88) Ding, L.; Sudakov, M.; Brancia, F. L.; Giles, R.; Kumashiro, S. *J. Mass Spectrom.* **2004**, *39*, 471-484.

(89) Wells, J. M.; Plass, W. R.; Patterson, G. E.; Zheng, O. Y.; Badman, E. R.; Cooks, R. G. *Anal. Chem.* **1999**, *71*, 3405-3415.

(90) Alfred, R. L.; Londry, F. A.; March, R. E. *Int. J. Mass Spectrom. Ion Proc.* **1993**, *125*, 171-185.

(91) Snyder, D. T.; Pulliam, C. J.; Cooks, R. G. *Rapid Commun. Mass Spectrom.* **2016**, *30*, 1190-1196.

(92) Syka, J. E. P.; Louris, J. N.; Kelley, P. E.; Stafford, G. C.; Reynolds, W. E., Method of operating ion trap detector in MS/MS mode, U.S. Patent 4,736,101, 1988.

(93) Bier, M. E.; Syka, J. E. P., Ion trap mass spectrometer system and method, U.S. Patent 5,420,425, 1995.

(94) Welling, M.; Schuessler, H. A.; Thompson, R. I.; Walther, H. *Int. J. Mass Spectrom.* **1998**, *172*, 95-114.

(95) Roth, B.; Frohlich, U.; Schiller, S. *Phys. Rev. Lett.* **2005**, *94*, 053001.

(96) Wang, M.; Quist, H. E.; Hansen, B. J.; Peng, Y.; Zhang, Z.; Hawkins, A. R.; Rockwood, A. L.; Austin, D. E.; Lee, M. L. *J. Am. Soc. Mass Spectrom.* **2011**, *22*, 369-378.

(97) Peng, Y.; Hansen, B. J.; Quist, H.; Zhang, Z.; Wang, M.; Hawkins, A. R.; Austin, D. E. *Anal. Chem.* **2011**, *83*, 5578-5584.

(98) Johnson, J. V.; Pedder, R. E.; Yost, R. A. *International Journal of Mass Spectrometry and Ion Processes* **1991**, *106*, 197-212.

(99) Snyder, D. T.; Pulliam, C. J.; Cooks, R. G. *Rapid Commun. Mass Spectrom.* **2016**, *30*, 800-804.

(100) Li, L.; Chen, T. C.; Ren, Y.; Hendricks, P. I.; Cooks, R. G.; Ouyang, Z. *Anal. Chem.* **2014**, *86*, 2909-2916.

(101) Wu, G.; Cooks, R. G.; Ouyang, Z.; Yu, M.; Chappell, W. J.; Plass, W. R. *J. Am. Soc. Mass. Spectrom.* **2006**, *17*, 1216-1228.

(102) Schwartz, J. C.; Syka, J. E.; Jardine, I. *J. Am. Soc. Mass Spectrom.* **1991**, *2*, 198-204.

(103) Schwartz, J. C.; Senko, M. W.; Syka, J. E. *J Am Soc Mass Spectrom* **2002**, *13*, 659-669.

(104) Xu, W.; Song, Q.; Smith, S. A.; Chappell, W. J.; Ouyang, Z. *J. Am. Soc. Mass Spectrom.* **2009**, *20*, 2144-2153.

(105) Franzen, J.; Gabling, R.; Heinen, G.; Weiss, G., Method of mass analyzing a sample by use of a quistor, U.S. Patent 4,882,484, Nov. 21, 1989, 1989.

(106) Snyder, D. T.; Pulliam, C. J.; Wiley, J. S.; Duncan, J.; Cooks, R. G. *J. Am. Soc. Mass Spectrom.* **2016**, *27*, 1243-1255.

(107) Johnson, J. V.; Pedder, R. E.; Yost, R. A. *Int. J. Mass Spectrom. Ion Proc.* **1991**, *106*, 197-212.

(108) Schlunegger, U. P.; Stoeckli, M.; Caprioli, R. M. *Rapid Commun Mass Spectrom* **1999**, *13*, 1792-1796.

(109) Ding, L.; Kumashiro, S. *Rapid Commun. Mass Spectrom.* **2006**, *20*, 3-8.

(110) Wells, J. M.; Plass, W. R.; Patterson, G. E.; Ouyang, Z.; Badman, E. R.; Cooks, R. G. *Anal. Chem.* **1999**, *71*, 3405-3415.

(111) Welling, M.; Schuessler, H. A.; Thompson, R. I.; Walther, H. *Int. J. Mass Spectrom. Ion Proc.* **1998**, *172*, 95-114.

(112) Cox, K. A.; Cleven, C. D.; Cooks, R. G. *Int. J. Mass Spectrom. Ion Proc.* **1995**, *144*, 47-65.

(113) Wells, J. M.; Plass, W. A.; Cooks, R. G. *Anal. Chem.* **2000**, *72*, 2677-2683.

(114) Plass, W. R.; Li, H.; Cooks, R. G. *Int. J. Mass Spectrom.* **2003**, *228*, 237-267.

(115) Wang, Y.; Franzen, J.; Wanczek, K. P. *Int. J. Mass Spectrom. Ion Proc.* **1993**, *124*, 125-144.

(116) March, R. E. *Rapid Commun. Mass Spectrom.* **1998**, *12*, 1543-1554.

(117) March, R. E. *Int. J. Mass Spectrom.* **2000**, *200*, 285-312.

(118) Fulford, J. E.; Nhu-Hoa, D.; Hughes, R. J.; March, R. E.; Bonner, R. F.; Wong, G. J. *J. Vac. Sci. Technol.* **1980**, *17*, 829.

(119) Franzen, J. *Int. J. Mass Spectrom. Ion Processes* **1994**, *130*, 15-40.

(120) Zhang, X.; Wang, Y.; Hu, L.; Guo, D.; Fang, X.; Zhou, M.; Xu, W. *J. Am. Soc. Mass Spectrom.* **2016**, *27*, 1256-1262.

(121) Chen, E. X.; Gehm, M.; Danell, R.; Wells, M.; Glass, J. T.; Brady, D. *J. Am. Soc. Mass Spectrom.* **2014**, *25*, 1295-1304.

(122) Lu, I. C.; Lin, J. L.; Lai, S. H.; Chen, C. H. *Anal. Chem.* **2011**, *83*, 8273-8277.

(123) Johnson, J. V.; Pedder, R. E.; Yost, R. A. *Int. J. Mass Spectrom. Ion Processes* **1991**, *106*, 197-212.

(124) Jiang, L. F.; Moini, M. *J. Am. Soc. Mass Spectrom.* **1992**, *3*, 842-846.

(125) Qiao, H.; Gao, C.; Mao, D.; Konenkov, N.; Douglas, D. J. *Rapid Commun. Mass Spectrom.* **2011**, *25*, 3509-3520.

(126) Kaiser, R. E.; Louris, J. N.; Amy, J. W.; Cooks, R. G. *Rapid Commun. Mass Spectrom.* **1989**, *3*, 225-229.

(127) Goeringer, D. E.; Whitten, W. B.; Ramsey, J. M.; Mcluckey, S. A.; Glish, G. L. *Anal. Chem.* **1992**, *64*, 1434-1439.

(128) Arnold, N. S.; Hars, C.; Meuzelaar, H. L. *J. Am. Soc. Mass Spectrom.* **1994**, *5*, 676-688.

(129) Tomachev, A. V.; Udseth, H. R.; Smith, R. D. *Rapid Commun. Mass Spectrom.* **2000**, *14*, 1907-1913.

(130) Knight, R. D. *Int. J. Mass Spectrom. Ion Phys.* **1983**, *51*, 127-131.

(131) Fulford, J. E.; Nhu-Hoa, D.; Hughes, R. J.; March, R. E.; Bonner, R. F.; Wong, G. J. *J. Vac. Sci. Technol.* **1980**, *17*, 829-835.

(132) Todd, J. F. J.; Penman, A. D.; Smith, R. D. *Int. J. Mass Spectrom. Ion Processes* **1991**, *106*, 117-135.

(133) Snyder, D. T.; Pulliam, C. J.; Cooks, R. G. *Rapid Commun. Mass Spectrom.* **2016**, *30*, 2369-2378.

(134) Snyder, D. T.; Peng, W.-P.; Cooks, R. G. *Chemical Physics Letters* **2017**, *668*, 69-89.

(135) Snyder, D. T.; Pulliam, C. J.; Cooks, R. G. *Int. J. Mass Spectrom.* **2017**, *422*, 154-161.

(136) Leshin, L. A.; Mahaffy, P. R.; Webster, C. R.; Cabane, M.; Coll, P.; Conrad, P. G.; Archer, P. D., Jr.; Atreya, S. K.; Brunner, A. E.; Buch, A.; Eigenbrode, J. L.; Flesch, G. J.; Franz, H. B.; Freissinet, C.; Glavin, D. P.; McAdam, A. C.; Miller, K. E.; Ming, D. W.; Morris, R. V.; Navarro-Gonzalez, R.; Niles, P. B.; Owen, T.; Pepin, R. O.; Squyres, S.; Steele, A.; Stern, J. C.; Summons, R. E.; Sumner, D. Y.; Sutter, B.; Szopa, C.; Teinturier, S.; Trainer, M. G.; Wray, J. J.; Grotzinger, J. P.; Team, M. S. L. S. *Science* **2013**, *341*, 1238937.

(137) Vasavada, A. R.; Grotzinger, J. P.; Arvidson, R. E.; Calef, F. J.; Crisp, J. A.; Gupta, S.; Hurowitz, J.; Mangold, N.; Maurice, S.; Schmidt, M. E.; Wiens, R. C.; Williams, R. M. E.; Yingst, R. A. *J. Geophys. Res.-Planet* **2014**, *119*, 1134-1161.

(138) Freissinet, C.; Glavin, D. P.; Mahaffy, P. R.; Miller, K. E.; Eigenbrode, J. L.; Summons, R. E.; Brunner, A. E.; Buch, A.; Szopa, C.; Archer, P. D.; Franz, H. B.; Atreya, S. K.; Brinckerhoff, W. B.; Cabane, M.; Coll, P.; Conrad, P. G.; Des Marais, D. J.; Dworkin, J. P.; Fairen, A. G.; Francois, P.; Grotzinger, J. P.; Kashyap, S.; ten Kate, I. L.; Leshin, L. A.; Malespin, C. A.; Martin, M. G.; Martin-Torres, F. J.; McAdam, A. C.; Ming, D. W.; Navarro-Gonzalez, R.; Pavlov, A. A.; Prats, B. D.; Squyres, S. W.; Steele, A.; Stern, J. C.; Sumner, D. Y.; Sutter, B.; Zorzano, M. P.; Team, M. S. *J. Geophys. Res.-Planet* **2015**, *120*, 495-514.

(139) Brinckerhoff, W. B.; Pinnick, V. T.; van Amerom, F. H. W.; Danell, R. M.; Arevalo, R. D.; Atanassova, M. S.; Li, X.; Mahaffy, P. R.; Cotter, R. J.; Goesmann, F.; Steininger, H.; Team, M. *2013 Ieee Aerospace Conference* **2013** Mars Organic Molecule Analyzer (MOMA) Mass Spectrometer for ExoMars 2018 and Beyond.

(140) Cai, Y.; Peng, W.-P.; Kuo, S. J.; Chang, H. C. *Int. J. Mass Spectrom.* **2002**, *214*, 63-73.

(141) Murphy, J. P., 3rd; Yost, R. A. *Rapid Commun. Mass Spectrom.* **2000**, *14*, 270-273.

(142) Wells, J. M.; Plass, W. R.; Cooks, R. G. *Anal. Chem.* **2000**, *72*, 2677-2683.

(143) Li, H. Y.; Peng, Y. N.; Plass, W. R.; Cooks, R. G. *Int. J. Mass Spectrom.* **2003**, *222*, 481-491.

(144) Dehmelt, H. G. *Adv. At. Mol. Phys.* **1968**, *3*, 53-72.

(145) Konig, S.; Fales, H. M. *J. Am. Soc. Mass Spectrom.* **1999**, *10*, 273-276.

(146) Fulford, J. E.; March, R. E. *Int. J. Mass Spectrom. Ion Phys.* **1978**, *26*, 155-162.

(147) McLuckey, S. A.; Goeringer, D. E.; Glish, G. L. *J. Am. Soc. Mass Spectrom.* **1991**, *2*, 11-21.

(148) Guan, S.; Marshall, A. G. *Int. J. Mass Spectrom. Ion Processes* **1996**, *157/158*, 5-37.

(149) Kenny, D. V.; Callahan, P. J.; Gordon, S. M.; Stiller, S. W. *Rapid Commun. Mass Spectrom.* **1993**, *7*.

(150) Goeringer, D. E.; Asano, K. G.; Mcluckey, S. A.; Hoekman, D.; Stiller, S. W. *Analytical Chemistry* **1994**, *66*, 313-318.

(151) Xue, B.; Sun, L.; Huang, Z.; Gao, W.; Fan, R.; Cheng, P.; Ding, L.; Ma, L.; Zhou, Z. *Analyst* **2016** 10.1039/c6an01118g.

(152) Singh, R.; Jayaram, V.; Reilly, P. T. A. *Int. J. Mass Spectrom.* **2013**, *343-344*, 45-49.

(153) Lopez, L. L.; Tiller, P. R.; Senko, M. W.; Schwartz, J. C. *Rapid Commun. Mass Spectrom.* **1999**, *13*, 663-668.

(154) Schwartz, J. C.; Syka, J. E. P.; Quarmby, S. T. In *The 53rd ASMS Conference on Mass Spectrometry and Allied Topics*: San Antonio, TX, 2005.

(155) Cunningham, C., Jr.; Glish, G. L.; Burinsky, D. J. *J. Am. Soc. Mass Spectrom.* **2006**, *17*, 81-84.

(156) Collin, O. L.; Beier, M.; Jackson, G. P. *Anal. Chem.* **2007**, *79*, 5468-5473.

(157) Laskay, U. A.; Hyland, J. J.; Jackson, G. P. *J. Am. Soc. Mass Spectrom.* **2007**, *18*, 749-761.

(158) Laskay, U. A.; Jackson, G. P. *Rapid Commun. Mass Spectrom.* **2008**, *22*, 2342-2348.

(159) Murrell, J.; Despeyroux, D.; Lammert, S. A.; Stephenson, J. L.; Goeringer, D. E. *J. Am. Soc. Mass Spectrom.* **2003**, *14*, 785-789.

(160) Qin, J.; Chait, B. T. *Anal. Chem.* **1996**, *68*, 2108-2112.

(161) Snyder, D. T.; Cooks, R. G. *J Am Soc Mass Spectrom* **2016**, *27*, 1906-1913.

(162) Vachet, R. W.; Glish, G. L. *Anal. Chem.* **1998**, *70*, 340-346.

(163) Brodbelt, J. S.; Wilson, J. J. *Mass Spectrom. Rev.* **2009**, *28*, 390-424.

(164) Brodbelt, J. S. *Chem. Soc. Rev.* **2014**, *43*, 2757-2783.

(165) Brodbelt, J. S. *Anal. Chem.* **2016**, *88*, 30-51.

(166) Dongre, A. R.; Somogyi, A.; Wysocki, V. H. *J. Mass Spectrom.* **1996**, *31*, 339-350.

(167) Lammert, S. A.; Cooks, R. G. *J. Am. Soc. Mass Spectrom.* **1991**, *2*, 487-491.

(168) Ma, X.; Ouyang, Z. *Trends Anal. Chem.* **2016** 10.1016/j.trac.2016.04.009.

(169) Guan, S. *J. Chem. Phys.* **1989**, *91*, 775-777.

(170) Sonl, M. H.; Cooks, R. G. *Anal. Chem.* **1994**, *66*, 2488-2496.

(171) Snyder, D. T.; Fedick, P. W.; Cooks, R. G. *Anal Chem* **2016**, *88*, 9572-9581.

(172) Snyder, D. T.; Cooks, R. G. *J. Am. Soc. Mass Spectrom.* **2016**, *27*, 1914-1921.

(173) Mach, P. M.; Wright, K. C.; Verbeck, G. F. *J. Am. Soc. Mass Spectrom.* **2015**, *26*, 281-285.

(174) O'Leary, A. E.; Hall, S. E.; Vircks, K. E.; Mulligan, C. C. *Anal. Methods* **2015** 10.1039/c5ay00511f.

(175) Mach, P. M.; McBride, E. M.; Sasiene, Z. J.; Brigance, K. R.; Kennard, S. K.; Wright, K. C.; Verbeck, G. F. *Anal. Chem.* **2015**, *87*, 11501-11508.

(176) Pulliam, C. J.; Wei, P.; Snyder, D. T.; Wang, X.; Ouyang, Z.; Pielak, R. M.; Graham Cooks, R. *Analyst* **2016**, *141*, 1633-1636.

(177) Huang, G.; Gao, L.; Duncan, J.; Harper, J. D.; Sanders, N. L.; Ouyang, Z.; Cooks, R. G. *J. Am. Soc. Mass Spectrom.* **2010**, *21*, 132-135.

(178) Sanders, N. L.; Kothari, S.; Huang, G. M.; Salazar, G.; Cooks, R. G. *Anal. Chem.* **2010**, *82*, 5313-5316.

(179) Takats, Z.; Wiseman, J. M.; Gologan, B.; Cooks, R. G. *Science* **2004**, *306*, 471-473.

(180) Wells, J. M.; Roth, M. J.; Keil, A. D.; Grossenbacher, J. W.; Justes, D. R.; Patterson, G. E.; Barket, D. J., Jr. *J. Am. Soc. Mass Spectrom.* **2008**, *19*, 1419-1424.

(181) Liu, J.; Wang, H.; Manicke, N. E.; Lin, J. M.; Cooks, R. G.; Ouyang, Z. *Anal. Chem.* **2010**, *82*, 2463-2471.

(182) Wang, H.; Liu, J.; Cooks, R. G.; Ouyang, Z. *Angew. Chem. Int. Ed. Engl.* **2010**, *49*, 877-880.

(183) Jjunju, F. P. M.; Li, A.; Badu-Tawiah, A.; Wei, P.; Li, L.; Ouyang, Z.; Roqan, I. S.; Cooks, R. G. *Analyst* **2013**, *138*, 3740.

(184) Liu, J.; Wang, H.; Cooks, R. G.; Ouyang, Z. *Anal. Chem.* **2011**, *83*, 7608-7613.

(185) Klampfl, C. W.; Himmelsbach, M. *Anal. Chim. Acta* **2015**, *890*, 44-59.

(186) Li, A. Y.; Hollerbach, A.; Luo, Q. J.; Cooks, R. G. *Angew. Chem. Int. Ed. Engl.* **2015**, *54*, 6893-6895.

(187) Hu, B.; So, P. K.; Chen, H.; Yao, Z. P. *Anal. Chem.* **2011**, *83*, 8201-8207.

(188) Gomez-Rios, G. A.; Pawliszyn, J. *Angew. Chem. Int. Ed. Engl.* **2014**, *53*, 14503-14507.

(189) Albert, A.; Engelhard, C. *Anal. Chem.* **2012**, *84*, 10657-10664.

(190) Zhai, Y.; Jiang, T.; Huang, G.; Wei, Y.; Xu, W. *Analyst* **2016** 10.1039/C6AN00956E.

(191) Harper, J. D.; Charipar, N. A.; Mulligan, C. C.; Zhang, X.; Cooks, R. G.; Ouyang, Z. *Anal. Chem.* **2008**, *80*, 9097-9104.

(192) Wiley, J. S.; Shelley, J. T.; Cooks, R. G. *Anal. Chem.* **2013**, *85*, 6545-6552.

(193) Hendricks, P. I.; Dalgleish, J. K.; Shelley, J. T.; Kirleis, M. A.; McNicholas, M. T.; Li, L.; Chen, T. C.; Chen, C. H.; Duncan, J. S.; Boudreau, F.; Noll, R. J.; Denton, J. P.; Roach, T. A.; Ouyang, Z.; Cooks, R. G. *Anal. Chem.* **2014**, *86*, 2900-2908.

(194) Na, N.; Zhao, M.; Zhang, S.; Yang, C.; Zhang, X. *J. Am. Soc. Mass Spectrom.* **2007**, *18*, 1859-1862.

(195) Jjunju, F. P.; Maher, S.; Li, A.; Badu-Tawiah, A. K.; Taylor, S.; Cooks, R. G. *J. Am. Soc. Mass Spectrom.* **2015**, *26*, 271-280.

(196) Johnson, R. C.; Cooks, R. G.; Allen, T. M.; Cisper, M. E.; Hemberger, P. H. *Mass Spectrom. Rev.* **2000**, *1*, 1-37.

(197) Riter, L. S.; Peng, Y.; Noll, R. J.; Patterson, G. E.; Aggerholm, T.; Cooks, R. G. *Anal. Chem.* **2002**, *74*, 6154-6162.

(198) Wei, Y.; Bian, C.; Ouyang, Z.; Xu, W. *Rapid Commun. Mass Spectrom.* **2015**, *29*, 701-706.

(199) Chen, C. H.; Chen, T. C.; Zhou, X.; Kline-Schoder, R.; Sorensen, P.; Cooks, R. G.; Ouyang, Z. *J. Am. Soc. Mass Spectrom.* **2015**, *26*, 240-247.

(200) Keil, A.; Talaty, N.; Janfelt, C.; Noll, R.; Gao, L.; Ouyang, Z.; Cooks, R. G. *Anal. Chem.* **2007**, *79*, 7734-7739.

(201) Tian, Y.; Higgs, J.; Li, A.; Barney, B.; Austin, D. E. *J. Mass Spectrom.* **2014**, *49*, 233-240.

(202) Wells, J. M.; Badman, E. R.; Cooks, R. G. *Anal. Chem.* **1998**, *70*, 438-444.

(203) Patterson, G. E.; Guymon, A. J.; Riter, L. S.; Everly, M.; Griep-Raming, J.; Laughlin, B. C.; Ouyang, Z.; Cooks, R. G. *Anal Chem* **2002**, *74*, 6145-6153.

(204) Ouyang, Z.; Wu, G.; Song, Y.; Li, H.; Plass, W. R.; Cooks, R. G. *Anal. Chem.* **2004**, *76*, 4595-4605.

(205) Contreras, J. A.; Murray, J. A.; Tolley, S. E.; Oliphant, J. L.; Tolley, H. D.; Lammert, S. A.; Lee, E. D.; Later, D. W.; Lee, M. L. *J. Am. Soc. Mass Spectrom.* **2008**, *19*, 1425-1434.

(206) Taylor, N.; Austin, D. E. *Int. J. Mass Spectrom.* **2012**, *321-322*, 25-32.

(207) Whitten, W. B.; Reilly, P. T.; Ramsey, J. M. *Rapid Commun. Mass Spectrom.* **2004**, *18*, 1749-1752.

(208) Song, Q.; Xu, W.; Smith, S. A.; Gao, L.; Chappell, W. J.; Cooks, R. G.; Ouyang, Z. *J. Mass Spectrom.* **2010**, *45*, 26-34.

(209) Kornienko, O.; Reilly, P. T. A.; Whitten, W. B.; Ramsey, J. M. *Rapid Commun. Mass Spectrom.* **1999**, *13*, 50-53.

(210) Cai, Y.; Peng, W. P.; Kuo, S. J.; Chang, H. C. *Int. J. Mass Spectrom.* **2002**, *214*, 63-73.

(211) Peng, W. P.; Cai, Y.; Lee, Y. T.; Chang, H. C. *Int. J. Mass Spectrom.* **2003**, *229*, 67-76.

(212) Gao, L.; Sugiarto, A.; Harper, J. D.; Cooks, R. G.; Ouyang, Z. *Anal. Chem.* **2008**, *80*, 7198-7205.

(213) Cooks, R. G.; Glish, G. L.; McLuckey, S. A.; Kaiser, R. E. *Chem. Eng. News* **1991**, *69*, 26-41.

(214) Ouyang, Z.; Noll, R. J.; Cooks, R. G. *Anal. Chem.* **2009**, *81*, 2421-2425.

(215) Lawton, Z. E.; Traub, A.; Fatigante, W. L.; Mancias, J.; O'Leary, A. E.; Hall, S. E.; Wieland, J. R.; Oberacher, H.; Gizzi, M. C.; Mulligan, C. C. *J. Am. Soc. Mass Spectrom.* **2016** 10.1007/s13361-016-1562-2.

(216) O'Leary, A. E.; Oberacher, H.; Hall, S. E.; Mulligan, C. C. *Anal. Methods* **2015**, *7*, 3331-3339.

(217) Mahaffy, P. R.; Webster, C. R.; Cabane, M.; Conrad, P. G.; Coll, P.; Atreya, S. K.; Arvey, R.; Barciniak, M.; Benna, M.; Bleacher, L.; Brinckerhoff, W. B.; Eigenbrode, J. L.; Carignan, D.; Cascia, M.; Chalmers, R. A.; Dworkin, J. P.; Errigo, T.; Everson, P.; Franz, H.; Farley, R.; Feng, S.; Frazier, G.; Freissinet, C.; Glavin, D. P.; Harpold, D. N.; Hawk, D.; Holmes, V.; Johnson, C. S.; Jones, A.; Jordan, P.; Kellogg, J.; Lewis, J.; Lyness, E.; Malespin, C. A.; Martin, D. K.; Maurer, J.; McAdam, A. C.; McLennan, D.; Nolan, T. J.; Noriega, M.; Pavlov, A. A.; Prats, B.; Raaen, E.; Sheinman, O.; Sheppard, D.; Smith, J.; Stern, J. C.; Tan, F.; Trainer, M.; Ming, D. W.; Morris, R. V.; Jones, J.; Gundersen, C.; Steele, A.; Wray, J.; Botta, O.; Leshin, L. A.; Owen, T.; Battel, S.; Jakosky, B. M.; Manning, H.; Squyres, S.; Navarro-González, R.; McKay, C. P.; Raulin, F.; Sternberg, R.; Buch, A.; Sorensen, P.; Kline-Schoder, R.; Coscia, D.; Szopa, C.; Teinturier, S.; Baffes, C.; Feldman, J.; Flesch, G.; Forouhar, S.; Garcia, R.; Keymeulen, D.; Woodward, S.; Block, B. P.; Arnett, K.; Miller, R.; Edmonson, C.; Gorevan, S.; Mumm, E. *Space Sci. Rev.* **2012**, *170*, 401-478.

(218) Schwartz, J. C.; Senko, M. W.; Syka, J. E. P. *J. Am. Soc. Mass Spectrom.* **2002**, *13*, 659-669.

(219) Badman, E. R.; Cooks, R. G. *Anal. Chem.* **2000**, *72*, 3291-3297.

(220) Patterson, G. E.; Guymon, A. J.; Riter, L. S.; Everly, M.; Griep-Raming, J.; Laughlin, B. C.; Ouyang, Z.; Cooks, R. G. *Anal. Chem.* **2002**, *74*, 6145-6153.

(221) Higgs, J. M.; Austin, D. E. *Int. J. Mass Spectrom.* **2014**, *363*, 40-51.

(222) Higgs, J. M.; Petersen, B. V.; Lammert, S. A.; Warnick, K. F.; Austin, D. E. *Int. J. Mass Spectrom.* **2016**, *395*, 20-26.

(223) Berton, A.; Traldi, P.; Ding, L.; Brancia, F. L. *J. Am. Soc. Mass Spectrom.* **2008**, *19*, 620-625.

(224) Brancia, F. L.; McCullough, B.; Entwistle, A.; Grossmann, J. G.; Ding, L. *J. Am. Soc. Mass Spectrom.* **2010**, *21*, 1530-1533.

(225) Bandelow, S.; Marx, G.; Schweikhard, L. *Int. J. Mass Spectrom.* **2013**, *336*, 47-52.

(226) Brabeck, G. F.; Reilly, P. T. A. *Int. J. Mass Spectrom.* **2014**, *364*, 1-8.

(227) Xu, F. X.; Wang, L.; Dai, X. H.; Fang, X.; Ding, C. F. *J. Am. Soc. Mass Spectrom.* **2014**, *25*, 556-562.

(228) Xue, B.; Ma, L.; Sun, L.; Gao, W.; Cheng, P.; Ding, L.; Huang, Z.; Zhou, Z. *Rapid Commun. Mass Spectrom.* **2016**, *30*, 1985-1990.

(229) Xu, F. X.; Dang, Q. K.; Dai, X. H.; Fang, X.; Wang, Y. Y.; Ding, L.; Ding, C. F. *J. Am. Soc. Mass Spectrom.* **2016**, *27*, 1351-1356.

(230) Snyder, D. T.; Cooks, R. G. *Int. J. Mass Spectrom.* **2017**, *417*, 1-7.

(231) Huo, X.; Chen, J.; Tang, F.; Yao, T.; Piao, S.; Ni, K.; Wang, X. **2017** 10.1002/rcm.7880.

(232) Senko, M. W.; Schwartz, J. C., Two-dimensional quadrupole ion trap, U.S. Patent US7180057 B1, 2007.

(233) Danell, R. M. In *58th ASMS Conference on Mass Spectrometry and Allied Topics*: Salt Lake City, UT, 2010.

(234) Tabert, A. M.; Goodwin, M. P.; Cooks, R. G. *J. Am. Soc. Mass Spectrom.* **2006**, *17*, 56-59.

(235) Snyder, D. T.; Cooks, R. G. *Rapid Commun Mass Spectrom* **2017**, *31*, 200-206.

(236) Evans-Nguyen, T.; Wang, D.; van Amerom, F., Continuous operation high speed ion trap mass spectrometer, U.S. Patent US20150034820 A1, 2015.

(237) Biemann, K. *Proc. Natl. Acad. Sci. U. S. A.* **2007**, *104*, 10310-10313.

(238) Bantscheff, M.; Boesche, M.; Eberhard, D.; Matthieson, T.; Sweetman, G.; Kuster, B. *Mol Cell Proteomics* **2008**, *7*, 1702-1713.

(239) Bateman, R. H.; Carruthers, R.; Hoyes, J. B.; Jones, C.; Langridge, J. I.; Millar, A.; Vissers, J. P. *J Am Soc Mass Spectrom* **2002**, *13*, 792-803.

(240) Sandra, K.; Devreese, B.; Van Beeumen, J.; Stals, I.; Claeyssens, M. *J. Am. Soc. Mass Spectrom.* **2004**, *15*, 413-423.

(241) de Hoffman, E. *J. Mass Spectrom.* **1996**, *31*, 129-137.

(242) Scrivens, J. H.; Rollins, K.; Jennings, R. C. K. *Rapid Commun Mass Spectrom* **1992**, *6*, 272-277.

(243) Gu, M.; Turecek, F. *Organic Mass Spectrometry* **1993**, *28*, 1135-1143.

(244) Le Blanc, J. C.; Hager, J. W.; Ilisiu, A. M.; Hunter, C.; Zhong, F.; Chu, I. *Proteomics* **2003**, *3*, 859-869.

(245) Hopfgartner, G.; Varesio, E.; Tschappat, V.; Grivet, C.; Bourgogne, E.; Leuthold, L. A. *J. Mass Spectrom.* **2004**, *39*, 845-855.

(246) Olsen, J. V.; Schwartz, J. C.; Griep-Raming, J.; Nielsen, M. L.; Damoc, E.; Denisov, E.; Lange, O.; Remes, P.; Taylor, D.; Splendore, M.; Wouters, E. R.; Senko, M.; Makarov, A.; Mann, M.; Horning, S. *Molecular & Cellular Proteomics* **2009**, *8*, 2759-2769.

(247) Sleno, L.; Volmer, D. A. *J. Mass Spectrom.* **2004**, *39*, 1091-1112.

(248) Steen, H.; Kuster, B.; Mann, M. *J. Mass Spectrom.* **2001**, *36*, 782-790.

(249) Yost, R. A.; Enke, C. G. *Anal Chem* **1979**, *51*, 1251-1264.

(250) Chernushevich, I. V.; Loboda, A. V.; Thomson, B. A. *J Mass Spectrom* **2001**, *36*, 849-865.

(251) Schoen, A. E.; Amy, J. W.; Ciupek, J. D.; Cooks, R. G.; Dobberstein, P.; Jung, G. *International Journal of Mass Spectrometry and Ion Processes* **1985**, *65*, 125-140.

(252) Carr, S. A.; Huddleston, M. J.; Annan, R. S. *Analytical Biochemistry* **1996**, *239*, 180-192.

(253) Borchers, C.; Parker, C. E.; Deterding, L. J.; Tomer, K. B. *J Chromatogr A* **1999**, *854*, 119-130.

(254) Williamson, B. L.; Marchese, J.; Morrice, N. A. *Mol. Cell. Proteomics* **2006**, *5*, 337-346.

(255) Rappsilber, J.; Friesen, W. J.; Paushkin, S.; Dreyfuss, G.; Mann, M. *Anal. Chem.* **2003**, *75*, 3107-3114.

(256) Aldini, G.; Regazzoni, L.; Orioli, M.; Rimoldi, I.; Facino, R. M.; Carini, M. *J. Mass Spectrom.* **2008**, *43*, 1470-1481.

(257) Ritchie, M. A.; Gill, A. C.; Deery, M. J.; Lilley, K. *J Am Soc Mass Spectrom* **2002**, *13*, 1065-1077.

(258) Steen, H.; Küster, B.; Fernandez, M.; Pandey, A.; Mann, M. *Anal. Chem.* **2001**, *73*, 1440-1448.

(259) Bollineni, R.; Fedorova, M.; Hoffmann, R. *J. Proteomics* **2011**, *74*, 2351-2359.

(260) Iglesias, A. H.; Santos, L. F.; Gozzo, F. C. *Anal Chem* **2010**, *82*, 909-916.

(261) Snyder, D. T.; Schilling, M. C.; Hochwender, C. G.; Kaufman, A. D. *Anal. Methods* **2015**, *7*, 870-876.

(262) Qu, J.; Wang, Y. M.; Luo, G. A.; Wu, Z. P. *J. Chromatogr. A* **2001**, *928*, 155-162.

(263) Fabre, N.; Claparols, C.; Richelme, S.; Angelin, M. L.; Fouraste, I.; Moulis, C. *J. Chromatogr. A* **2000**, *904*, 35-46.

(264) Brugger, B.; Erben, G.; Sandhoff, R.; Wieland, F. T.; Lehmann, W. D. *Proc. Natl. Acad. Sci. USA* **1997**, *94*, 2339-2344.

(265) Ejsing, C. S.; Duchoslav, E.; Sampaio, J.; Simons, K.; Bonner, R.; Thiele, C.; Ekroos, K.; Shevchenko, A. *Anal Chem* **2006**, *78*, 6202-6214.

(266) Shaner, R. L.; Allegood, J. C.; Park, H.; Wang, E.; Kelly, S.; Haynes, C. A.; Sullards, M. C.; Merrill, A. H., Jr. *J. Lipid Res.* **2009**, *50*, 1692-1707.

(267) Wang, X.; Sakuma, T.; Asafu-Adjaye, E.; Shiu, G. K. *Anal. Chem.* **1999**, *71*, 1579-1584.

(268) Martin, J. W.; Mabury, S. A.; O'Brien, P. J. *Chem. Biol. Interact.* **2005**, *155*, 165-180.

(269) Löffler, D.; Ternes, T. A. *J. Chromatogr. A* **2003**, *1000*, 583-588.

(270) Hirsch, R.; Ternes, T. A.; Haberer, K.; Mehlich, A.; Ballwanz, F.; Kratz, K. L. *J Chromatogr A* **1998**, *815*, 213-223.

(271) Stafford, G. C.; Kelley, P. E.; Syka, J. E. P.; Reynolds, W. E.; Todd, J. F. J. *International Journal of Mass Spectrometry and Ion Processes* **1984**, *60*, 85-98.

(272) Welling, M.; Schuessler, H. A.; Thompson, R. I.; Walther, H. *International Journal of Mass Spectrometry* **1998**, *172*, 95-114.

(273) Ding, L.; Sudakov, M.; Brancia, F. L.; Giles, R.; Kumashiro, S. *J Mass Spectrom* **2004**, *39*, 471-484.

(274) Roth, B.; Frohlich, U.; Schiller, S. *Phys Rev Lett* **2005**, *94*, 053001.

(275) Ouyang, Z.; Cooks, R. G. *Annu Rev Anal Chem* **2009**, *2*, 187-214.

(276) Snyder, D. T.; Pulliam, C. J.; Ouyang, Z.; Cooks, R. G. *Anal. Chem.*, DOI: 10.1021/acs.analchem.5b03070.

(277) Li, L.; Chen, T. C.; Ren, Y.; Hendricks, P. I.; Cooks, R. G.; Ouyang, Z. *Anal Chem* **2014**, *86*, 2909-2916.

(278) Makarov, A. A. *Anal Chem* **1996**, *68*, 4257-4263.

(279) Browne, D. L.; Wright, S.; Deadman, B. J.; Dunnage, S.; Baxendale, I. R.; Turner, R. M.; Ley, S. V. *Rapid Commun. Mass Spectrom.* **2012**, *26*, 1999-2010.

(280) Chen, C. H.; Lin, Z.; Tian, R.; Shi, R.; Cooks, R. G.; Ouyang, Z. *Anal Chem* **2015**, *87*, 8867-8873.

(281) Smith, J. N.; Noll, R. J.; Cooks, R. G. *Rapid Commun. Mass Spectrom.* **2011**, *25*, 1437-1444.

(282) Dumlao, M.; Sinues, P. M.-L.; Nudnova, M.; Zenobi, R. *Anal. Methods* **2014**, *6*, 3604.

(283) Urabe, T.; Takahashi, K.; Kitagawa, M.; Sato, T.; Kondo, T.; Enomoto, S.; Kidera, M.; Seto, Y. *Spectrochim. Acta. A Mol. Biomol. Spectrosc.* **2014**, *120*, 437-444.

(284) Giannoukos, S.; Brkic, B.; Taylor, S.; France, N. *J. Am. Soc. Mass Spectrom.* **2015**, *26*, 231-239.

(285) Brinckerhoff, W.; Danell, R.; Van Ameron, F.; Pinnick, V.; Li, X.; Arevalo, R.; Glavin, D.; Getty, S.; Mahaffy, P.; Chu, P. **2014** Development of a Linear Ion Trap Mass Spectrometer (LITMS) Investigation for Future Planetary Surface Missions.

(286) Wu, Q.; Tian, Y.; Li, A.; Austin, D. E. *International Journal of Mass Spectrometry* **2015**, *393*, 52-57.

(287) Gao, L.; Song, Q.; Patterson, G. E.; Cooks, R. G.; Ouyang, Z. *Anal. Chem.* **2006**, *78*, 5994-6002.

(288) Song, Q.; Kothari, S.; Senko, M. A.; Schwartz, J. C.; Amy, J. W.; Stafford, G. C.; Cooks, R. G.; Ouyang, Z. *Anal Chem* **2006**, *78*, 718-725.

(289) Zhang, C.; Chen, H.; Guymon, A. J.; Wu, G.; Cooks, R. G.; Ouyang, Z. *Int. J. Mass Spectrom.* **2006**, *255-256*, 1-10.

(290) Fico, M.; Yu, M.; Ouyang, Z.; Cooks, R. G.; Chappell, W. J. *Anal. Chem.* **2007**, *79*, 8076-8082.

(291) Wu, Q.; Li, A.; Tian, Y.; Zare, R. N.; Austin, D. E. *Anal. Chem.* **2016** 10.1021/acs.analchem.6b01830.

(292) Wu, Q.; Tian, Y.; Li, A.; Andrews, D.; Hawkins, A. R.; Austin, D. E. *J. Am. Soc. Mass Spectrom.* **2017** 10.1007/s13361-017-1607-1.

(293) Schwartz, J. C.; Wade, A. P.; Enke, C. G.; Cooks, R. G. *Anal. Chem.* **1990**, *62*, 1809-1818.

(294) Scrivens, J. H.; Rollins, K.; Jennings, R. C. K. *Rapid Commun. Mass Spectrom.* **1992**, *6*, 272-277.

(295) Borchers, C.; Parker, C. E.; Deterding, L. J.; Tomer, K. B. *J. Chromatogr. A* **1999**, *854*, 119-130.

(296) Eberlin, M. N. *Mass Spectrom. Rev.* **1997**, *16*, 113-144.

(297) McClellan, J. E.; Quarmby, S. T.; Yost, R. A. *Anal Chem* **2002**, *74*, 5799-5806.

(298) Swaney, D. L.; McAlister, G. C.; Coon, J. J. *Nat. Methods* **2008**, *5*, 959-964.

(299) Schroeder, M. J.; Shabanowitz, J.; Schwartz, J. C.; Hunt, D. F.; Coon, J. J. *Anal. Chem.* **2004**, *76*, 3590-3598.

(300) Bern, M.; Finney, G.; Hoopmann, M. R.; Merrihew, G.; Toth, M. J.; MacCoss, M. J. *Anal. Chem.* **2010**, *82*, 833-841.

(301) Juraschek, R.; Dulcks, T.; Karas, M. *J. Am. Soc. Mass Spectrom.* **1999**, *10*, 300-308.

(302) Lee, H.; Jhang, C. S.; Liu, J. T.; Lin, C. H. *J. Sep. Sci.* **2012**, *35*, 2822-2825.

(303) Lesiak, A. D.; Musah, R. A.; Cody, R. B.; Domin, M. A.; Dane, A. J.; Shepard, J. R. *Analyst* **2013**, *138*, 3424-3432.

(304) Presley, B. C.; Jansen-Varnum, S. A.; Logan, B. K. *Forensic Sci. Rev.* **2013**, *25*, 27-46.

(305) Snyder, D. T.; Fedick, P. W.; Cooks, R. G. *Anal. Chem.* **2016**, *88*, 9572-9581.

(306) Snyder, D. T.; Cooks, R. G. *Rapid Commun. Mass Spectrom.* **2017**, *31*, 200-206.

(307) Snyder, D. T.; Pulliam, C. J.; Wiley, J. S.; Duncan, J.; Cooks, R. G. *J. Am. Soc. Mass Spectrom.* **2016**, *27*, 1243-1255.

(308) Wang, Y.; Franzen, J.; Wanczek, K. P. *Int. J. Mass Spectrom. Ion Processes* **1993**, *124*, 125-144.

(309) Shay, B. J.; Eberlin, M. N.; Cooks, R. G.; Wesdemiotis, C. *J. Am. Soc. Mass Spectrom.* **1991**, *3*, 518-534.

(310) Sorrilha, A. E.; Gozzo, F. C.; Pimpim, R. S.; Eberlincor, M. N. *J. Am. Soc. Mass Spectrom.* **1996**, *7*, 1126-1137.

(311) Juliano, V. F.; Gozzo, F. C.; Eberlin, M. N.; Kascheres, C.; do Lago, C. L. *Anal. Chem.* **1996**, *68*, 1328-1334.

(312) Beynon, J. H.; Cooks, R. G.; Amy, J. W.; Baitinger, W. E.; Ridley, T. Y. *Anal. Chem.* **1973**, *45*, 1023A-1031A.

(313) Cooks, R. G.; Beynon, J. H.; Litton, J. F. *Org. Mass Spectrom.* **1975**, *10*, 503-506.

(314) Kruger, T. L.; Litton, J. F.; Kondrat, R. W.; Cooks, R. G. *Anal. Chem.* **1976**, *48*, 2113-2119.

(315) Beynon, J. H.; Cooks, R. G. *Int. J. Mass Spectrom. Ion Phys.* **1976**, *19*, 107-137.

(316) Kondrat, R. W.; Cooks, R. G.; McLaughlin, J. L. *Science* **1978**, *199*, 978-980.

(317) Syka, J. E.; Coon, J. J.; Schroeder, M. J.; Shabanowitz, J.; Hunt, D. F. *Proc. Natl. Acad. Sci. U.S.A.* **2004**, *101*, 9528-9533.

(318) Lawton, Z. E.; Traub, A.; Fatigante, W. L.; Mancias, J.; O'Leary, A. E.; Hall, S. E.; Wieland, J. R.; Oberacher, H.; Gizzi, M. C.; Mulligan, C. C. *J. Am. Soc. Mass Spectrom.* **2017**, *28*, 1048-1059.

(319) Vircks, K. E.; Mulligan, C. C. *Rapid Commun. Mass Spectrom.* **2012**, *26*, 2665-2672.

(320) Shortt, B. J.; Darrach, M. R.; Holland, P. M.; Chutjian, A. *J. Mass Spectrom.* **2005**, *40*, 36-42.

(321) Ferreira, C. R.; Yannell, K. E.; Mollenhauer, B.; Espy, R. D.; Cordeiro, F. B.; Ouyang, Z.; Cooks, R. G. *Analyst* **2016**, *141*, 5252-5255.

(322) Crutchfield, C. A.; Thomas, S. N.; Sokoll, L. J.; Chan, D. W. *Clin. Proteomics* **2016**, *13*, 1.

(323) Cooks, R. G. In *Collision Spectroscopy*; Springer US: New York, 1978, pp 357-450.

(324) Schinke, R. *Photodissociation Dynamics: Spectroscopy and Fragmentation of Small Polyatomic Molecules*; Cambridge University Press: New York, 1993 Photodissociation Dynamics: Spectroscopy and Fragmentation of Small Polyatomic Molecules.

(325) Cammarata, M. B.; Brodbelt, J. S. *Chem. Sci.* **2015**, *6*, 1324-1333.

(326) Little, D. P.; Speir, J. P.; Senko, M. W.; O'Connor, P. B.; McLafferty, F. W. *Anal. Chem.* **1994**, *66*, 2809-2815.

(327) Syka, J. E.; Coon, J. J.; Schroeder, M. J.; Shabanowitz, J.; Hunt, D. F. *Proc. Natl. Acad. Sci. U. S. A.* **2004**, *101*, 9528-9533.

(328) Mabud, M. A.; Dekrey, M. J.; Cooks, R. G. *Int. J. Mass Spectrom. Ion Processes* **1985**, *67*, 285-294.

(329) Chorush, R. A.; Little, D. P.; Beu, S. C.; Wood, T. D.; McLafferty, F. W. *Anal. Chem.* **1995**, *67*, 1042-1046.

(330) Kenttamaa, H. I.; Wood, K. V.; Busch, K. L.; Cooks, R. G. *Org. Mass Spectrom.* **1983**, *18*, 561-567.

(331) Schwartz, J. C.; Schey, K. L.; Cooks, R. G. *Int. J. Mass Spectrom. Ion Processes* **1990**, *101*, 1-20.

(332) Kondrat, R. W.; Mcclusky, G. A.; Cooks, R. G. *Anal. Chem.* **1978**, *50*, 2017-2021.

(333) Vincenti, M.; Schwartz, J. C.; Cooks, R. G.; Wade, A. P.; Enke, C. G. *Org. Mass Spectrom.* **1988**, *23*, 579-584.

(334) McLafferty, F. W. *Science* **1990**, *247*, 925-929.

(335) Wesdemiotis, C.; McLafferty, F. W. *Chem. Rev.* **1987**, *87*, 485-500.

(336) Terlouw, J. K.; Schwarz, H. *Angew. Chem. Int. Ed. Engl.* **1987**, *26*, 805-815.

(337) Zakett, D.; Schoen, A. E.; Kondrat, R. W.; Cooks, R. G. *J. Am. Chem. Soc.* **1979**, *101*, 6781-6783.

(338) Goldberg, N.; Schwarz, H. *Acc. Chem. Res.* **1994**, *27*, 347-352.

(339) Haag, R.; Schröder, D.; Zywietz, T.; Jiao, H.; Schwarz, H.; von Ragué Schleyer, P.; de Meijere, A. *Angew. Chem. Int. Ed. Engl.* **1996**, *35*, 1317-1319.

(340) Schröder, D.; Schalley, C. A.; Schwarz, H.; Goldberg, N.; Hrûsák, J. *Chem. Eur. J.* **1996**, *2*, 1235-1242.

(341) Snyder, D. T.; Cooks, R. G. *J. Am. Soc. Mass Spectrom.* **2017**, *28*, 1929-1938.

(342) Jarrell, T. M.; Marcum, C. L.; Sheng, H.; Owen, B. C.; O'Lenick, C.; Maraun, H.; Bozell, J. J.; Kenttämaa, H. I. *Green Chem.* **2014**, *16*, 2713-2727.

(343) Koizumi, H.; Whitten, W. B.; Reilly, P. T. A.; Koizumi, E. *Int. J. Mass Spectrom.* **2009**, *286*, 64-69.

(344) McClellan, J. E.; Quarmby, S. T.; Yost, R. A. *Anal. Chem.* **2002**, *74*, 5799-5806.

(345) Orians, C. M.; Fritz, R. S. *J. Chem. Ecol.* **1995**, *21*, 1245-1253.

(346) Boeckler, G. A.; Gershenzon, J.; Unsicker, S. B. *Phytochemistry* **2011**, *72*, 1497-1509.

(347) Paul, W.; Reinhard, H. P.; von Zahn, U. *Zeitschrift für Physik* **1958**, *152*, 143-182.

(348) Fulford, J. E.; Hoa, D.-N.; Hughes, R. J.; March, R. E.; Bonner, R. F.; Wong, G. J. *J. Vac. Sci. Technol.* **1980**, *17*, 829-835.

(349) Olsen, J. V.; Schwartz, J. C.; Griep-Raming, J.; Nielsen, M. L.; Damoc, E.; Denisov, E.; Lange, O.; Remes, P.; Taylor, D.; Splendore, M.; Wouters, E. R.; Senko, M.; Makarov, A.; Mann, M.; Horning, S. *Mol. Cell Proteomics* **2009**, *8*, 2759-2769.

(350) Makarov, A.; Denisov, E.; Kholomeev, A.; Balschun, W.; Lange, O.; Strupat, K.; Horning, S. *Anal. Chem.* **2006**, *78*, 2113-2120.

(351) Collings, B. A.; Campbell, J. M.; Mao, D.; Douglas, D. J. *Rapid Commun. Mass Spectrom.* **2001**, *15*, 1777-1795.

(352) Johnson, J. V.; Pedder, R. E.; Yost, R. A. *Int. J. Mass Spectrom. Ion Processes* **1991**, *106*, 197-212.

(353) Schwudke, D.; Oegema, J.; Burton, L.; Entchev, E.; Hannich, J. T.; Ejsing, C. S.; Kurzchalia, T.; Shevchenko, A. *Anal. Chem.* **2006**, *78*, 585-595.

(354) Snyder, D. T.; Pulliam, C. J.; Cooks, R. G. *Rapid Commun. Mass Spectrom.* **2016**, *30*, 2369-2378.

(355) Julian, R. K.; Cooks, R. G. *Anal. Chem.* **1993**, *65*, 1827-1833.

(356) March, R. E.; Todd, J. F. J. *Practical Aspects of Trapped Ion Mass Spectrometry, Vol. 4*; CRC Press Taylor & Francis Group: Boca Raton, FL, 2010; Vol. IV.

(357) Garcia-Reyes, J. F.; Harper, J. D.; Salazar, G. A.; Charipar, N. A.; Ouyang, Z.; Cooks, R. G. *Anal. Chem.* **2011**, *83*, 1084-1092.

(358) Jarmusch, A. K.; Pirro, V.; Kerian, K. S.; Cooks, R. G. *Analyst* **2014**, *139*, 4785-4789.

(359) Pirro, V.; Jarmusch, A. K.; Vincenti, M.; Cooks, R. G. *Anal. Chim. Acta* **2015**, *861*, 47-54.

(360) Hou, K.; Xu, W.; Xu, J.; Cooks, R. G.; Ouyang, Z. *Anal. Chem.* **2011**, *83*, 1857-1861.

(361) Dalgleish, J. K.; Hou, K.; Ouyang, Z.; Cooks, R. G. *Anal. Lett.* **2012**, *45*, 1440-1446.

(362) Kerian, K. S.; Jarmusch, A. K.; Cooks, R. G. *Analyst* **2014**, *139*, 2714-2720.

(363) Fedick, P. W.; Bain, R. M. *Forensic Chemistry* **2017**, *5*, 53-57.

(364) Badman, E. R.; Cooks, R. G. *J. Mass Spectrom.* **2000**, *35*, 659-671.

(365) Blain, M. G.; Riter, L. S.; Cruz, D.; Austin, D. E.; Wu, G.; Plass, W. R.; Cooks, R. G. *Int. J. Mass Spectrom.* **2004**, *236*, 91-104.

(366) Wu, Q.; Li, A.; Tian, Y.; Zare, R. N.; Austin, D. E. *Anal. Chem.* **2016**, *88*, 7800-7806.

(367) Tian, Y.; Decker, T. K.; McClellan, J. S.; Bennett, L.; Li, A.; De la Cruz, A.; Andrews, D.; Lammert, S. A.; Hawkins, A. R.; Austin, D. E. *J. Am. Soc. Mass Spectrom.* **2017** 10.1007/s13361-017-1759-z.

(368) Luebkemann, F.; Wanczek, K. P. *Int. J. Mass Spectrom.* **2009**, *281*, 150-156.

(369) Beauchamp, P.; Hörst, S.; Yelle, R.; Cable, M.; Neidholdt, E.; Beauchamp, J.; Hodyss, R.; Briois, C.; Thirkell, L.; Willis, P.; Nellis, G.; Gianchandani, Y.; Choukroun, M. In *International Workshop on Instrumentation for Planetary Missions*: Greenbelt, MD, 2014.

(370) Chen, E. X.; Russell, Z. E.; Amsden, J. J.; Wolter, S. D.; Danell, R. M.; Parker, C. B.; Stoner, B. R.; Gehm, M. E.; Glass, J. T.; Brady, D. J. *J. Am. Soc. Mass Spectrom.* **2015** 10.1007/s13361-015-1178-y.

(371) Amsden, J. J.; Herr, P. J.; Landry, D. M. W.; Kim, W.; Vyas, R.; Parker, C. B.; Kirley, M. P.; Keil, A. D.; Gilchrist, K. H.; Radauscher, E. J.; Hall, S. D.; Carlson, J. B.; Baldasaro, N.; Stokes, D.; Di Dona, S. T.; Russell, Z. E.; Grego, S.; Edwards, S. J.; Sperline, R. P.; Denton, M. B.; Stoner, B. R.; Gehm, M. E.; Glass, J. T. *J. Am. Soc. Mass Spectrom.* **2017** 10.1007/s13361-017-1820-y.

(372) Wright, S.; Malcolm, A.; Wright, C.; O'Prey, S.; Crichton, E.; Dash, N.; Moseley, R. W.; Zaczek, W.; Edwards, P.; Fussell, R. J.; Syms, R. R. *Anal. Chem.* **2015**, *87*, 3115-3122.

(373) Snyder, D. T.; Peng, W.-P.; Cooks, R. G. *Chem. Phys. Lett.* **2017**, *668*, 69-89.

(374) Snyder, D. T.; Kaplan, D. A.; Danell, R. M.; van Amerom, F. H. W.; Pinnick, V. T.; Brinckerhoff, W. B.; Mahaffy, P. R.; Cooks, R. G. *Analyst* **2017**, *142*, 2109-2117.

(375) Balsiger, H.; Altwegg, K.; Bochsler, P.; Eberhardt, P.; Fischer, J.; Graf, S.; Jäckel, A.; Kopp, E.; Langer, U.; Mildner, M.; Müller, J.; Riesen, T.; Rubin, M.; Scherer, S.; Wurz, P.; Wüthrich, S.; Arijs, E.; Delanoye, S.; Keyser, J. D.; Neefs, E.; Nevejans, D.; Rème, H.; Aoustin, C.; Mazelle, C.; Médale, J. L.; Sauvaud, J. A.; Berthelier, J. J.; Bertaux, J. L.; Duvet, L.; Illiano, J. M.; Fuselier, S. A.; Ghielmetti, A. G.; Magoncelli, T.; Shelley, E. G.; Korth, A.; Heerlein, K.; Lauche, H.; Livi, S.; Loose, A.; Mall, U.; Wilken, B.; Gliem, F.; Fiethe, B.; Gombosi, T. I.; Block, B.; Carignan, G. R.; Fisk, L. A.; Waite, J. H.; Young, D. T.; Wollnik, H. *Space Sci. Rev.* **2007**, *128*, 745-801.

(376) Rubin, M.; Altwegg, K.; Balsiger, H.; Bar-Nun, A.; Berthelier, J. J.; Bieler, A.; Bochsler, P.; Briois, C.; Calmonte, U.; Combi, M.; De Keyser, J.; Dhooghe, F.; Eberhardt, P.; Fiethe, B.; Fuselier, S. A.; Gasc, S.; Gombosi, T. I.; Hansen, K. C.; Hässig, M.; Jäckel, A.; Kopp, E.; Korth, A.; Le Roy, L.; Mall, U.; Marty, B.; Mousis, O.; Owen, T.; Rème, H.; Sémon, T.; Tzou, C. Y.; Waite, J. H.; Wurz, P. *Science* **2015**, *348*, 232.

(377) Zhai, Y.; Jiang, T.; Huang, G.; Wei, Y.; Xu, W. *Analyst* **2016**, *141*, 5404-5411.

(378) Venter, A.; Nefliu, M.; Graham Cooks, R. *Trends Anal. Chem.* **2008**, *27*, 284-290.

(379) Tabert, A. M.; Griep-Raming, J.; Guymon, A. J.; Cooks, R. G. *Anal Chem* **2003**, *75*, 5656-5664.

(380) Chaudhary, A.; van Amerom, F. H. W.; Short, R. T. *J. Microelectromech. Syst.* **2009**, *18*, 442-448.

(381) Xu, W.; Li, L.; Zhou, X.; Ouyang, Z. *Anal. Chem.* **2014**, *86*, 4102-4109.

(382) Austin, D. E.; Peng, Y.; Hansen, B. J.; Miller, I. W.; Rockwood, A. L.; Hawkins, A. R.; Tolley, S. E. *J. Am. Soc. Mass Spectrom.* **2008**, *19*, 1435-1441.

(383) Wu, Q.; Tian, Y.; Li, A.; Andrews, D.; Hawkins, A. R.; Austin, D. E. *J. Am. Soc. Mass Spectrom.* **2017**, *28*, 859-865.

(384) Franzen, J. *Int. J. Mass Spectrom. Ion Processes* **1991**, *106*, 63-78.

(385) Kotana, A. N.; Mohanty, A. K. *International Journal of Mass Spectrometry* **2015**, *386*, 15-23.

(386) Xue, B.; Sun, L.; Huang, Z.; Gao, W.; Fan, R.; Cheng, P.; Ding, L.; Ma, L.; Zhou, Z. *Analyst* **2016**, *141*, 5535-5542.

(387) Jiang, T.; Zhang, H.; Tang, Y.; Zhai, Y.; Xu, W.; Xu, H.; Zhao, X.; Li, D.; Xu, W. *Anal. Chem.* **2017**, *89*, 5578-5584.

(388) Snyder, D. T.; Cooks, R. G. *Int. J. Mass Spectrom.* **2017**, *417*, 1-7.

(389) Toschek, P. *Nature* **2017**, *545*, 290.

(390) Londry, F. A.; Wells, G. J.; March, R. E. *Rapid Commun. Mass Spectrom.* **1993**, *7*, 43-45.

(391) Li, G.; Li, D.; Cheng, Y.; Pei, X.; Zhang, H.; Wang, Y.; Sun, J.; Dong, M. *Rev. Sci. Instrum.* **2017**, *88*, 123108.

(392) Johnson, J. V.; Yost, R. A.; Kelley, P. E.; Bradford, D. C. *Anal. Chem.* **1990**, *62*, 2162-2172.

(393) Snyder, D. T.; Cooks, R. G. *Anal. Chem.* **2017**, *89*, 8148-8155.

(394) Snyder, D. T.; Szalwinski, L. J.; Cooks, R. G. *Anal. Chem.* **2017**, *89*, 11053-11060.

(395) Beynon, J. H.; Cooks, R.-G.; Amy, J.-W.; Baitinger, W.; Ridley, T. *Anal. Chem.* **1973**, *45*, 1023A-1031A.

(396) Schoen, A. E.; Amy, J. W.; Ciupek, J. D.; Cooks, R. G.; Dobberstein, P.; Jung, G. *Int. J. Mass Spectrom. Ion Processes* **1985**, *65*, 125-140.

(397) Louris, J. N.; Wright, L. G.; Cooks, R. G.; Schoen, A. E. *Anal. Chem.* **1985**, *57*, 2918-2924.

(398) Chernushevich, I. V.; Loboda, A. V.; Thomson, B. A. *J. Mass Spectrom.* **2001**, *36*, 849-865.

(399) Cody, R.; Burnier, R.; Freiser, B. *Anal. Chem.* **1982**, *54*, 96-101.

(400) Vincenti, M.; Schwartz, J.; Cooks, R.; Wade, A.; Enke, C. *J. Mass Spectrom.* **1988**, *23*, 579-584.

(401) Ross III, C. W.; Guan, S.; Grosshans, P. B.; Ricca, T. L.; Marshall, A. G. *J. Am. Chem. Soc.* **1993**, *115*, 7854-7861.

(402) van der Rest, G.; Marshall, A. G. *Int. J. Mass Spectrom.* **2001**, *210*, 101-111.

(403) Pfändler, P.; Bodenhausen, G.; Rapin, J.; Houriet, R.; Gäumann, T. *Chem. Phys. Lett.* **1987**, *138*, 195-200.

(404) Guan, S.; Jones, P. R. *J. Chem. Phys.* **1989**, *91*, 5291-5295.

(405) Pfandler, P.; Bodenhausen, G.; Rapin, J.; Walser, M. E.; Gaumann, T. *J. Am. Chem. Soc.* **1988**, *110*, 5625-5628.

(406) Agthoven, M. A.; Coutouly, M. A.; Rolando, C.; Delsuc, M. A. *Rapid Commun. Mass Spectrom.* **2011**, *25*, 1609-1616.

(407) Chiron, L.; van Agthoven, M. A.; Kieffer, B.; Rolando, C.; Delsuc, M. A. *Proc. Natl. Acad. Sci. USA* **2014**, *111*, 1385-1390.

(408) van Agthoven, M. A.; Chiron, L.; Coutouly, M.-A.; Sehgal, A. A.; Pelupessy, P.; Delsuc, M.-A.; Rolando, C. *Int. J. Mass Spectrom.* **2014**, *370*, 114-124.

(409) Bray, F.; Bouclon, J.; Chiron, L.; Witt, M.; Delsuc, M. A.; Rolando, C. *Anal. Chem.* **2017**, *89*, 8589-8593.

(410) Bensimon, M.; Zhao, G.; Gäumann, T. *Chem. Phys. Lett.* **1989**, *157*, 97-100.

(411) Floris, F.; van Agthoven, M. A.; Chiron, L.; Wootton, C. A.; Lam, P. Y. Y.; Barrow, M. P.; Delsuc, M. A.; O'Connor, P. B. *J. Am. Soc. Mass Spectrom.* **2018**, *29*, 207-210.

(412) van Agthoven, M. A.; Lynch, A. M.; Morgan, T. E.; Wootton, C. A.; Lam, Y. P. Y.; Chiron, L.; Barrow, M. P.; Delsuc, M. A.; O'Connor, P. B. *Anal. Chem.* **2018**, *90*, 3496-3504.

(413) van Agthoven, M. A.; Barrow, M. P.; Chiron, L.; Coutouly, M. A.; Kilgour, D.; Wootton, C. A.; Wei, J.; Soulby, A.; Delsuc, M. A.; Rolando, C.; O'Connor, P. B. *J. Am. Soc. Mass Spectrom.* **2015**, *26*, 2105-2114.

(414) van Agthoven, M. A.; Chiron, L.; Coutouly, M. A.; Delsuc, M. A.; Rolando, C. *Anal. Chem.* **2012**, *84*, 5589-5595.

(415) Floris, F.; van Agthoven, M.; Chiron, L.; Soulby, A. J.; Wootton, C. A.; Lam, Y. P.; Barrow, M. P.; Delsuc, M. A.; O'Connor, P. B. *J. Am. Soc. Mass Spectrom.* **2016**, *27*, 1531-1538.

(416) van Agthoven, M. A.; Wootton, C. A.; Chiron, L.; Coutouly, M. A.; Soulby, A.; Wei, J.; Barrow, M. P.; Delsuc, M. A.; Rolando, C.; O'Connor, P. B. *Anal. Chem.* **2016**, *88*, 4409-4417.

(417) Floris, F.; Vallotto, C.; Chiron, L.; Lynch, A. M.; Barrow, M. P.; Delsuc, M. A.; O'Connor, P. B. *Anal. Chem.* **2017**, *89*, 9892-9899.

(418) Agthoven, M. A.; O'Connor, P. B. *Rapid Commun. Mass Spectrom.* **2017**, *31*, 674-684.

(419) Snyder, D. T.; Szalwinski, L. J.; Wells, M.; Cooks, R. G. **2018** In preparation.

(420) Snyder, D. T.; Szalwinski, L. J.; Wells, M.; Cooks, R. G. **2018** Submitted.

(421) Snyder, D. T.; Szalwinski, L. J.; Hilger, R. T.; Cooks, R. G. *J. Am. Soc. Mass Spectrom.* **2018**, *29*, 1355-1364.

(422) Snyder, D. T.; Szalwinski, L. J.; Schrader, R.; Pirro, V.; Hilger, R. T.; Cooks, R. G. *J. Am. Soc. Mass Spectrom.* **2018**, *29*, 1345-1354.

(423) Xu, W.; Manicke, N. E.; Cooks, G. R.; Ouyang, Z. *JALA Charlottesv Va* **2010**, *15*, 433-439.

(424) Carette, M.; Perrier, P.; Zerega, Y.; Brincourt, G.; Payan, J. C.; Andre, J. *Int. J. Mass Spectrom.* **1997**, *171*, 253-261.

(425) Bebinger, M. *NPR* **2018** Fentanyl-laced cocaine becoming a deadly problem among drug users.

(426) Armenian, P.; Vo, K. T.; Barr-Walker, J.; Lynch, K. L. *Neuropharmacology* **2017** 10.1016/j.neuropharm.2017.10.016.

(427) McBride, E. M.; Keller, R. E.; Verbeck, G. F. *Int. J. Mass Spectrom.* **2018**, *428*, 55-61.

(428) Haramija, M. *J. Mass Spectrom.* **2018**, *53*, 264-277.

(429) Remes, P. M.; Syka, J. E. P.; Kovtoun, V. V.; Schwartz, J. C. *Int. J. Mass Spectrom.* **2015**, *377*, 368-384.

(430) Julian, R. K.; Reiser, H. P.; Cooks, R. G. *Int. J. Mass Spectrom. Ion Processes* **1993**, *123*, 85-96.

(431) Schwartz, J. C.; Louris, J. N., Method of detecting ions in an ion trap mass spectrometer, U.S. Patent 5,285,063, 1994.

VITA

Dalton Snyder was born in St. Louis, MO – along with his fraternal twin Dylan – and spent his childhood in southern Indiana where he graduated valedictorian of Gibson Southern High School in 2010. He received his BSc degree in Professional Chemistry and Applied Mathematics with *summa cum laude* honors from the University of Evansville (UE) in 2014. During his tenure at UE, he spent a considerable amount of time as a teaching/lab assistant in the chemistry, physics, and philosophy (under the notable Prof. Anthony Beavers) departments. Dalton also contributed to the NSF-funded textbook *Calculus: Resequenced for Students in STEM* by Dwyer and Gruenwald. Research under Prof. Arlen Kaufman was a seminal component of his undergraduate education, with varied topics including cold vapor atomic absorption of mercury in soils contaminated by coal-fired power plants, HPLC-MS/MS of pharmaceuticals, personal care products, and agrochemicals in local bodies of water, and ambient ionization mass spectrometry of *Populus* plants.

Dalton started his PhD studies at Purdue University in 2014 under Prof. R. Graham Cooks. He developed several new scan modes for the linear quadrupole ion trap, most notably secular frequency scanning, the inverse Mathieu q scan, precursor and neutral loss scans, logical MS/MS scans, and two-dimensional MS/MS scans. These developments led to no less than 23 peer-reviewed publications, >5 patent applications, and ~18 conference poster/oral presentations, including three first author oral presentations at the annual American Society for Mass Spectrometry Conference. Dalton collaborated with NASA Goddard Space Flight Center, FLIR Systems, Inc., and Merck, and, through a NASA Visiting Technologiest Experience, spent several weeks at Goddard implementing new scan modes on a breadboard of the Mars Organic Molecule Analyzer Linear Ion Trap. Dalton was a member of two university jazz bands, Phi Lambda Upsilon, the Golden Key International Honor Society, and the Turkey Run Analytical Chemistry Conference Organizing Committee (having organized the 2017 meeting).

PUBLICATIONS

1. Snyder, D. T.; Szalwinski, L. J.; Cooks, R. G. Two-dimensional mass spectrometry in a linear quadrupole ion trap via ion micropacket detection. *In preparation*.

2. Snyder, D. T.; Szalwinski, L. J.; Cooks, R. G. Two-dimensional mass spectrometry in a linear quadrupole ion trap via frequency tagging. *In preparation*.

3. Snyder, D. T.; Szalwinski, L. J.; Cooks, R. G. Improving performance metrics of ion trap precursor and neutral loss scans using triple resonance techniques. *In preparation*.

4. Snyder, D. T.; Szalwinski, L. J.; Cooks, R. G. Logical MS/MS: A new set of operations for tandem mass spectrometry. *Submitted.*

5. Snyder, D. T.; Szalwinski, L. J.; Cooks, R. G. Mass Spectrometry | Ion Traps. In *Encyclopedia of Analytical Science, 3rd Edition*. To be published in Feb. 2019.

6. Snyder, D. T.; Szalwinski, L. J.; Hilger, R.; Cooks, R. G. Implementation of precursor and neutral loss scans on a miniature ion trap mass spectrometer and performance comparison to a bench top linear ion trap. *J. Am. Soc. Mass Spectrom.* **2018**, *29*, 1355-1364. DOI: 10.1007/s13361-018-1922-1

7. Snyder, D. T.; Szalwinski, L. J.; Schrader, R.; Pirro, V.; Hilger, R.; Cooks, R. G. Precursor and neutral loss scans in an rf scanning linear quadrupole ion trap. *J. Am. Soc. Mass Spectrom.* **2018**, *29*, 1345-1354. DOI: 10.1007/s13361-018-1920-3

8. Snyder, D. T.; Szalwinski, L. J.; Cooks, R. G. Sequential and simultaneous MS/MS combinations and permutations in a linear quadrupole ion trap. *Anal. Chem.* **2017**, *89*, 11053-11060. DOI: 10.1021/acs.analchem.7b03064

9. Snyder, D. T.; Cooks, R. G. Single analyzer neutral loss scans in a linear quadrupole ion trap using orthogonal double resonance excitation. *Anal. Chem.* **2017**, *89*, 8148-8155. DOI: 10.1021/acs.analchem.7b01963

10. Snyder, D. T.; Cooks, R. G. Single analyzer precursor ion scans in a linear quadrupole ion trap using orthogonal double resonance excitation. *J. Am. Soc. Mass Spectrom.* **2017**, *28*, 1929-1938. DOI: 10.1007/s13361-017-1707-y

11. Snyder, D. T.; Kaplan, D.; Danell, R.; van Amerom, F.; Pinnick, V.; Brinckerhoff, W.; Mahaffy, P.; Cooks, R. G. Unique capabilities of ac frequency scanning and its application on a Mars Organic Molecule Analyzer linear ion trap. *Analyst.* **2017**, *142*, 2109-2117. DOI: 10.1039/C7AN00664K

12. Snyder, D. T.; Cooks, R. G. Improving mass assignments in quadrupole ion traps operated using ac scans: Theory and experimental validation. *Int. J. Mass Spectrom.* **2017**, *417*, 1-7. DOI: 10.1016/j.ijms.2017.05.001

13. Snyder, D. T.; Cooks, R. G. Ion isolation and multigenerational collision-induced dissociation using the inverse Mathieu q scan. *Rapid Commun. Mass Spectrom.* **2017**, *31*, 200-206. DOI: 10.1002/rcm.7782

14. Snyder, D. T.; Wen-Ping Peng; Cooks, R. G. Resonance methods in quadrupole ion traps. *Chem. Phys. Lett.* **2017***, 668*, 69-89. Invited Frontiers article. DOI: 10.1016/j.cplett.2016.11.011 *Cover Article.*

15. Pulliam, C. J.; Bain, R. Osswald, H.; Snyder, D. T.; Ayrton, S.; Fedick, P.; Flick, T. Cooks, R. G. Simultaneous on-line monitoring of multiple reactions using a miniature mass spectrometer. *Anal. Chem.* **2017**, *89*, 6969-6975. DOI: 10.1021/acs.analchem.7b00119

16. Snyder, D. T.; Pulliam, C. J.; Cooks, R. G. Extending the mass range of a miniature ion trap mass spectrometer using the inverse Mathieu q scan. *Int. J. Mass Spectrom.* **2017**, *422*, 154-161. DOI: 10.1016/j.ijms.2016.10.022

17. Snyder, D. T. Pulliam, C. J. Cooks, R. G. Linear mass scans in quadrupole ion traps using the inverse Mathieu q scan. *Rapid Commun. Mass Spectrom.* **2016**, *30*, 2369-2378. DOI: 10.1002/rcm.7710

18. Snyder, D. T.; Fedick, P.; Cooks, R. G. Multigenerational collision-induced dissociation for characterization of organic molecules. *Anal. Chem.* **2016**, *88*, 9572-9581. DOI: 10.1021/acs.analchem.6b02209

19. Snyder, D. T.; Cooks, R. G. Multigenerational broadband collision-induced dissociation of precursor ions in a linear quadrupole ion trap. *J. Am. Soc. Mass Spectrom.* **2016**, *27*, 1914-1921. DOI: 10.1007/s13361-016-1493-y

20. Snyder, D. T.; Cooks, R. G. Ion isolation in a linear ion trap using dual resonance frequencies. *J. Am. Soc. Mass Spectrom.* **2016**, *27*, 1906-1913. DOI: 10.1007/s13361-016-1494-x

21. Snyder, D. T.; Cooks, R. G. Successive resonances for ion ejection at arbitrary frequencies in an ion trap. *J. Am. Soc. Mass Spectrom.* **2016**, *27*, 1922-1928. DOI: 10.1007/s13361-016-1473-2

22. Snyder, D. T.; Pulliam, C. J. Cooks, R. G. Calibration procedure for secular frequency scanning in an ion trap. *Rapid Commun. Mass Spectrom.* **2016**, *30*, 1190-1196. DOI: 10.1002/rcm.7550

23. Snyder, D. T.; Pulliam, C. J.; Cooks, R. G. Single analyzer precursor scans using an ion trap. *Rapid. Commun. Mass Spectrom.* **2016**, *30*, 800-804. DOI: 10.1002/rcm.7500

24. Snyder, D. T.; Pulliam, C. J.; Wiley, J. S.; Duncan, J.; Cooks, R. G. Experimental Characterization of Secular Frequency Scanning in Ion Trap Mass Spectrometers. *J. Am. Soc. Mass Spectrom.* **2016**, *27*, 1243-1255. DOI: 10.1007/s13361-016-1377-1

25. Bag, S.*; Wei, P.*; Pulliam, C. J.; Snyder, D. T. Pielak, R. M.; Cooks, R. G. Analysis of bacteria using zero volt paper spray. *Anal. Methods* **2016**, *8*, 1770-1773. DOI: 10.1039/C6AY00063K

26. Pulliam, C. J.*; Wei, P.*; Snyder, D. T.; Wang, X.; Pielak, R. M.; Ouyang, Z.; Cooks, R. G. Rapid discrimination of bacteria using a miniature mass spectrometer. *Analyst.* **2016***, 141*, 1633-1636. DOI: 10.1039/C5AN02575C

27. Snyder, D. T.; Pulliam, C. J.; Cooks, R. G. Miniature and Fieldable Mass Spectrometers: Recent Advances. *Anal. Chem.* **2016**, *88*, 2-29. Invited review. DOI: 10.1021/acs.analchem.5b03070

406

analytical chemistry

Single Analyzer Neutral Loss Scans in a Linear Quadrupole Ion Trap Using Orthogonal Double Resonance Excitation

Dalton T. Snyder and R. Graham Cooks*

Purdue University Department of Chemistry, West Lafayette, Indiana 47907, United States

ABSTRACT: In this follow-up paper to our previous work on single analyzer precursor ion scans in a linear quadrupole ion trap (Snyder, D. T.; Cooks, R. G. Single analyzer precursor ion scans in a linear quadrupole ion trap using orthogonal double resonance excitation. *J. Am. Soc. Mass Spectrom.* **2017**, DOI: 10.1007/s13361-017-1707-y), we now report the development of single analyzer neutral loss scans in a linear quadrupole ion trap using orthogonal double resonance excitation. Methodologically, there are three key differences between single analyzer precursor ion scans and neutral loss scans under constant radiofrequency (rf) conditions: (1) in the latter experiment, both excitation and ejection frequencies must be scanned, whereas in the former the ejection frequency is fixed, (2) the need to maintain a constant neutral loss while incrementing both precursor and product ion masses, complicated by the complex relationship between secular frequency and mass, requires use of two simultaneous frequency scans, both linear in mass, and (3) because the ejection frequency is scanned, a third ac signal occurring between the ac excitation and ac ejection frequency scans must also be applied and scanned in order to reject artifact peaks caused by ejection of unfragmented precursor ions. Using this methodology, we demonstrate neutral loss scans on a commercial linear ion trap using mixtures of illicit drugs and acylcarnitines. We also demonstrate neutral loss scanning on a *Populus deltoides* leaf and on a lignin sample, both significantly more complex mixtures.

The beginnings of tandem mass spectrometry (MS/MS or MS^n) date back to the first mass-analyzed ion kinetic energy spectrometer (MIKES) developed at Purdue University.[1-5] Tandem MS, the production and mass analysis of fragment ions from mass-selected precursor ions, is particularly useful for complex mixture analysis and has served as the backbone of fields as diverse as proteomics,[6-8] forensics,[9,10] environmental monitoring,[11,12] and biomarker discovery.[13,14]

Among the activation methods for MS/MS are collision-induced dissociation (CID),[15] ultraviolet photodissociation,[16-18] infrared multiphoton dissociation,[19] electron transfer dissociation,[20] surface-induced dissociation,[21-23] and others. Collision-induced dissociation has been especially notable in the development of the suite of MS/MS scan modes which includes three prominent members, product ion scans, precursor ion scans, and neutral loss scans,[24,25] as well as other notable modes, doubly charged ion scans,[26] reaction intermediate scans,[27] multiple reaction monitoring,[28] and functional relationship scans.[29] Of interest in this work is the neutral loss scan, which is readily implemented in multianalyzer instruments such as the triple quadrupole[25] but not previously accessible with any single mass analyzer operated in a data-independent mode.

Although neutrals are not directly measurable by mass spectrometers, they are indirectly accessible by a variety of methods and they carry important analytical information. The two most prominent techniques for probing neutral species are

neutralization-reionization mass spectrometry (NRMS)[30-32] and the neutral loss scan.[33] The NRMS experiment neutralizes a mass-selected ion, usually by charge exchange or CID, and the resulting neutral undergoes energetic collisions that produce neutral fragments that are reionized and mass analyzed. Hypervalent and other unusual species can be produced and characterized,[34-36] a unique capability.

By contrast, in a neutral loss MS/MS experiment, a precursor ion is mass-selected by a first mass analyzer and undergoes activation to produce a product ion and a neutral. The product ion is mass selected for detection by a second analyzer. For the neutral loss scan, the relationship between the precursor ion mass-to-charge ratio (m/z) and the product ion m/z is fixed, that is, the neutral mass is constant, and as such it describes a shared molecular functionality of a group of precursor ions. In comparison, the precursor ion scan selects a fixed product ion m/z, which might also correspond to a common functionality in all precursor ions that yield this fragment.

Because mass selection of both precursor and product ion is necessitated in precursor ion and neutral loss scans, the prevailing wisdom in mass spectrometry has been that multiple mass analyzers are required. However, Yost et al. demonstrated in principle that a single 3D ion trap could perform a single

Table 1. Experimental Parameters for Neutral Loss Scans Performed in This Work

figure	RF modulation[a] (mV_{pp})	LMCO (Th)	scan rate (Th/s)	excitation amplitude (mV_{pp})	artifact reject amplitude (mV_{pp})	eject amplitude (mV_{pp})	excite delay[b] (ms)	artifact reject delay (ms)	eject delay (ms)	NL[c] (Da)
2b	210	100	1740	400	2700	1200	75	91.35	112.6	57
3b	150	70	1140	150	440	400	75	85.35	99.6	31
3c	150	70	1140	140	190	400	75	80.35	94.5	19
4b	210	100	1740	600	3400	1200	75	91.35	107.6	59
5b	300	200	2900	400	2000	1600	75	79.35	87	44
6b	200	110	1580	500	700	700	135	140	147	18

[a]RF modulation is the dc voltage substituted between the rf detector board and rf amplifier and is proportional to the rf amplitude (i.e., determines the LMCO). [b]Delay time indicates trigger delay between the beginning of the ionization phase to the application of the waveform. The difference between the excite delay and eject delay is directly proportional to the neutral loss mass. [c]NL = neutral loss.

analyzer precursor ion scan by using multiple simultaneous resonance frequencies corresponding to precursor and product ion.[37] In other words, the precursor ion is mass-selectively activated via CID by a first scanned resonance frequency, and product ions of a selected m/z (determined by the resonance frequency) are then simultaneously ejected upon their formation by a second fixed resonance frequency. The correlation between m/z and time is thus preserved in the ejection time of the product ion.

The first published implementation of the single analyzer precursor ion scan in a linear ion trap[38] used the Mini 12[39] miniature rectilinear ion trap mass spectrometer developed at Purdue University. In that experiment, the two resonance frequencies were applied in a parallel fashion on the same pair of electrodes; however, beat frequencies and unintentional ejection of precursor ions during excitation caused artifact peaks, which significantly hampered the utility of this scan mode. Subsequently, we developed an orthogonal version of the precursor scan experiment in which precursor ion excitation and product ion ejection frequencies were applied to orthogonal electrode pairs, thereby mitigating both problems simultaneously.[40]

Here we demonstrate the corresponding neutral loss scan mode in a single linear ion trap, also using orthogonal double resonance excitation. The implementation of neutral loss scans, as well as precursor ion scans, in a single mass analyzer is motivated by the constraints placed upon miniature and portable mass spectrometers,[41,42] for which simple, power-efficient electronics, lenient vacuum conditions, and small footprints are imperative. These considerations eliminate multiple-analyzer mass spectrometers as candidate analyzers in a portable system. The constraints are further exacerbated in space science, where power consumption and instrument volume are of the utmost concern.[43] The ultimate goal in this work is the eventual implementation of both precursor ion and neutral loss scans on the next-generation linear ion traps developed at NASA Goddard Space Flight Center for detection of organic compounds on Mars.

■ EXPERIMENTAL SECTION

Chemicals. Acetyl-L-carnitine (C_2 side chain) hydrochloride, propionyl-L-carnitine (C_3), isobutyryl-L-carnitine (C_4), isovaleryl-L-carnitine (C_5), and hexanoyl-L-carnitine (C_6) were purchased from Sigma-Aldrich (St. Louis, MO, U.S.A.). These compounds were dissolved and diluted in 50:50 methanol/water. Amphetamine, methamphetamine, 3,4-methylenedioxyamphetamine, and 3,4-methylenedioxymethamphetamine were purchased from Cerilliant (Round Rock, TX,

U.S.A.) and were diluted in methanol to concentrations between 0.25 and 1 ppm. Pierce ESI LTQ calibration mixture containing caffeine, the peptide MRFA, and Ultramark 1621[44] was obtained from Thermo Fisher (Rockford, IL, U.S.A.). Organosolv switchgrass lignin was prepared as previously described[45] and dissolved initially in 50:50 water/tetrahydrofuran but then diluted further in 50:50 methanol/water.

Ionization. Nanoelectrospray ionization (nESI) was used for production of analyte ions in the majority of this study. Typical operating parameters were 1500 V spray voltage using 5 μm nanospray tips pulled from borosilicate glass capillaries (1.5 mm O.D., 0.86 I.D.; Sutter Instrument Co., Novato, CA, U.S.A.) by a Flaming/Brown micropipette puller (model P-97; Sutter Instrument Co.).

A leaf from a *Populus deltoides* tree (latitude 40.464, longitude −86.968) was analyzed by leaf spray ionization tandem mass spectrometry.[46,47] For this experiment, a triangle (~8 mm height, 5 mm width) was cut from the leaf, held in a copper clip, and 5 kV was applied to the leaf after addition of 20 μL of methanol/water in order to generate ions for analysis.

The positive ion mode was used for all experiments. Ion injection time was generally set at 5 ms but was manually optimized to prevent trap overloading. Automatic gain control was not used in this study.

Instrumentation. A Thermo Scientific LTQ linear ion trap mass spectrometer (San Jose, CA, U.S.A.) with rf frequency tuned to 1.164 MHz was used for all experiments. The dimensions of the trap are x_0 = 4.75 mm, y_0 = 4 mm, and three axial sections of 12, 37, and 12 mm.[48] As described previously,[40] the commercial rf coil was modified with an extra Thermo LTQ low pass filter board (part 97055−91120) and Thermo LTQ balun board (part 97055−91130) in order for low voltage ac signals to be applied to both x and y electrodes of the linear ion trap.[48] As supplied commercially, the LTQ can only apply supplementary ac voltages to the x electrodes, the direction in which the detector lies, but in this study orthogonality of excitation and ejection signals is crucial to obtaining unambiguous results.

In contrast to our previous study on single analyzer precursor ion scans, the rf voltage in this study was fixed by substituting the rf modulation signal between the main rf amplifier board and the rf detector board with a DC signal from an external function generator. The DC signal was directly proportional to the output voltage from the coil, as indicated by the calibrated lower-mass cutoff (LMCO) and mass scan rate values (Table 1). For example, a modulation signal of 210 mV_{pp} provided a LMCO of ~100 Th. Due to electronic constraints, the amplitude of the modulation signal did not vary through the scan period and was constant through the ionization, ion
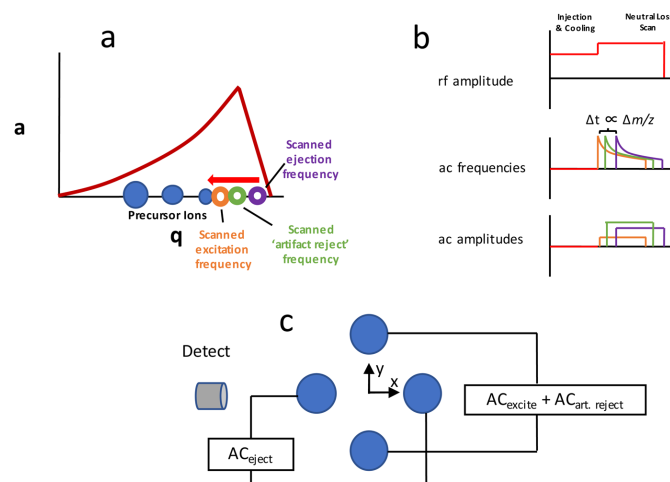
Figure 1. Methodology for single analyzer neutral loss scans in a linear quadrupole ion trap. (a) As shown on the Mathieu stability diagram, three supplementary ac frequencies are scanned simultaneously at the same mass scan rate in order to excite precursor ions and simultaneously eject product ions of a constant mass offset from the precursors, while a third intermediate frequency is scanned to reject artifactual unfragmented precursor ions. A scan table of the experiment is shown in (b), and (c) shows the directionality of the low voltage frequency sweeps (trapping rf not shown). Adapted with permission from ref 40. Copyright Springer 2017.

cooling, and mass scan time segments. The duty cycle of the modulation signal was ~90%, the remaining time being used to pulse the analyzer to zero voltage and thus clear the trap of ions after every scan.

Neutral loss scans were performed by simultaneously applying three swept-frequency sinusoidal inverse Mathieu q scans to the x and y electrodes of the linear ion trap, as shown in the Mathieu stability diagram in Figure 1a and the scan table in Figure 1b. In general, all the inverse Mathieu q scans started at Mathieu $q = 0.908$ (start frequency of 580 kHz) and ended at $q = 0.15$ (end frequency of 62 kHz) 300 ms later. These scans give an approximately linear relationship between excited/ejected ion m/z and time.[49,50] Note that because the same frequency sweeps were used throughout this study, a higher rf voltage (and, hence, LMCO) will result in lower activation time for each precursor ion since the scan rate is proportional to the rf voltage.

A first frequency sweep was used for ion excitation, a second frequency sweep was used for precursor ion rejection after its excitation (artifact rejection), and a third frequency sweep was used for product ion ejection. The former two ac signals were summed and applied to the y electrodes and the third signal was applied to the x electrodes (Figure 1c), namely, in the dimension in which ions are detected. The frequency sweeps were all calculated in Matlab and applied by two synced Keysight 33612A 2-channel waveform generators (Newark, SC, U.S.A.). For application of two simultaneous frequency sweeps to the y electrodes, the two channels of one of the generators were summed into a single channel, a built-in feature of these Keysight units. The second Keysight generator supplied the product ion ejection frequency sweep and the dc signal for rf modulation.

In order to maintain a constant mass offset between the excitation frequency sweep and the ejection frequency sweep, a requirement for a neutral loss scan, the delay time between application of the excitation sweep and ejection sweep had to be varied. Because $t \propto m/z$, to a close approximation, for the inverse Mathieu q scan, a time offset between two identical frequency sweeps corresponds to a constant mass offset throughout the mass scan. The time offset could be approximated from the calibrated mass scan rate. Once the time offset was selected and verified experimentally, the time offset between the excitation frequency sweep and the artifact reject sweep was made approximately half the offset between the excitation and ejection sweeps. The artifact rejection sweep ejects into the y electrodes precursor ions that survive the excitation sweep, as we will discuss later, and is an important difference between single analyzer precursor ion scans and neutral loss scans.

The function generators were triggered just before the ionization period using the triggers built into the LTQ "Diagnostics" menu, and the trigger delays were then adjusted so that the neutral loss scan started at the beginning of the LTQ's data acquisition period (i.e., mass scan). For a built-in scan function, the commercial "Ultrazoom" scan was chosen. However, the "Ultrazoom" selection as used here did not control the scan rate or rf amplitude; it only controlled the length of data acquisition and digitization rate of the detection electronics. Each spectrum displayed here is an average of 20 scans.

■ RESULTS AND DISCUSSION

Comparison between Single Analyzer Precursor Ion Scans and Neutral Loss Scans. In previous work we demonstrated single analyzer precursor ion scans in a linear ion trap using orthogonal double resonance excitation at constant rf amplitude, that is, using sweeps of the low voltage ac frequency.[40] In order to mass-selectively fragment precursor ions as a function of time, a first swept-frequency sinusoidal ac signal is applied to the y electrodes. To eject a particular
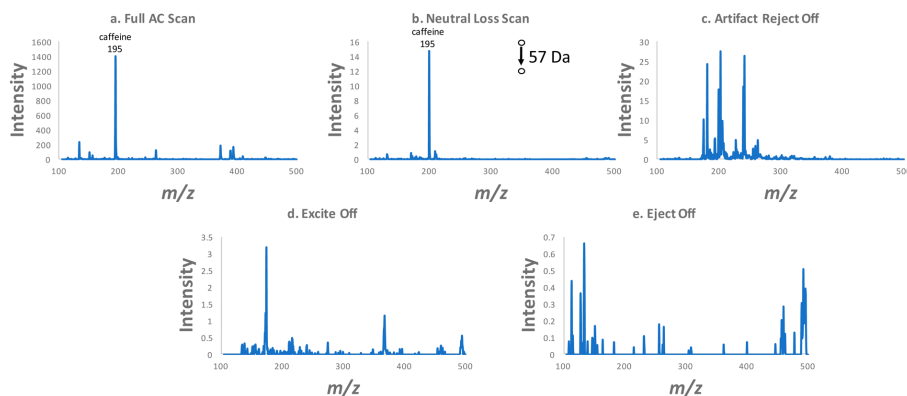
Figure 2. Only the combination of three ac frequency sweeps performed at the same mass scan rate gives an unambiguous neutral loss scan. (a) Full ac scan using LTQ ESI of caffeine in Pierce calibration mixture, (b) neutral loss scan of 57 Da, and neutral loss scans with (c) artifact reject frequency off, (d) precursor ion excitation frequency off, (e) product ion ejection frequency off. Note the different intensity scales.

product ion, a second ac signal with fixed frequency corresponding to that of the product ion is applied simultaneously to the x electrodes (direction in which ions are detected). The orthogonality of the excitation and ejection ac signals is key to preventing artifacts from being observed in the mass spectrum since precursor ions can be unintentionally ejected during the excitation frequency sweep. Thus, a signal is observed at the detector only when a precursor ion fragments to the product ion whose secular frequency is selected for ejection. Mass information is preserved in the ejection time of the product ion, which correlates to the fragmentation time of the precursor ion.

Neutral loss scans in a single linear ion trap have similarities to precursor ion scans but are significantly more complex. The difficulty stems from the following differences: (1) the ejection frequency must be scanned and hence it will eject both undesired precursor ions that survive fragmentation as well as the desired product ions formed during fragmentation, and (2) the excitation and ejection frequency sweeps must have a constant mass offset through the entire mass scan (a difficult task due to the complex relationship between secular frequency and ion m/z).

The first problem can be mitigated by scanning a third frequency for "artifact rejection" (Figure 1a,b). The artifact rejection frequency sweep must occur between the excitation and ejection frequency sweeps. Hence, during the simultaneous sweep of all three frequencies, precursor ions will first fragment because of the y-dimension excitation, neutral loss products will simultaneously be ejected into the detector by the dipolar x-direction ejection sweep, and leftover precursor ions will be ejected into the y electrodes by the artifact rejection sweep.

The second problem is maintenance of a constant mass offset between the excitation and ejection frequencies. The fact that the relationship between ion secular frequency and m/z cannot be described analytically but instead requires a numerical or analytical (i.e., a finite equation) approximation[51−53] makes calculation of the frequency sweeps difficult unless the relationship between m/z and time is linear, as is the case for the inverse Mathieu q scan.[49,50,54] By using this nonlinear frequency sweep for excitation, ejection, and artifact rejection, a simple experimental parameter, the delay time between the

frequency sweeps, then determines the mass of the neutral loss (Figure 1b). This fortunate relationship is only applicable to the inverse Mathieu q scan because $t \propto m/z$ and, therefore, $\Delta t \propto \Delta m/z$.

Of course, the amplitude of each of the three frequency sweeps needs to be adjusted according to the intended function. The excitation sweep should have the lowest amplitude so that it activates, not ejects, precursor ions. The artifact rejection and product ion ejection sweeps should both have higher amplitudes in order to eject precursor and product ions, respectively. The former should be adjusted to (1) prevent premature ejection of precursors but also (2) to efficiently eject precursors after activation. Importantly, the smaller the neutral loss mass, the closer each frequency sweep will be and, hence, the lower the amplitude that will be used for artifact rejection. The product ion ejection amplitude should be adjusted for sensitivity and resolution. In this work, the excitation signal was a few hundred millivolts, whereas the rejection and ejection sweeps were generally 3−6× higher in amplitude. See Table 1 for all experimental parameters.

To sum up the neutral loss scan experiment, a first inverse Mathieu q scan activates precursor ions, and simultaneous sweeps of two additional inverse Mathieu q scans with appropriate time delays reject leftover precursor ions and eject product ions of a constant mass offset. The three ac waveforms are identical inverse Mathieu q scans, which allows one to easily maintain a constant mass offset. The excitation and artifact reject sweeps are applied in the y dimension to reduce artifacts from ejection of precursor ions, and the ejection sweep is applied in the x direction, where the detector is placed (Figure 1c). The amplitude of each signal is adjusted for its intended function.

Validation of Neutral Loss Scanning by Double Resonance Excitation. In order to experimentally validate whether neutral loss scans are viable using a single linear ion trap, particularly with respect to artifact rejection, we began experiments with a very simple LTQ calibration mixture containing caffeine, the peptide MRFA, and Ultramark 1621 phosphazine molecules. To validate artifact rejection, only the low mass range (i.e., region surrounding the m/z of protonated caffeine) was considered. Figure 2a shows a full mass scan in

this mass range (LMCO = 100 Th) using a 300 ms inverse Mathieu q scan from Mathieu $q = 0.908$ to $q = 0.15$. Only caffeine, m/z 195, is present in high abundance and hence it should also be the only ion detected in a neutral loss scan of 57 Da (m/z 195 → 138). As shown in Figure 2b–e, only the neutral loss scan with all three ac frequency sweeps applied simultaneously gives an unambiguous mass spectrum (panel b). With the artifact rejection frequency off (Figure 2c), several peaks are observed to confound the data, and with either the excitation (Figure 2d) or ejection (Figure 2e) frequencies off, virtually no ions are detected. Note the different intensity scales for each plot. For the neutral loss scan, the full width at half-maximum (fwhm) for caffeine is 0.6 Da.

Screening of Illicit Drugs. Previously we demonstrated the application of precursor ion scans to amphetamine analysis and showed that amphetamine (amp) and methamphetamine (map) can be detected via a precursor ion scan of m/z 119, and 3,4-methylenedioxyamphetamine (mda) and 3,4-methylenedioxymethamphetamine (mdma) can be detected using a precursor ion scan of m/z 163.[40] Analogously, a neutral loss scan of 31 Da returns map and mdma (Figure 3b, compare to full scan in panel a), whereas a neutral loss scan of 17 Da (NH_3) reveals amp and mda, despite their low intensity (<25 counts) in the full mass scan. For the latter scan, differences in fragmentation efficiency or differences in precursor ion Mathieu q parameter can account for the relative intensity shifts from the full scan to the neutral loss scan. Remarkably, neither neutral loss scan shows beat frequency effects or other artifacts which may be caused by simultaneous excitation of multiple ions. Also note how cleanly the neutral loss scans of 31 and 17 Da distinguish the four amphetamines. The fwhm peak width in these spectra was ∼0.9 Da.

Screening of Acylcarnitines. In the premier demonstration of data-dependent ion trap precursor ion and neutral loss scanning, Yost et al. analyzed acylcarnitines, which offer similar product ions as well as similar neutral losses.[55] The Yost method required a complex sequence of scan segments and algorithms in order to select precursor ions for activation as well as to resonantly eject product ions without also ejecting other precursor ions. Although that method would be expected to yield higher sensitivity and resolution than the method proposed here (because each precursor ion is given more time on resonance and more time for product ion collisional cooling), the complexity and inefficiency of the scan with respect to electronics, data system, time, and hence power consumption makes it unsuitable for resource-constrained ion traps. Using the reported common neutral loss of 59 Da, we were able to perform a similar but data-independent neutral loss experiment with acetyl-, propionyl-, isobutyryl-, isovaleryl-, and hexanoyl-L-carnitine using a single ion injection (5 ms injection time) and a single 300 ms mass scan period. As shown in Figure 4b (compare to full scan in panel a), all of the acylcarnitines are detected, although only ∼4% of the precursor ion intensity is observed due to the short activation time. The intensity in the neutral loss scan can be increased by decreasing the scan rate, giving precursor ions longer resonance times and thus increasing the conversion of precursor ions to product ions. For example, if the scan rate is decreased by a factor of 3, then the efficiency of conversion of precursor ions to detected product ions becomes ∼10%. Other peaks were observed between the main analyte peaks. These correspond to the sodiated analytes, which clearly exhibit higher conversion of
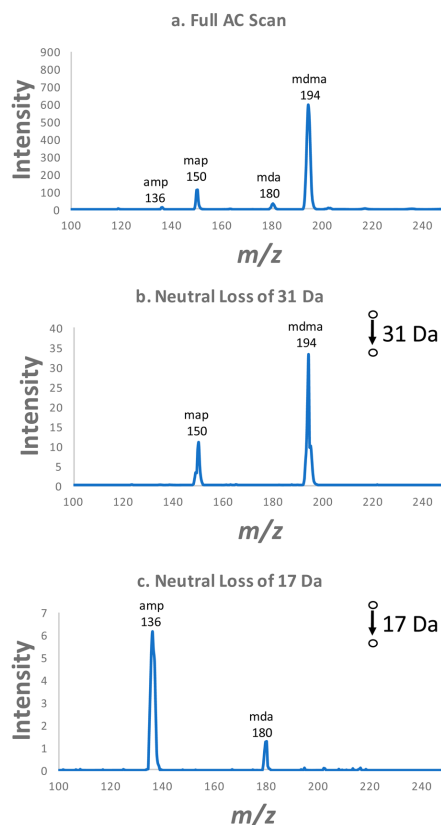

Figure 3. Single analyzer neutral loss scans of amphetamines: (a) full scan mass spectrum of amphetamine (amp), methamphetamine (map), 3,4-methylenedioxyamphetamine (mda), and 3,4-methylenedioxymethamphetamine (mdma); (b) neutral loss scan of 31 Da, and (c) neutral loss scan of 17 Da.

precursor ions to product ions, likely due to the stabilization of the molecules via a salt bridge interaction.

Screening of Phenolic Glycosides in a *Populus deltoides* Leaf. Moving to a complex mixture is a significant step for any scan mode, as additional complexity can easily result in addition of artifact peaks as well as suppression of analyte signal. As an initial demonstration of analysis of complex mixtures using a data-independent single analyzer neutral loss scan, we chose an individual leaf of a *Populus deltoides* tree.[47] The *Populus* genus is well-known to contain phenolic glycosides, which are defense chemicals that deter herbivores and decrease their fitness.[56,57] Previously they have been analyzed by leaf spray ionization tandem mass spectrometry using a triple quadrupole mass spectrometer.[47] Potassiated salicortin and HCH salicortin (structures in ref 47) were previously observed as the dominant ions in the full scan, as they were in this study (Figure 5a). It was also noted previously that neutral losses of 44 Da in the positive ion mode (CO_2, as confirmed by exact mass measurement on an LTQ
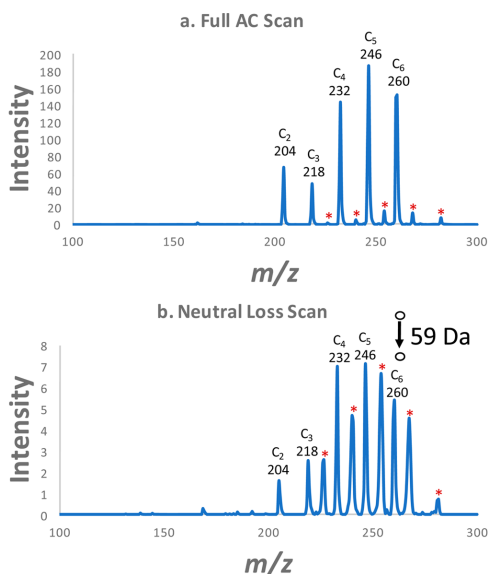
Figure 4. Single analyzer neutral loss scanning of acylcarnitines: (a) full ac scan of acetylcarnitine (m/z 204), propionylcarnitine (m/z 218), isobutyrylcarnitine (m/z 232), isovalerylcarnitine (m/z 246), and hexanoylcarnitine (m/z 260), and (b) neutral loss scan of 59 Da. Peaks marked with * are sodium adducts.
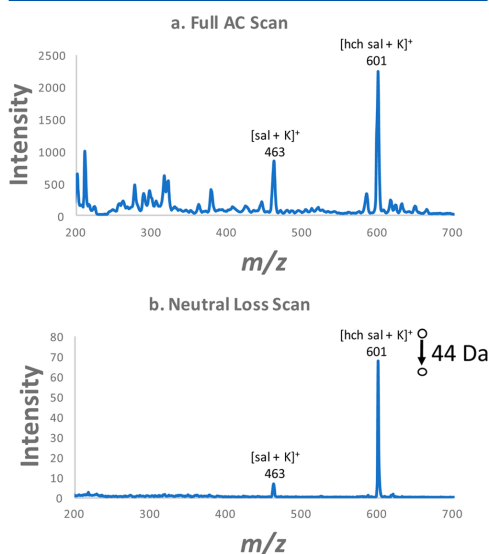

Figure 5. Single analyzer neutral loss scanning of a *Populus deltoides* leaf: (a) full scan mass spectrum and (b) neutal loss scan of 44 Da, targeting phenolic glycosides salicortin (sal) and HCH salicortin (hch sal).

Orbitrap XL with <1.0 ppm error) are common among the phenolic glycosides due to their unique (and shared) side chains, and hence, a neutral loss scan ought to filter out most other chemicals.

A neutral loss scan of 44 Da (Figure 5b) revealed both potassiated salicortin as well as the potassium adduct of HCH salicortin. About 3% of the precursor ions were converted to detected product ions, in line with the data in the previous case. Despite the chemical complexity of the leaf, virtually no other peaks were observed in the neutral loss spectrum, perhaps because losses of CO_2 are not common in the positive ion mode. The peak width in this case was ~1 Da fwhm.

Screening of Components in Switchgrass Lignin. The previous experiment provides evidence that a complex mixture can be vastly simplified using a single data-independent neutral loss scan in a single quadrupole ion trap. One might think, however, that ions of lower abundance than salicortin were not detected in the neutral loss scan because they were present at low concentrations. We, therefore, examined a mixture with a large set of ions of varying abundances that could be detected using a single neutral loss scan.

Organosolv switchgrass lignin is a complex mixture of phenolic compounds and carbohydrates, as well as other molecules with similar functionality, that has previously been characterized by HPLC-MS/MS in a linear quadrupole ion trap coupled to a Fourier transform ion cyclotron resonance mass spectrometer.[45] The study was performed primarily in negative ion mode because most of the ions produced in the positive ion mode lose 18 Da (water) in MS/MS, and hence, MS/MS spectra in positive mode do not distinguish the various classes of molecules. However, for the purposes of determining the dynamic range of the neutral loss scan, the positive ion mode provides a reasonable set of analytes for examination.

As previously described and as shown in Figure 6a, the full scan mass spectrum of organosolv lignin is complex, but most of the molecules present in the full scan lose 18 Da in MS/MS. As shown in Figure 6b, a neutral loss scan of 18 Da returns not just the ions of high abundance, but also those of low abundance. Of course, the ions of interest must be labile enough to fragment in a relatively short period of time (~1 ms), and so the neutral loss scan will inherently be biased against molecules that do not fragment readily. Another limitation of the ion trap neutral loss scan is that the selectivity is limited by secular frequency spacing and bandwidth. It is hence difficult to distinguish neutral losses of similar mass. As shown in Figure 6b, not only were water loss products detected, but also the loss of 17 Da (152 → 135). Exciting and ejecting ions at varying Mathieu q exacerbates this problem. The sensitivity is limited by the limited activation time that each ion experiences, which in these experiments varied from ~350 μs to 1 ms. As noted previously, however, the conversion efficiency of precursors to products can be increased by slowing the scan rate.

■ CONCLUSION

Since the initial development of linear quadrupole ion traps approximately a decade and a half ago,[48,58] it has been the prevailing wisdom that single ion traps cannot perform data-independent precursor and neutral loss scans, two of the three main types of MS/MS experiments. As we have shown in this and the related paper on precursor ion scans, quadrupole ion traps are extraordinarily versatile devices with access to all three major MS/MS scan types.
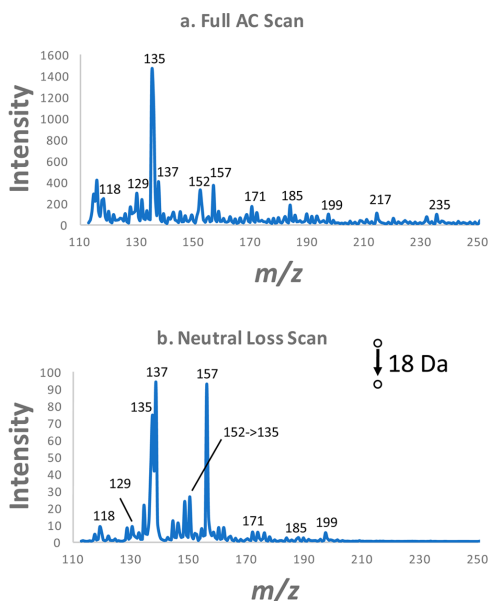
Figure 6. Single analyzer neutral loss scan of organosolv switchgrass lignin: (a) full scan mass spectrum and (b) neutral loss scan of 18 Da.

Compared to previous variants of data-dependent neutral loss scanning, this double resonance neutral loss scan offers high efficiency in terms of time, rf power, and sample consumption. The demonstrated method is completely data-independent and only requires a single mass scan segment and a single ion injection, making it particularly suitable for planetary exploration and other applications where significant constraints are imposed upon the instrument.

■ AUTHOR INFORMATION

Corresponding Author

*E-mail: cooks@purdue.edu.

ORCID ⓘ

R. Graham Cooks: 0000-0002-9581-9603

Notes

The authors declare no competing financial interest.

■ ACKNOWLEDGMENTS

■ REFERENCES

(1) Beynon, J. H.; Cooks, R. G.; Amy, J. W.; Baitinger, W. E.; Ridley, T. Y. *Anal. Chem.* **1973**, *45*, 1023A−1031A.

(2) Cooks, R. G.; Beynon, J. H.; Litton, J. F. *Org. Mass Spectrom.* **1975**, *10*, 503−506.

(3) Kruger, T. L.; Litton, J. F.; Kondrat, R. W.; Cooks, R. G. *Anal. Chem.* **1976**, *48*, 2113−2119.

(4) Beynon, J. H.; Cooks, R. G. *Int. J. Mass Spectrom. Ion Phys.* **1976**, *19*, 107−137.

(5) Kondrat, R. W.; Cooks, R. G.; McLaughlin, J. L. *Science* **1978**, *199*, 978−980.

(6) Schroeder, M. J.; Shabanowitz, J.; Schwartz, J. C.; Hunt, D. F.; Coon, J. J. *Anal. Chem.* **2004**, *76*, 3590−3598.

(7) Syka, J. E.; Coon, J. J.; Schroeder, M. J.; Shabanowitz, J.; Hunt, D. F. *Proc. Natl. Acad. Sci. U. S. A.* **2004**, *101*, 9528−9533.

(8) Swaney, D. L.; McAlister, G. C.; Coon, J. J. *Nat. Methods* **2008**, *5*, 959−964.

(9) Lawton, Z. E.; Traub, A.; Fatigante, W. L.; Mancias, J.; O'Leary, A. E.; Hall, S. E.; Wieland, J. R.; Oberacher, H.; Gizzi, M. C.; Mulligan, C. C. *J. Am. Soc. Mass Spectrom.* **2017**, *28*, 1048−1059.

(10) Vircks, K. E.; Mulligan, C. C. *Rapid Commun. Mass Spectrom.* **2012**, *26*, 2665−2672.

(11) Shortt, B. J.; Darrach, M. R.; Holland, P. M.; Chutjian, A. *J. Mass Spectrom.* **2005**, *40*, 36−42.

(12) Contreras, J. A.; Murray, J. A.; Tolley, S. E.; Oliphant, J. L.; Tolley, H. D.; Lammert, S. A.; Lee, E. D.; Later, D. W.; Lee, M. L. *J. Am. Soc. Mass Spectrom.* **2008**, *19*, 1425−1434.

(13) Ferreira, C. R.; Yannell, K. E.; Mollenhauer, B.; Espy, R. D.; Cordeiro, F. B.; Ouyang, Z.; Cooks, R. G. *Analyst* **2016**, *141*, 5252−5255.

(14) Crutchfield, C. A.; Thomas, S. N.; Sokoll, L. J.; Chan, D. W. *Clin. Proteomics* **2016**, *13*, 1.

(15) Cooks, R. G. *Collision Spectroscopy*; Springer: New York, 1978; pp 357−450.

(16) Schinke, R. *Photodissociation Dynamics: Spectroscopy and Fragmentation of Small Polyatomic Molecules*; Cambridge University Press: New York, 1993.

(17) Brodbelt, J. S. *Chem. Soc. Rev.* **2014**, *43*, 2757−2783.

(18) Cammarata, M. B.; Brodbelt, J. S. *Chem. Sci.* **2015**, *6*, 1324−1333.

(19) Little, D. P.; Speir, J. P.; Senko, M. W.; O'Connor, P. B.; McLafferty, F. W. *Anal. Chem.* **1994**, *66*, 2809−2815.

(20) Syka, J. E.; Coon, J. J.; Schroeder, M. J.; Shabanowitz, J.; Hunt, D. F. *Proc. Natl. Acad. Sci. U. S. A.* **2004**, *101*, 9528−9533.

(21) Mabud, M. A.; Dekrey, M. J.; Cooks, R. G. *Int. J. Mass Spectrom. Ion Processes* **1985**, *67*, 285−294.

(22) Chorush, R. A.; Little, D. P.; Beu, S. C.; Wood, T. D.; McLafferty, F. W. *Anal. Chem.* **1995**, *67*, 1042−1046.

(23) Dongre, A. R.; Somogyi, A.; Wysocki, V. H. *J. Mass Spectrom.* **1996**, *31*, 339−350.

(24) Schwartz, J. C.; Wade, A. P.; Enke, C. G.; Cooks, R. G. *Anal. Chem.* **1990**, *62*, 1809−1818.

(25) Yost, R. A.; Enke, C. G. *Anal. Chem.* **1979**, *51*, 1251−1264.

(26) Kenttamaa, H. I.; Wood, K. V.; Busch, K. L.; Cooks, R. G. *Org. Mass Spectrom.* **1983**, *18*, 561−567.

(27) Schwartz, J. C.; Schey, K. L.; Cooks, R. G. *Int. J. Mass Spectrom. Ion Processes* **1990**, *101*, 1−20.

(28) Kondrat, R. W.; Mcclusky, G. A.; Cooks, R. G. *Anal. Chem.* **1978**, *50*, 2017−2021.

(29) Vincenti, M.; Schwartz, J. C.; Cooks, R. G.; Wade, A. P.; Enke, C. G. *Org. Mass Spectrom.* **1988**, *23*, 579−584.

(30) McLafferty, F. W. *Science* **1990**, *247*, 925−929.

(31) Wesdemiotis, C.; McLafferty, F. W. *Chem. Rev.* **1987**, *87*, 485−500.

(32) Terlouw, J. K.; Schwarz, H. *Angew. Chem., Int. Ed. Engl.* **1987**, *26*, 805−815.

(33) Zakett, D.; Schoen, A. E.; Kondrat, R. W.; Cooks, R. G. *J. Am. Chem. Soc.* **1979**, *101*, 6781−6783.

(34) Goldberg, N.; Schwarz, H. *Acc. Chem. Res.* **1994**, *27*, 347−352.

(35) Haag, R.; Schröder, D.; Zywietz, T.; Jiao, H.; Schwarz, H.; von Ragué Schleyer, P.; de Meijere, A. *Angew. Chem., Int. Ed. Engl.* **1996**, *35*, 1317−1319.

(36) Schröder, D.; Schalley, C. A.; Schwarz, H.; Goldberg, N.; Hrûsák, J. *Chem. - Eur. J.* **1996**, *2*, 1235−1242.

(37) Johnson, J. V.; Pedder, R. E.; Yost, R. A. *Int. J. Mass Spectrom. Ion Processes* **1991**, *106*, 197−212.

(38) Snyder, D. T.; Pulliam, C. J.; Cooks, R. G. *Rapid Commun. Mass Spectrom.* **2016**, *30*, 800−804.

(39) Li, L.; Chen, T. C.; Ren, Y.; Hendricks, P. I.; Cooks, R. G.; Ouyang, Z. *Anal. Chem.* **2014**, *86*, 2909−2916.

(40) Snyder, D. T.; Cooks, R. G. *J. Am. Soc. Mass Spectrom.* **2017**, DOI: 10.1007/s13361-017-1707-y.

(41) Ouyang, Z.; Cooks, R. G. *Annu. Rev. Anal. Chem.* **2009**, *2*, 187−214.

(42) Snyder, D. T.; Pulliam, C. J.; Ouyang, Z.; Cooks, R. G. *Anal. Chem.* **2016**, *88*, 2−29.

(43) Brinckerhoff, W. B.; Pinnick, V. T.; van Amerom, F. H. W.; Danell, R. M.; Arevalo, R. D.; Atanassova, M. S.; Li, X.; Mahaffy, P. R.; Cotter, R. J.; Goesmann, F.; Steininger, H.; Team, M. Mars Organic Molecule Analyzer (MOMA) Mass Spectrometer for ExoMars 2018 and Beyond. *IEEE Aerospace Conference*, **2013**.

(44) Jiang, L. F.; Moini, M. *J. Am. Soc. Mass Spectrom.* **1992**, *3*, 842−846.

(45) Jarrell, T. M.; Marcum, C. L.; Sheng, H.; Owen, B. C.; O'Lenick, C.; Maraun, H.; Bozell, J. J.; Kenttämaa, H. I. *Green Chem.* **2014**, *16*, 2713−2727.

(46) Liu, J.; Wang, H.; Cooks, R. G.; Ouyang, Z. *Anal. Chem.* **2011**, *83*, 7608−7613.

(47) Snyder, D. T.; Schilling, M. C.; Hochwender, C. G.; Kaufman, A. D. *Anal. Methods* **2015**, *7*, 870−876.

(48) Schwartz, J. C.; Senko, M. W.; Syka, J. E. *J. Am. Soc. Mass Spectrom.* **2002**, *13*, 659−669.

(49) Snyder, D. T.; Pulliam, C. J.; Cooks, R. G. *Rapid Commun. Mass Spectrom.* **2016**, *30*, 2369−2378.

(50) Snyder, D. T.; Cooks, R. G. *Int. J. Mass Spectrom.* **2017**, *417*, 1.

(51) Koizumi, H.; Whitten, W. B.; Reilly, P. T. A.; Koizumi, E. *Int. J. Mass Spectrom.* **2009**, *286*, 64−69.

(52) March, R. E.; Todd, J. F. J. *Practical Aspects of Trapped Ion Mass Spectrometry*; CRC Press Taylor & Francis Group: Boca Raton, FL, 2010; Vol. *IV*.

(53) Snyder, D. T.; Pulliam, C. J.; Cooks, R. G. *Rapid Commun. Mass Spectrom.* **2016**, *30*, 1190−1196.

(54) Snyder, D. T.; Pulliam, C. J.; Cooks, R. G. *Int. J. Mass Spectrom.* **2016**, n/a.

(55) McClellan, J. E.; Quarmby, S. T.; Yost, R. A. *Anal. Chem.* **2002**, *74*, 5799−5806.

(56) Orians, C. M.; Fritz, R. S. *J. Chem. Ecol.* **1995**, *21*, 1245−1253.

(57) Boeckler, G. A.; Gershenzon, J.; Unsicker, S. B. *Phytochemistry* **2011**, *72*, 1497−1509.

(58) Hager, J. W. *Rapid Commun. Mass Spectrom.* **2002**, *16*, 512−526.